The Dissertation Committee for Nolan Wayne Waggoner Certifies that this is the approved version of the following dissertation:

Development of novel porous coordination polymers with interest in catalysis, structure directing agents, and magnetism

Committee:

Simon M. Humphrey, Supervisor

Michael J. Rose

Eric. V. Anslyn

Delia J. Milliron

Paul T. Wood

Development of novel porous coordination polymers with interest in catalysis, structure directing agents, and magnetism

by

Nolan Wayne Waggoner, B.S.

Dissertation

Presented to the Faculty of the Graduate School of

The University of Texas at Austin

in Partial Fulfillment

of the Requirements

for the Degree of

Doctor of Philosophy

The University of Texas at Austin

December 2016

Dedication

I would like to dedicate this dissertation to my beautiful wife. I believe persuading her to marry me will forever be my greatest achievement. I can't thank her enough for all of her support and patience.

"The greater danger for most of us lies not in setting our aim too high and falling short, but in setting our aim too low and achieving our mark."

-Michelangelo Buonarroti

Acknowledgements

With great appreciation and gratitude, I would like to thank the following individuals for their contributions and encouragement. First and foremost, I would like to thank my supervisor Professor Simon Humphrey. Without his guidance and faith in me, this work would not have been possible. I would also like to thank my committee members for taking the time out of their busy schedules to learn about my work. Your time spent exploring my research and giving feedback has not gone unnoticed and is greatly valued. Furthermore, I would like to thank Beau Saccoccia; his hard work as an undergraduate student in our group was pivotal to my success. I would like to extend my gratitude to Professors Paul Wood, Jon Sessler, Juergen Eckert, Brian Space, Vince Lynch, and Kim Dunbar for their efforts in our collaborative publications. Paul specifically taught me a great deal through our joint efforts and his time and thoughts were greatly respected.

Development of novel porous coordination polymers with interest in catalysis, structure directing agents, and magnetism

Nolan Wayne Waggoner, Ph.D.

The University of Texas at Austin, 2016

Supervisor: Simon M. Humphrey

Porous coordination polymers (PCPs) have emerged as a novel and versatile class of crystalline materials since the late 1990's due to their high porosity and tunable reactivity. Applications for these materials have spread to areas including gas storage and separations, sensing, magnetism, and more recently, catalysis. However, designing a PCP-based material for a specific application remains a struggle within this field due to their unpredictable self-assembly. In order to overcome this hurdle, linker design has become paramount to the process.

The Humphrey Group has developed a new class of PCPs called Phosphine Coordination Materials (PCMs). These materials incorporate one or more phosphorous sites within the linker to act as a point of functionalization. The lone pair of each P(III) site can act as a tunable handle, which allows for access to increased chemical versatility. With this larger goal in mind, the research discussed herein has been focused on the development of novel materials on three fronts: catalytically active linkers, employment of structure directing agents, and examination of PCMs in magnetism.

Several catalytically active organic linkers were developed for the purpose of taking known homogenous reactivity and applying that knowledge to a heterogeneous framework.

The linker systems described herein include *trans*-$RuCl_2(1,2\text{-}C_6H_4\text{-}((P\text{-}C_6H_4\text{-}p\text{-}CO_2H)_2)_2$, the ferrocene backbone system $Fe(C_5H_4)_2\text{-}(P\text{-}(C_6H_4\text{-}p\text{-}CO_2H)_2)_2$, and the extended building block $1,2\text{-}C_6H_4\text{-}(P\text{-}(p\text{-}C_6H_4\text{-}p\text{-}C_6H_4\text{-}CO_2H)_2)_2$.

The second study examined a $[Me\text{-}P\text{-}(C_6H_4\text{-}p\text{-}CO_2H)_3]^+ Cl^-$ linker to create a series of frameworks through variation of only the alkali hydroxide added during synthesis. This resulted in five frameworks, four of which were non-isostructural. Designated PCMs 6-9, the frameworks demonstrated unusual pore topology as well as the highest cryogenic oxygen uptake to date for a saturated metal site material.

Next, two isostructural materials termed Ln-PCM-21 were synthesized and their experimental bulk magnetic properties were studied. Afterwards, three theoretical models were considered in relation to this experimental data and their relatability was reported.

The final study explored the magnetic behavior of a set of 1-dimensional coordination polymers that conversely employed thiolate groups; referred to as Thiolate Coordination Materials (TCMs). One material, Fe-TCM-1, was extensively studied and two isostructural materials were attempted (Co^{II}, Mn^{II}), with interest in single-chain magnetic behavior.

Table of Contents

List of Tables

List of Figures

List of Schemes

Chapter 1: Introduction

EVOLUTION OF COORDINATION POLYMERS

Coordination polymers have been used in various applications for hundreds of years, with examples ranging from Prussian blue to modern porous materials.[1,2] However, many long-established materials were not considered as coordination polymers until the term was first published in the 1960's.[3] Coordination polymers are defined as one-, two-, or three-dimensional materials made up of macromolecular repeating units (Figure 1.1).[4] Historically, this group of materials has been divided into three major subdivisions; inorganic, organic, and porous coordination polymers.

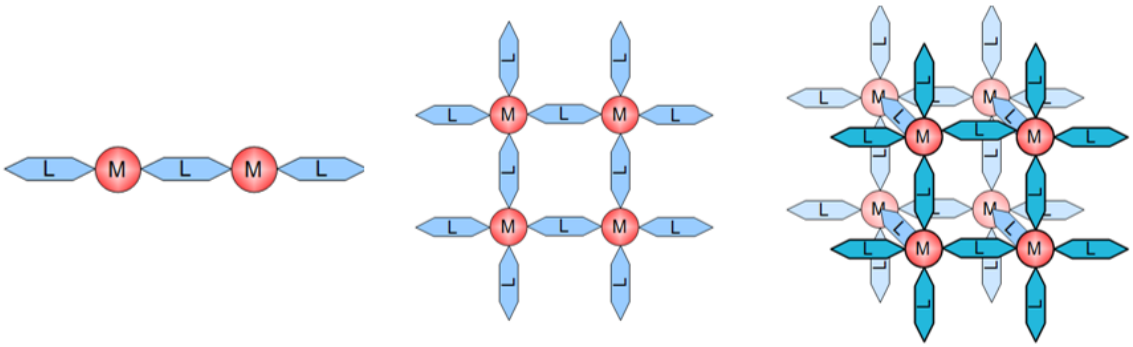

Figure 1.1. Visual depiction of a one-dimensional (Left), two-dimensional (Middle), and three-dimensional (Right) coordination polymer.[7]

A large variety of materials can be described as inorganic coordination polymers, including 1-dimensional organometallic chains and zeolites.[5,6] The former have been explored for applications ranging from electronics and magnetism, and have famously been employed as paint pigments.[1,8,9] Although zeolites have been of interest for over two centuries, their application and synthesis are still being explored today.[10] Zeolites are a

group of microporous and/or mesoporous aluminosilicate minerals that occur naturally and can also be synthesized.[11] They have been used commercially for a large variety of applications including selective adsorption and catalysis.[12,13] The utility of zeolites has been largely attached to their regular structures and high internal surface areas. However, these materials lack tunability due to their lack of surface functionality.

Carbon-based coordination polymers have had a great impact on an assortment of commercial processes as well, specifically in the fields of purification and extraction.[14,15] Activated carbon has been used the most extensively thus far, in a variety of grades and applications due to its high internal surface area (>1300 m^2/g). Unfortunately, this type of material lacks order in its structure in the solid-state, which can further hinder applicability.[16,17] Graphene has made great strides since its discovery in 1916 and it could allow for a theoretical internal surface area double that of activated carbon due to its highly regular structure.[18] However, its porous attributes have largely been overshadowed by its unique electronic properties, and synthetic modification has proven to be difficult.[19]

Porous coordination polymers (PCPs) are by far the most recently explored class of coordination polymers. They have ushered in a brand new era of coordination materials with their combination of immense internal surface areas, tunability, and regular structure.

HISTORY AND CHARACTERISTICS OF POROUS COORDINATION POLYMERS

PCPs, also referred to as metal-organic frameworks, were first published in the 1990's and have revitalized the field of porous materials, with interest continuing to grow over the last twenty years.[20] PCPs are microporous, crystalline materials fashioned through the coordination of organic linkers with typically anionic groups (*e.g.*, carboxylic or pyrazolate functionalities) connected through cationic metal nodes or clusters to create

infinite, porous frameworks (Figure 1.2). These ideally 3-dimensional materials are characteristically contain uniform pores with dimensions no larger than 2 nm, making the large majority of PCPs microporous. Microporous PCPs that can resist collapse upon activation have demonstrated impressive internal surface areas, with the highest published to date approaching 6500 m^2/g.[21] Since their first publication over twenty years ago interest in the field has increased exponentially, with over 24,000 publications to date referencing metal-organic frameworks.

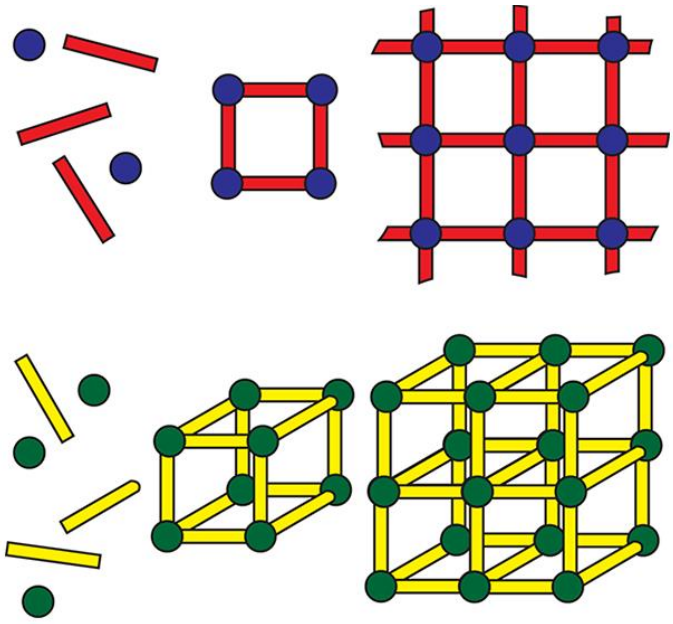

Figure 1.2. Visual representation of stepwise PCP self-assembly with linkers (rods) and connected through metal nodes (circles).[22]

The rapid and continued growth of PCP research has largely been due to their unparalleled chemical tunability and structural diversity, which are not available in zeolites and carbon-

based polymers. These unique characteristics allow for PCPs to access a wide range of advantageous chemical and physical properties not yet explored in porous materials.

Regardless of the popularity of attention PCPs have received, the self-assembly process that occurs during crystallization still not well understood. In an effort to overcome this hurdle there have been great efforts in reverse-engineering,[23,24] as well as theoretical modelling of materials in order to recognize patterns within their construction.[25-27] However, the process of designing PCPs for specific applications is still in its infancy, with much work to still be done.

DESIGN AND SYNTHESIS OF POROUS COORDINATION POLYMERS

PCP intelligent design

Despite the self-assembly of PCPs proving to be unpredictable, functionality control through choice of linker and metal salts during synthesis can allow for incorporation of desired reactivity, regardless of the resulting topology. PCPs are most commonly constructed using 3*d* transition metal or lanthanide (III) ions paired with organic linkers displaying hard, anionic functionality, which allows for covalent and ionic/electrostatic metal-ligand bonding. The resulting structures are ideally substitutionally-inert materials that have sufficient chemical and thermal stability for applications.[28] Metal ions and/or clusters of the 3*d* or 4*f* elements also facilitate ordered bonding between adjacent organic linkers, which in turn allows for the formation of polymers with a range of 3-D network topologies that can commonly display unparalleled regularity.[29] The geometry of organic linkers and the preferred coordination modes of the metal species tend to directly influence the resulting MOF structures, which can allow for a degree of control over the self-assembly process. A variety of work has been conducted

in the literature to better predict likely resulting topologies based on connectivity and the bond angles, as demonstrated by Cook *et al.* in 2013 (Figure 1.3).[22]

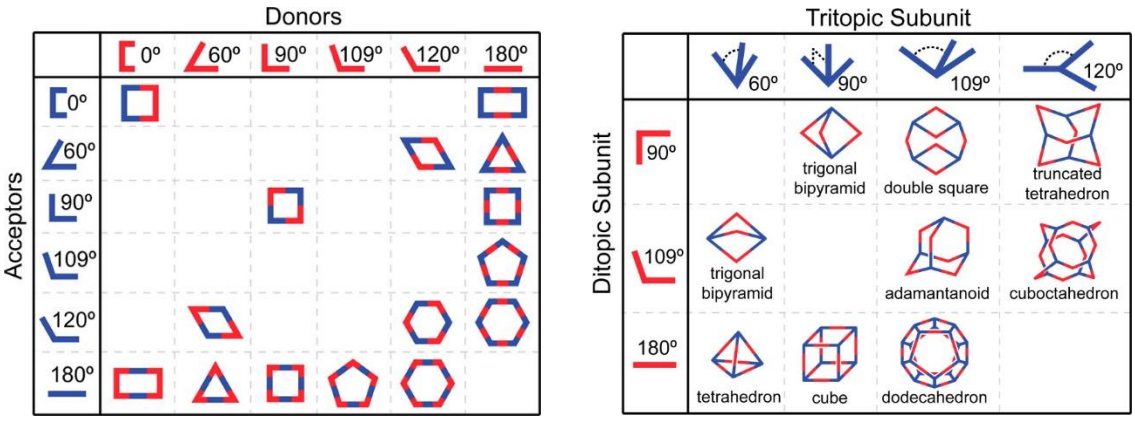

Figure 1.3. A variety of combinations of ditropic (Left) and tritopic (Right) building blocks and their resulting predicted combined geometries.[22]

This effect of intelligent design on topology can be more easily visualized in the comparison of MOF-5 and MOF-177.[30,31] In the case of the former, the linear organic linker 1,4-benzenedicarboxylate is shown to favor straight linkages between adjacent metal ions. Conversely, trigonal geometry within the linker 1,3,5-*tris*(4-carboxyphenyl)benzene will more likely promote trigonal (or hexagonal) symmetry elements in the resulting structure, as seen in MOF-177 (Scheme 1.1).[32]

Careful selection of reagents in PCP synthesis is just one of several techniques in use today to overcome the obstacles surrounding self-assembly. Synthesis of these materials, regardless of proper forethought, is not a precise art and a rational choice of precursors does not guarantee the formation of a PCP with desired structure and function. Along with these attempts to better understand the relationship between linker/metal node

geometry and resulting topology, research has also sought to enhance the adaptability of PCPs through *pre*- and *post*-synthetic modification techniques.

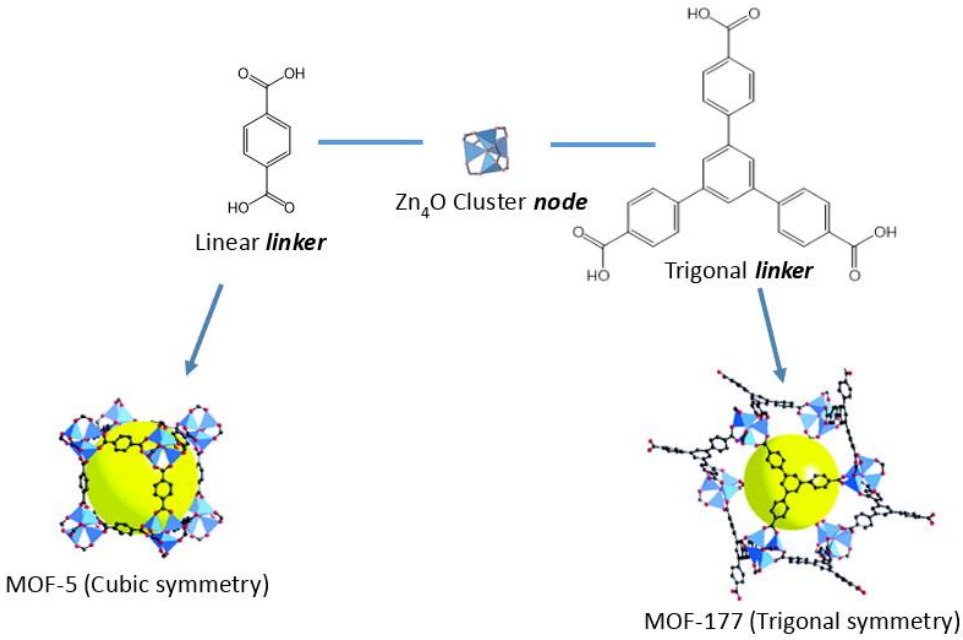

Scheme 1.1. Schematic illustration of how a linear linker can influence formation of a cubic structure (Left), in comparison to a trigonal ligand promoting trigonal or hexagonal symmetry (Right).

Pre-synthetic modification

Pre-synthetic modification in PCP development refers to functionalization or manipulation of a targeted site on the linker before it is incorporated into a framework. This term may seem to be ambiguous, with structural manipulation of a monomeric linker typically being indiscernible from previous synthetic steps. However, *pre*-synthetic modification specifically refers to the optional functionalization of a site that typically has a small effect on overall linker binding geometry, but a large influence on electronic

properties and applicability. In the literature, this modification process has been found to include groups such as halides, amines, alkyl groups, and similar simple moities to allow for increased analyte interactions,[33,34] gating effects,[35,36] and catalytic properties.[37-39] *Pre*-synthetic alterations can allow for several synthetic benefits in material design. Addition of a targeted functional group onto a linker before the PCP crystallization process can induce higher levels of symmetry, as seen in *bis*(phosphine) ligand systems with the addition of a chelating metal center (Figure 1.4).[40]

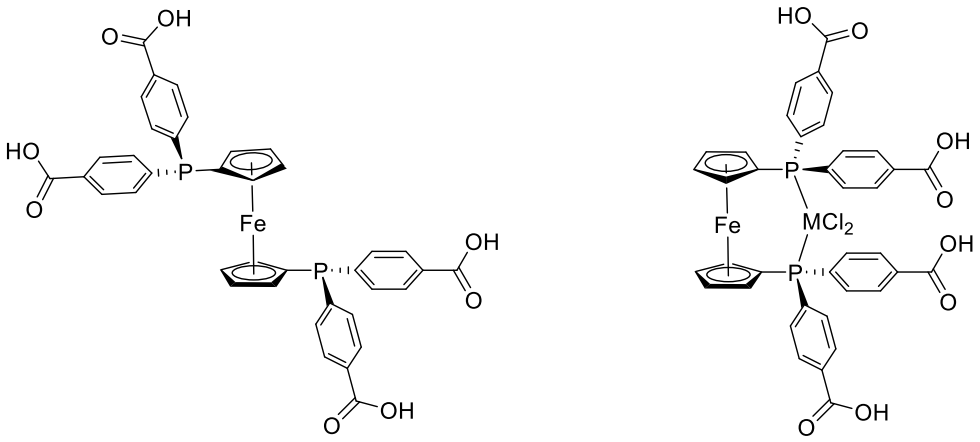

Figure 1.4. Depiction of a *bis*(phosphine) complex that has free rotation (Left) in comparison to a metalated complex that is locked into place symmetrically (Right).

Post-synthetic modification

Alternatively, some materials have demonstrated the ability to be functionalized after synthesis of the crystalline PCP through the process of *post*-synthetic modification (PSM). PSM was first demonstrated by Cohen and coworkers in 2007, proving that it was possible to modify a porous material in a heterogeneous manner after the formation of the crystalline solid.[41] Interestingly, the process of PSM can allow for the functionalization of

metal and/or ligand components without typically having an effect on the overall stability of a material. These crystal-to-crystal transformations can be hugely advantageous in PCP development, allowing for the same structure to be studied with multiple functionalities.[42,43] Additionally, this process can also allow for creation of modified materials that are not synthetically possible with a *pre*-functionalized approach.[44]

There are typically two possible locations within a framework that are considered for PSM; at the organic linker sites (covalent modification) or at the metal sites (coordinate covalent modification). Counter ion exchange is an alternative option for PSM that, as the name implies, can allow for the counter ion to be exchanged after the synthesis of a material. Covalent modification at the linker sites has been classically demonstrated throughout the PCP literature,[45-47] with a representative example by Jiang *et al.* in 2012; the PSM of 2-aminobenzene-1,4-dicarboxylate at the amine sites was shown *via* diazotization.[48] Coordinate covalent modification is equally as common, with one of the first and well-known examples coming from the work of Williams and coworkers with HKUST-1.[49] In this example, the copper clusters were found to by hydrated, and the coordinated water molecules could be easily exchanged. A third approach requires initial PSM functionalization on the linker, followed by the subsequent metalation of the added moiety (covalent and coordinate covalent modification) (Scheme 1.2). This approach can allow for chelating groups, such as hydroxides and carboxylates, along with unsaturated metal ions to be incorporated into saturated metal frameworks *post*-synthetically. There are many examples of this combined form of PSM in the literature, with applications including luminescence and catalysis.[50,51]

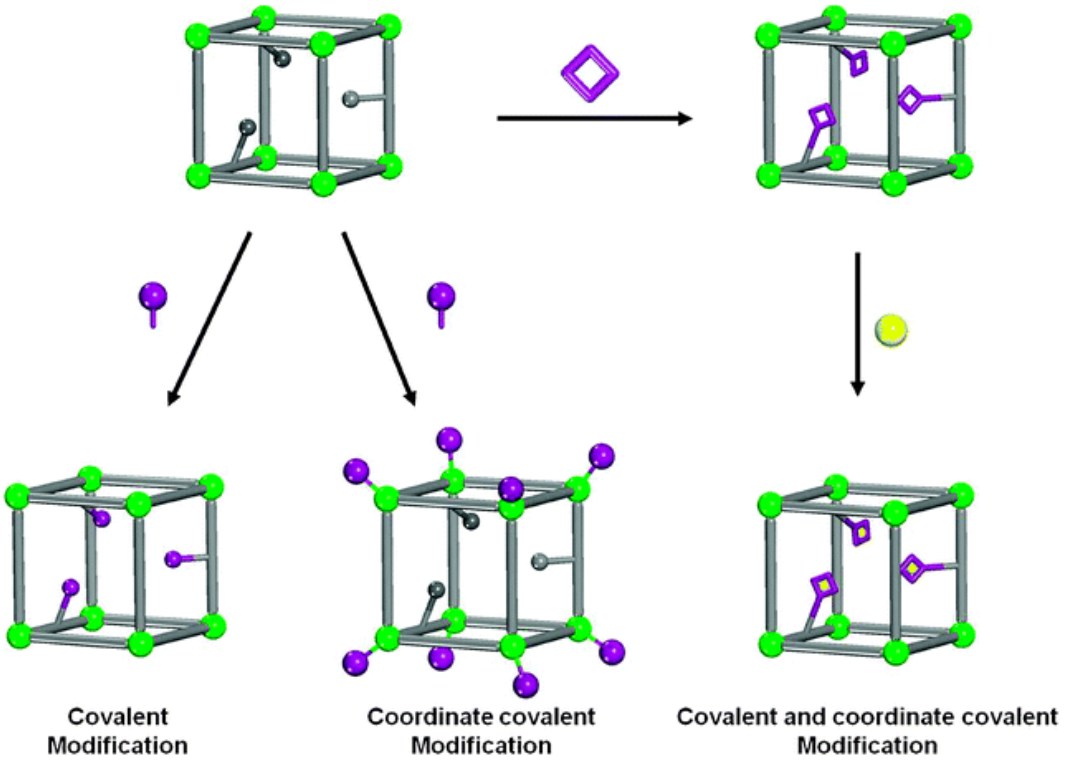

Scheme 1.2. Depiction of a PCP (Top left) that is manipulated through covalent (Left), coordinate covalent (Middle), and a combination of both PSM approaches (Right).[44]

PCP growth methods

In parallel with synthetic modification methods, there has also been a major focus on synthetic techniques for the preparation of PCPs. Conventional solvothermal heating is by far the most common technique employed in PCP growth. However, several other growth methods have been observed in the literature as well, which include microwave heating,[52] electrochemistry,[53] mechanochemistry,[54] and ultrasonic methods.[55] Within the realm of conventional heating, the reaction is typically carried out within the temperature range of 25 °C to 300 °C, contained in either scintillation vials or autoclaves. The resulting

PCP is most commonly isolated as a loose, crystalline solid. Others have has also begun to explore the development of thin films,[56] membranes,[57] and composites (Figure 1.5).[58,59]

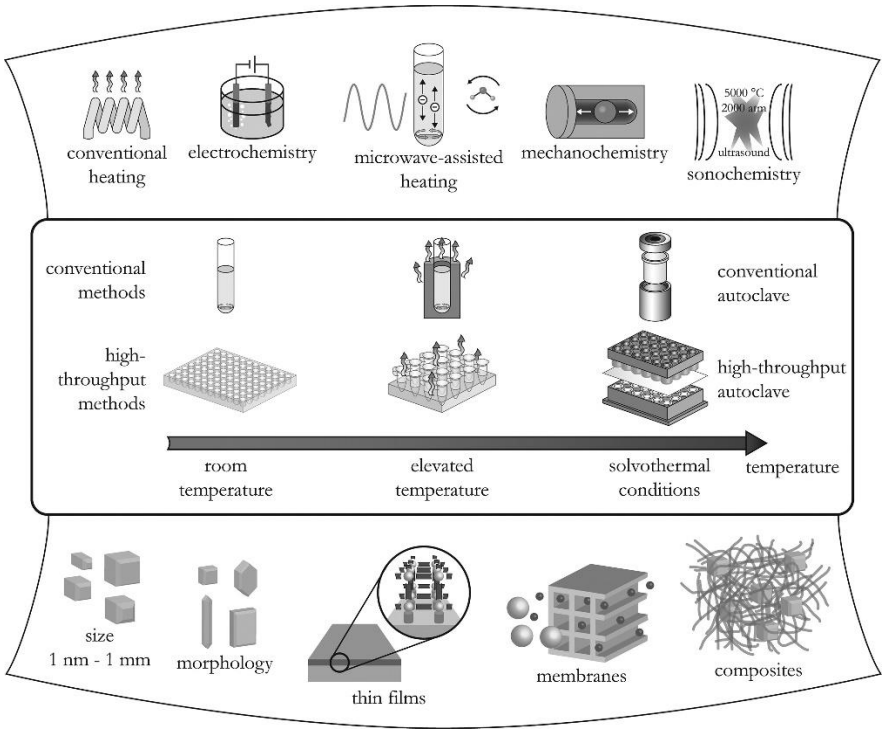

Figure 1.5. General overview of synthetic methods (Top), variability of temperatures and reaction vessels (Middle), and various forms of possible products (Bottom).[59]

Characterization methods

Thorough characterization of PCPs represents a critical time point along their developmental timeline. In order to gain a clear and full understanding of material properties and performance, a rigorous set of analytical techniques are required. The most influential analytical approaches allow for a great deal to be understood about the materials construction and applicability. Structural details are commonly explored through single crystal X-ray diffraction methods, while powder X-ray diffraction is employed to ensure

bulk purity. Even though both diffraction techniques are commonly utilized across various disciplines of chemistry, their employment with PCPs allows for a dramatic level of insight to be gained towards the self-assembly process of the resulting structures. Thermal stability is another important factor of interest when considering a variety of applications, and is commonly investigated through the use of thermogravimetric analysis (TGA). TGA measures a material's mass loss as the temperature is increased at a given ramp rate. The thermo-stability data of PCPs is helpful in understanding the amount of solvent free in the pores versus coordinated, and at what point the material shows full decomposition. More elaborate characterization techniques have been employed including inelastic neutron scattering for determination of primary physisorption sites,[60] and AC- and DC- SQUID magnetometry for the determination of magnetic properties.[61,62]

Gas sorption analysis

Sorption characteristics and internal surface area are considered among the most important attributes of a PCP. Initial sorption behavior is collected with a surface area analyzer, through the measurement of adsorption and desorption isotherms for a target analyte over a predetermined range of pressures. Before the process can begin, the solvent within the pores must be removed through activation of the PCP bulk material. Initial activation is achieved *via* exposure to ultra-high vacuum and a controlled heating process (ca. 50-300 °C). The activation procedure can be adapted to remove solvent within the pores or targeted coordinated solvent, depending on application and a material's ability to resist loss of porosity.

With an activated material, gas sorption capabilities can be measured for a number of analytes depending on interest. Commonly investigated gases include N_2, CO_2, CO,

CH_4, O_2, H_2, Ar, and a variety of organic and aqueous vapors. The analysis temperature can also be programmed by interest, with research from literature demonstrating customary ranges from 77 K – 673 K. Once the target analyte and analysis temperature are determined, sorption behavior is collected through the measurement of gas intercalated into a material (cc/g) over over pressure introduced into the sample cell (relative pressure). Pressures used in analysis can range dramatically, but typically fall into two categories: low pressure (0 to 1 atm) or high pressure (≤ 100 atm). From either measurement, a plot is generated with the gas uptake in cc/g on the Y-axis and the relative pressure of the sample cell on the X-axis (Figure 1.6). Maximum uptake and shape of isotherm data allows for insight into analyte capacity and overall behavior. The level of gravimetric capacity at low pressures is indicative of pore surface interactions and available surface area within a material.

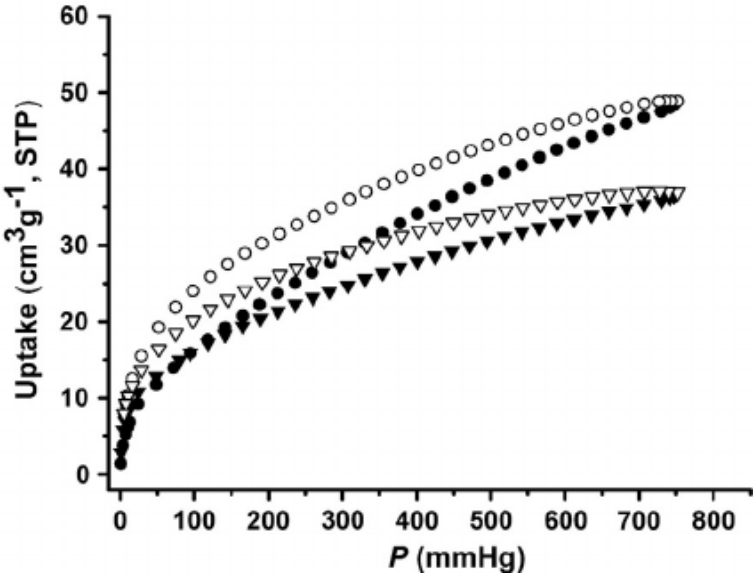

Figure 1.6. Representative low pressure adsorption (Closed) and desorption (Open) CO_2 isotherms for MOF-1 (Triangles) and MOF-2 (Circles).[63]

Internal surface area calculation

The internal surface area is calculated from the isotherm data collected from the surface area analyzer. This term is typically reported in m^2/g and is considered the standard reported value for comparison of materials across the field of PCPs. Cryogenic diatomic nitrogen or carbon dioxide are the most commonly employed analytes when calculating internal surface area, with analysis temperatures of 77 K and 196 K respectively.

In order to calculate the internal surface area from gas adsorption measurements, the Brunauer-Emmett-Teller (BET) mathematical theory is largely the most common method employed. The BET theory was initially published in 1938 in an attempt to explain physisorption behavior of an inert gas onto a solid surface of a given material.[64] The fundamentals of this theory were built upon three assumptions: gas molecules physically adsorb on a solid in layers infinitely, there is no interaction between each adsorption layer, and the Langmuir theory can be applied to each layer. These ideas can be combined mathematically in order to generate the BET equation (Equation 1.1) and the BET constant (Equation 1.2).

$$\frac{1}{\nu\left[\left(\frac{P_0}{P}\right)-1\right]} = \frac{c-1}{\nu_m c}\left(\frac{P}{P_0}\right) + \frac{1}{\nu_m c} \quad (1.1)$$

$$c = exp\left(\frac{E_1 - E_L}{RT}\right) \quad (1.2)$$

The BET equation allows for the creation of a BET plot, where $1/\nu[P_0/P)-1]$

versus P/P_0 from 0.05-0.35 atm ideally results in a linear relationship. Within the BET equation ν is equal to the adsorbed gas at the relative pressure at equilibrium (P) over saturation pressure (P_0), which can be used within the given pressure range to find the BET constant (c) as well as the volumetric quantity of gas needed for a monolayer dispersion (ν_m). The BET constant is equal to the heat of adsorption for the first monolayer (E_1) minus the heat of liquefaction (E_L) at a given temperature. In order to calculate ν_m and c, the slope (A) and y-intercept (I) of the BET plot is used (Equations 1.3 and 1.4, respectively).

$$\nu_m = \frac{1}{A+I} \quad (1.3)$$

$$c = 1 + \frac{A}{I} \quad (1.4)$$

The internal surface area can then be calculated, through the relationship of a materials BET specific surface area (S_{BET}) that relies on the mass of the solid sample that was analyzed (a), the adsorption cross section of the analyte (s), and Avogadro's number (N) (Equation 1.5).[64,65]

$$S_{BET} = \frac{(\nu_m N s)}{V a} \quad (1.5)$$

Gravimetric capacity

Weight percent or grams of adsorbate per grams of PCP, is also commonly calculated from the gas adsorption data in order to quantify a material's ability to perform storage and/or separations (Equation 1.6). Measurement of gravimetric capacity allows for normalized uptake of an analyte to be considered and compared to other materials as well.

Due to the popularity of this parameter in the literature, the creation of low density materials is commonly targeted for storage applications. However, high gravimetric adsorption of H_2 is naturally difficult due to the molecular weight of the analyte. Within the weight percent equation V represents the volumetric uptake, M_{gas} equals to the molecular weight of the analyte, and V_m is equivalent to the molar colume of an ideal gas (0 °C).

$$wt.\% = 100\% \times \frac{g_{gas}}{g_{mat}} = \frac{V \times M_{gas}}{V_m} \quad (1.6)$$

APPLICATIONS OF POROUS COORDINATION POLYMERS

PCPs display immense internal surface areas, uniform solid-state structure, small molecule programmability, and long range ordering. Such attributes have allowed for these materials to have a dramatic effect on a large assortment of applications, including gas storage and separations,[66,67] sensing,[68,69] catalysis,[70,71] and magnetism.[72,73] The specific applications discussed herein are either major contributors to PCP chemistry or directly apply to the research discussed in this dissertation.

Gas storage and separations

PCP application in targeted gas storage and purification has been at the forefront of interest since their discovery. For use of porous materials as storage devices, it is important to consider capacity at target pressures, speed of analyte release, as well as other factors. For storage applications, research has largely focused on hydrogen, with some efforts towards methane, and oxygen.[74-76] For the case of PCPs as separation agents, a general process would include passing a gas mixture over a packed column or fixed-bed that can

allow for different interactions to result in ideally individual elution of components. Strongly adsorbed components within the material could then be removed *via* desorption, to allow for the porous material to be reused.[77] Interest in purification materials has been industrially driven towards areas including carbon dioxide capture,[78] natural gas isolation,[79] separation of nitrogen and oxygen,[80] among many overs. The separation process is generally considered from two different approaches: bulk separation, which removes no less than 10 % of a specific fraction by weight, and purification, which applies to process that typically remove less than 2 weight % of a target analyte.[81]

Hydrogen storage

Hydrogen storage has been a large focal point in PCP gas sorption applications, with great promise in alternative energy. Hydrogen has the highest energy content per weight of any known element, containing nearly three times more energy by weight than gasoline. Unfortunately, when considering the same energetic comparison on a volumetric basis, the energy values are actually reversed. This lack of density in its liquid form presents a difficult hurdle in the field of hydrogen storage, with a common mid-sized car requiring 5 to 13 kg of hydrogen on board. Currently, tanks for automotive applications have been designed to withstand as high as 10,000 psi. However, this technology has inherent hazards and will need to be advanced further in order for hydrogen storage in automotive applications to continue to move forward.[82] PCPs have received a large amount of attention for hydrogen storage due to their impressive surface areas and tunable structures. The increase in surface areas for PCPs can allow for much closer hydrogen packing, resulting in a dramatic increase in overall storage capacity. Furthermore, their tunability through reagent control can be employed to manipulate physisorption

interactions as well.[83,84] Regardless, hydrogen storage is a difficult challenge to overcome and therefore, much of current research surrounding PCPs has focused on understanding the influence of PCP reagents and framework structure on overall hydrogen capacity.

Others have thus far looked into the utility of open metal sites,[85-87] small pore sizes,[88-90] nitrogen-rich environments or areas,[91,92] as well as incorporation of framework counterions for increasing hydrogen adsorption capacity in PCPs.[93,94] More recently, it has been hypothesized that polarized linkers or regions could increase hydrogen interactions as well.[95,96] With hydrogen adsorption measurement parameters within PCPs varying greatly, it is often difficult to compare materials directly without publication of gravimetric capacities. However, Lin and coworkers publication in 2012 claimed to have one of the highest total uptakes of hydrogen to date at room temperature.[97] This material, designated as (2) by Lin, utilized well-known copper paddle-wheel sub units along with an octa-carboxylate linker and a trizinc secondary building unit to allow high levels of interpenetration and open metal sites. The PCP demonstrated a total hydrogen uptake of 39 g/L (5.8 wt %) at 77 K, 90 bar, and 1.6 wt % uptake at 298 K. For more in depth discussions of current technology surround hydrogen storage in PCPs, the reader is directed to the selected reviews and book chapter on the topic.[86-88]

Carbon dioxide capture

Carbon dioxide capture is another topic of great interest, which investigates the bulk separation capacities of PCPs bulk remove a pollutant. The continued increase of atmospheric CO_2 levels from vehicle and industrial emissions is of great concern, with coal, natural gas, and petroleum making up 81 % of the United States energy usage as of 2010 (Figure 1.7).[98,99] Accounting for well over half of worldwide emissions, industrial

emissions are the greatest concern and current technology involves an unacceptable energy requirement for successful CO_2 capture. Initial processing is commonly approached through the employment of a combustion process in tandem with a carbon dioxide capture.[100] Both *pre*- and *post*-combustion have been explored, with a variety of capture mechanisms, which include adsorption, cryogenic distillation, and chemical looping.

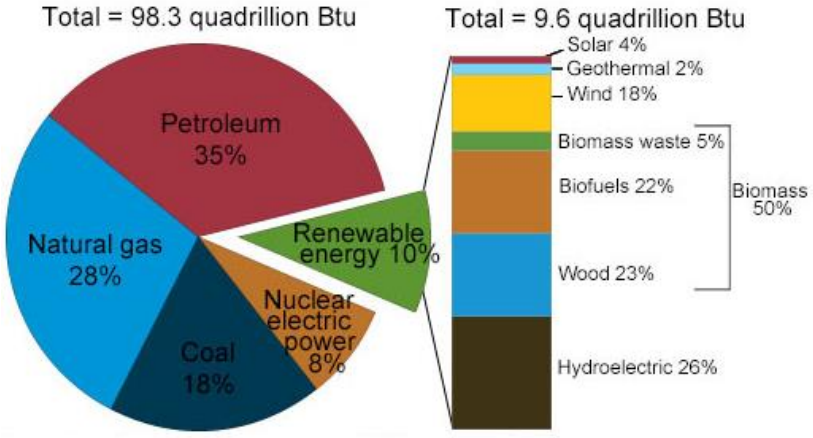

Figure 1.7. Graphical breakdown of energy sources in the United States as of 2014.[98]

Within the realm of adsorption materials, PCPs have gained significant momentum due to their inherent attributes.[101] Unfortunately, carbon dioxide separation properties are commonly discussed in the literature scientifically without considering aspects of their applicability. Due to this lack of consideration, it becomes difficult to consider a previously studied framework based off initial studies. Also, the demands of each specific process requiring carbon dioxide capture require vastly different attributes for a PCP to be successful (capacity, selectivity, stability, etc.). Consequently, the carbon capture material must be individually chosen for each specific application in order to maximize productivity.[102]

In 2005, Yaghi and coworker's published work on the material MOF-177, which demonstrated the highest carbon dioxide capacity found to date, at 33.5 mmol/g (298 K, 32 bar).[103] Although this material was not evaluated for separation capacity, it demonstrates the ability PCPs can have in overall CO_2 uptake. As a comparison, the highest performing zeolite (zeolite 13x) only adsorbs 7.4 mmol/g at the same conditions.[104] Several other materials were evaluated extensively for their adsorption capacities as well various aspects of selectivity in the cited review by Long and coworkers.[100]

Applications in sensing

Chemical sensors are in need of unremitting improvement in sensitivity and selectivity in order to approach and overcome today's ever-evolving detection needs. Reliability, portability, and cost are the primary focal points for sensor development, with the goal of lowering limits of detection and increasing tolerance of harsh conditions.[105] Fundamentally, chemical sensors provide analytical information about the chemical composition of a target gas or liquid analyte that surrounds the sensor. The target analyte is first physically introduced to the sensor and it interacts with the selective receptor sites in the sensor material, thus inducing a physical change in the sensing material. The analyte-sensor interactions should ideally be reversible and can range from weak intermolecular interactions to the formation of strong chemical bonds.[106,107] The prompted change in the sensor is then converted into a measurable output signal, employing methodologies such as electrochemical,[108] mechanochemical,[109] nondispersive infrared,[110] surface plasmon resonance,[111] and luminescence sensing.[112] Luminescent PCP sensors are by far the most common sensing method employed found in the literature within this family of materials, with impressive applicability in areas such as detection of ions,[113,114] pH,[115,116]

temperature,[117,118] solvents,[119,120] explosives,[121,122] and biomolecules.[123,124] A smaller number of examples have also focused on mechanically-induced signaling through the employment of PCPs as thin films. These systems are each carefully designed to take advantage of certain physical attributes that are unique to PCPs, which allow for a broad scope of chemical detection.[32] Work in mechanochemical sensing with PCPs has begun exploring their applications in microbalances,[125] microcantilevers,[126] and surface acoustic wave sensors.[127] A comprehensive review of current sensing technology with employment of PCPs has been published by Kreno *et al.*[128]

Applications in catalysis

PCP application in heterogeneous catalysis has shown everpresent interest in the literature, largely due to their ability to incorporate a vast variety of functionalities into organized pore structures.[20] Zeolites have been shown to be applicable in catalysis as well, showing greater overall thermal stability than PCPs, but lacking in tunability.[129] Therefore, employment of PCPs for catalysis typically aims for milder conditions with targeted conversions. Common techniques for the combination of heterogeneous catalysis and PCPs have investigated heterogenization of well-known homogeneous reactivities,[130] framework stabilization of short-lived species,[130] framework-encapsulation of molecular catalysts,[131] coupling of catalysis to chemical separations, [132] connection of a catalyst *via* nominally saturated metal nodes,[133] *post*-synthetic incorporation of reactive sites,[134-135] and substrate influence in size-selective catalysis.[136] Despite interest in PCP employment as heterogeneous catalysts dating back to their first publication, there have only been a few dozen examples of catalysis by crystalline, microporous PCPs to date.

In heterogeneous studies, it is crucial to differentiate between heterogeneous activity and the presence of dissolved homogeneous species. A series of controlled experiments are required in order to confirm PCP utility in catalysis. Monitoring of activity upon removal of the catalyst from the reaction mixture is a common technique for identifying the presence or absence of homogeneous species. Size selectivity studies are also highly useful, and can allow for circumstantial evidence for heterogeneous catalysis. Functionalization of only the surface of a material is also a common concern for PCP based catalysts. Identification of catalytic sites within a material by single crystal X-ray diffraction is the best method for overcoming this concern in tandem with size selection studies. However, many incorporation methods make collection of a functionalized crystal structure not possible. For certain materials, it is also important to consider activity arising from the presence of exposed node sites. The control studies described are considered a few vital examples for PCP catalysis, and several other studies are required depending on the reaction of interest and heterogeneous system.[137] A book chapter and recent reviews have been published that cover the current scope of PCPs in catalysis.[130, 137,138]

Porous coordination polymers and magnetism

Magnetochemistry has been of interest since the early 19th century and has become an immense field with interest in understanding magnetic properties of materials as well as refining those properties to work towards their application.[139] Bulk magnetism of a material typically falls into either non-ordered or ordered behavior. Within the former, a material can be defined as either diamagnetic or paramagnetic. Of all types of magnetic behavior, diamagnetism is the smallest in magnitude and is due to paired electrons causing a material to oppose an external magnetic field. Paramagnetism is caused by unpaired electrons within

a material and results in the opposite effect. A material displaying this type of behavior is drawn in the same direction as an external magnetic field due to the alignment of its unpaired electrons within that field. The majority of today's application in magnetism have arisen from materials that can display some form of ordered magnetism. Ordered magnetism is comprised of three primary sub-groups: ferromagnetism, antiferromagnetism, and ferrimagnetism (Figure 1.8).

Ferromegnetism is the alignment of electrons as magnetic electronic dipoles throughout a material *via* communication, commonly through superexchange interactions. Due to the alignment of electrons within a ferromagnetic material, a bulk magnetic moment is typically observed. Antiferromagnetism is the opposite effect, where neighboring electrons communicate to oppose one another which results in a bulk magnetic moment that is ideally zero.

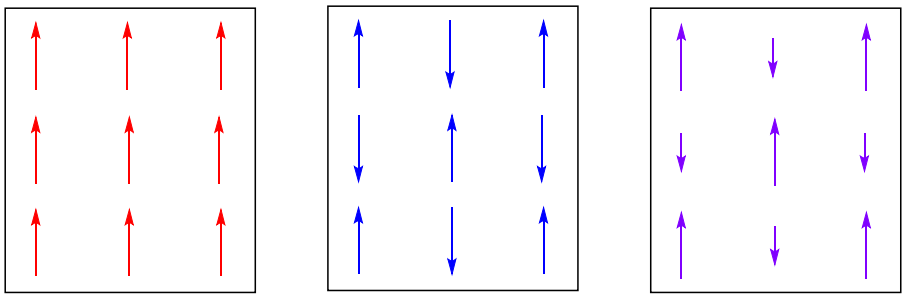

Figure 1.8. Visual representation of electrons within a ferromagnetic (Left), antiferromagnetic (Middle), and ferrimagnetic material (Right).

Ferrimagnetism is fundamentally a combination of the other two, with communication between neighboring metals resulting in opposing spins. However, for ferrimagnetic materials one direction of spins is stronger than the other, which results in a net magnetic moment > 0. For all forms of ordered magnetism, there is a certain temperature where a

material begins to display ordered behavior. Denoted as the Curie temperature (T_c) , this value is determined through magnetic measurements and the application of the Curie-Weiss law.[140]

Magnetic measurements of bulk solid materials are commonly carried out using a superconducting quantum interference device (SQUID). SQUIDs are highly sensitive magnetometers that can employ a constant field (DC) or alternating field (AC) to measure specific magnetic attributes of a bulk material. DC SQUIDs invstigate magnetic susceptibility of a material over a given temperature range and are applicable for measurement of a materials net magnetic moment and bulk behavior. The Curie-Weiss law can be applied to magnetic susceptibility data collected with constant current measurements in order to obtain important values (Equation 1.6, left). The Curie-Weiss law relates the magnetic susceptibility of a material (χ) to the Curie constant (C) over the temperature of a measurement (T) minus the Curie temperature in kelvin for $T \sim T_C$.

$$\chi = \frac{C}{T - T_C} \quad \text{or} \quad \chi = \frac{C}{T - \theta} \qquad (1.6)$$

When the Curie-Weiss law is applied with $T >> T_C$, the equation is slightly altered and Curie temperature is instead considered the Weiss constant (θ) (Equation 1.6, right). Therefore, depending on how the mathematical approach is applied, different information can be pulled from the data. The Curie constant can be calculated in multiple temperature ranges and gives the size of the magnetic moment per formula unit. The Curie temperature is typically assessed from the bulk magnetic susceptibility data directly as a peak is formed; this term is equal to the temperature that the material begins to show ordered magnetism. The Weiss constant is calculated from higher temperature magnetic susceptibility (ca. 200-

300 K) and its sign sheds light on short range magnetic interactions; θ = zero for paramagnetic materials, $\theta > 0$ for ferromagnetic materials, and $\theta < 0$ for antiferromagnetic materials.

AC-SQUIDs allow for an additional facet of a material to be investigated through its ability to vary the applied magnetic field as well as the temperature. This ability allows for the AC-SQUID to be able to probe for multiple ground states, blocking temperatures, spin relaxation times, and effective energy barriers of a material.[141] This data is commonly collected through a mathematical approach towards three different measurements. The most common measurement looks at the AC-magnetic susceptibility of a material over a series of external field energies (ca. 1-1500 Hz) over a small temperature range that encompasses the Curie temperature (Figure 1.9, top). The data collected at different frequencies allows for determination of spin relaxation times and ground state(s). Field dependence magnetization can be taken as well, which investigates how much a material will resist spin reversal upon reversal of the external field (Figure 1.9, bottom). This measurement can be performed at multiple temperatures in order to determine the point that the material will no longer resist change of spin direction; this is known as the spin reorientation barrier, or blocking temperature. The blocking temperature is very similar to the Curie temperature by definition, but have been shown to vary experimentally. The Blocking temperature is considered a more applicable value when considering application of a material.

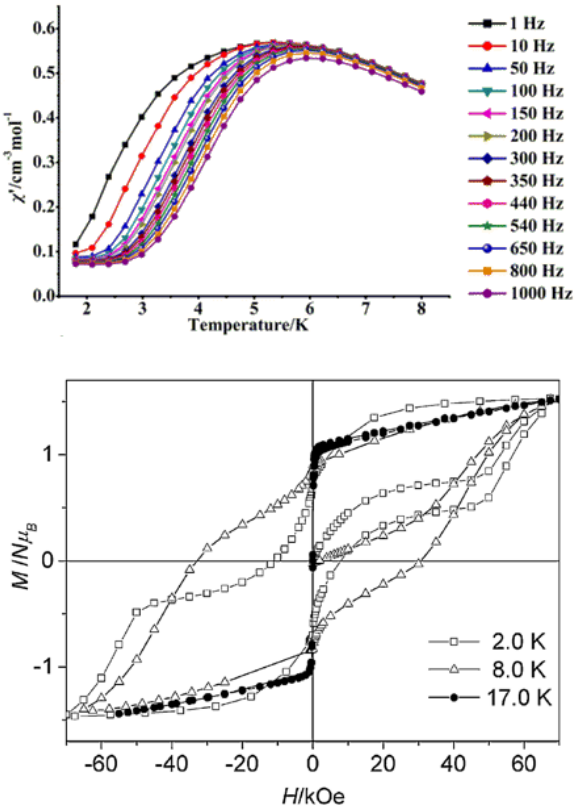

Figure 1.9. An example of a variable frequency AC-magnetic susceptibility plot (Top),[142] and field dependence of magnetization with a display of hysteresis loops (Bottom).[143]

The area of magnetism within solid-state materials has experienced a rejuvenation of growth in the literature over the last twenty years, with single-molecule magnets, single-chain magnets, and PCPs at the forefront of interest.[144-146] Magnetic materials that incorporate interlocked building blocks are considered among the top candidates for nanodevices that employ mechanical information, electronic information, or sensing functions. Currently, a major struggle in the field of magnetic materials for electronic applications is due to organization of magnetic centers.[147] PCPs provide a unique opportunity to employ highly regular, magnetically active nodal sites into a material in an approach to overcome this obstacle. The physical regularity and tunability of PCPs has

allowed for significant attention to be targeted towards their application as novel magnetic materials. Initial interest in magnetic properties began in 2000, largely due to their distinctive solid-state attributes.[148] Building block units that comprise the uniform structures of PCPs allow for the unique opportunity of probing internal structure interactions as well as additive magnetic characteristics. Ideally, PCPs acting as magnetic devices could act as a new generation of solid-state data storage devices. Chemically-driven PCPs have been found in the literature that demonstrate the ability of guest materials adsorbed into a material to affectively tune magnetic behavior.[149] Guest-PCP interactions have been shown to influence the possibility of spin crossover within a material as well.[150] From a different perspective, influence of magnetism in PCPs has also been shown possible by physical methods including heating,[151] and pressure.[152] Applications in magnetism that employ PCPs make up an exciting field that will continue to grow as their attributes are further studied and understood. For further information on the topic, see one of the comprehensive reviews cited.[153,154]

PHOSPHINE COORDINATION MATERIALS

An additional approach towards material tunability has been targeted over the last seven years through the incorporation of phosphorous sites into polymerizable linkers to create a new sub-family of PCPs that can access an exciting area of solid-state chemistry.[155] These polymers, referred to as phosphine coordination materials (PCMs), allow for access to an immense area of P(III) and P(V) chemistry that has largely not yet been explored in the area of PCPs. Inclusion of phosphorous into linkers for PCP development is advantageous from several viewpoints. Most importantly, the lone pair on P(III) is an ideal site for *pre*- or *post*-synthetic addition of a great assortment of functionalities. Additionally,

the vast majority of linkers used for PCP growth to date have displayed planar geometries while phosphine sites allow for access to trigonal pyramidal geometry (Figure 1.10).

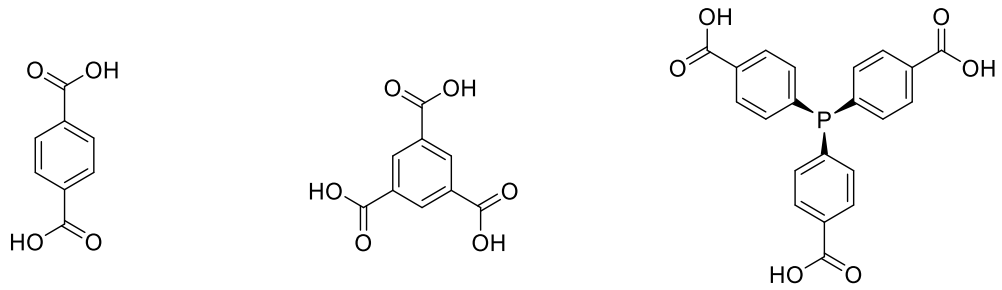

Figure 1.10. A visual representation of the common linkers terephthalic acid (Left), trimesic acid (Middle), in comparison to 4,4',4"-phosphinetriyltribenzoic acid ($ptbcH_3$) (Right).

The natural 3-dimensionality of phosphine ligands can in turn promote 3-dimesnional growth of a crystalline material as well as allow for access to novel PCP topologies not yet observed with traditional linkers. The phosphorous sites within a PCM can also act as a characterization handle during *pre*- or *post*-synthetic modification *via* ^{31}P-NMR spectroscopy. Due to the location of phosphorous in the building units, they can also act as a nodal site within a PCM as it connects the polymerizing arms of a single ligand (Figure 1.11). The inclusion of phosphorous as nodes within a material can produce lower density materials, which is crucial in consideration of gravimetric capacity.

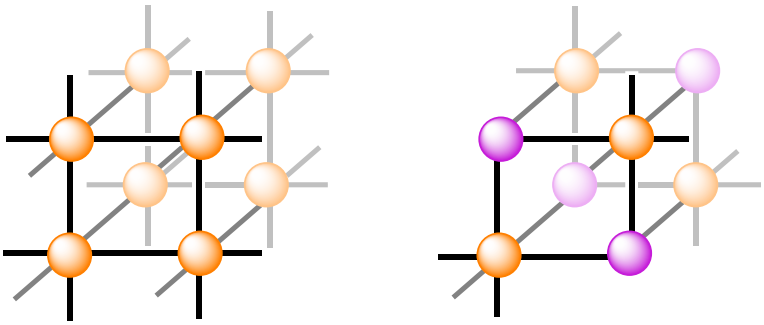

Figure 1.11. Visual representation of a framework comprised of only metal nodes (Left), and then half occupancy with metal nodes and phosphine nodes (Right).

Advantages of phosphine-based building units

With the vast area of phosphorous chemistry accessible for PCM manipulation and development, the Humphrey group has established a large library of both P(III) and P(V) based linkers. Targeted linkers for PCM development have largely employed carboxylate groups for polymerization. The triphenylphosphine derivative $ptbcH_3$ was the first building unit of interest, and lead to further exploration of various P(III) linkers to access increased electron density from the free lone pairs as well as the possibility of *post*-synthetic modification (Figure 1.12, top row).[155-157] These P(III) linkers have been explored with extended polymerization arms, different binding constituents (eg. phosphonate and amide functionalities), and various carboxylate positions. A *pre*-synthetic approach for building unit development has been approached from two sides.

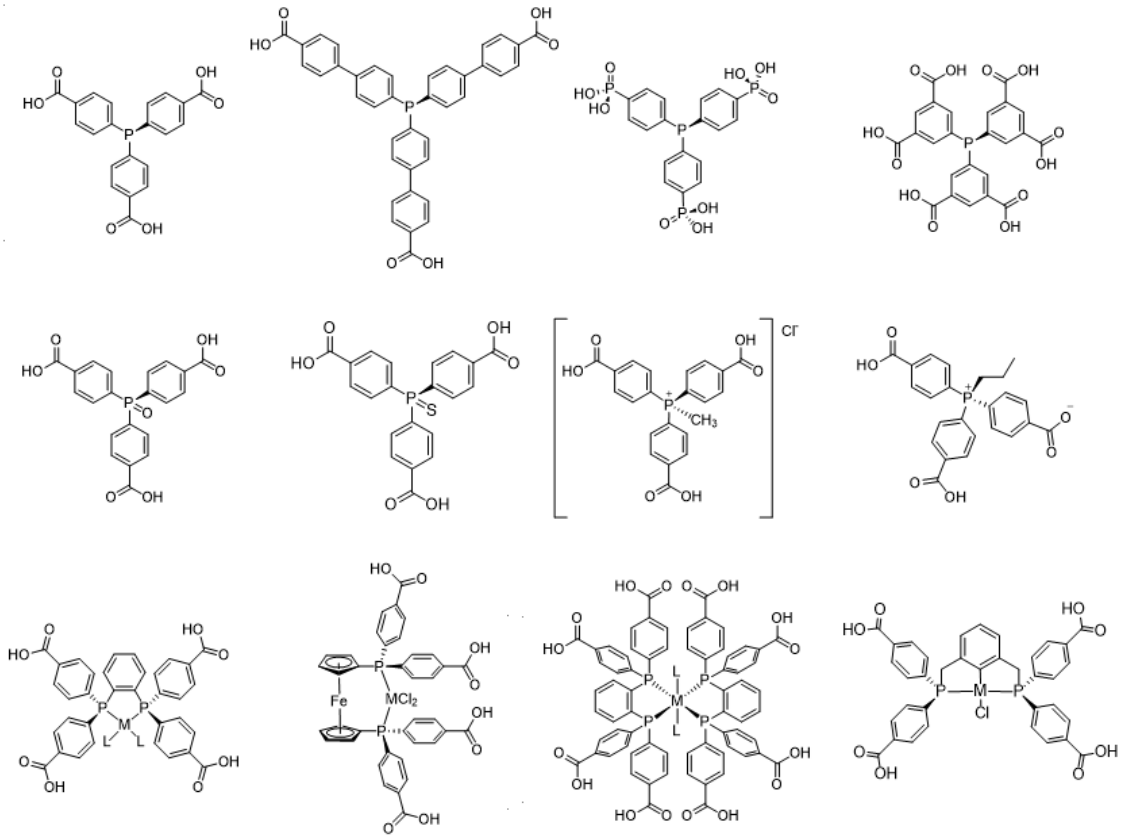

Figure 1.12. Selected overview of building units for PCM development.

First, simple addition of chalcogenide and alkyl functionalities was of interest and allowed for a great deal of materials to be developed (Figure 1.12, Middle row).[60,158-161] More recently, a second set of *pre*-synthetically functionalized linkers were of interest that allowed for inclusion of a catalytic-metal center (Figure 1.12, Bottom row).[162,163]

Overview of PCMs based on employed linker

The following section is meant to provide an overview of the most impressive PCMs explored to date. These materials will be organized based on the employed linker, and will include the highlights of their abilities. Each PCM has a designated number (PCM-X) and is referred to as such.

4,4',4"-phosphinetriyltribenzoic acid ($ptbcH_3$)

Due to its simplicity and similarity to triphenylphosphine, the linker $ptbcH_3$ (Figure 1.12, top row, left) was utilized in the synthesis of several PCMs. In 2009, PCM-1 through PCM-3 were reported with the employment of zinc(II) acetate ($Zn(OAc)_2$) and $ptbcH_3$.[155] PCM-1 was synthesized with no additional reagents in *N,N*-dimethylformamide (DMF) and it demonstrated hexagonal sheets based on fused M_3L_3 rings each adopting a regular chair confirmation, with each phosphine site pointing in the same direction (Figure 1.13).

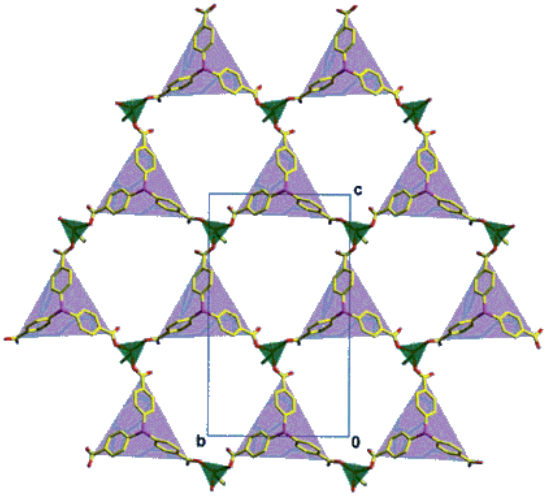

Figure 1.13. View of a single 2-dimensional honeycomb layer in PCM-1; trigonal pyramidal phosphine ligands are shown as violet triangles, with zinc tetrahedra drawn in green.[155]

PCM-2 and -3 took a similar approach with the employment of $Zn(OAc)_2$ and $ptbH_3$, with the synthetic alteration falling in solvent conditions along with the addition of base. PCM-2 required the addition of trimethylamine into a solvent mixture of DMF, ethanol, and water. This 2-dimensional material produced pairs of 6,3-connected sheets with nodal hydroxide inclusion and $HNME_2$ caps preventing polymerization in the final dimension. PCM-3 employed very similar conditions to PCM-2, with the replacement of triethylamine with pyrazine. This change of base allowed for the substitution of $HNMe_2$ with pyrazine, which resulted in a more symmetrical material. Otherwise the crystallography of both PCM-2 and -3 were the same (Figure 1.14).

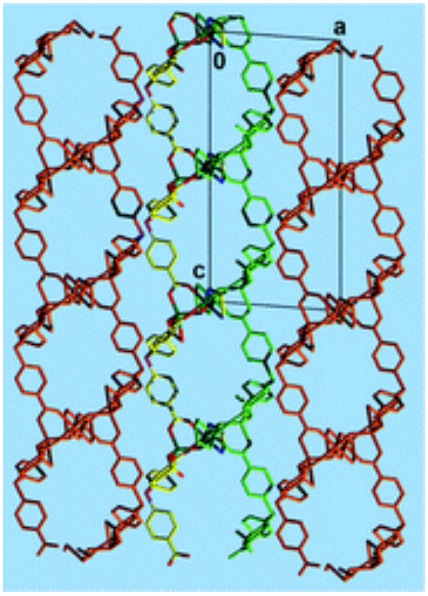

Figure 1.14. View in the ac plane for PCM-3 showing the close-packed array of bilayers.[155]

PCM-10 was published in 2014, and it was a $ptbcH_3$-based material that was extensively studied for *post*-synthetic addition of functionality.[156] PCM-10 is a calcium-

based material with 3-dimensional structure, which allowed for a greater level of overall stability in relation to previous ptbcH_3-based materials. The non-functionalized material PCM-10 was *post*-synthetically modified to incorporate gold chloride, oxide, and methyl functionalities. The latter functional group allowed for further modification due to its induced ionic character; fluoride, tetrafluoroborate, and hexafluorophosphate were individually exchanged as counter ions to observe their effect on gas sorption behavior (Scheme 1.3).

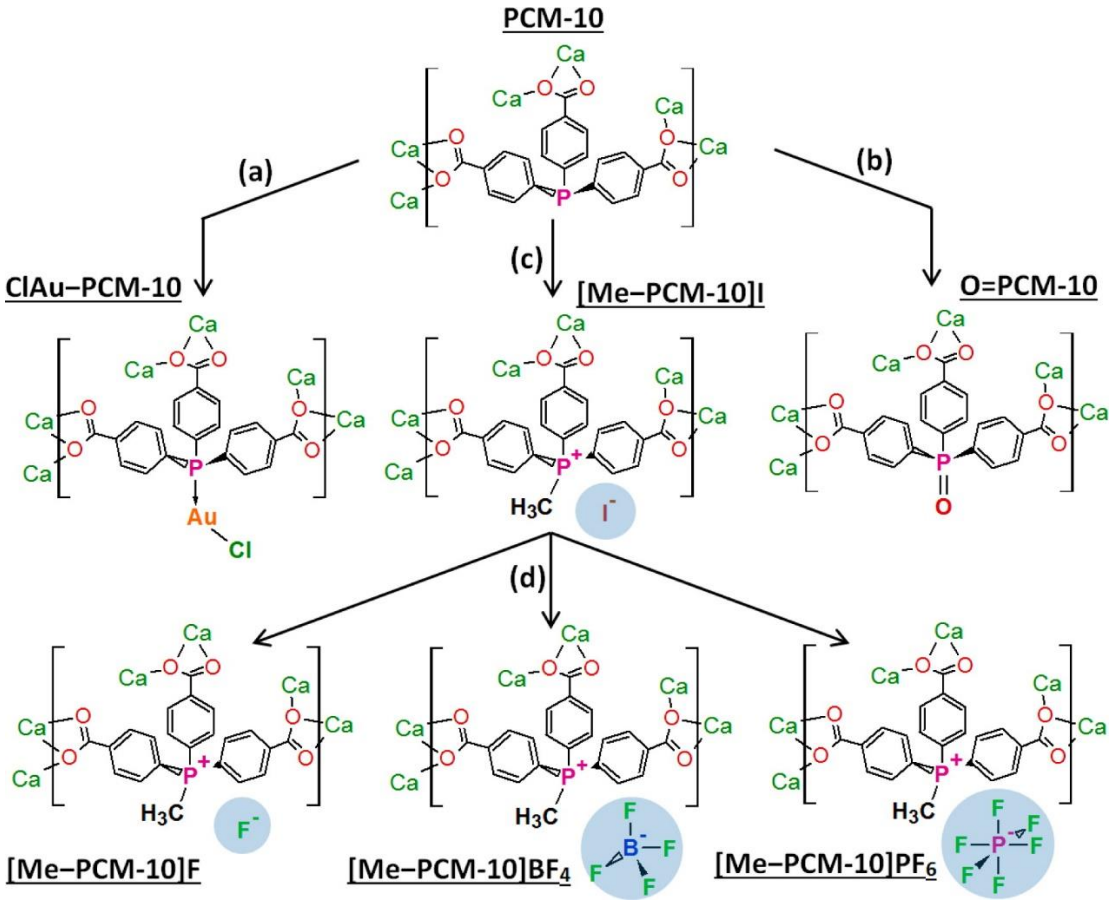

Scheme 1.3. Summary of PSMs applied to PCM-10.[156]

The effect of *post*-synthetic modifications of PCM-10 was observed with specific interest of increasing carbon dioxide affinity and overall hydrogen uptake. The heat of adsorption for CO_2 was calculated and used to better understand manipulability of its affinity. The gold functionalized material, Cl-Au-PCM-10, demonstrated a nominal increase in H_2 uptake up to 4.72 weight % in comparison to 0.63 weight % of the original PCM-10 (77 K, 0.975 atm).[157]

More recently, a series of isostructural materials has been developed that can employ the lanthanide rare-earth metals as well as yttrium for polymerization. This succession of isostructural materials, termed Ln-PCM-22, displays hexagonal symmetry *via* Ln_3L_3 rings that form 2-dimensional sheets similar to that seen in PCM-1. Unlike previously discussed materials, each individual Ln-PCM-22 has shown the ability to act as a 3-dimensional structure through interlayer hydrogen bonding of coordinated water to neighboring carboxylate groups. As commonly seen with lanthanide materials, the major interest of these PCMs has been targeted towards applications in luminescent sensing. Even more interesting, Ln-PCM-22 can be synthesized with a mixture of lanthanide species incorporated into a single material, which in turn can allow for tuning of its emission. Several mixed-lanthanide structures of PCM-22 have demonstrated an impressive ability to discern between vast assortments of solvents through each liquid providing a different emission 'fingerprint' from the submerged material. An impressive study is in draft and will be published later this year.[157]

Phosphonium and oxide linkers

The methyl phosphonium linker, $[Me\text{-}P(\text{-}C_6H_4\text{-}p\text{-}CO_2H)_3]^+Cl^-$ ($[mptbcH_3]Cl$) (Figure 1.12, center row, third from left), has been of interest in a variety of studies, including two individual analyses reported here in. PCM-6 through PCM-9 were studied together as an individual report, which allowed for an interesting perspective into the use of structure directing agents during synthesis; this study is discussed in great detail in Chapter 3.[158] PCM-14 is based off of calcium coordination in the creation of a highly dense material that was published in 2012.[159] This material demonstrated 3-fold symmetry, with each carboxylate group mono-coordinated to separate calcium nodes along with the incorporation of three coordinated water molecules per node. The internal surface area of PCM-14 displayed extreme temperature dependence, with ideal activation occurring at 180 °C. Further gas sorption studies showed that PCM-14 allowed for stark CO_2 selectivity over H_2, N_2, and O_2. In another study, two isostructural materials of Ln-PCM-21 were magnetically investigated and compared to theoretical models; the extensive details of this analysis can be found in Chapter 4.[160]

A phosphorous (V) linker based off of the carboxylated triphenylphosphine oxide ($optbcH_3$) (Figure 1.12, center row, left) has shown dramatic success in the area of PCMs as well. PCM-16 was published in 2012 by I. A. Ibarra *et al*. and it has remained one of the most impressive materials that employs $optbcH_3$.[161] The 3-dimensional polymer is synthesized using dysprosium(II) with the addition of hydrochloric acid. The acidic synthesis environment allowed for degradation of DMF to create the counterion Me_2NH_2. PCM-16 was found by X-ray diffraction to be anionic in nature with $Me_2NH_2^+$ in the pores to balance the anionic framework. The cation was found to *post*-synthetically exchangeable with NH_4^+, which in turn resulted in the increase of internal surface area by CO_2 from 1511 m^2/g to 1814 m^2/g (196 K, 0.975 atm), which is the highest yet observed for PCMs. PCM-

16 also demonstrated the highest O_2 uptake of any saturated-metal PCP found to date in the literature (65.1 wt. %, 77K, 0.975 atm), along with impressive H_2 uptake of 2.7 wt. % (77 K, 0.975 atm). The increased hydrogen uptake was further studied in collaboration with Space and coworkers *via* inelastic neutron scattering.[60] This study proved that the nitrogen containing counterion is hugely advantageous in hydrogen uptake, demonstrating interaction constants similar to materials with open metal sites present.

Pre-synthetically metalated linkers

As the most complex building units attempted to date, linkers with *pre*-synthetically metalated sites have proven the most challenging in development of novel PCPs. However, there have been two examples to date that have been successful in the creation of novel materials. The isostructural materials designated M-PCM-18 (M = Pd, Pt) were synthesized with a zinc precursor and a benzene backbone *bis*(phosphine) ligand with palladium(II) or platinum(II) metalation (Figure 1.11, bottom row, left).[162] M-PCM-18 displays significant symmetry, with a 2/*m* mirror plan that induces disorder with the indistinguishable inversion of the benzene ring and MCl_2 plane (Figure 1.15).

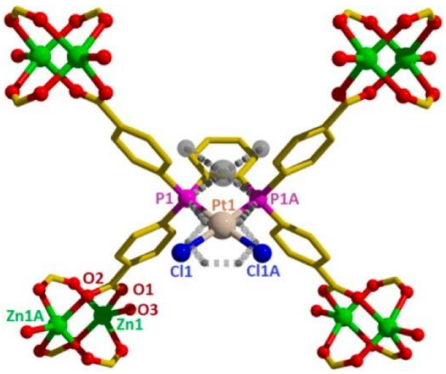

Figure 1.15. Pt-PCM-18 crystal structure with Zn^{II} paddlewheel nodes and puckered square grit net.[162]

Both isostructural materials demonstrated unusual and reversible H_2 sorption at 150 °C. Furthermore, the activation of Pt-Cl bonds in Pt-PCM-18 was demonstrated to provide organometallic species.

A novel material, designated PCM-36, was very recently created that allowed for the inclusion 1,3-benzene-(P-(C_6H_6-*p*-CO_2H)$_2$)$_2$ PdCl (Figure 1.11, bottom row, right) as the linker with cobalt(II) coordination. PCM-36 is the first demonstration in the literature of a 3-dimensional PCP that directly incorporates a pincer linker, making its creation a feat on its own. The extended crystal structure revealed the presence of micropores in all three dimensions, with the largest openings on the *ac*-plane allowing for two accessible Pd-Cl sites (Figure 1.16). *Post*-synthetic modification of the Pd-Cl bond was demonstrated within the material to provide Pd-CH_3 and Pd-N_3 functionalities. The former showed rapid CO_2 insertion (298 K, 1 atm), while the latter completely resisted CO insertion due to highly selective sorption behavior.[163]

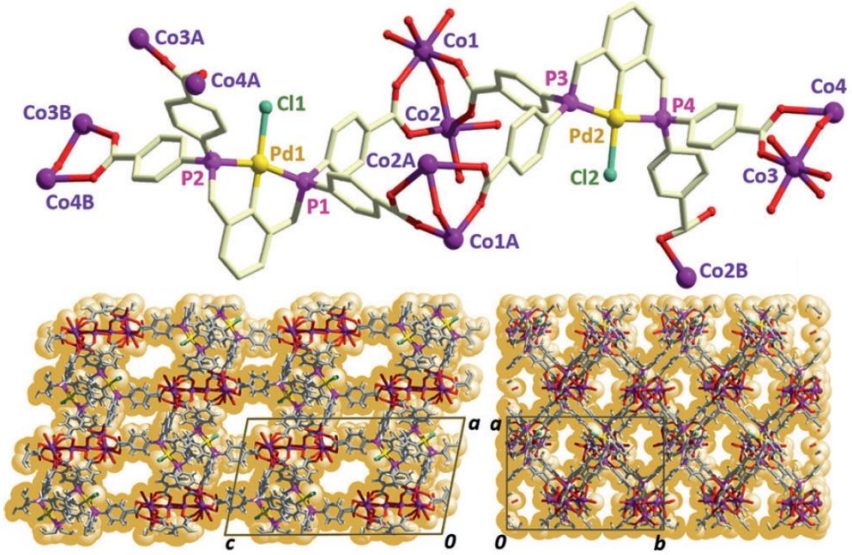

Figure 1.16. The asymmetric unit of PCM-36 showing (Top), space-fill representation of the *ac*-plane (Bottom left), and an alternative view down the *ab*-plane (Bottom right).[163]

REFERENCES

1. *Chemistry of Transition Metal Cyanide Compounds: Modern Perspectives - Progress in Inorganic Chemistry*, Volume 45, Dunbar, K.R.; Heintz, R. A., John Wiley & sons, Inc., 2007.
2. Zhou, H. -C.; Long, J. R.; Yaghi, O. M. *Chem. Rev.* **2012**, *112* (2), 673-674.
3. Bailar Jr, J. C. *Prep. Inorg. React.* **1964**, *1*, 1-27.
4. Batten, S. R.; Champness, N. R.; Chen, X.-M.; Garcia-Martinez, J.; Kitagawa, S.; Öhrström, L.; O'Keeffe, M.; Paik, S. M.; Reedijk, J. *Pure Appl. Chem.* **2013**, *85* (8), 1715–1724.
5. Chen, M; Zhao, H.; Sañudo, E. C.; Liu, C. -S.; Du, M. *Inorg Chem.* **2016**, *55* (8), 3715-3717.
6. Corma, A. *Chem. Rev*. **1997**, *97* (6), 2373–2420.
7. Wikipedia, the free encyclopedia; https://en.wikipedia.org/wiki/Coordination_polymer (accessed: July 27, 2016).
8. Lu, X.; Zhang, W.; Wang, C.; Wen, T.-C.; Wei, Y. *Prog. Polym. Sci.* **2011**, *36* (5), 671–712.
9. Chen, C. T.; Suslick, K. S. *Coord. Chem. Rev.* **1993**, *128* (1-2), 293-322.
10. Kitagawa, S.; Kitaura, R.; Noro, S. *Angew. Chem., Int. Ed.* **2004**, *43* (18), 2334–2375.
11. Rollmann, L. D.; Valyocsik, E. W.; Shannon, R. D. In *Inorganic Syntheses*; Murphy, D. W., Interrante, L. V., Eds.; John Wiley & Sons, Inc., 1995; pp 227–234.
12. Blanchard, G.; Maunaye, M.; Martin, G. *Water Res.* **1984**, *18* (12), 1501–1507.
13. Čejka, J.; Morris, R. E.; Serrano, D. P. *Catal. Sci. Technol.* **2016**, *6* (8), 2465–2466.
14. Jiang, M.; Ning, P.; Wang, Z. H.; Bai, Y. W.; Chen, W.; Zhang, W.; Wang, R. B. *Adv. Mater. Res.* **2012**, *476–478*, 1862–1866.

15. Siriwardane, R. V.; Shen, M.-S.; Fisher, E. P.; Poston, J. A. *Energy Fuels* **2001**, *15* (2), 279–284.
16. Bansal, R. C.; Goyal, M. *Activated Carbon Adsorption*; CRC Press, 2005.
17. Cecen, F.; Aktas, Ö. *Activated Carbon for Water and Wastewater Treatment*: Integration of Adsorption and Biological Treatment; John Wiley & Sons, 2011.
18. Bonaccorso, F.; Colombo, L.; Yu, G.; Stoller, M.; Tozzini, V.; Ferrari, A. C.; Ruoff, R. S.; Pellegrini, V. *Science* **2015**, *347* (6217), 1246501.
19. Cooper, D. R.; D'Anjou, B.; Ghattamaneni, N.; Harack, B.; Hilke, M.; Horth, A.; Majlis, N.; Massicotte, M.; Vandsburger, L.; Whiteway, E.; Yu, V.; *Int. Scholarly Res. Not.* **2012**.
20. Hoskins, B. F.; Robson, R. *J. Am. Chem. Soc.* **1990**, *112* (4), 1546–1554.
21. Furukawa, H.; Ko, N.; Go, Y. B.; Aratani, N.; Choi, S. B.; Choi, E.; Yazaydin, A. Ö.; Snurr, R. Q.; O'Keeffe, M.; Kim, J.; Yaghi, O. M. *Science* **2010**, *329* (5990), 424–428.
22. Cook, T. R.; Zheng, Y.-R.; Stang, P. J. *Chem. Rev.* **2013**, *113* (1), 734–777.
23. O'Keeffe, M. O.; Yaghi, O. M. *Chem. Rev.* **2012**, *112* (2), 675-702.
24. Bowes, C. L.; Ozin, G. A. *Adv. Mater.* **1996**, *8* (1), 13–28.
25. Tafipolsky, M.; Amirjalayer, S.; Schmid, R. *Microporous Mesoporous Mater.* **2010**, *129* (3), 304–318.
26. *Chapter 1: Crystal Growth and Nucleation*, Cubillas, P.; Anderson, M. W. In Zeolites and Catalysis; Čejka, J., Corma, A., Zones, S., Eds.; Wiley-VCH Verlag GmbH & Co. KGaA, 2010; pp 1–55.
27. Meng, W.; Li, H.; Xu, Z.; Du, S.; Li, Y.; Zhu, Y.; Han, Y.; Hou, H.; Fan, Y.; Tang, M. *Chem. Eur. J.* **2014**, *20* (10), 2945–2952.
28. Ma, J.; Huang, X.; Song, X.; Liu, W. *Chem. Eur. J.* **2013**, *19* (11), 3590–3595.

29. Zhang, R.; Ji, S.; Wang, N.; Wang, L.; Zhang, G.; Li, J.-R. *Angew. Chem., Int. Ed.* **2014**, *53* (37), 9775–9779.

30. Rowsell, J. L. C.; Eckert, J.; Yaghi, O. M. *J. Am. Chem. Soc.* **2005**, *127* (42), 14904–14910.

31. Chae, H. K.; Siberio-Pérez, D. Y.; Kim, J.; Go, Y.; Eddaoudi, M.; Matzger, A. J.; O'Keeffe, M.; Yaghi, O. M. *Nature* **2004**, *427* (6974), 523–527.

32. Waggoner, N. W.; Bohnsack, A. M.; Humphrey, S. M. Metal-organic frameworks for applications as sensing materials. In *Functional Metallosupramolecular Materials*, Hardy, J. G., Schacher, F. H., Eds.; Royal Society of Chemistry, Cambridge, United Kingdom, 2015, 192-245.

33. Salih, Z. I.; Guo, Y.-J.; Zheng, J.-J.; Zhao, X. *Comput. Theor. Chem.* **2015**, *1058*, 28–33.

34. Ko, N.; Choi, P. G.; Hong, J.; Yeo, M.; Sung, S.; Cordova, K. E.; Park, H. J.; Yang, J. K.; Kim, J. *J. Mater. Chem. A* **2015**, *3* (5), 2057–2064.

35. Kobalz, M.; Lincke, J.; Kobalz, K.; Erhart, O.; Bergmann, J.; Lässig, D.; Lange, M.; Möllmer, J.; Gläser, R.; Staudt, R.; Krautscheid, H. *Inorg. Chem.* **2016**, *55* (6), 3030–3039.

36. Mondal, S. S.; Thomas, A.; Holdt, H.-J. *Microporous Mesoporous Mater.* **2015**, *216*, 2–12.

37. Yuan, S.; Chen, Y.-P.; Qin, J.-S.; Lu, W.; Zou, L.; Zhang, Q.; Wang, X.; Sun, X.; Zhou, H.-C. *J. Am. Chem. Soc.* **2016**, *138* (28), 8912–8919.

38. Canivet, J.; Vandichel, M.; Farrusseng, D. *Dalton Trans.* **2016**, *45* (10), 4090–4099.

39. Eddaoudi, M.; Kim, J.; Rosi, N.; Vodak, D.; Wachter, J.; O'Keeffe, M.; Yaghi, O. M. *Science* **2002**, *295* (5554), 469–472.

40. Bohnsack, A. M. Novel Multifunctional Porous Coordination Polymers from Pre-synthetically Modified Organophosphorous Ligands, The University of Texas at Austin, TX, May 2015.
41. Wang, Z.; Cohen, S. M. *J. Am. Chem. Soc.* **2007**, *129* (41), 12368–12369.
42. Lin, Y.; Kong, C.; Chen, L. *RSC Adv.* **2016**, *6* (39), 32598–32614.
43. Li, H.-Y.; Wei, Y.-L.; Dong, X.-Y.; Zang, S.-Q.; Mak, T. C. W. *Chem. Mater.* **2015**, *27* (4), 1327–1331.
44. Tanabe, K. K.; Cohen, S. M. *Chem. Soc. Rev.* **2011**, *40* (2), 498–519.
45. Xu, L.; Luo, Y.; Sun, L.; Pu, S.; Fang, M.; Yuan, R. -X.; Du, H. -B. *Dalton Trans.* **2016**, *45* (20), 8614-8621.
46. Gotthardt, M. A.; Grosjean, S.; Brunner, T. S.; Kotzel, J.; Gänzler, A. M.; Wolf, S.; Bräse, S.; Kleist, W. *Dalton Trans.* **2015**, *44* (38), 16802–16809.
47. Bernt, S.; Guillerm, V.; Serre, C.; Stock, N. *Chem. Commun.* **2011**, *47* (10), 2838–2840.
48. Jiang, D.; Keenan, L. L.; Burrows, A. D.; Edler, J. *Chem. Commun.* **2012**, *48* (99), 12053-12055.
49. Chui, S. S.-Y.; Lo, S. M.-F.; Charmant, J. P. H.; Orpen, A. G.; Williams, I. D. *Science* **1999**, *283* (5405), 1148–1150.
50. Abdelhameed, R. M.; Carlos, L. D.; Silva, A. M. S.; Rocha, J. *Chem. Commun.* **2013**, *49* (44), 5019–5021.
51. Kardanpour, R.; Tangestaninejad, S.; Mirkhani, V.; Moghadam, M.; Mohammadpoor-Baltork, I.; Zadehahmadi, F. J. *Solid State Chem.* **2016**, *235*, 145–153.
52. Saccoccia, B.; Bohnsack, A. M.; Waggoner, N. W.; Cho, K. H.; Lee, J. S.; Hong, D.-Y.; Lynch, V. M.; Chang, J.-S.; Humphrey, S. M. *Angew. Chem. Int. Ed.* **2015**, *54* (18), 5394–5398.

53. Schäfer, P.; Veen, M. A. van der; Domke, K. F. *Chem. Commun.* **2016**, *52* (25), 4722–4725.

54. Julien, P. A.; Užarević, K.; Katsenis, A. D.; Kimber, S. A. J.; Wang, T.; Farha, O. K.; Zhang, Y.; Casaban, J.; Germann, L. S.; Etter, M.; Dinnebier, R. E.; James, S. L.; Halasz, I.; Friščić, T. *J. Am. Chem. Soc.* **2016**, *138* (9), 2929–2932.

55. Haque, E.; Khan, N. A.; Park, J. H.; Jhung, S. H. *Chem. Eur. J.* **2010**, *16* (3), 1046–1052.

56. Zacher, D.; Shekhah, O.; Wöll, C.; Fischer, R. A. *Chem. Soc. Rev.* **2009**, *38* (5), 1418–1429.

57. Rui, Z.; James, J. B.; Kasik, A.; Lin, Y. S. *AIChE J.* **2016**, ahead of print.

58. Wang, C.; Lee, M.; Liu, X.; Wang, B.; Chen, J. P.; Li, K. *Chem. Commun.* **2016**, *52* (57), 8869–8872.

59. Stock, N.; Biswas, S. *Chem. Rev.* **2012**, *112* (2), 933–969.

60. Forrest, K. A.; Pham, T.; Georgiev, P. A.; Embs, J. P.; Waggoner, N. W.; Hogan, A.; Humphrey, S. M.; Eckert, J.; Space, B. *Chem. Mater.* **2015**, *27* (22), 7619–7626.

61. Li, M.-X.; Zhang, Y.-F.; He, X.; Shi, X.-M.; Wang, Y.-P.; Shao, M.; Wang, Z.-X. *Cryst.Growth Des.* **2016**, *16* (5), 2912–2922.

62. Wang, S.; Cao, T.; Yan, H.; Li, Y.; Lu, J.; Ma, R.; Li, D.; Dou, J.; Bai, J. *Inorg. Chem.* **2016**, *55* (11), 5139–5151.

63. Alduhaish, O.; Li, B.; Nesterov, V.; Chen, B. *Inorg Chem.* **2014**, *45*, 89-92.

64. Brunauer, S.; Emmett, P. H.; Teller, E. *J. Am. Chem. Soc.* **1938**, *60* (2), 309–319.

65. Sing, K. S. W. *Adv. Colloid Interface Sci.* **1998**, *76–77*, 3–11.

66. Zhao, Y.-P.; Li, Y.; Cui, C.-Y.; Xiao, Y.; Li, R.; Wang, S.-H.; Zheng, F.-K.; Guo, G.-C. *Inorg. Chem.* **2016**, *55* (15), 7335–7340.

67. Wang, C.; Lee, M.; Liu, X.; Wang, B.; Paul Chen, J.; Li, K. *Chem. Commun.* **2016**, *52* (57), 8869–8872.

68. Du, P.-Y.; Gu, W.; Liu, X. *Inorg. Chem.* **2016**, *81* (8), 885-892.

69. Yang, J.; Ye, H.; Zhao, F.; Zeng, B. ACS *Appl. Mater. & Interfaces* **2016**, *8* (31), 20407–20414.

70. Wu, P.; Guo, X.; Cheng, L.; He, C.; Wang, J.; Duan, C. *Inorg. Chem.* **2016**, *55* (16), 8153-8159.

71. Sawano, T.; Lin, Z.; Boures, D.; An, B.; Wang, C.; Lin, W. *J. Am. Chem. Soc.* **2016**, *138* (31), 9783–9786.

72. Samui, A.; Chowdhuri, A. R.; Mahto, T. K.; Sahu, S. K. *RSC Adv.* **2016**, *6* (71), 66385–66393.

73. Wu, Y.-L.; Guo, F.-S.; Yang, G.-P.; Wang, L.; Jin, J.-C.; Zhou, X.; Zhang, W.-Y.; Wang, Y.-Y. *Inorg. Chem.* **2016**, *55* (13), 6592–6596.

74. Ozturk, Z.; Kose, D. A.; Sahin, Z. S.; Ozkan, G.; Asan, A. *Int. J. Hydrogen Energy* **2016**, *41* (28), 12167–12174.

75. Chang, G.; Wen, H.; Li, B.; Zhou, W.; Wang, H.; Alfooty, K.; Bao, Z.; Chen, B. *Cryst. Growth Des.* **2016**, *16* (6), 3395–3399.

76. Abdelhameed, R. M.; Carlos, L. D.; Silva, A. M. S.; Rocha, J. *Chem. Commun.* **2013**, *49* (44), 5019–5021.

77. Li, J.-R.; Kuppler, R. J.; Zhou, H.-C. *Chem. Soc. Rev.* **2009**, *38* (5), 1477–1504.

78. Wang, J.; Lin, Y.; Yue, Q.; Tao, K.; Kong, C.; Chen, L. *RSC Adv.* **2016**, *6* (58), 53017–53024.

79. Duan, X.; Zhang, Q.; Cai, J.; Yang, Y.; Cui, Y.; He, Y.; Wu, C.; Krishna, R.; Chen, B.; Qian, G. *J. Mater. Chem. A* **2014**, *2* (8), 2628–2633.

80. Verma, P.; Maurice, R.; Truhlar, D. G. *J. Phys. Chem. C* **2015**, *119* (51), 28499–28511.

81. Yang, R. T., *Adsorbents: Fundamentals and Applications*, John Wiley & Sons, Hoboken, 2003.

82. Sing, K. Colloids and Surfaces A: Physicochemical and Engineering Aspects 2001, 187–188, 3–9.

83. Rowsell, J. L. C.; Yaghi, O. M. *Angew. Chem., Int. Ed.* **2005**, *44* (30), 4670–4679.

84. Murray, L. J.; Dincă, M.; Long, J. R. *Chem. Soc. Rev.* **2009**, *38* (5), 1294–1314.

85. Chen, B.; Ockwig, N. W.; Millward, A. R.; Contreras, D. S.; Yaghi, O. M. *Angew. Chem., Int. Ed.* **2005**, *44* (30), 4745–4749.

86. Rowsell, J. L. C.; Yaghi, O. M. *J. Am. Chem. Soc.* **2006**, *128* (4), 1304–1315.

87. Dietzel, P. D. C.; Georgiev, P. A.; Eckert, J.; Blom, R.; Strässle, T.; Unruh, T. *Chem. Commun.* **2010**, *46* (27), 4962–4964.

88. Kesanli, B.; Cui, Y.; Smith, M. R.; Bittner, E. W.; Bockrath, B. C.; Lin, W. *Angew. Chem., Int. Ed.* **2005**, *44* (1), 72–75.

89. Ma, S.; Sun, D.; Ambrogio, M.; Fillinger, J. A.; Parkin, S.; Zhou, H.-C. *J. Am. Chem. Soc.* **2007**, *129* (7), 1858–1859.

90. Nugent, P.; Pham, T.; McLaughlin, K.; Georgiev, P. A.; Lohstroh, W.; Embs, J. P.; Zaworotko, M. J.; Space, B.; Eckert, J. *J. Mater. Chem. A* **2014**, *2* (34), 13884–13891.

91. Li, B.; Zhang, Z.; Li, Y.; Yao, K.; Zhu, Y.; Deng, Z.; Yang, F.; Zhou, X.; Li, G.; Wu, H.; Nijem, N.; Chabal, Y. J.; Lai, Z.; Han, Y.; Shi, Z.; Feng, S.; Li, J. *Angew. Chem. Int. Ed.* **2012**, *51* (6), 1412–1415.

92. Luebke, R.; Weseliński, Ł. J.; Belmabkhout, Y.; Chen, Z.; Wojtas, Ł.; Eddaoudi, M. *Crys. Growth Des.* **2014**, *14* (2), 414–418.

93. Liu, Y.; Eubank, J. F.; Cairns, A. J.; Eckert, J.; Kravtsov, V. C.; Luebke, R.; Eddaoudi, M. *Angew. Chem., Int. Ed.* **2007**, *46* (18), 3278–3283.

94. Nouar, F.; Eckert, J.; Eubank, J. F.; Forster, P.; Eddaoudi, M. *J. Am. Chem. Soc.* **2009**, *131* (8), 2864–2870.

95. Tsivion, E.; Long, J. R.; Head-Gordon, M. *J. Am. Chem. Soc.* **2014**, *136* (51), 17827–17835.

96. Barman, S.; Khutia, A.; Koitz, R.; Blacque, O.; Furukawa, H.; Iannuzzi, M.; Yaghi, O. M.; Janiak, C.; Hutter, J.; Berke, H. *J. Mater. Chem. A* **2014**, *2* (44), 18823–18830.

97. Liu, D.; Wu, H.; Wang, S.; Xie, Z.; Li, J.; Lin, W. *Chem. Sci.* **2012**, *3* (10), 3032–3037.

98. U. S. Energy Information Administration; http://www.eia.gov/energy_in_brief/article/major_energy_sources_and_users.cfm. (accessed: August 1, 2016)

99. Sumida, K.; Rogow, D. L.; Mason, J. A.; McDonald, T. M.; Bloch, E. D.; Herm, Z. R.; Bae, T.-H.; Long, J. R. *Chem. Rev.* **2012**, *112* (2), 724–781.

100. D'Alessandro, D. M.; Smit, B.; Long, J. R. *Angew. Chem., Int. Ed.* **2010**, *49* (35), 6058–6082.

101. Li, J.-R.; Ma, Y.; McCarthy, M. C.; Sculley, J.; Yu, J.; Jeong, H.-K.; Balbuena, P. B.; Zhou, H.-C. *Coord. Chem. Rev.* **2011**, *255* (15–16), 1791–1823.

102. Pirngruber, G. D.; Llewellyn, P. L. In Metal-Organic Frameworks; Farrusseng, D., Ed.; Wiley-VCH Verlag GmbH & Co. KGaA, 2011; pp 99–119.

103. Millward, A. R.; Yaghi, O. M. *J. Am. Chem. Soc.* **2005**, *127* (51), 17998–17999.

104. Cavenati, S.; Grande, C. A.; Rodrigues, A. E. *J. Chem. Eng. Data* **2005**, *50*, 369-376.

105. Korotcenkov, G. *Chemical Sensors: Comprehensive Sensor Technologies*, Vol 6, Chemical Sensors Applications; Momentum Press: New York, 2011**.**

106. Gouma, P. -I., *Nanomaterials for Chemical Sensors and Biotechnology*, Pan Stanford Publishing, Singapore, 2009.

107. Gründler, P., *Chemical Sensors*; Springer Berlin Heidelberg: Berlin, Heidelberg, 2007.

108. Hosseini, H.; Ahmar, H.; Dehghani, A.; Bagheri, A.; Tadjarodi, A.; Fakhari, A. R. *Biosens. Bioelectron.* **2013**, *42*, 426–429.

109. Allendorf, M. D.; Houk, R. J. T.; Andruszkiewicz, L.; Talin, A. A.; Pikarsky, J.; Choudhury, A.; Gall, K. A.; Hesketh, P. J. *J. Am. Chem. Soc.* **2008**, *130* (44), 14404–14405.

110. Dinh, T.-V.; Choi, I.-Y.; Son, Y.-S.; Kim, J.-C. *Sens. Actuators, B* **2016**, *231*, 529–538.

111. Kreno, L. E.; Hupp, J. T.; Van Duyne, R. P. *Anal. Chem.* **2010**, *82* (19), 8042–8046.

112. Rocha, J.; Carlos, L. D.; Paz, F. A. A.; Ananias, D. *Chem. Soc. Rev.* **2011**, *40* (2), 926–940.

113. Chen, B.; Wang, L.; Zapata, F.; Qian, G.; Lobkovsky, E. B. *J. Am. Chem. Soc.* **2008**, *130* (21), 6718–6719.

114. Manna, B.; Chaudhari, A. K.; Joarder, B.; Karmakar, A.; Ghosh, S. K. *Angew. Chem., Int. Ed.* **2013**, *52* (3), 998–1002.

115. Harbuzaru, B. V.; Corma, A.; Rey, F.; Jordá, J. L.; Ananias, D.; Carlos, L. D.; Rocha, J. *Angew. Chem., Int. Ed.* **2009**, *48* (35), 6476–6479.

116. Farha, O. K.; Mulfort, K. L.; Hupp, J. T. *Inorg. Chem.* **2008**, *47* (22), 10223–10225.

117. Zhu, Q.; Shen, C.; Tan, C.; Sheng, T.; Hu, S.; Wu, X. *Chem. Commun.* **2012**, *48* (4), 531–533.

118. Cui, Y.; Xu, H.; Yue, Y.; Guo, Z.; Yu, J.; Chen, Z.; Gao, J.; Yang, Y.; Qian, G.; Chen, B. *J. am. Chem. Soc.* **2012**, *134* (9), 3979–3982.

119. Wang, H.-M.; Liu, H.-P.; Chu, T.-S.; Yang, Y.-Y.; Hu, Y.-S.; Liu, W.-T.; Ng, S. W. *RSC Adv.* **2014**, *4* (27), 14035–14041.

120. Guo, Z.; Xu, H.; Su, S.; Cai, J.; Dang, S.; Xiang, S.; Qian, G.; Zhang, H.; O'Keeffe, M.; Chen, B. *Chem. Commun.* **2011**, *47* (19), 5551–5553.

121. Wang, B.; Lv, X.-L.; Feng, D.; Xie, L.-H.; Zhang, J.; Li, M.; Xie, Y.; Li, J.-R.; Zhou, H.-C. *J. Am. Chem. Soc.* **2016**, *138* (19), 6204–6216.

122. Hu, Y.; Ding, M.; Liu, X.-Q.; Sun, L.-B.; Jiang, H.-L. *Chem. Commun.* **2016**, *52* (33), 5734–5737.

123. Chen, L.; Zheng, H.; Zhu, X.; Lin, Z.; Guo, L.; Qiu, B.; Chen, G.; Chen, Z.-N. The *Analyst* **2013**, *138* (12), 3490.

124. Wei, X.; Zheng, L.; Luo, F.; Lin, Z.; Guo, L.; Qiu, B.; Chen, G. *J. Mater. Chem. B* **2013**, *1* (13), 1812.

125. Khoshaman, A. H.; Bahreyni, B. *Sens. Actuators, B* **2012**, *162* (1), 114–119.

126. Venkatasubramanian, A.; Lee, J.-H.; Stavila, V.; Robinson, A.; Allendorf, M. D.; Hesketh, P. J. *Sens. Actuators, B* **2012**, *168*, 256–262.

127. Robinson, A. L.; Stavila, V.; Zeitler, T. R.; White, M. I.; Thornberg, S. M.; Greathouse, J. A.; Allendorf, M. D. *Anal. Chem.* **2012**, *84* (16), 7043–7051.

128. Kreno, L. E.; Leong, K.; Farha, O. K.; Allendorf, M.; Van Duyne, R. P.; Hupp, J. T. *Chem. Rev.* **2012**, *112* (2), 1105–1125.

129. Farha, O. K.; Spokoyny, A. M.; Mulfort, K. L.; Hawthorne, M. F.; Mirkin, C. A.; Hupp, J. T. *J. Am. Chem. Soc.* **2007**, *129*, 12680-12681.

130. Ma, L.; Abney, C.; Lin, W. *Chem. Soc. Rev.* **2009**, *38* (5), 1248–1256.

131. Alkordi, M. H.; Liu, Y.; Larsen, R. W.; Eubank, J. F.; Eddaoudi, M. *J. Am. Chem. Soc*. **2008**, *130* (38), 12639–12641.

132. Nuzhdin, A. L.; Dybtsev, D. N.; Bryliakov, K. P.; Talsi, E. P.; Fedin, V. P. *J. Am. Chem. Soc.* **2007**, *129* (43), 12958–12959.

133. Fujita, M.; Kwon, Y. J.; Washizu, S.; Ogura, K. *J. Am. Chem. Soc.* **1994**, *116* (3), 1151–1152.

134. Wu, C.-D.; Hu, A.; Zhang, L.; Lin, W. *J. Am. Chem. Soc.* **2005**, *127* (25), 8940–8941.

135. Farha, O. K.; Mulfort, K. L.; Hupp, J. T. *Inorg. Chem.* **2008**, *47* (22), 10223–10225.

136. Horike, S.; Dincă, M.; Tamaki, K.; Long, J. R. *J. Am. Chem. Soc.* **2008**, *130* (18), 5854–5855.

137. Lee, J.; Farha, O. K.; Roberts, J.; Scheidt, K. A.; Nguyen, S. T.; Hupp, J. T. *Chem. Soc. Rev.* **2009**, *38* (5), 1450–1459.

138. Wee, L. H.; Alaerts, L.; Martens, J. A.; De Vos, D. In *Metal-Organic Frameworks*; Farrusseng, D., Ed.; Wiley-VCH Verlag GmbH & Co. KGaA: Weinheim, Germany, 2011; pp 191–212.

139. Faraday, M. *Experimental Researches in Chemistry and Physics*, Richard Taylor and William Francis: London, U.K., 1859.

140. Orchard, A. F. *Magnetochemistry*, Oxford University Press: New York, USA, 2003.

141. Drung, D.; Abmann, C.; Beyer, J.; Kirste, A.; Peters, M.; Ruede, F.; Schurig, T. *IEEE Trans. Appl. Supercond.* **2007**, *17* (2), 699–704.

142. Liu, K.; Li, H.; Zhang, X.; Shi, W.; Cheng, P. *Inorg. Chem.* **2015**, *54* (21), 10224–10231.

143. Wu, Y.-L.; Guo, F.-S.; Yang, G.-P.; Wang, L.; Jin, J.-C.; Zhou, X.; Zhang, W.-Y.; Wang, Y.-Y. *Inorg. Chem.* **2016**, *55* (13), 6592–6596.

144. Vaz, M. G. F.; Cassaro, R. A. A.; Akpinar, H.; Schlueter, J. A.; Lahti, P. M.; Novak, M. A. *Chemistry **2014,** 20* (18), 5460–5467.

145. Chen, M.; Zhao, H.; Sañudo, E. C.; Liu, C.-S.; Du, M. *Inorg. Chem.* **2016**, *55* (8), 3715–3717.

Bartolomé, E.; Bartolomé, J.; Arauzo, A.; Luzón, J.; Badía, L.; Cases, R.; Luis, F.; Melnic, S.; Prodius, D.; Shova, S.; Turta, C. *J. Mater. Chem. C* **2016**, *4* (22), 5038–5050.

146. Su, L.; Song, W.-C.; Zhao, J.-P.; Liu, F.-C. *Chem. Commun.* **2016**, *52* (56), 8722–8725.

147. Coronado, E.; Gaviña, P.; Tatay, S. *Chem. Soc. Rev.* **2009**, *38* (6), 1674–1689.

148. Chen, B.; Eddaoudi, M.; Reineke, T. M.; Kampf, J. W.; O'Keeffe, M.; Yaghi, O. M. *J. Am. Chem. Soc.* **2000**, *122* (46), 11559–11560.

149. Motokawa, N.; Matsunaga, S.; Takaishi, S.; Miyasaka, H.; Yamashita, M.; Dunbar, K. R. *J. Am. Chem. Soc.* **2010**, *132* (34), 11943–11951.

150. Halder, G. J. *Science* **2002**, *298* (5599), 1762–1765.

151. Coronado, E.; Giménez-Marqués, M.; Mínguez Espallargas, G. *Inorg. Chem.* **2012**, *51* (7), 4403–4410.

152. Yang, J.; Zhou, L.; Cheng, J.; Hu, Z.; Kuo, C.; Pao, C.-W.; Jang, L.; Lee, J.-F.; Dai, J.; Zhang, S.; Feng, S.; Kong, P.; Yuan, Z.; Yuan, J.; Uwatoko, Y.; Liu, T.; Jin, C.; Long, Y. *Inorg. Chem.* **2015**, *54* (13), 6433–6438.

153. Coronado, E.; Espallargas, G. M. *Chem. Soc. Rev.* **2013**, *42* (4), 1525–1539.

154. Huang, Y.-G.; Jiang, F.-L.; Hong, M.-C. *Coord. Chem. Rev.* **2009**, *253* (23–24), 2814–2834.

155. Humphrey, S. M.; Allan, P. K.; Oungoulian, S. E.; Ironside, M. S.; Wise, E. R. *Dalton Trans.* **2009**, *No. 13*, 2298–2305.

156. Nuñez, A. J.; Chang, M. S.; Ibarra, I. A.; Humphrey, S. M. *Inorg. Chem.* **2014**, *53* (1), 282–288.

157. Dunning, S. D.; Nuñez, A. J.; Moore, M. D.; Waggoner, N. W.; Lytwak, L. A.; Steiner, A.; Lynch, V. M.; Holliday, B. J.; Humphrey, S. M. *J. Am. Chem. Soc.* **2016**, in draft.

158. Waggoner, N. W.; Allen, P. K.; Lynch, V. M.; Kornfuehrer, T.; Humphrey, S. M. *Chem. Sci.* **2016**, in draft.

159. Ibarra, I. A.; Tan, K. E.; Lynch, V. M.; Humphrey, S. M. *Dalton Trans.* **2012**, 41 (*14*), 3920–3923.

160. Waggoner, N. W.; Saccoccia, B.; Ibarra, I. A.; Lynch, V. M.; Wood, P. T.; Humphrey, S. M. *Inorg. Chem.* **2014**, *53* (24), 12674–12676.

161. Ibarra, I. A.; Yoon, J. W.; Chang, J.-S.; Lee, S. K.; Lynch, V. M.; Humphrey, S. M. *Inorg. Chem.* **2012**, *51* (22), 12242–12247.

162. Bohnsack, A. M.; Ibarra, I. A.; Bakhmutov, V. I.; Lynch, V. M.; Humphrey, S. M. *J. Am. Chem. Soc.* **2013**, *135* (43), 16038–16041.

163. He, J.; Waggoner, N. W.; Dunning, S. D.; Stiener, A.; Lynch, V. M.; Humphrey, S. M. *Angew. Chem., Int. Ed.* **2016**, accepted.

Chapter 2: Development of unusual linkers for catalysis and gas storage

In this study, three individual linker systems were developed and characterized in order to explore new methods for inclusion of catalytically-active metals into PCPs. The initial system investigated was a group (VIII) metalated *trans*-di(*bis*(phosphine)) linker. This branch of complexes has shown literature precedence for chemisorption behavior upon activation and plausibility for hydrogenation catalysis.[1] The next system of interest took the well-known complex 1,1'-*bis*(diphenylphosphino)ferrocene (dppf) and adapted the extending phenyl rings to be polymerizable with *p*-carboxylate groups. The dppf complex metalated with palladium (II) and platinum (II) dichloride has shown significant catalytic applicability in a variety of coupling reactions.[2,3] The final linker of interest took another look at the complex 4,4',4",4"'-(1,2-phenylenebis(phosphinotriyl))tetrabenzoic acid (bbcb) that was previously synthesized within the group,[4] and expanded that system with an additional phenyl ring extension off of each arm. This extended linker, designated b-bbcb, allows for access to the possibility of larger pores while still incorporating catalytic Pd (II) or Pt (II) sites; this type of complex has demonstrated catalytic plausibility for coupling reactions as well as polymerization.[5,6] The development of these more complex linker systems with incorporation of catalytically interesting metals could usher in a new arena of PCMs with a wide variety of potential applications.

INTRODUCTION

Despite exploration of the field starting in the 18th century, heterogeneous catalysis has remained one of the largest areas of interest in chemistry today. Heterogeneous catalysis has displayed an impressive array of applications including alternative fossil fuel generation and refinement,[7-9] diatomic hydrogen manufacturing,[10,11] and removal of air

pollutants.[12,13] More recent research has focused on improvement of chemical production including ethanol as well as various hydrogenation products.[14-16] PCPs have drawn significant attention in the area of catalysis over the last 20 years, due to their uniform, size selective pores as well as their ability to incorporate a monumental number of well-defined, catalytically active sites within their framework structures. Additionally, PCPs allow for a great range of synthetic variability due to the inclusion of the organic linker component, making them significantly more adaptable than zeolites for use in catalysis.[17] Despite their many marketable attributes, research surrounding PCP-based catalysts has only recently begun to progress.[18-20] The slow progress in the development of PCP catalysts has largely been due to the complexity of chemistry surrounding these self-assembled materials, as well as the fact that small pore sizes typical in PCPs limit the number of possible reagents.[21] Furthermore, PCPs have been shown to display largely poor thermal stability in comparison to similar materials such as zeolites, creating concern for applicability in high-energy catalysis. Development of thermally robust PCPs for structurally demanding catalytic reactions is an ongoing effort.[22-25] The unpredictable nature of how each PCP will self-assemble creates a dilemma from a design perspective for promotion of spatially available catalytically active sites. There has been some progress in designing porous materials for catalysis through development of a better understanding within mechanisms of interest, as well as advancements in characterization techniques to identify key factors in active site chemistry.[21]

In an effort to overcome this difficulty of programing PCPs for use in catalysis, research to date has largely taken one of two approaches: PCPs with *post*-synthetically incorporated catalytic sites,[26-31] or the use of catalytically active metal sites as nodes along with the variation of linkers that can help facilitate catalysis through their functionality.[32-34] Both techniques have shown promise, although the former tends to further limit access

into pores due to microporosity. There has been much less focus, however, on use of linkers that incorporate catalytically active metals into their structures before polymerization. In one of the few examples published to date, Lin and coworkers demonstrated the inclusion of the BINAP functionality into a linker that was polymerized through the naphthalene backbone; this linker was coordinated with zirconium nodes to afford a UiO-type topology that demonstrated highly enantioselective cyclization reaction capabilities.[35,36] In another recent example, W. Xi *et al.* showed incorporation of a chiral vanadium-metallosalen catalyst as a ligand into a framework with both zinc and cadmium that demonstrate the ability to perform asymmetric organic transformations.[37] These two studies were the only true examples found to date in the literature that demonstrated incorporation of catalytically-active metals within the linkers prior to PCP growth, indicating the immense amount of research that is still needed available in this third area of catalytic-PCP development.

In this study, the focus was to synthesize and characterize a series of polymerizable linkers that incorporated a catalytically active metal center. Literature precedence was also a large influence in the choice for each system that was investigated. The initial system looked at the development of a group (VIII) *trans*-di(*bis*(phosphine)) complex. When considering potential applications, chemisorption behavior and hydrogenation capabilities were the primary interests for this linker system. An asymmetric version of this *trans*-di(*bis*(phosphine)) complex was attempted as well, which resulted in an interesting kinetic versus thermodynamic sub-study to better understand the chemistry behind linker formation. The next linker of interest took the well-known dppf complex incorporating a group (X) metal and looked at incorporating this functionality into a polymerizable linker. Interest for this complex was hopeful for coupling reaction applications. The final study attempted to extend the polymerization arms of a well-known group (X) *bis*(phophine)

linker in an attempt to facilitate the creation of a larger pore window. This extended, benzene backbone complex could allow for increased pore size, and therefore allow for a greater range of reactants to have access to all of the active metal sites. All three complexes were successfully synthesized and characterized. Exhaustive PCM trials have shown promise, but have proven more difficult than other frameworks due to their higher levels of coordination.

A GROUP (VIII) *TRANS*-DI(*BIS*(PHOSPHINE)) LINKER

Interest in group (VIII) monomeric complexes with *trans*-di(*bis*(ligand)) coordination around the equatorial sites can be found in the literature as early as the 1970's.[38-40] These complexes have commonly employed *bis*(phosphines) as the chelated ligands and halides at the axial sites. Continued interest has been seen for these monomeric species due to their ability to be easily 'activated' through single chloride removal (Scheme 2.1). The resulting open metal site has shown significant applicability in diatomic molecule association for N_2 and H_2, as well as in catalysis for hydrogenation and hydrogenolysis.[41-44]

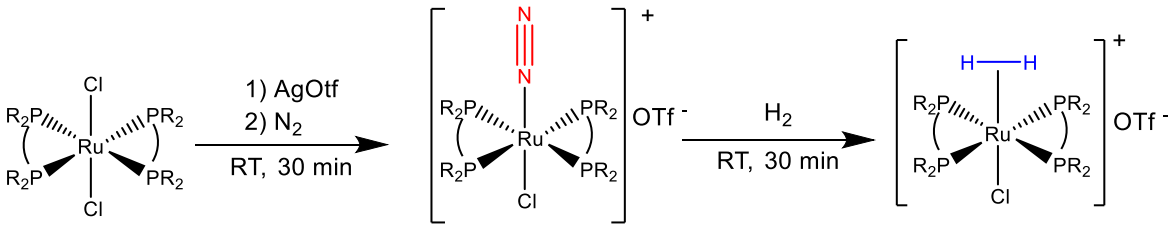

Scheme 2.1. Schematic representation of a *trans*-di(*bis*(phosphine)) complex (Left), activation followed by association of diatomic nitrogen (Middle), and exchange with diatomic hydrogen (Right).

For the case of H_2 association to a group (VIII) metal center, the diatomic hydrogen associates to the metal center in an η^2 fashion. The H_2 net σ bonding molecular orbital on H_2 is donating its electron density towards the metal center's e_g orbital, depleting electron density on the diatomic hydrogen. Meanwhile, one of the metal's t_2g orbitals is back-donating to the antibonding σ* orbital on H_2. Although the energy difference between these two orbitals is higher than a traditional π-backbonding interaction, the t_2g − σ* back donation still allows for a degree of increased electron density to be redistributed back onto the diatomic hydrogen (Figure 2.1). Typically, in this type of complex the σ interaction is expected to outweigh the back bonding that is occurring, which results in the H_2 becoming more acidic than its free form.1

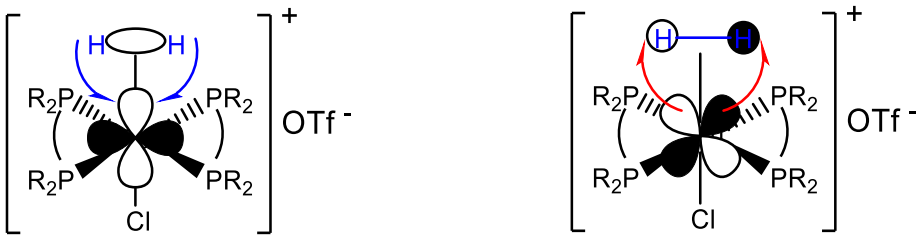

Figure 2.1. Representation of η^2-bound H_2 with σ donation into the metal center e_g orbital (Left, blue e^- movement), and backbonding donation from the t_2g orbital on the metal center to the σ* orbital from H_2 (Right, red e^- movement).

When considering the interaction of N_2 with a group (VIII) open metal site, there is different picture due to diatomic nitrogen associating end on with the metal center. This association geometry allows for a more traditional ligand interaction, with a N_2 lone pair from one side of the molecule allowing for σ to e_g donation from N_2 for the primary interaction. However, nitrogen has accessible, unfilled *p*-orbital space, which then can allow for a much higher degree of backbonding to occur from a metal center t_2g orbital

back into the π* orbital on N_2 (Figure 2.2). Naturally, the degree of backbonding still strongly relies on the relative energy of those *p*-orbitals. Regardless there is a higher plausibility of back-donation in this case than in H_2, which can change the interactions with the former in comparison to the latter dramatically.

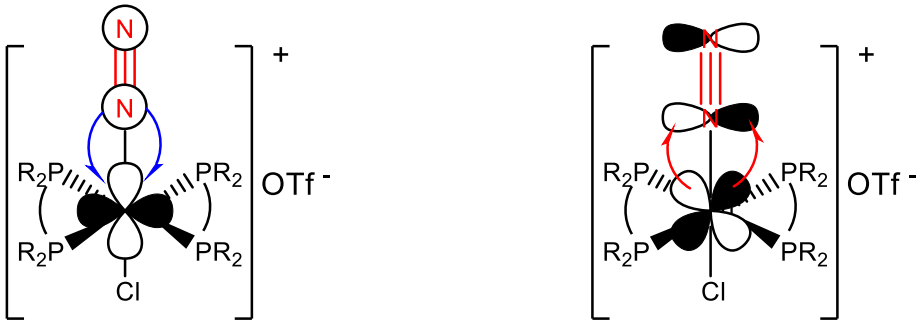

Figure 2.2. Representation of end-on association of N_2, with σ to e_g donation from diatomic nitrogen to the metal center (Left, blue e^- movement), and back-donation of electron density from a t_2g metal orbital back to the π* (Right, red e^- movement).

Trans-group (VIII) *bis*(phophine) complexes have shown great promise towards catalysis as well, with interest geared towards hydrogenolysis and a variation of hydrogenation reactions. Naturally, when considering ruthenium catalysis, there are a great degree of reaction pathways to consider due to the ability of ruthenium to access a much larger amount of oxidation states than many other common catalytic metal centers. Ruthenium catalysts can access common oxidative addition/reductive elimination $2e^-$-pathways seen with other catalysts, along with redox pathways that only require $1e^-$ movement as well. A catalyst with this level of variability can allow for very small changes in ligand make-up and environment to result in monumental changes in catalyst

performance. However, investigation of previous studies can help gain a knowledge base of what has been possible thus far with similar complexes.

The literature example that stood out for hydrogenolysis within this class of compounds came from Takei *et al.* in 2003.[1] Takei published a paper that demonstrated the complex $RuCl(\eta^2\text{-}H_2)(dppe)_2$ (dppe = 1,2 *bis*-(diphenylphosphino)ethane) acting as the active catalyst (10 mol%) in the conversion of 1-trimethylsilyloxy-1-cyclohexene under 1 atm of H_2 to cyclohexanone and its corresponding trialkylsilane. Several other trimethyl silylethers were investigated in this study, and the mechanism for the hydrogenolysis that was occurring was proposed as well (Scheme 2.2).

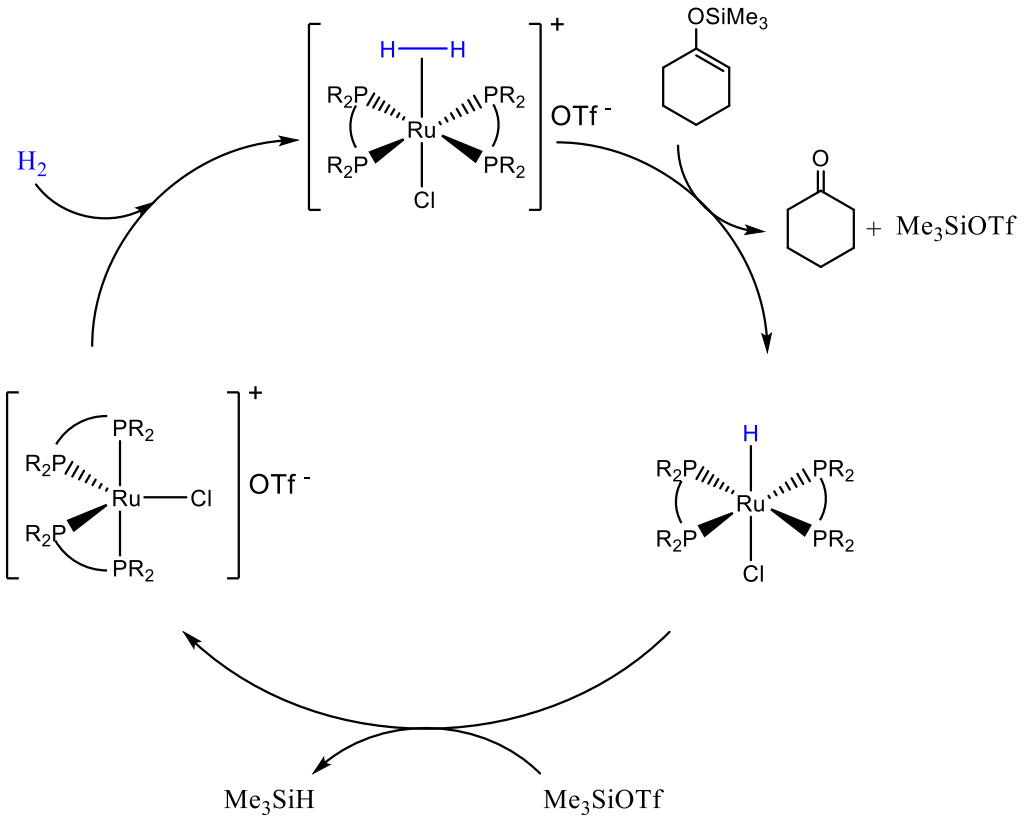

Scheme 2.2. Hydrogenolysis cycle as portrayed in the publication by Takei *et al.*[1]

Another area of catalysis that was found to employ *trans*-group (VIII) *bis*(phophine) complexes investigated various degrees of hydrogenation. In 1997, Baiker and coworkers demonstrated $RuCl_2(dppe)_2$ (2.44 mol%) catalyzing the synthesis of DMF and methyl formate through hydroaminylation in a solvent-free environment.[45] Baiker's work showed a turn over frequency of 360,000 h^{-1} and 830 h^{-1} at 373 K for the two products respectively, which was the highest output to date. Similar work to this publication was reviewed and investigated by Jessop *et al*. in 1995 and 1996 respectively.[46,47] However, other ruthenium complexes catalysts have shown the ability to decompose DMF, which further demonstrates the complexity of catalysis with group (VIII) complexes.[48,49]

Regardless of research around *trans*-group (VIII) *bis*(phophine) complexes and their properties dating back nearly 50 years, their abilities in associating diatomic species as well as in catalysis have never been demonstrated within a polymeric framework to date. It was this fact along with an impressive amount of monomeric studies that sparked interest in taking the reactivity of these complexes and attempting to apply that reactivity within a heterogeneous catalyst as a PCP. The diatomic interactions that the group (VIII) complexes are known for have the plausibility to demonstrate very interesting chemisorption properties upon cleavage of a halide site within the polymeric material. Furthermore, as discussed above, applying homogeneous reactivity into a porous, heterogeneous material can allow for very interesting progress in selectivity and overall output.

Results and discussion

This study was approached synthetically broken down into three different portions; precursor synthesis, complex synthesis, and complex variations. Each component was carefully characterized to ensure purity moving forward.

Precursor synthesis

Before the synthesis of the metalated linker was considered, the precursor 1,2-*bis*(dichlorophosphino)benzene (1,2-dcpb, **3**) was a concern. This compound was sold as a reagent by only one provider, and had doubled price over a year. With this concern in mind, gaining confidence in the synthesis to avoid purchase of the reagent 1,2-dcpb became a high priority. From the literature, there was one predominant route for the synthesis of 1,2-dcpb. Ding and coworkers reported the most recent update of this procedure in 2008.[50] This method used 1,2-dibromobenzene along with the stepwise replacement of halides with *bis(*diethylamino)phosphine groups; this method employed fractional distillation as the primary purification technique (Scheme 2.3).

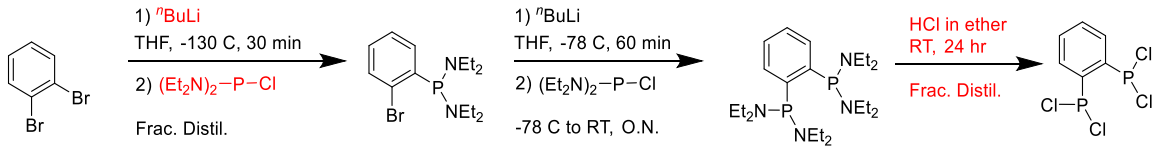

Scheme 2.3. The reaction pathway published by Ding and coworkers for the synthesis of 1,2 dcpb.[50]

Upon investigation of this synthetic pathway, it became clear that there were areas of improvement and adjustment that could be undertaken to create a more efficient process. Through this process, the ^{n}BuLi to $(Et_2N)_2$-P-Cl proportionality was first idealized in the initial step to avoid the unneeded production of benzyne and di-lithiated biproducts. More importantly, the final deprotection step was completely reconsidered. The reagent 4M HCl in diethyl either is not commercially available at that concentration, requiring a tank of HCl to saturate a solution of diethyl ether before use. To avoid this cost-intensive process, use

of phosphine trichloride (PCl_3) was considered as an alternative deprotection reagent. The use of PCl_3 was not only significantly more affordable, it also allowed for the $(Et_2N)_2$-P-Cl precursor to be created as the final product was produced. Then, the excess PCl_3, $(Et_2N)_2$-P-Cl, and 1,2-dcpb could be separated *via* fractional distillation to afford all three products, allowing for a significantly more efficient process. This alternative was attempted and the product 1,2-dcpb (**3**) was synthesized and confirmed by ^{31}P ^{1}H, and ^{13}C and NMR (Figure B.7-B.9). The upscaling of the production of 1,2-dcpb to replace reagent purchase is an ongoing effort. However, the idealization of proportions for the initial lithiation and the alternative deprotection method were successfully shown in this study and will help pave the way to self-production of 1,2-dcpb for the group indefinitely.

Linker development

The group (VIII) *trans*-1,2-di(*bis*(phosphine)) complex that was of interest in this study was *trans*-di(*bis*(4,4',4",4"'-(1,2-phenylenedi(phosphinotriyl)tetrabenzoic acid)) ruthenium dichloride ($PdCl_2(bbcb)_2$) (**6**, Figure 2.3A). This linker was chosen due to its benzene-backbone allowing for the promotion of *bis*(phosphine) chelation to the metal center, while the benzene-carboxylate arms allowed for an extended 'arm' length, which can help with maintaining porosity within a polymerized material.

The bbcb (**5**) ligand system had been previously synthesized within the group and was published with group (X) metalation for incorporation into a sub-group of PCMs.[4] The synthetic process reported by Bohnsack *et al*. was adapted and updated during work in this study as per experimental procedures below. The metalation process proved slightly difficult, likely due to steric bulk of the bbcb ligands. However, the $RuCl_2(bbcb)_2$ complex was successfully isolated as the thermodynamically favored product and was fully

characterized *via* FT-IR spectroscopy (Figure A.3), ^{31} P, ^{1}H, ^{13}C, NMR (Figure B.19−B.21), and single crystal X-ray crystallography (Table C.1−C.4) (Figure 2.3B,C).

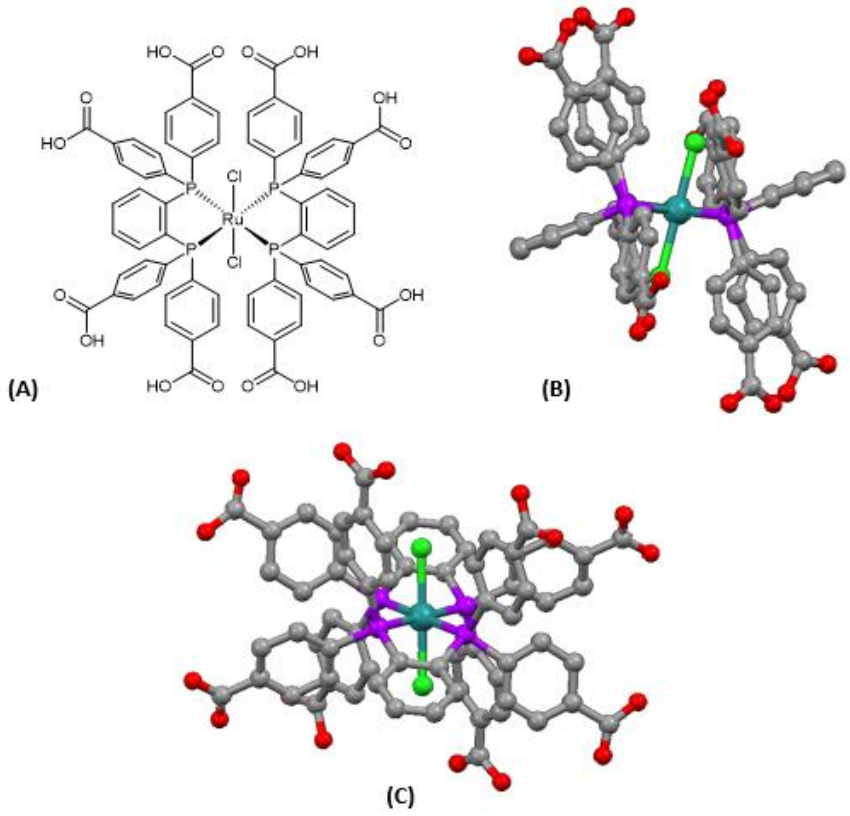

Figure 2.3. Visual representation of $RuCl_2(bbcb)_2$ (**6**) (**A**), X-ray crystal structure of the complex side-on (**B**), and face-on (**C**).

The crystallographic structure of $RuCl_2(bbcb)_2$ showed that the benzene rings were clearly under some form of stress in this complex, with the backbone showing 28.88−30.82° of flex out of the Ru1·P1·P2 plane. The bite angle of the bbcb *bis*(phosphines) seemed slightly shallow as well, with a P1·Ru1·P2 angle of 81.14°, and a P2·Ru1·P1 angle of 98.86° between the two bbcb chelates. However, the Cl1·Ru1 ·Cl2

angle was found to be 180.00° and the benzene-carboxylate arms were showed surprising regularity, with four of the arms pointing upwards and the other four facing downward in a double tabletop-like fashion. The regularity of the benzene arms can statistically help with material formation and their arrangement could help to promote 3-dimensionality as well.

In the literature, several examples of UiO-type materials employing zirconium have demonstrated 4-connected nodal systems.[51-54] This type of connectivity showed strong similarities to the plausible polymerization of $RuCl_2(bbcb)_2$, and was one of several metal systems of interest for PCM growth. Over the course of three years, 276 PCM-growth trials were performed with a variety of 3*d* and lanthanide metals, solvents, temperatures, secondary ligands, etc., being employed. Unfortunately, a PCM was not produced. However, these trials have given great insight into how these materials prefer to crystallize and have also provided several promising routes to work on for group continuation of attempts towards PCM growth. The use of ruthenium within linkers for PCP growth is in its adolescence in the literature, and continuation of this field will no doubt push the field of PCP-heterogeneous catalysis into a new era.

Asymmetric linker study

With the time-intensive process of $RuCl_2(bbcb)_2$ (**6**) PCM growth trials underway, a second linker was also considered in order to push this study forward on multiple fronts simultaneously. An asymmetric version of complex (**6**) was considered for this second linker, which would maintain the reactivity of interest while exploring a different carboxylate geometry for PCP growth (Figure 2.4). Asymmetric di(*bis*(phosphine)) complexes were found to be much more rare in the literature than its symmetric

counterparts. Only a handful of studies were found that looked at the combination of a *bis*(amine) and *bis*(phosphine),[55-57] and no examples were found that employed two different types of *bis*(phosphine) ligands on one group (VIII) metal center.

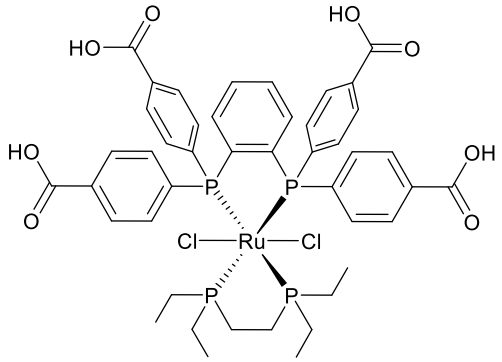

Figure 2.4. Visual representation of the asymmetric linker of interest $RuCl_2$(bbcb)(depe).

The use of one carboxylated-bbcb *bis*(phosphine) would allow for adequate polymerization into a 3-dimensional material on its own. Therefore, the other sites around the equatorial plane could be bound by anything else to keep the linker stable for polymerization. In an attempt to maintain a similar binding structure to $RuCl_2(bbcb)_2$ while taking up the smallest amount of space possible, the secondary ligand 1,2-*bis*(diethylphosphino)ethane (depe) was chosen.

The synthesis of the asymmetric linker $RuCl_2$(bbcb)(depe) was first attempted with the stepwise *in-situ* addition of the *bis*(phosphines) separately. With the understanding that depe would act as a notably better lewis base over bbcb, the latter was added first to help promote coordination of both chelates (Scheme 2.4).

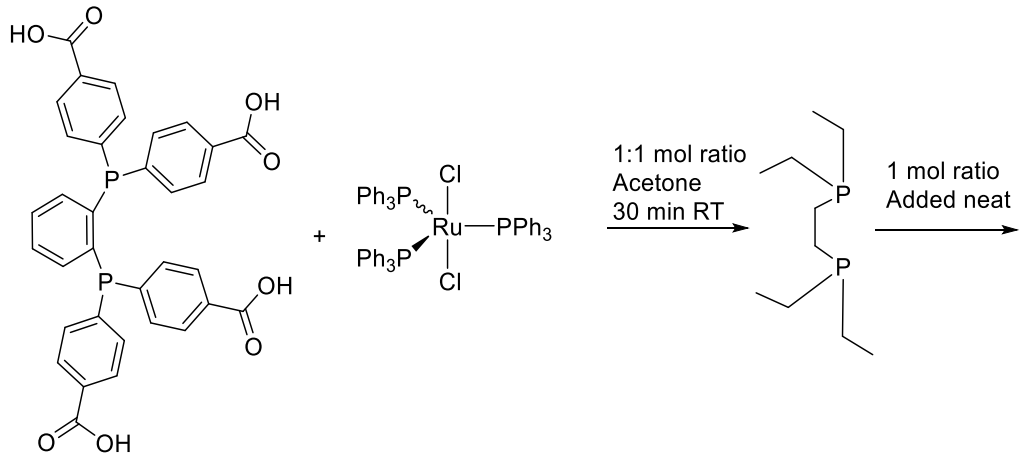

Scheme 2.4. Reaction scheme for stepwise *in-situ* synthesis of $RuCl_2(bbcb)(depe)$.

This reaction was attempted in a variety of solvents including acetone, tetrahydrofuran, and DMF with reflux for a minimum of two days. In every case the two complexes $RuCl_2(bbcb)_2$ and $RuCl_2(depe)_2$ were formed, suggesting these two species were the thermodynamic products. To further prove this hypothesis, $RuCl_2(bbcb)_2$ and $RuCl_2(depe)_2$ were synthesized individually, then placed together to reflux in solution; the reaction showed no conversion of the two complexes. However, EIC mass spectrometry was performed on the isolated from the reaction seen in Figure 2.8, and $RuCl_2(bbcb)(depe)$ was observed along with the other two symmetric products.

Next, variable temperature ^{31}P-NMR was performed for $RuCl_2(depe)_2$ + bbcb and $RuCl_2(bbcb)_2$ + depe (Figure 2.5) separately from −80 °C upwards in an attempt to find a temperature where the kinetic product $RuCl_2(bbcb)(depe)$ could be isolated. The latter study was of most interest, with a high likelihood that $RuCl_2(bbcb)_2$ exchanging with depe due to its lewis basicity. There was a small shift and broadening of peaks seen in the study, which is common in variable temperature NMR. The only changes seen as temperature

was varied was the formation of a small amount of $RuCl_2(bbcb)$ (~22 ppm, 3) and *cis*-$RuCl_2(depe)_2$ (~60 ppm, 3−5).

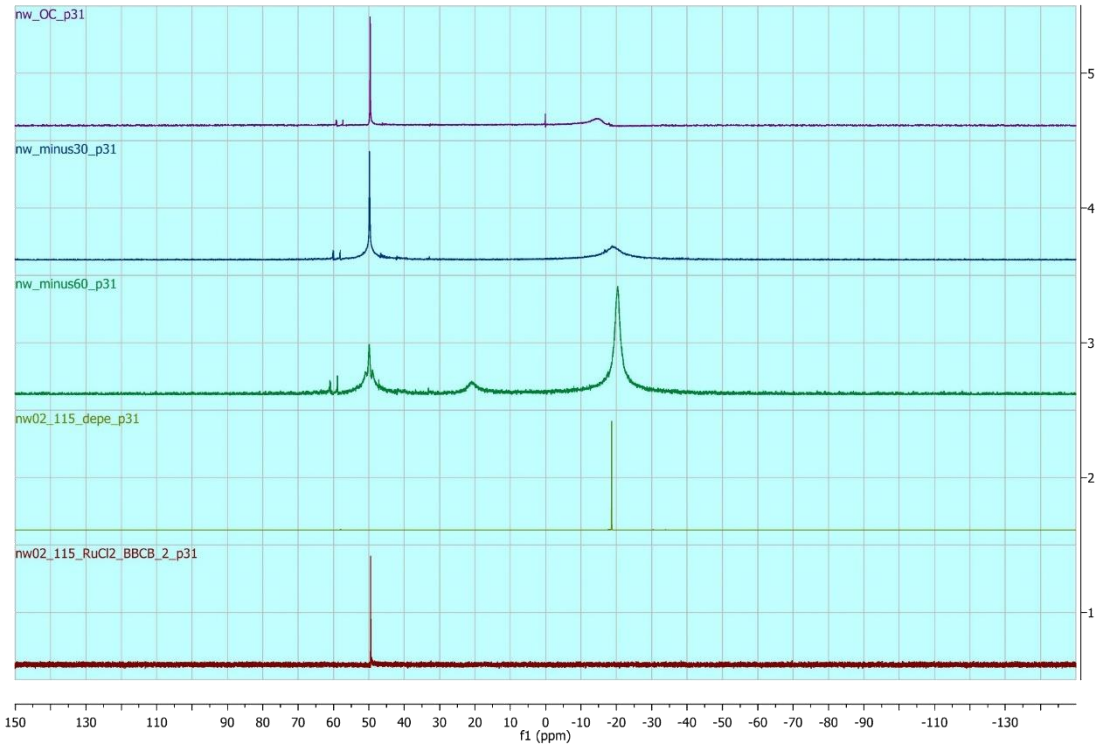

Figure 2.5. Variable temperature ^{31}P-NMR spectra for $RuCl_2(bbcb)_2$ (1)+ depe (2) in *d*-MeOH for −60 °C (3), −30 °C (4), and 0 °C (5).

With mass spectrometry data from the previously explored reaction suggesting that there is a notable amount of $RuCl_2(bbcb)(depe)$ being formed, it is unlikely that there would be none formed in the variable temperature NMR studies performed. With this in mind, it was probable that the ^{31}P-NMR shift of the asymmetric complex fell so closely to its symmetric relatives $RuCl_2(bbcb)_2$ and $RuCl_2(depe)_2$ (50.1 ppm and 48.8 respectively) that their chemical shifts were not distinguishable in the room temperature or especially in the variable temperature measurements.

Although the complex $RuCl_2$(bbcb)(depe) proved difficult to isolate, this investigation gave great insight into asymmetric di(*bis*(phosphine)) linker development and will continue to be explored by the Humphrey group for possible PCM incorporation in the future.

Experimental data

General

All synthetic methods for linker development were performed under a nitrogen atmosphere through the use of standard schlenk techniques. The precursor 1-chloro-N,N,N',N'-tetraethylphosphinediamine was synthesized per the literature.[58] As-purchased phosporous trichloride (PCl_3) (Sigma Aldrich, ≥99 %) was distilled before use (40 °C, passive vacuum). The reagents *n*-butyllithium (nBuLi) (2.5 M in hexanes, Sigma Aldrich), 1,2-dibromobenzene (1,2-dbb) (Oakwood Chemical, ≥98 %), 1,4-dibromobenzene (1,4-dbb) (Oakwood Chemical, ≥99 %), ammonium chloride (NH_4Cl) (Fisher Chemical, ACS grade), magnesium sulfate anhydrous ($MgSO_4$) (Fisher Chemical, ≥98 %), solid carbon dioxide (Praxair), and hydrochloric acid (Fisher chemical, ACS grade), hexanes (Fisher chemical, ACS grade) and dichloromethane (DCM) (Fisher chemical, ACS grade) were used as received. The precursor 1,2-*bis*(dichlorophosphino)benzene (1,2-dcpb) (Sigma Aldrich, ≥96 %) was used as received in the synthesis of bbcb. Tetrahydrofuran (THF) (Fisher chemical, HPLC grade) was distilled (dried over sodium in a still) and collected over sieves (4A). Diethyl ether was freeze-pump-thawed and acetone (Fischer Chemical, ACS grade) as well as all aqueous solutions were degassed with nitrogen for 30 min prior to use. $RuCl_2(PPh_3)_3$ and *trans*-$RuCl_2(depe)_2$ was prepared as per the literature.[59,60] Solution ^{1}H-NMR and ^{31}P-NMR were collected in-house using an Agilent MR 400MHz

spectrometer; ^{13}C-NMR was collected with a Varian Inova 500 MHz; FT-IR spectra were obtained direction from solid samples using a Nicolet iS*50 spectrophotometer with an attenuated total reflectance apparatus; thermogravimetric analysis (TGA) data was collected with a TA Instruments Q50 system for the temperature range of 25 °C to 800 °C. Procedure for bbcb was adapted from a previous publication in the group.[4]

X-ray Crystallography

A suitable crystal were mounted on a nylon thread loop in perfluoropolyether oil and attached to the diffractometer. The data was collected at 100 K. Data collection, unit cell refinement, and data collection were performed using direct methods, with full-matrix least squares on F^2 using SHELXL-2013. All data was collected using Mo Kα radiation (0.7093 Å) on a Nonius Kappa CCD diffractometer with a Bruker Apex II CCD, and a 600 low-temperature attachment employing Bruker's Apex II (2010) operating system. The structural analysis was performed using Mercury 3.1 (Build RC5).

Procedure for 1-(2-bromophenyl)-N,N,N',N'-tetraethylphosphinediamine (1)

A solution of THF (150 mL) and nBuLi (1.6 M in hexanes, 51.37 mmol) was added to a 100 mL round-bottomed flask. A second solution of 1,2-dbb (6.00 mL, 50.36 mmol) in THF (50 mL) was placed in the attached air-free dropping funnel. The nBuLi/THF mixture was cooled to −130 °C with a pentane/liquid N_2 bath while being stirred vigorously. Once the solution had equilibrated to the target temperature, the 1,2-dbb/THF solution was added dropwise over 45 min. The resulting yellow, slightly heterogeneous mixture was allowed to stir at −130 °C for 30 more min, while the dropping funnel was rinsed with a small amount of THF (*ca*. 5 mL). Then, a solution of N,N,N',N'-

tetraethylphosphinediamine (10.97 mL, 52.88 mmol) in THF (60 mL) was placed into the rinsed dropping funnel and slowly added to the reaction over 20 min. The pale yellow solution was allowed to continue stirring and acclimate to room temperature overnight. The reaction was pulled down to an oil *via* and diethyl ether (*ca*. 100 mL) was added *via* cannula, then stirred for 1−2 hrs. The lithium salts were air-free filtered away from the wanted solution and the diethyl ether was removed *in vacuo* to afford the crude product. The deep yellow oil was purified *via* fractional vacuum distillation (150 °C, 0.5 mmHg) to yield the product as a colorless oil (9.25 g, 28.79 mmol). Yield: 57.6 %. ^{31}P-NMR (C_6D_6, 161.8 MHz) δ = 96.464 ppm; ^{1}H-NMR (C_6D_6, 400.1 MHz) δ = 7.448−7.477 (dt, 1H), 7.403-7.424 (m, 1H), 7.013−7.119 (t, 1H), 6, 6.697−6.746 (m, 1H), 2.895−3.073 (m, 8H), 0.964−1.023 (m, 12H) ppm; ^{13}C-NMR (C_6D_6, 150.9 MHz): δ = 143.512 (s, Ar), 133.024 (s, Ar), 132.834 (s, Ar), 131.416 (s, Ar), 129.680 (s, Ar), 127.882 (s, Ar), 127.579 (s, Ar), 44.340 (s, Al), 44.158 (s, Al), 15.301 (s, Al).

Procedure for 1,1'-(1,2-phenylene)bis(N,N,N',N'-tetraethylphosphinediamine) (2)

The colorless oil (**1**) (2.90 mL, 11.63 mmol) was diluted with THF (30 mL) in a 100 mL round-bottomed flask. The stirred solution was cooled to −78 °C with a dry ice/acetone bath before nBuLi (1.6 M in hexanes,11.63 mmol) was added dropwise over 10 min. The deep orange suspension was allowed to stir for 1.5 hrs at −78 °C, before the addition of N,N,N',N'-tetraethylphosphinediamine (2.44 mL, 11.63 mmol) in THF (6 mL) slowly over 10 min. The resulting slightly yellow solution was allowed to stir and acclimate to room temperature overnight. All solvent was removed *in vacuo*, then diethyl either (25 mL) was added to the oil. After stirring or 1.5 hours, the resulting lithium salts were removed *via* air-free filtration and the diethyl ether was removed online to afford the

product as a yellow oil (4.656 g, 10.91 mmol). Yield: 94.1 %. ^{31}P-NMR (C_6D_6, 161.8 MHz) δ = 97.460 ppm; ^{1}H-NMR (C_6D_6, 400.1 MHz): δ = 7.725−7.767 (m, 2H), 7.209−7.249 (m, 2H), 2.986−3.140 (m, 16H), 1.067 (t, 24H) ppm; ^{13}C-NMR (C_6D_6, 150.9 MHz): δ = 145.666 (s, Ar), 130.870 (s, Ar), 130.817 (s, Ar), 127.412 (s, Ar), 126.957 (s, Ar), 43.551 (s, Al), 14.513 (s, Al) ppm.

Procedure for 1,2-bis(dichlorophosphino)benzene (3)

The precursor (**2**) (1.00 g, 2.34 mmol) with PCl_3 (23.99 mL, 82.37 mmol) was carefully added to a 200 mL round-bottomed flask. The oil/solution mixture was refluxed while stirring with a condenser attached for 16 hrs. The deep orange solution was allowed to cool, then the PCl_3 was then the solution was purified *via* fractional vacuum distillation (120 °C, 0.5 mmHg) to afford the product as a colorless oil. Due to the high reactivity of the product, it was taken directly for analytical analysis; this made a yield calculation not possible. ^{31}P-NMR (C_6D_6, 161.8 MHz) δ = 151.696 ppm; ^{1}H-NMR (C_6D_6, 400.1 MHz): δ = 7.757−7.798 (m, 2H), 6.856−6.879 (m 2H) ppm; ^{13}C-NMR (C_6D_6, 150.9 MHz): δ = 143.956 (t, Ar), 130.151 (t, Ar) ppm.

Procedure for 1,2-bis(di(4-bromophenyl)phosphino)benzene (bbcb-Br) (4)

The reagent 1,4-dbb (6.91 g, 29.30 mmol) was placed into a 250 mL round-bottomed flask and was dissolved in THF (125 mL). The solution was cooled to −78 °C with a dry ice/acetone bath before nBuLi (1.6 M in hexanes, 29.30 mmol) was added dropwise over 25 min. The white suspension was allowed to stir for 1 hour, then a solution of 1,2-dcpb (2.00 g, 7.15 mmol) in THF (*ca*. 5 mL) was slowly added over 15 min. The resulting pale yellow solution was left to stir and acclimate to room temperature overnight. Salt extraction was performed with an aqueous solution of NH_4Cl (50 mL, 1 M) in H_2O,

followed by drying of the organic layer over $MgSO_4$ for 15 min. before filtration. The filtrate was pulled down to afford a yellow oil. The oil was column purified (1:1 DCM:hexanes) over silica to afford the product as a white solid (4.592 g, 6.03 mmol). Yield: 84.4 %. ^{31}P-NMR ($CDCl_3$, 161.8 MHz) $\delta = -16.464$ ppm; ^{1}H-NMR ($CDCl_3$, 400.1 MHz): δ = 7.359 (d, 8H), 7.308 (m, 2H), 7.031 (m, 2H), 6.973 (m, 8H) ppm; ^{13}C-NMR ($CDCl_3$, 150.9 MHz): δ = 142.653 (t, Ar), 135.405 (t, Ar), 135.100 (t, Ar), 134.017 (t, Ar), 129.683 (s, Ar), 123.702 (s, Ar) ppm; FT-IR (solid/cm^{-1}): ν_{max} = 3044 (w), 2954 (w), 2925 (w), 2852 (w), 1638 (w), 1568 (m), 1554 (w), 1473 (s), 1438 (m), 1424 (w), 1382 (s), 1343 (w), 1297 (w), 1261 (m), 1181 (m), 1107 (w), 1094 (m), 1068 (s), 1007 (s), 944 (w), 808 (s), 757 (m), 735 (m), 723 (s), 702 (w), 663 (w), 628 (w), 568 (w), 553 (w), 512 (s), 501 (s), 436 (w), 401 (w).

Procedure for 4,4',4",4"'-(1,2-phenylenebis(phosphinotriyl))tetrabenzoic acid (bbcb) (5)

The previously synthesized (**4**) (2.48 g, 3.26 mmol) was placed into a 500 mL round-bottomed flask and dissolved in THF (350 mL). The solution was cooled to −78 °C with a dry ice/acetone bath, then nBuLi (1.6 M in hexanes, 16.30 mmol) was added dropwise over 15 min. The grapefruit colored suspension was allowed to stir at −78 °C for an additional 2 hrs after the addition. Crushed dry ice (*ca*. 100 g) along with diethyl ether (100 mL) was added, and the reaction was allowed to acclimate to room temperature overnight while stirring. The white suspension was air-free filtered and dried and the solid was dissolved in H_2O (*ca*. 250 mL). Upon acidification with HCl (12.1 M, 1 pipette), a pale yellow solid was isolated *via* air-free filtration to afford the product (1.86 g, 3.00 mmol). Yield: 92.1 %. ^{31}P-NMR (D_2O, 161.8 MHz) $\delta = -12.961$ ppm; ^{1}H-NMR (D_2O, 400.1 MHz): δ = 7.857 (d, 8H), 7.422 (m, 2H), 7.216 (m, 8H), 7.003 (m, 2H) ppm; ^{13}C-

NMR (D_2O, 150.9 MHz): δ = 167.365 (s, CO_2H), 141.967 (t, Ar), 141.936 (s, Ar), 134.536 (s, Ar), 133.826 (t, Ar), 131.621 (s, Ar), 131.385 (s, Ar), 129.859 (s, Ar) ppm; FT-IR (solid/cm^{-1}): ν_{max} = 3436 (br), 3164 (br), 3044 (w), 2961 (w), 2654 (w), 2537 (w), 1683 (w), 1592 (s), 1557 (m), 1495 (w), 1413 (m), 1395 (s), 1313 (w), 1288 (m), 1261 (m), 1225 (s), 1179 (s), 1126 (w), 1109 (m), 1085 (m), 1016 (s), 912 (w), 850 (m), 793 (m), 759 (s), 731 (w), 694 (s), 677 (s), 632 (w), 514 (s).

Procedure for trans-di(bis(4,4',4",4"'-(1,2-phenylenedi(phosphinotriyl)tetrabenzoic acid)) ruthenium dichloride ($PdCl_2(bbcb)_2$) (6)

To a 200 mL round-bottomed flask, (**5**) (1.30 g, 2.09 mmol) and $RuCl_2(PPh_3)_3$ (0.95 g, 0.99 mmol) was added, and dissolved with acetone (125 mL). The suspension was stirred for 1 hr, resulting in a deep red solution. The reaction was heated to reflux with a condenser for 16 hrs. Upon cooling, the slightly lighter solution was concentrated down (*ca*. 20 mL) before diethyl ether (150 mL) was added and stirred vigorously. The product was isolated by centrifugation to yield a bright yellow solid (1.06 g, 0.75 mmol). Yield: 75.3 %. ^{31}P-NMR (DMSO-d6, 161.8 MHz) δ = 50.261 ppm; ^{1}H-NMR (DMSO-d6, 400.1 MHz): δ = 13.101 (4H, CO_2H), 7.416 (d, 16H, 7.381 (s, 4H), 7.231 (m, 4H), 7.048 (m, 16H). ppm; ^{13}C-NMR (DMSO-d6 150.9 MHz): δ = 167.105 (s, CO_2H), 136.535 (s, Ar), 136.084 (s, Ar), 135.337 (s, Ar), 133.780 (s, Ar), 129.401 (s, Ar) ppm; FT-IR (solid/cm^{-1}): ν_{max} = 3042 (b), 2658 (w), 2532 (w), 2119 (bw), 1938 (w), 1685 (s), 1593 (s), 1557 (m), 1493 (m), 1394 (s), 1312 (w), 1220 (s), 1178 (s), 1106 (s), 1081 (s), 1016 (s), 962 (m), 917 (bw), 849 (m), 789 (w), 758 (s), 732 (w), 693 (sh), 676 (s), 632 (sh), 514 (s).

A FERROCENE-BACKBONE LINKER WITH GROUP (X) METALATION

The catalytic utility of *bis*(phosphine) complexes extends back to as early as the 1950's, with interest in complexes such as 1,1'-*bis*(diphenylphosphino) ferrocene (dppf), 1,2-*bis*(diphenylphosphino)ethane (dppe), 2,3-O-isopropylidene-2,3-dihydroxy-1,4-*bis*(diphenylphosphino)butane (DIOP), and Ethane-1,2-diylbis[(2-methoxyphenyl) phenylphosphane (DIPAMP) (Figure 2.6).[61-63] The backbone-structures seen above have been studied for several applications in catalysis, with the focus geared towards understanding the relationship between the bite angle of the *bis*(phosphine) and catalytic properties. The natural bite angle, defined as the ideal chelation angle that is governed by the ligand backbone, can dramatically influence the *bis*(phosphine) steric and electronic attributes.[64]

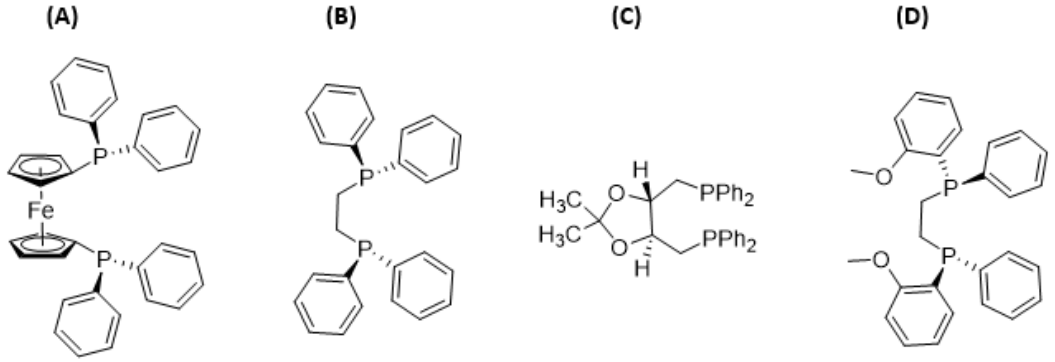

Figure 2.6. Visual representation of the ligands dppf (A), dppe (B), DIOP (C), and DIPAMP (D).

A certain level of instability is needed for catalyst maximum performance, in order to avoid a getting stuck at an irreversibly stable intermediate in a catalytic cycle. Unmetallated dppf has been found in the literature to have a natural bite angle of 99 °, allowing for an active

catalytic complex to be formed with the strained coordination of palladium(II) dichloride. For divalent group (X) metals in chelated phosphine complexes such as those described, a 90 ° bite angle typically allows for increased stability within square planar geometries; smaller and larger bite angles will destabilize a square planar complex with favor being directed towards tetrahedral or trigonal geometries and zerovalent metal species.[65]

The monomeric complex 1,1'-*bis*(diphenylphosphino) ferrocene (dppf) with palladium(II) metalation has shown great promise in the area of catalysis dating back to the early 1980's, with specific interest in coupling reactions.[66-69] In earlier work, Suzuki and coworkers published a study in 1989 that compared the catalytic coupling output of $PdCl_2$(dppf) at different conditions and environments in comparison to another phosphine catalyst.[70] The study focused on the functionalizing alkenes, arenes, and cycloalkenes through hydrocarbon-coupling in classic Suzuki fashion; it demonstrated PdC_2(dppf) was able to perform better than the catalyst system $Pd(PPh_3)_4$ at an operating temperature 15 ° cooler than the latter. In a more recent study, T. Ishiyama *et al*. discussed the use of a dppf-based catalyst for the cross-coupling of an alkoxydiboron coupound with haloarenes.[71] This 1995 publication allowed for a direct route to arylboronic esters without the need for Grignard or lithium-based reagents. The two examples described are a small demonstration of the powerful catalytic attributes dppf-complexes have demonstrated over the last several decades.

Results and discussion

In this study, *bis*(*p*-carboxylate-biphenylphosphino)ferrocene palladium dichloride ($PdCl_2$(dppf-CO_2H)) (**9**) was the target linker, with platinum metalation (**10**) being of interest as well (Figure 2.7, left). With carboxylate groups extending from the phenyl arms,

the MCl_2(dppf-CO_2H) complex can allow for polymerization of the $PdCl_2$(dppf) functionality into a PCP. The palladium and platinum complexes were successfully synthesized and characterized *via* FT-IR spectroscopy (Figures A1.6−A1.7) and ^{31}P, ^{1}H, and ^{13}C-NMR (Figures A2.30−A2.35). The X-ray crystal structure of $PdCl_2$(dppf-CO_2H) (**9**) was collected as well (Tables 3.5−3.8) (Figure 2.7, right).

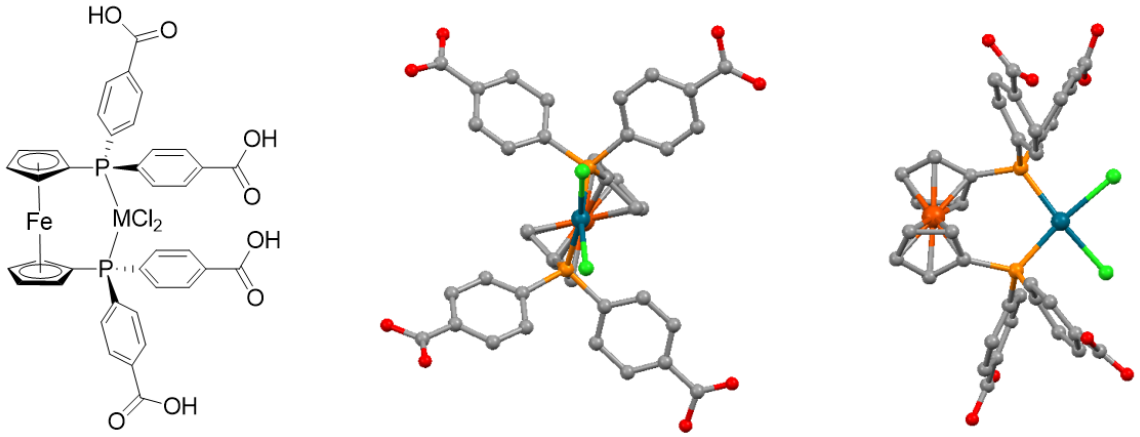

Figure 2.7. Visual representation of MCl_2(dppf-CO_2H) (**9**) (Left), and X-ray crystal structure of the complex (**9**) down the M−Fe bond (Middle), and perpendicular (Right).

The X-ray crystal structure of $PdCl_2$(dppf-CO_2H) demonstrated a bite angle of 101.6 °. This greater degree of strain on the ferrocene backbone was likely due to the carboxylate groups pulling benzene ring electron density away from the phosphine sites. This degree of strain away from 90 ° could allow for access to catalytic properties not seen to date with $PdCl_2$(dppf) systems. Furthermore, the four carboxylate groups naturally sit in a uniform distribution around the complex, which can help to promote 3-dimensional growth.

Framework development attempts were undertaken for both palladium (II) and platinum (II) complexes over the past two years, with amorphous growth overtaking

crystalline material development. This fast formation of non-crystalline solid pointed towards strong interactions between the linker and metal salts. Crystallizing agents such as triethyl amine and other bases were employed without much success. However, the development of PCMs based on dppf-CO_2H linkers is in its adolescence and has a bright future within the Humphrey research group. With information gained through trials, successful synthesis of a PCM will likely require less than or equal to room temperature conditions in tandem with some sort of base to slow crystallization.

Experimental data

General

All ligand syntheses were performed under a nitrogen atmosphere using standard schlenk techniques. *N*-butyllithium (^{n}BuLi) (1.6 M in hexanes, Sigma Aldrich) and N,N,N',N'-tetramethylethylenediamine (TMEDA) (Sigma Aldrich, ~99 %) were used as received. Ferrocene (Acros, ≥98 %) was purified via sublimation. The precursor *bis*(4-bromophenyl)chlorophosphine was prepared as per the literature.[72] Ammonium chloride (NH_4Cl) (Fisher Chemical, ACS grade), hydrochloric acid (Fisher Chemical, ACS grade), magnesium sulfate anhydrous ($MgSO_4$) (Fisher Chemical, ≥98 %), and solid carbon dioxide (Praxair) were used as received. Both $Pd(COD)Cl_2$ and $Pt(COD)Cl_2$ were synthesized *via* literature procedures.[73,74] Tetrahydrofuran (THF) (Fisher Chemical, HPLC grade), diethyl ether (BDH, ACS grade), and hexanes (Fisher Chemical, ACS grade) were obtained from Fisher Scientific and dried/degassed using a Solvent Purification System (Innovative Technologies). N, N'-dimethylformamide (DMF) (Fisher Chemical, ACS grade), ethanol (EtOH) (Pharmco-Aaper, ACS grade), and all aqueous solutions were sparged with N_2 for no less than 30 minutes prior to use. Solution ^{13}C-NMR and

gHSQCAD 2D-NMR were collected in-house using a Varian DirectDrive 600 MHz spectrometer; solution ^{31}P NMR and ^{1}H-NMR were collected in-house as well on an Agilent MR 400 MHz spectrometer; FT-IR spectra were obtained directly from solid samples using a Nicolet IS*50 spectrophotometer fitted with an attenuated total reflectance apparatus; thermogravimetric analysis (TGA) data was collected with a TA Instruments Q50 system for the temperature range of 25 °C to 800 °C. Elemental microanalyses were performed by QTI Intertek (New Jersey) or Midwest Microlab LLC (Indianapolis).

X-ray crystallography

A suitable crystal was mounted on a nylon thread loop in perfluoropolyether oil and attached to the diffractometer. The data was collected at 100 K. Data collection, unit cell refinement, and data reduction were performed using direct methods, with full-matrix least squares refinement, and data reduction were performed using Apex II (Bruker AXS, Inc. 2010). All data was collected using Mo Kα radiation (0.7093 Å) on a Nonius Kappa CCD diffractometer with a Bruker Apex II CCD, and a 600 low-temperature attachment. The structural analysis was performed using Mercury 3.1 (Build RC5).

Procedure for 1,1'-bis(di(4-bromodiphenyl)phosphino)ferrocene (dppf-Br) (7)

In a 100 mL round bottomed flask, ferrocene (1.03 g, 5.53 mmol) was dissolved in hexanes (28.0 mL). Once dissolved, nBuLi (1.60 M in hexanes, 12.00 mmol) was added drop-wise followed by TMEDA (1.72 mL, 11.5 mmol) and the cloudy orange/red mixture was heated to 60 °C for 1 hr with a reflux condenser attached. The reaction was then cooled to room temperature before the addition of THF (11.3 mL), which formed a suspension. The mixture was cooled to −50 °C *via* a controlled dry ice/acetone bath before the drop-

wise addition of *bis*(4-bromophenyl)chlorophosphine (4.61 g, 12.2 mmol) dissolved in THF (6 mL). The heterogeneous mixture was allowed to stir and warm to room temperature overnight. The red suspension was washed with aqueous NH_4Cl (10 %, 50 mL; HCl, 6 drps), then dried over $MgSO_4$ (*ca*. 50 g). The filtrate was dried *in vacuo* to yield a golden red solid. Yield: 71.5 %. ^{31}P-NMR ($CDCl_3$, 161.8 MHz) δ = −19.371 ppm; ^{1}H-NMR ($CDCl_3$, 400.1 MHz): δ = 7.40 (dd, 8H), 7.09 (dd, 8H), 4.29 (t, 4H), 3.89 (q, 4H); 137.41 ppm; ^{13}C-NMR ($CDCl_3$, 150.9 MHz): δ = 137.41 (d, Ar), 134.80 (d, Ar), 131.42 (d, Ar), 123.44 (s, Ar), 75.63 (d, Cp), 73.67 (d, Cp), 72.65 (d, Cp); FT-IR (solid/cm^{-1}): ν_{max} = 3069 (w), 2927 (w), 1902 (w), 1637 (w), 1604 (w), 1568 (m), 1474 (s), 1434 (sh), 1413 (w), 1379 (s), 1296 (w), 1260 (w), 1193 (w), 1180 (w), 1160 (m), 1107 (m), 1093 (m), 1066 (s), 1028 (m), 1007 (s), 887 (w), 808 (s), 743 (m), 719 (s), 698 (sh), 887 (w), 573 (sh), 543 (sh), 515 (sh), 491 (s), 432 (sh).

Procedure for 4,4',4",4"'-(1,1'-ferrocenebis(phosphinotriyl)tetrabenzoic acid (dppf-CO_2H) (8)

In a 500 mL round bottomed flask, **7** (2.5 g, 2.9 mmol) was dissolved in THF (300 mL), then cooled to −78 °C *via* a dry ice/acetone bath. A solution of nBuLi (1.60 M in hexanes, 13.1 mmol) was added dropwise to the mixture. The resulting brown slurry was allowed to stir at −78 °C for 4 hrs, after which an excess of crushed dry ice (*ca*. 200 g) was added followed by diethyl ether (100 mL). The mixture was allowed to stir and slowly acclimate to room temperature overnight. The resulting yellow slurry was then filtered under nitrogen to yield the deprotonated carboxylate salt. The dried solid was dissolved in H_2O (100 mL) and HCl (12.1 M, 1 pipette) was added. The product was then filtered under nitrogen and dried *in vacuo* to afford a deep orange powder (1.7 g, 2.4 mmol). Yield: 81.5 %. ^{31}P-NMR (DMSO-d6, 161.8 MHz) δ = −17.444 ppm; ^{1}H-NMR (DMSO-d6, 400.1

MHz): δ = 12.998 (s, 4H), 7.874 (m, 8H), 7.336 (m, 8H), 4.257 (m, 4H), 4.022 (m, 4H); ^{13}C-NMR (DMSO-d6, 100.6 MHz): δ = 143.644 (d, Ar), 133.050 (d, Ar), 130.994 (s, CO_2H), 129.046 (d, Ar), 74.648 (d, Cp), 73.738 (d, Cp), 72.457 (d, Cp); FT-IR (solid/cm^{-1}): ν_{max} = 2927 (br), 2512 (b), 1926 (br), 1686 (s), 1594 (s), 1541 (m), 1492 (w), 1393 (s), 1312 (sh), 1262 (br, s), 1179 (m), 1162 (m), 1128 (sh), 1107 (m), 1087 (m), 1028 (w), 1016 (m), 851 (sh), 813 (m), 763 (s), 744 (m), 719 (w), 695 (s), 633 (m), 523 (sh), 483 (s).

Procedure for bis(p-carboxylate-biphenylphosphino)ferrocene palladium dichloride ($PdCl_2$(dppf-CO_2H)) (9)

In a 100 mL schlenk flask, (**8**) (0.300 g, 0.411 mmol) and Pd(COD)Cl_2 (0.130 g, 0.451 mmol) were dissolved in THF (25 mL). The reaction was refluxed at 66 °C overnight with a condenser attached. Upon cooling, the solution was concentrated *via* schlenk vacuum and the solid was dissolved in ethanol (30 mL). The yellow slurry was then filtered through celite and concentrated by rotary evaporation to afford a deep red solid (0.348 g, 0.350 mmol). Yield, 85.0 %. ^{31}P-NMR (DMSO-d6, 161.8 MHz) δ = 33.766 ppm; ^{1}H-NMR (DMSO-d6, 400.1 MHz): δ = 8.030 (m, 8H), 7.591 (m, 8H), 4.611 (m, 4H), 4.353 (m, 4H); ^{13}C-NMR (DMSO-d6, 100.6 MHz): δ = 136.519 (s, Ar), 135.321 (s, Ar), 133.729 (s, CO_2H), 129.385 (s, Ar), 76.619 (s, Cp), 75.175 (s, Cp), 73.074 (s, Cp); FT-IR (solid/cm^{-1}): ν_{max} = 3438 (b), 2964 (w), 2869 (w), 2612 (bw), 2498 (bw), 2111 (b), 1930 (bw), 1694 (s), 1634 (w), 1599 (m), 1562 (m), 1481 (w), 1436 (m), 1393 (s), 1259 (w), 1221 (m), 1166 (m), 1127 (m), 1086 (s), 1038 (m), 1015 (m), 877 (w), 859 (w), 802 (s), 761 (s), 687 (s), 634 (m), 554 (M), 487 (s).

Procedure for bis(p-carboxylate-biphenylphosphino)ferrocene platinum dichloride ($PtCl_2$(dppf-CO_2H)) (10)

In a 100 mL schlenk flask, (**8**) (0.250 g, 0.342 mmol) and $Pt(COD)Cl_2$ (0.141 g, 0.376 mmol) were dissolved in THF (50 mL). The reaction was refluxed at 66 °C with a reflux condenser attached overnight. Upon cooling, the solution was concentrated *via* schlenk vacuum and solid was dissolved in ethanol (30 mL). The slurry was then filtered through celite and concentrated by rotary evaporation to afford an orange solid (0.305 g, 0.280 mmol). Yield: 82.9 %. ^{31}P-NMR (DMSO-d6, 161.8 MHz) δ = 12.507 ppm; ^{1}H-NMR (DMSO-d6, 400.1 MHz): δ = 8.626 (m, 8H), 8.141 (m, 8H), 5,168 (m, 4H), 4,879 (m, 4H); ^{13}C-NMR (DMSO-d6, 100.6 MHz): δ = 136.519 (s, Ar), 135.321 (s, Ar), 133.729 (s, CO_2H), 129.385 (s, Ar), 76.619 (s, Cp), 75,175 (s, Cp), 73.074 (s, Cp); FT-IR (solid/cm^{-1}): ν_{max} = 3440 (b), 2964 (w), 2870 (w), 2613 (bw), 2499 (bw), 2113 (b), 1932 (bw), 1695 (s), 1634 (w), 1599 (m), 1562 (m), 1483 (w), 1438 (m), 1394 (s), 1259 (w), 1221 (m), 1166 (m), 1127 (m), 1089 (s), 1038 (m), 1015 (m), 877 (w), 859 (w), 802 (s), 763 (s), 687 (s), 634 (m), 554 (m), 536 (m), 426 (w).

A PHENYL-EXTENDED BENZENE-BACKBONE LIGAND WITH GROUP (X) METALATION

As described previously, *bis*(phosphine) complexes with group (X) metalation have been gaining momentum in cross-coupling catalysis, with small changes in the backbone structure dramatically influencing catalytic performance. Cross-coupling reactions have been studied with these complexes as catalysts, with special interest in complexes that can access acute or obtuse bite angles that flex away from the more stable 90 ° moieties. The natural bite angle of the ligand 1,2-*bis*(diphenylphosphino)benzene (dppb) was found to be 101 °; this large deviation from 90 ° adds instability to the complex while lowering the LUMO energy, making electronic transitions more readily accessible.[73] Despite the many

favorable attributes of metal complexes with dppb ligands, only a few examples in the literature were found where these were used for catalysis.[5,6] Investigation of group (X) *bis*(phosphine) catalysts in homogeneous applications has shed light on how these complexes can be manipulated to enhance catalytic performance. In an effort to drive these area of complexes towards heterogeneous applications, a linker comprised of a *bis*(phosphine) backbone with group X metalation was targeted for this study. More specifically, the study focused on the development of a 1,2-substituted benzene backbone linker that utilized extended carboxylate arms to help promote the possibility of larger pore windows within a framework.

Results and discussion

The linker 4',4''',4'''',4''''''-(1,2-phenylene*bis*(phosphino))tetrakis((1,1-biphenyl]-3-carboxylic acid)) palladium dichloride ($PdCl_2$(b-bbcb)) (**13**) was explored in this study (Figure 2.8). This complex was designed to incorporate the functionality found in bbcb as described in the first project of this chapter with group (X) metalation, along with the addition of a second benzene ring on each carboxylate arm to enlarge the possible pore size of a polymerized material.

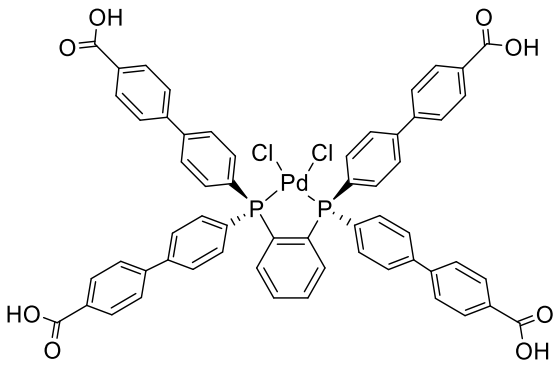

Figure 2.8. Visual representation of $PdCl_2$(b-bbcb) (**13**).

The complex (**13**) was successfully synthesized and characterized *via* FT-IR spectroscopy (Figure A.10), as well as ^{31}P, ^{1}H, and ^{13}C-NMR (Figure B.43−B.46). The key point of difficulty with this complex was solubility. Due to the extended nature of the organic portion and the four carboxylic acid groups, solubility became very low for the metalated complex. This resulted in difficulty with crystallization of the monomer as well as in PCM trials.

In the initial stages of PCM trials, luck was found with the reaction of $PdCl_2$(b-bbcb) with $Zn(NO_3)_2 \cdot 6H_2O$ in a 3:3:1 mixture of DMF, THF, and water to create square plate-like crystals referred to as PCM-41. Multiple attempts were made to obtain the structure of PCM-41 with both X-ray and synchrotron technology. Unfortunately, the structure has not been solved to date. However, the X-ray powder diffraction pattern of the bulk material was collected and peaks at low angles were found, suggesting that large openings were present within the material (Figure 2.9).

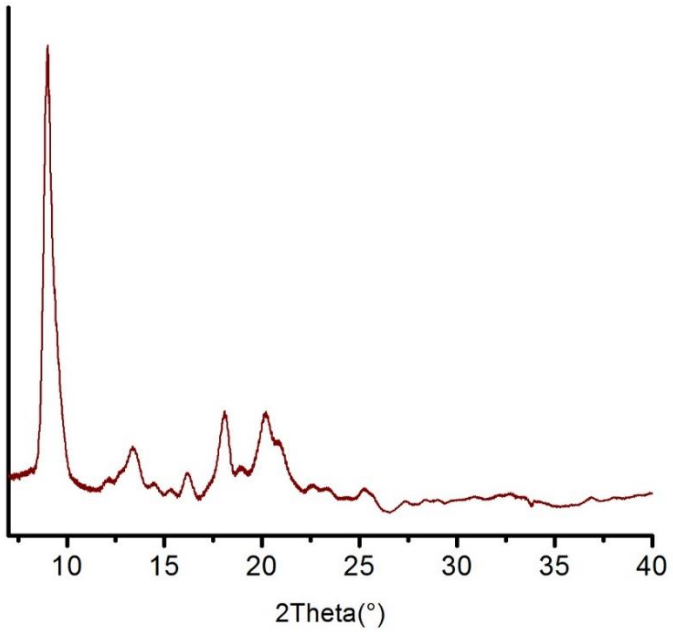

Figure 2.9. PXRD pattern of PCM-41 from 4−40 ° 2θ.

Afterwards, the thermogravimetric analysis (TGA) of PCM-41 was performed (Figure 2.10). This analysis demonstrated fast removal of non-coordinated solvent accounting for a 21.0 % mass loss, suggesting a moderately large void volume. A large plateau was observed after the initial solvent loss, with stability up to approximately 370 °C before net decomposition.

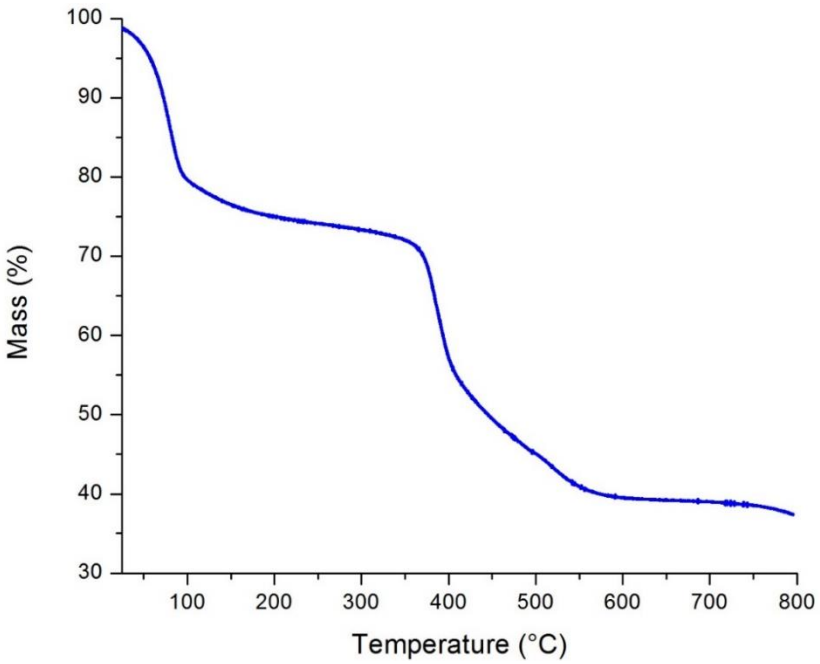

Figure 2.10. Thermogravimetric analysis of PCM-41 from 25−800 °C.

The synthesis of PCM-41 has proven difficult to reproduce, which has inhibited further characterization of the material. PCM trials have continued in an attempt to produce PCM-41 more reliably as well as explore the possibility of other PCPs. The b-bbcb backbone has great promise for PCP growth with the incorporation of catalytically active metals.

Experimental data

General

All synthetic methods for linker development were performed under a nitrogen atmosphere through the use of standard schlenk techniques. The reagents 4,4' dibromobiphenyl (EMD Millipore, 98 %), *n*-butyllithium (nBuLi) (2.5 M in hexanes, Sigma Aldrich), 1,2-*bis*(dichlorophosphino)benzene (1,2 DCPB) (Sigma Aldrich, ≥96 %), hydrochloric acid (Fisher chemical, ACS grade), solid carbon dioxide (Praxair), and zinc(II) nitrate hexahydrate (Sigma Aldrich, ≥98 %) were used as received. The metalation precursor $Pd(COD)Cl_2$ was synthesized as per the literature.[59] Tetrahydrofuran (THF) (Fisher Chemical, HPLC grade) was distilled (dried over sodium in a still) and collected over sieves (4A) for use. Diethyl ether (BDH, ACS grade) was dried over sieves (4A). Hexanes (Fisher chemical, ACS grade), dichloromethane (DCM) (Fisher chemical, ACS grade), N,N'-dimethylformamide (DMF) (Fisher chemical, ACS grade), and THF for solvothermal growth were used as received. Solution ^{31}P-NMR was collected in-house using an Agilent MR 400MHz spectrometer; Solution ^{1}H-NMR, ^{13}C-NMR, and gHSQCAD 2D-NMR were collected in-house using a Varian DirectDrive 600 MHz spectrometer; FT-IR spectra were obtained directly from solid samples using a Nicolet iS*50 spectrophotometer with an attenuated total reflectance apparatus; thermogravimetric analysis (TGA) data was collected with a TA Instruments Q50 system for the temperature range of 25 °C to 800 °C.

Powder X-ray diffraction (PXRD)

Phase purity of the as synthesized material PCM-41 was confirmed through the analysis of the bulk crystalline solid, which was placed in a borosilicate tube and spun in

situ to prevent preferential orientation of the crystallites. The spectrum was collected on a Rigaku R-Axis Spider diffractometer with an image plate detector. Rigaku RINT data collection and 2DP software was used to convert 2 dimensional powder diffraction patterns. This system used Cu Kα (radiation (1.5406 Å). Reflection data was collected in the range of 5.0−40.0° 2θ.

Procedure for 1,2-bis(di(4'-bromo-[1,1'biphenyl]-4-yl)phosphino)benzene (b-bbcb-Br) (11)

The reagent 4,4' dibromobiphenyl (9.142 g; 29.300 mmol) was dissolved in THF (250 mL) in a 500 mL round bottomed flask, then cooled to −78 °C *via* a dry ice/acetone bath. A solution of nBuLi (2.50 M in hexanes, 29.3 mmol) was added dropwise over 15 min. The resulting green, heterogeneous mixture was allowed to stir at −78 °C for 1 hr. A solution of 1,2 DCPB (2.0g, 7.146 mmol) in THF (*ca*. 5 mL) was added dropwise to the reaction over 15 min. The resulting pink, slightly heterogeneous reaction was pulled down to an oil, and diethyl ether (*ca*. 200 mL) was added to precipitate salt impurities. This suspension was allowed to stir for 1−2 hrs, air-free filtered, then concentrated *in vacuo* to afford a pink/off-white solid. The product was isolated *via* column chromatography (6:1 Hexanes:DCM) on silica to afford a white crystalline solid (2.436 g, 2.284 mmol). Yield: 32.9 %. ^{31}P-NMR ($CDCl_3$, 161.9): δ = −14.145 ppm; ^{1}H-NMR ($CDCl_3$, 400.1 MHz): δ = 7.523 (dt, 8H), 7.415 (d, 8H), 7.384 (m, 2H), 7.358 (dt, 8H), 7.313 (m, 8H), 7.262 (m, 2H) ppm; ^{13}C-NMR ($CDCl_3$, 100.6 MHz): δ = 143.508 (t, Ar), 139.934 (s, Ar), 139.254 (s, Ar), 136.026 (t, Ar), 134.639 (t, Ar), 134.242 (t, Ar), 131.939 (s, Ar), 129.289 (s, Ar), 128.531 (s, Ar), 126.771 (t, Ar) ppm; FT-IR (solid/cm^{-1}): ν_{max} = 3020 (bw), 2935 (bw), 1897 (w), 1593 (w), 1569 (w), 1543 (w), 1498 (w), 1475 (s), 1339 (sh), 1379 (m), 1307 (w), 1258

(w), 1194 (w), 1179 (w), 1096 (m), 1074 (s), 1011 (sh), 1000 (s), 845 (s), 804 (s), 765 (sh), 754 (s), 733 (m), 685 (sh), 660 (w), 639 (w), 626 (w), 510 (s).

Procedure for 4',4'",4"",4""",4"""'-(1,2-phenylenebis(phosphino))tetrakis((1,1-biphenyl]-3-carboxylic acid)) (b-bbcb) (12)

The synthesized reagent **11** (2.436 g, 2.284 mmol) was placed into a 500 mL round bottomed flask and dissolved in THF (300 mL). This solution was cooled to −78 °C *via* a dry ice/acetone bath, and nBuLi (2.5 M in hexanes, 11.421 mmol) was added dropwise over 15 min. The resulting brown, heterogeneous mixture was allowed to stir at −78 °C for 2 hrs. Diethyl ether (100 mL) and an excess of crushed dry ice (*ca*. 150 g) were added to the suspension, which caused the reaction to lighten in color quickly. The reaction was allowed to stir and warm to room temperature under nitrogen, with the dry ice/acetone bath evaporating overnight. The product was isolated *via* air-free filtration and dried under a stream of nitrogen. The off-white solid was dissolved in degassed H_2O (*ca*. 150 mL). The solution was cooled to 0 °C, and HCl (12.1 N, 1 pipette) was added in a nitrogen environment. The precipitated product was collected *via* air-free filtration and was dried under a stream of nitrogen to afford a yellow powder (2.051 g, 2.213 mmol). Yield: 97.2 %. ^{31}P-NMR (DMSO-d6, 161.9): δ = −15.449 ppm; ^{1}H-NMR (DMSO-d6, 400.1 MHz): δ = 7.927 (d, 8H), 7.640 (d 8H), 7.573 (d, 8H), 7.361 (dd, 2H), 7.192 (t, 8H), 7.095 (t, 2H) ; ^{13}C-NMR (DMSO-d6, 100.6 MHz): δ = 167.451 (s, CO_2H), 143.847 (s, Ar), 143.437 (t, Ar), 139.652 (s, Ar), 139.449 (s, Ar), 136.691 (s, Ar), 134.542 (t, Ar), 132.781 (t, Ar), 130.779 (s, Ar), 130.338 (t, Ar), 127.584 (t, Ar), 127.160 (t, Ar) ppm; FT-IR (solid/cm^{-1}): ν_{max} = 3379 (br), 3018 (br), 2659 (w), 2533 (w), 1926 (w), 1684 (s), 1607 (s), 1572 (m), 1518 (sh), 1484 (m), 1416 (s), 1386 (s), 1312 (sh), 1230 (s), 1176 (s), 1098 (s), 1018 (w), 1003 (s), 864 (m), 821 (s), 770 (s), 741 (s), 699 (m), 657 (m), 628 (w), 576 (sh), 553 (s), 525 (s).

Procedure for 4',4'",4"",4""",4"""'-(1,2-phenylenebis(phosphino))tetrakis((1,1-biphenyl]-3-carboxylic acid)) palladium dichloride ($PdCl_2$(b-bbcb)) (13)

The synthesized reagent **12** (500 mg, 0.539 mmol) and $Pd(COD)Cl_2$ (169 mg, 0.593 mmol) were dissolved in THF (150 mL) in a 200 mL schlenk flask. Once fitted with a reflux condenser, this yellow heterogeneous mixture was allowed to reflux at 66 °C overnight. The visibly unchanged reaction was allowed to cool, then filtered through celite. The yellow solution was concentrated *in vacuo* and washed with a copious amount of hexanes to yield the product as a yellow powder (602 mg, 0.524 mmol). Yield: 97.4%. ^{31}P-NMR (DMSO-d6, 161.9): δ = 64.093 ppm; ^{1}H-NMR (DMSO-d6, 400.1 MHz): δ = 8.440 (d, 8H), 8.362 (m, 16H), 8.271 (d, 8H), 8.131 (d, 2H), 7.892 (t, 2H) ppm; ^{13}C-NMR (DMSO-d6, 100.6 MHz): δ = 167.443 (s, CO_2H), 143.149 (s, Ar), 134.975 (t, Ar), 131.081 (s), 130.532 (s, Ar), 129.618 (s, Ar), 129.032 (t, Ar), 128.858 (s, Ar), 128.205 (m, Ar) 128.113 (m, Ar), 127.726 (s, Ar), 127.507 (t, Ar) ; FT-IR (solid/cm^{-1}): ν_{max} = 3052 (w), 2925 (bw), 8260 (w), 1652 (s), 1607 (s), 1562 (s), 1494 (sh), 1392 (s), 1287 (sh), 1252 (m), 1180 (m), 1101 (s), 1061 (m), 1003 (s), 831 (s), 783 (s), 764 (s), 728 (m), 707 (m), 7674 (m), 659 (m), 561 (s), 540 (sh), 426 (m).

Procedure for PCM-41 (14)

$PdCl_2$(b-bbcb) (**13**) (22 mg, 0.02 mmol) and $Zn(NO_3)_2{\cdot}H_2O$ (21 mg, 0.07 mmol) were placed in a 20mL scintillation vial, then dissolved in DMF:THF:water. (3:3:1, 7 mL). The yellow solution was sealed in the scintillation vial then heated to 45 °C with a graphite thermal bath for 3 days. The plate-like crystals were collected *via* filtration. Yield: 10 mg. FT-IR (solid/cm^{-1}): ν_{max} = 3379 (br), 3017 (br), 2659 (bw), 2533 (bw), 1926 (w), 1684 (s), 1601 (s), 1572 (m), 1545 (sh), 1518 (w), 1485 (m), 1416 (s), 1386 (s), 1312 (sh), 1230 (s),

1176 (s), 1098 (s), 1018 (w), 1003 (s), 864 (m), 821 (s), 770 (s), 741 (s), 699 (m), 657 (w), 628 (w), 553 (sh), 525 (s), 491 (s).

CONCLUSIONS

In this study, three novel linker systems were designed and synthesized with the goal of incorporating catalytically active metal sites into porous coordination polymers. There have been very few examples in the literature of linkers with active metal sites present, which leaves a great deal of room for growth in the world of PCPs and heterogeneous catalysis. The first system that was explored in this study built upon the well-characterized reactivity of *trans*-di(*bis*(phosphine)) group (VIII) complexes.This functionality was incorporated into a polymerizable linker. The ligand precursor 1,2-dcpb and the desired complex $RuCl_2(bbcb)_2$ were successfully synthesized and fully characterized, and numerous attempts were made to synthesize PCMs using $RuCl_2(bbcb)_2$ as a linker. The asymmetric complex $RuCl_2(bbcb)(depe)$ was also examined with the intention of developing a second linker system. Although this complex was found to be thermodynamically unfavorable, an interesting analysis of the $RuCl_2(bbcb)(depe)$ complex was performed by variable temperature NMR, which gave insight into the kinetic versus thermodynamic favorability of products in this reaction. The second complex, $MCl_2(dppf\text{-}CO_2H)$ (M = Pd, Pt), was successfully synthesized and characterized as well. Efforts to incorporate this complex into PCMs will continue in an effort to draw comparisons to its monomeric counterpart. The final system built upon previous work in the group in an attempt to extend the arms of the linker system to allow for larger possible pore sizes. The novel linker, referred to $PdCl_2$(b-bbcb), was successfully synthesized, characterized, and

incorporated into the framework PCM-41. Although this project has been slow to develop, it will no doubt contribute to this new sub-family of catalytically active PCMs in the future.

REFERENCES

1. Takei, I.; Nishibayashi, Y.; Ishii, Y.; Mizobe, Y.; Uemura, S.; Hidai, M. *J. Organomet. Chem.* **2003**, *679* (1), 32–42.
2. Miyaura, N.; Ishiyama, T.; Sasaki, H.; Ishikawa, M.; Sato, M.; Suzuki, A. *J. Am. Chem. Soc.* **1989**, *111* (1), 314–321.
3. Jiang, N.; Ragauskas, A. J. *Tetrahedron Let.* **2006**, *47* (2), 197–200.
4. Bohnsack, A. M.; Ibarra, I. A.; Bakhmutov, V. I.; Lynch, V. M.; Humphrey, S. M. *J. Am. Chem. Soc.* **2013**, *135* (43), 16038–16041.
5. Pagot, M.; Toniolo, L.; Antonetti, C.; Forte, C.; Galletti, A. M. R. *J. Mol. Catal. A: Chem.* **2015**, *410*, 202–208.
6. Zhang, S.; Wang, L.; Feng, X.; Bao, M. *Org. Biomol. Chem.* **2014**, *12* (37), 7233–7237.
7. Xie, W.; Peng, H.; Chen, L. *Appl. Catal., A* **2006**, *300* (1), 67–74.
8. Kim, H.-J.; Kang, B.-S.; Kim, M.-J.; Park, Y. M.; Kim, D.-K.; Lee, J.-S.; Lee, K.-Y. *Catal. Today* **2004**, *93–95*, 315–320.
9. Lin, Y.-C.; Huber, G. W. *Energy Environ. Sci.* **2008**, *2* (1), 68–80.
10. Herrmann, J.-M. *Top. Catal.* **2005** *34* (1–4), 49–65.
11. Jiang, N.; Ragauskas, A. J. *Tetrahedron Let.* **2006**, *47* (2), 197–200.
12. Weitkamp, E. A.; Lambe, A. T.; Donahue, N. M.; Robinson, A. L. *Environ. Sci. Technol.* **2008**, *42* (21), 7950–7956.
13. Yu, Q. L.; Ballari, M. M.; Brouwers, H. J. H. *Appl. Catal., B* **2010**, *99* (1–2), 58–65.
14. Subramani, V.; Gangwal, S. K. *Energy Fuels* **2008**, *22* (2), 814–839.

15. Sheldon, R. A.; Downing, R. S. *Appl. Catal., A* **1999**, *189* (2), 163–183.

16. Claus, P. *Appl. Catal., A* **2005**, *291* (1–2), 222–229.

17. Lee, J.; Farha, O. K.; Roberts, J.; Scheidt, K. A.; Nguyen, S. T.; Hupp, J. T. *Chem. Soc. Rev.* **2009**, *38* (5), 1450–1459.

18. Ma, L.; Abney, C.; Lin, W. *Chem. Soc. Rev.* **2009**, *38* (5), 1248–1256.

19. Horike, S.; Dincă, M.; Tamaki, K.; Long, J. R. *J. Am. Chem. Soc.* **2008**, *130* (18), 5854–5855.

20. Wu, C.-D.; Hu, A.; Zhang, L.; Lin, W. *J. Am. Chem. Soc.* **2005**, *127* (25), 8940–8941.

21. Cormas, A.; García, H.; Llabrés i Xamena, F. X. *Chem. Rev.* **2010**, *110* (8), 4606–4655.

22. Huang, X.-C.; Lin, Y.-Y.; Zhang, J.-P.; Chen, X.-M. *Angew. Chem., Int. Ed.* **2006**, *45* (10), 1557–1559.

23. Comotti, A.; Bracco, S.; Sozzani, P.; Horike, S.; Matsuda, R.; Chen, J.; Takata, M.; Kubota, Y.; Kitagawa, S. *J. Am. Chem. Soc.* **2008**, *130* (41), 13664–13672.

24. He, Y.; Xiang, S.; Zhang, Z.; Xiong, S.; Fronczek, F. R.; Krishna, R.; O'Keeffe, M.; Chen, B. *Chem. Commun.* **2012**, *48* (88), 10856–10858.

25. Jiang, J.-J.; Pan, M.; Liu, J.-M.; Wang, W.; Su, C. *Inorg. Chem.* **2010**, *49* (21), 10166–10173.

26. Wang, C.; Xie, Z.; deKrafft, K. E.; Lin, W. *J. Am. Chem. Soc.* **2011**, *133* (34), 13445–13454.

27. Liu, J.; Chen, L.; Cui, H.; Zhang, J.; Zhang, L.; Su, C.-Y. *Chem. Soc. Rev.* **2014**, *43* (16), 6011–6061.

28. Lu, G.; Li, S.; Guo, Z.; Farha, O. K.; Hauser, B. G.; Qi, X.; Wang, Y.; Wang, X.; Han, S.; Liu, X.; DuChene, J. S.; Zhang, H.; Zhang, Q.; Chen, X.; Ma, J.; Loo, S. C. J.; Wei, W. D.; Yang, Y.; Hupp, J. T.; Huo, F. *Nat. Chem.* **2012**, *4* (4), 310–316.

29. Jiang, H.-L.; Akita, T.; Ishida, T.; Haruta, M.; Xu, Q. *J. Am. Chem. Soc.* **2011**, *133* (5), 1304–1306.

30. Dhakshinamoorthy, A.; Garcia, H. *Chem. Soc. Rev.* **2012**, *41* (15), 5262–5284.

31. Manna, K.; Zhang, T.; Greene, F. X.; Lin, W. *J. Am. Chem. Soc.* **2015**, *137* (7), 2665–2673.

32. Marx, S.; Kleist, W.; Baiker, A. *J. Catal.* **2011**, *281* (1), 76–87.

33. Siu, P. W.; Brown, Z. J.; Farha, O. K.; Hupp, J. T.; Scheidt, K. A. *Chem. Commun.* **2013**, *49* (93), 10920–10922.

34. Timofeeva, M. N.; Panchenko, V. N.; Jun, J. W.; Hasan, Z.; Matrosova, M. M.; Jhung, S. H. *Appl. Catal., A* **2014**, *471*, 91–97.

35. Falkowski, J. M.; Sawano, T.; Zhang, T.; Tsun, G.; Chen, Y.; Lockard, J. V.; Lin, W. *J. Am. Chem. Soc.* **2014**, *136* (14), 5213–5216.

36. Sawano, T.; Thacker, N. C.; Lin, Z.; McIsaac, A. R.; Lin, W. *J. Am. Chem. Soc.* **2015**, *137* (38), 12241–12248.

37. Xi, W.; Liu, Y.; Xia, Q.; Li, Z.; Cui, Y. *Chem. Eur. J.* **2015**, *21* (36), 12581–12585.

38. Douglas, P. G.; Feltham, R. D.; Metzger, H. G. *J. Chem. Soc. 1970*, *No. 14*, 889b–890.

39. Quinby, M. S.; Feltham, R. D. Inorg. Chem. 1972, 11 (10), 2468–2476.

40. Coe, B. J.; Chery, M.; Beddoes, R. L.; Hope, H.; White, P. S. *Dalton Trans.* **1996**, *No. 20*, 3917–3924.

41. Kubas, G. J.; Ryan, R. R.; Swanson, B. I.; Vergamini, P. J.; Wasserman, H. J. *J. Am. Chem. Soc.* **1984**, *106* (2), 451–452.

42. Lee, D.-H.; Patel, B. P.; Crabtree, R. H.; Clot, E.; Eisenstein, O. *Chem. Commun.* **1999**, *No. 3*, 297–298.

43. Landau, S. E.; Morris, R. H.; Lough, A. J. *Inorg. Chem.* **1999**, *38* (26), 6060–6068.

44. Abdur-Rashid, K.; Lough, A. J.; Morris, R. H. *Organometallics* **2000**, *19* (14), 2655–2657.

45. Kröcher, O.; Köppel, R. A.; Baiker, A. *Chem. Commun.* **1997**, *No. 5*, 453–454.

46. Jessop, P. G.; Ikariya, T.; Noyori, R. *Chem. Rev.* **1995**, *95* (2), 259–272.

47. Jessop, P. G.; Hsiao, Y.; Ikariya, T.; Noyori, R. *J. Am. Chem. Soc.* **1996**, *118* (2), 344–355.

48. Standfest-Hauser, C. M.; Mereiter, K.; Schmid, R.; Kirchner, K. *Organometallics* **2004**, *23* (9), 2194–2196.

49. Kahrovic, E.; Orioli, P.; Bruni, B.; Di Vaira, M.; Messori, L. *Inorg. Chim. Acta* **2003**, *355*, 420–423.

50. Zhao, B.; Peng, X.; Wang, Z.; Xia, C.; Ding, K. *Chem. Eur. J.* **2008**, *14* (26), 7847–7857.

51. Kandiah, M.; Nilsen, M. H.; Usseglio, S.; Jakobsen, S.; Olsbye, U.; Tilset, M.; Larabi, C.; Quadrelli, E. A.; Bonino, F.; Lillerud, K. P. *Chem. Mater.* **2010**, *22* (24), 6632–6640.

52. Valenzano, L.; Civalleri, B.; Chavan, S.; Bordiga, S.; Nilsen, M. H.; Jakobsen, S.; Lillerud, K. P.; Lamberti, C. *Chem. Mater.* **2011**, *23* (7), 1700–1718.

53. Wu, H.; Chua, Y. S.; Krungleviciute, V.; Tyagi, M.; Chen, P.; Yildirim, T.; Zhou, W. *J. Am. Chem. Soc.* **2013**, *135* (28), 10525–10532.

54. Vermoortele, F.; Bueken, B.; Le Bars, G.; Van de Voorde, B.; Vandichel, M.; Houthoofd, K.; Vimont, A.; Daturi, M.; Waroquier, M.; Van Speybroeck, V.; Kirschhock, C.; De Vos, D. E. *J. Am. Chem. Soc.* **2013**, *135* (31), 11465–11468.

55. Forman, G. S.; Ohkuma, T.; Hems, W. P.; Noyori, R. *Tetrahedron Lett.* **2000**, *41* (49), 9471–9475.

56. Hu, A.; Ngo, H. L.; Lin, W. *J. Am. Chem. Soc.* **2003**, *125* (38), 11490–11491.

57. Henschke, J. P.; Burk, M. J.; Malan, C. G.; Herzberg, D.; Peterson, J. A.; Wildsmith, A. J.; Cobley, C. J.; Casy, G. *Adv. Synth. Catal.* **2003**, *345* (1–2), 300–307.

58. Punji, B.; Mague, J. T.; Balakrishna, M. S. *Inorg. Chem.* **2007**, *46* (24), 10268–10275.

59. Hallman, P. S.; Stephenson, T. A.; Wilkinson, G. In *Inorganic Syntheses*; Parry, R. W., Ed.; John Wiley & Sons, Inc., **1970**; pp 237–240.

60. Samouei, H.; Miloserdov, F. M.; Escudero-Adán, E. C.; Grushin, V. V. *Organometallics* **2014**, *33* (24), 7279–7283.

61. Issleib, K; Müller D. W. *Chem. Ber.* **1959**, *92*, 3175-3182.

62. Kagan, H. B.; Dang-Tuan-Phat. *J. Am. Chem. Soc.* **1972**, *94* (18), 6429–6433.

63. Knowles, W. S. *Angew. Chem., Int. Ed.* **2002**, *41* (12), 1998–2007.

64. Casey, C. P.; Whiteker, G. T. *Isr. J. Chem.* **1990**, *30*, 299-304.

65. Gensow, M.-N. B.; Freixa, Z.; van Leeuwen, P. W. N. M. *Chem. Soc. Rev.* **2009**, *38* (4), 1099–1118.

66. Fuchikami, T.; Ohishi, K.; Ojima, I. *J. Org. Chem.* **1983**, *48* (21), 3803–3807.

67. Molander, G. A.; Biolatto, B. *J. Org. Chem.* **2003**, *68* (11), 4302–4314.

68. Hamann, B. C.; Hartwig, J. F. *J. Am. Chem. Soc.* **1997**, *119* (50), 12382–12383.

69. Driver, M. S.; Hartwig, J. F. *J. Am. Chem. Soc.* **1996**, *118* (30), 7217–7218.

70. Miyaura, N.; Ishiyama, T.; Sasaki, H.; Ishikawa, M.; Sato, M.; Suzuki, A. *J. Am. Chem. Soc.* **1989**, *111* (1), 314–321.

71. Ishiyama, T.; Murata, M.; Miyaura, N. *J. Org. Chem.* **1995**, *60* (23), 7508–7510.

72. de Pater, J. J. M.; Maljaars, C. E. P.; de Wolf, E.; Lutz, M.; Spek, A. L.; Deelman, B.-J.; Elsevier, C. J.; van Koten, G. *Organometallics* **2005**, *24* (22), 5299–5310.

73. Donahue, C. M.; McCollom, S. P.; Forrest, C. M.; Blake, A. V.; Bellott, B. J.; Keith, J. M.; Daly, S. R. *Inorg. Chem.* **2015**, *54* (12), 5646–5659.

74. Drew, D.; Doyle, J. R.; Shaver, A. G. In *Inorganic Syntheses*; Angelici, R. J., Ed.; John Wiley & Sons, Inc., **1990**; pp 346–349.

Chapter 3: PCP variability through the use of structure directing agents

An unusual series of PCPs have been developed through the variation of the alkali hydroxide added during synthesis. Four of the five novel materials were found to be non-isostructural, resulting in the frameworks designated PCM-6 to PCM-9. These PCPs were created through the addition of lithium hydroxide through cesium hydroxide, respectively, as structure directing agents to an otherwise unaltered set of reaction conditions. These materials were investigated with interest in crystallographic differences caused by the addition of the alkali hydroxide as well as how these changes would affect stability and gas adsorption capabilities. PCMs 6 to 9 were found to have impressive oxygen uptake, competing with the highest cryogenic uptake to date for a saturated metal PCP.

INTRODUCTION

In the field of PCPs, there have been many methods developed to promote porosity and material growth. Use of a templating agent is a common technique that has been applied to zeolites and PCPs alike.[1-3] Traditional templating occurs through the templating agent molding its shape or geometry on the host structure, and is relatively rare.[4,5] More broadly, certain solvents such as tetrahydrofuran and the more exotic morpholine have shown utility as templating agents as well.[6,7] Alternatively, structure directing agents (SDAs) are a less straightforward approach to influencing framework formation. SDAs are defined as organic or inorganic cationic species that are added during synthesis and prove crucial to the formation of the PCP. These agents do not show signs of templating, but they are required for framework formation to occur.[8-10] Since it is more difficult to predetermine the applicability of an SDA before PCP formation, the final product can prove much less predictable than common templating agents. In this study, we attempted to use lithium

through cesium cations to act as templating agents within the creation of PCMs 6 to 9. Surprisingly, these five materials demonstrated that the alkali hydroxides were in fact employed as SDAs and, in some cases, a reactant.

Worldwide, diatomic oxygen is used in a variety of highly demanding applications, with 100 million tons being produced each year. These applications include steel manufacturing and chemical production processes, which account for 80 % of annual usage.[11] Industrial processes for oxygen isolation from air have traditionally relied on energy-intensive cryogenic distillations.[12] The desire to overcome this inefficient process has led to growing interest over the last decade in the evolution of materials for diatomic oxygen physisorption and separation.[13,14] The key to unlocking PCPs utility in oxygen purification lies in understanding not only preferential interaction with O_2, but how to increase overall adsorption as well. There has been a recent push in research to understand the utility of open metal sites to overcome the battle of favored interaction of N_2 over O_2.[15-17] However, very little is understood about the effect of linkers on that oxygen uptake at this time.

The rational design of PCPs through network design has been thoroughly investigated. Despite their unpredictable nature, a great deal is now understood about achieving desired network topologies through the favorability of certain organic linkers interacting with a specific inorganic node.[18] The vast majority of published PCPs known to date are created through the use *poly*-carboxylated aromatic ligands. This type of linker is inherently planar and has a tendency to promote less desirable 2-D porous sheets. To overcome this behavior and achieve 3-D framework connectivity, two or more ligands are commonly used.[19,20] Other techniques that work to overcome this hurdle embrace the inclusion of a secondary pillaring ligand,[21,22] or trust in the metal nodes to facilitate growth past sheet formation.[23,24] Less commonly, carboxylate functional groups can be encouraged

to rotate out-of-plane in respect to its aromatic ring, to generate a linker that can in fact promote 3-dimensionality. This behavior can be encouraged with high steric bulk within the ligand in order to promote loss of π-conjugation. Linker systems commonly demonstrate a loss of planarity such as this when they contain two or more adjacent carboxylate groups, for example the ligand 1,2,3,4,5,6-benzenehexacarboxylate is used to form a variety of 3-D materials.[25,26]

In the literature, much less attention has been focused on the use of intrinsically 3-D linkers that can aid in the reduced formation of less desirable 2-D materials. There have been a handful of tetrahedral linkers utilized for PCP development found in the literature.[27-29] For example, Robson and co-workers in 1989 demonstrated the use of $C(C_6H_4\text{-}p\text{-}CN)_4$ to create a diamond-like polymer through coordination with Cu^+.[30] More recent examples of tetrahedral systems include incorporation of $Si(C_6H_4\text{-}p\text{-}CO_2H)_4$ by Qui and coworkers into a lanthanide based framework in 2013;[31] the similar carbon based linker $C(C_6H_4\text{-}p\text{-}C_1N_4)_4$ was coordinated with a Cu^+/Cu^{2+} mixed system by Long and coworkers in 2008.[32] The unusual $C(CH_2\text{-}O\text{-}C_6H_4\text{-}p\text{-}CO_2H)_4$ ligand was reacted with various proportions of Cd^{2+} by Tian *et al*. in 2010 to create a series of materials as well.[33]

In this work, the methyl phosphonium derivative $[Me\text{-}P(\text{-}C_6H_4\text{-}p\text{-}CO_2H)_3]^+Cl^-$ ($[mptbcH_3]Cl$) was employed as the linker. This structure was achieved through monomeric conversion of the trilithium salt phosphanotriylbenzenecarboxylate with iodomethane followed by aqueous HCl work up ($ptbLi_3$; $P(C_6H_4\text{-}p\text{-}CO_2Li)_3$). The fully deprotonated tricarboxylate, $mptbc^{2-}$, is a 3-connected trigonal PCM building block that allows for the designed synthesis of open 3-D polymers based on fused networks of M_2L_2 molecular squares (Figure 3.1). This type of crystallographic stoichiometry is achievable due to the $mptbc^{2-}$ ligand acting as a dianion, owing to a single -1 charge being offset by a formal +1 charge on the central P(V) atom.

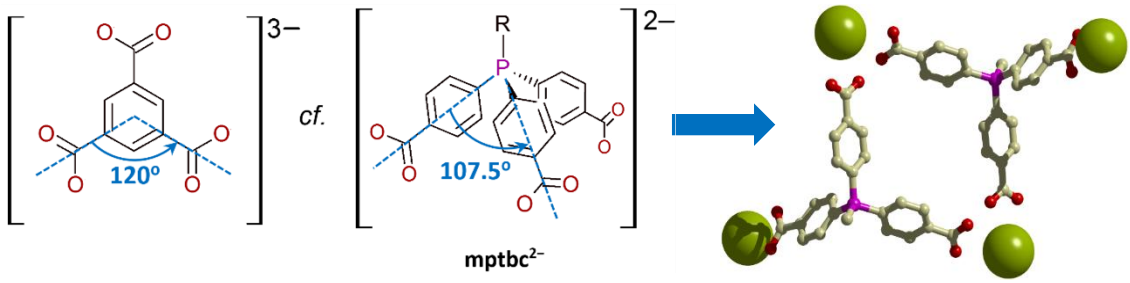

Figure 3.1: The important geometric differences between routine planar tricarboxylate ligands (Left) and (*tris-p*-carboxylated)phosphine derivatives such as the phosphonium dianion $mptbc^{2-}$ (Middle); the latter favor the generation of a 3-D array of fused M_2L_2 molecular squares due to the generation of a dianion (Right).

The dianionic nature of the ligand allows for an overall reduction in the resulting PCM density simply due to the fact that fewer metal ions are needed to achieve charge balance. Of even more interest, we found that the use of different alkali hydroxide solutions added during synthesis resulted in the formation of four distinct and infinitely porous 3-D network types that demonstrated these M_2L_2 squares and were obtained under otherwise identical reaction conditions (Scheme 3.1).

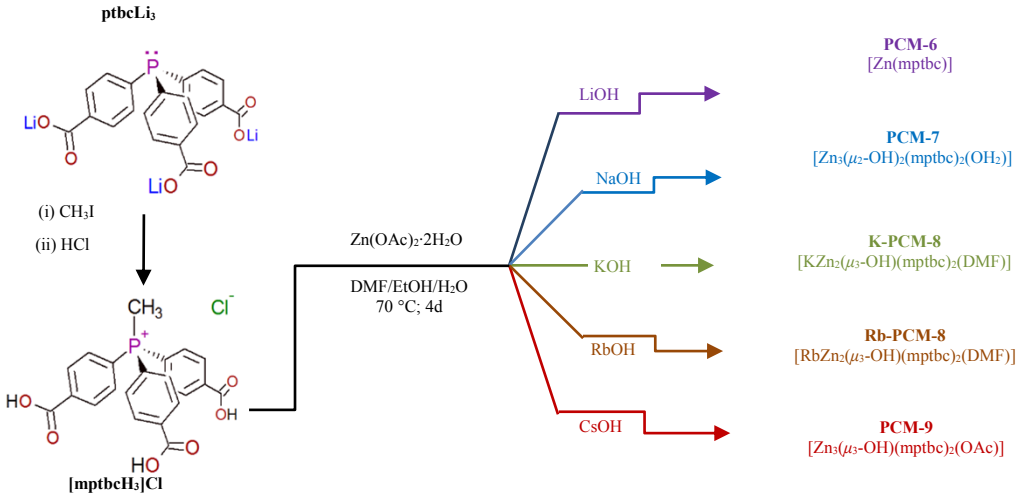

Scheme 3.1. Synthetic method used to prepare five Zn(II)-phosphonium PCMs, based on four unique network types. Method for the conversion of the free phosphine ligand $ptbcLi_3$ into the phosphonium chloride derivative $[mptbcH_3]Cl$ (Left). The five possible structural outcomes based solely on the identity of the alkali hydroxide employed (Right).

RESULTS AND DISCUSSION

Synthesis and structures of the Zn^{II}-phosphonium PCMs

The $[mptbcH_3]Cl$ building block described above is readily soluble in both aqueous and polar organic solvents. In this work, the linker was deprotonated with a mixed solvent system consisting of *N*,*N*-dimethylformamide (DMF), ethanol, and deionized water (4:1:1) using a less than stoichiometric amount of alkali-metal hydroxide (MOH; M = Li, Na, K, Rb, Cs) to obtain the dianionic species $mptbc^{2-}$, followed by addition of 1.0 molar equivalents of Zn(II) acetate. Heating of the resulting solutions to 70 °C for 4 days gave substantial yields of colorless crystalline materials. Interestingly, X-ray structural analysis of the products revealed that the variation of the MOH employed had a profound effect on

the reaction outcome, as summarized in Scheme 3.1. The alkali hydroxide variation resulted in the formation of four related but distinct materials, with only KOH and RbOH producing isostuctural versions of the same material, designated PCM-8. These materials were the only new PCMs identified in this study in which the alkali metal ion actually incorporated itself into the PCM; the ionic radii of K^+ and Rb^+ are similar and therefore commonly exhibit similar chemical behavior.[34] In all other instances, the MOH precursors seem to act as SDAs,[10] perhaps *via* thermodynamic effects related to the formation of byproducts (*e.g.*, MCl species that are generated from initial reaction with [mptbcH_3]Cl).

Working in descending order, the use of LiOH afforded PCM-6, which demonstrated the simplest connectivity that might be predicted using the trigonal pyramidal mptbc^{2-} ligand along with isolated Zn(II) ions. PCM-6 crystallizes into the orthorhombic space group *Pnna* and the asymmetric unit contains one ligand associated to a single tetrahedrally coordinated zinc(II) center, which also connects to three adjacent mpbc^{2-} groups as seen in Figure 3.2a. The comprehensive structure is shown to be quadruply interpenetrated, in which two sets of pairs of eclipsed nets imitate the zeolite type ABW. Zeolite frameworks of the type ABW are traditionally based on 4 and 8 membered rings.[35] Because PCM-6 has the crystallographic stoichiometry M_2P_2, its structure is based on 4-membered ring much like those of ABW materials. PCM-6 demonstrates guest-accessible square pores along the crystallographic *b*- and *c*- axes, with diagonal van der Waals openings of 8.8 and 9.4 Å, respectively (P· · ·P; Figure 3.2b−d).

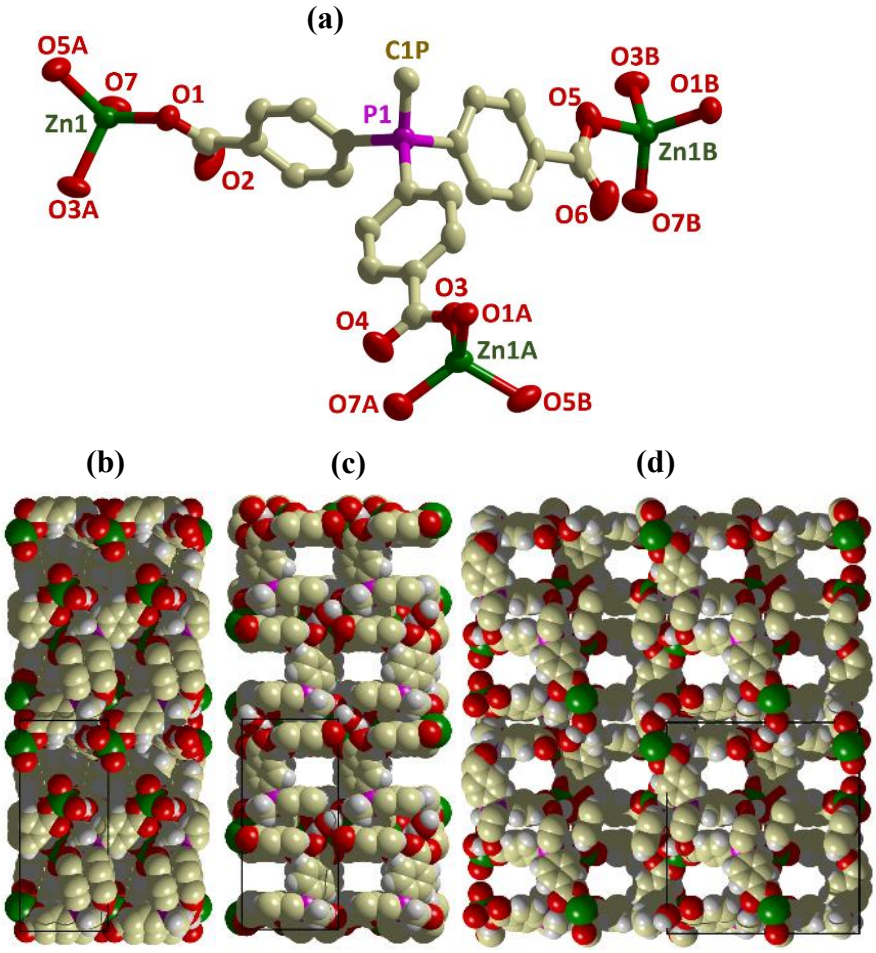

Figure 3.2. Asymmetric unit of the material PCM-6 (a); View of the PCM-6 extended network on the crystallographic *a*-axis (b), *b*-axis (c), and *c*-axis (d).

Reactions that were performed using the assumed *in-situ* precursor Na_2[mptbc], which was obtained via deprotonation of [mptbcH_3]Cl with NaOH, gave rise to the material PCM-7. This material had the formula unit [$Zn_3(\mu_2\text{-}OH)_2$(mptbc)$_2$], and crystallized in the monoclinic space group $P2_1/c$. PCM-7 was found to incorporate both tetrahedral and 5-coordinate zinc(II) sites, with the M_2P_2 squares being formed by linear $[Zn_3(\mu_2\text{-}OH)_2]^{4+}$ nodes at alternating corners, where the central Zinc (II) atom (Zn1) is monohydrated (Figure 3.3a).

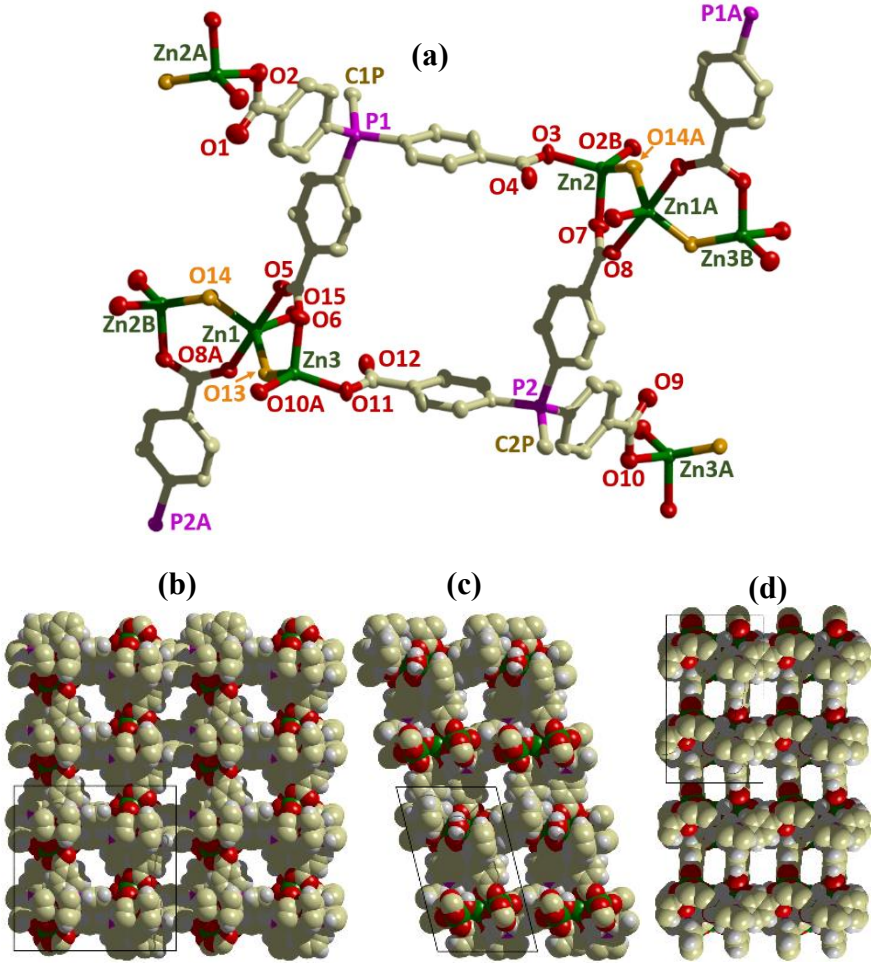

Figure 3.3. Crystallographic representation of the asymmetric unit for PCM-7 (a). View of PCM-7 extended network on the *a*-axis (b), *b*-axis (c), and *c*-axis (d).

For this material, each Zn_3 cluster bridges to six P-nodes, providing a distorted octahedral node (Figure 3.4a), which then links to two further adjacent M_2P_2 squares. When compared to PCM-6, the higher degree of connectivity in PCM-7 results in a non-interpenetrated polymer that allows for M_2P_2 windows in all three crystallographic axes with van der Waals diagonal openings between 9.1 and 13.2 Å (Figure 3.4b−d).

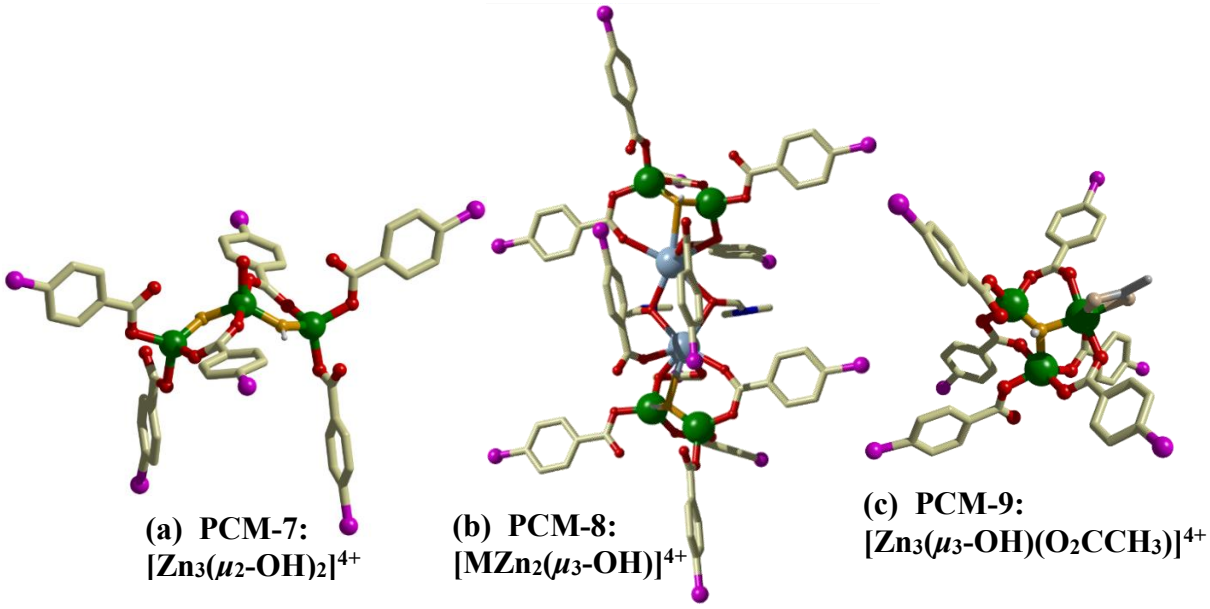

Figure 3.4. Crystallographic representation of the nodal system $[Zn_3(\mu_2\text{-}OH)_2]^{4+}$ for PCM-7 (a), $[MZn_2(\mu_3\text{-}OH)]^{4+}$ seen in the isostructural PCM-8 (M = K, Rb) (b), and $Zn(\mu_3\text{-}OH)(O_2CCH_3)]^{4+}$ seen in PCM-9 (c).

Deprotonation of the methyl phosphonium linker using either KOH or RbOH, followed by the reaction with $Zn(OAc)_2$ gave a single product with the formula unit $[MZn_2(\mu_3\text{-}OH)(mptbc)_2(DMF)]$ (PCM-8(M); M = K, Rb). The isostructural materials PCM-8(K) and PCM-8(Rb) crystallize into the orthorhombic space group *Pbcn* (Z = 8). The network topology of PCM-8 is similar to that of PCM-7, having 6,3-connectivity resulting in square pores in all three directions (Figure 3.5).

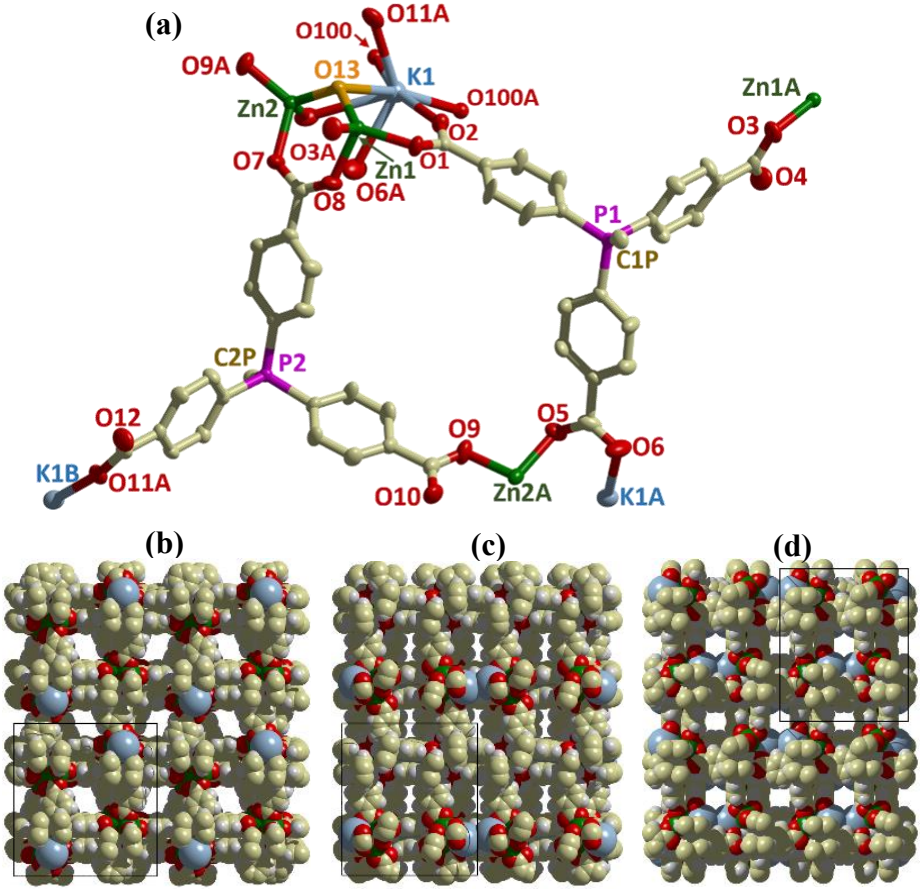

Figure 3.5. Crystallographic representation of the asymmetric unit for the isostructural materials PCM-8(K) and PCM-8(Rb) (a). View of PCM-8 extended network on the *a*-axis (b), *b*-axis (c), and *c*-axis (d).

Despite their similarities, one major difference between these materials is the identity of the metal nodes; for PCM-8, the metal nodes at alternating corners of each M_2P_2 window are based on triangular $[MZn_2(\mu_3\text{-}OH)]^{4+}$ clusters that provide a *pseudo*-octahedral connectivity (Figures 3.4b & 3.5a). Triangular $[M_3(\mu_3\text{-}OH)]^{5+}$ clusters are common in coordination chemistry[36] and have been observed frequently in PCPs,[37-39] but to the best of our knowledge there are no examples of heterobimetallic trimers containing K^+ or Rb^+ ions. Interestingly, charge balance is achieved by the replacement of a single zinc (II) ion in each

trimeric cluster with an alkali metal ion of similar size, which creates a cluster with an overall +4 charge that is countered by two $mptbc^{2-}$ anions. On the other hand, PCM-7 was able to achieve charge balance through the incorporation of a second OH^- group. Making use of their expanded coordination sphere, K^+ and Rb^+ within PCM-8 demonstrated pairs of triangles bridging into larger dimers through M_2O_2 squares mediated by the aldehyde-*O* atoms from the adjoining DMF molecules.

In the final reaction, the presumed *in-situ* precursor Cs_2[mptbc], created through the reaction of [$mptbcH_3$]Cl and CsOH, reacted with zinc(II) to give the fourth unique structure. This material, designated PCM-9, crystallized into the space group $P\bar{1}$ with the asymmetric unit [$Zn_3((\mu_3\text{-}OH)(mptbc)_2(O_2CCH_3)$]. PCM-9 exhibited 3-D porosity with accessible M_2P_2 squares accessible in all dimensions (Figure 3.6).

The structure of PCM-9 is similar to those of PCMs 7-8. However, due to Cs^+ having a significantly expanded ionic radius it was not able to incorporate itself into the framework. Instead, a more common Zn_3 cluster with a bridging μ_3-OH group was observed that once again resulted, unexpectedly, in an overall charge of +4 with the incorporation of a single terminal acetate ligand as seen in Figure 3.6a. This was likely driven by charge balance to compensate for the net -2 charge from each deprotonated methyl phosphonium ligand. The $[Zn_3((\mu_3\text{-}OH)(O_2CCH_3)]^{4+}$ metal cluster sites in PCM-9 acted as classic octahedral 6-connected nodes, which resulted in 6,3-connectivity containing more slanted pores than seen by other materials mentioned.

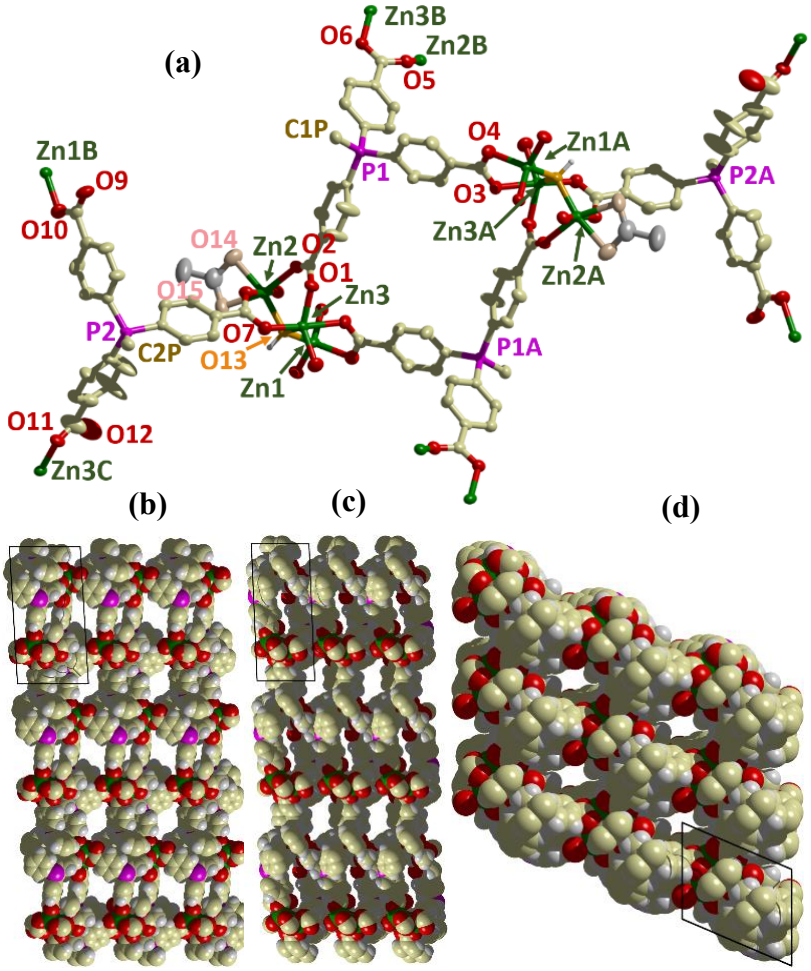

Figure 3.6. Crystallographic representation of the asymmetric unit for PCM-9 (a). View of PCM-9 extended network on the *a*-axis (b), *b*-axis (c), and *c*-axis (d).

Guest sorption and selectivity properties of PCMs 6−9

Before gas sorption studies were performed, the mother solution for each framework was solvent exchanged with ethanol. The thermal stability of PCM's 6−9 was found to be around 400 °C for each material through thermogravimetric analysis (TGA) as seen in Figure 3.7. Initial solvent loss was observed in the *post*-activation TGA of each material. This suggested that solvent was still coordinated to the frameworks after

activation for autosorb analysis. Higher activation temperatures during gas sorption studies demonstrated loss of porosity, which confirmed that coordinated solvent was in fact paramount to each material's porous stability. All gas adsorption measurements were performed in-house on a Quantachrome AS1 instrument and uptake and separation studies were performed using CO_2, N_2, O_2, H_2, and CH_4. The uptake and oddities of each probe gas are discussed below.

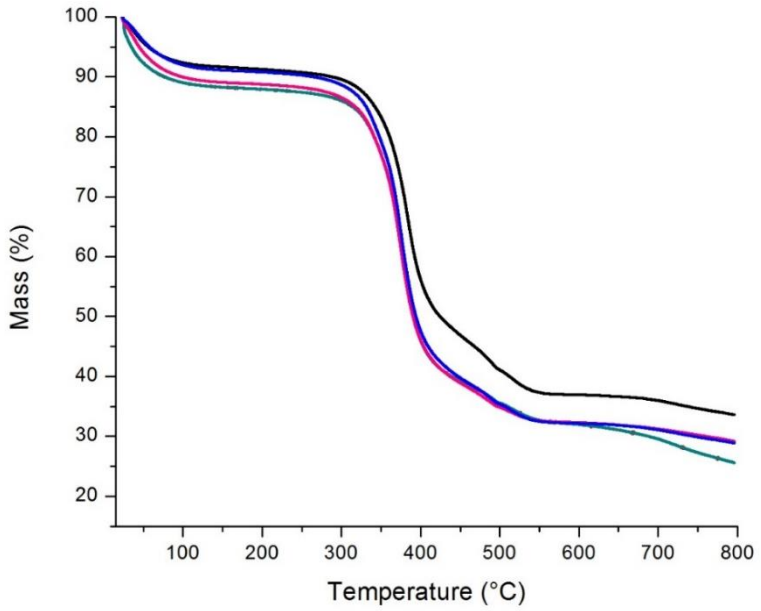

Figure 3.7. TGA analysis of *post*-activation materials from 25−800 °C for PCM-6 (Black), PCM-7 (Red), PCM-8(K) (Green), PCM-8(Rb)(Pink), PCM-9 (Blue).

Carbon dioxide

Carbon dioxide sorption at cryogenic temperatures serves as the benchmark analysis for PCMs in order to calculate internal surface areas. The overlay of CO_2 adsorption isotherms at 196 K for PCMs 6−9 is shown in Figure 3.8. From these isotherms, BET internal surface areas were calculated (0.05−0.30 atm) to be 1129 m^2/g, 1082 m^2/g,

858 m^2/g, 735 m^2/g, and 975 m^2/g for PCMs 6-9 respectively. These values are considered competitive with previously reported PCMs, with PCM-16 demonstrating the current highest value of 1811 m^2/g.[40] In each case, a typical Type 1 isotherm was observed with significant saturation occurring by 0.2 atm.

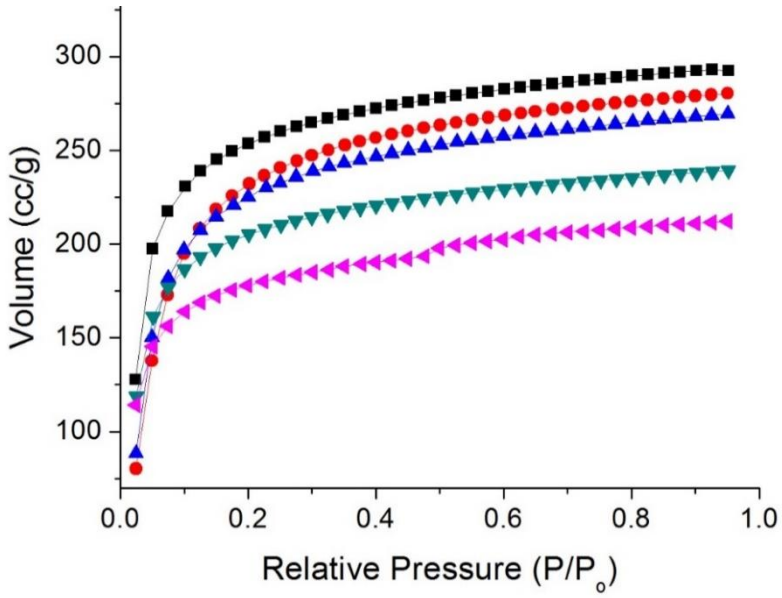

Figure 3.8. Cryogenic CO_2 adsorption isotherms collected at 196 K for PCM-6 (Black squares), PCM-7 (Red circles), PCM-8(K) (Green down triangles), PCM-8(Rb)(Pink left triangles), PCM-9 (Blue triangles) from 0.025−0.975 atm.

Nitrogen

Diatomic nitrogen was investigated next in a similar fashion; each material's sorption behavior was monitored at 77 K and the overlay of adsorption isotherms can be seen in Figure 3.9. Even though these isotherms generally still followed Type 1 isotherm behavior, they showed nearly instant saturation for N_2. Furthermore, regardless of all five materials demonstrating a lower BET surface area by nitrogen uptake, PCMs 6−9 all show

a higher cc/g maximum uptake for nitrogen in comparison to carbon dioxide. The only oddity in the ordering of the N_2 isotherms for these frameworks was found with the increased uptake of PCM-7 over PCM-6.

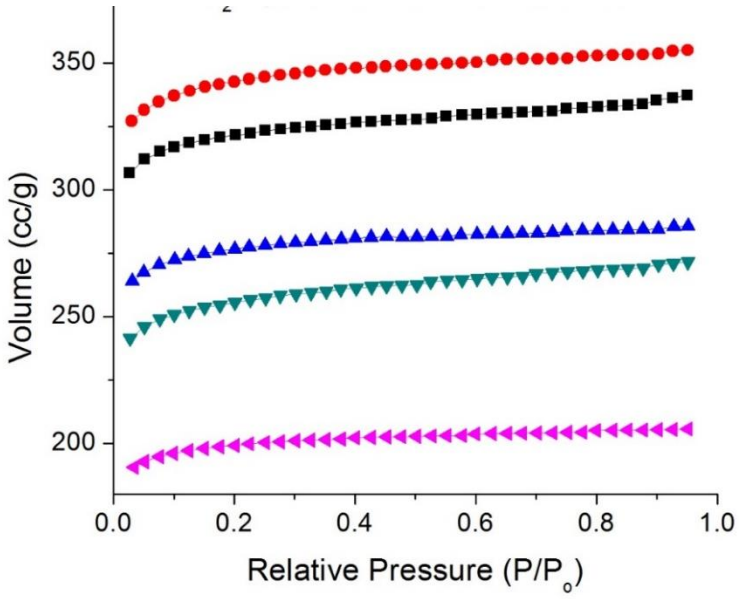

Figure 3.9. Cryogenic N_2 adsorption isotherms collected at 77 K for PCM-6 (Black squares), PCM-7 (Red circles), PCM-8(K) (Green down triangles), PCM-8(Rb) (Pink left triangles), PCM-9 (Blue triangles) from 0.025−0.975 atm.

Oxygen

Diatomic oxygen sorption studies were investigated next and resulted in fast saturation of each material, similar to behavior for nitrogen. The cc/g uptake of diatomic oxygen was found to be the highest of all five gases studied. The cryogenic O_2 adsorption isotherms for PCM's 6−9 are shown in Figure 3.10 below. As discussed earlier, previous materials that have demonstrated higher than normal oxygen uptake have largely incorporated unsaturated metal sites.[5-7] However, a much smaller group of materials have

shown an increase in this value without any open metal sites present. PCM's 6−9 are a demonstration of the latter.

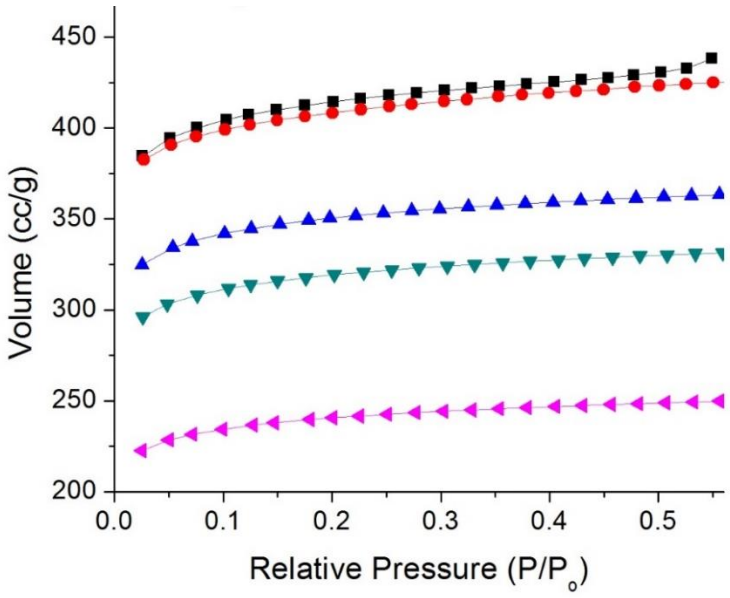

Figure 3.10. Cryogenic O_2 adsorption isotherms collected at 77 K for PCM-6 (black squares), PCM-7 (Red circles), PCM-8(K) (Green down triangles), PCM-8(Rb) (Pink left triangles), PCM-9 (Blue triangles) from 0.025−0.550 atm.

The weight percent uptake was calculated for the cryogenic oxygen adsorption at 0.550 atm for each of the five materials; PCMs 6−9 were found to adsorb 62.6 wt. %, 58.4 wt. %, 48.1 wt. %, 36.2 wt. %, and 52.9 wt. % (g O_2/g sample %) respectively. PCM-6 displayed the highest uptake of the five materials, with a molar uptake of 19.6 mmol/g. This is comparable to the highest cryogenic oxygen uptake of any PCP to date without open metal sites present (19.8 mmol/g; Dy-PCM-16).[40] The high O_2 uptake for PCM-6 was even more impressive given the fact that its CO_2 internal surface area was 62 % that of Dy-PCM-16. With oxygen uptake being affected more dramatically than any other gas, a

secondary factor must be accounted for to explain the disproportional increase in cryogenic gas sorption. Previous examples of saturated-metal materials with elevated oxygen sorption properties have included Yang and co-workers with the fluorinated material FMOF-1 and Park *et al.* with their SNU-9 framework that incorporated a carboxylated benzophenone linker.[41,42] In all cases found, a polarized bond was incorporated into the linker. While a P=O bond isn't as polarized as the other examples, the net polar nature of the bond seems to a factor nevertheless. With this thought process in mind, we believe that the highly polarized nature of the P^{+}−Me bond in the linker is likely responsible for this increase in oxygen sorption behavior. Unfortunately, the relationship between polarized bonds within linkers and gas sorption properties of diatomic oxygen has largely been unexplored. However, this characteristic within PCPs has recently been published in relation to H_2 studies and could shed light on the sorption behavior observed in this study.[41,42]

Hydrogen

Hydrogen adsorption was of interest next and displayed very slow saturation with a type 1 isotherm. The H_2 cryogenic isotherm for PCMs 6 to 9 is shown below in Figure 3.11. Slow saturation with no plateau was observed in all cases. However, all five materials demonstrated a notably high hydrogen uptake, with values of 2.06 wt. %, 2.12 wt. %, 1.64 wt. %, 1.28 wt. %, and 1.58 wt. % respectively. PCM-7 performed the best for H_2 adsorption with a maximum uptake of 10.5 mmol/g (77 K, 0.975 atm). This increased level of hydrogen uptake across PCMs 6−9 is likely related to the increase oxygen sorption behavior observed as well. In a theoretical study from 2014, Tsivion *et al.* used DFT calculations to demonstrate π-donor orbital interactions with H_2.[43] In a separate example,

Berke and coworkers publication from the same year discussed the specific importance of polarized components in linkers to increase H_2 uptake.[45] In both examples, there was a large emphasis on the need for polarization of H_2 itself in order increase sorption behaviour outside of open metal sites. From both theoretical and experimental results, it was observed that inclusion of a polarized component within a linker can in turn influence polarization of diatomic hydrogen. Therefore, the increased adsorption observed for H_2 and possibly O_2 is likely due to the polarity of the P^{+}−Me bond within the linker for PCMs 6 to 9 as described above.

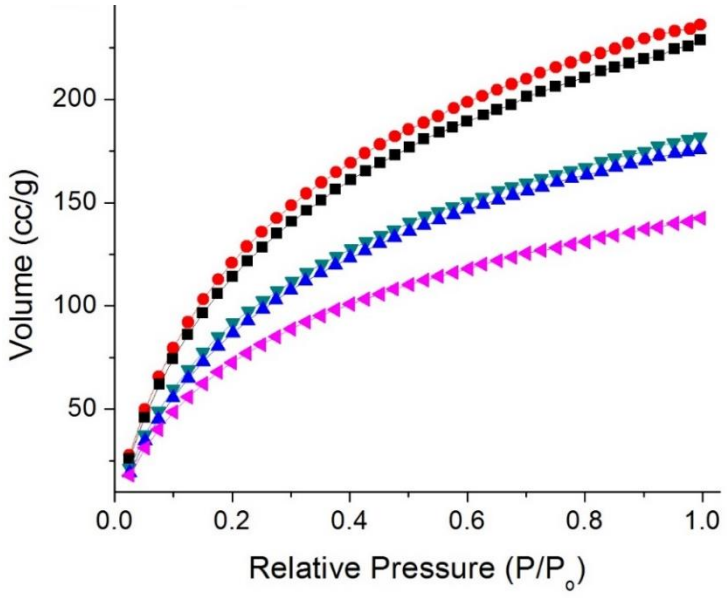

Figure 3.11. Cryogenic H_2 adsorption isotherms collected at 77 K for PCM-6 (Black squares), PCM-7 (Red circles), PCM-8(K) (Green down triangles), PCM-8(Rb) (Pink left triangles), PCM-9 (Blue triangles) from 0.025−0.975 atm.

Methane

The final gas studied was methane, which demonstrated similar adsorption behavior to hydrogen. This slow saturation with no plateau for each material can be seen in Figure 3.13. PCM-7 was the only oddity in this CH_4 data, with a lower than expected sorption behavior.

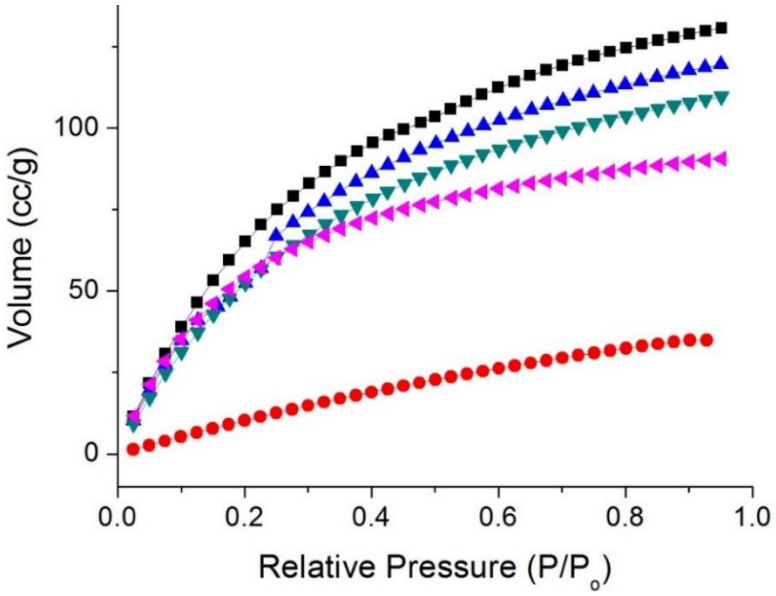

Figure 3.12. Cryogenic CH_4 adsorption isotherms collected at 196 K for PCM-6 (Black squares), PCM-7 (Red circles), PCM-8(K) (Green down triangles), PCM-8(Rb) (Pink left triangles), PCM-9 (Blue triangles) from 0.025−0.975 atm.

Due to the large difference in uptake between CO_2 and CH_4 at cryogenic temperatures for PCMs 6 to 9, room temperature measurements were then also investigated for possible applications in separations chemistry. The comparative isotherms for each material can be seen in Figures 3.13−3.17 respectively. The separation capacities were calculated by IAST methods.[44] Unfortunately, PCMs 6−9 demonstrated a modest separation capacity overall.

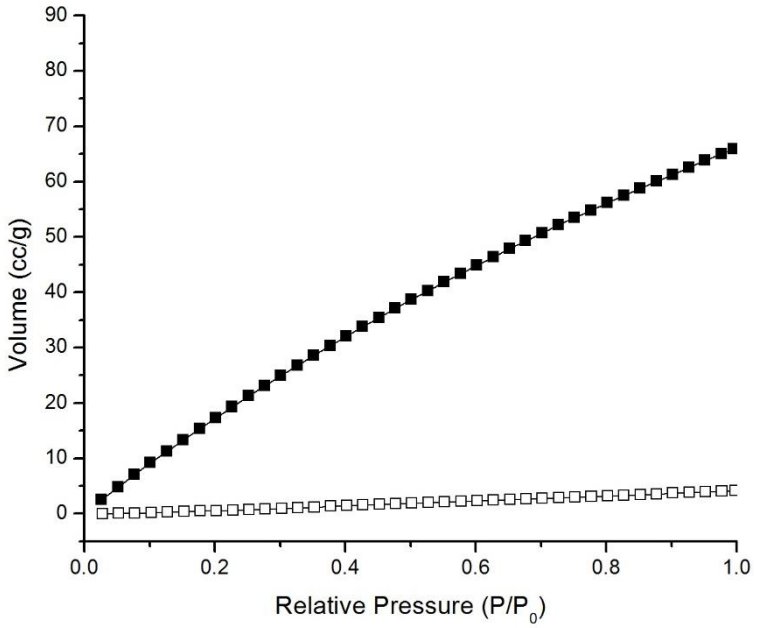

Figure 3.13. Gas adsorption measurements at 25 °C for EtOH-exchanged PCM-6 for CO_2 (Filled) versus CH_4 (Open) from 0.05−0.975 atm; separation capacity of 4.51:1.

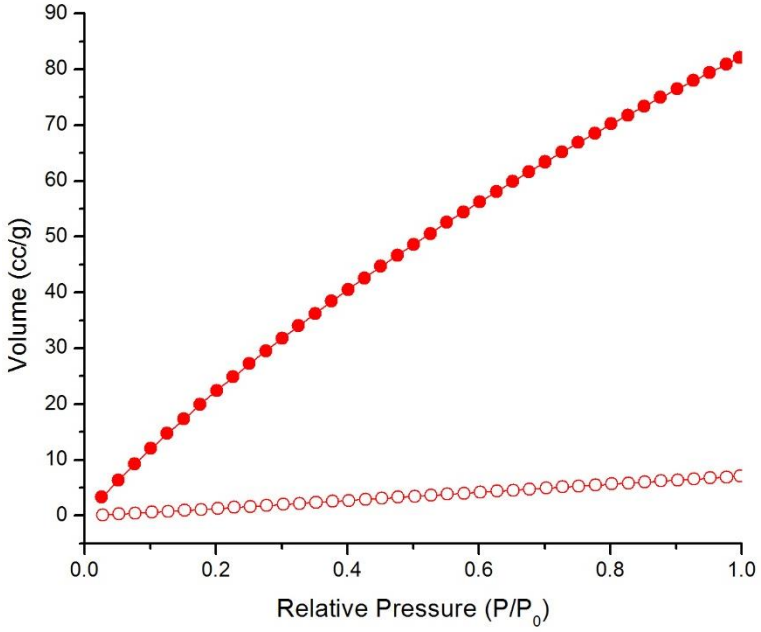

Figure 3.14. Gas adsorption measurements at 25 °C for EtOH-exchanged PCM-7 for CO_2 (Filled) versus CH_4 (Open) from 0.05−0.975 atm.; separation capacity of 4.50:1.

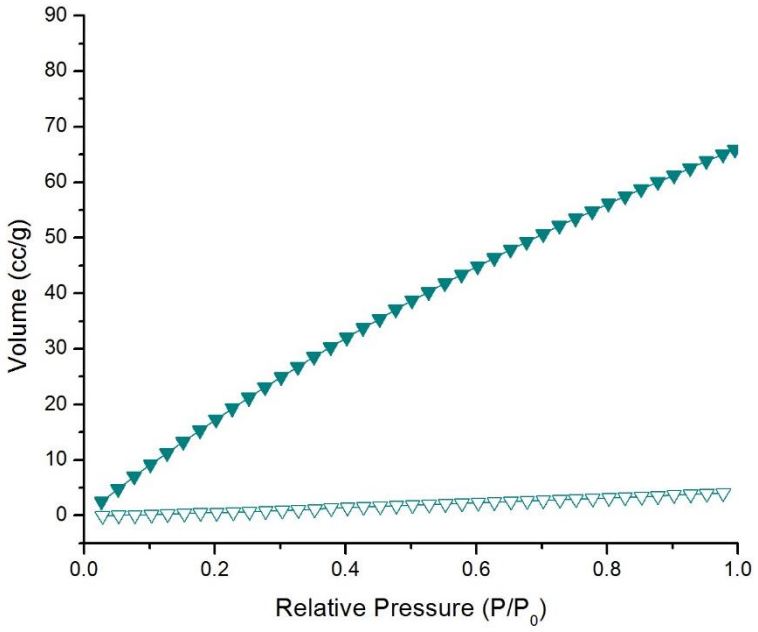

Figure 3.15. Gas adsorption measurements at 25 °C for EtOH-exchanged PCM-8(K) for CO_2 (Filled) versus CH_4 (Open) from 0.05−0.975 atm.; separation capacity of 4.12:1.

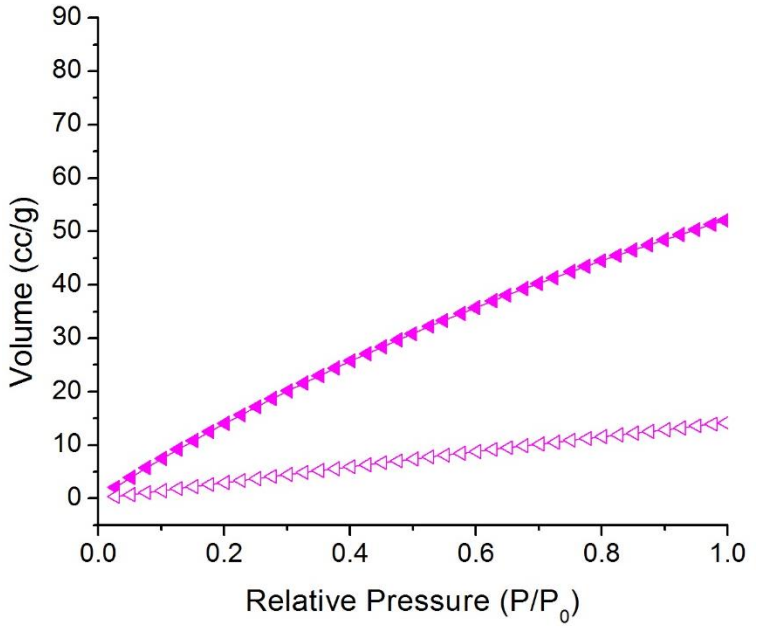

Figure 3.16. Gas adsorption measurements at 25 °C for EtOH-exchanged PCM-8(Rb) for CO_2 (Filled) versus CH_4 (Open) from 0.05−0.975 atm.; separation capacity of 4.16:1.

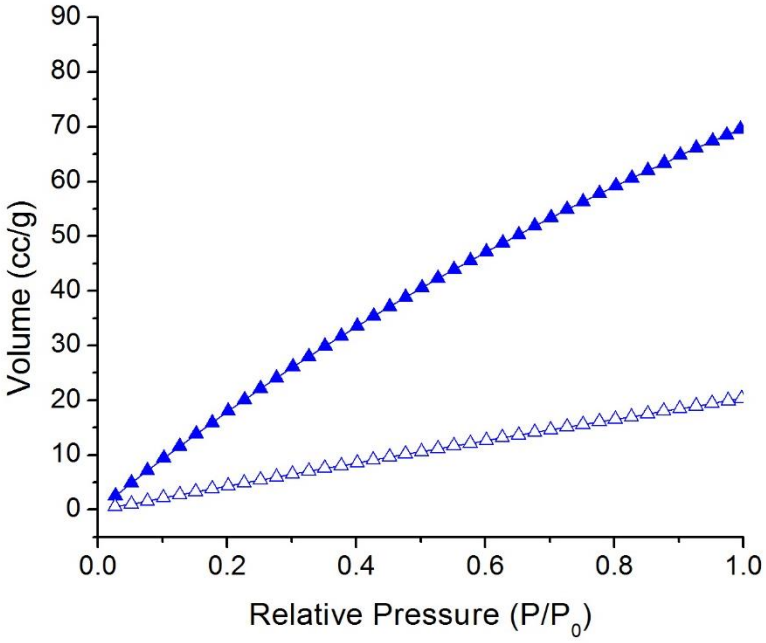

Figure 3.17. Gas adsorption measurements at 25 °C for EtOH-exchanged PCM-9 for CO_2 (Filled) versus CH_4 (Open) from 0.05−0.975 atm.; separation capacity of 3.81:1.

CONCLUSIONS

Five novel PCPs, four of which were non-isostructural, were successfully synthesized through the simple addition of a variety of alkali-metal hydroxide solutions. PCM's 6−9 were created through the addition of LiOH through CsOH respectively, while keeping all other synthetic conditions consistent. Through the use of a unique methyl phosphonium linker, the creation of lower density materials with open square pores was accomplished. In turn, this allowed for PCMs 6 to 9 to demonstrate promising guest-host interaction leading to new applications for gas storage and separations. The series performed impressively for oxygen uptake, with a maximum of 19.6 mmol/g (62.6 % by weight) uptake for PCM-6 (0.550 atm, 77 K). This value is nearly identical to the current

highest performing PCP that does not include open metal sites. Furthermore, these materials performed notably for hydrogen adsorption as well, with a maximum of 10.5 mmol/g (2.12 % by weight) for PCM-7 (0.975 atm, 77 K). This behavior is most likely due to the polarized P^{+}−Me bond allowing for more favorable interactions with both O_2 and H_2. Further exploration of polarized groups and their influence on oxygen adsorption properties is of interest for future work due to a lack of presence in the literature with focus on linker influence. The series of PCMs 6−9 provides interesting insight into the structural effects on materials of very small synthetic changes.

EXPERIMENTAL DATA

General

All synthetic methods for linker development were performed under a nitrogen atmosphere through the use of standard Schlenk techniques. The reagents 1,4-dibromobenzene (Oakwood Chemical, ≥99 %), n-butyllithium (nBuLi) (2.5 M in hexanes, Sigma Aldrich), lithium hydroxide (LiOH) (Sigma Aldrich, ≥98 %), sodium hydroxide (NaOH) (Fisher Chemical, ACS grade), potassium hydroxide (KOH) (Fisher Chemical, ACS grade), rubidium hydroxide (RbOH) (Sigma Aldrich, 50 wt. % solution in water, ≥99 %), cesium hydroxide (CsOH) (Sigma Aldrich, 50 wt. % in water, ≥99 %), sodium chloride (NaCl) (Fisher Chemical, ≥99 %), magnesium sulfate anhydrous ($MgSO_4$) (Fisher Chemical, ≥98 %), silica (Agela Technologies, 80 μm), hydrochloric acid (Fisher Chemical, ACS grade), solid carbon dioxide (Praxair), Iodomethane (MeI) (Alfa Aesar, 99.5 % stab. with copper), and zinc acetate dihydrate (Alfa Aesar, ≥97 %) were used as received. Phosphorous trichloride (Sigma Aldrich, ≥99 %) was purified through vacuum distillation (40 °C, passive vacuum). Tetrahydrofuran (THF) (Fisher Chemical, HPLC

grade) was distilled (dried over sodium in still) and collected over sieves (4A) for use. Dichloromethane (DCM) (Fisher Chemical, ACS grade), hexanes (Fisher Chemical, ACS grade), N,N-dimethylformamide (DMF) (Fisher Chemical, ACS grade), ethanol (EtOH) (Pharmco-Aaper, ACS grade), were used as received and all aqueous solutions along with diethyl ether (BDH, ACS grade) were purged with nitrogen for 30 min prior to use. Solution ^{1}H-NMR and ^{31}P-NMR were collected in-house using an Agilent MR 400 MHz spectrometer; ^{13}C-NMR was collected with a Varian Inova 500 MHz; FT-IR spectra were obtained directly from solid samples using a Nicolet iS*50 spectrophotometer with an attenuated total reflectance apparatus; thermogravimetric analysis (TGA) data was collected with a TA Instruments Q50 system for the temperature range of 25 °C to 800 °C. Elemental Analysis was performed by Midwest Microlab LLC (Indianapolis).

X-ray crystallography

Suitable single crystals were mounted on a nylon thread loop in perfluoropolyether oil and attached to the diffractometer. The data was collected at 180 K. Structures were solved using direct methods, with full-matrix least squares refinement. All data was collected on an Enraf-Nonium Kappa CCD single crystal diffractometer with an Oxford Cryosystems cryostream device collected using Co Kα radiation (1.7889 Å).

Powder X-ray diffraction (PXRD).

The PXRD model data was generated using the Sim PowPatt function in the PLATON software from the hkl reflection data collected in the single crystal experiments. Phase purity of the as synthesized materials PCM-6 and PCM-9 were confirmed through analysis of each material loaded as a bulk onto a nylon thread loop with mineral oil and

spun *in situ* to prevent preferential orientation of the crystallites. Spectra for these materials was collected on an Agilent SuperNova with AtlassS2 CCD using CrysAlisPro V171.38.27t. These samples were collected using Cu Kα radiation (1.5406 Å). Reflection data was collected in the range of 5.0−40.0° 2θ.

Phase purity of the as synthesized materials PCM-7 and PCM-8(K and Rb) was confirmed through the analysis of the powdered crystalline samples, which were placed in borosilicate tubes and spun in situ to prevent preferential orientation of the crystallites. Spectra were collected on a STOE STADi-P diffractometer with a linear position sensitive detector. This system operated in Debye-Scherrer geometry using Co Kα radiation (1.7902 Å). Reflection data was collected with WinXPow software from 5.0−40.0° 2θ using multiple scans, which were subsequently averaged.

Gas sorption isotherms

Samples were *pre*-treated under ultra-high vacuum in a clean system with a diaphragm and turbo pumping system. Isotherms for CO_2, N_2, O_2, and H_2 were collected utilizing ultra-high purity gases (Praxair, 99.995 %). Surface areas were then calculated using the Brauner-Emmett Teller method for CO_2, based on adsorption data points in the range $P/P_o = 0.05−0.030$.

Procedure for *tris*(4-bromophenyl)phosphine (tBrtpp) (15)

The reagent 1,4 dibromobenzene (12.46 g; 52.81 mmol) was dissolved in THF (350 mL) in a 1000 mL round bottomed flask, then cooled to −78 °C via an acetone/dry ice bath. A solution of nBuLi (2.5 M in hexanes; 52.81 mmol) was added dropwise to the reaction over 30 min. The resulting white, heterogeneous mixture was allowed to stir for 1 hr at −78

°C. Phosphorous trichloride (1.54 mL, 17.60 mmol) was then added dropwise over 15 min. The resulting clear solution was washed with an aqueous NaCl solution (10 %, 150 mL), before being dried over $MgSO_4$. Once filtered, the solvent was removed *in vacuo* to yield a yellow oil. The oil was isolated via column purification (40:1, hexanes:DCM) on silica to afford a white crystalline solid (3.661 g, 7.337 mmol). Yield, 41.70%. ^{31}P NMR ($CDCl_3$, 161.9): δ = −8.579; ^{1}H-NMR ($CDCl_3$, 400.1 MHz): δ = 7.466 (d, 6H), 7.119 (t, 6H); ^{13}C NMR (CDCl3, 100.6 MHz): δ = 166.980 (s, Ar), 140.120 (s, Ar), 133.980 (d, Ar), 130.669 (d, Ar), 123.223 (s, Ar)162; FT-IR (solid/cm^{-1}): ν_{max} = 3041 (w), 2923 (w), 1852 (w), 1903 (w), 1789 (w), 1637 (w), 1566 (m), 1472 (s), 1380 (s), 1297 (w), 1260 (w), 1178 (w), 1103 (w) 1065 (s), 1006 (s), 947 (w), 831 (s), 815 (s), 722 (s), 709, (s), 701 (m), 528 (m), 506 (s), 485 (m), 471 (m), 452 (m).

Procedure for lithium 4,4',4"-phosphinetriyltribenzoate (pbtcLi$_3$) (16)

tBrtpp (**15**) (2.29 g, 4.59 mmol) was placed into a 1000 mL round bottomed flask and dissolved in THF (250 mL). The solution was then cooled to −78 °C via an acetone/dry ice bath before the dropwise addition of nBuLi (2.5 M in hexanes, 14.68 mmol) over 10 min. The resulting pink heterogeneous mixture was then allowed to stir at −78 °C for an additional 4 hrs. Diethyl ether (75 mL) along with excess crushed dry ice (ca. 100 g) was added to the solution, which caused the heterogeneous mixture to lighten in color slightly. The reaction was left under nitrogen and was allowed to slowly warm up to room temperature while stirring with the acetone/dry ice bath evaporating overnight. The product was isolated via centrifugation, then dried under nitrogen to afford a white powder (1.84 g; 4.47 mmol). Yield: 97.35 %. ^{31}P NMR (D_2O, 161.9 MHz): δ = -7.719; ^{1}H NMR (D_2O, 400.1 MHz): δ = 7.628 (dd, 6H), 7.185 (td, 6H); ^{13}C NMR (D2O, 100.6 MHz): δ = 174.869

(s), 138.855 (d, Ar), 136.979 (s, Ar), 133.378 (d, Ar), 128.929 (d, Ar); FT-IR (solid/cm^{-1}): ν_{max} = 3345 (b), 2975 (w), 2874 (w), 1584 (s), 1538 (s), 1390 (s), 1304 (w), 1275 (w), 1090 (w), 1046 (m), 1016 (w), 891 (w), 847 (m), 775 (s), 721 (m), 701 (m), 634 (w), 545 (w).

Procedure for *tris*(4-carboxyphenyl)(methyl)phosphonium chloride ([mptbcH$_3$]Cl) (17)

pbtcLi$_3$ (**16**) (658 mg, 1.60 mmol) was placed into H_2O (6 mL) in a glass reactor tube fitted with a magnetic stir bar and screw cap. A solution of MeI (0.20 mL, 3.21 mmol) in DCM (5 mL) was added, and the biphasic reaction was spun into an emulsion at room temperature for 24 hrs. The organic phase was removed via pipette; the aqueous phase was rinsed into a 50 mL round bottom flask with H_2O (ca. 30 mL). The diluted aqueous solution was cooled to 0 °C, then acidified (pH 2) with an HCl solution (1.0 M) to yield a white precipitate. This solid was isolated by filtration, washed with diethyl ether, and dried under vacuum (525 mg, 0.98 m mol). Yield: 61.19%. ^{31}P (DMSO, 161.9 MHz): δ = 23.821; ^{1}H NMR (DMSO, 400.1 MHz): δ = 8.8208 (dd, 6H), 7.898 (dd, 6H), 3.401 (s, CO_2H), 3.251 (d, 3H); 13C NMR (d-DMSO, 150.9 MHz): δ = 166.587 (s), 137.523 (d, Ar), 134.410 (d, Ar), 130.783 (d, Ar), 123.881 (d, Ar), 7.634 (d); FT-IR (solid/cm^{-1}): ν_{max} = 3392 (b), 2986 (w), 2913 (w), 2604 (w), 2485 (w), 1934 (w), 1705 (m), 1560 (w), 1564 (w), 1545 (w), 1497 (w), 1394 (m), 1254 (m), 1185 (w), 1103 (m), 1013 (m), 903 (m), 858 (m), 809 (w), 759 (s), 707 (s), 688 (s), 630 (w), 549 (m), 514 (m), 490 (m).

Procedure for PCM-6 (18)

[mptbcH$_3$]Cl (**17**) (40 mg, 1.0 mmol) was dissolved in a solution of DMF:EtOH:DI water (1:1:1, 2.5 mL). Two drops of LiOH (1 M) was added and then the solution was shaken. A second solution of zinc(II) acetate dihydrate (20 mg, 1.6 mmol) in DMF (2.5 mL) was then added. The white, heterogeneous suspension was heated in a 20 mL sealed glass vial at 80 °C through the employment of a graphite thermal bath for 3−5 days. Once gelling had ceased, the crystalline product was collected through decantation. Washes with ethanol and short bursts of sonication were performed until solution was clear and only product remained. Yield: 40 mg. Anal. Found: C, 47.80; H, 3.36; N, 0.00 %. [PCM-6]·4H$_2$O; ($C_{22}H_{23}O_{10}P_1Zn_1$) requires: C, 48.59; H, 4.26; N, 0.00 %; FT-IR (solid/cm^{-1}): ν_{max} = 3250 (b), 2984 (w), 2912 (w), 1592 (s), 1546 (s), 1496 (w), 1366 (s), 1317 (w), 1284 (w), 1189 (w), 1139 (w), 1105 (m), 1015 (m), 890 (m), 862 (w), 840 (m), 767 (s), 730 (s), 691 (m), 629 (w), 541 (m), 479 (m).

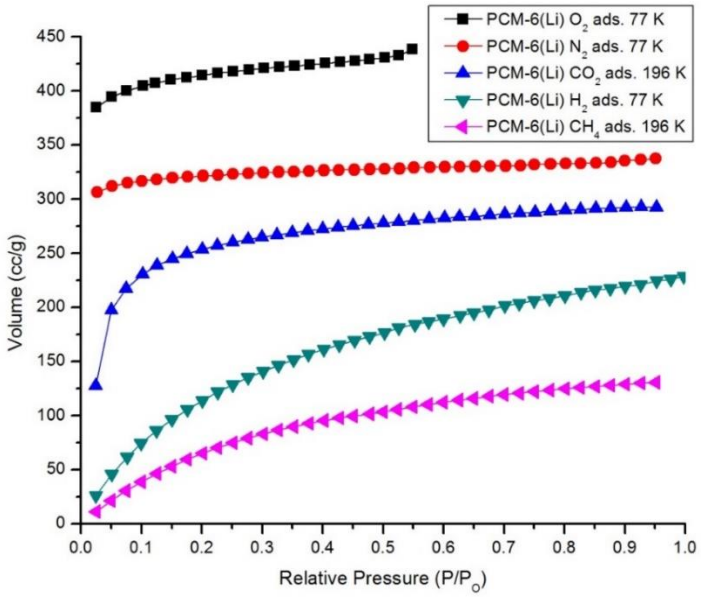

Figure 3.18. Cryogenic adsorption isotherms for PCM-6 (**18**) for O_2 (Black square), N_2 (Red circle), CO_2 (Blue triangle), H_2 (Green down triangle), and CH_4 (Pink left triangle).

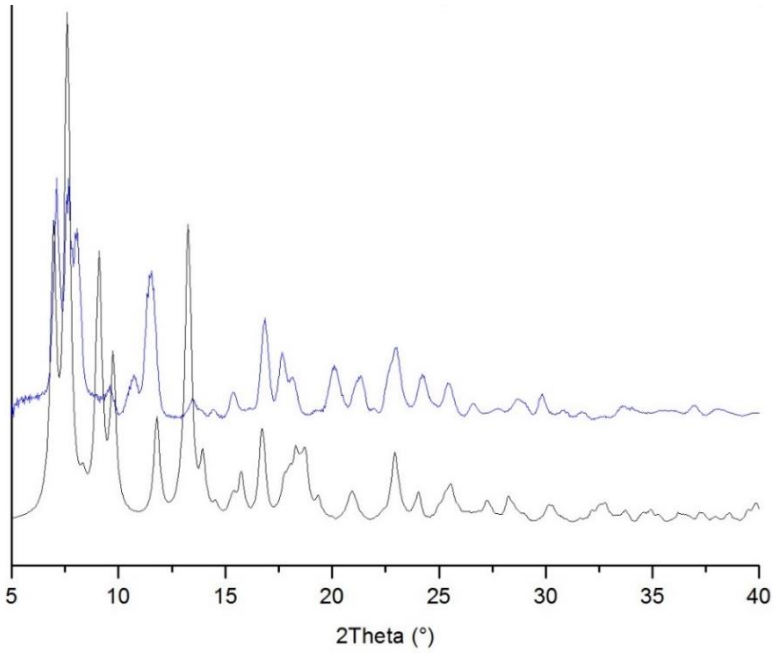

Figure 3.19. PXRD comparison of the model pattern (Black) vs PCM-6 (**18**) bulk pattern (Blue).

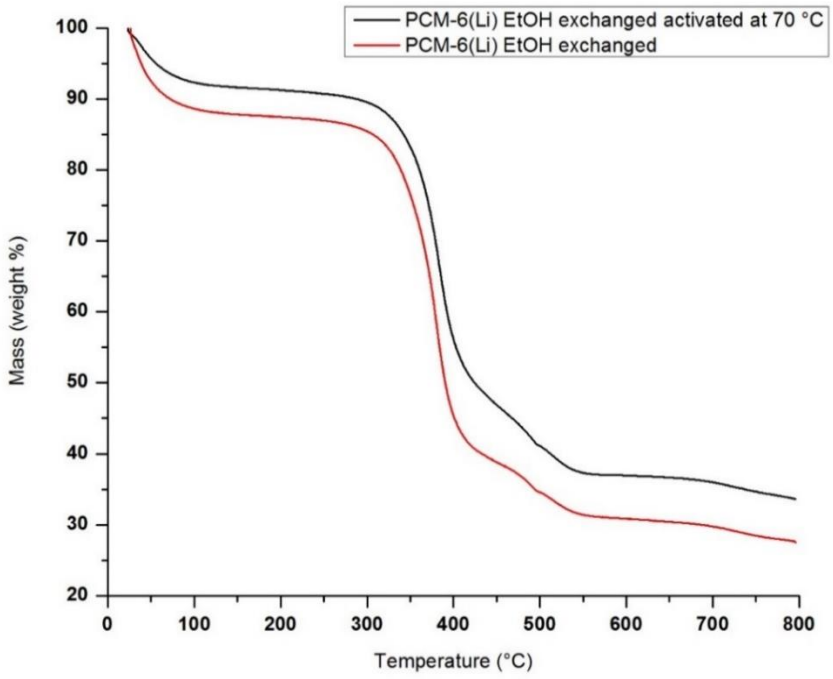

Figure 3.20. TGA of *pre*-activated (Red) and *post*-activated (Black) PCM-6 (**18**).

Procedure for PCM-7 (19)

[mptbcH3]Cl (**17**) (40 mg, 1.0 mmol) was dissolved in a solution of DMF:EtOH:DI water (1:1:1, 2.5 mL). Two drops of NaOH (1 M) was added to the homogenous solution then shaken. A second solution of zinc(II) acetate dihydrate (20 mg, 1.6 mmol) in DMF (2.5 mL) was then added. The white, heterogeneous suspension was heated in a 20 mL sealed glass vial at 80 °C through the employment of a graphite thermal bath for 3−5 days. Once gelling had ceased, the crystalline product was collected through decantation. Washes with ethanol and short bursts of sonication were performed until solution was clear and only product remained. Yield: 38 mg. Anal. Found: C, 43.73; H, 4.49; N, 0.31 %. [PCM-7]·8H_2O; ($C_{44}H_{50}O_{23}P_2Zn_3$) requires: C, 43.86; H, 4.18; N, 0.00 %; FT-IR (solid/cm^{-1}): ν_{max} = 3362 (b), 3072 (w), 2984 (w), 2912 (w), 1592 (s), 1547 (s), 1496 (w), 1362 (s), 1317, (w), 1284 (w), 1189 (w), 1139 (w), 1105 (s), 1015 (m), 900 (m), 862 (w), 840 (m), 766 (s), 731 (s), 691 (m), 630 (w), 542 (m), 479 (m).

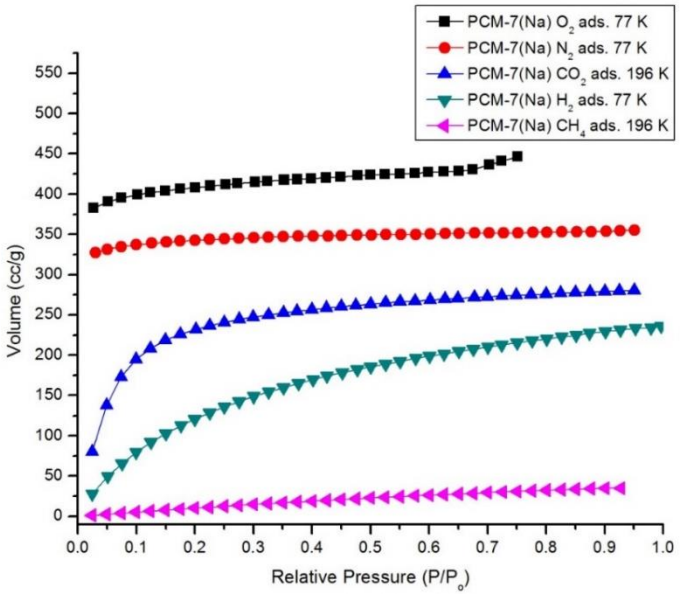

Figure 3.21. Cryogenic adsorption isotherms for PCM-7 (**19**) for O_2 (Black square), N_2 (Red circle), CO_2 (Blue triangle), H_2 (Green down triangle), and CH_4 (Pink left triangle).

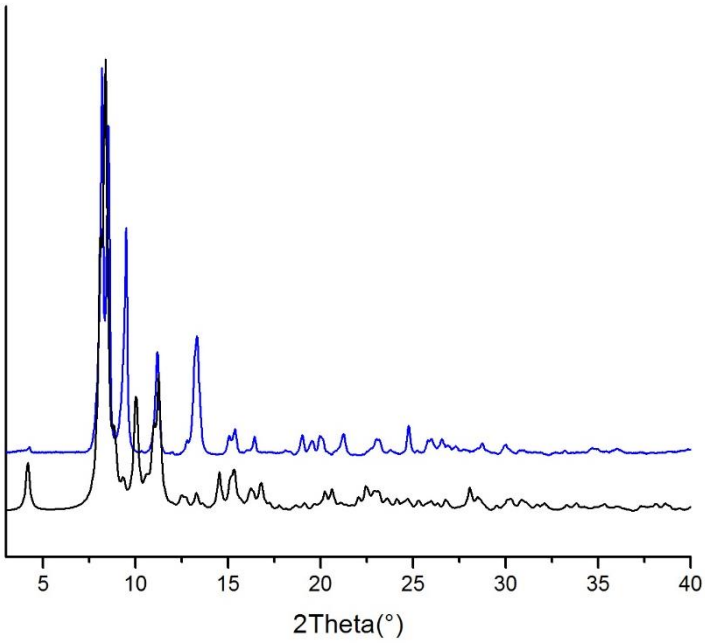

Figure 3.22. PXRD comparison of the model pattern (Black) vs PCM-7 (**19**) bulk pattern (Blue).

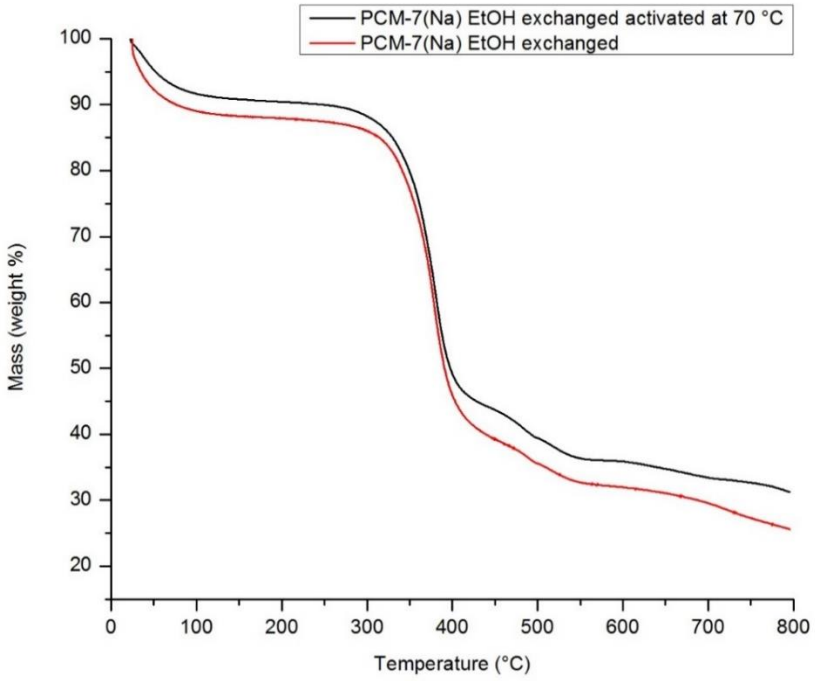

Figure 3.23. TGA of *pre*-activated (red) and *post*-activated (Black) PCM-7 (**19**).

Procedure for PCM-8(K) (20)

[mptbcH3]Cl (40 mg, 1.0 mmol) was dissolved in a solution of DMF:EtOH:DI water (1:1:1, 2.5 mL). Two drops of KOH (1 M) was added to the solution then shaken. A second solution of zinc(II) acetate dihydrate (20 mg, 1.6 mmol) in DMF (2.5 mL) was then added. The white, heterogeneous suspension was heated in a 20 mL sealed glass vial at 80 °C through the employment of a graphite thermal bath for 3−5 days. Once gelling had ceased, the crystalline product was collected through decantation. Washes with ethanol and short bursts of sonication were performed until solution was clear and only product remained. Yield: 38 mg. Anal. Found: C, 44.88; H, 4.28; N, 0.00 %. [PCM-8(K)]·10H_2O·(-1DMF); ($C_{44}H_{51}O_{23}P_2Zn_2K_1$) requires: C, 44.80; H, 4.36; N, 0.00 %; FT-IR (solid/cm^{-1}): ν_{max} = 3220 (b), 3082 (w), 2986 (w), 2915 (w), 2120 (b), 1592 (s), 1544 (s), 1498 (w), 1368 (s), 1316 (w), 1283 (w), 1191 (w), 1137 (w), 1106 (s), 1015 (m), 980 (w), 908 (m), 863 (w), 841 (m), 766 (s), 730 (s), 690 (m), 630 (w), 545 (m), 479 (m).

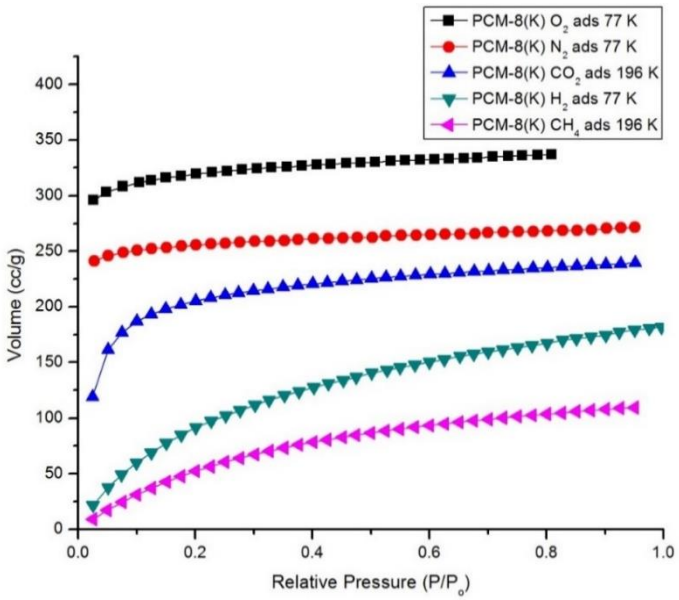

Figure 3.24. Cryogenic adsorption isotherms for PCM-8(K) (**20**) for O_2 (Black square), N_2 (Red circle), CO_2 (Blue triangle), H_2 (Green down triangle), and CH_4 (Pink left triangle).

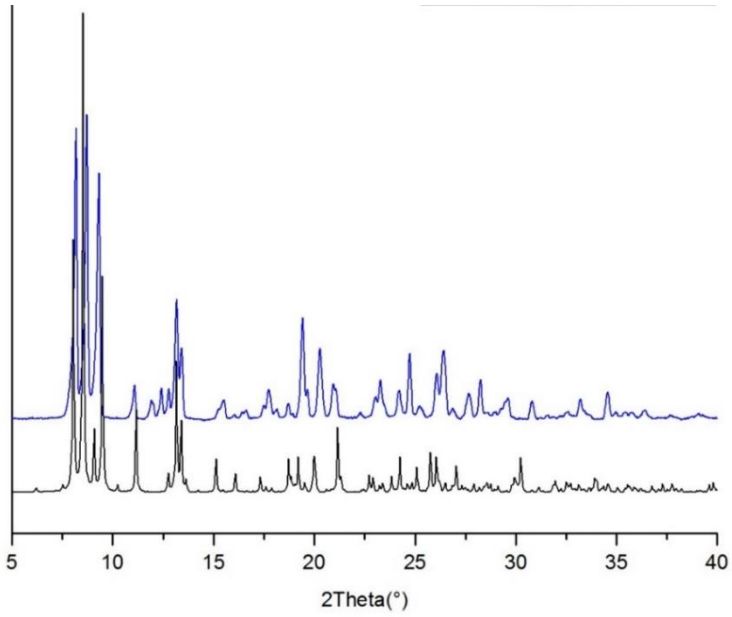

Figure 3.25. PXRD comparison of the model pattern (Black) vs PCM-8(K) (**20**) bulk pattern (Blue).

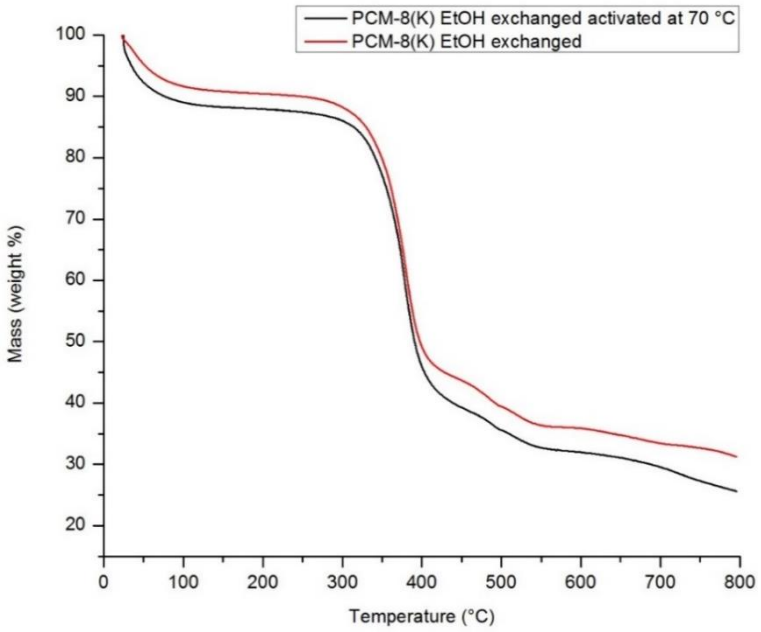

Figure 3.26. TGA of *pre*-activated (Red) and *post*-activated (Black) PCM-8(K) (**20**).

Procedure for PCM-8(Rb) (21)

[mptbcH3]Cl (**17**) (40 mg, 1.0 mmol) was dissolved in a solution of DMF:EtOH:DI water (1:1:1, 2.5 mL). Three drops of RbOH (1 M) was added to the solution then shaken. A second solution of zinc(II) acetate dihydrate (20 mg, 1.6 mmol) in DMF (2.5 mL) was then added. The white, heterogeneous suspension was heated in a 20 mL sealed glass vial at 80 °C through the employment of a graphite thermal bath for 3−5 days. Once gelling had ceased, the crystalline product was collected through decantation. Washes with ethanol and short bursts of sonication were performed until solution was clear and only product remained. Yield: 28 mg. Anal. Found: C, 44.96; H, 4.28; N, 0.00 %. [PCM-8(Rb)] $\cdot 7.5H_2O \cdot 1EtOH$; ($C_{46}H_{52}O_{21.5}P_2Zn_2Rb_1$) requires: C, 45.02; H, 4.27; N, 0.00 %; FT-IR (solid/cm^{-1}): ν_{max} = 3374 (b), 3064 (w), 2978 (w), 2908 (w), 2120 (b), 1593 (s), 1547 (s),

1496 (w), 1355 (s), 1188, (w), 1138 (w), 1104 (s), 1014 (m), 900 (m), 861 (w), 838 (m), 766 (s), 730 (s), 691 (m), 630 (w), 542 (m), 479 (m).

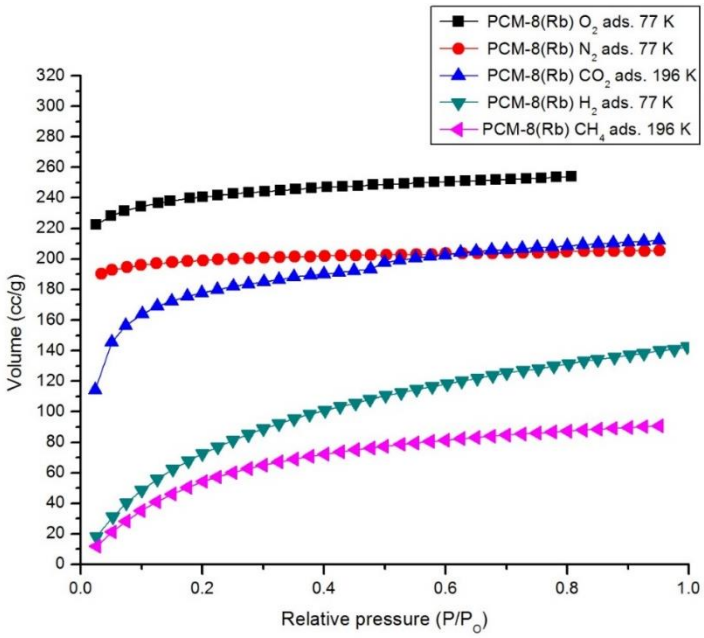

Figure 3.27. Cryogenic adsorption isotherms for PCM-8(Rb) (**21**) for O_2 (Black square), N_2 (Red circle), CO_2 (Blue triangle), H_2 (Green down triangle), and CH_4 (Pink left triangle).

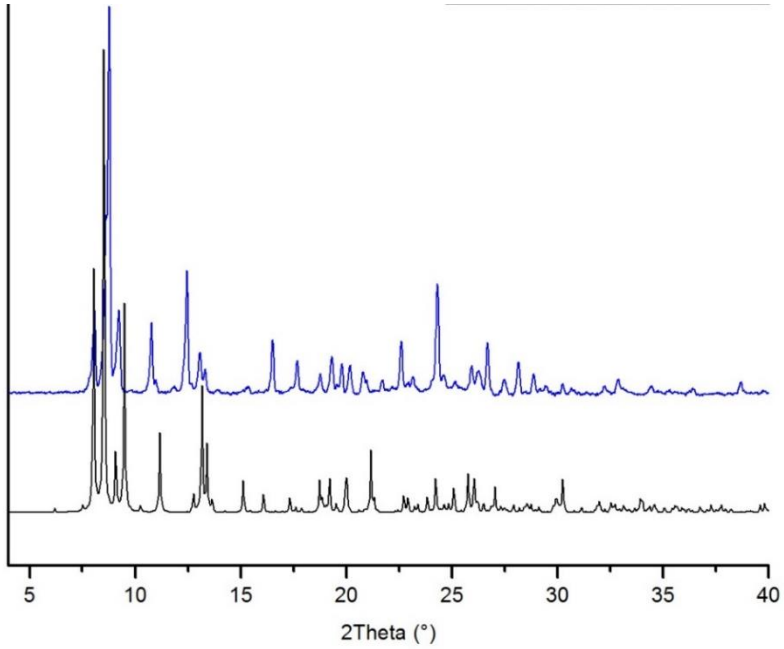

Figure 3.28. PXRD comparison of the model pattern (Black) vs PCM-8(Rb) (**21**) bulk pattern (Blue).

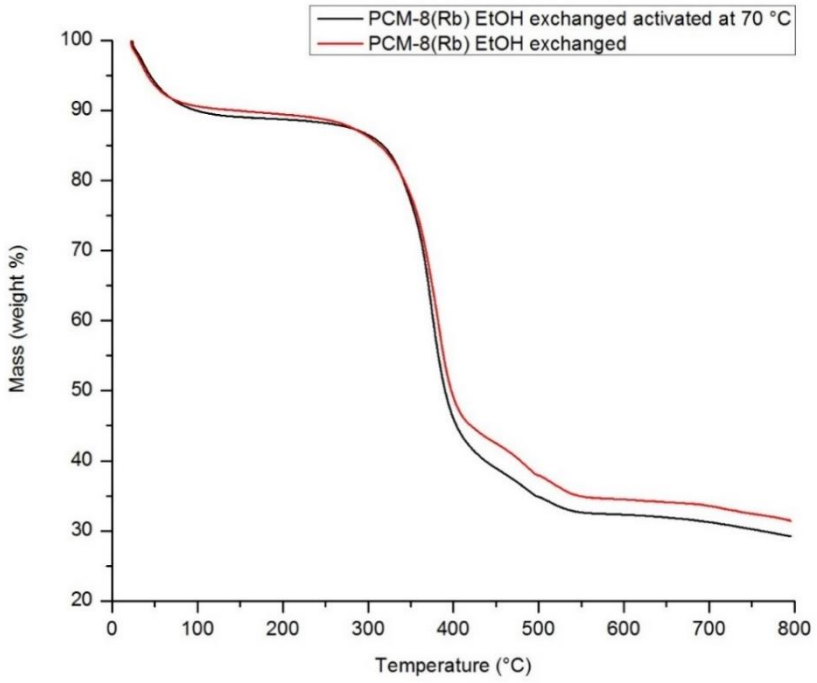

Figure 3.29. TGA of *pre*-activated (Red) and *post*-activated (Black) PCM-8(Rb) (**21**).

Procedure for PCM-9 (22)

[mptbcH3]Cl (**17**) (40 mg, 1.0 mmol) was dissolved in a solution of DMF:EtOH:DI water (1:1:1, 2.5 mL). Two drops of CsOH (1 M) was added to the solution then shaken. A second solution of zinc(II) acetate dihydrate (20 mg, 1.6 mmol) in DMF (2.5 mL) was then added. The white, heterogeneous suspension was heated in a 20 mL sealed glass vial at 80 °C through the employment of a graphite thermal bath for 3−5 days. Once gelling had ceased, the crystalline product was collected through decantation. Washes with ethanol and short bursts of sonication were performed until solution was clear and only product remained. Yield: 38 mg. Anal. Found: C, 45.29; H, 4.34; N, 0.00 %. [PCM-9] $\cdot 8H_2O \cdot 1EtOH$; ($C_{48}H_{54}O_{24}P_2Zn_3$) requires: C, 45.28; H, 4.28; N, 0.00 %. FT-IR (solid/cm^{-1}): ν_{max} = 3381 (b), 3085 (w), 2977 (w), 2907 (w), 2108 (b), 1950 (w), 1830 (w), 1655 (w), 1613 (s), 1550 (s), 1496(w), 1366 (s), 1316 (w), 1284 (w), 1254 (w), 1186 (w), 1138 (w), 1106 (s), 1046 (m), 1015 (m), 987 (w), 912 (m), 901 (m), 864 (w), 845 (m), 790 (w), 767 (s), 734 (s), 692 (m), 657 (w), 630 (w), 583 (w), 541 (m), 487 (m).

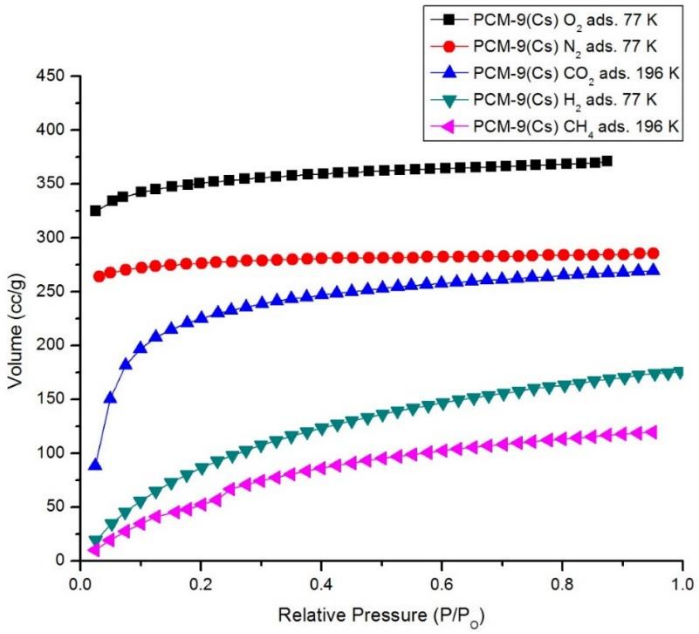

Figure 3.30. Cryogenic adsorption isotherms for PCM-9 (**22**) for O_2 (Black square), N_2 (Red circle), CO_2 (Blue triangle), H_2 (Green down triangle), and CH_4 (Pink left triangle).

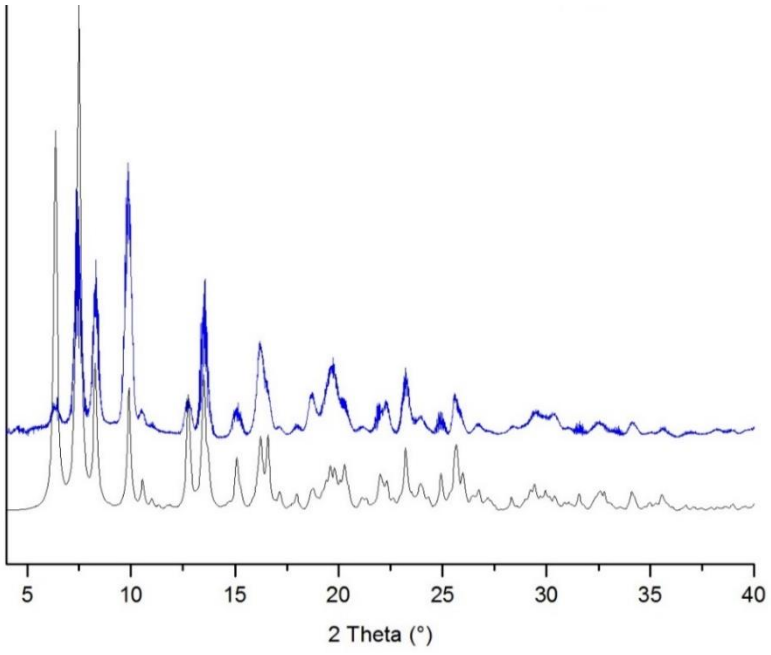

Figure 3.31. PXRD comparison of the model pattern (Black) vs PCM-9 (**22**) bulk pattern (Blue).

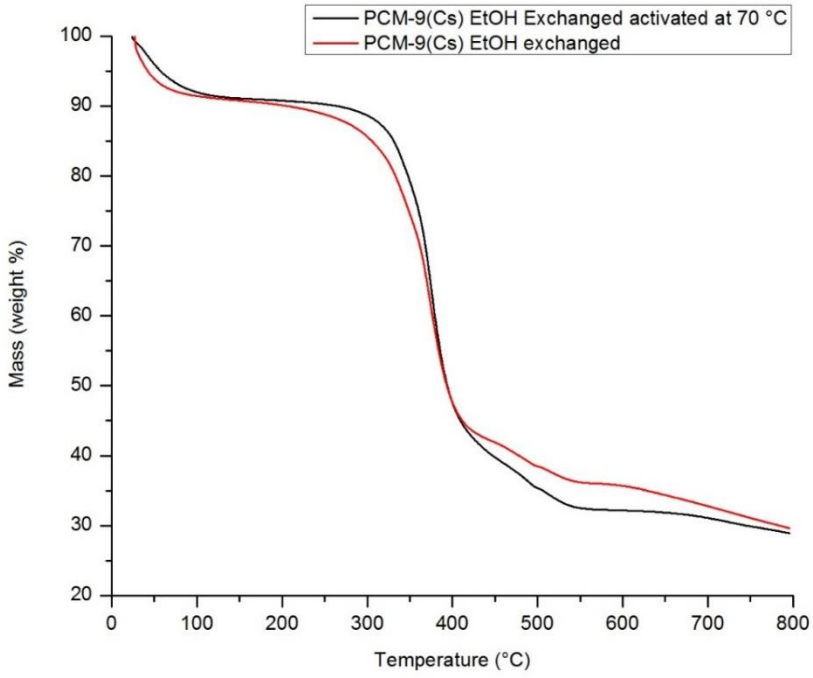

Figure 3.32. TGA of *pre*-activated (red) and *post*-activated (Black) PCM-9 (**22**).

REFERENCES

1. Cooper, E. R.; Andrews, C. D.; Wheatley, P. S.; Webb, P. B.; Wormald, P.; Morris, R. E. *Nature* **2004**, *430* (7003), 1012–1016.
2. Beck, J. S.; Vartuli, J. C.; Kennedy, G. J.; Kresge, C. T.; Roth, W. J.; Schramm, S. E. *Chem. Mater.* **1994**, *6* (10), 1816–1821.
3. Parnham, E. R.; Morris, R. E. *Acc. Chem. Res.* **2007**, *40* (10), 1005–1013.
4. Fang, Q.; Zhu, G.; Xue, M.; Wang, Z.; Sun, J.; Qiu, S. *Cryst. Growth Des.* **2008**, *8* (1), 319–329.
5. Schaate, A.; Klingelhöfer, S.; Behrens, P.; Wiebcke, M. *Cryst. Growth Des.* **2008**, *8* (9), 3200–3205.
6. Ding, R.; Huang, C.; Lu, J.; Wang, J.; Song, C.; Wu, J.; Hou, H.; Fan, Y. *Inorg. Chem.* **2015**, *54* (4), 1405–1413.

7. Tian, Y.-Q.; Zhao, Y.-M.; Chen, Z.-X.; Zhang, G.-N.; Weng, L.-H.; Zhao, D.-Y. *Chem. Eur. J.* **2007**, *13* (15), 4146–4154.
8. Jackson, S. L.; Rananaware, A.; Rix, C.; Bhosale, S. V.; Latham, K. *RSC Adv.* **2015**, *5* (102), 84134–84141.
9. Liu, Y.; Kravtsov, V. C.; Eddaoudi, M. *Angew. Chem., Int. Ed.,* **2008**, *47* (44), 8446–8449.
10. Plabst, M.; Köhn, R.; Bein, T. *CrystEngComm* **2010**, *12* (6), 1920–1926.
11. Emsley, J. Nature's Building Blocks: An A-Z Guide to the Elements; OUP Oxford, 2011.
12. Gaffney, T. R. *Current Opinion in Solid State and Materials Science* **1996**, *1* (1), 69–75.
13. Sava Gallis, D. F.; Parkes, M. V.; Greathouse, J. A.; Zhang, X.; Nenoff, T. M. *Chem. Mater.* **2015**, *27* (6), 2018–2025.
14. Murray, L. J.; Dinca, M.; Yano, J.; Chavan, S.; Bordiga, S.; Brown, C. M.; Long, J. R. *J. Am. Chem. Soc.* **2010**, *132* (23), 7856–7857.
15. Southon, P. D.; Price, D. J.; Nielsen, P. K.; McKenzie, C. J.; Kepert, C. J. *J. Am. Chem. Soc.* **2011**, *133* (28), 10885–10891.
16. Parkes, M. V.; Greathouse, J. A.; Hart, D. B.; Gallis, D. F. S.; Nenoff, T. M. *Phys. Chem. Chem. Phys.* **2016**, *18* (16), 11528–11538.
17. Verma, P.; Maurice, R.; Truhlar, D. G. *J. Phys. Chem. C* **2015**, *119* (51), 28499–28511.
18. Wang, C.; Liu, D.; Lin, W. *J. Am. Chem. Soc.* **2013**, *135* (36), 13222–13234.
19. Du, M.; Jiang, X.-J.; Zhao, X.-J. *Inorg. Chem.* **2007**, *46* (10), 3984–3995.
20. Chevreau, H.; Devic, T.; Salles, F.; Maurin, G.; Stock, N.; Serre, C. *Angew. Chem. Int. Ed.* **2013**, *52* (19), 5056–5060.
21. Choi, H. J.; Suh, M. P. *J. Am. Chem. Soc.* **2004**, *126* (48), 15844–15851.

22. Lee, C. Y.; Farha, O. K.; Hong, B. J.; Sarjeant, A. A.; Nguyen, S. T.; Hupp, J. T. *J. Am. Chem. Soc.* **2011**, *133* (40), 15858–15861.

23. Natarajan, S.; Mahata, P. *Chem. Soc. Rev.* **2009**, *38* (8), 2304–2318.

24. Du, P.-Y.; Gu, W.; Liu, X. *Inorg. Chem.* **2016**, *55* (16), 7826–7828.

25. Taylor, K. M. L.; Jin, A.; Lin, W. *Angew. Chem., Int. Ed.* **2008**, *47* (40), 7722–7725.

26. Volkringer, C.; Henry, N.; Grandjean, S.; Loiseau, T. *J. Am. Chem. Soc.* **2012**, *134* (2), 1275–1283.

27. Ibarra, I. A.; Tan, K. E.; Lynch, V. M.; Humphrey, S. M., *Dalton Trans.* **2012**, *41* (14), 3920–3923.

28. Thallapally, P. K.; Tian, J.; Radha Kishan, M.; Fernandez, C. A.; Dalgarno, S. J.; McGrail, P. B.; Warren, J. E.; Atwood, J. L. *J. Am. Chem. Soc.* **2008**, *130* (50), 16842–16843.

29. Liang, L.-L.; Ren, S.-B.; Zhang, J.; Li, Y.-Z.; Du, H.-B.; You, X.-Z. *Dalton Trans.* **2010**, *39* (33), 7723.

30. Hoskins, B. F.; Robson, R. *J. Am. Chem. Soc.* **1989**, *111* (15), 5962–5964.

31. Li, Y.; Xue, M.; Guo, L.; Huang, L.; Chen, S.; Qiu, S. *Inorg. Chem. Commun.* **2013**, *28*, 25–30.

32. Dincă, M.; Dailly, A.; Long, J. R. *Chem. Eur. J.* **2008**, *14* (33), 10280–10285.

33. Nuñez, A. J.; Chang, M. S.; Ibarra, I. A.; Humphrey, S. M. *Inorg. Chem.* **2014**, *53* (1), 282–288.

34. Kaltsoyannis, N. *J. Chem. Soc., Dalton Trans.* **1997**, No. 1, 1–12.

35. Norby, P.; Fjellvåg, H. *Zeolites* **1992**, *12* (8), 898–908.

36. Kuznetsov, D. A.; Fedyanin, I. V.; Komarova, N. S.; Shilov, G. V.; Martynenko, V. M.; Vasilev, S. G.; Krivenko, A. G.; Lyssenko, K. A.; Bazhenova, T. A. *Eur. J. Inorg. Chem.* **2015** (*4*), 715–724.

37. Hausdorf, S.; Baitalow, F.; Böhle, T.; Rafaja, D.; Mertens, F. O. R. L. *J. Am. Chem. Soc.* **2010**, *132* (32), 10978–10981.
38. Liu, B.; Shioyama, H.; Akita, T.; Xu, Q. *J. Am. Chem. Soc.* **2008**, *130* (16), 5390–5391.
39. Chen, B.; Wang, X.; Zhang, Q.; Xi, X.; Cai, J.; Qi, H.; Shi, S.; Wang, J.; Yuan, D.; Fang, M. *J. Mater. Chem.* **2010**, *20* (18), 3758–3767.
40. Ibarra, I. A.; Yoon, J. W.; Chang, J.-S.; Lee, S. K.; Lynch, V. M.; Humphrey, S. M. *Inorg. Chem.* **2012**, *51* (22), 12242–12247.
41. Yang, C.; Wang, X.; Omary, M. A. *J. Am. Chem. Soc.* **2007**, *129* (50), 15454–15455.
42. Park, H. J.; Suh, M. P. *Chem. Commun.* **2010**, *46* (4), 610–612.
43. Tsivion, E.; Long, J. R.; Head-Gordon, M. *J. Am. Chem. Soc.* **2014**, *136* (51),
44. 17827–17835.
45. Barman, S.; Khutia, A.; Koitz, R.; Blacque, O.; Furukawa, H.; Iannuzzi, M.; Yaghi, O. M.; Janiak, C.; Hutter, J.; Berke, H. *J. Mater. Chem. A* **2014**, *2*, 18823–18830.
46. Myers, A. L.; Prausnitz, J. M. *AIChE* **1965**, *11* (1), 121–127.

Chapter 4: Exploration of PCPs for applications in magnetism

Two novel, isostructural phosphine coordination materials were synthesized and investigated with interest in magnetism. These materials, designated Ln-PCM-21, were created through the reaction of either a praseodymium (Pr) or neodymium (Nd) precursor along with the linker *tris*(4-carboxyphenyl)methyl phosphonium chloride ($[mptbcH_3]^+$ Cl^-). The deprotonated version of the linker, $mptbc^{2-}$, allows for access to unique metal-to-linker crystallographic ratios not yet explored within phosphine coordination materials. Both materials Ln-PCM-21 (Ln = Pr or Nd) (**23**, **24**) were found to be cationic and contain unusual Ln-O-Ln bridged clusters. After careful characterization, magnetic susceptibility data for both analogues was collects and compared to three different models based off of varying approaches.[1] The work encompassed in this chapter was published in 2014 in the Journal of Inorganic Chemistry.[a]

INTRODUCTION

Incorporation of rare earth metals into porous materials allows for access to an incredible array of capabilities not accessible by transition metals. Lanthanide-based porous coordination polymers (Ln-PCPs) have become of great interest in recent years due to their magnetic properties, thermal stability, and their advantageous high emission quantum yields.[2-6] Furthermore, a wide range of coordination numbers are accessible by lanthanides, resulting in a great array of framework topologies. The coordination number and geometry can be largely influenced by linker chemistry, making these materials highly

[a] Waggoner, Nolan. W. (Primary Author); Saccoccia, Beau (Primary Undergraduate/Key Scientific Contributor); Ibarra, Illich. A. (Gas Sorption Analysis); Lynch, Vincent. M. (X-Ray Crystallography); Wood, Paul. T. (Magnetic Modelling Calculations); Humphrey, Simon. M. (Primary Advisor) *Inorg. Chem.* **2014**, *53* (24), 12674–12676.

adaptable.[7] However, regardless of this growing interest in Ln-PCPs, they still remain less common in the literature than traditional transition metal porous materials.[8,9]

Recently, the exploration of magnetic materials has been a rapidly expanding field, with focus being drawn towards novel single-molecule magnets (SMMs) and single-chain magnets (SCMs).[10-14] These materials, also known as molecular nanomagnets, are inorganic compounds that demonstrate superparamagnetic behavior at relatively low temperatures, referred to as blocking temperatures.[15,16] The utility of an ideal SMM comes from both a high level of magnetic anisotropy and a low level of communication between individual molecules. Magnetic anisotropy can be increased by a high spin ground state as well as a high level of zero-field splitting.[17] If this localized magnetic ability can be accessed at ambient temperatures (as opposed to cryogenic temperatures), huge applications including high-density information storage, spintronics, and quantum computing could be further explored.[18] To deter molecules or clusters from influencing one another, they are typically placed in a regular fashion onto a substrate or incorporated into a polymeric material in a fashion that minimizes communication between centers to prevent magnetic relaxation. In order for a material or structure to function as molecular nanomagnet, it must contain or include isolated molecules or clusters that demonstrate slow relaxation of magnetization and a B-H hysteresis loop.[19,20]

Interest in lanthanide based magnetism has recently grown significantly, primarily due to the expected differences in behavior in relation to traditional transition metal complexes. Use of lanthanide rare-earth metals allows for access to higher possible quantum numbers and the lack of covalency minimizes ligand field effects in polymerized systems. Due to the latter, ligand bonding does not quench the orbital contribution to the magnetic moment. These two factors can be combined for lanthanide clusters in Ln-PCPs to allow for a greater possible magnetization to become accessible.[21] Furthermore, the level

of magnetism can be hugely influenced by the number of lanthanide centers per cluster and nodal symmetry as well. Inclusion of odd numbered clustering allows for induced spin frustration, maximizing the possibility of magnetism. Subsequently, higher levels of symmetry of the net Ln-node leads to more degenerate energy levels, resulting in fewer magnetic quenching pathways.

Within the literature, there is a growing amount of examples that explore the magnetic properties arising within Ln-PCPs. For dimer clusters, A. Bhunia *et al.* showed a series of salen based PCPs that employed lanthanide dimers in 1-D chains that were studied for their magnetic properties in 2011.[22] In another example Zhang and coworkers demonstrated in 2012 the magnetic ability of a variety of lanthanides in a paddlewheel orientation with the use of the linker 5-(4-carboxy-2-nitrophenoxy)isophthalic acid.[23] Examples of larger clustering are numerous in the literature as well,[24-26] including the work done by A. K. Jami *et al.* in 2013, which demonstrated the use of a Dy_4 hydroxo cluster that displayed slow relaxation.[27] A series of Ln_7 based clusters were investigated by Yang and coworkers in 2013 for their net magnetic behavior.[28] However, to the best of our knowledge, there is only one example to date in the literature of a linear Ln_3 cluster. Thompson and coworkers published a molecular Dy_3 species in 2012 that demonstrated SMM behavior with the utilization of a tritopic pyridine *bis*(hydrazine) ligand scaffold to stabilize the cluster.[29]

In this study a set of two isostructural materials, Ln-PCM-21, were isolated through our continued interest in the assembly of lanthanide based phosphine coordination materials (Ln-PCMs) for applications in sensing. However, these frameworks demonstrate perfectly linear $[Ln_3]^{9+}$ trimers for both Pr^{3+} ad Nd^{3+}, being brought together by the ligand $[Me\text{-}P(\text{-}C_6H_4\text{-}p\text{-}CO_2H)_3]^+Cl^-$ ($[mptbcH_3]Cl$); making them ideal candidates for interest in magnetism. Further isostructural materials were attempted with other Ln^{3+} nitrate

precursors, though no other crystalline products were yielded; this suggested that formation of Ln-PCM-21 was highly sensitive to Ln^{3+} ionic size. As seen in the case of PCM's 6−9 in chapter 3, the [mptbcH$_3$]Cl linker allows for incorporation a pseudo-tetrahedral geometry into the framework and its fully deprotonated charge of −2 ($mptbc^{2-}$) can promote uncommon PCM crystallographic metal-to-ligand ratios.

RESULTS AND DISCUSSION

Ln-PCM-21 synthesis and structure analysis

The [mptbcH$_3$]$^+$Cl$^-$ ligand, created upon reaction of its respective lithium salt with MeI and aqueous acidic workup, was reacted with 2.55 molar equivalents of Ln(NO$_3$)$_2$ metal salt in a solution of *N*,*N*-dimethylformamide, water, acetonitrile (3:2:2). This solution was heated at 85 °C for 5 days, providing moderate yields of crystalline colorless rods (Scheme 4.1).

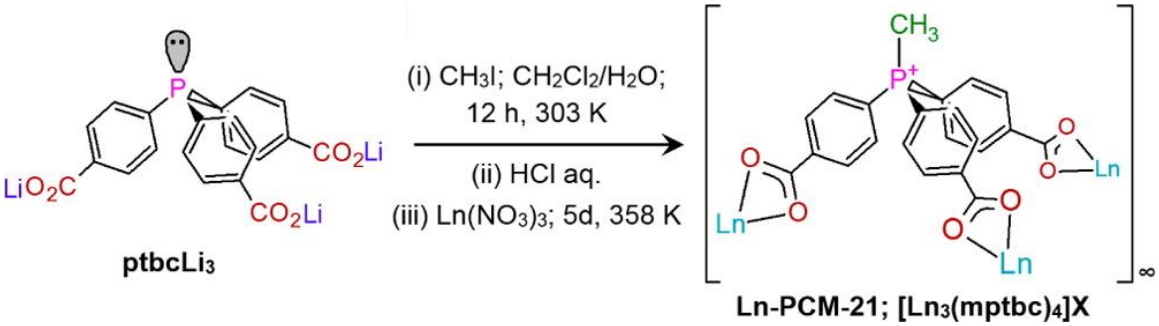

Scheme 4.1. Preparation of the phosphonium chloride linker and synthesis of Ln-PCM-21.

Upon X-ray structural analysis, both the Pr-PCM-21 (**23**) and Nd-PCM-21 (**24**) frameworks resulted in the formula unit [Ln$_3$(mptbc)$_4$]X·solvent, where the cationic frameworks are countered by a 1:1 mixture of Cl$^-$ and NO$_3^-$ anions confirmed by ICP-MS,

elemental analysis, and TGA. Due to the isostructural nature of these materials, all structural details discussed below can be assumed applicable in both cases. Single X-ray diffraction of Ln-PCM-21 revealed that it crystallized in the rhombohedral $R\bar{3}c$ space group, with two crystallographically distinct methyl-phosphonium ligands and Ln^{3+} sites present in the asymmetric unit (Figure 4.1a). The carboxylate groups acted as the oxide source in the development of Ln-O-Ln bridges, with additional bridging occurring between Ln1 and Ln2 centers. In the crystal structure, $mptbc^{2-}$ was found to be nearly perfectly tetrahedral at the P atom, with bonds showing little to no flexing with angles of 108.6(2) and 109.1(3)°. The expanded polymer in Ln-PCM-21 had Ln_2P_2 rings seen in the asymmetric unit, fused to adjacent Ln_2P_2 rings by perfectly linear $[Ln_3]^{9+}$ clusters at opposite corners (Figure 4.1b,c).

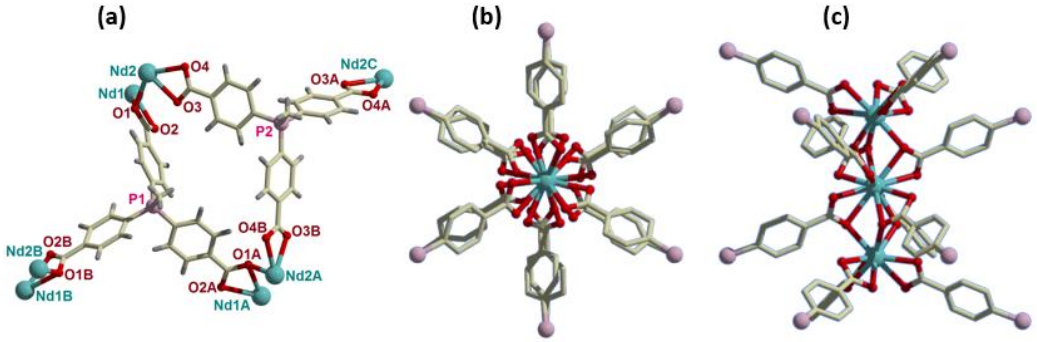

Figure 4.1. Asymmetric unit of Nd-PCM-21 (**24**) (a); Side-on projection of $[Ln_3]^{9+}$ cluster complex with P atoms (purple) drawn with cutoff bonds to the other three substituents (b); front view of same $[Ln_3]^{9+}$ cluster along the Nd2-Nd1-Nd2 axis (c).

Each Ln_3 cluster contains a central Nd1 atom that is chelated by 6-carboxylate groups, resulting in 6-fold symmetry and a 12-coordinate icosahedron (Figure 4.2a). Completing the trimer cluster, two 9-coordinate Nd2 sites are bridged to Nd1 with three carboxylate

oxides on each side (Figure 4.2b); the Nd1-O distances ranged from 2.447(5) −2.685(5) Å. These Nd2 sites demonstrate monocapped square-antiprismatic coordination geometry, with a Nd1-Nd2 internuclear distance of 3.911(5) Å.

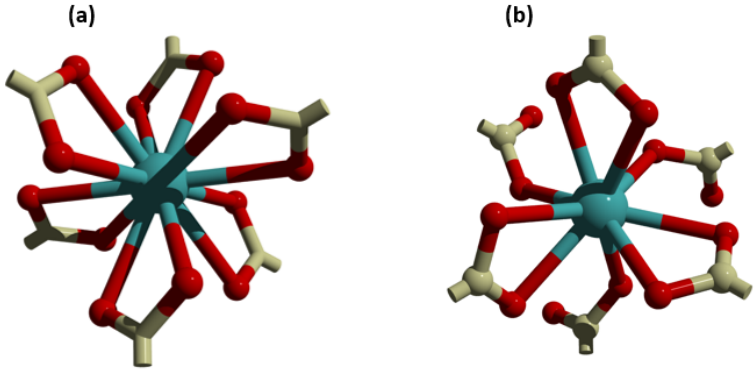

Figure 4.2. Coordination geometry of the 12-coordinate Nd1 site (a); coordination geometry of the 9-coordinate Nd2 sites.

The extended structure of Ln-PCM-21 demonstrated 2-D bilayer sheets, with six uniquely oriented sheets allowing for an oddly long c-axis (1.4.37(3) Å; Figure 4.3). Due to the layered format of the material, this led to the modest BET internal surface areas (0.05−0.30 atm) of 121 M^2/g and 132 M^2/g for Pr and Nd respectively.

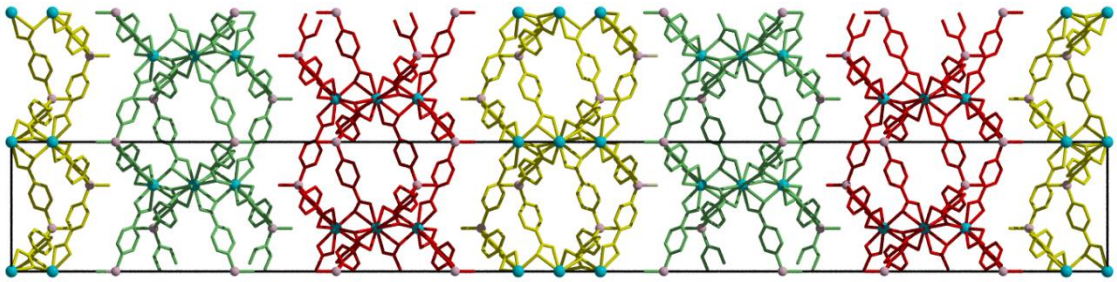

Figure 4.3. Nd-PCM-21 (**23**) extended framework structure along the c-axis with the six unique layer orientations.

Ln-PCM-21 magnetism

Experimental magnetic susceptibility

The field-cooled magnetic susceptibility of both Pr-PCM-21 and Nd-PCM-21 were investigated, with an external field of 100 Oe from 5−300 K. The linear high-temperature data was fitted to the Curie-Weiss law (Equation 4.1), where magnetic susceptibility (χ) is equal to the Curie constant (*C*) over absolute temperature minus the Curie temperature ($T-T_c$). When $T >> T_c$, the Curie Weiss law is slightly altered, with the Weiss constant (θ) replacing the latter T_c term to distinguish the difference between the two terms; this allowed for Weiss constants to be calculated (Figure 4.4 and 4.5 respectively).

$$\chi = \frac{C}{T - Tc} \qquad (4.1)$$

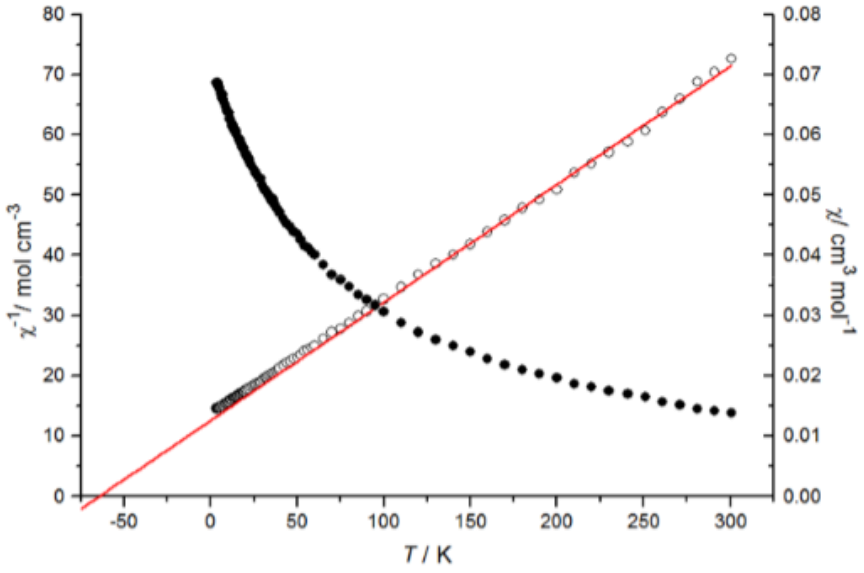

Figure 4.4. Plot of χ_m versus T (left axis) and χ_m^{-1} versus T for (**23**) Pr-PCM-21; *C* = 5.10(6) cm^3 /mol · K; θ = −64(3) K.

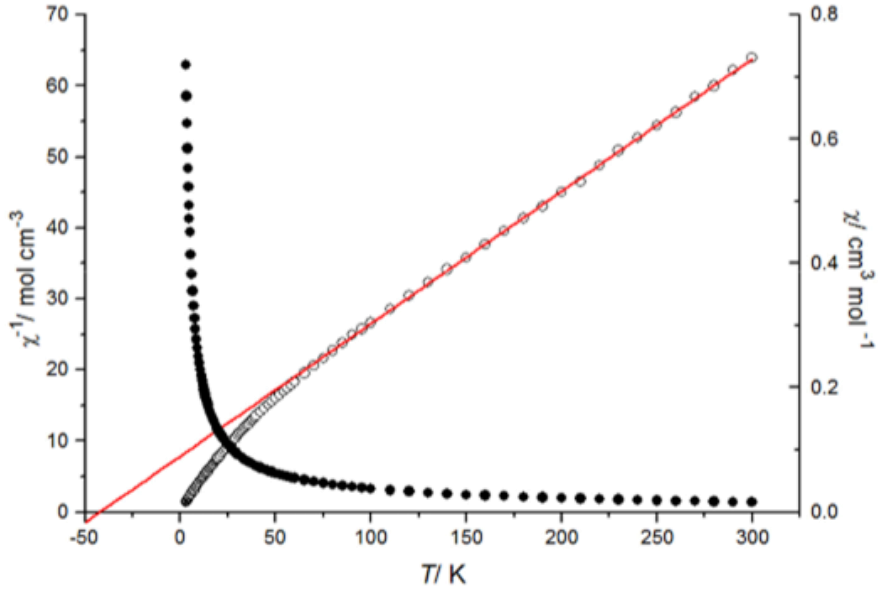

Figure 4.5. Plot of χ_m versus T (left axis) and χ_m^{-1} versus T for Nd-PCM-21 (**24**); C = 5.36(2) cm^3 /mol · K; θ = −42(1) K.

The materials created from Pr^{3+} and Nd^{3+} provided Weiss constants of −64(3) and −42(1) K respectively. The plots of $\chi_m T$ versus T for both materials were consistent with a negative Weiss constant value, and the high temperature values showed consistency as well. A negative Weiss constant is indicative of antiferrimagnetic interactions occurring within the material. That is, at lower temperatures the materials Ln-PCM-21 demonstrated opposing magnetic moments, with some of those moments being unequal resulting in continue spontaneous magnetism.

Magnetic susceptibility models

In order to begin modelling, a simplified perspective of the each trimer was considered (Figure 4.6). In order to understand the materials Ln-PCM-21 deviating from pure Curie law behavior the following explanations were considered; thermal population

of excited states within the ^3H and ^4I energy states, exchange interactions occurring between neighboring ions, and zero-field splitting (ZFS) with consideration of the J = 4 and $^9/_2$ into m_J states for Pr and Nd respectively.

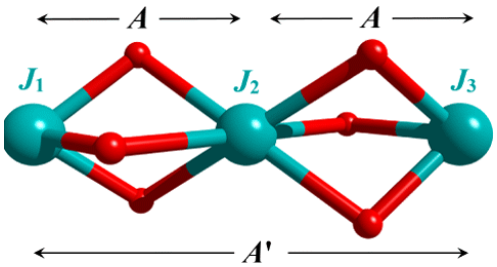

Figure 4.6. Simplified $[Ln_3]^{9+}$ cluster magnetic model and coupling constants for Ln-PCM-21.

In the case of these frameworks, thermal population was the least likely occurrence. This is due to population of even the lowest energies for each material becoming highly unlikely, with first-excited-state energy gaps of 400 cm^{-1} and 450 cm^{-1} resulting from spin-orbit coupling constants (λ) of 400 cm^{-1} and 350 cm^{-1} for Pr^{3+} and Nd^{3+} respectively. Furthermore, thermal population of excited *J* states results in a general increase in magnetization as well as a positive Weiss constant. Therefore, thermal population was ruled out as a possibility within the frameworks Ln-PCM-21. From the remaining two possible interactions, three modelling viewpoints were taken into consideration; superexchange, zero-field splitting (ZFS), and ZFS with the addition of a mean-field-theory term.

For the first model considered, it was assumed that superexchange between neighboring ions across oxide bridges within a cluster was the only important factor. Traditionally, superexchange occurs between two cationic species through a non-magnetic anion bridge allowing for interaction of present spin states, as was first described by H. A.

Kramers in 1934.[30] However, lanthanide species such as those present in clusters within Ln-PCM-21, demonstrate highly ionic binding characteristics.[31] With such little covalency present within the clusters, this traditional approach to spin state interactions becomes far less important. Instead, primary consideration was given to the interaction of the *J*-states present for each lanthanide species, which allowed for interactions through space instead of directly through the oxide bridge bonds. This was mathematically accomplished through the use of the isotropic spin Hamiltonian (equation 4.2), where *A* was equal to the coupling constant and the *J* states were considered instead of spin-states; this along with Kambé vector coupling was used to calculate all possible *J*-state interactions (Equation 4.3), with N_{Av} = avogadro's constant, *g* = gyromagnetic ratio, β = bohr magneton, K_B = boltzman's constant, and T = temperature.

$$E = -A[J_T(J_T+1) - J^+(J^++1) - J_2(J_2+1)]; J_T = J^+ + J_2 \; and \; J^+ = J_1 + J_3 \quad (4.2)$$

$$\chi T = \left(\frac{N_{Av}\cdot g^2\cdot \beta^2}{3k_B}\right)\cdot\left[\frac{\left\{\sum J_T(J_T+1)(2J+1)e^{\left(-\frac{A}{k_BT}\right)}\right\}}{\left\{\sum(2J_T+1)e^{\left(-\frac{A}{k_BT}\right)}\right\}}\right] \quad (4.3)$$

Through the use of the gyromagnetic ratio (Equation 4.4), the *g* value for both Pr^{3+} and Nd^{3+} were calculated (Equations 4.5).

$$g = \frac{3}{2}\cdot\left\{\frac{S(S+1)-L(L+1)}{2J(J+1)}\right\} \quad (4.4)$$

$$g_{^3H_4}^{Pr^{3+}} = \frac{3}{2} + \left\{\frac{(1\cdot2)-(5\cdot6)}{2\cdot4\cdot5}\right\} = 0.800 \qquad g_{^3H_4}^{Nd^{3+}} = \frac{3}{2} + \left\{\frac{(3/2\cdot5/2)-(6\cdot7)}{2\cdot9/12\cdot11/2}\right\} = 0.727$$

(4.5)

With the employment of these expressions in mind, the overall expressions for the magnetic susceptibility of each material due to superexchange were then calculated (equations 4.6 and 4.7)

$$\chi T_{mol}^{Pr^{3+}} = 0.080 \cdot \left[\frac{\left\{ \begin{array}{c} \sum 3900\, e^{\left(\frac{64A}{k_B T}\right)} + 3036\, e^{\left(\frac{40A}{k_B T}\right)} + 2310\, e^{\left(\frac{18A}{k_B T}\right)} + 1710\, e^{\left(\frac{-2A}{k_B T}\right)} + 1224\, e^{\left(\frac{-20A}{k_B T}\right)} \\ +840\, e^{\left(\frac{-36A}{k_B T}\right)} + 546\, e^{\left(\frac{-50A}{k_B T}\right)} + 330\, e^{\left(\frac{-62A}{k_B T}\right)} + 180\, e^{\left(\frac{-72A}{k_B T}\right)} + 3036\, e^{\left(\frac{56A}{k_B T}\right)} \\ +2310\, e^{\left(\frac{34A}{k_B T}\right)} + 1710\, e^{\left(\frac{14A}{k_B T}\right)} + 1224\, e^{\left(\frac{-4A}{k_B T}\right)} + 840\, e^{\left(\frac{-20A}{k_B T}\right)} + 546\, e^{\left(\frac{-34A}{k_B T}\right)} \\ +330\, e^{\left(\frac{-46A}{k_B T}\right)} + 180\, e^{\left(\frac{-56A}{k_B T}\right)} + 84\, e^{\left(\frac{-64A}{k_B T}\right)} + 2310\, e^{\left(\frac{48A}{k_B T}\right)} + 1710\, e^{\left(\frac{28A}{k_B T}\right)} \\ +1224\, e^{\left(\frac{10A}{k_B T}\right)} + 840\, e^{\left(\frac{-6A}{k_B T}\right)} + 546\, e^{\left(\frac{-20A}{k_B T}\right)} + 330\, e^{\left(\frac{-32A}{k_B T}\right)} + 180\, e^{\left(\frac{-42A}{k_B T}\right)} \\ +84\, e^{\left(\frac{-50A}{k_B T}\right)} + 30\, e^{\left(\frac{-56A}{k_B T}\right)} + 1710\, e^{\left(\frac{40A}{k_B T}\right)} + 1124\, e^{\left(\frac{22A}{k_B T}\right)} + 840\, e^{\left(\frac{6A}{k_B T}\right)} \\ +546\, e^{\left(\frac{-8A}{k_B T}\right)} + 330\, e^{\left(\frac{-20A}{k_B T}\right)} + 180\, e^{\left(\frac{-30A}{k_B T}\right)} + 84\, e^{\left(\frac{-38A}{k_B T}\right)} + 30\, e^{\left(\frac{-44A}{k_B T}\right)} \\ +6\, e^{\left(\frac{-48A}{k_B T}\right)} + 1224\, e^{\left(\frac{32A}{k_B T}\right)} + 840\, e^{\left(\frac{16A}{k_B T}\right)} + 546\, e^{\left(\frac{2A}{k_B T}\right)} + 330\, e^{\left(\frac{-10A}{k_B T}\right)} \\ +180\, e^{\left(\frac{-20A}{k_B T}\right)} + 84\, e^{\left(\frac{-28A}{k_B T}\right)} + 30\, e^{\left(\frac{-34A}{k_B T}\right)} + 6\, e^{\left(\frac{-38A}{k_B T}\right)} + 840\, e^{\left(\frac{24A}{k_B T}\right)} \\ +546\, e^{\left(\frac{10A}{k_B T}\right)} + 330\, e^{\left(\frac{-2A}{k_B T}\right)} + 180\, e^{\left(\frac{-12A}{k_B T}\right)} + 84\, e^{\left(\frac{-20A}{k_B T}\right)} + 30\, e^{\left(\frac{-26A}{k_B T}\right)} \\ +6\, e^{\left(\frac{-30A}{k_B T}\right)} + 546\, e^{\left(\frac{16A}{k_B T}\right)} + 330\, e^{\left(\frac{4A}{k_B T}\right)} + 180\, e^{\left(\frac{-6A}{k_B T}\right)} + 84\, e^{\left(\frac{-14A}{k_B T}\right)} \\ +30\, e^{\left(\frac{-20A}{k_B T}\right)} + 330\, e^{\left(\frac{8A}{k_B T}\right)} + 180\, e^{\left(\frac{-2A}{k_B T}\right)} + 84\, e^{\left(\frac{-10A}{k_B T}\right)} + 180 \end{array} \right\}}{\left\{ \begin{array}{c} \sum 25\, e^{\left(\frac{64A}{k_B T}\right)} + 23\, e^{\left(\frac{40A}{k_B T}\right)} + 21\, e^{\left(\frac{18A}{k_B T}\right)} + 19\, e^{\left(\frac{-2A}{k_B T}\right)} + 17\, e^{\left(\frac{-20A}{k_B T}\right)} \\ +15\, e^{\left(\frac{-36A}{k_B T}\right)} + 13\, e^{\left(\frac{-50A}{k_B T}\right)} + 11\, e^{\left(\frac{-62A}{k_B T}\right)} + 9\, e^{\left(\frac{-72A}{k_B T}\right)} + 23\, e^{\left(\frac{56A}{k_B T}\right)} \\ +21\, e^{\left(\frac{34A}{k_B T}\right)} + 19\, e^{\left(\frac{14A}{k_B T}\right)} + 17\, e^{\left(\frac{-4A}{k_B T}\right)} + 15\, e^{\left(\frac{-20A}{k_B T}\right)} + 13\, e^{\left(\frac{-34A}{k_B T}\right)} \\ +11\, e^{\left(\frac{-46A}{k_B T}\right)} + 9\, e^{\left(\frac{-56A}{k_B T}\right)} + 7\, e^{\left(\frac{-64A}{k_B T}\right)} + 21\, e^{\left(\frac{48A}{k_B T}\right)} + 19\, e^{\left(\frac{28A}{k_B T}\right)} \\ +17\, e^{\left(\frac{10A}{k_B T}\right)} + 15\, e^{\left(\frac{-6A}{k_B T}\right)} + 13\, e^{\left(\frac{-20A}{k_B T}\right)} + 11\, e^{\left(\frac{-32A}{k_B T}\right)} + 9\, e^{\left(\frac{-42A}{k_B T}\right)} \\ +7\, e^{\left(\frac{-50A}{k_B T}\right)} + 5\, e^{\left(\frac{-56A}{k_B T}\right)} + 19\, e^{\left(\frac{40A}{k_B T}\right)} + 17\, e^{\left(\frac{22A}{k_B T}\right)} + 15\, e^{\left(\frac{6A}{k_B T}\right)} \\ +13\, e^{\left(\frac{-8A}{k_B T}\right)} + 11\, e^{\left(\frac{-20A}{k_B T}\right)} + 9\, e^{\left(\frac{-30A}{k_B T}\right)} + 7\, e^{\left(\frac{-38A}{k_B T}\right)} + 5\, e^{\left(\frac{-44A}{k_B T}\right)} \\ +3\, e^{\left(\frac{-48A}{k_B T}\right)} + 17\, e^{\left(\frac{32A}{k_B T}\right)} + 15\, e^{\left(\frac{16A}{k_B T}\right)} + 13\, e^{\left(\frac{2A}{k_B T}\right)} + 11\, e^{\left(\frac{-10A}{k_B T}\right)} \\ +9\, e^{\left(\frac{-20A}{k_B T}\right)} + 7\, e^{\left(\frac{-28A}{k_B T}\right)} + 5\, e^{\left(\frac{-34A}{k_B T}\right)} + 3\, e^{\left(\frac{-38A}{k_B T}\right)} + 1\, e^{\left(\frac{-40A}{k_B T}\right)} \\ +15\, e^{\left(\frac{24A}{k_B T}\right)} + 13\, e^{\left(\frac{10A}{k_B T}\right)} + 11\, e^{\left(\frac{-2A}{k_B T}\right)} + 9\, e^{\left(\frac{-12A}{k_B T}\right)} + 7\, e^{\left(\frac{-20A}{k_B T}\right)} \\ +5\, e^{\left(\frac{-26A}{k_B T}\right)} + 3\, e^{\left(\frac{-30A}{k_B T}\right)} + 13\, e^{\left(\frac{16A}{k_B T}\right)} + 11\, e^{\left(\frac{4A}{k_B T}\right)} + 9\, e^{\left(\frac{-6A}{k_B T}\right)} \\ +7\, e^{\left(\frac{-4A}{k_B T}\right)} + 5\, e^{\left(\frac{-20A}{k_B T}\right)} + 11\, e^{\left(\frac{8A}{k_B T}\right)} + 9\, e^{\left(\frac{-2A}{k_B T}\right)} + 7\, e^{\left(\frac{-10A}{k_B T}\right)} + 9 \end{array} \right\}} \right]$$

(4.6)

$$\chi T_{mol}^{Nd^{3+}} = 0.066 \cdot \frac{\left\{\begin{array}{c} \sum 5481\ e^{\left(\frac{81A}{k_BT}\right)} + 4387.5\, e^{\left(\frac{54A}{k_BT}\right)} + 3450\, e^{\left(\frac{29A}{k_BT}\right)} + 2656.5\, e^{\left(\frac{6A}{k_BT}\right)} + 1995\, e^{\left(\frac{-15A}{k_BT}\right)} \\ +1453.5\, e^{\left(\frac{-34A}{k_BT}\right)} + 1020\, e^{\left(\frac{-51A}{k_BT}\right)} + 682.5\, e^{\left(\frac{-66A}{k_BT}\right)} + 429\, e^{\left(\frac{-79A}{k_BT}\right)} + 247.5\, e^{\left(\frac{-90A}{k_BT}\right)} \\ +4387.5\, e^{\left(\frac{72A}{k_BT}\right)} + 3450\, e^{\left(\frac{47A}{k_BT}\right)} + 2656.5\, e^{\left(\frac{24A}{k_BT}\right)} + 1995\, e^{\left(\frac{3A}{k_BT}\right)} + 1453.5\, e^{\left(\frac{-16A}{k_BT}\right)} \\ +1020\, e^{\left(\frac{-33A}{k_BT}\right)} + 682.5\, e^{\left(\frac{-48A}{k_BT}\right)} + 429\, e^{\left(\frac{-61A}{k_BT}\right)} + 247.5\, e^{\left(\frac{-72A}{k_BT}\right)} + 126\, e^{\left(\frac{-81A}{k_BT}\right)} \\ +3450\, e^{\left(\frac{63A}{k_BT}\right)} + 2656.5\, e^{\left(\frac{40A}{k_BT}\right)} + 1995\, e^{\left(\frac{19A}{k_BT}\right)} + 1453.5\, e^{\left(\frac{0A}{k_BT}\right)} + 1020\, e^{\left(\frac{-17A}{k_BT}\right)} \\ +682.5\, e^{\left(\frac{-32A}{k_BT}\right)} + 429\, e^{\left(\frac{-45A}{k_BT}\right)} + 247.5\, e^{\left(\frac{-56A}{k_BT}\right)} + 126\, e^{\left(\frac{-65A}{k_BT}\right)} + 52.5\, e^{\left(\frac{-72A}{k_BT}\right)} \\ +2656.5\, e^{\left(\frac{54A}{k_BT}\right)} + 1995\, e^{\left(\frac{33A}{k_BT}\right)} + 1453.5\, e^{\left(\frac{14A}{k_BT}\right)} + 1020\, e^{\left(\frac{-3A}{k_BT}\right)} + 682.5\, e^{\left(\frac{-18A}{k_BT}\right)} \\ +429\, e^{\left(\frac{-31A}{k_BT}\right)} + 247.5\, e^{\left(\frac{-42A}{k_BT}\right)} + 126\, e^{\left(\frac{-51A}{k_BT}\right)} + 52.5\, e^{\left(\frac{-58A}{k_BT}\right)} + 15\, e^{\left(\frac{-63A}{k_BT}\right)} \\ +1995\, e^{\left(\frac{45A}{k_BT}\right)} + 1453.5\, e^{\left(\frac{26A}{k_BT}\right)} + 1020\, e^{\left(\frac{9A}{k_BT}\right)} + 682.5\, e^{\left(\frac{-6A}{k_BT}\right)} + 429\, e^{\left(\frac{-19A}{k_BT}\right)} \\ +247.5\, e^{\left(\frac{-30A}{k_BT}\right)} + 126\, e^{\left(\frac{-39A}{k_BT}\right)} + 52.5\, e^{\left(\frac{-46A}{k_BT}\right)} + 15\, e^{\left(\frac{-51A}{k_BT}\right)} + 1.5\, e^{\left(\frac{-54A}{k_BT}\right)} \\ +1453.5\, e^{\left(\frac{36A}{k_BT}\right)} + 1020\, e^{\left(\frac{19A}{k_BT}\right)} + 682.5\, e^{\left(\frac{4A}{k_BT}\right)} + 429\, e^{\left(\frac{-9A}{k_BT}\right)} + 247.5\, e^{\left(\frac{-20A}{k_BT}\right)} \\ +126\, e^{\left(\frac{-29A}{k_BT}\right)} + 52.5\, e^{\left(\frac{-36A}{k_BT}\right)} + 15\, e^{\left(\frac{-41A}{k_BT}\right)} + 1.5\, e^{\left(\frac{-44A}{k_BT}\right)} + 1020\, e^{\left(\frac{27A}{k_BT}\right)} \\ +682.5\, e^{\left(\frac{12A}{k_BT}\right)} + 429\, e^{\left(\frac{-1A}{k_BT}\right)} + 247.5\, e^{\left(\frac{-12A}{k_BT}\right)} + 126\, e^{\left(\frac{-21A}{k_BT}\right)} + 52.5\, e^{\left(\frac{-28A}{k_BT}\right)} \\ +15\, e^{\left(\frac{-33A}{k_BT}\right)} + 682.5\, e^{\left(\frac{18A}{k_BT}\right)} + 429\, e^{\left(\frac{5A}{k_BT}\right)} + 247.5\, e^{\left(\frac{-6A}{k_BT}\right)} + 126\, e^{\left(\frac{-15A}{k_BT}\right)} \\ +52.5\, e^{\left(\frac{-22A}{k_BT}\right)} + 429\, e^{\left(\frac{9A}{k_BT}\right)} + 247.5\, e^{\left(\frac{-2A}{k_BT}\right)} + 157.5\, e^{\left(\frac{-11A}{k_BT}\right)} + 247.5 \end{array}\right\}}{\left\{\begin{array}{c} \sum 28\ e^{\left(\frac{81A}{k_BT}\right)} + 26\, e^{\left(\frac{54A}{k_BT}\right)} + 24\, e^{\left(\frac{29A}{k_BT}\right)} + 22\, e^{\left(\frac{6A}{k_BT}\right)} + 20\, e^{\left(\frac{-15A}{k_BT}\right)} \\ +18\, e^{\left(\frac{-34A}{k_BT}\right)} + 16\, e^{\left(\frac{-51A}{k_BT}\right)} + 14\, e^{\left(\frac{-66A}{k_BT}\right)} + 12\, e^{\left(\frac{-79A}{k_BT}\right)} + 10\, e^{\left(\frac{-90A}{k_BT}\right)} \\ +26\, e^{\left(\frac{72A}{k_BT}\right)} + 24\, e^{\left(\frac{47A}{k_BT}\right)} + 22\, e^{\left(\frac{24A}{k_BT}\right)} + 20\, e^{\left(\frac{3A}{k_BT}\right)} + 18\, e^{\left(\frac{-16A}{k_BT}\right)} \\ +16\, e^{\left(\frac{-33A}{k_BT}\right)} + 14\, e^{\left(\frac{-48A}{k_BT}\right)} + 12\, e^{\left(\frac{-61A}{k_BT}\right)} + 10\, e^{\left(\frac{-72A}{k_BT}\right)} + 8\, e^{\left(\frac{-81A}{k_BT}\right)} \\ +24\, e^{\left(\frac{63A}{k_BT}\right)} + 22\, e^{\left(\frac{40A}{k_BT}\right)} + 20\, e^{\left(\frac{19A}{k_BT}\right)} + 18\, e^{\left(\frac{0A}{k_BT}\right)} + 16\, e^{\left(\frac{-17A}{k_BT}\right)} \\ +14\, e^{\left(\frac{-32A}{k_BT}\right)} + 12\, e^{\left(\frac{-45A}{k_BT}\right)} + 10\, e^{\left(\frac{-56A}{k_BT}\right)} + 8\, e^{\left(\frac{-65A}{k_BT}\right)} + 6\, e^{\left(\frac{-72A}{k_BT}\right)} \\ +22\, e^{\left(\frac{54A}{k_BT}\right)} + 20\, e^{\left(\frac{33A}{k_BT}\right)} + 18\, e^{\left(\frac{14A}{k_BT}\right)} + 16\, e^{\left(\frac{-3A}{k_BT}\right)} + 14\, e^{\left(\frac{-18A}{k_BT}\right)} \\ +12\, e^{\left(\frac{-31A}{k_BT}\right)} + 10\, e^{\left(\frac{-42A}{k_BT}\right)} + 8\, e^{\left(\frac{-51A}{k_BT}\right)} + 6\, e^{\left(\frac{-58A}{k_BT}\right)} + 4\, e^{\left(\frac{-63A}{k_BT}\right)} \\ +20\, e^{\left(\frac{45A}{k_BT}\right)} + 18\, e^{\left(\frac{26A}{k_BT}\right)} + 16\, e^{\left(\frac{9A}{k_BT}\right)} + 14\, e^{\left(\frac{-6A}{k_BT}\right)} + 12\, e^{\left(\frac{-19A}{k_BT}\right)} \\ +10\, e^{\left(\frac{-30A}{k_BT}\right)} + 8\, e^{\left(\frac{-39A}{k_BT}\right)} + 6\, e^{\left(\frac{-46A}{k_BT}\right)} + 4\, e^{\left(\frac{-51A}{k_BT}\right)} + 2\, e^{\left(\frac{-54A}{k_BT}\right)} \\ +18\, e^{\left(\frac{36A}{k_BT}\right)} + 16\, e^{\left(\frac{19A}{k_BT}\right)} + 14\, e^{\left(\frac{4A}{k_BT}\right)} + 12\, e^{\left(\frac{-9A}{k_BT}\right)} + 10\, e^{\left(\frac{-20A}{k_BT}\right)} \\ +8\, e^{\left(\frac{-29A}{k_BT}\right)} + 6\, e^{\left(\frac{-36A}{k_BT}\right)} + 4\, e^{\left(\frac{-41A}{k_BT}\right)} + 2\, e^{\left(\frac{-44A}{k_BT}\right)} + 16\, e^{\left(\frac{27A}{k_BT}\right)} \\ +14\, e^{\left(\frac{12A}{k_BT}\right)} + 12\, e^{\left(\frac{-1A}{k_BT}\right)} + 10\, e^{\left(\frac{-12A}{k_BT}\right)} + 8\, e^{\left(\frac{-21A}{k_BT}\right)} + 6\, e^{\left(\frac{-28A}{k_BT}\right)} \\ +4\, e^{\left(\frac{-33A}{k_BT}\right)} + 14\, e^{\left(\frac{18A}{k_BT}\right)} + 12\, e^{\left(\frac{5A}{k_BT}\right)} + 10\, e^{\left(\frac{-6A}{k_BT}\right)} + 8\, e^{\left(\frac{-15A}{k_BT}\right)} \\ +6\, e^{\left(\frac{-22A}{k_BT}\right)} + 12\, e^{\left(\frac{9A}{k_BT}\right)} + 10\, e^{\left(\frac{-2A}{k_BT}\right)} + 8\, e^{\left(\frac{-11A}{k_BT}\right)} + 10 \end{array}\right\}}$$

(4.7)

For the second model system, only tetragonal zero-field splitting of Ln^{3+} ions was considered. With respect to the Ln-PCM-21 frameworks, each Ln^{3+} cation was considered individually, assuming no interactions between these ions. The magnetic susceptibility for each ion in a cluster was then summed to give net values. Therefore, the only magnetic susceptibility of interest with this model was a result of the additive net-orbital distortion occurring from each cation, summed as a cluster. The ZFS equation employed (Equation 4.8) used the same constants N_{Av}, g, β, k_B; the D-tensor (D) was included as well, which took into account the spin anisotropy of each individual ion for a given value of the J-states (X in this case). The Pr^{3+} and Nd^{3+} ground terms of $J = 4$ and $^9/_2$ were split into m_J values = 4, 3, 2, 1, 0 and $^9/_2, ^7/_2, ^5/_2, ^3/_2, ^1/_2$ states respectively for the ZFS expression (Equation 4.9 and 4.10).

$$\chi T_{mol}^{Ln^{3+}} = \left(\frac{N_{Av} \cdot g^2 \cdot \beta^2}{3k_B}\right) \cdot \left[\frac{\left\{\sum m_J(m_J+1)(2m_J+1)e^{\left(-D/k_BT\right)}\right\}}{\left\{\sum(2m_J+1)e^{\left(-D/k_BT\right)}\right\}}\right] \quad (4.8)$$

$$\chi T_{mol}^{Pr^{3+}} = 0.72 \cdot \left[\frac{\left\{2e^{(-D/X)}+8e^{(-4D/X)}+18e^{(-9D/X)}+32e^{(-16D/X)}\right\}}{\left\{1+2e^{(-D/X)}+2e^{(-4D/X)}+2e^{(-9D/X)}+2e^{(-16D/X)}\right\}}\right] \quad (4.9)$$

$$\chi T_{mol}^{Nd^{3+}} = 0.05 \cdot \left[\frac{\left\{81e^{(-81D/4X)}+49e^{(-49D/4X)}+25e^{(-25D/4X)}+9e^{(-9D/4X)}\right\}}{\left\{1+1e^{(-49D/4X)}+1e^{(-25D/4X)}+1e^{(-9D/4X)}+1e^{(-D/4X)}\right\}}\right] \quad (4.10)$$

The final mathematic approach for the prediction of magnetic susceptibility behavior for Ln-PCM-21 took the ideals from the ZFS approach, then added in a small amount of interaction between the individual cations for a cluster referred to as a mean-field theory term (Equation 4.11). This interaction, also denoted as an exchange interaction constant (A), can be empirically calculated from each of the equations and allows for a better understanding of the degree of long range interactions that are plausible for a material. The expressions with these energy states included are shown below as well (Equation 4.12, 4.13).

$$\chi T_{ZFS+MFT}^{Ln^{3+}} = \frac{\chi T_{ZFS}^{Ln^{3+}}}{1-\left(\frac{2zJ'}{N_{Av}g^2\beta^2}\right)\chi T_{ZFS}^{Ln^{3+}}} \quad (4.11)$$

$$\chi T_{mol}^{Pr^{3+}} = \left[\frac{0.72\cdot\left\{\left[\frac{\left\{2e^{(-D/X)}+8e^{(-4D/X)}+18e^{(-9D/X)}+32e^{(-16D/X)}\right\}}{\left\{1+2e^{(-D/X)}+2e^{(-4D/X)}+2e^{(-9D/X)}+2e^{(-16D/X)}\right\}}\right]\right\}}{\left\{1-A\cdot 0.72\left[\frac{\left\{2e^{(-D/X)}+8e^{(-4D/X)}+18e^{(-9D/X)}+32e^{(-16D/X)}\right\}}{\left\{1+2e^{(-D/X)}+2e^{(-4D/X)}+2e^{(-9D/X)}+2e^{(-16D/X)}\right\}}\right]\right\}}\right] \quad (4.12)$$

$$\chi T_{mol}^{Nd^{3+}} = \left[\frac{0.05\cdot\left\{\left[\frac{\left\{81e^{(-81D/4X)}+49e^{(-49D/4X)}+25e^{(-25D/4X)}+9e^{(-9D/4X)}+1e^{(-D/4X)}\right\}}{\left\{1e^{(-49D/4X)}+1e^{(-25D/4X)}+1e^{(-9D/4X)}+1e^{(-D/X)}\right\}}\right]\right\}}{\left\{1-A\cdot 0.05\left[\frac{81e^{(-81D/4X)}+49e^{(-49D/4X)}+25e^{(-25D/4X)}+9e^{(-9D/4X)}+1e^{(-D/4X)}}{\left\{1e^{(-49D/4X)}+1e^{(-25D/4X)}+1e^{(-9D/4X)}+1e^{(-D/X)}\right\}}\right]\right\}}\right] \quad (4.13)$$

Comparison of experimental vs modeled magnetic susceptibility

Once all of the expressions were confirmed, the three models (superexchange, ZFS, and ZFS + MFT) were then inlayed with the experimental data (Figure 4.7, 4.8). The R^2 value of fit for each model system can be found in Table 4.1.

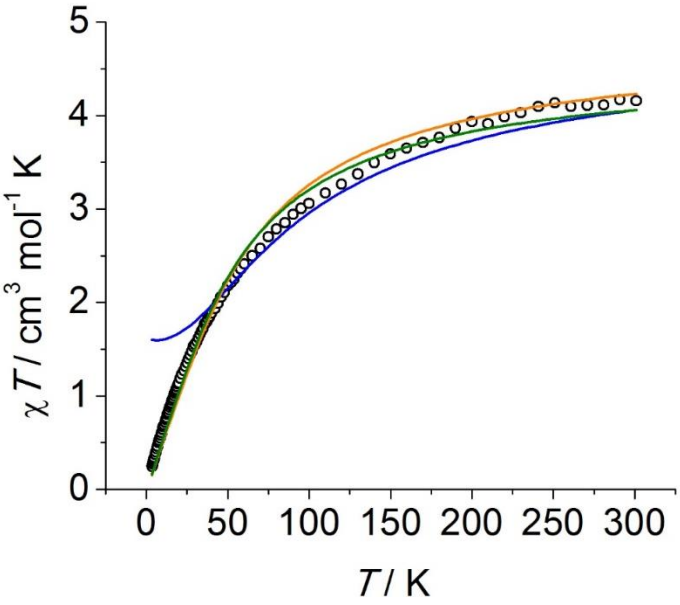

Figure 4.7. Plots of observed $\chi_m T$ versus T (Black) for Pr-PCM-21 (**23**) and model systems for superexchange (Blue), ZFS model (Orange), and ZFS + MFT model (Green).

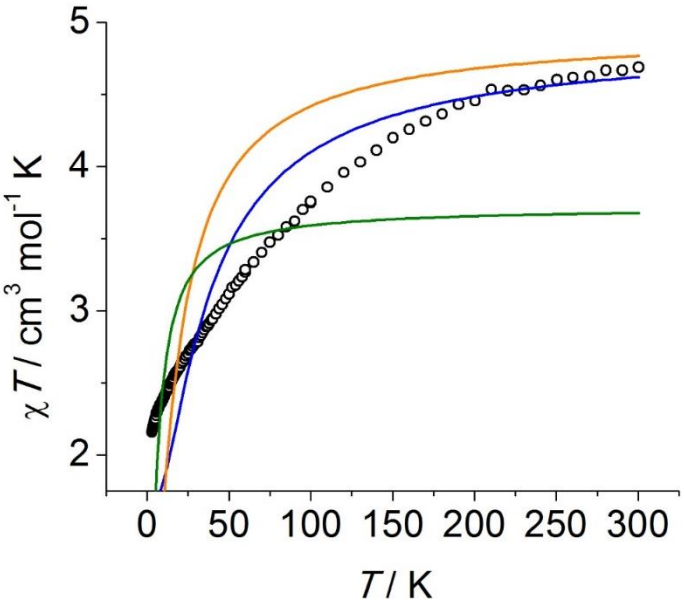

Figure 4.8. Plots of observed $\chi_m T$ versus T (Black) for Nd-PCM-21 (**24**) and model systems for superexchange (Blue), ZFS model (Orange), and ZFS + MFT model (Green).

Material	SE Model	ZFS Model	XFS & MFT
Pr-PCM 21	0.910	0.990	0.993
Nd-PCM 21	0.710	0.490	0.530

Table 4.1. R^2 line-fit values for the three model expressions studied.

In this comparison of modeled and experimental data, the superexchange fit was modest in both cases, with Pr^{3+} outperforming Nd^{3+}. When superexchange is undeniably the most important factor, $\chi_m T$ will typically remain close to its limiting high-temperature value with decreasing T. In turn, this would indicate that the thermal energy is still much larger in magnitude than the strength of the exchange interactions. However, in the

experimental data, the observed $\chi_m T$ did not behave in this fashion, with rapid decay at higher temperatures, and that rate slowing once at lower temperatures. This behavior has been seen in previous studies,[32] and resulted in R^2-fit values of 0.910 and 0.710 for Pr-PCM-21 and Nd-PCM-21 respectively. Therefore, superexchange did not appear to be the most important factor in magnetic susceptibility. This was expected, as lack of significant covalency should result in only weak magnetic exchange interactions as seen in other Ln-clustering.[33] As discussed, the coupling constant (A) from the each equation can be empirically calculated to learn more about the level of interactions taking place for that model system; the value from Equation 4.3 was found to be −2.8(3) cm^{-1} and −0.80(4) cm^{-1} for Pr-PCM-21 and Nd-PCM-21 respectively. These values were considered reasonable, given the inherent ionic nature of the Ln-bonding, although the superexchange model did not fit the data set across the full temperature range.

For the investigation of tetragonal ZFS, the results varied greatly between the isostructural Pr^{3+} and Nd^{3+} frameworks; R^2-fit values were found to be 0.990 and 0.490 respectively. For the former, it became clear that consideration of tetragonal ZFS was much more likely to be a key factor in overall magnetic susceptibility, with a large improvement in fit. For Pr-PCM-21, the value of the spin anisotropy D-tensor was calculated to be 7.2(1) K which aligns well with moderate ionic distortion resulting in magnetic susceptability.[34,35] For the case of Nd-PCM-21, the line fit was dramatically worsened, with the model being significantly misshapen compared to the data series. The likely reasoning behind this lack of correlation was found in other studies of electron paramagnetic resonance studies. Previous examples in the literature for Pr^{3+} demonstrated near tetragonal splitting as modeled.[36] However, in the case of Nd^{3+}, the anisotropy was found to act more so rhombic in its anisotropic distortion.[37] The rhombic model was considered, but there are simply too

many factors to consider for such a complex. Regardless, the D-tensor value for Nd^{3+} through the tetragonal ZFS model able to be determine and was found to be 1.7(1) K.

The final approach to modeling the data employed the ZFS method with a mean-field theory term model expression, which gave an even more dichotomized result, with R^2-fit values of 0.993 and 0.530 when compared with the experimental data. The former, Pr-PCM-21, showed a slightly better fit with a calculated D-tensor value of 6.8(1) K and an A value of −0.012(2) K. Interestingly, this demonstrates that the spin anisotropy for both the ZFS and ZFS+MFT models to be highly similar. The interaction term was found to be quite small although helpful for the fit, pointing towards a very small amount of interaction occurring between the tetragonal distorted Ln^{3+} ions. For the case of Nd^{3+}, since the distortion was ruled to be more complex than previously hypothesized for the original ZFS model, adding the MFT term was not ultimately very helpful. However, it gave rise to D = 0.73(7) K and an A = −0.0 K; though these values are largely not applicable with the model demonstrating such a poor fit.

With the coupling constants from the superexchange model and the ZFS+MFT model (as the MFT term) both showing small values, it is highly unlikely that any long range ordering between clusters was occurring for either framework. The closest $[Ln_3]^{9+}\cdots[Ln_3]^{9+}$ distance was found to be 12.6 Å, even with a strong interaction constant, through space coupling interactions drops off very quickly with increased separation.

CONCLUSIONS

Two novel, isostructural Ln-PCPs were successfully synthesized and were found to incorporate highly unusual, perfectly linear $[Ln_3]^{9+}$ clusters of interest for magnetic applications. These two materials, designated Ln-PCM-21 (Ln = Pr, Nd), were fully

characterized, and then the field-cooled magnetic susceptibility was measured for each sample form 5−300 K employing a field of 100 Oe. The reciprocal of this data was used to fit the Curie-Weiss law, providing Curie constants of −64(3) K and −42(1) K for Pr and Nd respectively. This antiferromagnetic behavior was modeled using three different approaches; assuming superexchange was the only important factor, looking at tetragonal zero-field splitting of each individual cation, and taking that ZFS approach then adding a mean-field theory term to allow for some interaction to be considered. For Pr-PCM-21, the ZFS+MFT model expression fit the experimental data set the best, with an R^2-fit value of 0.993 (D-tensor = 6.8(1) K, A = −0.012(2) K). For Nd-PCM-21, the superexchange model fit best, but only due to the ZFS taking into account tetragonal distortion when Nd^{3+} likely demonstrates rhombic distortion (R^2 = 0.710; A = -.80(4) cm^{-1} or −1.1 K). With these results in mind, the Pr-PCM-21 magnetic susceptibility data was successfully modeled, while in the Nd-PCM-21 a more complex mathematic approach is needed.

EXPERIMENTAL DATA

General

All reactions were conducted in 20 mL sealed glass scintillation vials and heated *via* immersion in a thermal graphite bath. The rare-earth metal precursors $Pr(NO_3)_3{\cdot}6H_2O$ (Sigma, Aldrich, ≥99.9%) and $Nd(NO_3)_3{\cdot}6H_2O$ (Sigma, Aldrich, ≥99.9%) were used as received. N,N-dimethylformamide (DMF) (VWR, ACS grade) and acetonitrile (MeCN) (Fisher Scientific, ACS grade) were used as received. A full description of synthesis and characterization for the ligand $mptbcH_3]^+Cl^-$ can be found in the experimental data section of Chapter 3. FT-Infrared spectroscopy was collected directly from solid samples using a Nicolet iS*50 spectrophotometer with an attenuated total reflectance apparatus; autosorb

gas adsorption analysis was performed in house employing a Quantachrome AS1 instrument; thermogravimetric analysis was collected in house with a TA instruments Q50 system for the temperature range of 25 °C to 800 °C. Elemental Analysis was performed by Midwest Microlab LLC (Indianapolis).

X-ray crystallography

Suitable single crystals were mounted on a glass fibre in perfluoropolyether oil and attached to the diffractometer, and collected at 100 K using a Rigaku XStream low-temperature apparatus. The data for Nd-PCM-21 was collected on a Rigaku AFC-12 with a Saurn 724+ CCD using a graphite monochromator and MoKα radiation (0.7107) Å. Data reduction was performed using Rigaku Americas Corporation's Crystal Clear v1.4 package. The structure was solved using SIR97 and refined using Shelx-2013. CCDC 10226261.

Powder X-ray diffraction (PXRD)

The phase purity and thermal stability of Pr-PCM-21 and Nd-PCM-21 were confirmed by analysis of the crystalline samples inserted into individual 0.7 mm borosilicate capillaries and spun *in situ* to prevent preferential orientation of crystals. Spectra were recorded employing a Stoe Stadi-P diffractometer operation in Deby-Scherrer orientation and fitted with a scintillation count detector. The X-ray source was monochromated CoKα radiation (1.7889 Å). Fifty independent datasets of reflection data were collected for the range 5.0 – 40° 2θ and were subsequently averaged. The PXRD patterns were compared directly to the corresponding simulated pattern for Nd-PCM-21

that was generated using the SimPowPatt facility in PLATON using hkl reflection data obtained from the single crystal measurement.

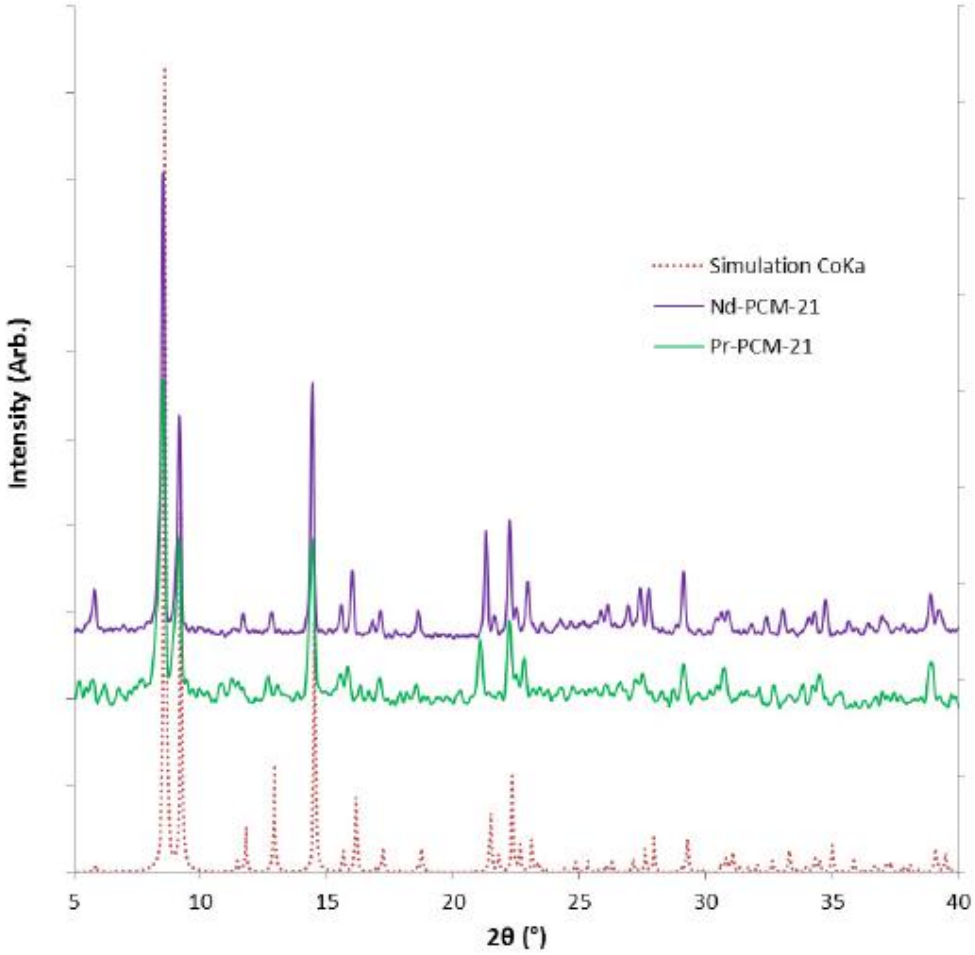

Figure 4.9. Overlay of PXRD data for Pr-PCM-21(Green) and Nd-PCM-21 (Purple) versus the model pattern (Red) calculated from the Nd-PCM-21 single crystal structure data.

Thermogravimetric analysis

Measurements were performed using a ramp rate of 1.0 °C min^{-1} using 99.9995+ % N_2 as the carrier gas. For Pr-PCM-21 an initial mass loss of 5.8 % was observed between 25−61 °C corresponding to a 8 H_2O per formula unit loss; a second distinct mass loss of 10.1 % was observed between 70−155 °C, which corresponds to the removal of 4 DMF molecules. This data was supported by elemental analyses. For Nd-PCM-21, the profile for solvent loss slightly varied, and indicated a larger H_2O/DMF ratio, which is supported by C, H, N microanalyses. An additional second mass loss of 3.9 % was observed between 89−152 °C; this corresponds to 2 DMF molecules. It should be noted that the single crystal X-ray structure was found to contain 2 well-ordered DMF molecules per formula unit, which agrees with TGA and EA results (Figure 4.10).

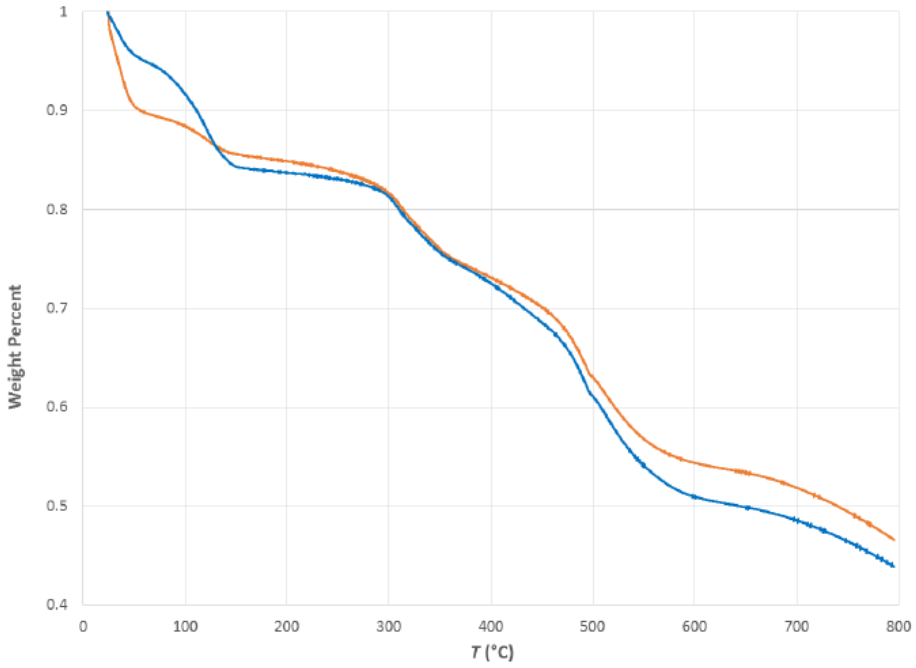

Figure 4.10. TGA traces for as-synthesized Pr-PCM-21 (**23**) (Blue) and Nd-PCM-21 (**24**) (Orange).

Gas sorption isotherms

Samples were *pre*-treated under ultra-high vacuum in a clean system with a diaphragm and turbo pumping system. Isotherms for CO_2, N_2, O_2, and H_2 were collected utilizing ultra-high purity gases (Praxair, 99.995 %). Surface areas were then calculated using the Brauner-Emmett Teller method for CO_2, based on adsorption data points in the range $P/P_o = 0.05-0.030$. The sorption isotherms are included below (Figure 4.11, 4.12).

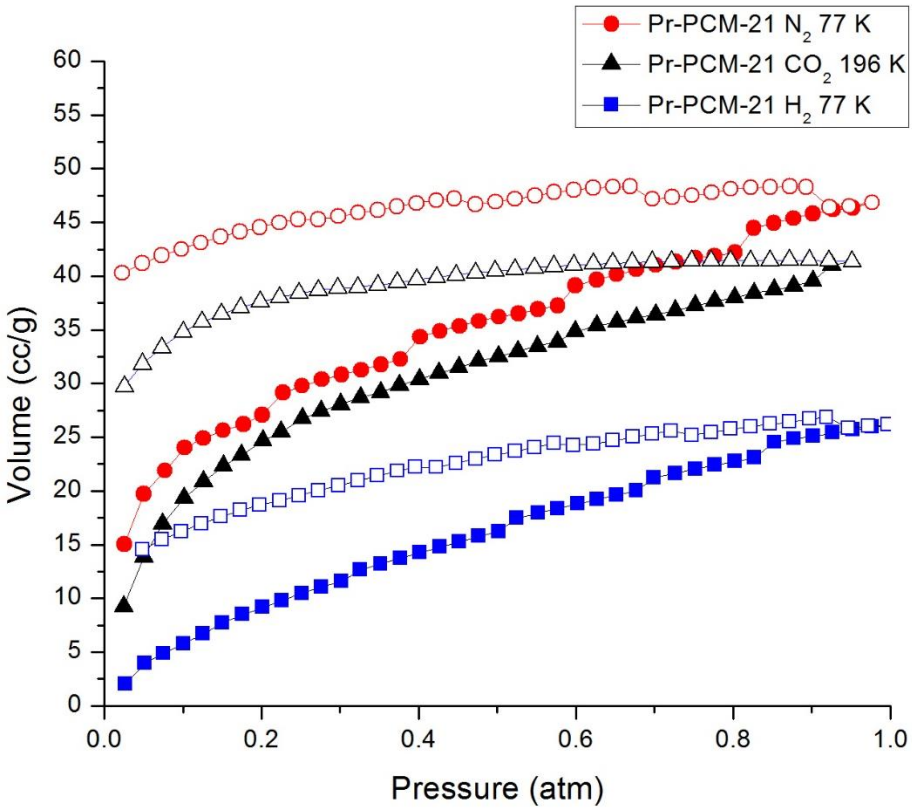

Figure 4.11. Adsorption-desorption isotherms for Pr-PCM-21 (**23**) for the gases CO_2 (Black triangles), H_2 (Blue squares), N_2 (Red circles). Closed symbols denote adsorption, with open for desorption data.

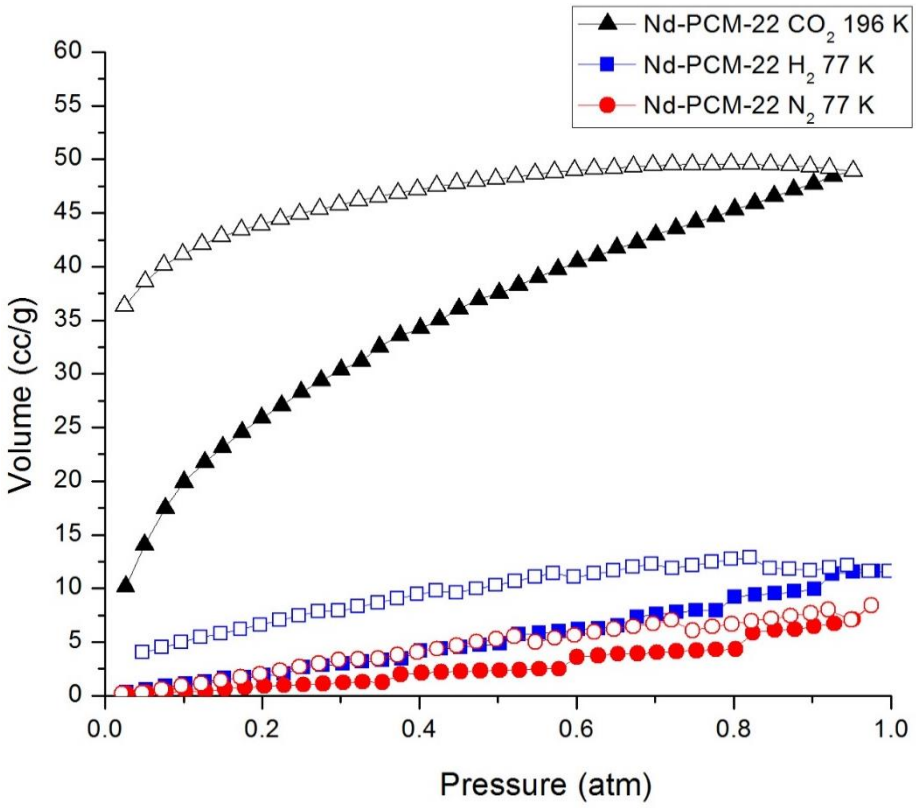

Figure 4.12. Adsorption-desorption isotherms for Nd-PCM-21 (**24**) for the gases CO_2 (Black triangles), H_2 (Blue squares), N_2 (Red circles). Closed symbols denote adsorption, with open for desorption data.

SQUID magnetometry

Variable-temperature magnetic measurements were performed on pure crystalline samples for both Pr-PCM-21 and Nd-PCM-21 analogues. The samples were individually loaded into gelatin capsules and the magnetic susceptibility was measured with a Quantum Design MPMs-5 magnetometer over the temperature range of 4−300 K with an external applied field of 100 Oe. The data was corrected for diamagnetism using Pascal's constants.[38] Models were fitted to the observed data and refined against least squares using he fitting function in Origin v. 8.0.

Procedure for Pr-PCM-21 (23)

The ligand $[mptbcH3]^{+}Cl^{-}$ (20 mg, 49 μmol) and $Pr(NO_3)_3{\cdot}6H_2O$ (55 mg, 126 μmol) were co-dissolved upon stirring in a mixture of DMF (3 mL), H_2O (2 mL), and MeCN (2 mL). The solution was then heated at 358 K for 5 days to yield colorless rods. The product was isolated by decantation and washing with fresh mother solution. Yield: 14 mg. Anal. Found: C, 47.4; H, 4.30; N, 2.30; Cl, 0.63 %. [Pr-PCM-21]0.5Cl,0.5(NO_3)·4DMF·8H_2O; ($C_{100}H_{104}Cl_{0.5}N_{4.5}Pr_3O_{36.5}P_4$) requires: C, 47.7; H, 4.16; N, 2.50; Cl, 0.70 %. FT-IR (solid/cm^{-1}): ν_{max} = 1623 (m), 1627 (m), 1542 (s), 1497 (w), 1358 (s), 1314 (m), 1110, 1020 (m) 908 (m), 845 (m), 770 (s), 738 (s), 689 (s).

Procedure for Nd-PCM-21 (24)

The same method as described above for Nr-PCM-21 was employed, but $Pr(NO_3)_3{\cdot}6H_2O$ (55 mg, 125 μmol) was used as the precious earth-metal precursor. This reaction produced target colorless needle-like crystals that were isolated again by decantation and washing with fresh mother solution. Yield: 12 mg. Anal. found: C, 44.8; H, 3.82; N, 1.75; Cl, 0.80 %. [Nd-PCM-21]0.5Cl,0.5(NO_3)·2DMF·15H_2O; ($C_{94}H_{132}Cl_{0.5}N_{2.5}Nd_3O_{42.5}P_4$) requires: C, 44.7; H, 4.15; N, 1.39; Cl, 0.70 %. FT-IR (solid/cm^{-1}): ν_{max} = 1625 (m), 1629 (m), 1540 (s), 1501 (w), 1358 (s), 1308 (m), 1107, 1017 (m), 898 (m), 842 (m), 772 (s), 737 (s), 686 (s).

REFERENCES

1. Waggoner, N. W.; Saccoccia, B.; Ibarra, I. A.; Lynch, V. M.; Wood, P. T.; Humphrey, S. M. *Inorg. Chem.* **2014**, *53* (24), 12674–12676.
2. Ding, B.; Liu, S. X.; Cheng, Y.; Guo, C.; Wu, X. X.; Guo, J. H.; Liu, Y. Y.; Li, Y. *Inorg. Chem.* **2016**, *55* (9), 4391–4402.
3. Zhang, X.; Vieru, V.; Feng, X.; Liu, J.-L.; Zhang, Z.; Na, B.; Shi, W.; Wang, B.-W.; Powell, A. K.; Chibotaru, L. F.; Gao, S.; Cheng, P.; Long, J. R. *Angew. Chem. Int. Ed.* **2015**, *54* (34), 9861–9865.
4. Li, Y.; Zhang, S.; Song, D. *Angew. Chem. Int. Ed.* **2013**, *52* (2), 710–713.
5. Cui, Y.; Xu, H.; Yue, Y.; Guo, Z.; Yu, J.; Chen, Z.; Gao, J.; Yang, Y.; Qian, G.; Chen, B. *J. Am. Chem. Soc.* **2012**, *134* (9), 3979–3982.
6. Rocha, J.; Carlos, L. D.; Paz, F. A. A.; Ananias, D. *Chem. Soc. Rev.* **2011**, *40* (2), 926–940.
7. Cotton, S. *Lanthanide and Actinide Chemistry*; John Wiley & Sons: Hoboken, **2013**; 2-3.
8. Harbuzaru, B. V.; Corma, A.; Rey, F.; Atienzar, P.; Jordá, J. L.; García, H.; Ananias, D.; Carlos, L. D.; Rocha, J. *Angew. Chem., Int. Ed.* **2008**, *47* (6), 1080–1083.
9. Chen, Y.; Ma, S. *Rev. Inorg. Chem.* **2012**, *32* (2–4), 81–100.
10. Bogani, L.; Wernsdorfer, W. *Nat Mater* **2008**, *7* (3), 179–186.
11. Ishikawa, N.; Sugita, M.; Ishikawa, T.; Koshihara, S.; Kaizu, Y. *J. Am. Chem. Soc.* **2003**, *125* (29), 8694–8695.
12. Chorazy, S.; Rams, M.; Nakabayashi, K.; Sieklucka, B.; Ohkoshi, S. *Chem. Eur. J.* **2016**, *22* (22), 7371–7375.
13. Jiang, Z.-X.; Liu, J.-L.; Chen, Y.-C.; Liu, J.; Jia, J.-H.; Tong, M.-L. *Chem. Commun.* **2016**, *52* (37), 6261–6264.

14. Pedersen, K. S.; Ariciu, A.-M.; McAdams, S.; Weihe, H.; Bendix, J.; Tuna, F.; Piligkos, S. *J. Am. Chem. Soc.* **2016**, *138* (18), 5801–5804.
15. Sessoli, R.; Gatteschi, D.; Caneschi, A.; Novak, M. A. *Nature* **1993**, *365* (6442), 141–143.
16. Coulon, C.; Miyasaka, H.; Clérac, R. *Single-Molecule Magnets and Related Phenomena*; Winpenny, R., Ed.; *Structure and Bonding*; Springer Berlin Heidelberg, **2006**; pp 163–206.
17. Benelli, C.; Gatteschi, D. *Introduction to Molecular Magnetism: From Transition Metals to Lanthanides*; John Wiley & Sons, **2015**.
18. Liu, K.; Zhang, X.; Meng, X.; Shi, W.; Cheng, P.; Powell, A. K. *Chem. Soc. Rev.* **2016**, *45* (9), 2423–2439.
19. Miller, J. S.; Gatteschi, D. *Chem. Soc. Rev.* **2011**, *40* (6), 3065–3066.
20. *Hysteresis in Magnetism: For Physicists, Materials Scientists, and Engineers*, Bertotti, G.; Gulf Professional Publishing USA, **1998**.
21. Woodruff, D. N.; Winpenny, R. E. P.; Layfield, R. A. *Chem. Rev.* **2013**, *113* (7), 5110–5148.
22. Bhunia, A.; Lan, Y.; Mereacre, V.; Gamer, M. T.; Powell, A. K.; Roesky, P. W. *Inorg. Chem.* **2011**, *50* (24), 12697–12704.
23. Su, S.; Wang, S.; Song, X.; Song, S.; Qin, C.; Zhu, M.; Hao, Z.; Zhao, S.; Zhang, H. *Dalton Trans.* **2012**, *41* (16), 4772–4779.
24. Sessoli, R.; Powell, A. K. *Coord. Chem. Rev.* **2009**, *253* (19–20), 2328–2341.
25. Layfield, R. A. *Organometallics* **2014**, *33* (5), 1084–1099.
26. Singh-Wilmot, M. A.; Sinclair, R. A.; Andrews, M.; Rowland, C.; Cahill, C. L.; Murugesu, M. *Polyhedron* **2013**, *53*, 187–192.
27. Jami, A. K.; Baskar, V.; Sañudo, E. C. *Inorg. Chem.* **2013**, *52* (5), 2432–2438.

28. Fang, W.-H.; Cheng, L.; Huang, L.; Yang, G.-Y. *Inorg. Chem.* **2013**, *52* (1), 6–8.
29. Anwar, M. U.; Tandon, S. S.; Dawe, L. N.; Habib, F.; Murugesu, M.; Thompson, L. K. *Inorg. Chem.* **2012**, *51* (2), 1028–1034.
30. H. A. Kramers, *Physica,* **1934**, *1*, 182-192.
31. *Lanthanides and actinides in molecular magnetism*, First edition.; Layfield, R. A., Murugesu, M., Eds.; Wiley-VCH Verlag GmbH & Co. KGaA: Weinheim, Germany, **2015**.
32. Cepeda, J.; Balda, R.; Beobide, G.; Castillo, O.; Fernández, J.; Luque, A.; Pérez-Yáñez, S.; Román, P.; Vallejo-Sánchez, D. *Inorg. Chem.* **2011**, *50* (17), 8437–8451.
33. Zhou, X.; Xia, S.; Tanner, P. A. J. Phys. Chem. B 2007, 111 (30), 8677–8679.
34. *Molecular nanomagnets and related phenomena*; Gao, S., Affronte, M., Eds.; Structure and Bonding; Springer: Berlin, **2015**.
35. Zhang, P.; Guo, Y.-N.; Tang, J. *Coord. Chem. Rev.* **2013**, *257* (11–12), 1728–1763.
36. Kaczmarek, S. M.; Tomaszewicz, E.; Moszyński, D.; Jasik, A.; Leniec, G. *Mat. Chem. Phys.* **2010**, *124* (1), 646–651.
37. Mingalieva, L. V.; Voronkova, V. K.; Galeev, R. T.; Sukhanov, A. A.; Melnik, S.; Prodius, D.; Turta, K. I. *Appl. Magn. Reson.* **2009**, *37* (1–4), 737–750.
38. Kahn, O. *Molecular magnetism*, Wiley-VCH, Chichester, **1993**.

Chapter 5: Thiolate coordination materials with anticipated impressive magnetic behavior

Very recently, a new area of coordination polymers has been explored within the Humphrey group with interest in thiolate coordination materials (TCMs) and their predictably exciting magnetic properties. These materials have become of renewed interest in collaboration with Professor Paul Wood from the University of Cambridge. Despite the short timeline of this study, an isostructural set of 1-dimensional polymers has been discovered, termed M-TCM-1 (M = Fe, Co*, Mn*). Optimization of synthetic routes is still in progress for the Co^{II} and Mn^{II} analogs. However, Fe-TCM-1 has been successfully synthesized and characterized, with specific interest in its magnetic behavior. The crystal structure of Fe-TCM-1 demonstrated bond angles that are indicative of extraordinary magnetic behavior, Curie temperatures, and blocking temperatures in relation to the Goodenough-Kanamori rules. Due to the high symmetry and bonding characteristics of this material, there is a high likelihood it will demonstrate significantly elevated magnetic temperatures.

INTRODUCTION

Exploration of novel magnetic materials continues to be of great interest in a variety of industrial applications surrounding data storage and electronics. Efforts continue to pursue smaller and smaller magnetic units, leading to interest in control over single magnetic domains on the atomic level.[1,2] Below a certain size, these individual sites can display field hysteresis loops when they possess a significant, 1-dimensional magnetic anisotropy (also known as *ising* dimensionality). Unfortunately, looking to smaller magnetic materials has its disadvantages. Reduction of the particle size can in turn reduce

magnetic anisotropy to an equal level of thermal energy. Due to this struggle in miniaturization, dictated by the superparamagnetic limit, magnetic applications are thus lost past a certain size boundary.[3,4] To overcome this hurdle in micro-magnetic materials, discovery of single-molecule magnets (SMMs) is considered an important step towards tomorrow's memory devices.[5] In a material, a series of SMMs are held within a system in ideally a paramagnetic fashion. Below its magnetic Curie temperature, a SMM can display ordered magnetization with overall magnetic behavior promoted by high spin ground states and large ising-spin anisotropy. Regardless, the primary difficulty with the development of SMMs in applications has been due to issues with their aligned incorpation into a material.[6,7]

Single-chain magnets (SCMs) have been explored more recently, with initial interest starting in the early 2000s.[8] SCMs are defined as isolated 1-dimensional chains that can be individually magnetized in the absence of an applied magnetic field.[9] Like their monomeric predecessors, SCMs require a minimum temperature in order to achieve ordered magnetic behavior. However, the additive magnetic properties of each individual chain can be significantly larger than seen in SMMs, allowing for a higher level of applicability at elevated temperatures. An impressive array of 1-dimesional models have been expansively reviewed in the literature,[10] as well as in comparison to experimental studies.[11,12] Common model approaches include treatment of a system as a classical-spin Heisenberg chain,[13,14] an Ising chain,[15,16] or an anisotropic Heisenberg chain.[17,18]

In consideration of general superexchange behavior, the Goodenough-Kanamori (G. K.) rules have done impressively well at prediction of ordered magnetic performance. First established in 1959, the G. K. rules have provided impressive guidelines for the accurate prediction of superexchange behavior in magnetic materials. This method considers the probability of increased magnetic interaction between cationic sites due to

their relative angle in relation to one another.[19] The G. K. rules are based upon four pillars: (1) the spin angular momentum is conserved in both a real or virtual electronic transfer, (2) The Pauli exclusion principle restricts electron transfer from/to half-filled orbitals or multiple-electron transfers from the same anionic bridge, (3) The intraatomic spin-spin potential exchange interaction (ferromagnetic) is what determines overall behavior when the Pauli exclusion principle does not apply, (4) due to the fact that spins are only oriented in one of two fashions, the angular dependence for electron-spin transfer between cations becomes predicable.[20] In a more direct approach, the G. K. rules have allowed for the value of a given cation-anion-cation angle to give insight into a material's magnetic properties. In the case of a cation-anion-cation bridging angle that is 180 ° within a polymer, the rules predict that it will display strong antiferromagnetic behavior (Figure 5.1).

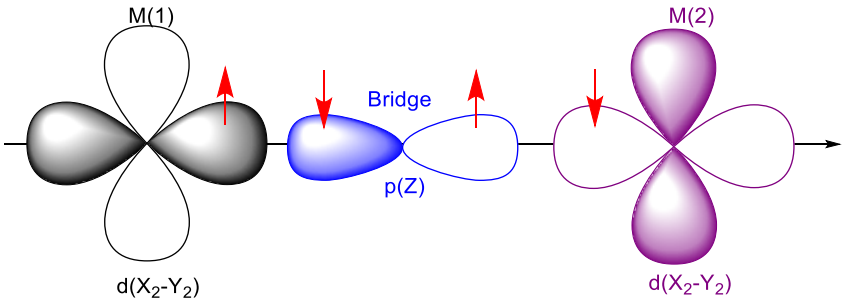

Figure 5.1. A visual, orbital representation of superexchange across a 180 ° bridge.

Conversely, a perpendicular bond angle between two metal cations through an anionic bridge will result in a different effect. In polymeric systems that display 90 ° angles across cation-anion-cation bridges, a bulk ferromagnetic effect is predicted (Figure 5.2). The ferromagnetic behavior predicted and observed for 90 ° bridging is typically smaller in magnitude than that antiferromagnetic behavior seeh in linear systems, but both examples predict immense improvement in magnetic properties due to these geometric relationships.

Additionally, the Curie and blocking temperatures are predicted in increase as well, due to increase magnetic order *via* increased orbital overlap. Naturally, net magnetic properties can be dramatically influenced by multiplicity among other factors. However, the G. K. rules have shown great resilience since their introduction and have been proven highly applicable to predict the improvment of net magnetic behavior.[21-23]

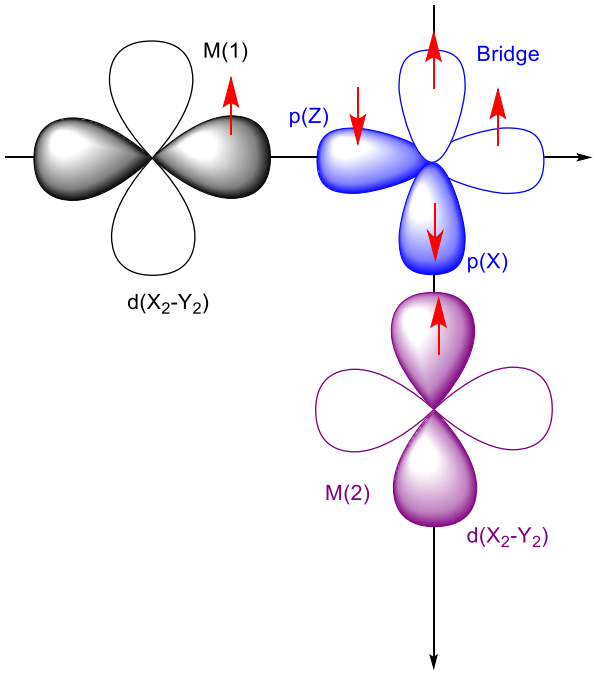

Figure 5.2. A visual, orbital representation of superexchange across a 90 ° bridge.

There are a common series of SQUID measurements that are typically investigated in order to better understand a material's magnetic properties. Initially, bulk magnetic properties are typically probed using a set external field energy while measuring the magnetic susceptibility of a material (χ, *y*-axis) over a temperature range (ca. 5−300 K, *x*-axis). In tandem with the Curie-Weiss law, these plots can give information on bulk behavior, Curie temperature, Weiss constant, and the magnitude of the magnetic moment

(as seen in Chapter 4). AC-SQUID measurements can then be carried out in order to obtain information such as effective energy barriers, blocking temperatures, ground states, and spin relaxation times.

Regardless of their need for excessively low operation temperatures, single-chain magnets have become ever-present in the literature. In 2005, T. Kajiwara *et al*. domnstrated a series of coordination polymers, with most impressive of which based off of Fe^{II}/Fe^{III} centers connected through *bis*(2-pyridylcarbonyl)amine linkers.[24] The high-spin iron(II) and low-spin iron(III) sites were shown to alternate through the polymer backbone in a 1:1 fashion through analysis of the compound's Mössbauer spectrum. The twisting planes of the 1-dimensional chain allowed for slow reversal of magnetization, with a blocking temperature estimated at 1.3 K. The AC-magnetic susceptibility was also investigated from 1.5−4.5 K at eight different frequencies from 5−997 Hz.

In another example, Clérac and coworkers published a trinuclear single-chain magnet that incorporated Mn^{III}-Fe^{III}-Me^{III} units.[25] The repeating unit was found to be $(NEt_4)[Mn_2(salmen)_2(MeOH)_2Fe(CN)_6]$ with $salmen^{2-}$ equal to *rac*-N,N'-(1-methylethylene)*bis*(salicylideneiminate) (Figure 5.3). The variable field magnetic susceptibility was measured to afford a spin relaxation of time of $\tau_0 = 2.5 \times 10^{-7}$ s. The blocking temperature was found *via* investigation of the field dependence of magnetization, with loss of hysteresis behavior at 1.4 K.

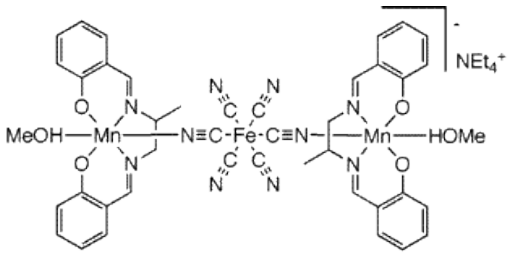

Figure 5.3. $(NEt_4)[Mn_2(salmen)_2(MeOH)_2Fe(CN)_6]$ repeating unit from the work of Clérac and coworkers.[25]

More recently, Novak and coworkers have demonstrated the highest blocking temperature reported to date for a single-chain magnet.[26] The material described was comprised of a 1:1 ratio of $[Co(hfac)_2]$ (hfac = fluoroacetylacetonate) and a nitrronylnitroxide radical linked to pyrene to afford a 1-dimensional polymer that demonstrated strong antiferromagnetic superexchange. Two separate relaxation times were calculated from variable field AC-magnetic susceptibility measurements, with the intrinsic $\tau_0 = (7 \pm 5) \times 10^{-10}$ s, and the lower temperature value of $\tau_0 = (6 \pm 3) \times 10^{-12}$ s. Through investigation of field dependence of magnetization, a record breaking blocking temperature of 14 K was determined due to loss of hysteresis. Due to a high level of chain isolation, no evidence of ordered magnetism was observed for this material. Although 14 K is still far from applicable, the work done within this report demonstrated interesting techniques for creating a material with individual magnetic sites that resist spin-reversal to a record breaking temperature.

RESULTS AND DISCUSSION

The recrystallized ligand 2-mna was dissolved in basic deionized water, followed by the addition of an aqueous $FeCl_2$ solution in a 1:2.6:4 ratio (ligand:metal:base). The resulting rust-colored slurry was heated to 200 °C for 18 hours to yield deep red crystals of the 1-dimensional polymer, Fe-TCM-1. The Fe^{II} product demonstrated impressive aqueous and thermal stability, with thermogravimetric analysis (TGA) showing stark resilience out to approximately 375 °C (Figure 5.4).

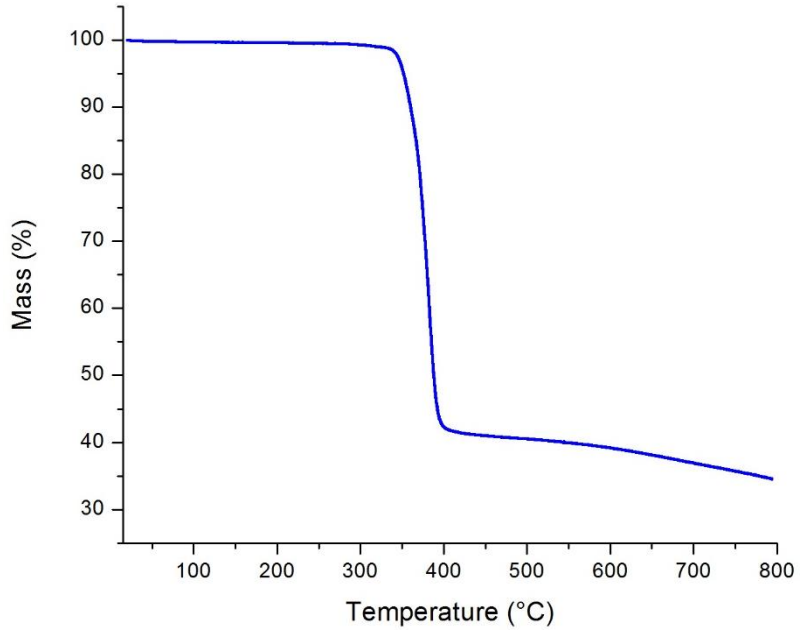

Figure 5.4. TGA analysis from 25−800 °C for Fe-TCM-1.

The X-ray crystal structure of Fe-TCM-1 revealed exciting regularity of its 1-dimensional construction, with bond angles akin to ideal Goodenough-Kanamori conditions. The solid-state structure crystallized in the monoclinic $P2_1/n$ space group, with approximate cell dimensions of $a = 3.7$, $b = 12.3$, $c = 13.7$ Å, with $\alpha, \gamma = 90$ °, $\beta = 95.2$ °. The crystal structure of Fe-TCM-1 was found to have the formula $Fe(2\text{-mna})_2$ with the cyclic nitrogen protonated (Figure 5.5A). This resulted in the pyridine-based ligand acting as a singly charged pyridinium thiolatocarboxylate species. The Fe-TCM-1 structure was found to consist of 1-dimensional polymeric chains with doubly-bridged iron(II) cations through sulfur anions. The backbone of the polymer down the *a*-axis is comprised of Fe_2S_2 squares falling in the same plane (Figure 5.5C). The Fe1-S1-Fe1 angle within the Fe_2S_2 squares were found to be 90.21 °. With a coupling angle so close to the ideal G.K. value of 90 °, this suggests a high likelihood of ferromagnetic behavior.

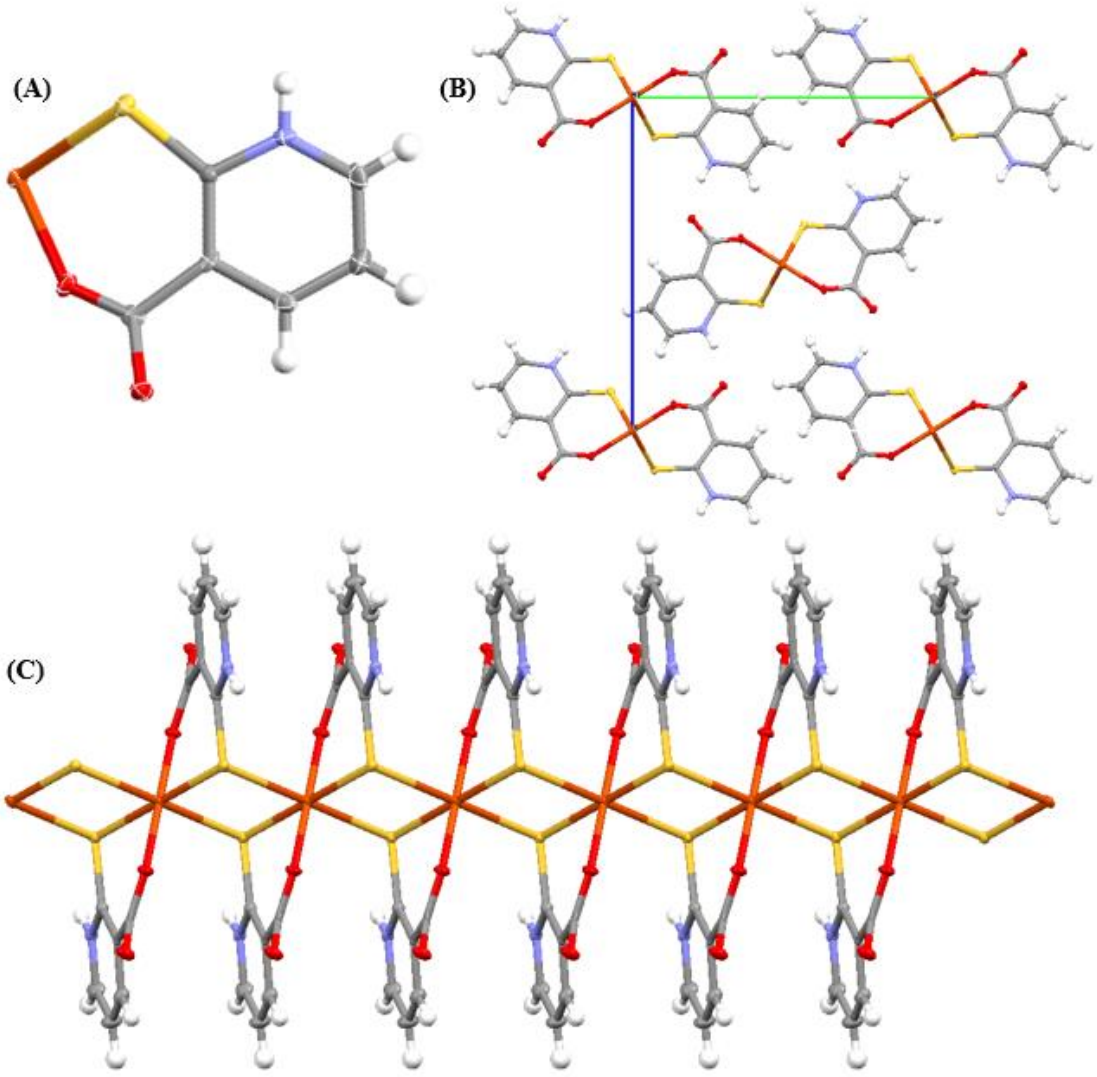

Figure 5.5. Ellipsoid crystallographic representation of the asymmetric unit (A), view of the 1-dimensional polymer down the *a*-axis (B), and along the *b*-axis (C). Hydrogen atoms were added to structure for clarity.

The axial positions of each octohedral Fe^{II} site are bound to carboxylate functionalities of individual 2-mna ligands, creating flexed 6-membered rings consisting of the atoms Fe1·S1·C2·C3·C7·O1. Individual chains were found to crystalize in a freely packed,

staggered fashion, with a closest contact value of 1.930(3) Å coming from the carboxylate O2 to the thiolate H1A of the adjacent polymer (Figure 5.5B). Selected bond angles and lengths are provided in table 5.1.

Fe1·S1·Fe1 angle	**90.21(4) °**	Fe1−S1 distance	**2.515(1) Å**
S1·Fe1·S1 angle	**89.79(4) °**	Fe1−O1 distance	**1.995(3) Å**
S1·Fe1·O1 angle	**87.4(1)/92.6(1) °**	Fe1·Fe1 distance	**3.6490(6) Å**

Table 5.1. Selected bond angles and lengths for Fe-TCM-1.

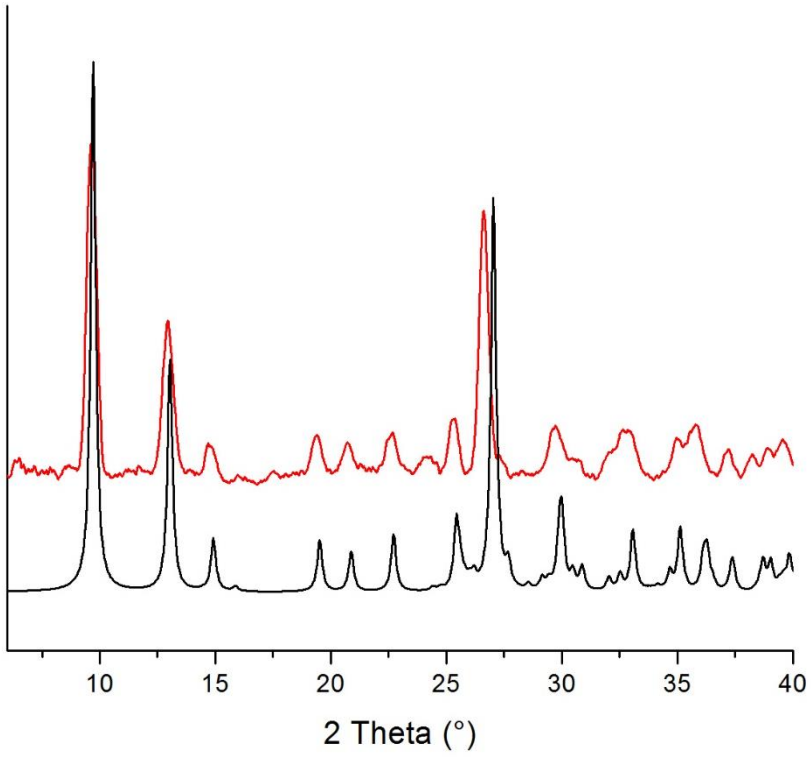

Figure 5.6. PXRD comparison of the model pattern (Black) vs Fe-TCM-1 (**25**) bulk pattern (Red).

The solid-state properties of Fe-TCM-1 were then further investigated. The FT-IR spectrum was collected (Figure A.25) along with the powder X-ray diffraction (PXRD) pattern (Figure 5.6). The PXRD pattern was compared to the 2-dimensional model pattern generated from the single-crystal structure. The model and experimental patterns showed great comparability, confirming bulk purity of the crystalline material.

CONCLUSIONS AND FUTURE OUTLOOK

In this recent study, a novel sub-group of coordination polymers was pioneered, termed TCMs. More specifically, the first reported TCM from the Humphrey group was successfully synthesized through the connection of Fe^{II} cations through two sulfur bridges to create a very symmetrical polymer. The crystal structure of Fe-TCM-1 demonstrated Fe1−S1−Fe1 bond angles of 90.21 °, which in turn provides a high probability of ferromagnetic behavior and increased blocking temperatures per the Goodenough-Kanamori rules. This material has been further characterized by TGA, PXRD, and FT-IR to confirm thermal stability and bulk purity.

Currently, DC- and AC-magnetic studies are underway in collaboration with the Dunbar group at Texas A&M University. There is specific interest in determining the value of the Weiss constant, Curie temperature, spin relaxation times, blocking temperature, and overall magnetic behavior. It is our goal to have this work published in collaboration with the Dunbar group and Prof. Paul Wood shortly in the coming months.

EXPERIMENTAL DATA

General

All reactions were carried out in 23.0 mL Teflon©-lined autoclaves, purchased from Parr Corp., Illinois. All solids were purged with N_2 flow for no less than 15 minutes before solvation. Solutions were sparged during mixing process as well until autoclaves were sealed to prevent and/or reduce decomposition. The reagent 2-mercaptopyridine-3-carboxylic acid (2-mna) (Sigma Aldrich, Technical grade) was recrystallized from boiling, deionized water and dried under vacuum before use. Iron(II) chloride tetrahydrate (Acros Organics, ≥99 %), Cobalt(II) chloride anhydrous (EMD Millipore, ≥99 %), and potassium hydroxide (KOH) (Fisher Chemical, ACS grade) were used as received. Deionized water and the KOH solution were sparged with N_2 for no less than 15 minutes prior to use. FT-IR spectra were obtained directly from solid samples using a Nicolet iS*50 spectrophotometer with an attenuated total reflectance apparatus; thermogravimetric analysis (TGA) data was collected with a TA Instruments Q50 system for the temperature range of 25 °C to 800 °C; the solid-state UV/Visible spectra was collected on a Cary 5000 UV/Vis NIR spectrometer with specular reflectance.

X-ray crystallography

The single crystal X-ray diffraction data was collected at 100 K on a Nonius Kappa CCD diffractometer with a using a μ-focus Mo Kα radiation source (λ = 0.7093 Å). Data collection, unit cell refinement, and data reduction were performed using Apex II (Bruker AXS, Inc. 2010). The structure of Fe-TCM-1 (**25**) solved by direct methods using the SIR2014 program and refined by full-matrix least-squares on F^2 with anisotropic displacement parameters for all non-H atoms using SHELXL-2013. The structural analysis

was performed using Mercury 3.1 (Build RC5). The hydrogen atoms were placed in fixed, calculated positions with isotropic displacement parameters set to 1.2 x U_{eq} with respect to the attached atom.

Powder X-ray diffraction (PXRD)

The PXRD model data was generated using the Sim PowPatt function in the PLATON software from the hkl reflection data collected in the single crystal experiments. Phase purity of Fe-TCM-1 was confirmed through analysis of the bulk polycrystalline material, which was placed in borosilicate tubes and spun *in situ* to prevent preferential orientation of the crystallites. Spectrum was collected on a Rigaku R-Axis Spider diffractometer with an image plate detector with CrystalClear V1.40 operating system. The system operated in Debye-Scherrer geometry using Cu K α radiation (1.5418 Å). Reflection data was collected from 6.0−40.0 ° 2θ. The experimental data was generated up using Rigaku's 2DP software for converting the 2-dimensional powder diffraction image into a conventional 1-dimensional powder pattern.

Procedure for Fe-TCM-1 (25)

A stirred solution of 2-mna (155 mg, 1.0 mmol) and KOH (1.0 M, 4.0 mmol) in H_2O (2.0 mL) was prepared in a 20 mL autoclave liner. A separate solution of $FeCl_2{\cdot}4H_2O$ (507 mg, 2.6 mmol) in H_2O (4.0 mL) was prepared and added to the stirred solution. The orange slurry was sealed and the autoclave reaction vessel was heated to 200 °C for 18 hrs, then allowed to cool to room temperature (ca. 0.5 °C min^{-1}). The black mixture was washed with H_2O followed by decanting to yield the crude product Fe-TCM-1 (**25**). The crystalline solid was further purified *via* magnetic removal of FeO_3 to yield deep red, rod-like

crystals.Yield: 40 mg. FT-IR (solid/cm^{-1}): ν_{max} = 3069 (m), 2598 (br), 2070 (w), 1988 (w), 1618 (sh), 1599 (m), 1560 (s), 1486 (s), 1435 (sh), 1368 (s), 1319 (s), 1229 (s), 1204 (sh), 1149 (sh), 1133 (s), 1077 (sh), 1039 (s), 952 (s) 860 (m), 824 (s), 766 (s), 749 (s), 638 (s), 544 (s), 503 (s), 472 (s).

REFERENCES

1. Kodama, R. H. *Magn. Magn. Mater.* **1999**, *200*, 359-372.
2. Thompson, D. A.; Best, J. S. *IBM J. Res. Develop.* **2000**, *44* (3), 311-322.
3. Weller, D.; Moser, A. *IEEE Trans. Magn.* **1999**, *35* (6), 4423-4439.
4. Skumryev, V.; Stoyanov, S.; Zhang, Y.; Hadjipanayis, G.; Givord, D.; Nogués, J. *Nature* **2003**, *423* (6942), 850–853.
5. *Single-Molecule Magnets and Related Phenomena*; Winpenny, R., Ed.; Structure and Bonding; Springer-Verlag: Berlin/Heidelberg, 2006; Vol. 122, pp 164-206.
6. Gatteschi, D.; Sessoli, R. *Angew. Chem., Int. Ed.* **2003**, *42* (3), 268–297.
7. Christou, G.; Gatteschi, D.; Hendrickson, D. N.; Sessoli, R. *MRS Bullet.* **2000**, *25* (11), 66–71.
8. Mukherjee, P. S.; Maji, T. K.; Mostafa, G.; Mallah, T.; Chaudhuri, N. R. *Inorg. Chem.* **2000**, *39* (22), 5147–5150.
9. Clérac, R.; Miyasaka, H.; Yamashita, M.; Coulon, C. *J. Am. Chem. Soc.* **2002**, *124* (43), 12837–12844.
10. Coulon, C.; Miyasaka, H.; Clérac, R. In *Single-Molecule Magnets and Related Phenomena*; Winpenny, R., Ed.; Structure and Bonding; Springer Berlin Heidelberg, **2006**; pp 163–206.
11. Sun, H.-L.; Wang, Z.-M.; Gao, S. *Coord. Chem. Rev.* **2010**, *254* (9–10), 1081–1100.

12. Waggoner, N. W.; Saccoccia, B.; Ibarra, I. A.; Lynch, V. M.; Wood, P. T.; Humphrey, S. M. *Inorg. Chem.* **2014**, *53* (24), 12674–12676.
13. Lisnyi, B.; Strečka, J. *J. Magn. Magn. Mater.* **2015**, *377*, 502–510.
14. Peters, D.; McCulloch, I. P.; Selke, W. *Phys. Rev. B* **2009**, *79* (13), 132406.
15. Maignan, A.; Hardy, V.; Hébert, S.; Drillon, M.; Lees, M. R.; Petrenko, O.; Paul, D. M. K.; Khomskii, D. *J. Mater. Chem.* **2004**, *14* (8), 1231–1234.
16. Sun, H.-L.; Wang, Z.-M.; Gao, S. *Chem. Eur. J.* **2009**, *15* (7), 1757–1764.
17. Yamamoto, S.; Miyashita, S. *Phys. Rev. B* **1994**, *50* (9), 6277–6288.
18. Sakai, T.; Takahashi, M. *Phys. Rev. B* **1998**, *50* (9), 6277-6288.
19. Weihe, H.; Güdel, H. U. *Inorg. Chem.* **1997**, *36* (17), 3632–3639.
20. Goodenough, J. *Scholarpedia* **2008**, *3* (10), 7382.
21. Poudeu, P. F. P.; Takas, N.; Anglin, C.; Eastwood, J.; Rivera, A. *J. Am. Chem. Soc.* **2010**, *132* (16), 5751–5760.
22. Lebernegg, S.; Schmitt, M.; Tsirlin, A. A.; Janson, O.; Rosner, H. *Phys. Rev. B* **2013**, *87* (15), 155111.
23. Bensch, W.; Sander, B.; Kremer, R. K.; Kockelmann, W. *J. Solid State Chem.* **2001**, *158* (2), 198–207.
24. Kajiwara, T.; Nakano, M.; Kaneko, Y.; Takaishi, S.; Ito, T.; Yamashita, M.; Igashira-Kamiyama, A.; Nojiri, H.; Ono, Y.; Kojima, N. *J. Am. Chem. Soc.* **2005**, *127* (29), 10150–10151.
25. Ferbinteanu, M.; Miyasaka, H.; Wernsdorfer, W.; Nakata, K.; Sugiura, K.; Yamashita, M.; Coulon, C.; Clérac, R. *J. Am. Chem. Soc.* **2005**, *127* (9), 3090–3099.
26. Vaz, M. G. F.; Cassaro, R. A. A.; Akpinar, H.; Schlueter, J. A.; Lahti, P. M.; Novak, M. A. *Chemistry* **2014**, *20* (18), 5460–5467.

Appendix A: FT-IR spectra

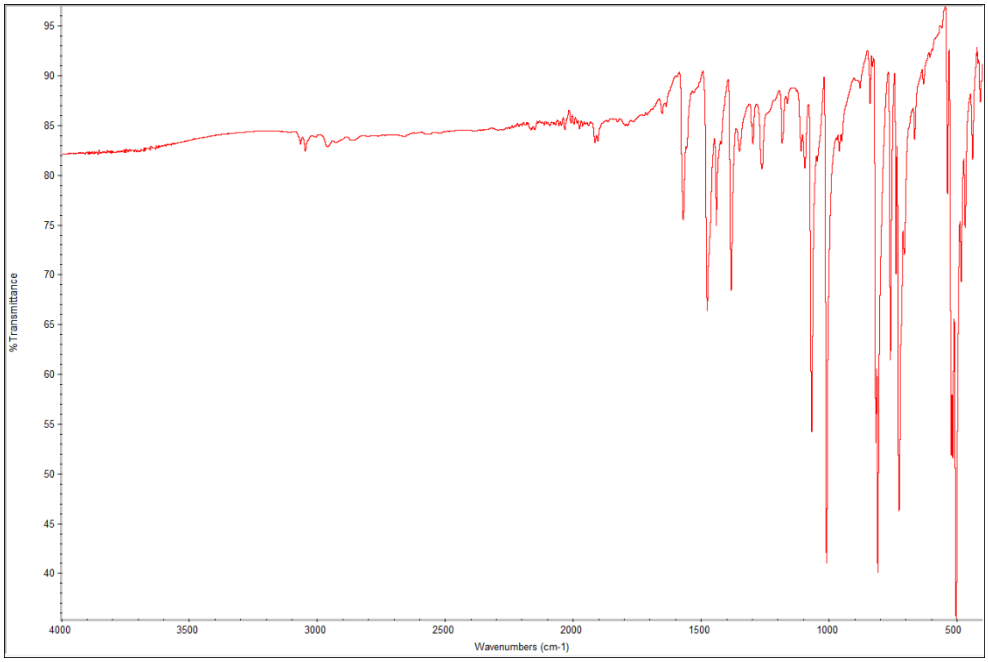

Figure A.1. Infrared spectrum of bbcb-Br(**4**) from 450−4000 cm^{-1}.

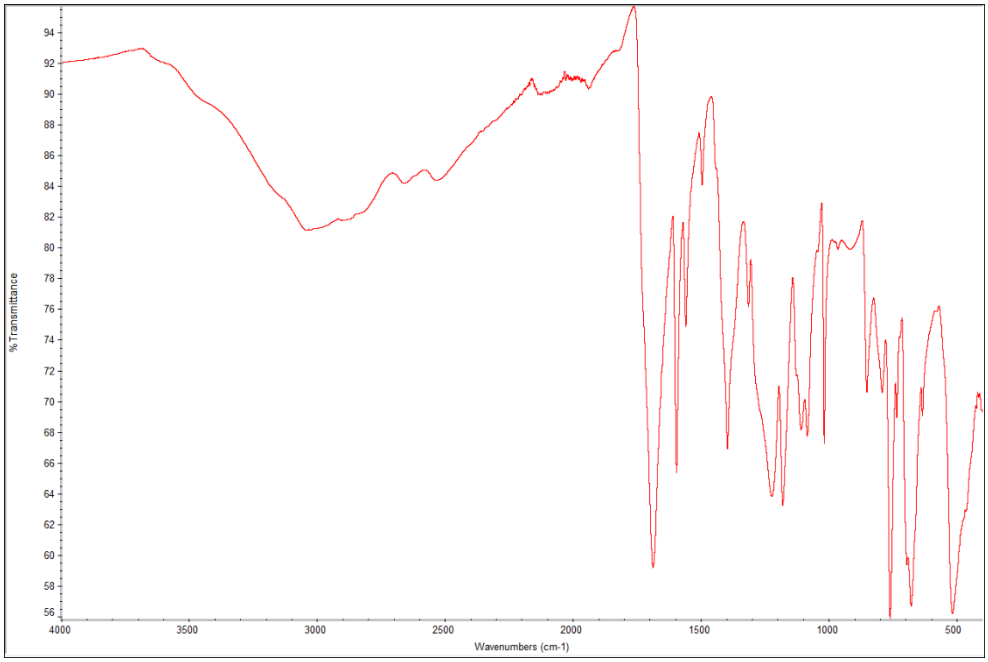

Figure A.2. Infrared spectrum of bbcb (**5**) from 450−4000 cm^{-1}.

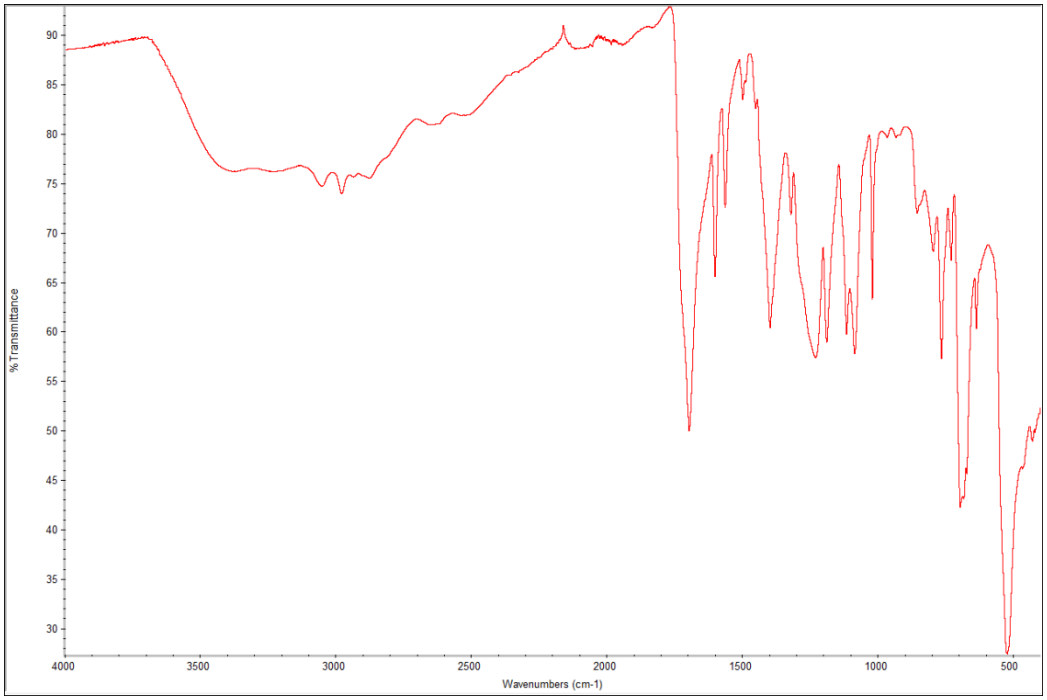

Figure A.3. Infrared spectrum of $PdCl_2(bbcb)_2$ (**6**) from 450−4000 cm^{-1}.

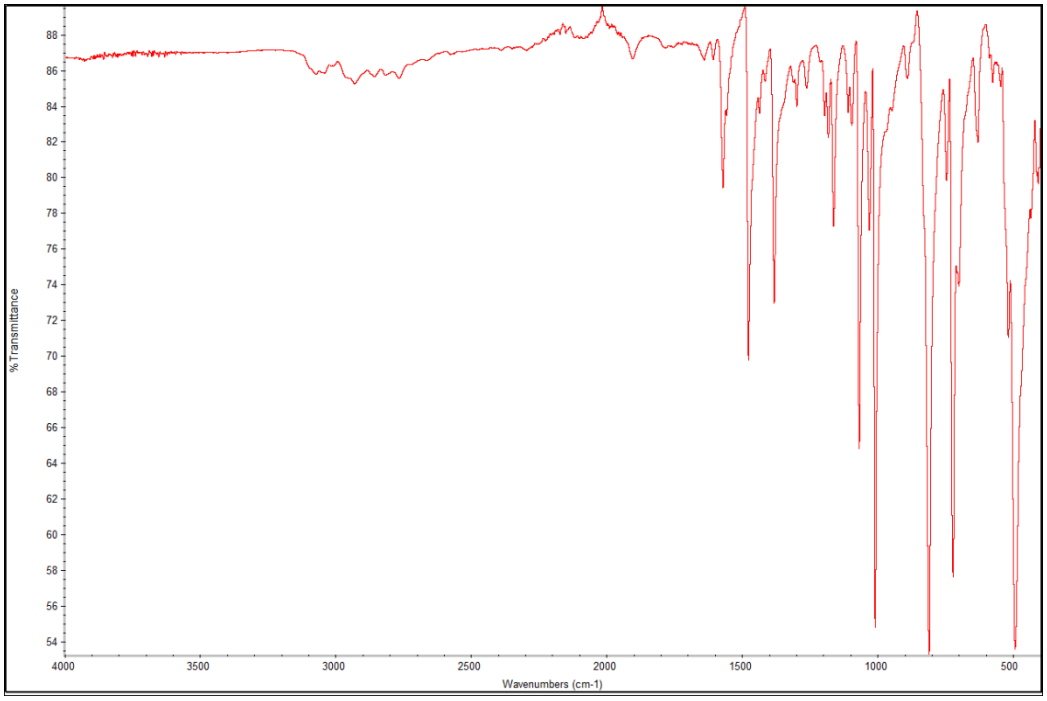

Figure A.4. Infrared spectrum of dppf-Br (**7**) from 450−4000 cm^{-1}.

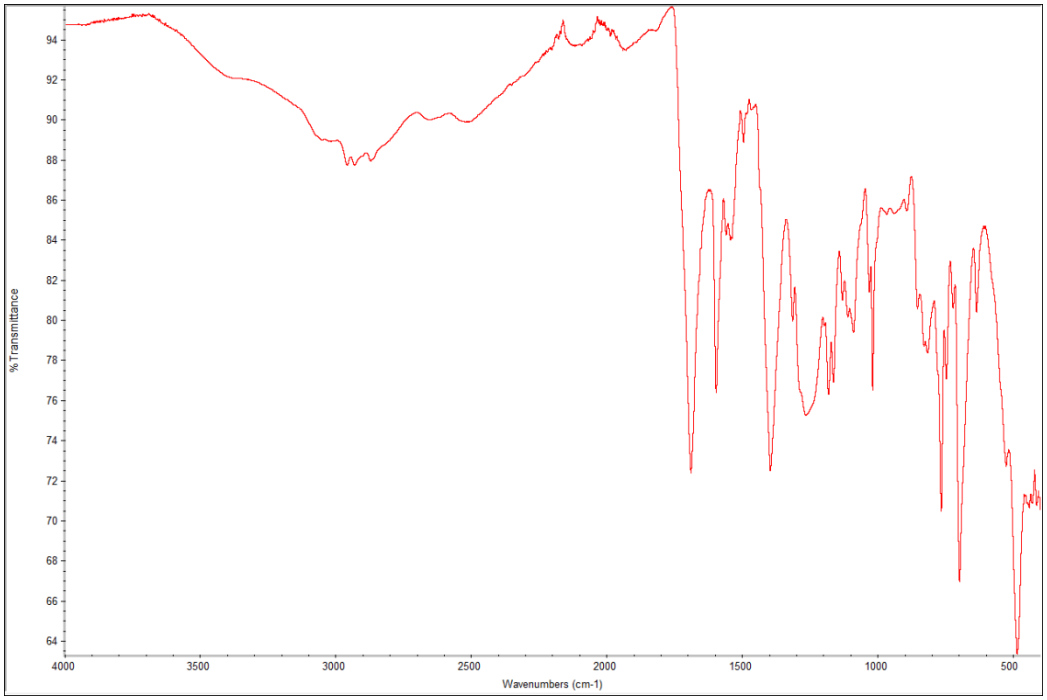

Figure A.5. Infrared spectrum of dppf-CO_2H (**8**) from 450−4000 cm^{-1}.

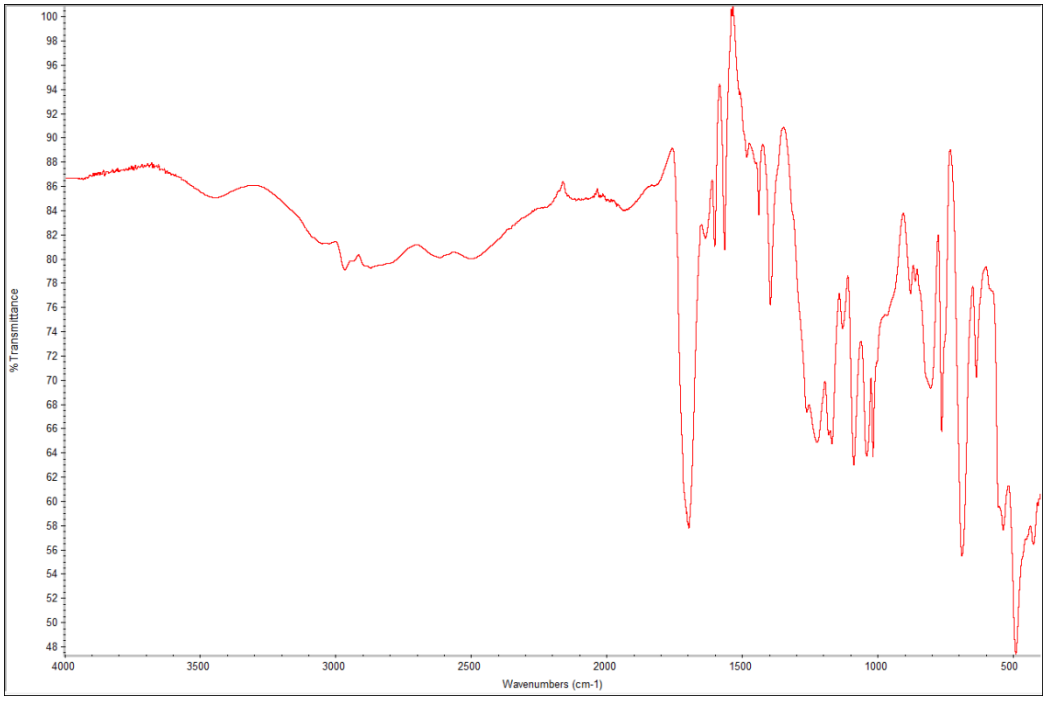

Figure A.6. Infrared spectrum of $PdCl_2$(dppf-CO_2H) (**9**) from 450−4000 cm^{-1}.

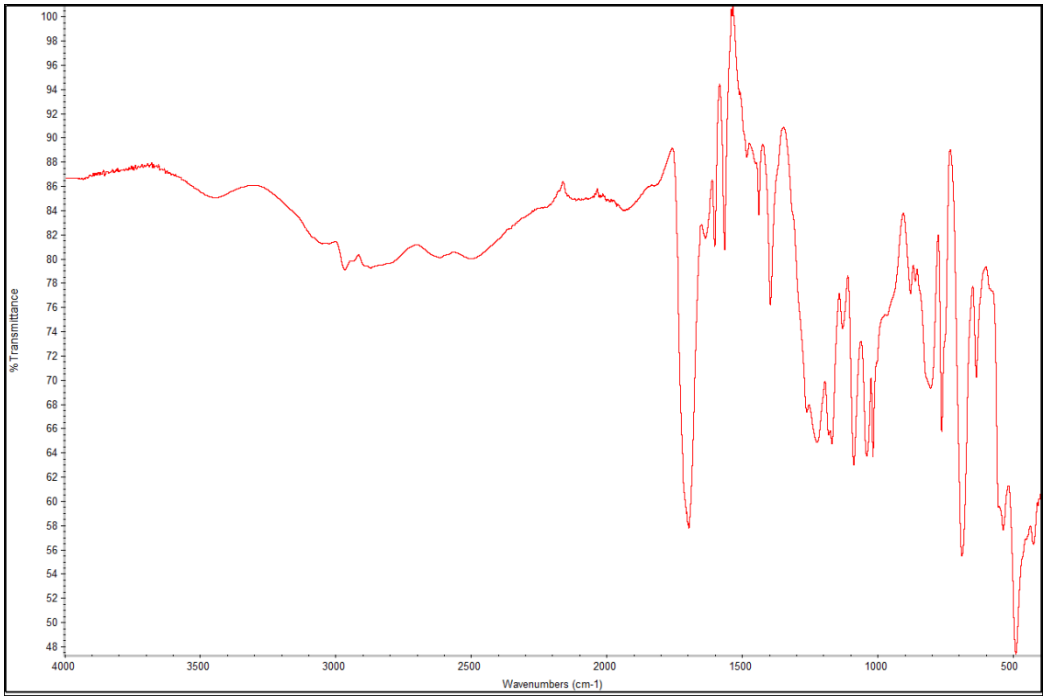

Figure A.7. Infrared spectrum of $PtCl_2$(dppf-CO_2H) (**10**) from 450−4000 cm^{-1}.

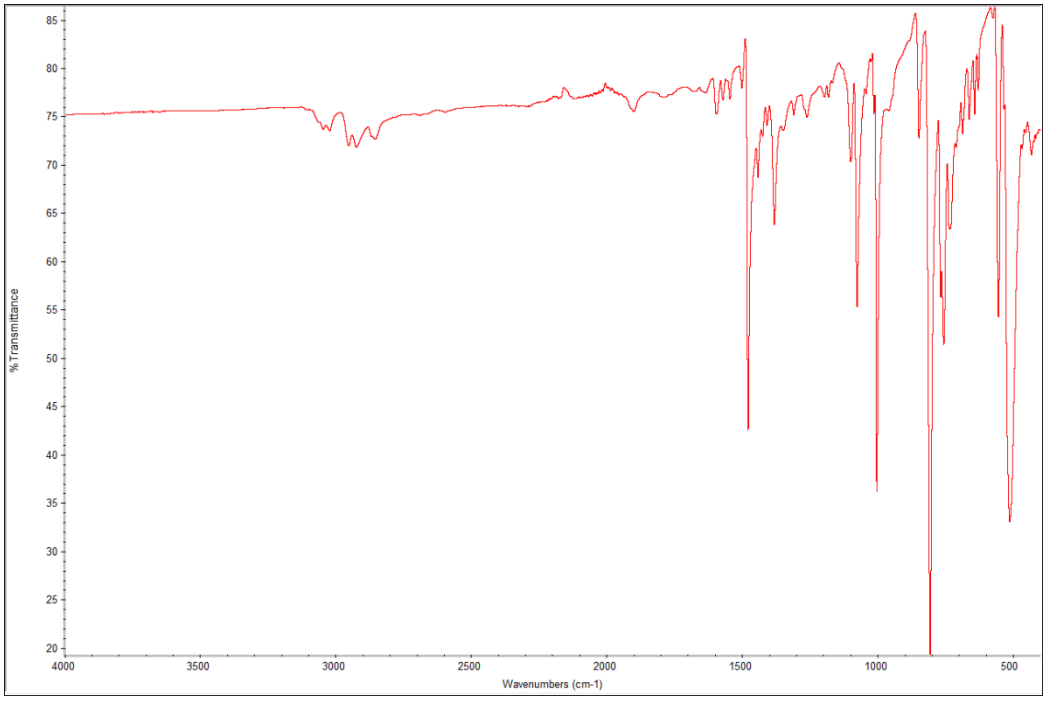

Figure A.8. Infrared spectrum of b-bbcb-Br (**11**) from 450−4000 cm^{-1}.

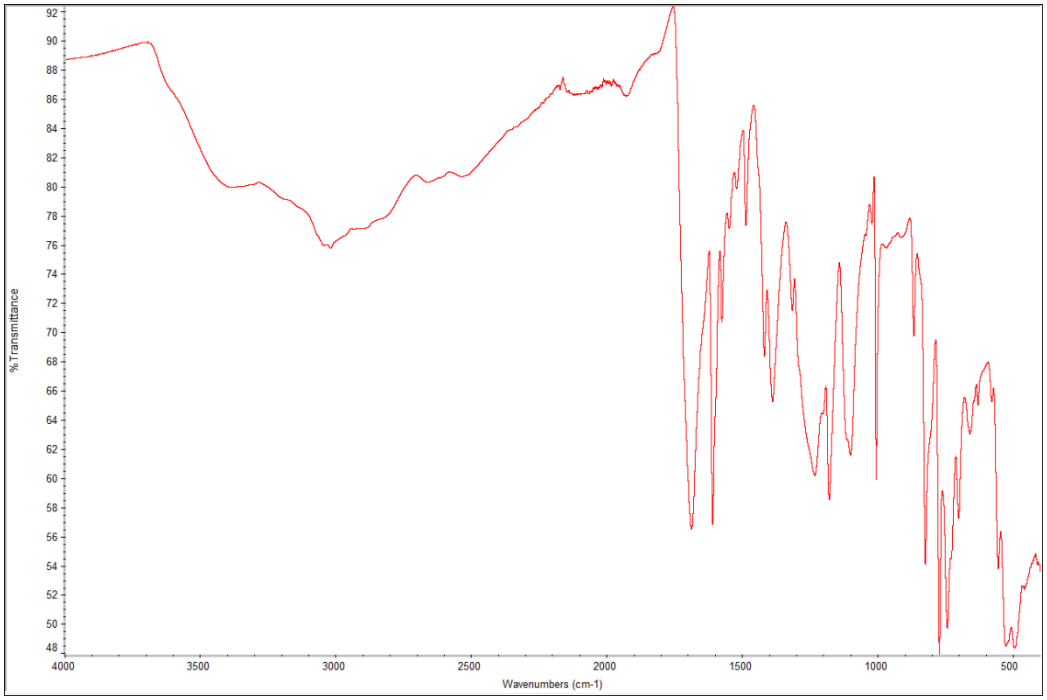

Figure A.9. Infrared spectrum of b-bbcb (**12**) from 450−4000 cm^{-1}.

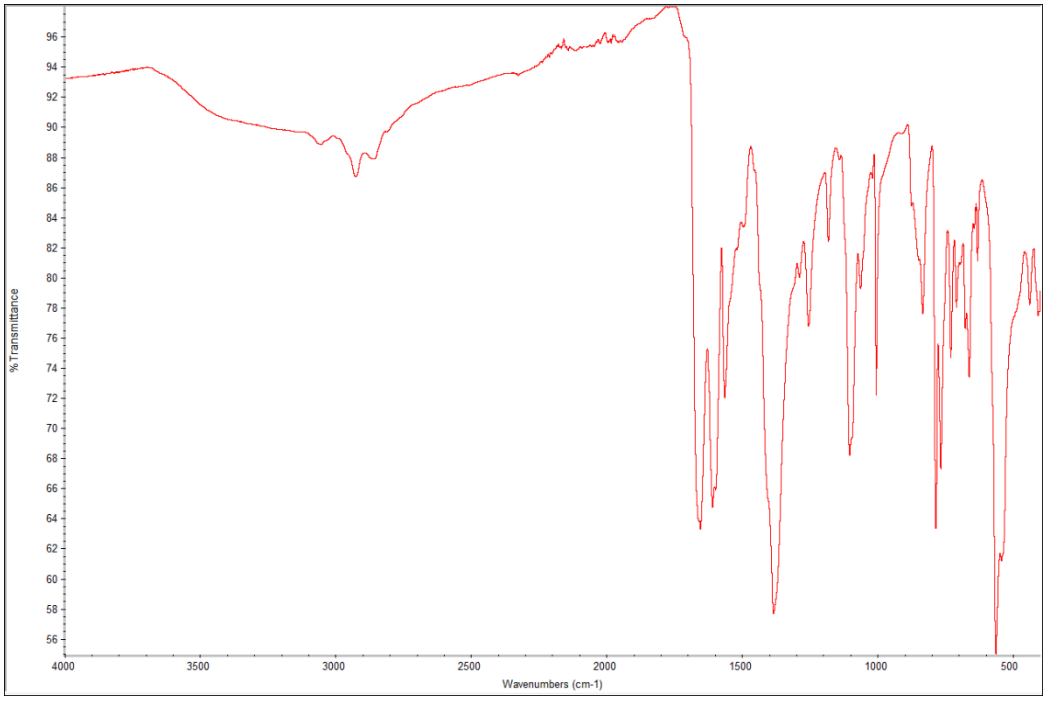

Figure A.10. Infrared spectrum of $PdCl_2$(b-bbcb) (**13**) from 450−4000 cm^{-1}.

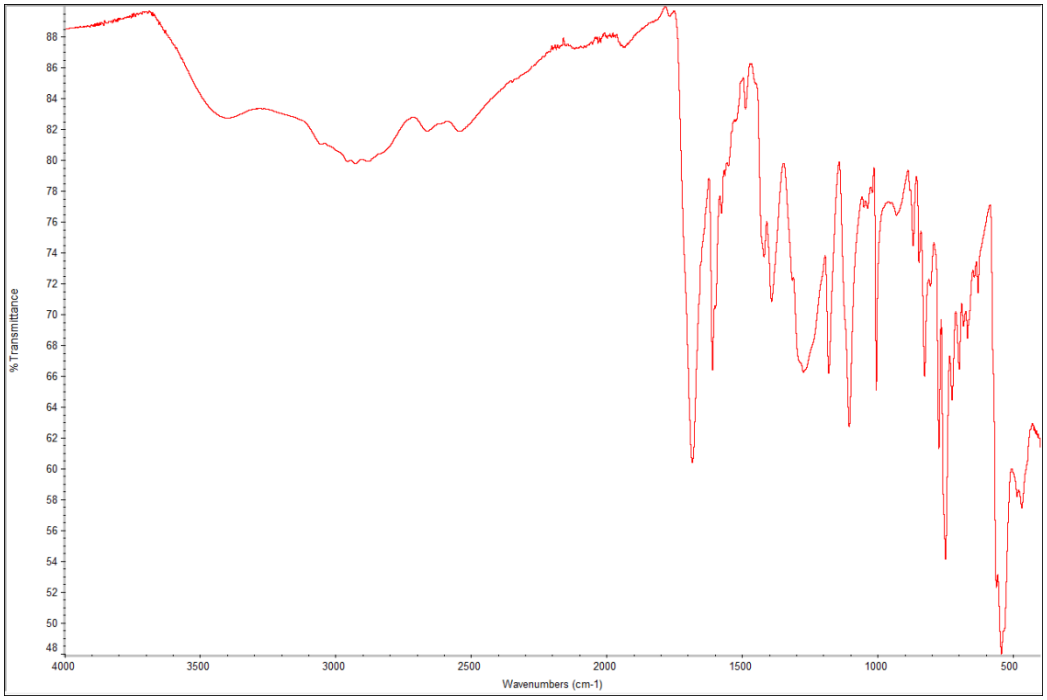

Figure A.11. Infrared spectrum of PCM-41 (**14**) from 450−4000 cm^{-1}.

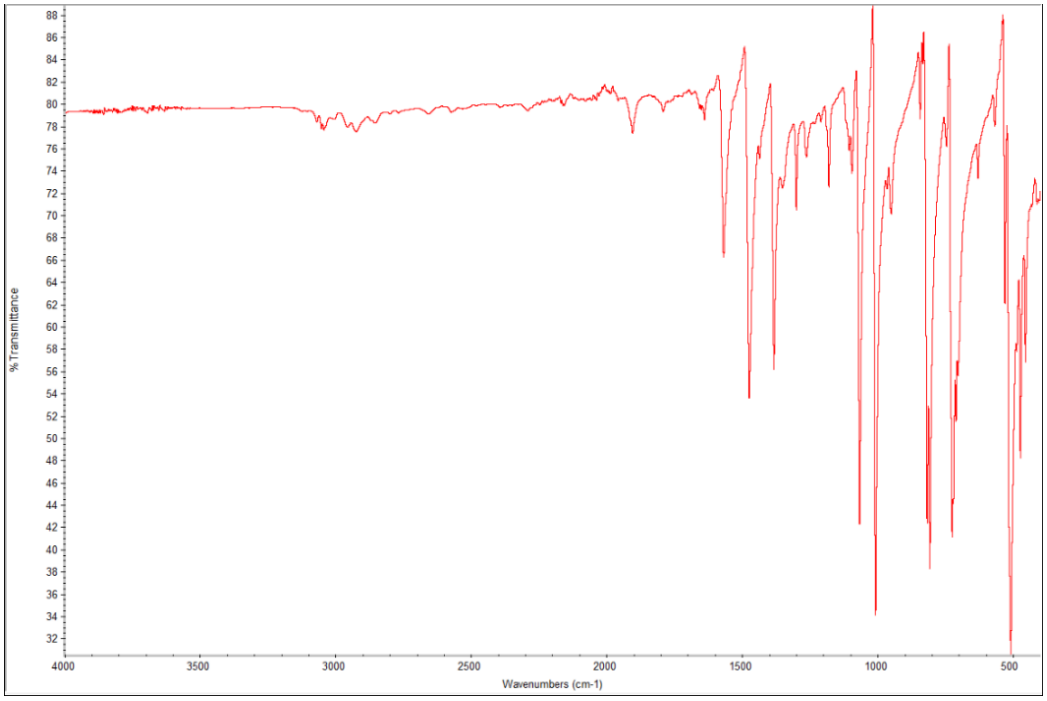

Figure A.12. Infrared spectrum of tBrtpp (**15**) from 450−4000 cm^{-1}.

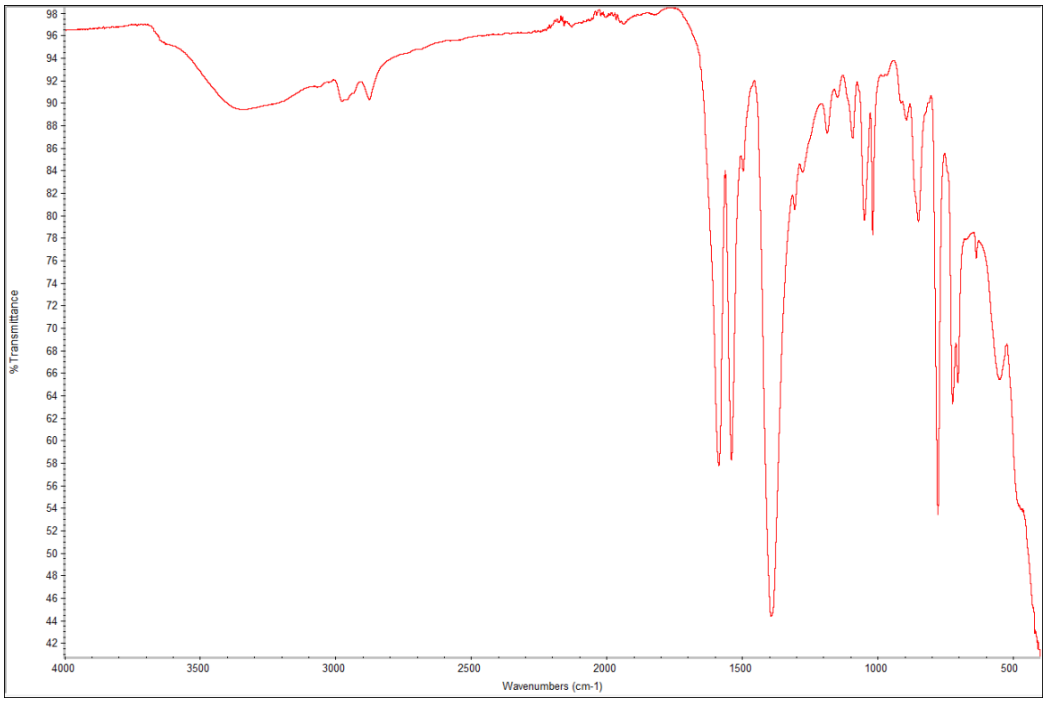

Figure A.13. Infrared spectrum of $pbtcLi_3$ (**16**) from 450−4000 cm^{-1}.

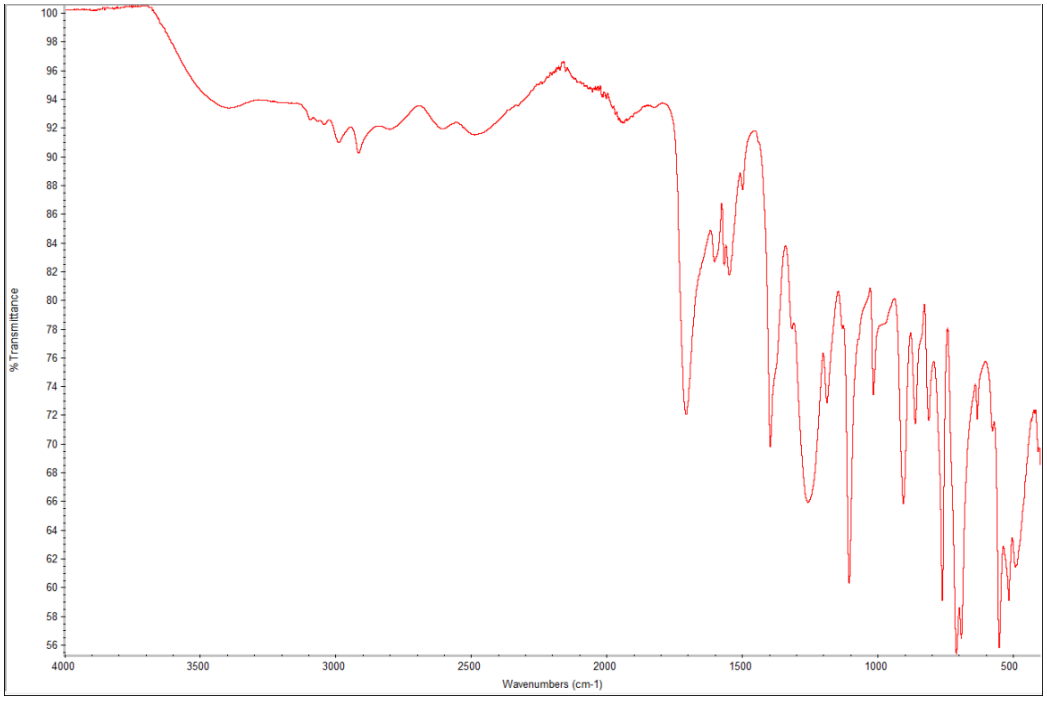

Figure A.14. Infrared spectrum of $[mptbcH_3]Cl$ (**17**) from 450−4000 cm^{-1}.

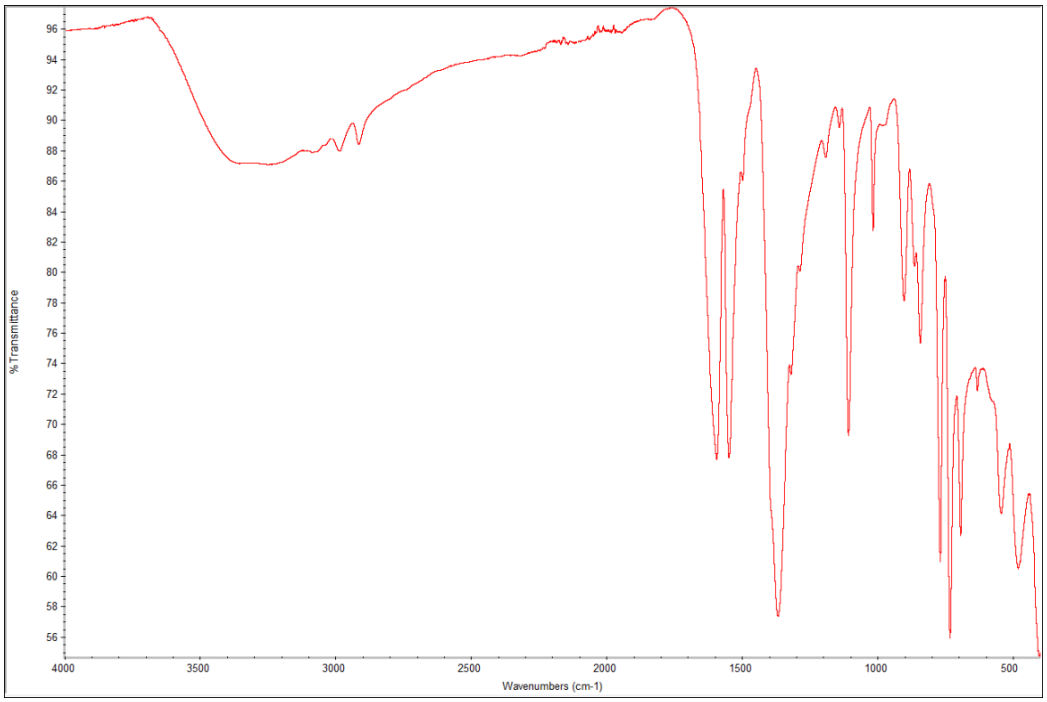

Figure A.15. Infrared spectrum of PCM-6 (**18**) from 450−4000 cm^{-1}.

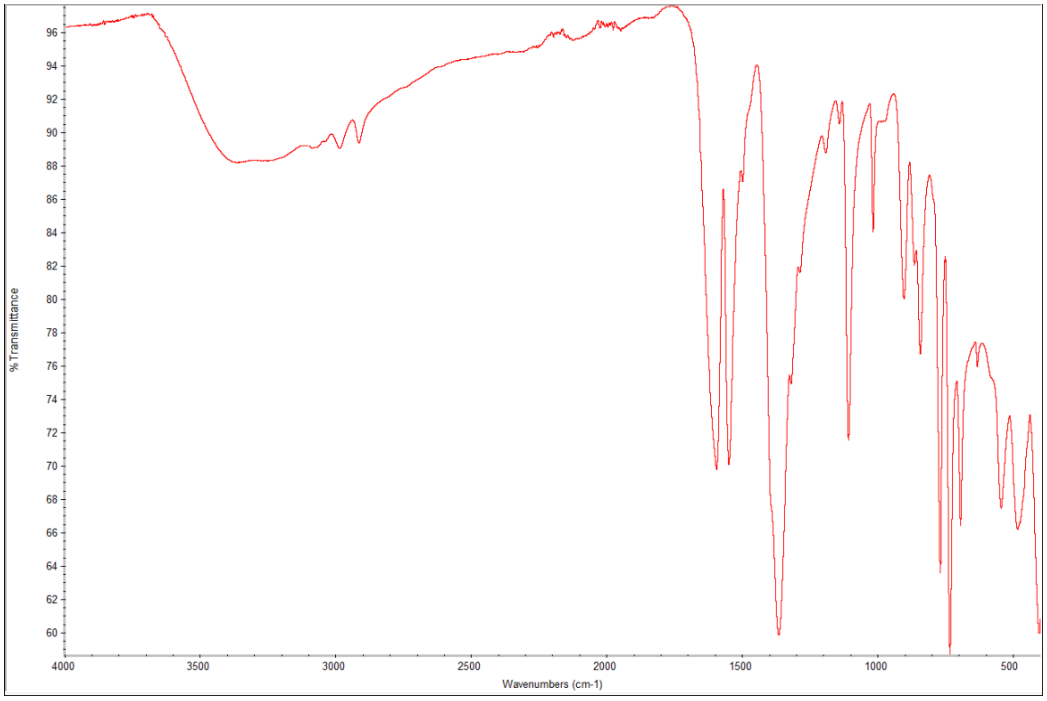

Figure A.16. Infrared spectrum of PCM-7 (**19**) from 450−4000 cm^{-1}.

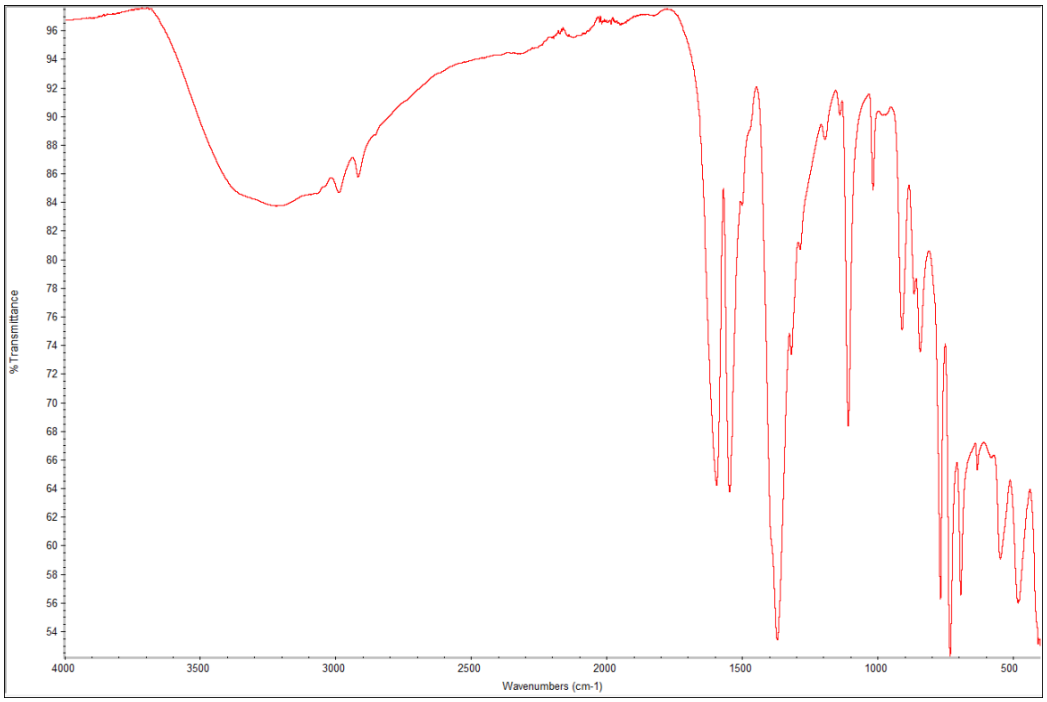

Figure A.17. Infrared spectrum of PCM-8(K) (**20**) from 450−4000 cm^{-1}.

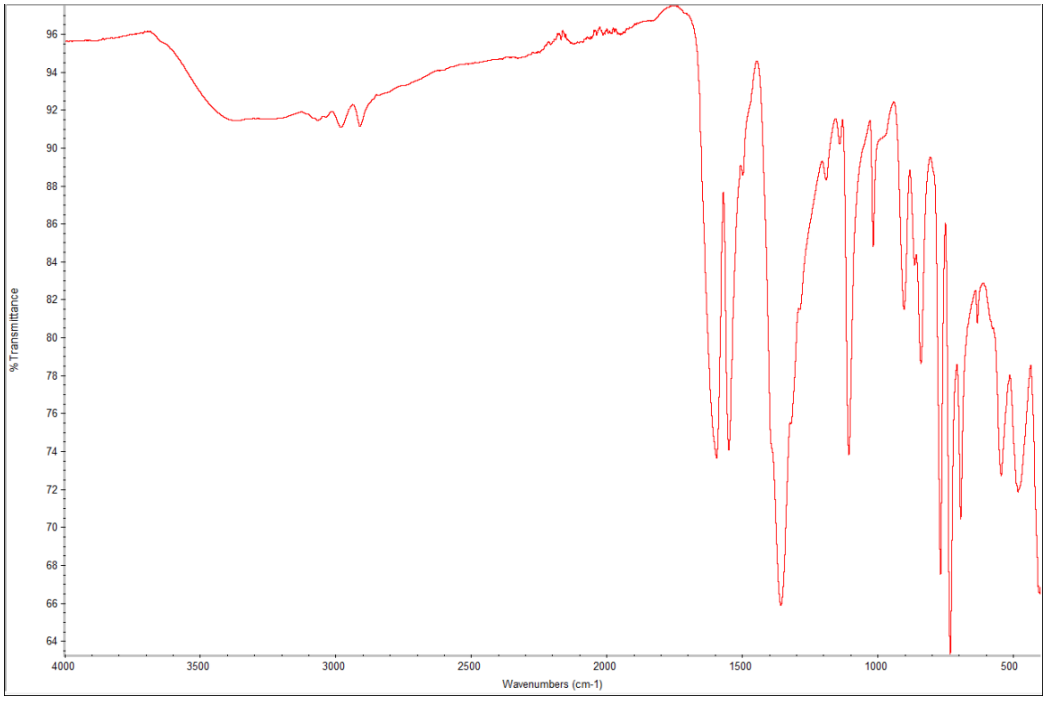

Figure A.18. Infrared spectrum of PCM-8(Rb) (**21**) from 450−4000 cm^{-1}.

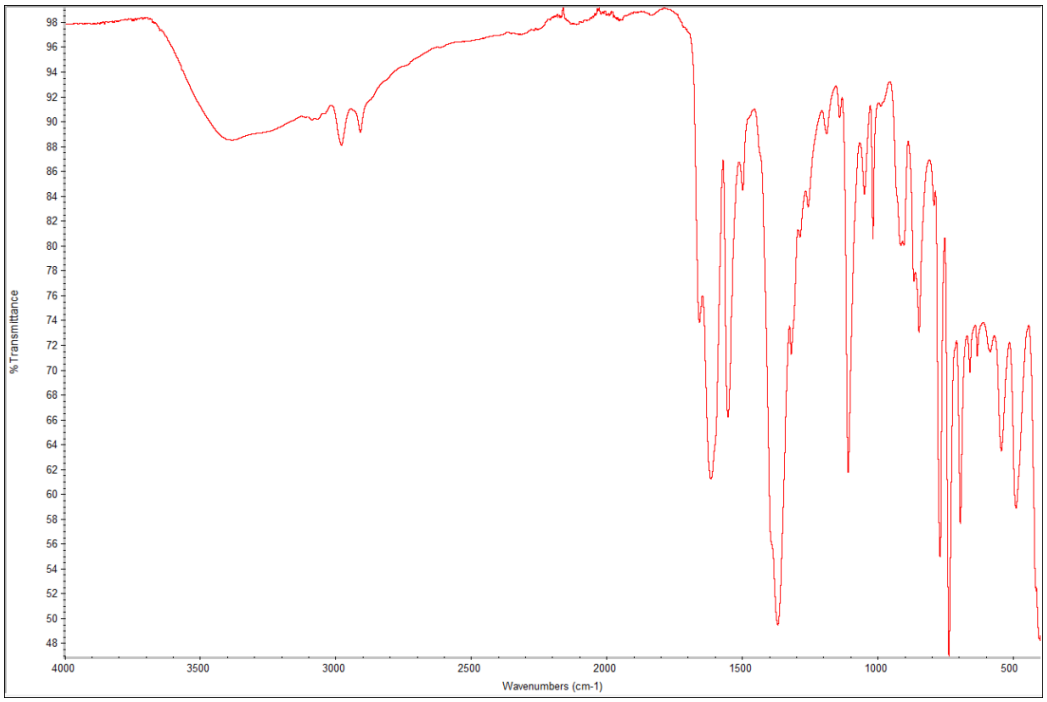

Figure A.19. Infrared spectrum of PCM-9 (**22**) from 450−4000 cm^{-1}.

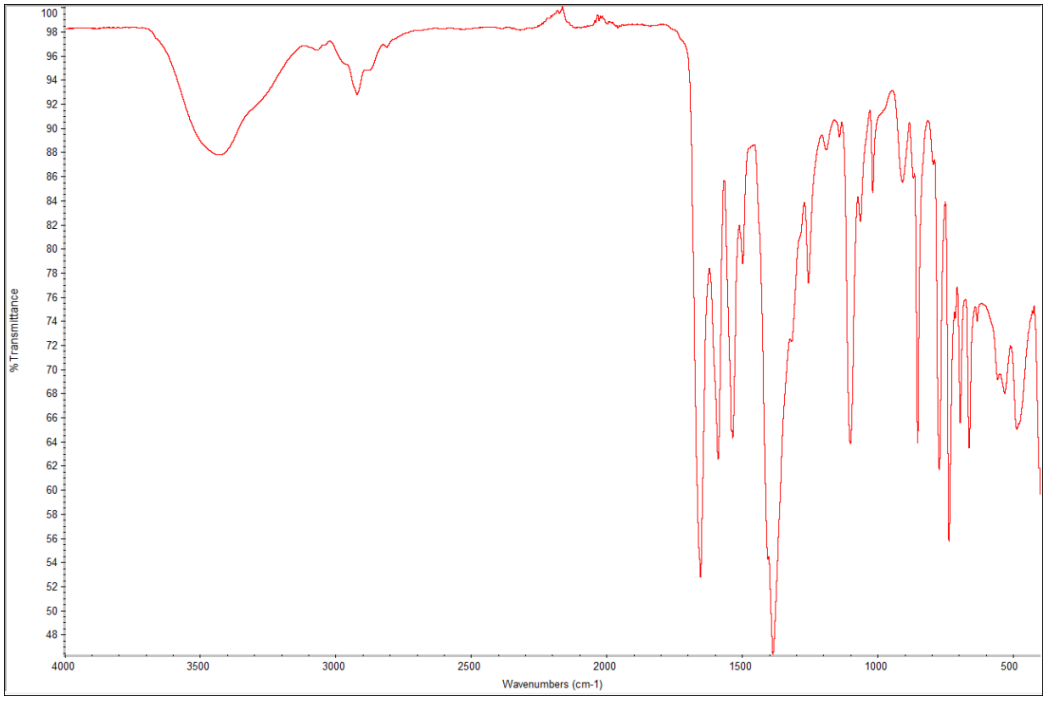

Figure A.20. Infrared spectrum of Pr-PCM-21 (**23**) from 450−4000 cm^{-1}.

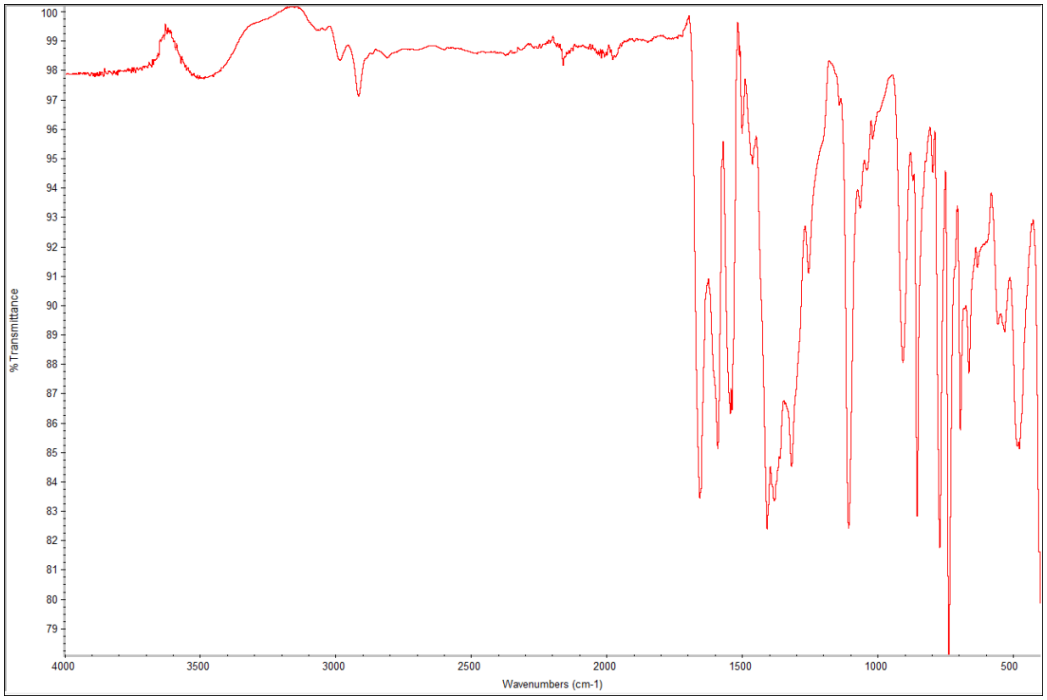

Figure A.21. Infrared Spectrum Nd-PCM-21 (**24**) from 450−4000 cm^{-1}.

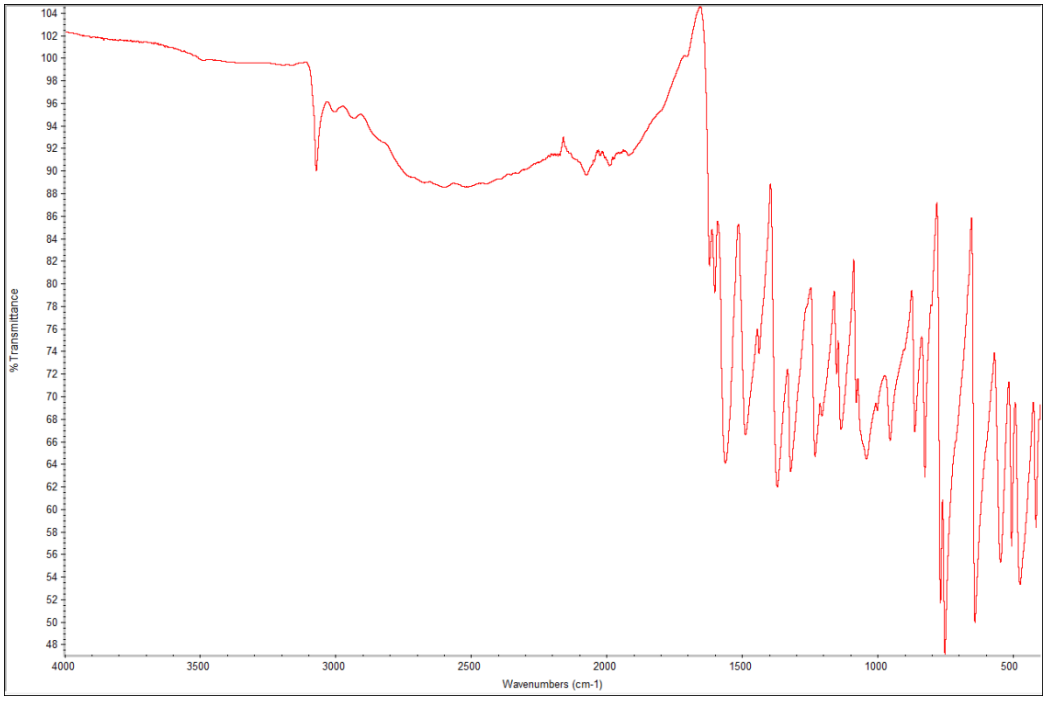

Figure A.22. Infrared spectrum of Fe-TCM-1 (**25**) from 450−4000 cm^{-1}.

Appendix B: NMR spectra

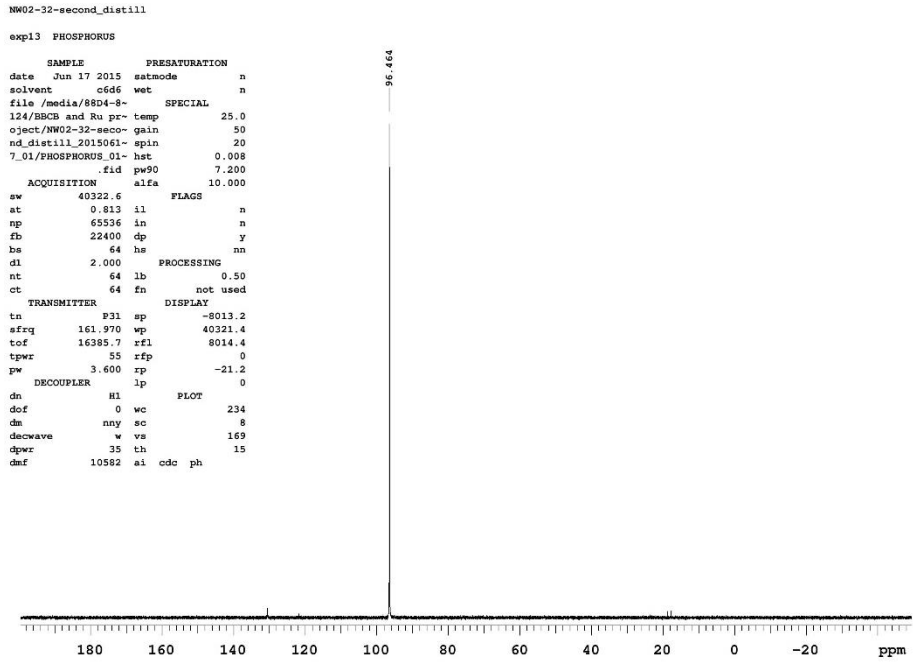

Figure B.1. ^{31}P-NMR spectrum of (**1**) in C_6D_6.

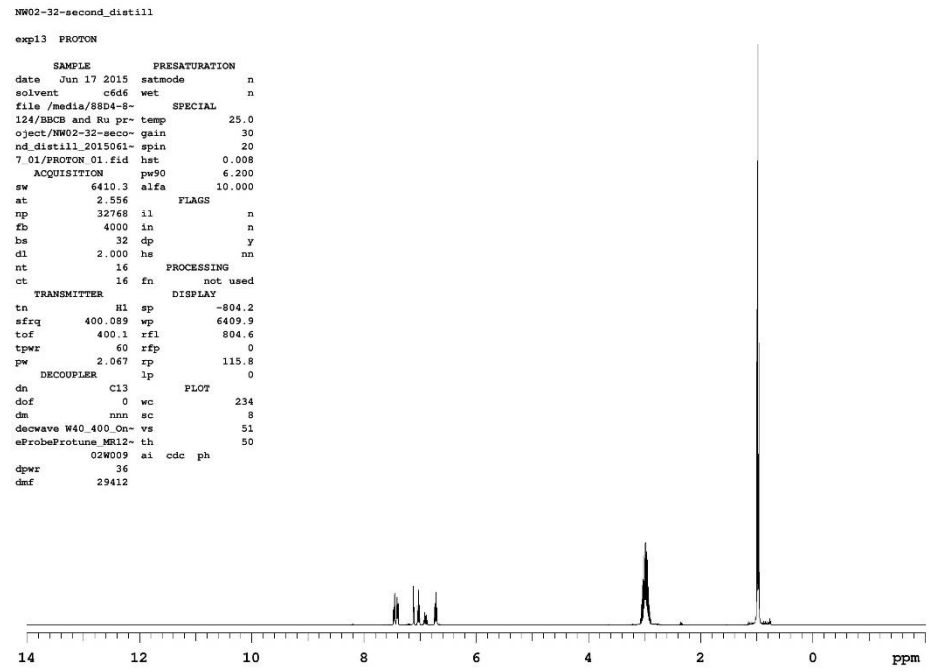

Figure B.2. ^{1}H-NMR spectrum of (**1**) in C_6D_6.

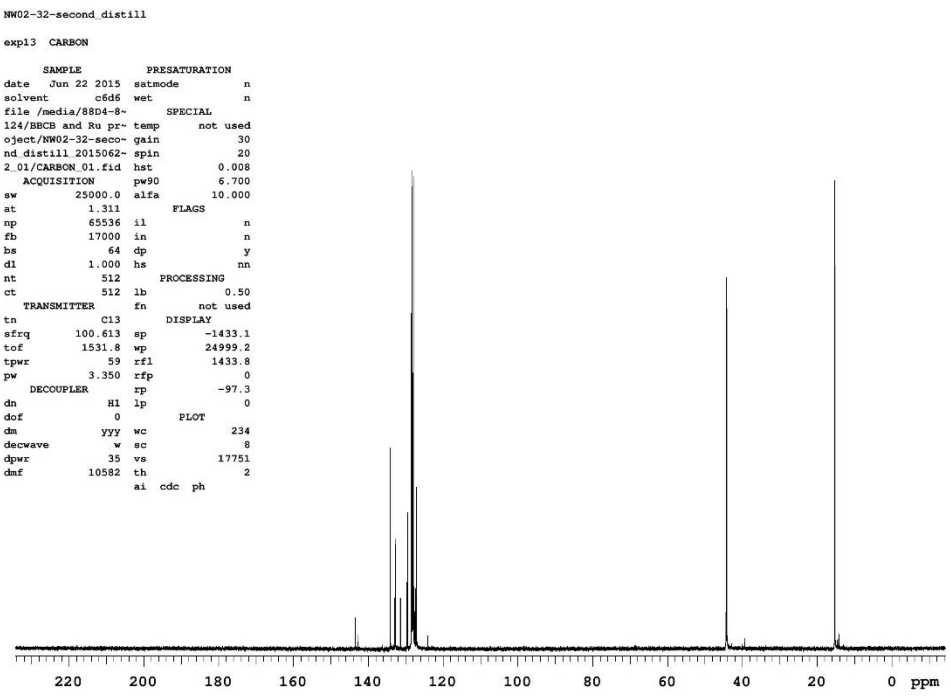

Figure B.3. ^{13}C-NMR spectrum of (**1**) in C_6D_6.

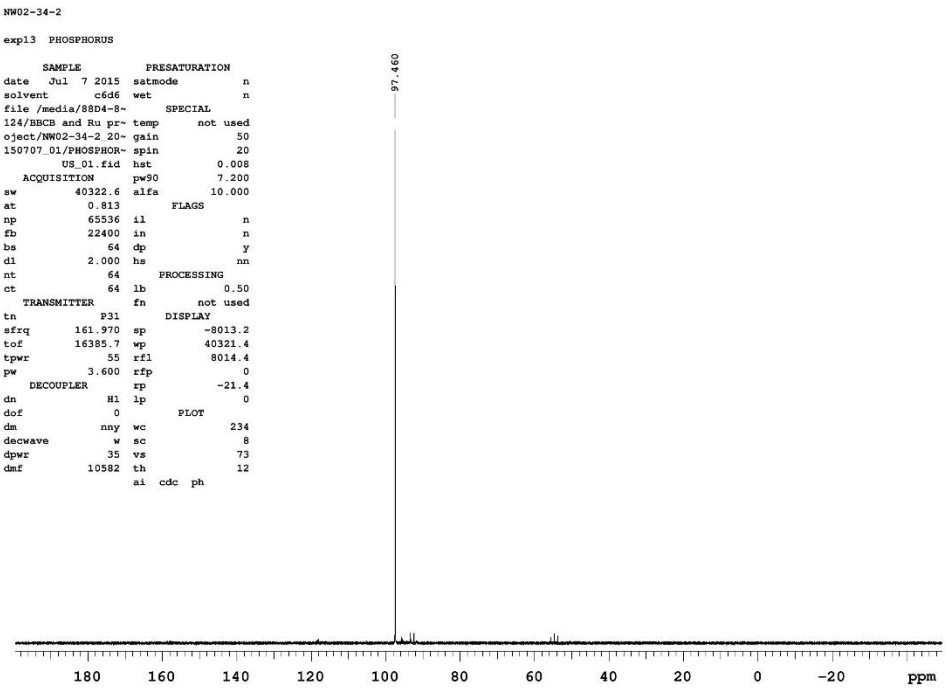

Figure B.4. ^{31}P-NMR spectrum of (**2**) in C_6D_6.

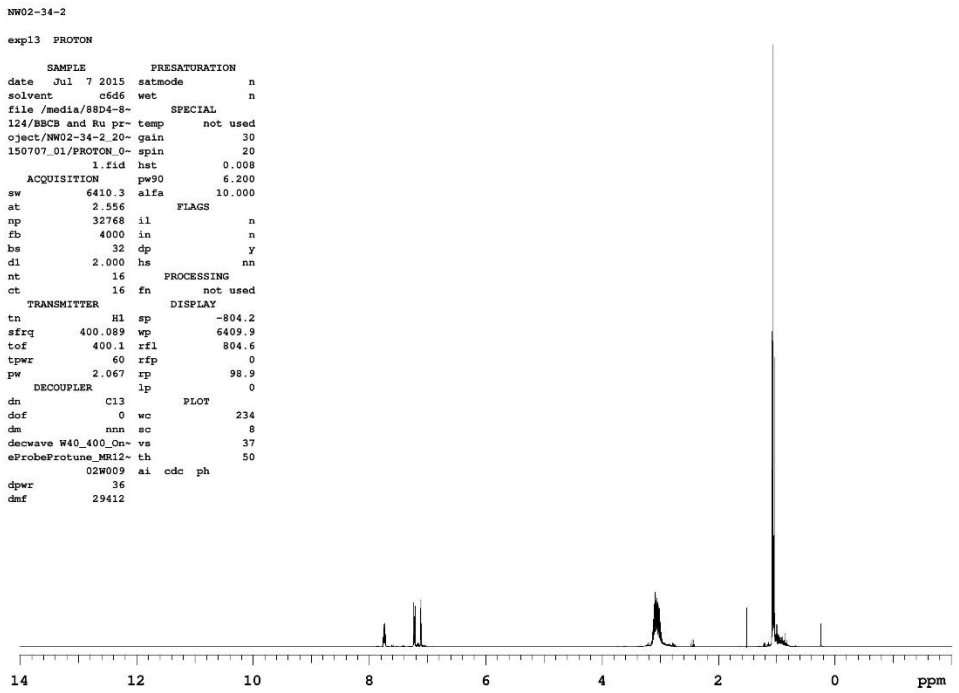

Figure B.5. ^{1}H-NMR spectrum of (**2**) in C_6D_6.

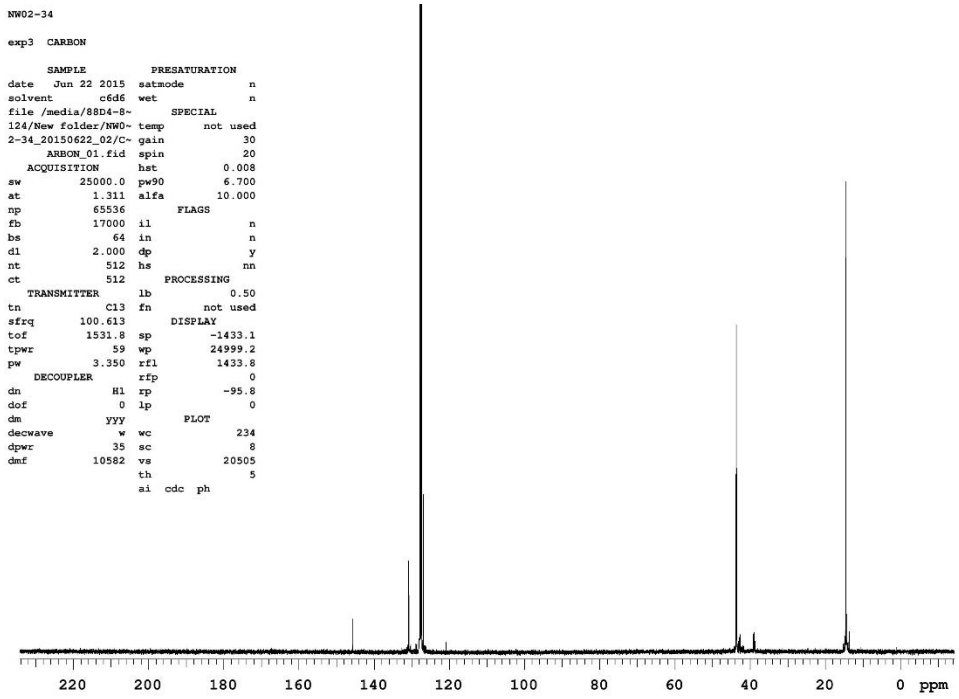

Figure B.6. ^{13}C-NMR spectrum of (**2**) in C_6D_6.

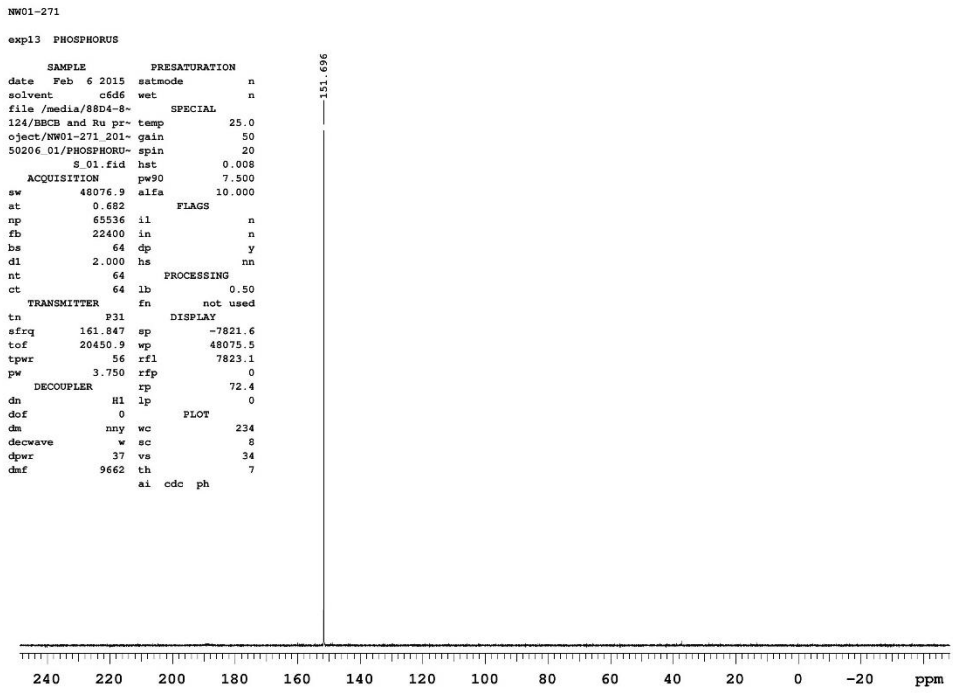

Figure B.7. ^{31}P-NMR spectrum of 1,2-dcpb (**3**) in C_6D_6.

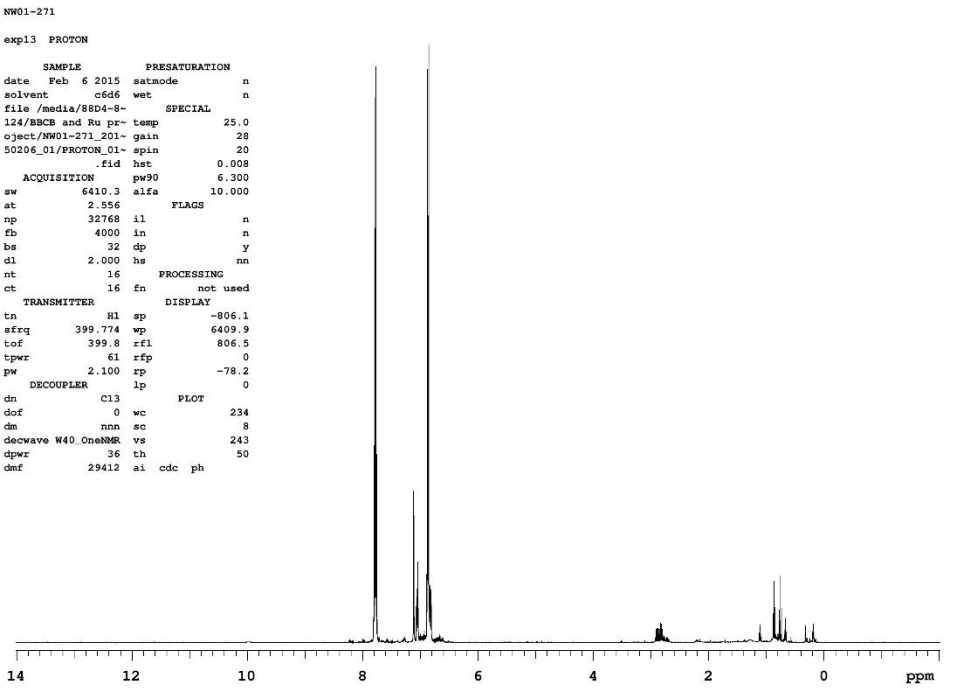

Figure B.8. ^{1}H-NMR spectrum of 1,2-dcpb (**3**) in C_6D_6.

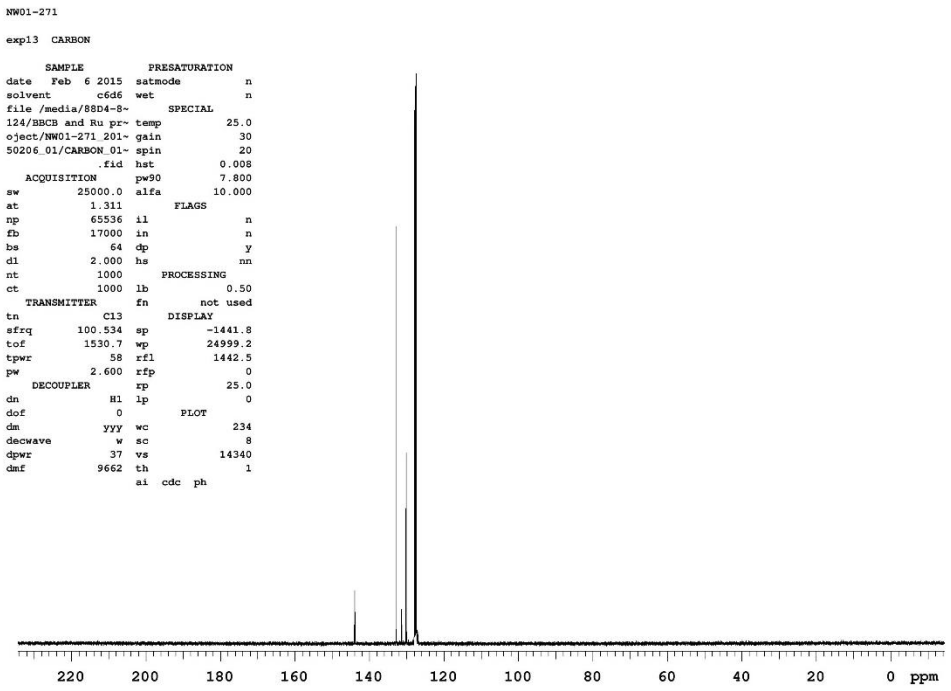

Figure B.9. ^{13}C-NMR spectrum of 1,2-dcpb (**3**) in C_6D_6.

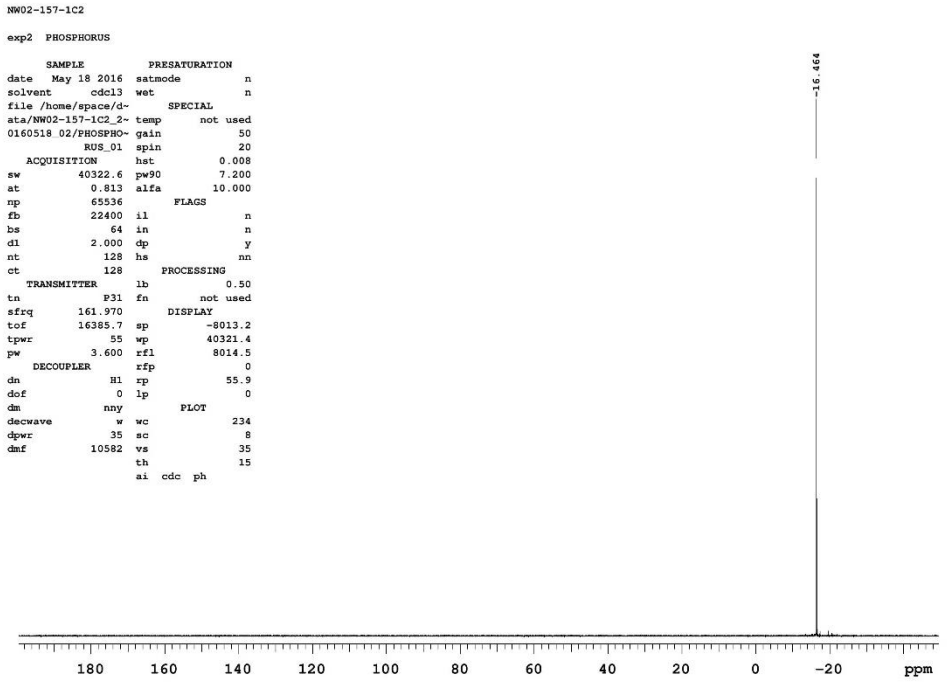

Figure B.10. ^{31}P-NMR spectrum of bbcb-Br (**4**) in $CDCl_3$.

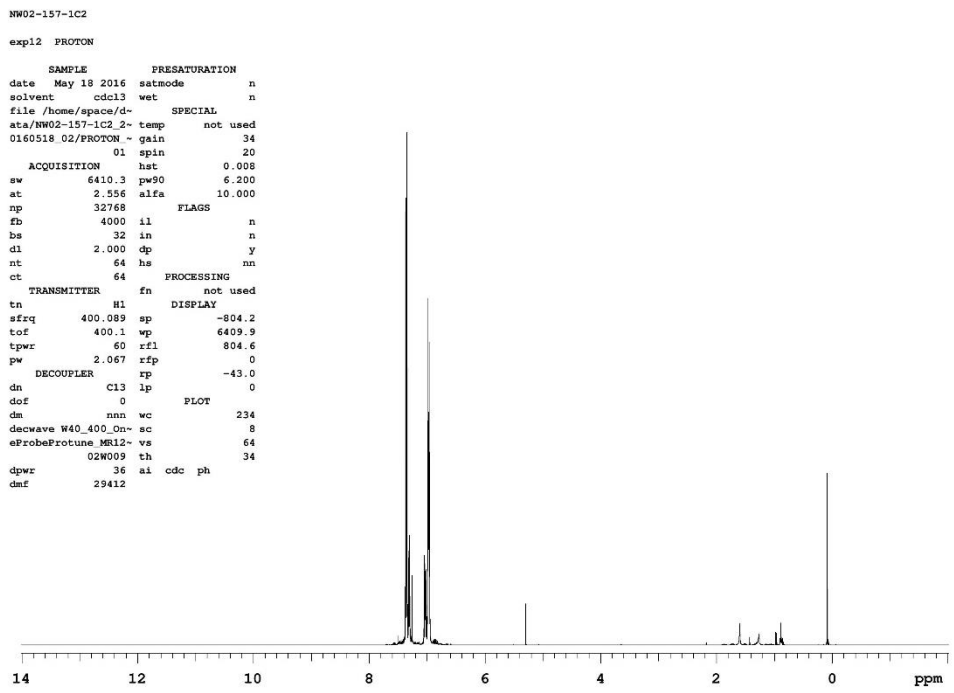

Figure B.11. ^{1}H-NMR spectrum of bbcb-Br (**4**) in $CDCl_3$.

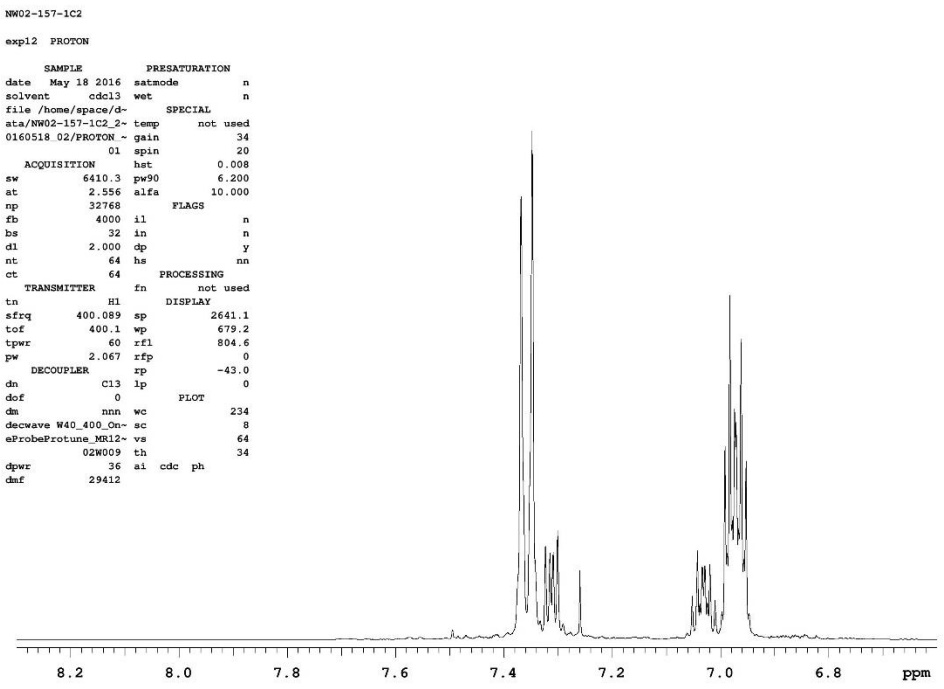

Figure B.12. ^{1}H expanded NMR spectrum of bbcb-Br (**4**) in $CDCl_3$.

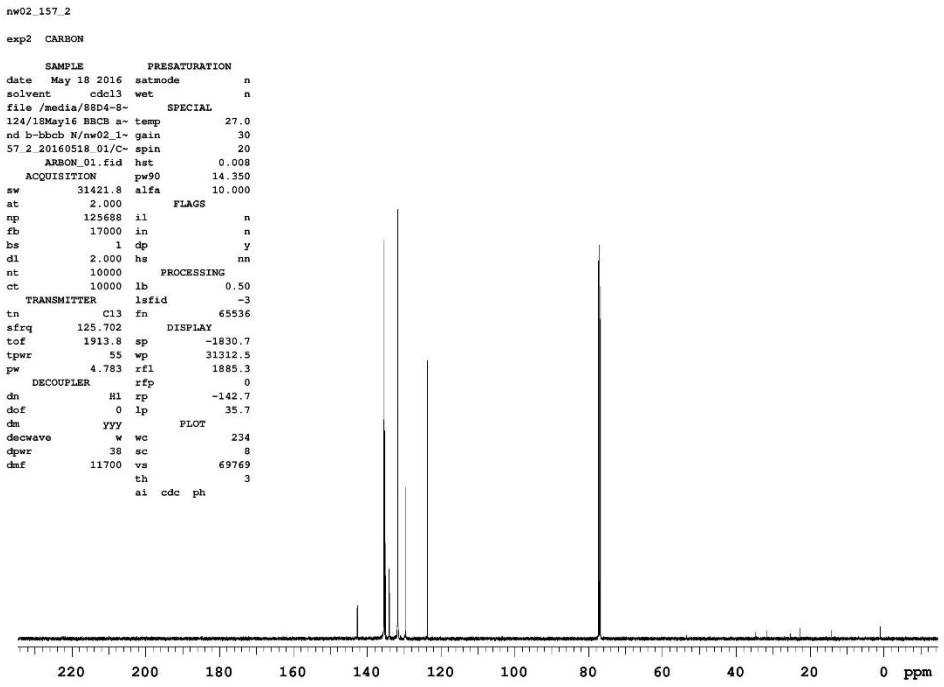

Figure B.13. ^{13}C-NMR spectrum of bbcb-Br (**4**) in $CDCl_3$.

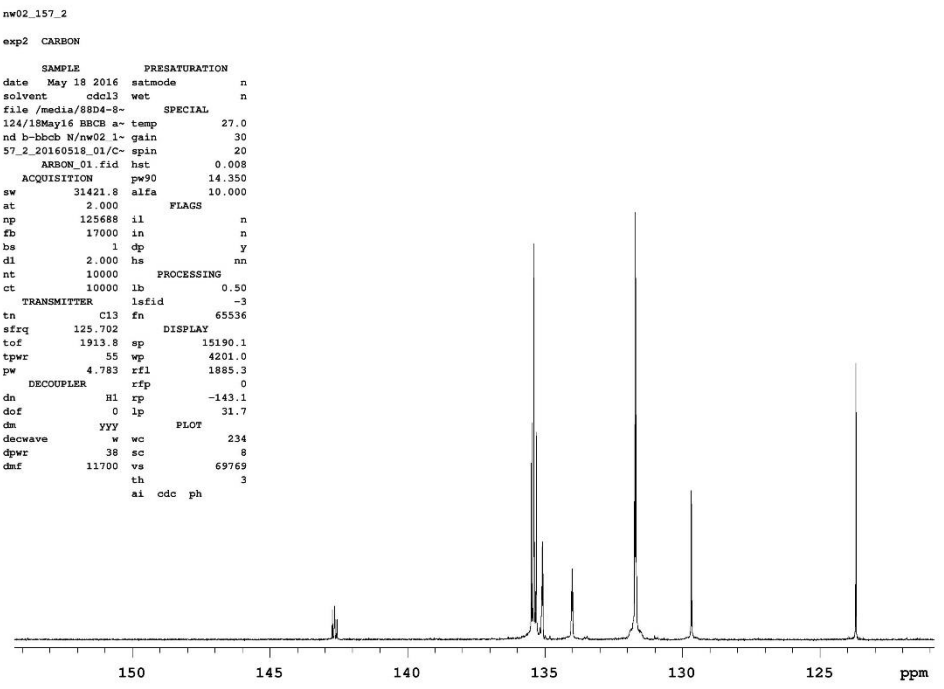

Figure B.14. ^{13}C expanded NMR spectrum of bbcb-Br (**4**) in $CDCl_3$.

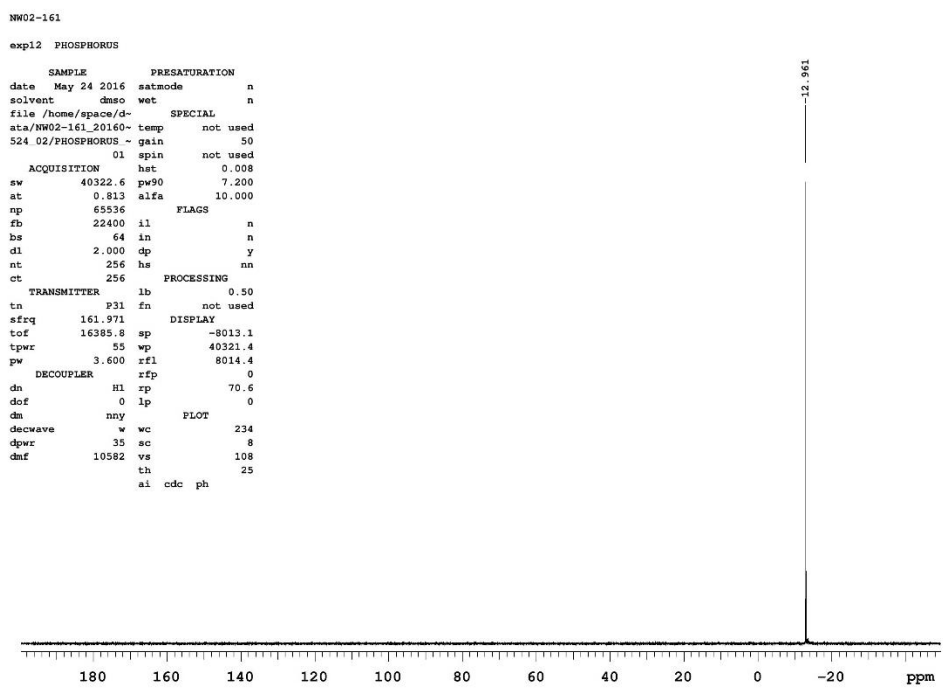

Figure B.15. ^{31}P-NMR spectrum of bbcb (**5**) in DMSO-d6.

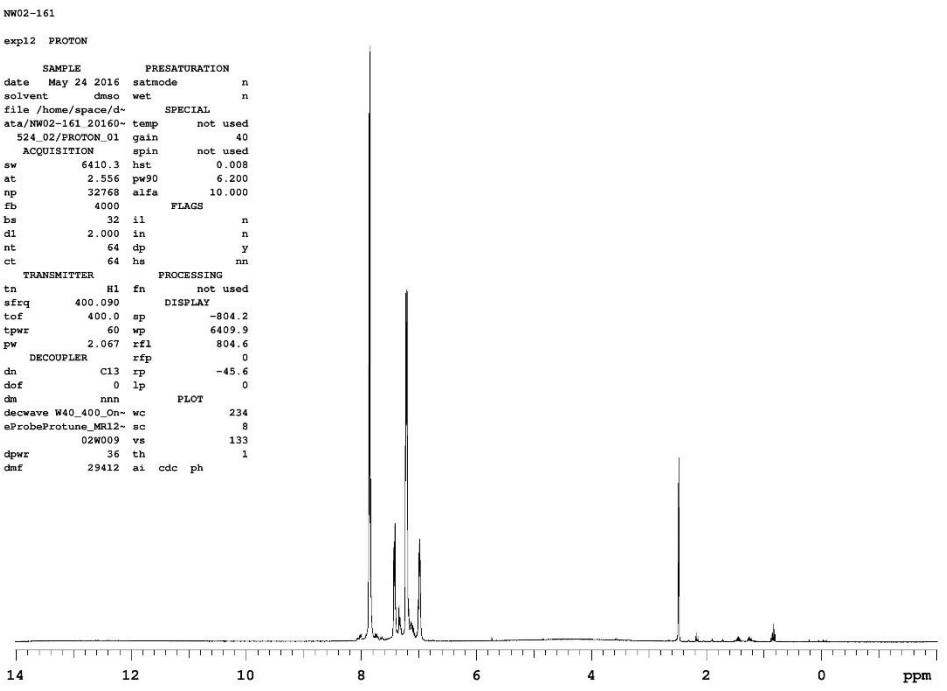

Figure B.16. ^{1}H-NMR spectrum of bbcb (**5**) in DMSO-d6

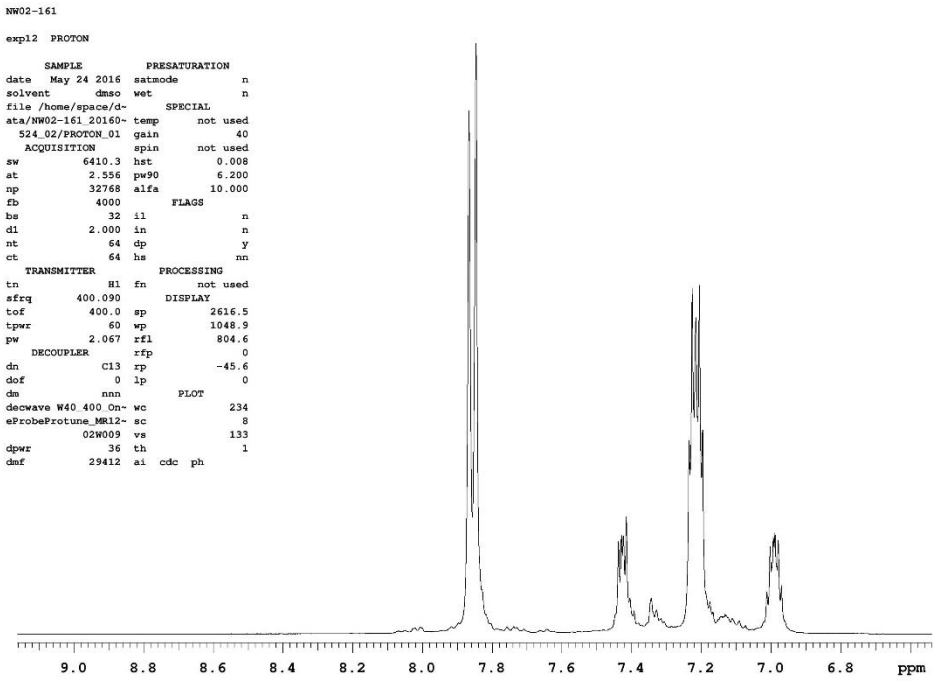

Figure B.17. ^{1}H expanded NMR spectrum of bbcb (**5**) in DMSO-d6.

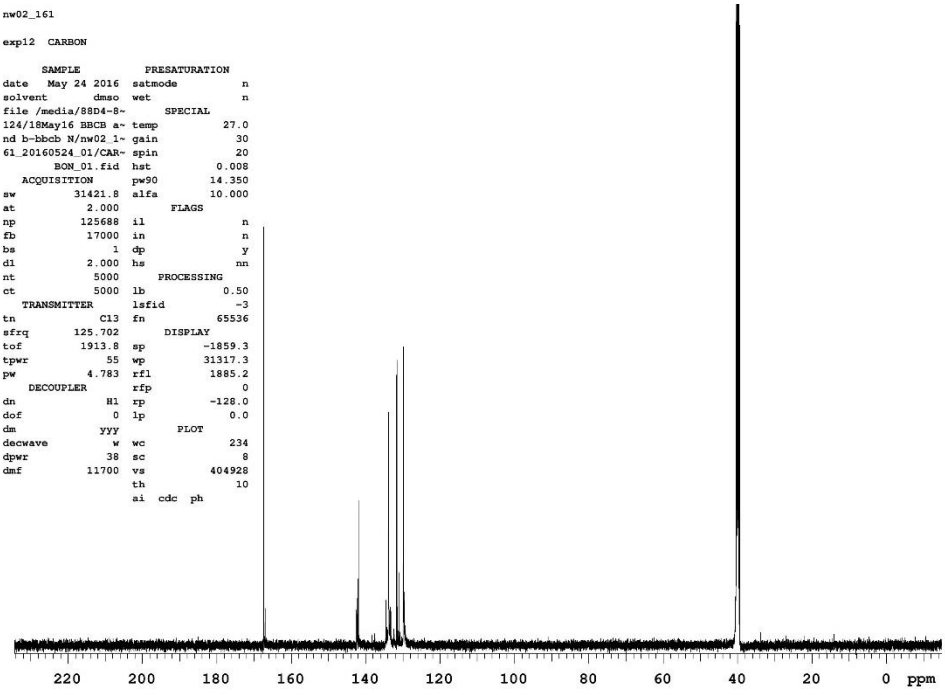

Figure B.18. ^{13}C-NMR spectrum of bbcb (**5**) in DMSO-d6.

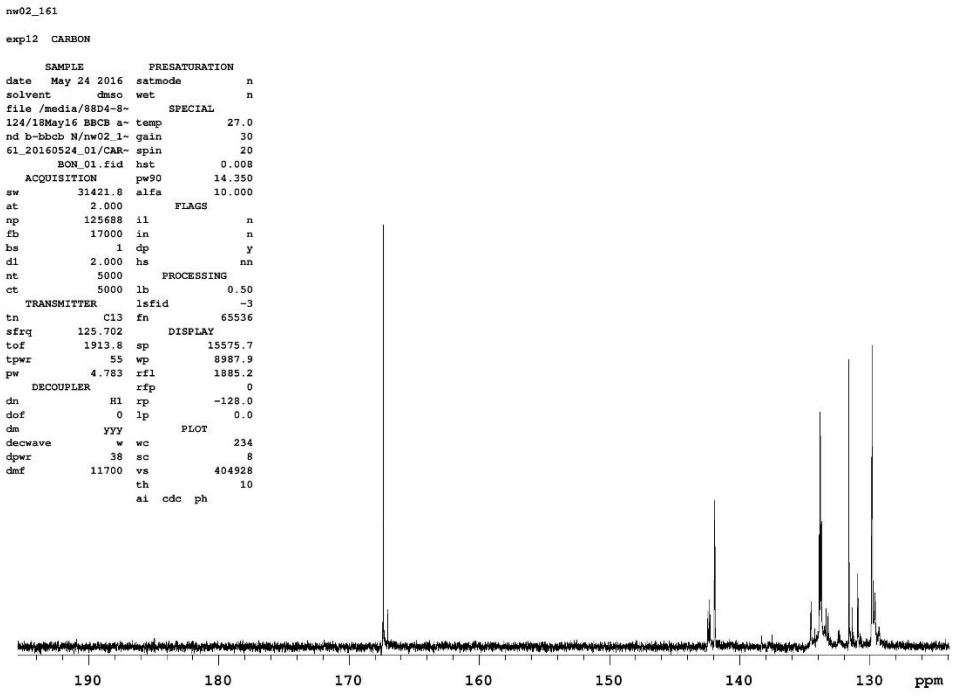

Figure B.19. ^{13}C expanded NMR spectrum of bbcb (**5**) in DMSO-d6.

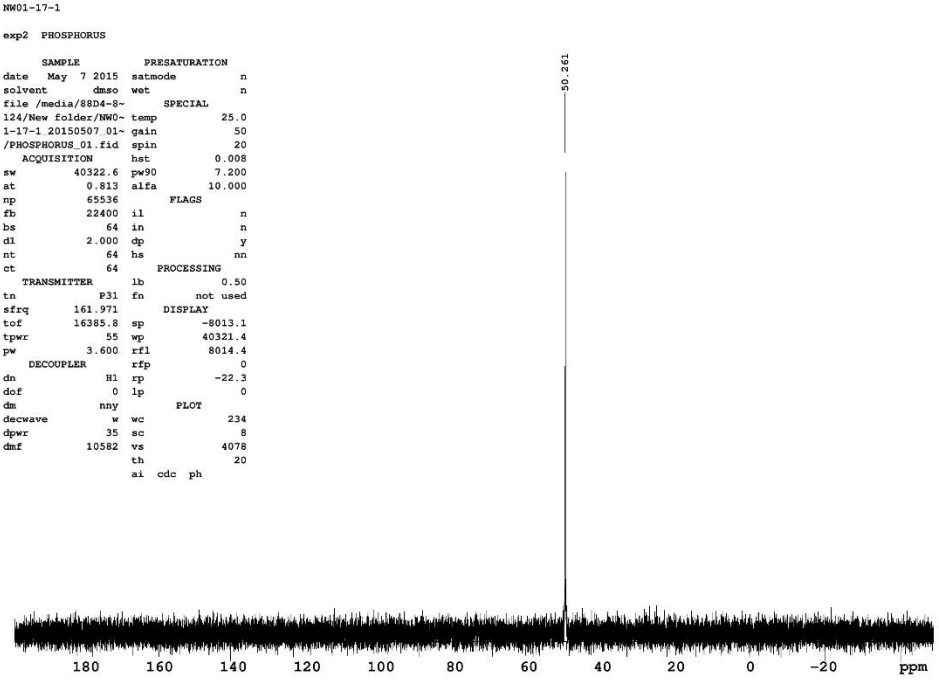

Figure B.20. ^{31}P-NMR spectrum of $RuCl_2(bbcb)_2$ (**6**) in DMSO-d6.

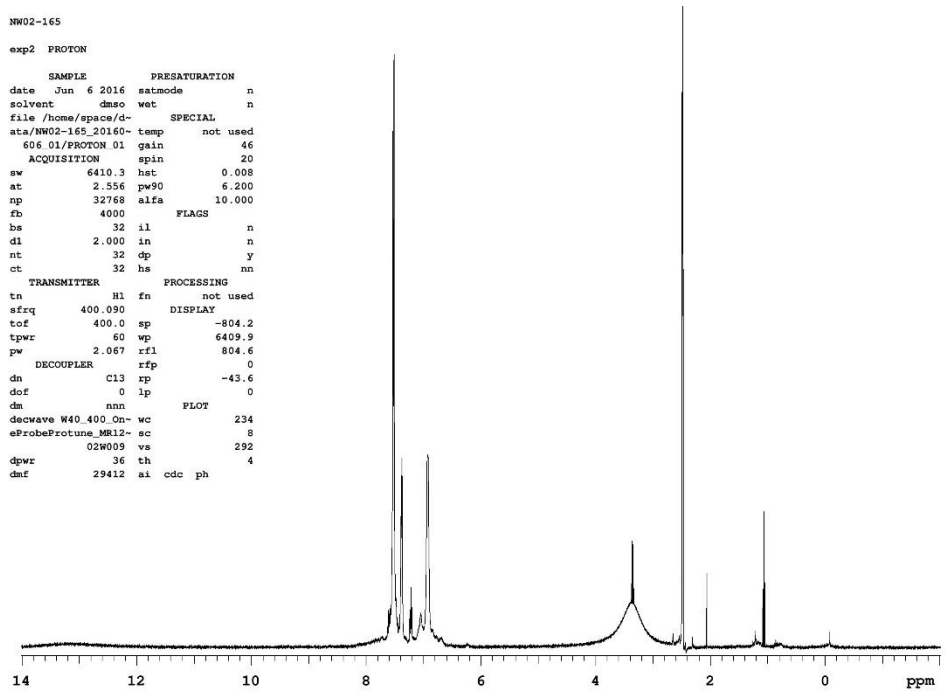

Figure B.21. ^{1}H-NMR spectrum of $RuCl_2(bbcb)_2$ (**6**) in DMSO-d6.

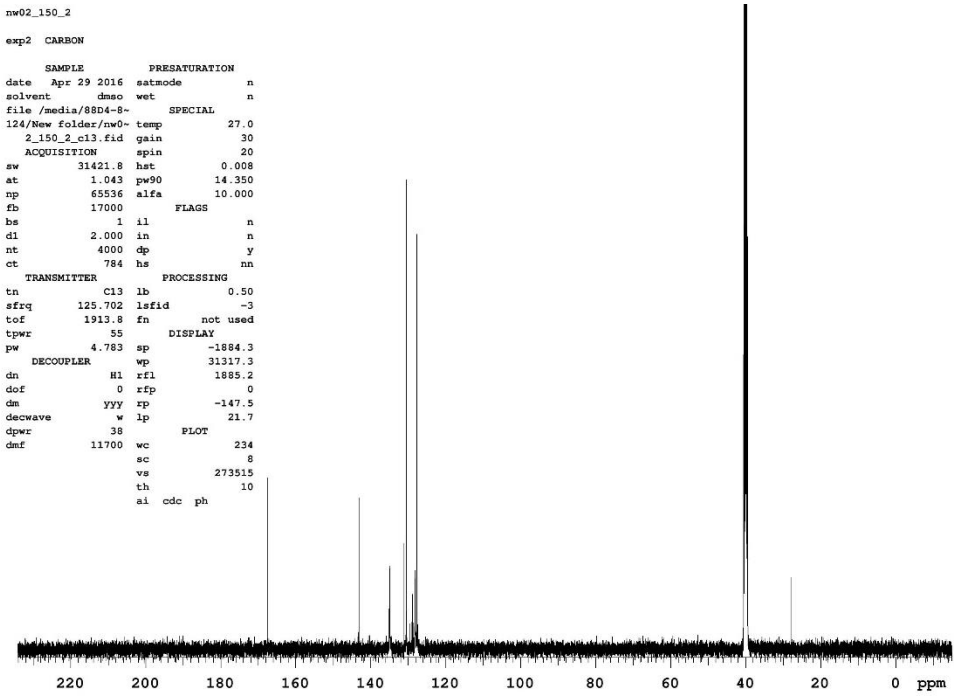

Figure B.22. ^{13}C-NMR spectrum of $RuCl_2(bbcb)_2$ (**6**) in DMSO-d6.

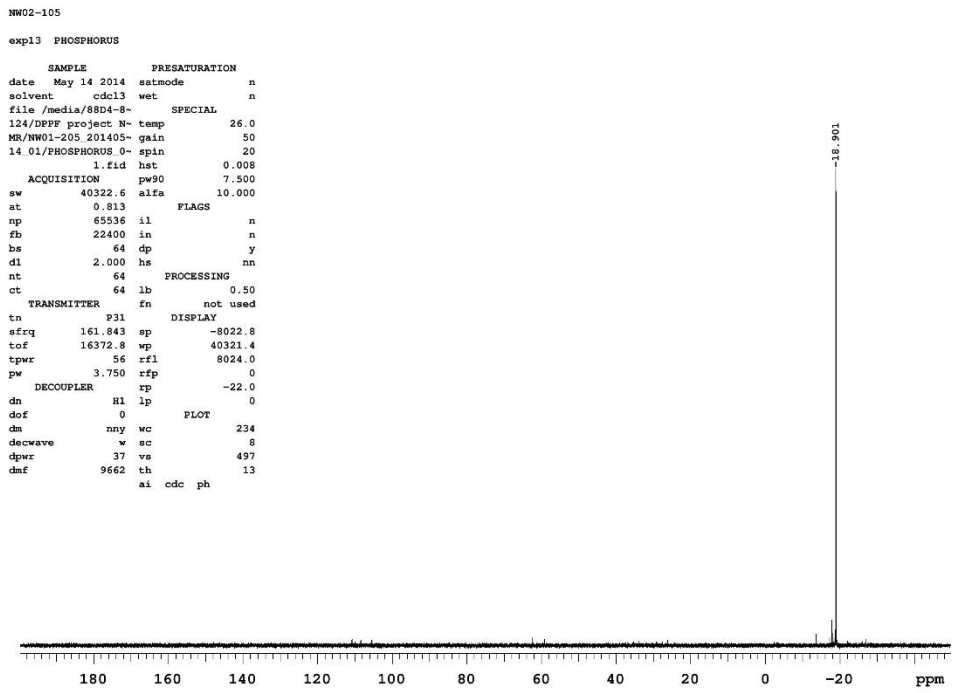

Figure B.23. ^{31}P-NMR spectrum of dppf-Br (**7**) in $CDCl_3$.

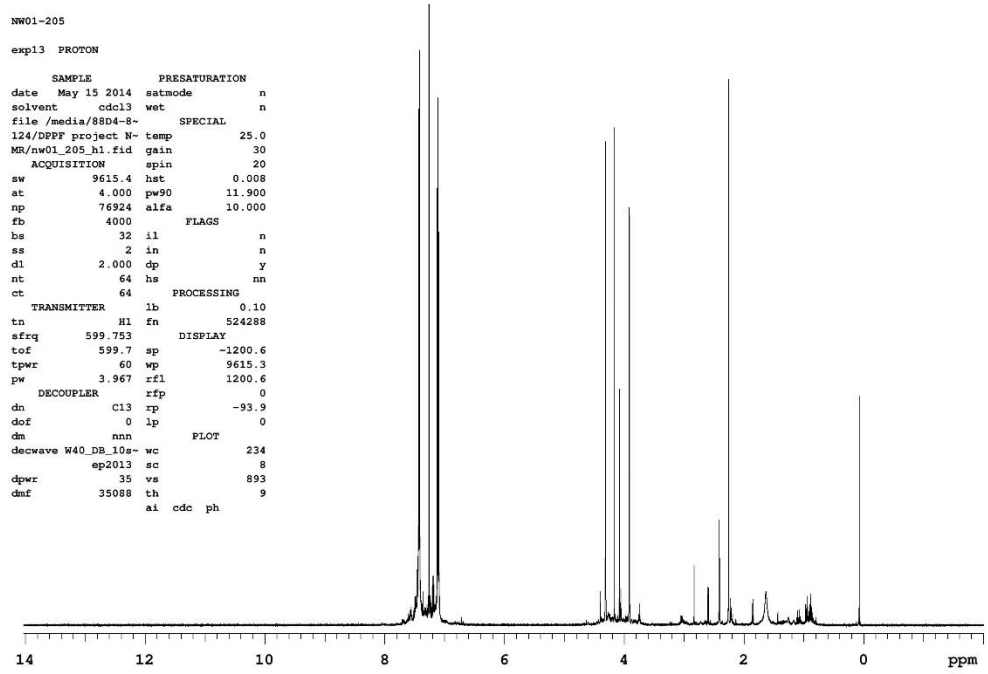

Figure B.24. ^{1}H-NMR spectrum of dppf-Br (**7**) in $CDCl_3$.

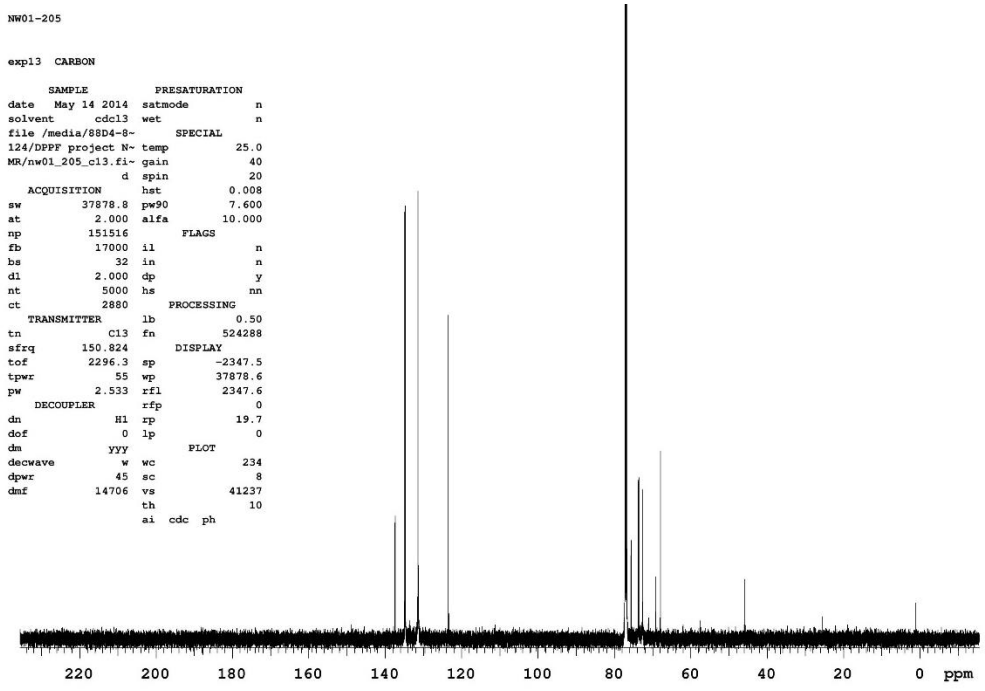

Figure B.25. ^{13}C-NMR spectrum of dppf-Br (**7**) in $CDCl_3$.

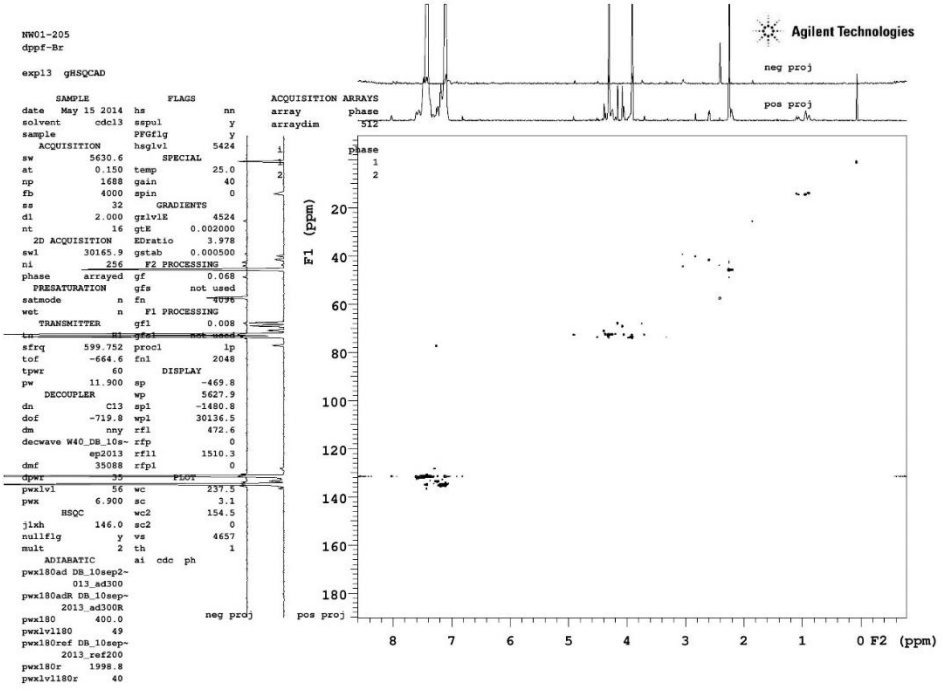

Figure B.26. 2-D gHSQCAD spectrum of dppf-Br (**7**) in $CDCl_3$.

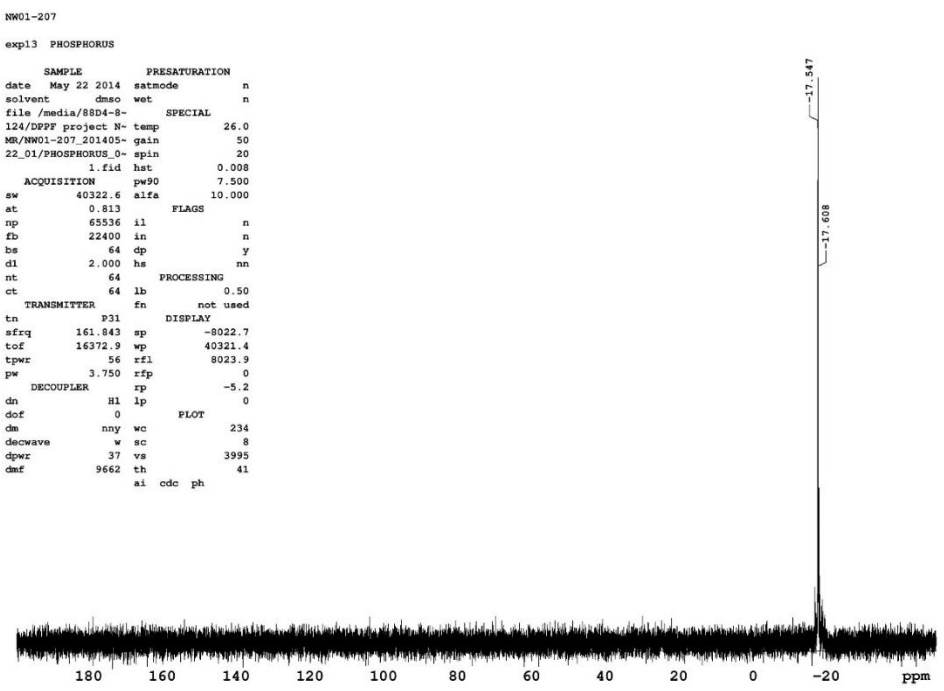

Figure B.27. ^{31}P-NMR spectrum of dppf-CO_2H (**8**) in DMSO-d6.

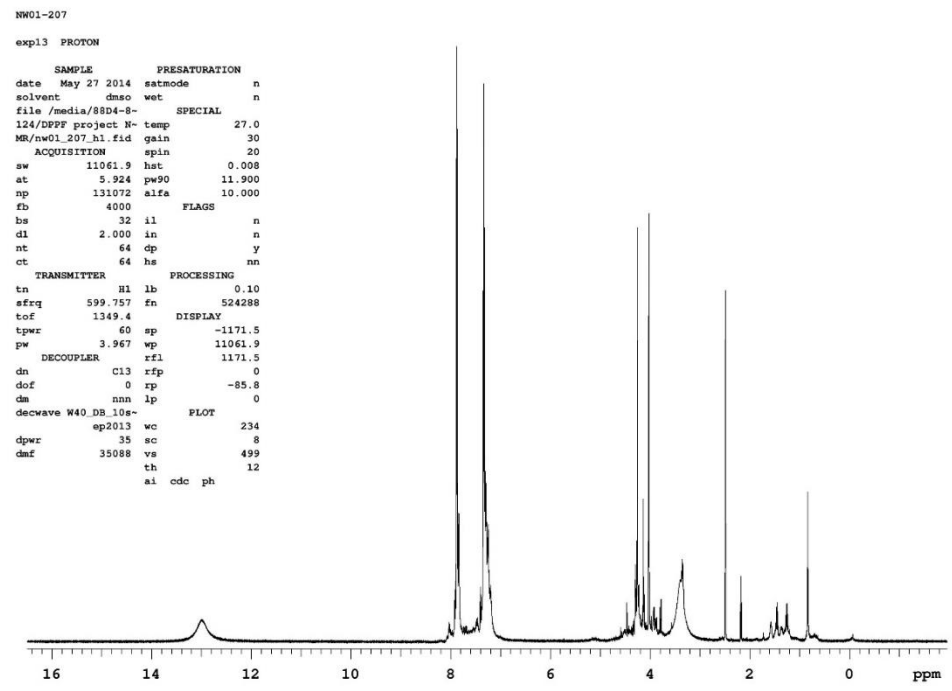

Figure B.28. ^{1}H-NMR spectrum of dppf-CO_2H (**8**) in DMSO-d6.

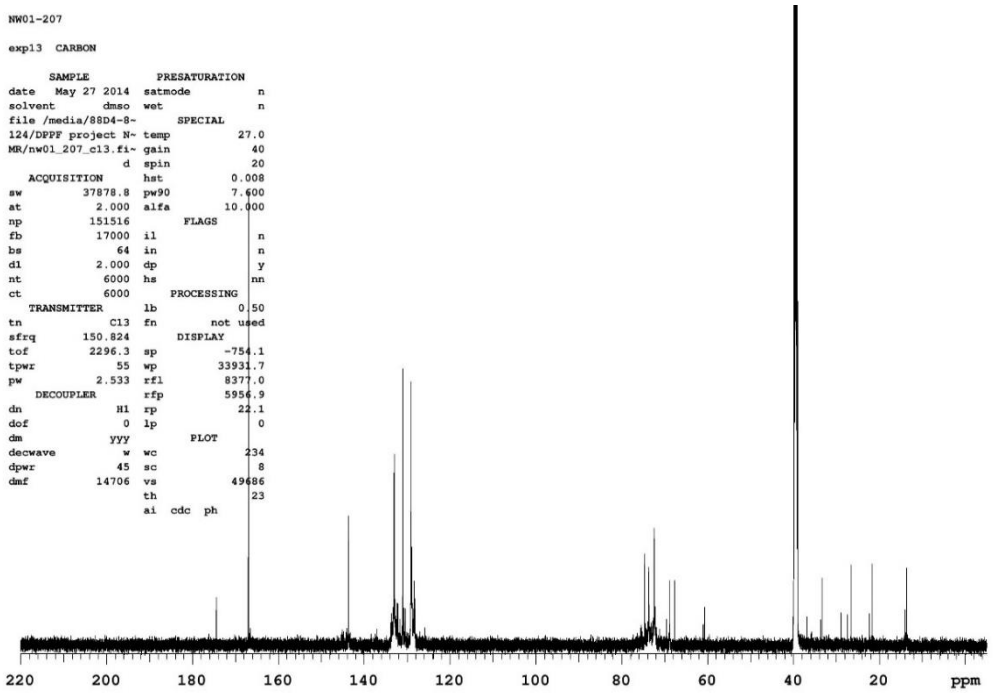

Figure B.29. ^{13}C-NMR spectrum of dppf-CO_2H (**8**) in DMSO-d6.

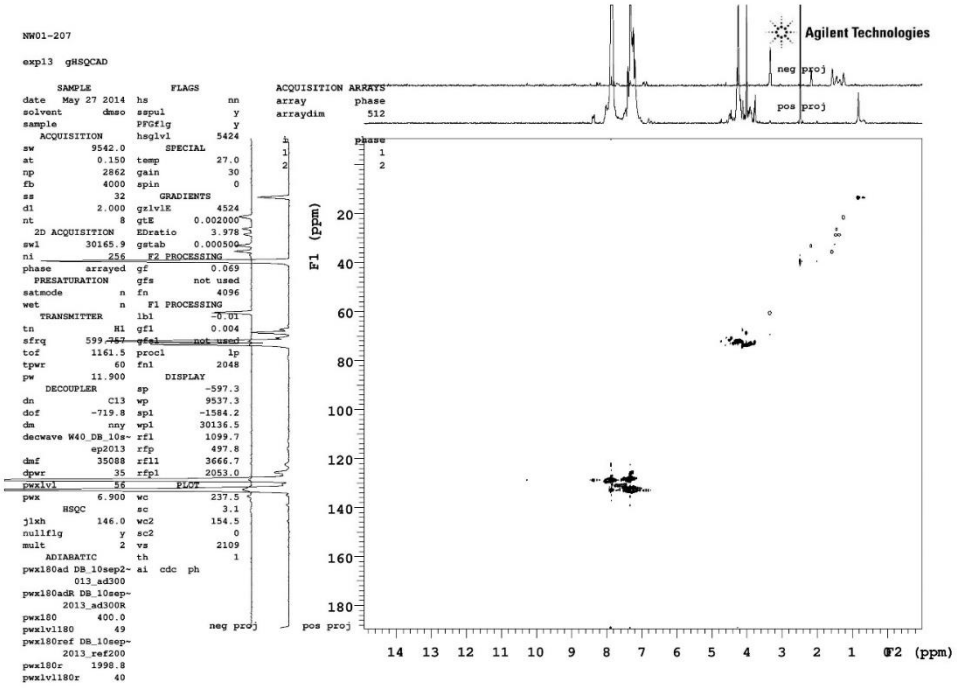

Figure B.30. gHSQCAD spectrum of dppf-CO_2H (**8**) in DMSO-d6.

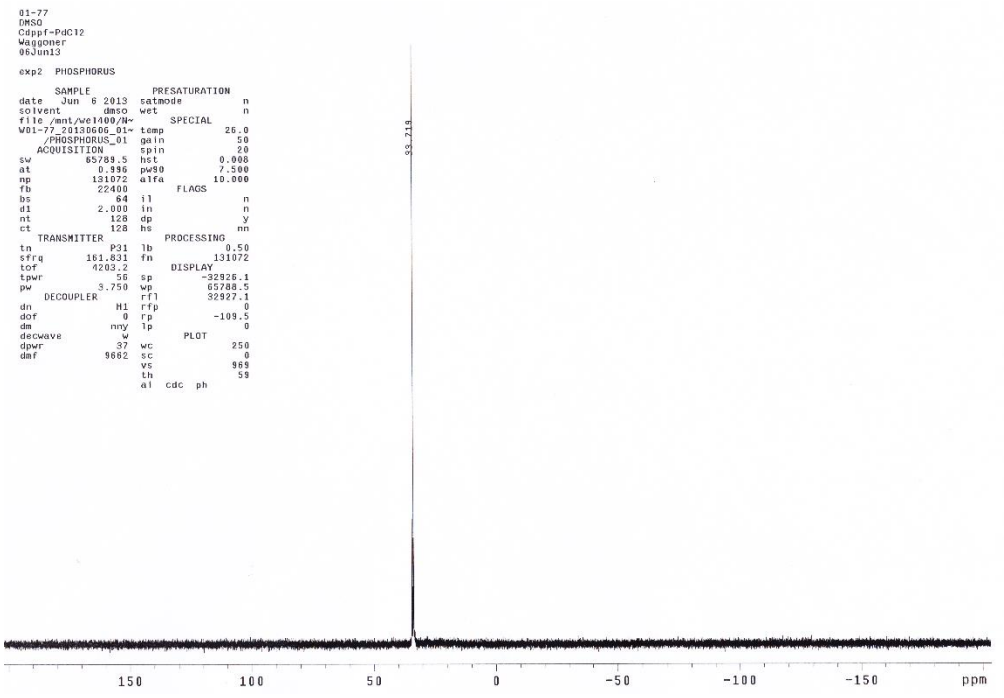

Figure B.31. ^{31}P-NMR spectrum of $PdCl_2$(dppf-CO_2H) (**9**) in DMSO-d6.

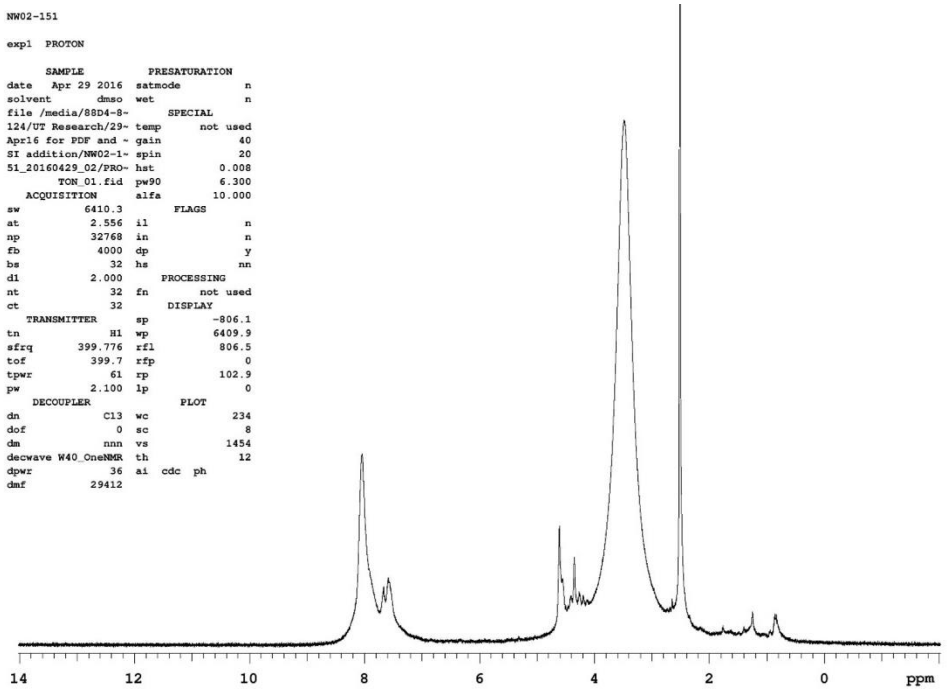

Figure B.32. ^{1}H-NMR spectrum of $PdCl_2$(dppf-CO_2H) (**9**) in DMSO-d6.

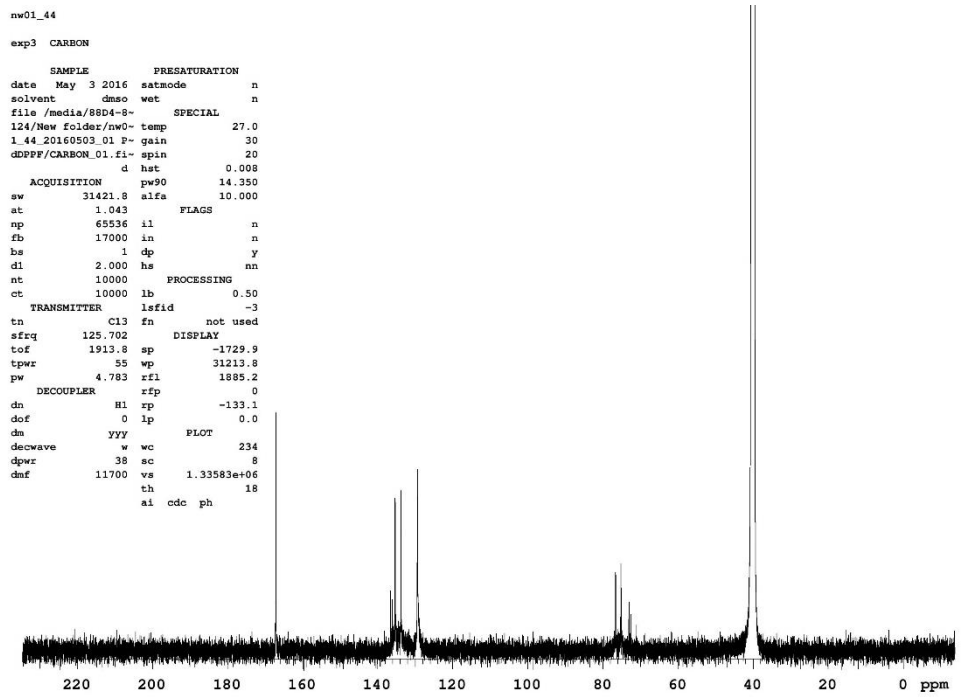

Figure B.33. ^{13}C-NMR spectrum of $PdCl_2$(dppf-CO_2H) (**9**) in DMSO-d6.

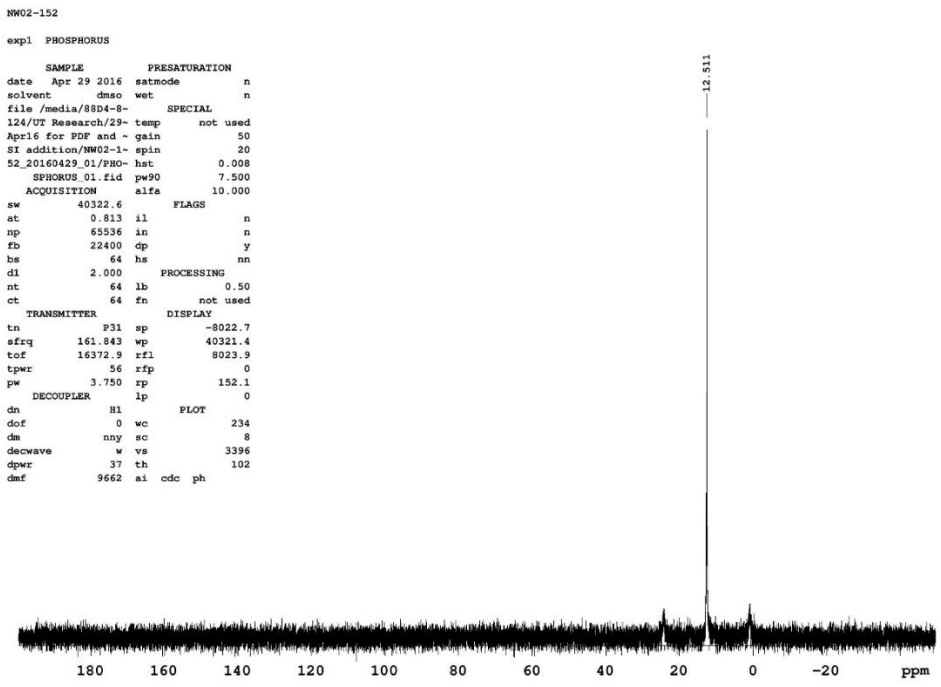

Figure B.34. ^{31}P-NMR spectrum of $PtCl_2$(dppf-CO_2H) (**10**) in DMSO-d6.

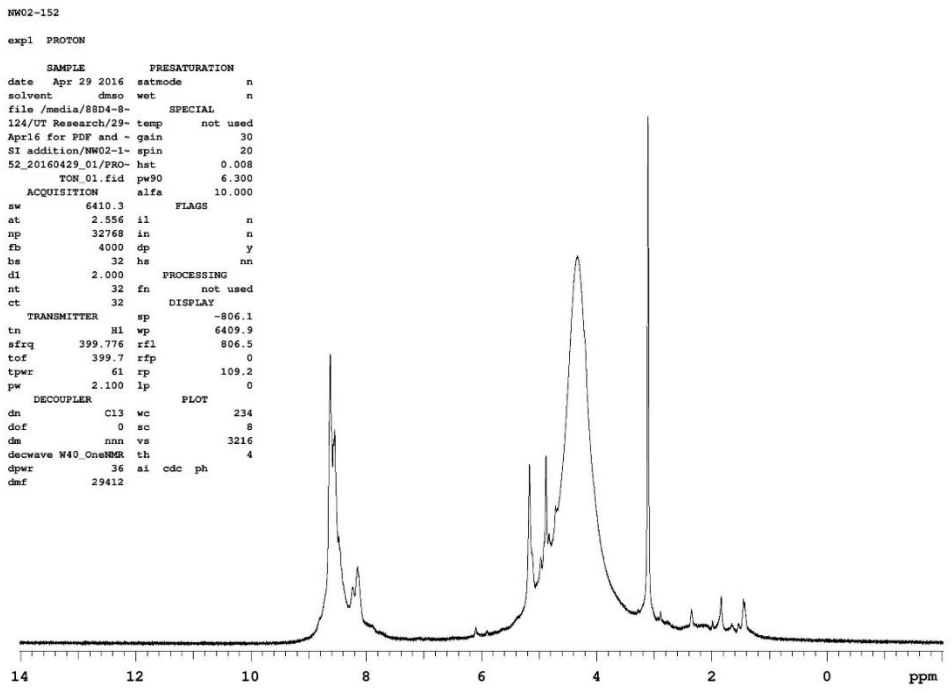

Figure B.35. ^{1}H-NMR spectrum of $PtCl_2$(dppf-CO_2H) (**10**) in DMSO-d6.

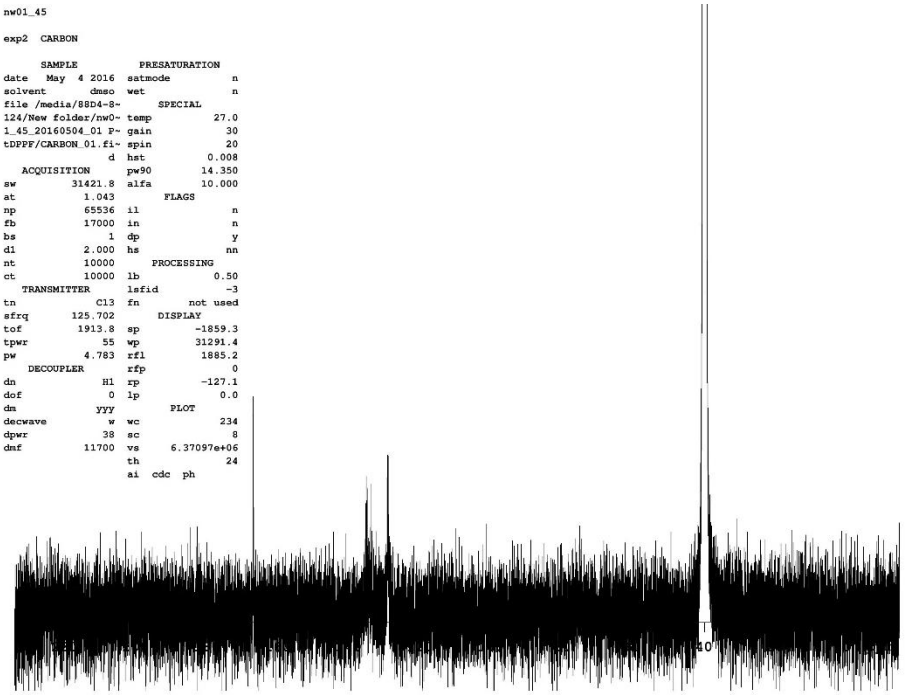

Figure B.36. ^{13}C-NMR spectrum of $PtCl_2$(dppf-CO_2H) (**10**) in DMSO-d6.

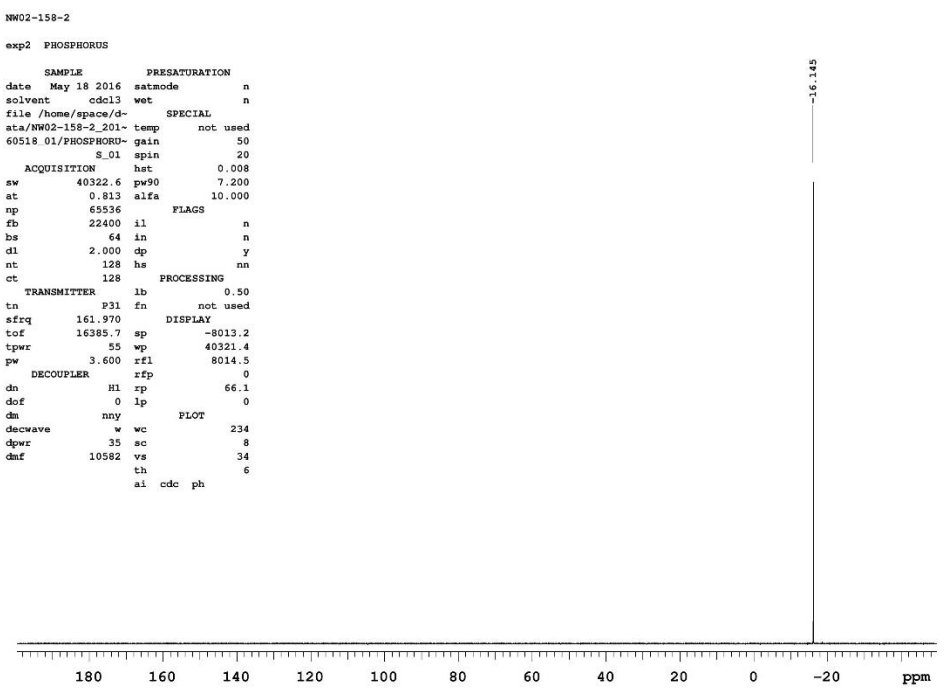

Figure B.37. ^{31}P-NMR spectrum of b-bbcb-Br (**11**) in $CDCl_3$.

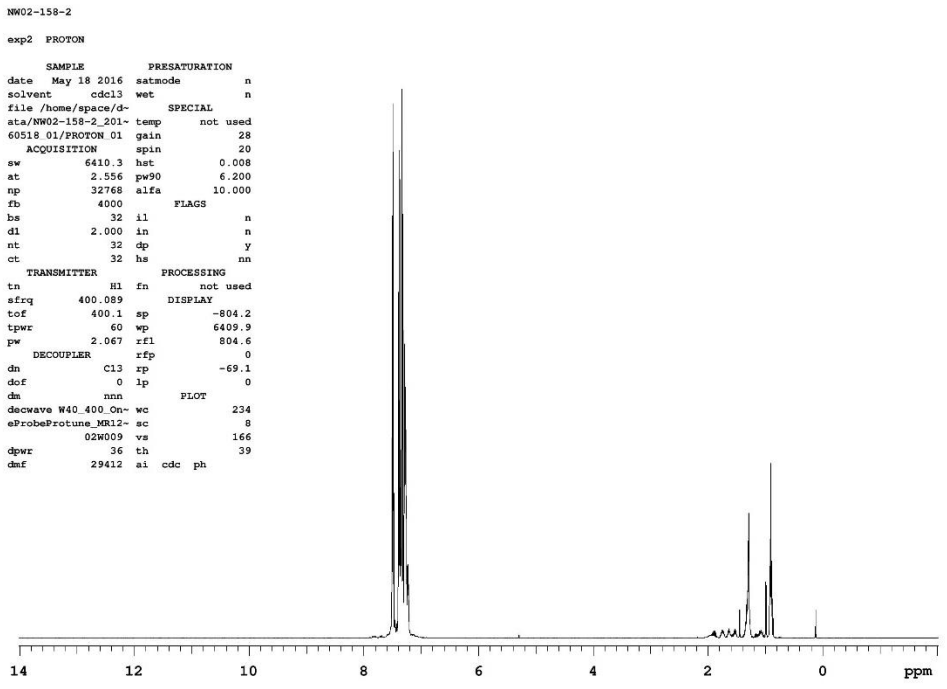

Figure B.38. ^{1}H-NMR spectrum of b-bbcb-Br (**11**) in $CDCl_3$.

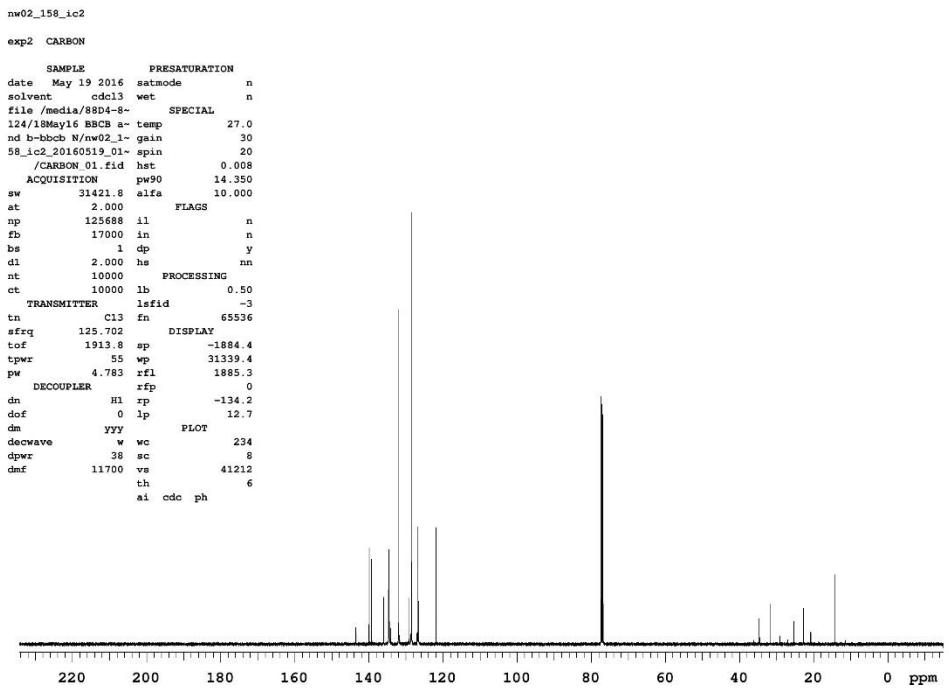

Figure B.39. ^{13}C-NMR spectrum of b-bbcb-Br (**11**) in $CDCl_3$.

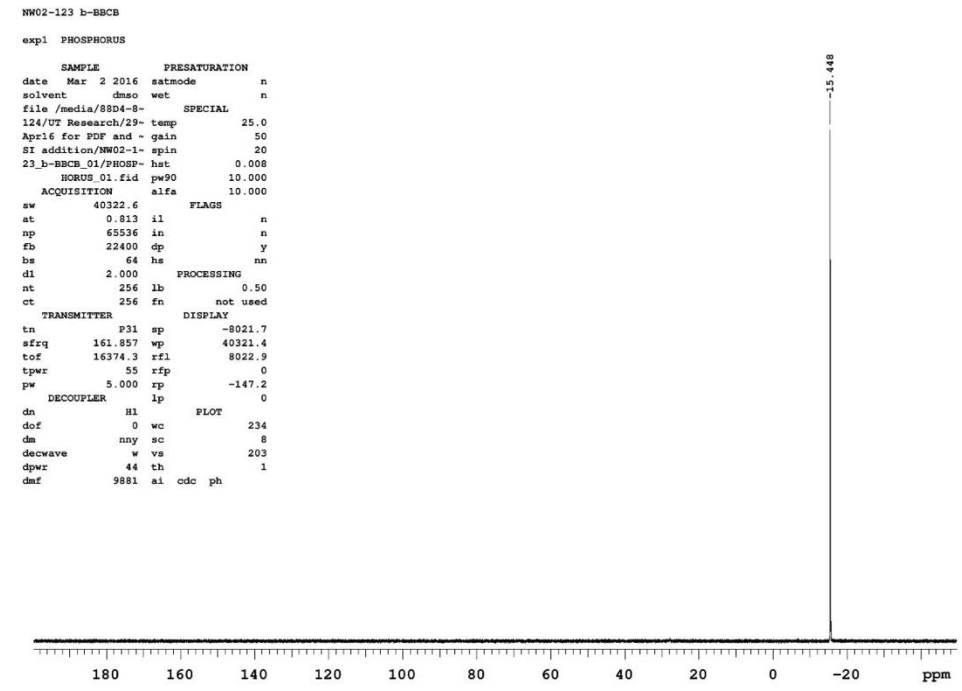

Figure B.40. ^{31}P-NMR spectrum of b-bbcb (**12**) in DMSO-d6.

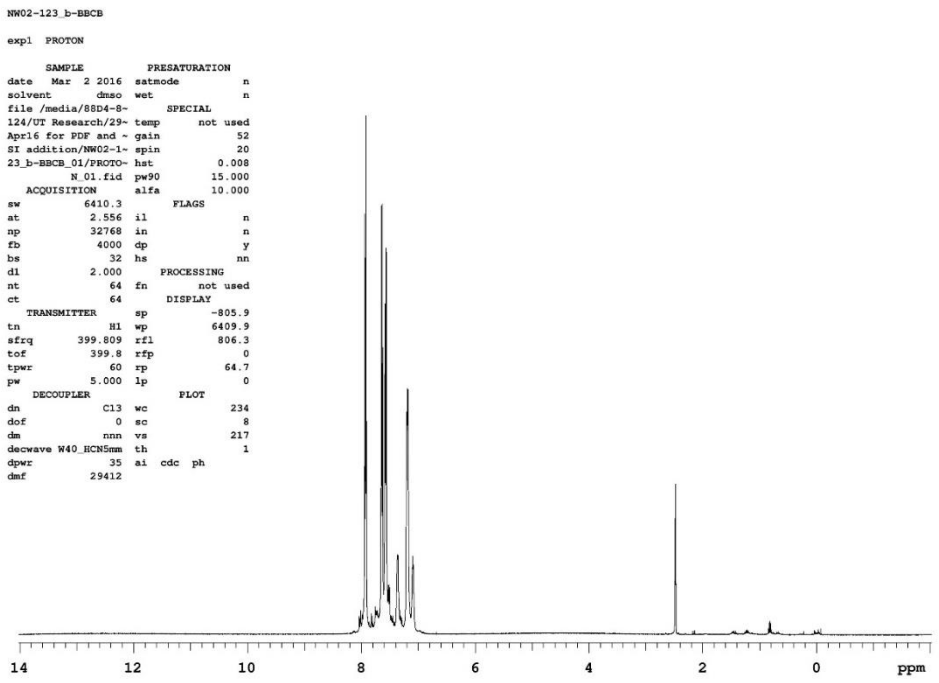

Figure B.41. ^{1}H-NMR spectrum of b-bbcb (**12**) in DMSO-d6.

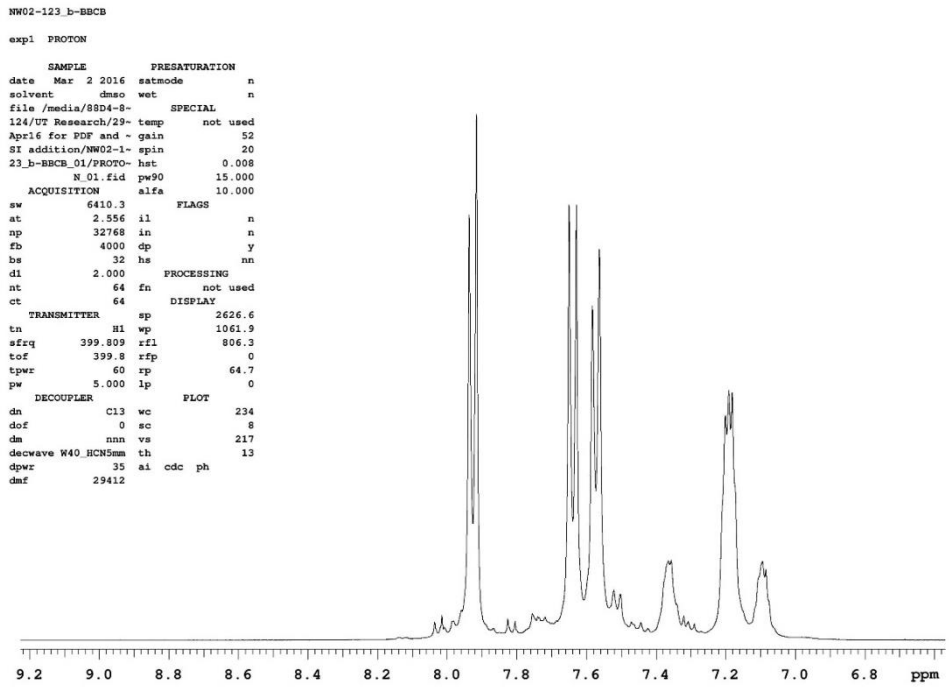

Figure B.42. ^{1}H-NMR expanded spectrum of b-bbcb (**12**) in DMSO-d6.

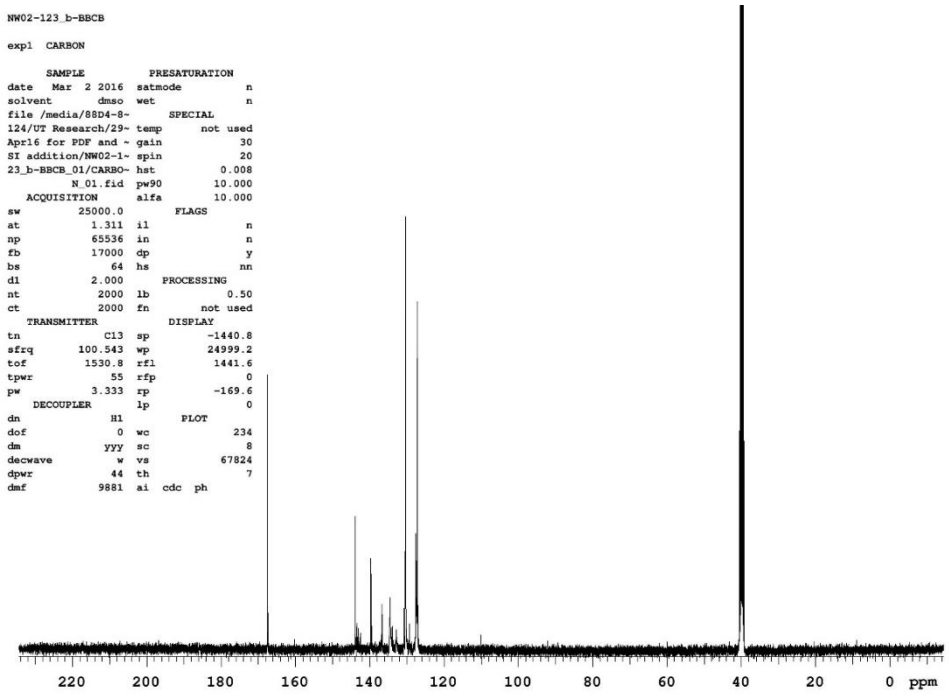

Figure B.43. ^{13}C-NMR spectrum of b-bbcb (**12**) in DMSO-d6.

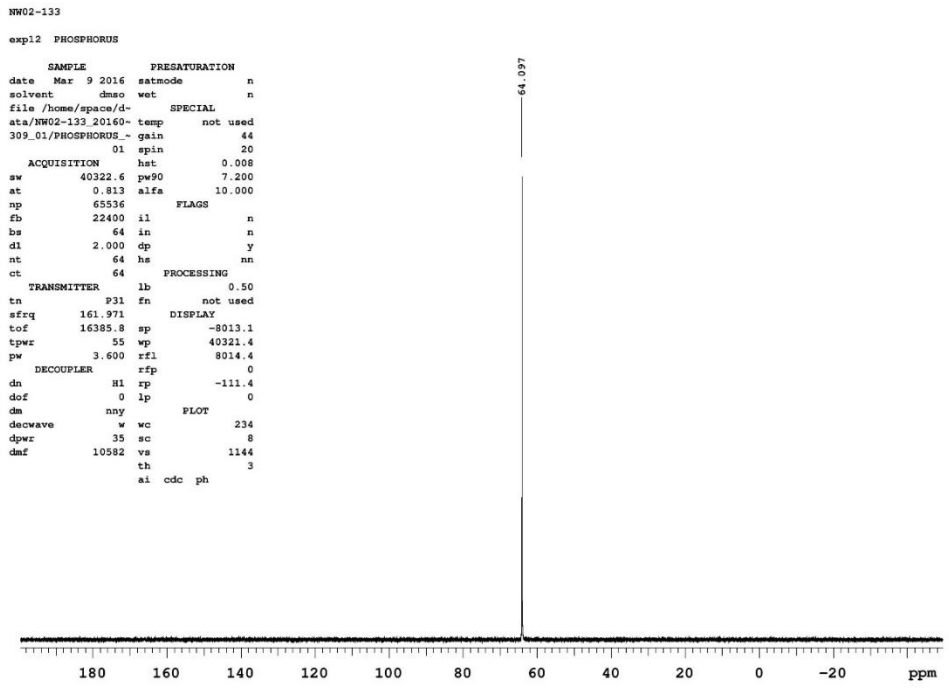

Figure B.44. ^{31}P-NMR spectrum of $PdCl_2$(b-bbcb) (**13**) in DMSO-d6.

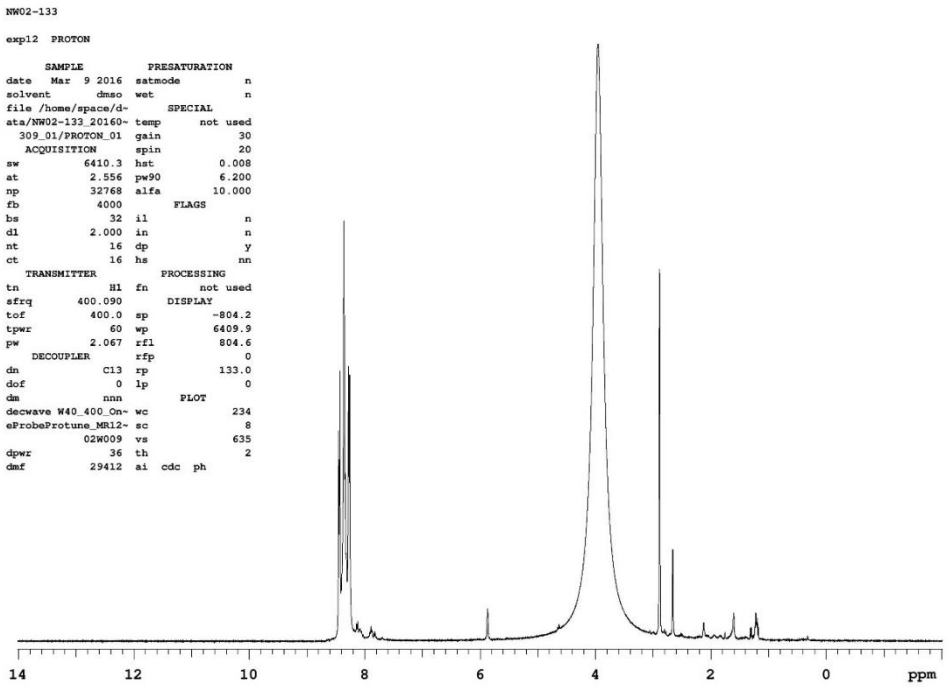

Figure B.45. ^{1}H-NMR spectrum of $PdCl_2$(b-bbcb) (**13**) in DMSO-d6.

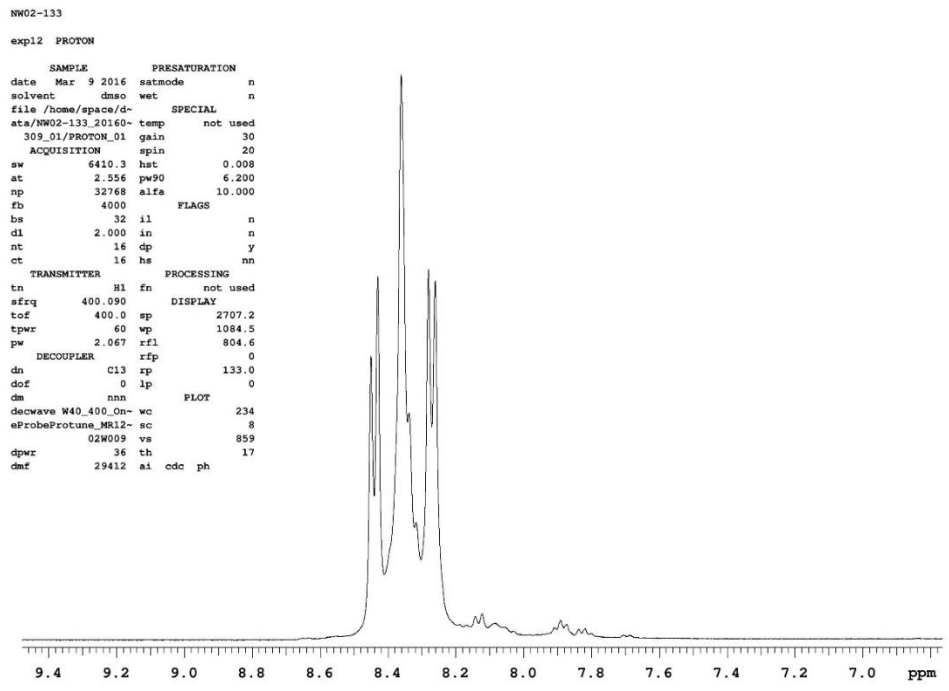

Figure B.46. ^{1}H-NMR expanded spectrum of $PdCl_2$(b-bbcb) (**13**) in DMSO-d6.

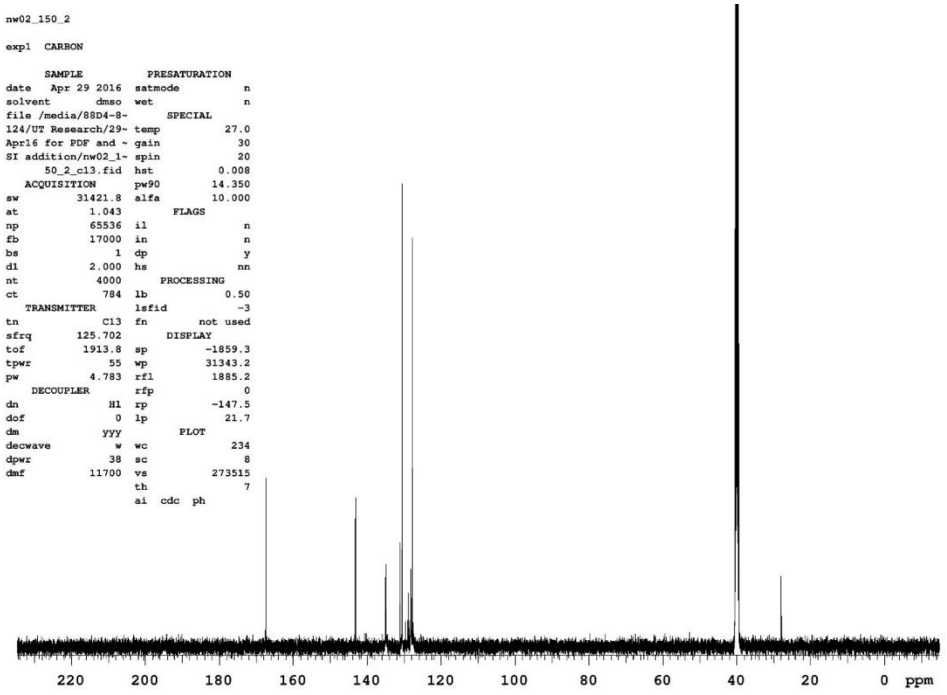

Figure B.47. ^{13}C-NMR spectrum of $PdCl_2$(b-bbcb) (**13**) in DMSO-d6.

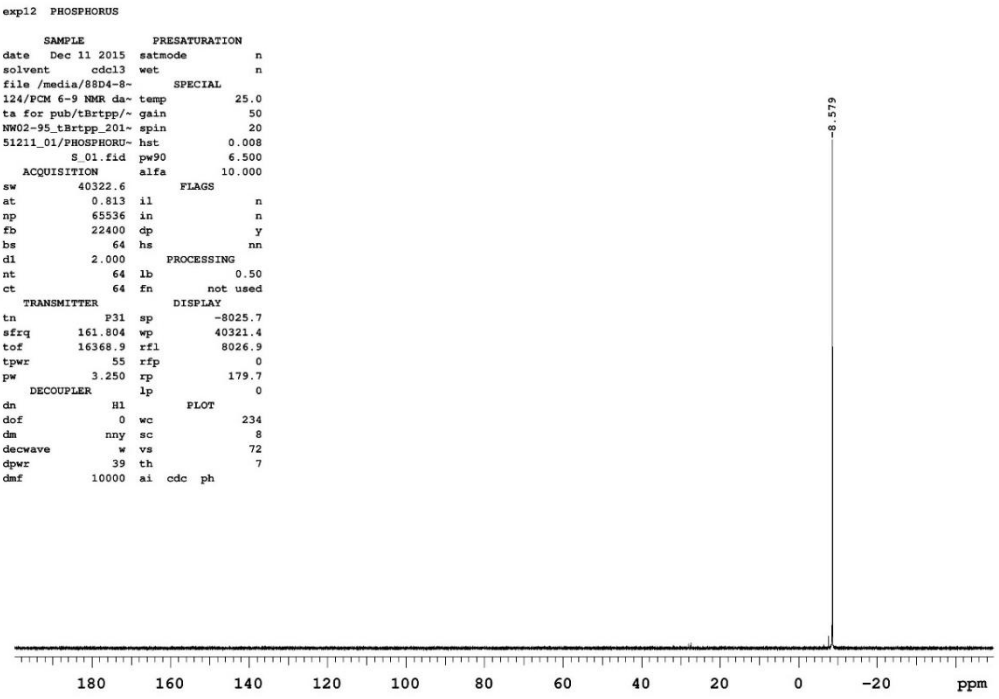

Figure B.48. ^{31}P-NMR spectrum of tBrtpp (**14**) in $CDCl_3$.

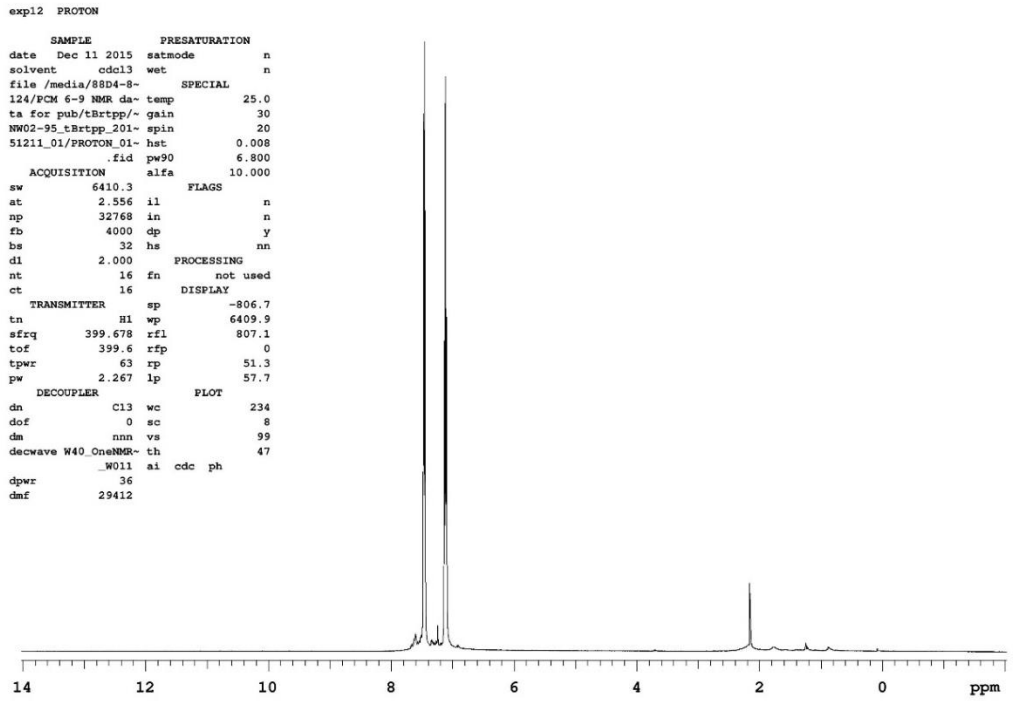

Figure B.49. ^{1}H-NMR spectrum of tBrtpp (**14**) in $CDCl_3$.

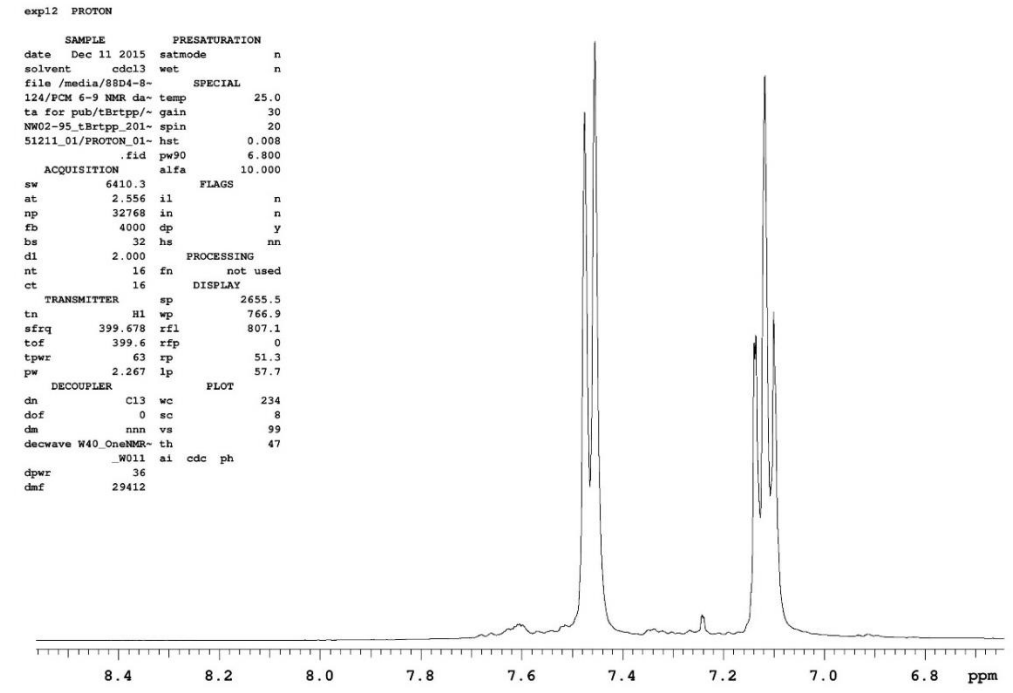

Figure B.50. ^{1}H-NMR expanded spectrum of tBrtpp (**14**) in $CDCl_3$.

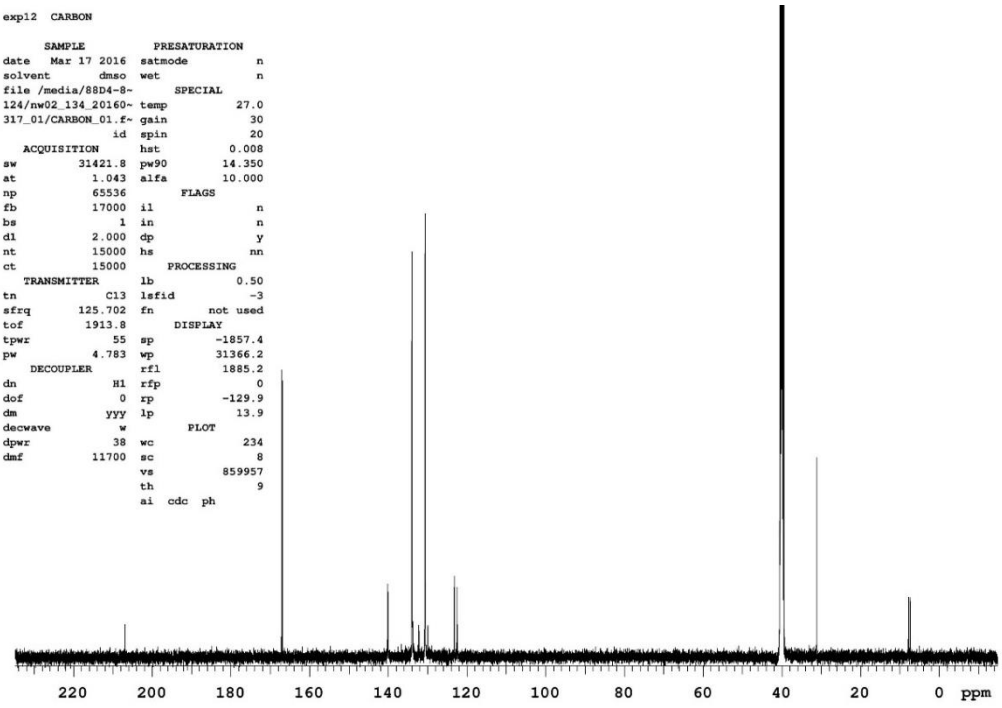

Figure B.51. ^{13}C-NMR spectrum of tBrtpp (**14**) in $CDCl_3$.

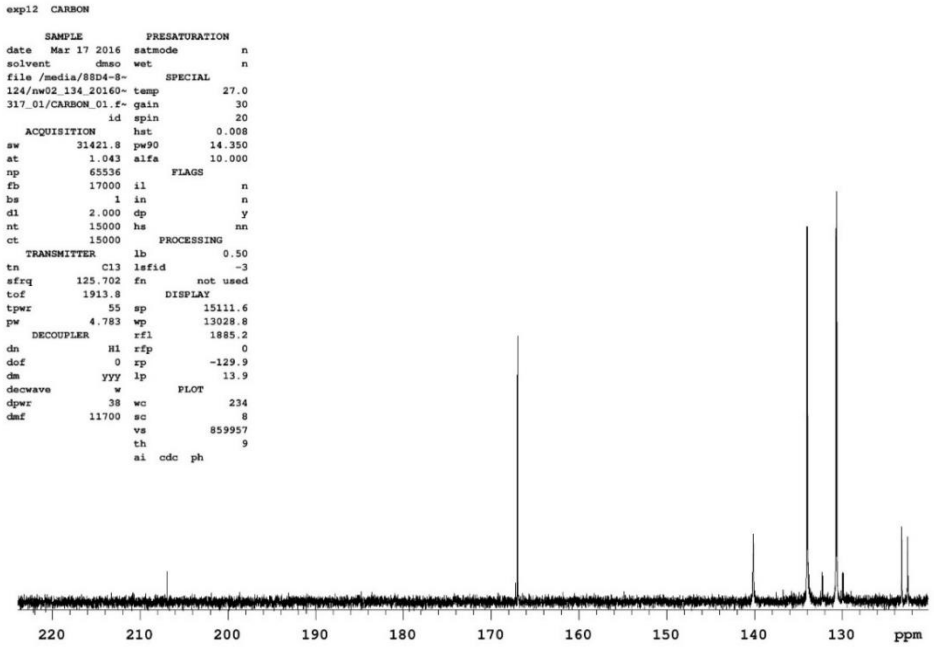

Figure B.52. ^{13}C-NMR expanded spectrum of tBrtpp (**14**) in $CDCl_3$.

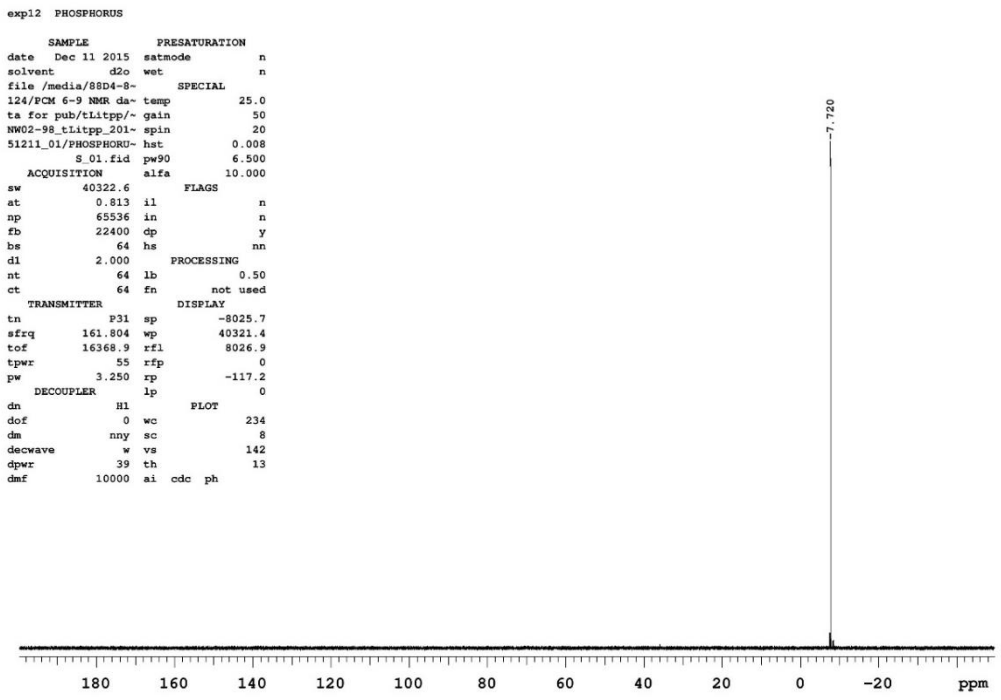

Figure B.53. ^{31}P-NMR spectrum of pbtcLi$_3$ (**15**) in D_2O.

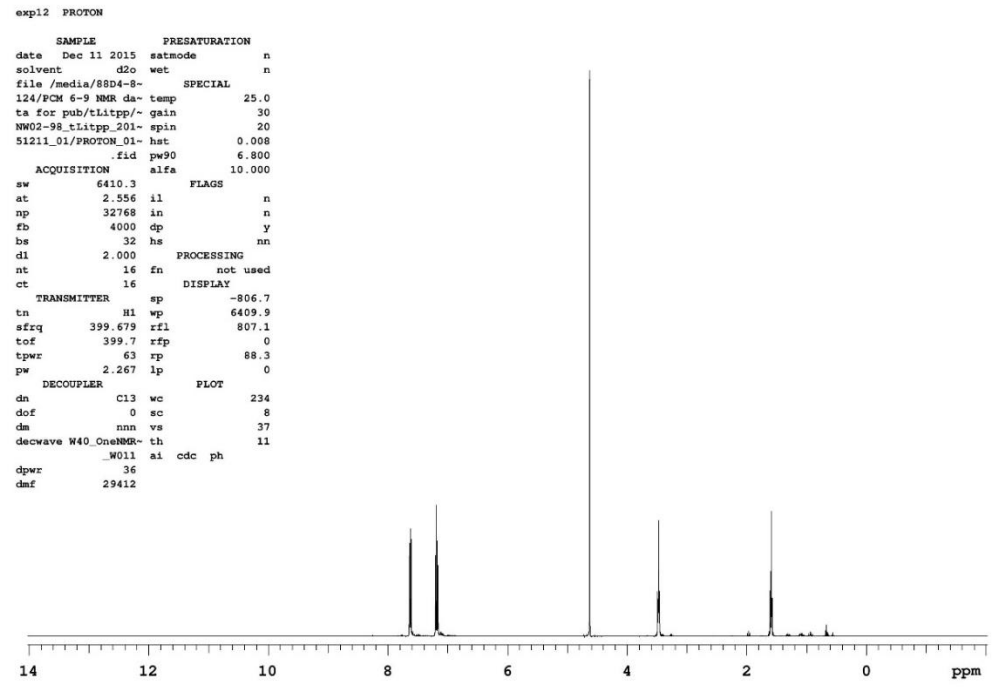

Figure B.54. ^{1}H-NMR spectrum of pbtcLi$_3$ (**15**) in D_2O.

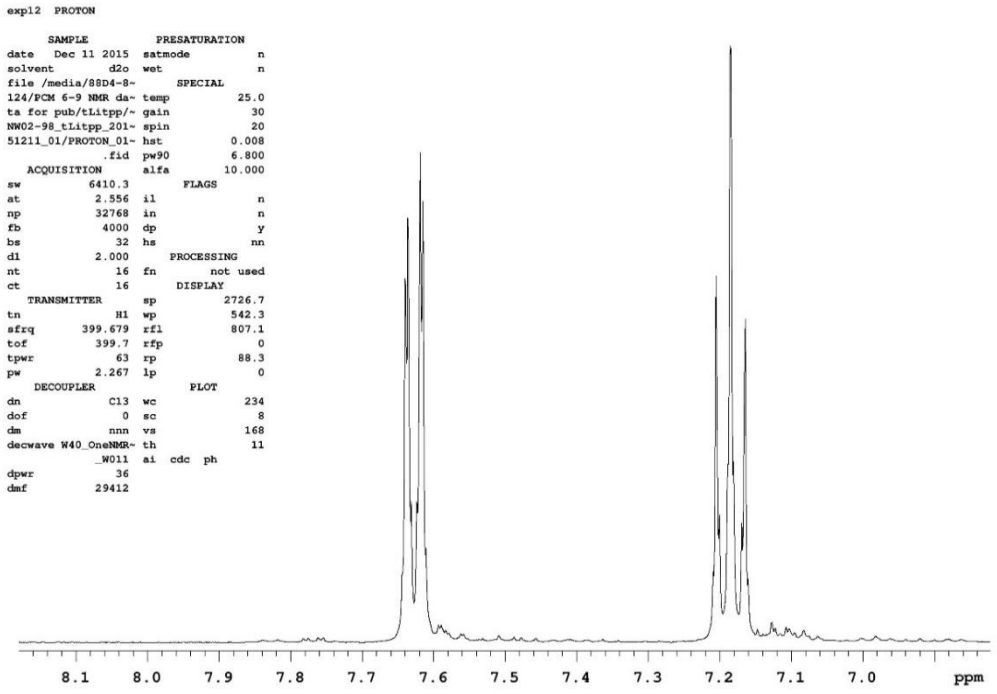

Figure B.55. ^{1}H-NMR expanded spectrum of pbtcLi$_3$ (**15**) in D_2O.

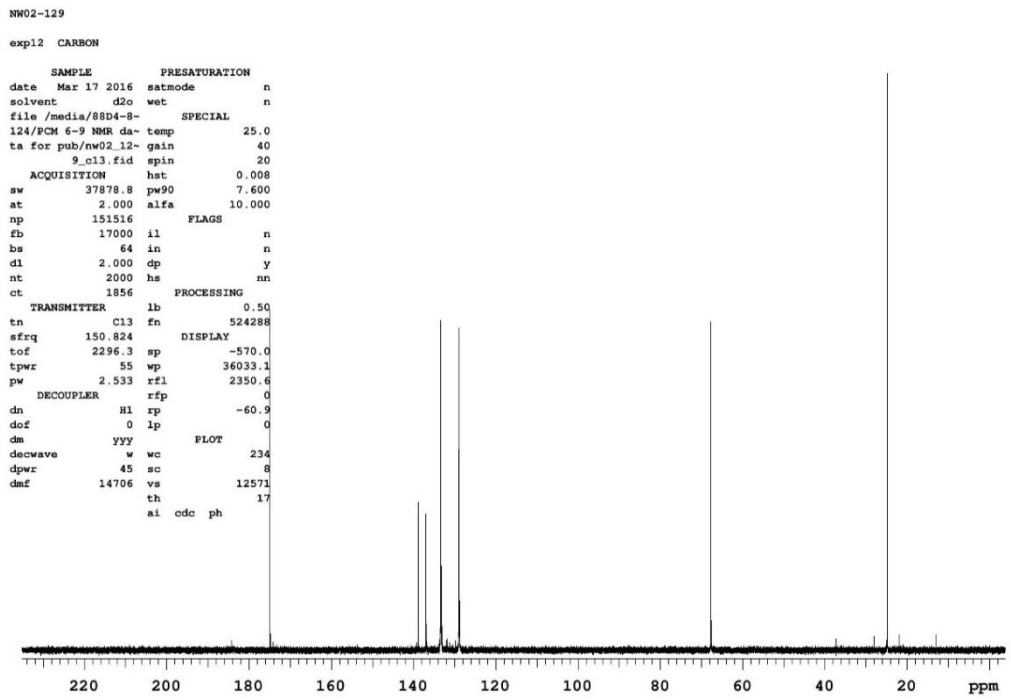

Figure B.56. ^{13}C-NMR spectrum of pbtcLi$_3$ (**15**) in D_2O.

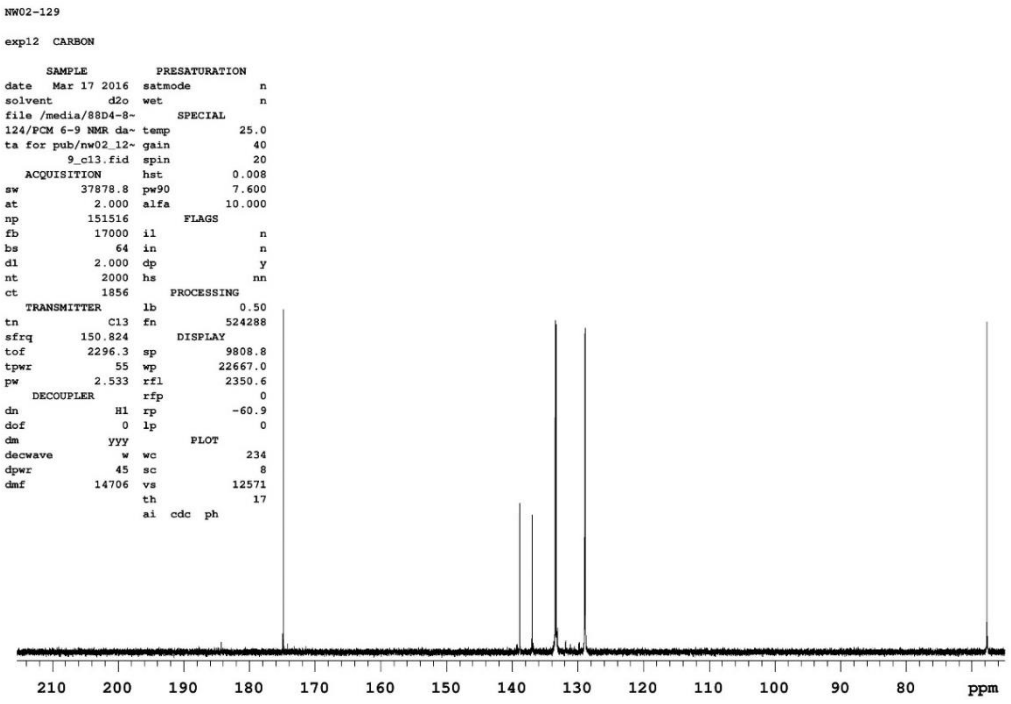

Figure B.57. ^{13}C-NMR expanded spectrum of pbtcLi$_3$ (**15**) in D_2O.

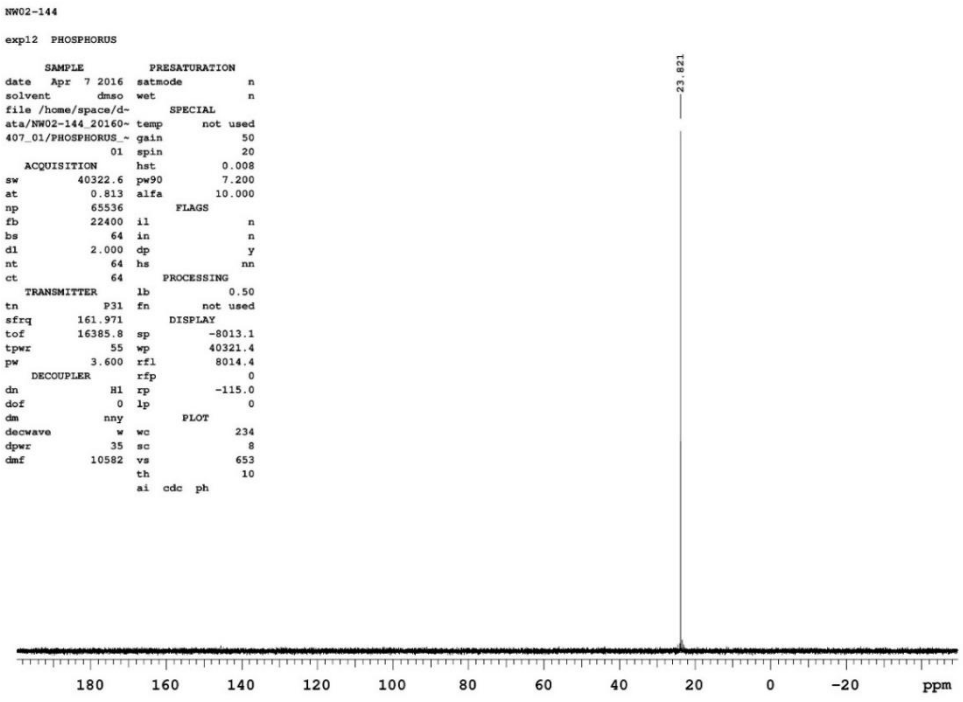

Figure B.58. ^{31}P-NMR spectrum of [mptbcH$_3$]Cl (**16**) in DMSO-d6.

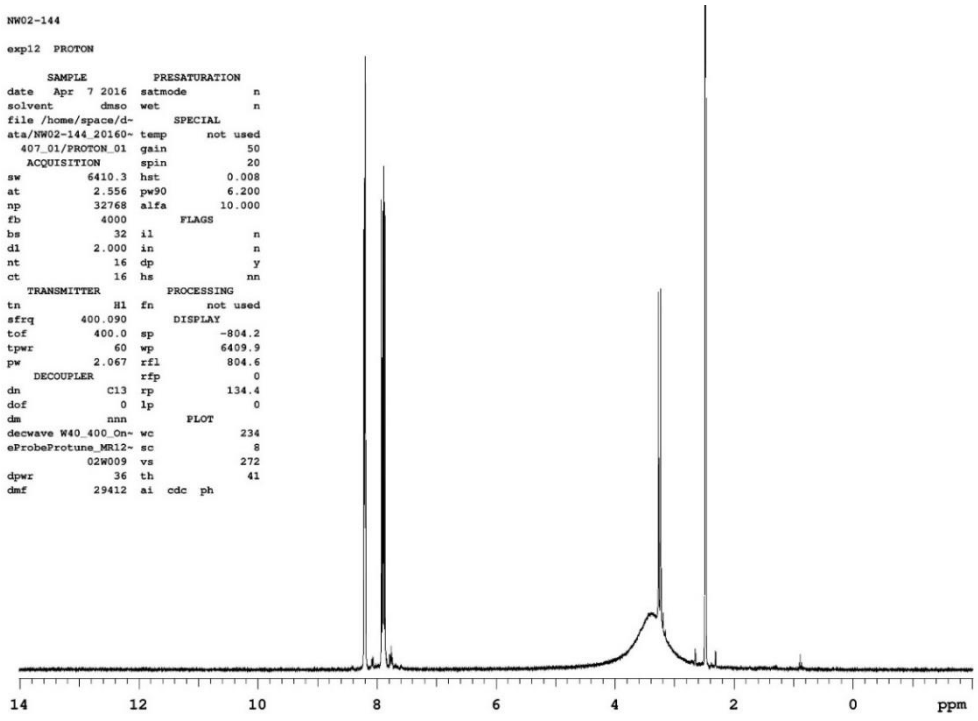

Figure B.59. ^{1}H-NMR spectrum of [mptbcH_3]Cl (**16**) in DMSO-d6.

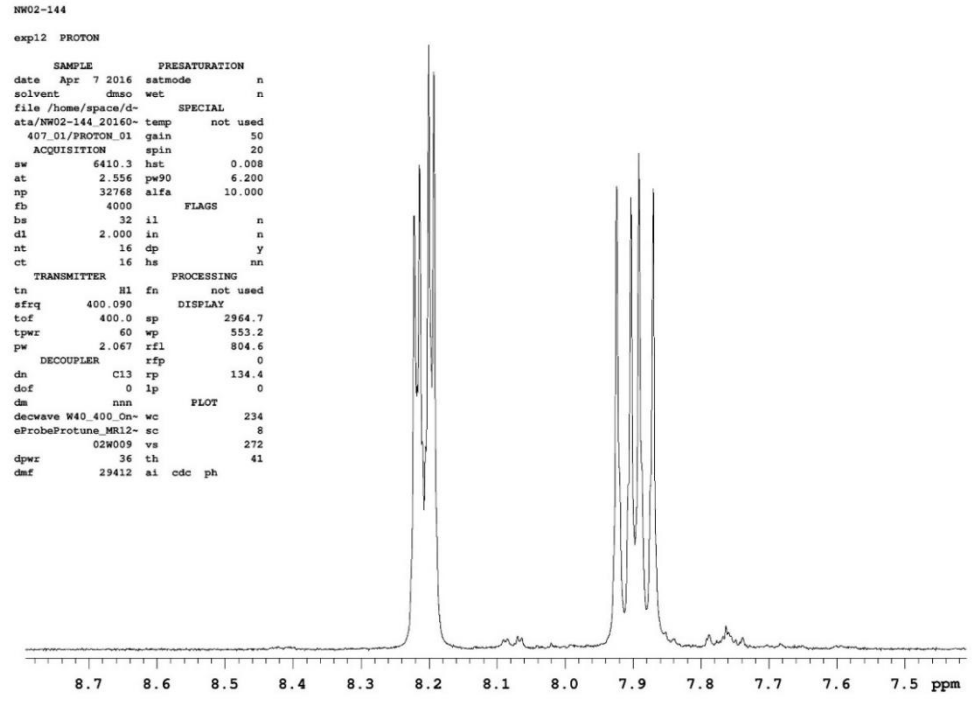

Figure B.60. ^{1}H-NMR expanded aromatic region of [mptbcH_3]Cl (**16**) in DMSO-d6.

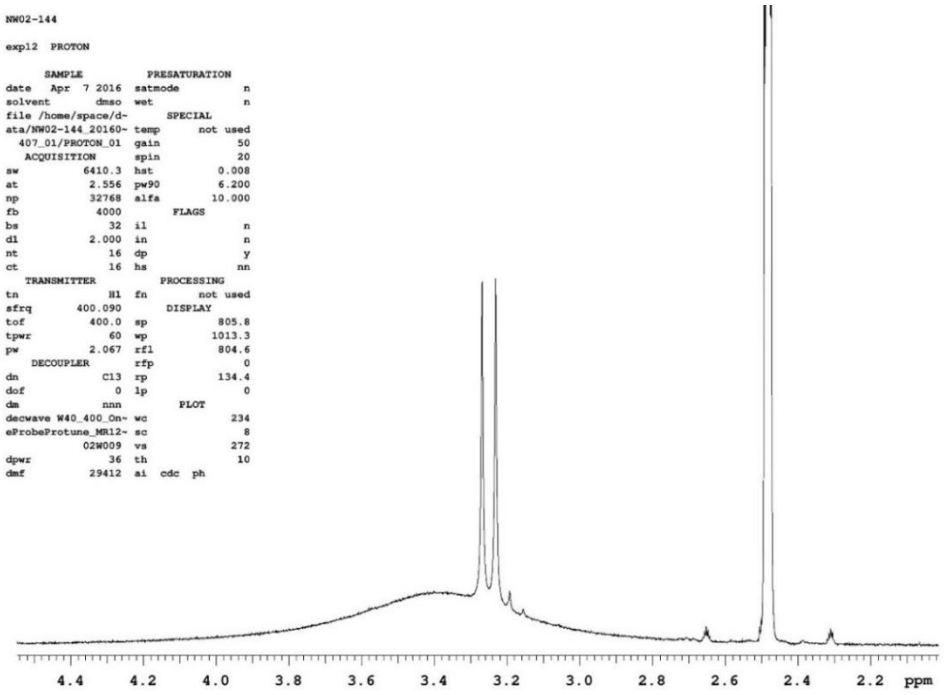

Figure B.61. ^{1}H-NMR expanded aliphatic region of [mptbcH$_3$]Cl (**16**) in DMSO-d6

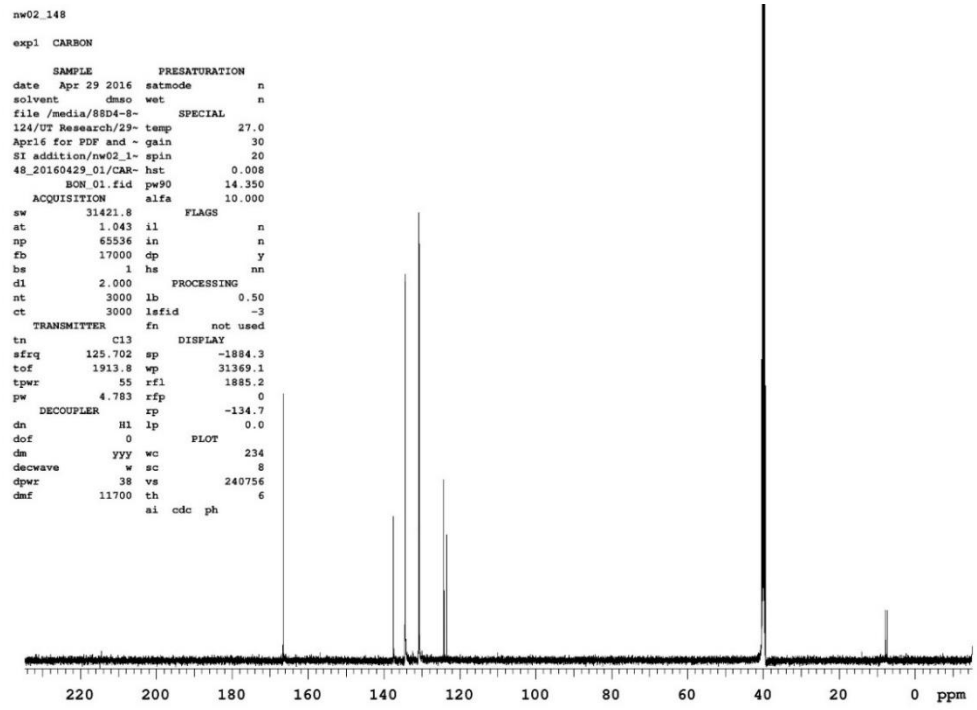

Figure B.62. ^{13}C-NMR spectrum of [mptbcH$_3$]Cl (**16**) in DMSO-d6.

Appendix C: Crystallographic data

Table C.1. Crystal data and structure refinement for $RuCl_2(bbcb)_2$ (**6**).

Identification code	SH13040	
Empirical formula	C34 H0 Cl0 O8 P2 Ru0.50	
Formula weight	648.81	
Temperature	153(2) K	
Wavelength	0.71073 Å	
Crystal system	Triclinic	
Space group	P -1	
Unit cell dimensions	a = 15.1162(13) Å	a= 91.709(4)°.
	b = 15.4177(11) Å	b= 101.900(5)°.
	c = 18.6493(12) Å	g = 99.293(5)°.
Volume	4188.1(5) $Å^3$	
Z	4	
Density (calculated)	1.029 Mg/m^3	
Absorption coefficient	0.314 mm^{-1}	
F(000)	1280	
Crystal size	0.085 x 0.338 x 0.339 mm^3	
Theta range for data collection	1.592 to 24.999°.	
Index ranges	-17<=h<=17, -18<=k<=18, -22<=l<=22	
Reflections collected	99929	
Independent reflections	14743 [R(int) = 0.2274]	
Completeness to theta = 24.999°	99.9 %	
Refinement method	Full-matrix least-squares on F^2	
Data / restraints / parameters	14743 / 0 / 823	
Goodness-of-fit on F^2	1.399	
Final R indices [I>2sigma(I)]	R1 = 0.1391, wR2 = 0.3731	
R indices (all data)	R1 = 0.2907, wR2 = 0.4810	
Extinction coefficient	n/a	
Largest diff. peak and hole	2.496 and -0.788 $e.Å^{-3}$	

Table C.2. Atomic coordinates (x 10^4) and equivalent isotropic displacement parameters ($Å^2$x 10^3) for $RuCl_2(bbcb)_2$ (**6**). U(eq) is defined as one third of the trace of the orthogonalized U^{ij} tensor.

	x	y	z	U(eq)
C(1)	-655(19)	3286(12)	1050(9)	89(8)
C(1A)	3370(40)	-1720(20)	2970(20)	177(18)
C(5)	-3914(14)	-340(12)	-322(10)	60(5)
C(6)	1600(14)	7247(12)	4744(10)	64(5)
C(7)	-3435(14)	-853(13)	126(10)	63(5)
C(8)	-845(15)	2405(10)	1142(9)	62(6)
C(9)	-2322(15)	-2492(13)	1587(12)	69(6)
C(10)	-94(15)	5979(10)	2771(9)	61(6)
C(11)	-1884(17)	7937(16)	4515(12)	93(7)
C(12)	-1383(13)	7441(12)	4201(10)	60(5)
C(13)	-675(12)	1821(10)	646(7)	43(4)
C(14)	-3561(15)	509(14)	-438(11)	72(6)
C(15)	-992(13)	2482(11)	3710(9)	52(5)
C(16)	-1425(16)	5534(10)	1802(9)	55(5)
C(17)	303(19)	-3594(12)	-471(9)	96(9)
C(18)	-380(16)	313(10)	3185(8)	56(6)
C(19)	1316(16)	8530(11)	3744(10)	67(6)
C(20)	-769(14)	-1631(10)	1745(8)	52(5)
C(21)	1891(15)	-735(13)	1576(10)	74(6)
C(22)	-2268(14)	2397(13)	2646(9)	65(5)
C(23)	1480(15)	2723(12)	4339(11)	71(6)
C(24)	-194(17)	185(11)	3993(9)	55(5)
C(25)	-1840(20)	5257(14)	1006(14)	86(8)
C(27)	1711(16)	5142(14)	3656(12)	79(7)
C(28)	-3046(17)	1860(16)	2130(12)	84(7)
C(29)	183(15)	662(9)	2096(8)	55(5)
C(30)	-928(13)	6846(10)	4615(9)	50(5)

C(31)	2760(20)	9490(20)	4310(20)	138(12)
C(32)	2251(17)	8026(14)	4797(12)	87(7)
C(33)	-2332(16)	-2714(12)	860(13)	78(6)
C(34)	-2021(15)	5551(12)	2288(10)	68(6)
C(36)	2093(15)	8661(12)	4284(13)	72(6)
C(37)	-1949(14)	3273(11)	2476(9)	60(5)
C(38)	644(15)	7770(11)	3708(9)	63(6)
C(39)	957(13)	3221(11)	4660(8)	47(5)
C(40)	-1442(15)	289(11)	2032(9)	61(6)
C(41)	353(15)	559(11)	2880(8)	62(6)
C(42)	1893(18)	-2328(16)	2241(12)	83(7)
C(44)	1016(16)	4366(13)	3463(10)	69(6)
C(45)	-1157(14)	3728(11)	2960(8)	60(5)
C(46)	305(14)	-2155(10)	-44(7)	58(5)
C(47)	-1298(16)	184(11)	2797(9)	66(6)
C(48)	-1634(15)	5779(12)	3028(9)	59(5)
C(49)	-794(12)	-1844(9)	996(7)	39(4)
C(50)	2060(30)	4930(30)	2490(19)	156(16)
C(51)	-674(14)	6002(9)	3283(8)	46(5)
C(52)	-2616(17)	865(13)	-78(10)	79(7)
C(53)	-687(13)	3316(11)	3560(8)	54(5)
C(54)	-2090(13)	323(10)	370(8)	48(5)
C(55)	791(13)	7140(10)	4211(9)	46(5)
C(56)	1949(17)	2135(13)	4725(11)	80(7)
C(57)	2653(16)	-1592(16)	2457(11)	71(6)
C(58)	-1561(16)	-2368(12)	576(9)	68(6)
C(59)	-1806(16)	2025(13)	3244(13)	81(7)
C(60)	1142(15)	-2210(13)	1724(9)	67(6)
C(61)	1149(13)	-1413(10)	1388(7)	47(5)
C(62)	-4802(18)	-712(15)	-768(13)	81(7)
C(63)	-3140(20)	-2910(20)	1890(20)	115(10)
C(64)	2643(15)	-863(14)	2119(12)	74(6)
C(66)	870(19)	3884(16)	2781(11)	98(8)

C(67)	2310(20)	5454(18)	3229(17)	124(11)
C(68)	-2543(17)	-548(12)	468(10)	71(6)
C(100)	-496(16)	5735(9)	2023(9)	50(5)
C(101)	1430(30)	4157(19)	2318(16)	137(14)
C(102)	-705(14)	520(9)	1698(8)	43(5)
C(103)	116(17)	-3038(10)	39(9)	79(7)
C(104)	-1563(15)	-1972(12)	2031(11)	66(6)
O(1A)	4070(20)	-1100(20)	3207(17)	241(17)
O(1B)	-3796(16)	-3292(18)	1548(14)	179(12)
O(2A)	3486(14)	-2414(17)	3368(13)	160(8)
O(2B)	-3065(16)	-2650(17)	2581(14)	159(9)
O(3)	-917(11)	57(10)	4283(6)	88(5)
O(4)	-1369(13)	5348(8)	540(7)	92(5)
O(5)	-3304(11)	1103(10)	2208(10)	105(6)
O(8)	-2727(16)	4983(13)	863(9)	135(8)
O(9)	-3396(12)	2279(11)	1533(9)	112(6)
O(12)	3437(16)	9626(13)	4869(13)	156(8)
O(13)	2616(13)	10069(10)	3841(10)	108(6)
O(14)	594(11)	209(9)	4345(6)	78(4)
O(15)	-5230(11)	-254(10)	-1261(9)	98(5)
O(16)	-5199(11)	-1470(12)	-658(9)	107(5)
P(3)	-877(4)	624(2)	702(2)	43(1)
P(4)	160(3)	-1292(2)	638(2)	34(1)
P(6)	317(4)	4018(3)	4148(2)	47(1)
P(7)	-139(3)	6222(2)	4257(2)	36(1)
Ru(1)	0	0	0	37(1)
Ru(2)	0	5000	5000	41(1)
Cl(1)	1311(3)	1006(2)	701(2)	47(1)
Cl(2)	-1638(3)	4684(3)	4494(2)	50(1)
O(20)	3230(30)	5930(20)	2110(20)	280(20)
C(105)	2790(50)	5330(30)	2090(30)	250(30)
O(19)	2510(30)	4900(20)	1380(20)	370(20)

Table C.3. Bond lengths [Å] and angles [°] for $RuCl_2(bbcb)_2$ (**6**).

C(1)-C(17)#1	1.37(3)	C(18)-C(41)	1.35(3)
C(1)-C(8)	1.37(2)	C(18)-C(24)	1.50(2)
C(1A)-O(1A)	1.29(4)	C(19)-C(36)	1.36(3)
C(1A)-O(2A)	1.33(4)	C(19)-C(38)	1.41(3)
C(1A)-C(57)	1.34(5)	C(20)-C(49)	1.42(2)
C(5)-C(14)	1.37(3)	C(20)-C(104)	1.44(3)
C(5)-C(7)	1.35(2)	C(21)-C(61)	1.38(2)
C(5)-C(62)	1.44(3)	C(21)-C(64)	1.40(3)
C(6)-C(55)	1.39(2)	C(22)-C(59)	1.38(3)
C(6)-C(32)	1.41(3)	C(22)-C(37)	1.43(2)
C(7)-C(68)	1.37(3)	C(22)-C(28)	1.47(3)
C(8)-C(13)	1.36(2)	C(23)-C(56)	1.37(3)
C(9)-C(33)	1.39(3)	C(23)-C(39)	1.39(2)
C(9)-C(104)	1.38(3)	C(24)-O(14)	1.23(2)
C(9)-C(63)	1.53(4)	C(24)-O(3)	1.31(2)
C(10)-C(51)	1.43(2)	C(25)-O(4)	1.23(3)
C(10)-C(100)	1.41(2)	C(25)-O(8)	1.31(3)
C(11)-C(12)	1.36(3)	C(27)-C(67)	1.36(3)
C(11)-C(56)#2	1.45(3)	C(27)-C(44)	1.44(3)
C(12)-C(30)	1.39(2)	C(28)-O(5)	1.19(2)
C(13)-C(46)#1	1.43(2)	C(28)-O(9)	1.36(2)
C(13)-P(3)	1.830(15)	C(29)-C(102)	1.37(2)
C(14)-C(52)	1.46(3)	C(29)-C(41)	1.45(2)
C(15)-C(53)	1.35(2)	C(30)-C(39)#2	1.37(2)
C(15)-C(59)	1.42(3)	C(30)-P(7)	1.859(17)
C(16)-C(34)	1.41(3)	C(31)-O(12)	1.29(3)
C(16)-C(100)	1.36(3)	C(31)-O(13)	1.28(4)
C(16)-C(25)	1.51(3)	C(31)-C(36)	1.49(4)
C(17)-C(103)	1.36(2)	C(32)-C(36)	1.40(3)
C(17)-C(1)#1	1.36(3)	C(33)-C(58)	1.41(3)
C(18)-C(47)	1.41(3)	C(34)-C(48)	1.39(2)

C(37)-C(45)	1.41(2)	C(63)-O(2B)	1.32(3)
C(38)-C(55)	1.38(2)	C(66)-C(101)	1.36(3)
C(39)-C(30)#2	1.37(2)	C(102)-P(3)	1.837(14)
C(39)-P(6)	1.852(17)	P(3)-Ru(1)	2.334(4)
C(40)-C(102)	1.39(2)	P(4)-Ru(1)	2.371(4)
C(40)-C(47)	1.42(2)	P(6)-Ru(2)	2.334(4)
C(42)-C(60)	1.37(3)	P(7)-Ru(2)	2.383(4)
C(42)-C(57)	1.46(3)	Ru(1)-P(3)#1	2.334(4)
C(44)-C(66)	1.41(3)	Ru(1)-P(4)#1	2.371(4)
C(44)-P(6)	1.857(18)	Ru(1)-Cl(1)#1	2.421(4)
C(45)-C(53)	1.42(2)	Ru(1)-Cl(1)	2.421(4)
C(46)-C(103)	1.36(2)	Ru(2)-P(6)#2	2.335(4)
C(46)-C(13)#1	1.43(2)	Ru(2)-P(7)#2	2.383(4)
C(46)-P(4)	1.882(15)	Ru(2)-Cl(2)	2.424(5)
C(48)-C(51)	1.41(2)	Ru(2)-Cl(2)#2	2.424(5)
C(49)-C(58)	1.38(2)	O(20)-C(105)	1.05(5)
C(49)-P(4)	1.812(16)	C(105)-O(19)	1.41(6)
C(50)-C(101)	1.37(5)		
C(50)-C(67)	1.52(5)	C(17)#1-C(1)-C(8)	121.4(16)
C(50)-C(105)	1.52(7)	O(1A)-C(1A)-O(2A)	109(4)
C(51)-P(7)	1.827(15)	O(1A)-C(1A)-C(57)	122(3)
C(52)-C(54)	1.42(2)	O(2A)-C(1A)-C(57)	129(4)
C(53)-P(6)	1.842(19)	C(14)-C(5)-C(7)	123.1(19)
C(54)-C(68)	1.44(2)	C(14)-C(5)-C(62)	117(2)
C(54)-P(3)	1.788(19)	C(7)-C(5)-C(62)	119.7(18)
C(55)-P(7)	1.844(17)	C(55)-C(6)-C(32)	119.7(18)
C(56)-C(11)#2	1.45(3)	C(68)-C(7)-C(5)	120.3(18)
C(57)-C(64)	1.31(3)	C(13)-C(8)-C(1)	119.2(16)
C(60)-C(61)	1.40(2)	C(33)-C(9)-C(104)	121(2)
C(61)-P(4)	1.863(17)	C(33)-C(9)-C(63)	117(2)
C(62)-O(15)	1.31(2)	C(104)-C(9)-C(63)	122(2)
C(62)-O(16)	1.27(2)	C(51)-C(10)-C(100)	119.1(19)
C(63)-O(1B)	1.12(3)	C(12)-C(11)-C(56)#2	121(2)

C(11)-C(12)-C(30)	119.4(18)	C(39)#2-C(30)-P(7)	116.7(13)
C(8)-C(13)-C(46)#1	118.5(14)	O(12)-C(31)-O(13)	122(3)
C(8)-C(13)-P(3)	124.3(12)	O(12)-C(31)-C(36)	116(3)
C(46)#1-C(13)-P(3)	117.2(11)	O(13)-C(31)-C(36)	121(2)
C(5)-C(14)-C(52)	118.5(19)	C(36)-C(32)-C(6)	119(2)
C(53)-C(15)-C(59)	117.5(18)	C(58)-C(33)-C(9)	118(2)
C(34)-C(16)-C(100)	122.9(16)	C(16)-C(34)-C(48)	117.9(19)
C(34)-C(16)-C(25)	118(2)	C(32)-C(36)-C(19)	120.3(19)
C(100)-C(16)-C(25)	119(2)	C(32)-C(36)-C(31)	121(2)
C(103)-C(17)-C(1)#1	121.7(16)	C(19)-C(36)-C(31)	118(2)
C(47)-C(18)-C(41)	124.3(15)	C(45)-C(37)-C(22)	116.1(17)
C(47)-C(18)-C(24)	118.3(18)	C(55)-C(38)-C(19)	119.5(18)
C(41)-C(18)-C(24)	117.4(19)	C(30)#2-C(39)-C(23)	120.0(16)
C(36)-C(19)-C(38)	120.7(17)	C(30)#2-C(39)-P(6)	117.6(13)
C(49)-C(20)-C(104)	117.8(17)	C(23)-C(39)-P(6)	122.3(12)
C(61)-C(21)-C(64)	118.4(18)	C(102)-C(40)-C(47)	120.8(19)
C(59)-C(22)-C(37)	121.0(18)	C(18)-C(41)-C(29)	117.9(19)
C(59)-C(22)-C(28)	119.9(19)	C(60)-C(42)-C(57)	119(2)
C(37)-C(22)-C(28)	118.8(17)	C(66)-C(44)-C(27)	121.5(19)
C(56)-C(23)-C(39)	121.6(18)	C(66)-C(44)-P(6)	121.0(18)
O(14)-C(24)-O(3)	123.8(16)	C(27)-C(44)-P(6)	117.5(14)
O(14)-C(24)-C(18)	120.8(19)	C(53)-C(45)-C(37)	121.3(17)
O(3)-C(24)-C(18)	115(2)	C(103)-C(46)-C(13)#1	121.6(15)
O(4)-C(25)-O(8)	125(2)	C(103)-C(46)-P(4)	123.3(13)
O(4)-C(25)-C(16)	121(3)	C(13)#1-C(46)-P(4)	115.1(11)
O(8)-C(25)-C(16)	114(2)	C(18)-C(47)-C(40)	116.4(19)
C(67)-C(27)-C(44)	124(2)	C(51)-C(48)-C(34)	121.3(18)
O(5)-C(28)-O(9)	123(2)	C(58)-C(49)-C(20)	119.3(16)
O(5)-C(28)-C(22)	122(2)	C(58)-C(49)-P(4)	124.5(12)
O(9)-C(28)-C(22)	114(2)	C(20)-C(49)-P(4)	115.8(12)
C(102)-C(29)-C(41)	119.2(17)	C(101)-C(50)-C(67)	126(2)
C(12)-C(30)-C(39)#2	120.6(15)	C(101)-C(50)-C(105)	129(4)
C(12)-C(30)-P(7)	122.1(13)	C(67)-C(50)-C(105)	104(4)

C(48)-C(51)-C(10)	119.0(15)	C(16)-C(100)-C(10)	119.8(17)
C(48)-C(51)-P(7)	122.4(13)	C(50)-C(101)-C(66)	120(3)
C(10)-C(51)-P(7)	118.3(15)	C(29)-C(102)-C(40)	121.3(15)
C(54)-C(52)-C(14)	119.2(18)	C(29)-C(102)-P(3)	117.3(13)
C(15)-C(53)-C(45)	121.9(18)	C(40)-C(102)-P(3)	121.4(15)
C(15)-C(53)-P(6)	122.6(14)	C(17)-C(103)-C(46)	117.5(17)
C(45)-C(53)-P(6)	115.4(13)	C(20)-C(104)-C(9)	120.9(18)
C(52)-C(54)-C(68)	117.3(19)	C(54)-P(3)-C(13)	103.3(8)
C(52)-C(54)-P(3)	122.4(14)	C(54)-P(3)-C(102)	104.4(8)
C(68)-C(54)-P(3)	119.8(14)	C(13)-P(3)-C(102)	101.9(6)
C(6)-C(55)-C(38)	120.4(17)	C(54)-P(3)-Ru(1)	114.3(5)
C(6)-C(55)-P(7)	119.0(13)	C(13)-P(3)-Ru(1)	109.2(5)
C(38)-C(55)-P(7)	120.2(15)	C(102)-P(3)-Ru(1)	121.6(6)
C(23)-C(56)-C(11)#2	116.9(19)	C(49)-P(4)-C(61)	101.2(7)
C(64)-C(57)-C(1A)	122(3)	C(49)-P(4)-C(46)	102.3(7)
C(64)-C(57)-C(42)	120(2)	C(61)-P(4)-C(46)	98.2(7)
C(1A)-C(57)-C(42)	118(3)	C(49)-P(4)-Ru(1)	119.2(5)
C(49)-C(58)-C(33)	122.9(17)	C(61)-P(4)-Ru(1)	125.1(5)
C(22)-C(59)-C(15)	122.2(18)	C(46)-P(4)-Ru(1)	106.9(5)
C(61)-C(60)-C(42)	119(2)	C(44)-P(6)-C(53)	101.0(9)
C(21)-C(61)-C(60)	121.4(17)	C(44)-P(6)-C(39)	102.6(9)
C(21)-C(61)-P(4)	119.8(13)	C(53)-P(6)-C(39)	103.7(8)
C(60)-C(61)-P(4)	118.7(14)	C(44)-P(6)-Ru(2)	123.3(6)
O(15)-C(62)-O(16)	119(2)	C(53)-P(6)-Ru(2)	115.8(6)
O(15)-C(62)-C(5)	121(2)	C(39)-P(6)-Ru(2)	108.2(5)
O(16)-C(62)-C(5)	120(2)	C(51)-P(7)-C(30)	103.5(8)
O(1B)-C(63)-O(2B)	123(4)	C(51)-P(7)-C(55)	100.5(8)
O(1B)-C(63)-C(9)	125(4)	C(30)-P(7)-C(55)	99.4(7)
O(2B)-C(63)-C(9)	112(3)	C(51)-P(7)-Ru(2)	118.2(5)
C(57)-C(64)-C(21)	122(2)	C(30)-P(7)-Ru(2)	106.0(5)
C(101)-C(66)-C(44)	118(3)	C(55)-P(7)-Ru(2)	125.8(6)
C(27)-C(67)-C(50)	110(3)	P(3)-Ru(1)-P(3)#1	180.00(16)
C(7)-C(68)-C(54)	121.6(19)	P(3)-Ru(1)-P(4)#1	81.24(13)

P(3)#1-Ru(1)-P(4)#1	98.76(13)	P(6)-Ru(2)-P(7)#2	81.16(13)
P(3)-Ru(1)-P(4)	98.76(13)	P(6)#2-Ru(2)-P(7)#2	98.84(13)
P(3)#1-Ru(1)-P(4)	81.24(13)	P(7)-Ru(2)-P(7)#2	180.0
P(4)#1-Ru(1)-P(4)	180.0	P(6)-Ru(2)-Cl(2)	93.05(16)
P(3)-Ru(1)-Cl(1)#1	93.31(15)	P(6)#2-Ru(2)-Cl(2)	86.94(16)
P(3)#1-Ru(1)-Cl(1)#1	86.69(15)	P(7)-Ru(2)-Cl(2)	80.73(14)
P(4)#1-Ru(1)-Cl(1)#1	100.08(13)	P(7)#2-Ru(2)-Cl(2)	99.27(14)
P(4)-Ru(1)-Cl(1)#1	79.92(13)	P(6)-Ru(2)-Cl(2)#2	86.95(16)
P(3)-Ru(1)-Cl(1)	86.69(15)	P(6)#2-Ru(2)-Cl(2)#2	93.05(16)
P(3)#1-Ru(1)-Cl(1)	93.31(15)	P(7)-Ru(2)-Cl(2)#2	99.27(14)
P(4)#1-Ru(1)-Cl(1)	79.92(13)	P(7)#2-Ru(2)-Cl(2)#2	80.73(14)
P(4)-Ru(1)-Cl(1)	100.08(13)	Cl(2)-Ru(2)-Cl(2)#2	180.0
Cl(1)#1-Ru(1)-Cl(1)	180.0	O(20)-C(105)-O(19)	113(6)
P(6)-Ru(2)-P(6)#2	180.0(2)	O(20)-C(105)-C(50)	137(6)
P(6)-Ru(2)-P(7)	98.83(13)	O(19)-C(105)-C(50)	104(5)
P(6)#2-Ru(2)-P(7)	81.16(13)		

Symmetry transformations used to generate equivalent atoms:
#1 -x,-y,-z #2 -x,-y+1,-z+1

Table C.4. Anisotropic displacement parameters ($Å^2 x\ 10^3$)for $RuCl_2(bbcb)_2$ (**6**). The anisotropic displacement factor exponent takes the form: $-2p^2[\ h^2a^{*2}U^{11} + ... + 2\ h\ k\ a^*\ b^*\ U^{12}\ ]$.

	U^{11}	U^{22}	U^{33}	U^{23}	U^{13}	U^{12}
C(1)	200(30)	38(11)	34(10)	2(8)	43(13)	13(14)
C(1A)	250(50)	110(30)	190(40)	80(30)	120(40)	0(30)
C(5)	66(15)	38(11)	59(12)	-9(9)	-3(11)	-20(10)
C(6)	66(15)	57(12)	60(12)	6(10)	13(11)	-15(11)
C(7)	53(14)	64(13)	60(12)	12(10)	-7(10)	-5(11)

C(8)	124(18)	21(9)	37(9)	-1(8)	7(10)	16(10)
C(9)	73(17)	68(14)	68(14)	40(11)	24(13)	-3(12)
C(10)	129(18)	24(9)	37(9)	16(7)	28(11)	18(10)
C(11)	110(20)	90(17)	81(16)	15(13)	13(14)	25(15)
C(12)	72(15)	46(11)	72(12)	4(10)	19(11)	38(11)
C(13)	77(13)	30(9)	15(7)	14(7)	2(8)	-4(8)
C(14)	65(16)	81(16)	65(13)	2(11)	8(11)	6(12)
C(15)	56(13)	37(10)	56(10)	-19(9)	13(9)	-12(9)
C(16)	97(18)	29(9)	31(9)	16(7)	2(11)	4(10)
C(17)	220(30)	28(10)	40(10)	4(9)	39(14)	17(13)
C(18)	127(19)	27(9)	17(8)	3(7)	31(11)	3(10)
C(19)	98(18)	31(10)	65(12)	12(9)	10(12)	-5(11)
C(20)	90(16)	36(10)	37(9)	25(8)	19(10)	23(10)
C(21)	88(17)	65(13)	52(12)	-1(10)	0(11)	-21(12)
C(22)	71(15)	67(14)	46(10)	2(10)	-10(10)	6(12)
C(23)	93(17)	39(11)	88(14)	6(10)	20(13)	28(12)
C(24)	105(18)	39(10)	24(9)	4(8)	30(11)	1(11)
C(25)	130(30)	44(13)	82(18)	28(12)	16(18)	6(14)
C(27)	89(18)	64(14)	111(17)	54(12)	59(14)	39(13)
C(28)	89(19)	79(17)	79(15)	22(14)	-9(14)	26(15)
C(29)	114(18)	20(8)	23(8)	1(7)	10(10)	-4(10)
C(30)	79(14)	26(9)	51(10)	10(8)	22(10)	16(9)
C(31)	60(20)	130(30)	180(30)	20(20)	-40(20)	-12(19)
C(32)	100(20)	56(13)	100(17)	25(12)	27(14)	-8(13)
C(33)	99(19)	40(11)	94(16)	41(11)	22(14)	-1(11)
C(34)	101(17)	48(12)	47(11)	19(9)	-3(11)	9(11)
C(36)	68(16)	39(11)	104(17)	25(11)	12(14)	-3(11)
C(37)	89(16)	37(10)	50(11)	-12(9)	16(11)	-3(10)
C(38)	106(18)	37(10)	44(10)	3(8)	18(11)	3(11)
C(39)	78(14)	40(10)	28(8)	7(7)	14(9)	15(10)
C(40)	115(18)	34(10)	43(10)	12(8)	34(11)	20(11)
C(41)	124(19)	37(10)	29(9)	4(7)	33(11)	3(11)
C(42)	100(20)	94(18)	76(15)	18(13)	34(14)	48(17)

C(44)	111(19)	58(13)	54(12)	24(10)	49(12)	16(13)
C(45)	89(16)	46(11)	35(9)	0(8)	-9(10)	13(11)
C(46)	113(17)	32(9)	18(8)	0(7)	-1(9)	1(10)
C(47)	111(19)	42(11)	30(9)	7(8)	-8(11)	-2(11)
C(48)	81(17)	49(11)	42(10)	15(8)	-8(10)	19(11)
C(49)	67(13)	18(8)	28(8)	6(6)	7(8)	-4(8)
C(50)	230(40)	180(40)	140(30)	100(30)	130(30)	100(30)
C(51)	86(16)	24(9)	27(8)	11(7)	7(9)	8(9)
C(52)	120(20)	58(13)	61(12)	18(10)	14(13)	9(13)
C(53)	82(15)	46(11)	36(9)	6(8)	18(9)	14(10)
C(54)	90(15)	30(9)	25(8)	8(7)	16(9)	11(9)
C(55)	76(14)	23(9)	42(9)	1(7)	27(10)	5(9)
C(56)	130(20)	56(13)	64(13)	20(10)	25(13)	40(14)
C(57)	69(17)	83(16)	55(12)	28(12)	-8(11)	15(14)
C(58)	100(19)	46(11)	43(10)	21(9)	-10(11)	1(12)
C(59)	95(19)	46(12)	101(17)	22(12)	18(15)	11(12)
C(60)	92(18)	67(13)	39(10)	23(9)	-1(11)	16(12)
C(61)	83(15)	35(9)	17(7)	6(7)	10(8)	-9(9)
C(62)	90(20)	64(15)	91(16)	27(13)	23(15)	25(15)
C(63)	70(20)	160(30)	120(30)	60(20)	0(20)	30(20)
C(64)	63(16)	71(15)	77(14)	22(12)	-8(12)	7(12)
C(66)	170(30)	106(18)	46(12)	27(12)	41(14)	70(18)
C(67)	180(30)	110(20)	150(20)	84(18)	120(20)	70(20)
C(68)	110(20)	53(12)	50(11)	6(9)	29(12)	0(12)
C(100)	89(17)	16(8)	46(10)	12(7)	15(11)	9(9)
C(101)	230(40)	84(19)	140(20)	37(18)	140(30)	30(20)
C(102)	85(15)	23(8)	19(8)	-5(6)	7(9)	8(9)
C(103)	190(20)	9(8)	41(10)	5(7)	17(12)	15(11)
C(104)	76(16)	47(11)	83(14)	38(11)	20(13)	25(11)
O(1A)	170(30)	190(30)	280(30)	140(20)	-90(20)	-60(20)
O(1B)	88(18)	220(30)	190(20)	89(19)	-22(16)	-43(17)
O(2A)	91(16)	180(20)	190(20)	55(19)	9(15)	6(15)
O(2B)	140(20)	210(20)	150(19)	83(19)	74(17)	35(17)

O(3)	126(14)	107(12)	43(7)	23(7)	39(8)	26(10)
O(4)	179(18)	44(8)	51(8)	3(6)	28(10)	8(9)
O(5)	90(13)	46(9)	154(15)	7(9)	-8(11)	-21(8)
O(8)	150(20)	137(17)	85(12)	33(11)	12(13)	-51(15)
O(9)	102(14)	108(13)	95(12)	-7(10)	-21(10)	-20(10)
O(12)	150(20)	117(16)	180(20)	72(15)	31(17)	-35(14)
O(13)	129(16)	62(10)	121(13)	36(9)	20(11)	-14(10)
O(14)	96(13)	99(11)	31(7)	13(7)	-1(8)	10(9)
O(15)	89(13)	72(10)	112(12)	2(9)	-7(10)	-11(9)
O(16)	87(13)	105(13)	107(12)	11(10)	5(10)	-31(10)
P(3)	90(4)	24(2)	15(2)	8(2)	12(2)	6(2)
P(4)	62(3)	23(2)	12(2)	6(2)	5(2)	-2(2)
P(6)	77(4)	32(2)	36(2)	12(2)	18(2)	12(2)
P(7)	50(3)	27(2)	33(2)	12(2)	12(2)	4(2)
Ru(1)	77(2)	19(1)	11(1)	5(1)	8(1)	-3(1)
Ru(2)	66(2)	27(1)	31(1)	10(1)	14(1)	7(1)
Cl(1)	83(3)	29(2)	21(2)	2(2)	5(2)	-11(2)
Cl(2)	65(3)	39(2)	45(2)	13(2)	10(2)	5(2)
O(20)	390(50)	160(30)	410(40)	110(30)	320(40)	70(30)
C(105)	520(100)	110(40)	180(50)	30(40)	200(50)	80(50)
O(19)	570(60)	240(40)	380(40)	-70(30)	370(40)	-80(40)

Table C.5. Crystal data and structure refinement for $PdCl_2$(dppf-CO_2H) (**8**).

Identification code	SH12051
Empirical formula	C30 H0 Cl2 Fe O8 P2 Pd
Formula weight	783.39
Temperature	293(2) K
Wavelength	71.073 pm
Crystal system	Monoclinic
Space group	P 21/c

Unit cell dimensions	a = 1465.81(13) pm	a= 90°.
	b = 1109.87(9) pm	b= 90.342(2)°.
	c = 2776.4(2) pm	g = 90°.
Volume	4.5166(7) nm^3	
Z	4	
Density (calculated)	1.152 Mg/m^3	
Absorption coefficient	0.941 mm^{-1}	
F(000)	1520	
Crystal size	0.200 x 0.200 x 0.200 mm^3	
Theta range for data collection	3.135 to 27.483°.	
Index ranges	-18<=h<=19, -14<=k<=14, -36<=l<=36	
Reflections collected	59351	
Independent reflections	10328 [R(int) = 0.1107]	
Completeness to theta = 25.242°	99.8 %	
Refinement method	Full-matrix least-squares on F^2	
Data / restraints / parameters	10328 / 0 / 469	
Goodness-of-fit on F^2	1.412	
Final R indices [I>2sigma(I)]	R1 = 0.1312, wR2 = 0.3726	
R indices (all data)	R1 = 0.1781, wR2 = 0.4039	
Extinction coefficient	n/a	
Largest diff. peak and hole	4.089 and -0.628 e.$Å^{-3}$	

Table C.6. Atomic coordinates (x 10^4) and equivalent isotropic displacement parameters (pm^2x 10^{-1}) for $PdCl_2$(dppf-CO_2H) (**8**). U(eq) is defined as one third of the trace of the orthogonalized U^{ij} tensor.

	x	y	z	U(eq)
Pd(1)	5581(1)	7010(1)	1515(1)	43(1)
Fe(1)	4320(1)	3542(1)	1356(1)	45(1)
Cl(1)	5009(2)	8952(2)	1633(1)	58(1)

P(2)	6236(2)	5171(2)	1561(1)	43(1)
P(1)	4142(2)	6541(2)	1259(1)	43(1)
Cl(2)	7059(2)	7791(3)	1624(1)	69(1)
O(1)	354(7)	7294(11)	2604(4)	90(3)
O(2)	8844(9)	2788(13)	-201(4)	107(4)
O(3)	8552(8)	4536(15)	-543(4)	118(5)
O(4)	3522(7)	11223(8)	-307(3)	71(2)
O(6)	3924(9)	9720(9)	-816(3)	96(4)
O(7)	8322(7)	5324(10)	3743(3)	79(3)
O(8)	1373(7)	7157(9)	3207(3)	79(3)
O(1A)	9553(9)	5033(13)	3277(5)	121(5)
C(4)	8147(9)	5171(10)	2893(4)	59(3)
C(5)	8568(9)	5198(13)	2431(5)	67(3)
C(6)	3140(10)	3201(11)	977(5)	62(3)
C(7)	3891(9)	3204(10)	652(4)	56(3)
C(8)	1905(8)	7069(10)	2406(4)	53(3)
C(9)	7202(8)	5175(10)	2943(4)	50(3)
C(10)	8467(11)	3836(18)	-220(5)	84(5)
C(11)	4356(9)	4326(10)	698(4)	54(3)
C(12)	7909(9)	4159(15)	229(4)	70(4)
C(13)	7995(8)	5204(12)	2028(4)	55(3)
C(14)	7391(9)	5196(13)	227(4)	64(3)
C(15)	6644(9)	5124(9)	2542(4)	54(3)
C(16)	4129(10)	8100(10)	-80(4)	59(3)
C(17)	2803(9)	6945(10)	2540(4)	56(3)
C(18)	4318(9)	2821(10)	2048(4)	53(3)
C(19)	3071(8)	4288(11)	1206(4)	52(3)
C(20)	4802(8)	2031(10)	1721(4)	55(3)
C(21)	3498(8)	6865(10)	2195(4)	50(3)
C(22)	3843(8)	5023(10)	1030(4)	51(3)
C(23)	3713(9)	10167(12)	-381(4)	60(3)
C(24)	8713(10)	5161(14)	3344(5)	71(4)
C(25)	1659(8)	7023(11)	1933(4)	57(3)

C(26)	1196(9)	7179(12)	2781(4)	62(3)
C(27)	4764(8)	4011(11)	2035(4)	52(3)
C(28)	5536(8)	2688(10)	1513(4)	49(3)
C(29)	4196(9)	7238(11)	300(4)	58(3)
C(30)	5495(7)	3919(9)	1696(3)	41(2)
C(109)	3260(8)	6791(9)	1712(4)	45(2)
C(104)	7039(8)	5139(9)	2071(4)	45(2)
C(108)	3896(8)	7532(10)	753(4)	49(3)
C(101)	6895(8)	4786(11)	1038(3)	50(3)
C(100)	6884(9)	5502(13)	620(4)	64(3)
C(105)	3759(8)	9195(11)	-10(4)	53(3)
C(107)	3411(9)	8618(11)	821(4)	62(3)
C(110)	2360(9)	6858(10)	1573(4)	56(3)
C(106)	3352(10)	9487(11)	450(4)	67(4)
C(103)	7929(9)	3382(15)	623(4)	72(4)
C(102)	7440(9)	3735(12)	1034(4)	63(3)

Table C.7. Bond lengths [pm] and angles [°] for $PdCl_2$(dppf-CO_2H) (**8**).

Pd(1)-P(2)	225.9(3)	Fe(1)-C(18)	208.3(11)
Pd(1)-P(1)	228.3(3)	Fe(1)-C(7)	208.3(11)
Pd(1)-Cl(1)	233.6(3)	Fe(1)-C(20)	208.1(11)
Pd(1)-Cl(2)	235.1(3)	P(2)-C(30)	180.4(11)
Fe(1)-C(22)	200.1(11)	P(2)-C(101)	180.1(11)
Fe(1)-C(30)	200.3(10)	P(2)-C(104)	183.5(11)
Fe(1)-C(11)	202.4(10)	P(1)-C(108)	181.8(11)
Fe(1)-C(19)	204.9(12)	P(1)-C(109)	183.0(11)
Fe(1)-C(27)	205.7(11)	P(1)-C(22)	185.2(11)
Fe(1)-C(28)	206.3(11)	O(1)-C(26)	133.2(16)
Fe(1)-C(6)	205.5(14)	O(2)-C(10)	128.8(19)

O(3)-C(10)	119.2(19)	C(25)-C(110)	144.8(16)
O(4)-C(23)	122.2(15)	C(27)-C(30)	143.5(15)
O(6)-C(23)	134.4(14)	C(28)-C(30)	145.8(14)
O(7)-C(24)	126.2(15)	C(29)-C(108)	137.5(14)
O(8)-C(26)	120.9(15)	C(109)-C(110)	137.4(17)
O(1A)-C(24)	125.4(18)	C(108)-C(107)	141.2(16)
C(4)-C(9)	139.2(17)	C(101)-C(100)	140.5(14)
C(4)-C(5)	142.8(17)	C(101)-C(102)	141.4(17)
C(4)-C(24)	149.7(17)	C(105)-C(106)	144.8(15)
C(5)-C(13)	139.5(17)	C(107)-C(106)	141.5(16)
C(6)-C(19)	136.8(16)	C(103)-C(102)	140.6(16)
C(6)-C(7)	142.8(19)		
C(7)-C(11)	142.5(17)	P(2)-Pd(1)-P(1)	101.70(11)
C(8)-C(25)	136.2(16)	P(2)-Pd(1)-Cl(1)	168.11(11)
C(8)-C(17)	137.2(18)	P(1)-Pd(1)-Cl(1)	85.53(11)
C(8)-C(26)	148.0(16)	P(2)-Pd(1)-Cl(2)	86.25(12)
C(9)-C(15)	137.8(15)	P(1)-Pd(1)-Cl(2)	166.76(11)
C(10)-C(12)	153.9(18)	Cl(1)-Pd(1)-Cl(2)	88.51(12)
C(11)-C(22)	142.2(15)	C(22)-Fe(1)-C(30)	109.8(5)
C(12)-C(14)	138(2)	C(22)-Fe(1)-C(11)	41.4(4)
C(12)-C(103)	139.4(19)	C(30)-Fe(1)-C(11)	107.9(5)
C(13)-C(104)	140.9(16)	C(22)-Fe(1)-C(19)	42.8(5)
C(14)-C(100)	136.7(16)	C(30)-Fe(1)-C(19)	140.9(4)
C(15)-C(104)	143.3(14)	C(11)-Fe(1)-C(19)	70.8(5)
C(16)-C(105)	134.6(16)	C(22)-Fe(1)-C(27)	108.3(4)
C(16)-C(29)	142.8(16)	C(30)-Fe(1)-C(27)	41.4(4)
C(17)-C(21)	140.5(15)	C(11)-Fe(1)-C(27)	135.0(5)
C(18)-C(20)	145.2(17)	C(19)-Fe(1)-C(27)	111.2(4)
C(18)-C(27)	147.4(16)	C(22)-Fe(1)-C(28)	140.6(5)
C(19)-C(22)	147.9(17)	C(30)-Fe(1)-C(28)	42.0(4)
C(20)-C(28)	142.5(16)	C(11)-Fe(1)-C(28)	111.2(5)
C(21)-C(109)	138.5(14)	C(19)-Fe(1)-C(28)	176.4(5)
C(23)-C(105)	149.3(16)	C(27)-Fe(1)-C(28)	69.8(4)

C(22)-Fe(1)-C(6)	68.2(5)	C(30)-P(2)-Pd(1)	116.8(3)
C(30)-Fe(1)-C(6)	177.0(5)	C(101)-P(2)-Pd(1)	113.5(4)
C(11)-Fe(1)-C(6)	69.1(5)	C(104)-P(2)-Pd(1)	109.3(3)
C(19)-Fe(1)-C(6)	38.9(4)	C(108)-P(1)-C(109)	107.5(5)
C(27)-Fe(1)-C(6)	141.0(5)	C(108)-P(1)-C(22)	103.9(5)
C(28)-Fe(1)-C(6)	138.4(5)	C(109)-P(1)-C(22)	102.0(5)
C(22)-Fe(1)-C(18)	136.9(4)	C(108)-P(1)-Pd(1)	106.3(4)
C(30)-Fe(1)-C(18)	69.6(4)	C(109)-P(1)-Pd(1)	114.0(4)
C(11)-Fe(1)-C(18)	176.8(5)	C(22)-P(1)-Pd(1)	122.1(4)
C(19)-Fe(1)-C(18)	109.7(5)	C(9)-C(4)-C(5)	121.6(11)
C(27)-Fe(1)-C(18)	41.7(4)	C(9)-C(4)-C(24)	117.7(11)
C(28)-Fe(1)-C(18)	68.5(5)	C(5)-C(4)-C(24)	120.7(12)
C(6)-Fe(1)-C(18)	113.4(5)	C(13)-C(5)-C(4)	117.3(12)
C(22)-Fe(1)-C(7)	67.7(4)	C(19)-C(6)-C(7)	110.5(11)
C(30)-Fe(1)-C(7)	137.1(5)	C(19)-C(6)-Fe(1)	70.3(7)
C(11)-Fe(1)-C(7)	40.6(5)	C(7)-C(6)-Fe(1)	70.9(7)
C(19)-Fe(1)-C(7)	67.5(5)	C(11)-C(7)-C(6)	108.4(10)
C(27)-Fe(1)-C(7)	175.5(5)	C(11)-C(7)-Fe(1)	67.5(6)
C(28)-Fe(1)-C(7)	111.8(5)	C(6)-C(7)-Fe(1)	68.8(7)
C(6)-Fe(1)-C(7)	40.4(5)	C(25)-C(8)-C(17)	120.3(10)
C(18)-Fe(1)-C(7)	142.7(5)	C(25)-C(8)-C(26)	119.9(11)
C(22)-Fe(1)-C(20)	177.8(5)	C(17)-C(8)-C(26)	119.6(11)
C(30)-Fe(1)-C(20)	69.6(4)	C(15)-C(9)-C(4)	120.4(11)
C(11)-Fe(1)-C(20)	140.8(5)	O(3)-C(10)-O(2)	125.0(15)
C(19)-Fe(1)-C(20)	136.5(5)	O(3)-C(10)-C(12)	121.0(16)
C(27)-Fe(1)-C(20)	69.7(5)	O(2)-C(10)-C(12)	114.0(13)
C(28)-Fe(1)-C(20)	40.2(5)	C(7)-C(11)-C(22)	106.2(11)
C(6)-Fe(1)-C(20)	112.5(5)	C(7)-C(11)-Fe(1)	72.0(7)
C(18)-Fe(1)-C(20)	40.8(5)	C(22)-C(11)-Fe(1)	68.5(6)
C(7)-Fe(1)-C(20)	114.3(5)	C(14)-C(12)-C(103)	121.9(12)
C(30)-P(2)-C(101)	108.1(5)	C(14)-C(12)-C(10)	119.2(12)
C(30)-P(2)-C(104)	102.1(5)	C(103)-C(12)-C(10)	118.9(14)
C(101)-P(2)-C(104)	105.8(5)	C(5)-C(13)-C(104)	121.8(11)

C(100)-C(14)-C(12)	120.5(12)	C(18)-C(27)-Fe(1)	70.1(6)
C(9)-C(15)-C(104)	119.7(11)	C(20)-C(28)-C(30)	107.9(10)
C(105)-C(16)-C(29)	121.6(10)	C(20)-C(28)-Fe(1)	70.6(6)
C(21)-C(17)-C(8)	121.3(11)	C(30)-C(28)-Fe(1)	66.8(6)
C(20)-C(18)-C(27)	107.9(10)	C(108)-C(29)-C(16)	119.8(11)
C(20)-C(18)-Fe(1)	69.5(6)	C(28)-C(30)-C(27)	109.1(9)
C(27)-C(18)-Fe(1)	68.2(6)	C(28)-C(30)-P(2)	128.6(8)
C(6)-C(19)-C(22)	106.0(10)	C(27)-C(30)-P(2)	122.3(8)
C(6)-C(19)-Fe(1)	70.7(8)	C(28)-C(30)-Fe(1)	71.2(6)
C(22)-C(19)-Fe(1)	66.8(6)	C(27)-C(30)-Fe(1)	71.3(6)
C(18)-C(20)-C(28)	108.5(10)	P(2)-C(30)-Fe(1)	125.5(5)
C(18)-C(20)-Fe(1)	69.6(6)	C(110)-C(109)-C(21)	120.2(10)
C(28)-C(20)-Fe(1)	69.2(6)	C(110)-C(109)-P(1)	119.8(8)
C(17)-C(21)-C(109)	119.0(11)	C(21)-C(109)-P(1)	120.0(9)
C(11)-C(22)-C(19)	108.8(10)	C(13)-C(104)-C(15)	119.0(10)
C(11)-C(22)-P(1)	126.3(9)	C(13)-C(104)-P(2)	124.6(8)
C(19)-C(22)-P(1)	124.6(8)	C(15)-C(104)-P(2)	116.3(9)
C(11)-C(22)-Fe(1)	70.2(6)	C(29)-C(108)-C(107)	119.3(10)
C(19)-C(22)-Fe(1)	70.3(6)	C(29)-C(108)-P(1)	120.0(9)
P(1)-C(22)-Fe(1)	120.7(6)	C(107)-C(108)-P(1)	120.7(7)
O(4)-C(23)-O(6)	124.0(11)	C(100)-C(101)-C(102)	117.7(11)
O(4)-C(23)-C(105)	125.9(11)	C(100)-C(101)-P(2)	121.8(9)
O(6)-C(23)-C(105)	110.1(11)	C(102)-C(101)-P(2)	120.5(8)
O(1A)-C(24)-O(7)	126.7(14)	C(101)-C(100)-C(14)	120.9(12)
O(1A)-C(24)-C(4)	114.6(12)	C(16)-C(105)-C(106)	119.9(10)
O(7)-C(24)-C(4)	118.7(13)	C(16)-C(105)-C(23)	124.7(10)
C(8)-C(25)-C(110)	119.0(11)	C(106)-C(105)-C(23)	115.4(11)
O(8)-C(26)-O(1)	123.7(11)	C(106)-C(107)-C(108)	120.8(10)
O(8)-C(26)-C(8)	122.6(12)	C(109)-C(110)-C(25)	119.8(11)
O(1)-C(26)-C(8)	113.7(11)	C(107)-C(106)-C(105)	117.8(11)
C(30)-C(27)-C(18)	106.6(10)	C(102)-C(103)-C(12)	117.1(14)
C(30)-C(27)-Fe(1)	67.3(6)	C(103)-C(102)-C(101)	121.8(12)

Table C.8. Anisotropic displacement parameters ($pm^2 x\ 10^{-1}$)for $PdCl_2$(dppf-CO_2H) (**8**). The anisotropic displacement factor exponent takes the form: $-2p^2[\ h^2a^{*2}U^{11} + ... + 2\ h\ k\ a^*\ b^*\ U^{12}\ ]$.

	U^{11}	U^{22}	U^{33}	U^{23}	U^{13}	U^{12}
Pd(1)	51(1)	41(1)	37(1)	2(1)	4(1)	-1(1)
Fe(1)	51(1)	44(1)	39(1)	-1(1)	-4(1)	3(1)
Cl(1)	80(2)	42(1)	53(2)	0(1)	13(1)	3(1)
P(2)	50(2)	46(2)	33(1)	1(1)	1(1)	4(1)
P(1)	52(2)	45(1)	31(1)	-2(1)	-1(1)	6(1)
Cl(2)	61(2)	68(2)	78(2)	9(2)	-3(2)	-19(2)
O(1)	59(6)	139(9)	73(6)	-33(6)	13(5)	-20(6)
O(2)	97(9)	150(12)	75(7)	1(7)	23(6)	21(8)
O(3)	88(8)	217(14)	50(6)	25(8)	13(5)	47(9)
O(4)	111(8)	55(5)	47(5)	9(4)	-10(5)	2(5)
O(6)	177(12)	70(6)	41(5)	1(4)	25(6)	-9(7)
O(7)	84(7)	107(7)	46(5)	9(5)	-10(5)	-14(6)
O(8)	82(7)	113(8)	43(5)	-13(5)	7(4)	-25(6)
O(1A)	93(9)	157(12)	111(9)	-32(8)	-52(7)	43(8)
C(4)	73(9)	51(7)	51(6)	-8(5)	-17(6)	13(6)
C(5)	60(8)	87(9)	54(7)	-8(6)	-5(6)	-10(7)
C(6)	70(9)	50(7)	66(8)	-8(5)	-7(6)	8(6)
C(7)	66(8)	51(7)	52(6)	-10(5)	-24(6)	9(6)
C(8)	53(7)	59(7)	48(6)	-7(5)	4(5)	-13(6)
C(9)	53(7)	56(6)	41(5)	5(5)	-5(5)	-18(5)
C(10)	83(11)	121(13)	47(7)	7(8)	-2(7)	34(10)
C(11)	78(8)	49(6)	35(5)	-4(4)	-18(5)	13(6)
C(12)	53(7)	119(12)	38(6)	4(7)	-15(5)	1(8)
C(13)	43(6)	78(8)	44(6)	3(5)	-4(5)	1(6)
C(14)	54(7)	95(10)	42(6)	6(6)	4(5)	15(7)
C(15)	82(9)	47(6)	31(5)	2(4)	-9(5)	-12(6)
C(16)	85(9)	51(7)	40(6)	2(5)	-8(6)	3(6)

C(17)	68(8)	59(7)	40(6)	-16(5)	8(5)	-14(6)
C(18)	67(8)	50(6)	42(6)	5(5)	-2(5)	-2(6)
C(19)	50(7)	57(7)	50(6)	-6(5)	-14(5)	3(5)
C(20)	52(7)	57(7)	55(6)	18(5)	-6(5)	-5(6)
C(21)	62(7)	56(6)	32(5)	-3(4)	7(5)	-14(5)
C(22)	59(7)	53(6)	40(5)	-9(4)	-1(5)	11(5)
C(23)	70(8)	63(8)	46(6)	9(5)	-5(6)	-9(6)
C(24)	57(8)	103(11)	54(7)	9(7)	-5(6)	6(8)
C(25)	45(6)	72(8)	53(6)	3(5)	5(5)	4(6)
C(26)	50(7)	82(9)	54(7)	-16(6)	2(5)	-9(6)
C(27)	47(6)	59(7)	51(6)	12(5)	-7(5)	2(5)
C(28)	55(7)	45(6)	48(6)	1(4)	-13(5)	15(5)
C(29)	73(8)	67(7)	35(5)	-9(5)	15(5)	4(6)
C(30)	46(6)	45(6)	33(5)	-5(4)	-3(4)	6(5)
C(109)	56(7)	40(5)	38(5)	2(4)	-6(5)	3(5)
C(104)	51(6)	42(5)	41(5)	0(4)	-3(4)	-3(5)
C(108)	64(7)	48(6)	33(5)	-1(4)	-3(5)	5(5)
C(101)	49(6)	72(7)	28(5)	4(5)	-9(4)	3(6)
C(100)	59(8)	87(9)	45(6)	27(6)	-1(5)	-3(7)
C(105)	66(8)	57(7)	37(5)	-3(5)	3(5)	-14(6)
C(107)	88(9)	63(7)	35(5)	4(5)	7(6)	26(7)
C(110)	58(7)	61(7)	49(6)	-9(5)	4(5)	2(6)
C(106)	97(10)	58(7)	45(6)	-7(5)	-2(6)	15(7)
C(103)	61(8)	123(11)	32(5)	-3(6)	-1(5)	-3(8)
C(102)	57(8)	73(8)	59(7)	-4(6)	10(6)	8(7)

Table C.9. Crystal data and structure refinement for pcm-6(Li) (**17**).

Identification code	PCM-6	
Empirical formula	C22 H17 N0 O7 P Zn	
Formula weight	489.69	
Temperature	180(2) K	
Wavelength	0.71073 Å	
Crystal system	Orthorhombic	
Space group	P n n a	
Unit cell dimensions	a = 23.2254(4) Å	a= 90°.
	b = 25.4124(6) Å	b= 90°.
	c = 10.6738(2) Å	g = 90°.
Volume	6299.8(2) $Å^3$	
Z	8	
Density (calculated)	1.033 Mg/m^3	
Absorption coefficient	0.859 mm^{-1}	
F(000)	2000	
Crystal size	0.100 x 0.100 x 0.100 mm^3	
Theta range for data collection	3.536 to 23.997°.	
Index ranges	-26<=h<=26, -27<=k<=29, -12<=l<=12	
Reflections collected	32451	
Independent reflections	4918 [R(int) = 0.0614]	
Completeness to theta = 23.997°	99.3 %	
Refinement method	Full-matrix least-squares on F^2	
Data / restraints / parameters	4918 / 6 / 290	
Goodness-of-fit on F^2	1.045	
Final R indices [I>2sigma(I)]	R1 = 0.0668, wR2 = 0.1681	
R indices (all data)	R1 = 0.0910, wR2 = 0.1803	
Extinction coefficient	n/a	
Largest diff. peak and hole	0.952 and -0.507 $e.Å^{-3}$	

Table C.10. Atomic coordinates (x 10^4) and equivalent isotropic displacement parameters ($Å^2$x 10^3) for pcm-6(Li) (**17**). U(eq) is defined as one third of the trace of the orthogonalized U^{ij} tensor.

	x	y	z	U(eq)
Zn(1)	4445(1)	3843(1)	14860(1)	48(1)
P(1)	3891(1)	5863(1)	8418(1)	46(1)
O(1)	4305(1)	4197(1)	13260(3)	50(1)
O(2)	4296(2)	4950(2)	14289(4)	92(1)
O(3)	1301(1)	6211(1)	5751(4)	59(1)
O(4)	1021(1)	5759(2)	7427(4)	74(1)
O(5)	5327(2)	8121(1)	9503(3)	66(1)
O(6)	4437(2)	8439(2)	9496(4)	82(1)
O(7)	4939(1)	4172(2)	16150(4)	65(1)
C(1)	3968(2)	5506(2)	9871(4)	42(1)
C(1P)	4278(2)	5541(2)	7212(5)	53(1)
C(2)	3866(2)	5756(2)	11000(5)	54(1)
C(3)	3935(2)	5491(2)	12104(5)	54(1)
C(4)	4108(2)	4971(2)	12104(4)	48(1)
C(5)	4200(2)	4722(2)	10977(5)	51(1)
C(6)	4130(2)	4984(2)	9844(5)	49(1)
C(7)	4237(2)	4690(2)	13315(5)	57(1)
C(8)	3150(2)	5912(2)	7982(5)	49(1)
C(9)	2719(2)	5695(2)	8727(5)	56(1)
C(10)	2148(2)	5725(2)	8325(5)	58(1)
C(11)	2016(2)	5975(2)	7204(5)	50(1)
C(12)	2439(2)	6199(2)	6487(5)	56(1)
C(13)	3017(2)	6163(2)	6871(5)	57(1)
C(14)	1391(2)	5978(2)	6774(5)	54(1)
C(15)	4158(2)	6517(2)	8654(4)	46(1)
C(16)	3786(2)	6916(2)	8970(5)	56(1)
C(17)	3985(2)	7417(2)	9196(5)	60(1)

C(18)	4566(2)	7524(2)	9159(5)	50(1)
C(19)	4948(2)	7122(2)	8845(5)	60(1)
C(20)	4749(2)	6615(2)	8576(5)	53(1)
C(21)	4777(3)	8072(2)	9401(5)	61(2)

Table C.11. Bond lengths [Å] and angles [°] for pcm-6(Li) (**17**).

Zn(1)-O(5)#1	1.946(4)	C(2)-C(3)	1.367(7)
Zn(1)-O(1)	1.957(3)	C(2)-H(2A)	0.9500
Zn(1)-O(7)	1.978(3)	C(3)-C(4)	1.380(7)
Zn(1)-O(3)#2	1.981(3)	C(3)-H(3A)	0.9500
P(1)-C(1P)	1.770(5)	C(4)-C(5)	1.376(7)
P(1)-C(8)	1.788(4)	C(4)-C(7)	1.507(7)
P(1)-C(15)	1.792(5)	C(5)-C(6)	1.390(7)
P(1)-C(1)	1.805(5)	C(5)-H(5A)	0.9500
O(1)-C(7)	1.265(6)	C(6)-H(6A)	0.9500
O(2)-C(7)	1.239(6)	C(8)-C(13)	1.381(7)
O(3)-C(14)	1.258(6)	C(8)-C(9)	1.392(7)
O(3)-Zn(1)#3	1.981(3)	C(9)-C(10)	1.396(6)
O(4)-C(14)	1.239(6)	C(9)-H(9A)	0.9500
O(5)-C(21)	1.287(6)	C(10)-C(11)	1.388(7)
O(5)-Zn(1)#4	1.946(4)	C(10)-H(10A)	0.9500
O(6)-C(21)	1.227(7)	C(11)-C(12)	1.370(7)
O(7)-H(7A)	1.025(17)	C(11)-C(14)	1.522(6)
O(7)-H(7B)	1.023(17)	C(12)-C(13)	1.407(7)
C(1)-C(6)	1.379(7)	C(12)-H(12A)	0.9500
C(1)-C(2)	1.384(7)	C(13)-H(13A)	0.9500
C(1P)-H(1C)	0.9800	C(15)-C(16)	1.373(7)
C(1P)-H(1B)	0.9800	C(15)-C(20)	1.398(6)
C(1P)-H(1A)	0.9800	C(16)-C(17)	1.376(7)

C(16)-H(16A)	0.9500	P(1)-C(1P)-H(1A)	109.5
C(17)-C(18)	1.378(7)	H(1C)-C(1P)-H(1A)	109.5
C(17)-H(17A)	0.9500	H(1B)-C(1P)-H(1A)	109.5
C(18)-C(19)	1.393(7)	C(3)-C(2)-C(1)	120.3(5)
C(18)-C(21)	1.499(7)	C(3)-C(2)-H(2A)	119.9
C(19)-C(20)	1.399(7)	C(1)-C(2)-H(2A)	119.9
C(19)-H(19A)	0.9500	C(2)-C(3)-C(4)	120.4(5)
C(20)-H(20A)	0.9500	C(2)-C(3)-H(3A)	119.8
		C(4)-C(3)-H(3A)	119.8
O(5)#1-Zn(1)-O(1)	107.92(15)	C(5)-C(4)-C(3)	119.0(4)
O(5)#1-Zn(1)-O(7)	112.10(16)	C(5)-C(4)-C(7)	120.1(4)
O(1)-Zn(1)-O(7)	120.65(16)	C(3)-C(4)-C(7)	120.7(5)
O(5)#1-Zn(1)-O(3)#2	105.51(15)	C(4)-C(5)-C(6)	121.5(5)
O(1)-Zn(1)-O(3)#2	107.80(15)	C(4)-C(5)-H(5A)	119.3
O(7)-Zn(1)-O(3)#2	101.63(15)	C(6)-C(5)-H(5A)	119.3
C(1P)-P(1)-C(8)	109.4(2)	C(1)-C(6)-C(5)	118.3(5)
C(1P)-P(1)-C(15)	110.8(2)	C(1)-C(6)-H(6A)	120.8
C(8)-P(1)-C(15)	107.7(2)	C(5)-C(6)-H(6A)	120.8
C(1P)-P(1)-C(1)	110.1(2)	O(2)-C(7)-O(1)	123.6(5)
C(8)-P(1)-C(1)	110.7(2)	O(2)-C(7)-C(4)	119.3(5)
C(15)-P(1)-C(1)	108.1(2)	O(1)-C(7)-C(4)	117.1(5)
C(7)-O(1)-Zn(1)	115.8(3)	C(13)-C(8)-C(9)	120.9(4)
C(14)-O(3)-Zn(1)#3	122.0(3)	C(13)-C(8)-P(1)	118.1(4)
C(21)-O(5)-Zn(1)#4	112.2(4)	C(9)-C(8)-P(1)	121.0(4)
Zn(1)-O(7)-H(7A)	101.1(14)	C(8)-C(9)-C(10)	119.0(5)
Zn(1)-O(7)-H(7B)	100.0(14)	C(8)-C(9)-H(9A)	120.5
H(7A)-O(7)-H(7B)	147(3)	C(10)-C(9)-H(9A)	120.5
C(6)-C(1)-C(2)	120.5(4)	C(11)-C(10)-C(9)	120.0(5)
C(6)-C(1)-P(1)	119.5(4)	C(11)-C(10)-H(10A)	120.0
C(2)-C(1)-P(1)	120.1(4)	C(9)-C(10)-H(10A)	120.0
P(1)-C(1P)-H(1C)	109.5	C(12)-C(11)-C(10)	120.9(4)
P(1)-C(1P)-H(1B)	109.5	C(12)-C(11)-C(14)	120.8(5)
H(1C)-C(1P)-H(1B)	109.5	C(10)-C(11)-C(14)	118.3(4)

C(11)-C(12)-C(13)	119.6(5)	C(16)-C(17)-C(18)	120.3(5)
C(11)-C(12)-H(12A)	120.2	C(16)-C(17)-H(17A)	119.8
C(13)-C(12)-H(12A)	120.2	C(18)-C(17)-H(17A)	119.8
C(8)-C(13)-C(12)	119.6(5)	C(17)-C(18)-C(19)	119.1(5)
C(8)-C(13)-H(13A)	120.2	C(17)-C(18)-C(21)	119.9(5)
C(12)-C(13)-H(13A)	120.2	C(19)-C(18)-C(21)	121.0(5)
O(4)-C(14)-O(3)	125.7(4)	C(18)-C(19)-C(20)	120.9(5)
O(4)-C(14)-C(11)	119.2(5)	C(18)-C(19)-H(19A)	119.5
O(3)-C(14)-C(11)	115.1(5)	C(20)-C(19)-H(19A)	119.5
C(16)-C(15)-C(20)	120.0(4)	C(15)-C(20)-C(19)	118.5(5)
C(16)-C(15)-P(1)	120.2(3)	C(15)-C(20)-H(20A)	120.8
C(20)-C(15)-P(1)	119.7(4)	C(19)-C(20)-H(20A)	120.8
C(15)-C(16)-C(17)	121.1(4)	O(6)-C(21)-O(5)	124.0(5)
C(15)-C(16)-H(16A)	119.5	O(6)-C(21)-C(18)	120.6(5)
C(17)-C(16)-H(16A)	119.5	O(5)-C(21)-C(18)	115.4(5)

Symmetry transformations used to generate equivalent atoms:
#1 -x+1,y-1/2,z+1/2 #2 -x+1/2,-y+1,z+1 #3 -x+1/2,-y+1,z-1
#4 -x+1,y+1/2,z-1/2

Table C.12. Anisotropic displacement parameters ($Å^2 x\ 10^3$)for pcm-7(Li) (**17**). The anisotropic displacement factor exponent takes the form: $-2p^2[\ h^2a^{*2}U^{11} + ... + 2\ h\ k\ a^*\ b^*\ U^{12}\ ]$.

	U^{11}	U^{22}	U^{33}	U^{23}	U^{13}	U^{12}
Zn(1)	36(1)	50(1)	57(1)	4(1)	6(1)	3(1)
P(1)	28(1)	46(1)	65(1)	9(1)	-9(1)	-6(1)
O(1)	47(2)	41(2)	63(2)	8(2)	-1(2)	4(2)
O(2)	150(4)	60(3)	66(3)	5(2)	-22(3)	19(3)
O(3)	37(2)	69(2)	71(2)	16(2)	-15(2)	-4(2)

O(4)	34(2)	104(3)	84(3)	33(2)	-8(2)	-12(2)
O(5)	64(2)	65(2)	68(2)	11(2)	-14(2)	-27(2)
O(6)	91(3)	49(3)	106(3)	6(2)	-34(3)	-12(2)
O(7)	38(2)	79(3)	77(2)	-15(2)	3(2)	-2(2)
C(1)	26(2)	43(3)	58(3)	10(2)	-10(2)	-7(2)
C(1P)	39(2)	53(3)	67(3)	8(3)	1(2)	-7(2)
C(2)	43(3)	44(3)	75(4)	7(3)	-9(2)	6(2)
C(3)	48(3)	57(3)	57(3)	-5(3)	-2(2)	6(2)
C(4)	42(2)	45(3)	56(3)	-1(2)	-10(2)	2(2)
C(5)	43(3)	37(3)	72(4)	2(3)	-14(2)	4(2)
C(6)	37(2)	51(3)	58(3)	2(2)	-9(2)	3(2)
C(7)	51(3)	69(4)	52(3)	-2(3)	-4(2)	4(3)
C(8)	36(2)	46(3)	65(3)	2(3)	-9(2)	-4(2)
C(9)	29(2)	66(3)	72(3)	23(3)	-8(2)	-5(2)
C(10)	34(2)	71(4)	71(3)	20(3)	-9(2)	-5(2)
C(11)	37(2)	46(3)	67(3)	3(3)	-9(2)	-4(2)
C(12)	53(3)	57(3)	59(3)	17(3)	-19(3)	-9(2)
C(13)	44(3)	66(4)	61(3)	16(3)	-7(2)	-10(2)
C(14)	40(3)	51(3)	70(4)	5(3)	-14(3)	1(2)
C(15)	36(2)	46(3)	57(3)	13(2)	-15(2)	-14(2)
C(16)	37(3)	52(3)	80(4)	6(3)	-2(2)	-8(2)
C(17)	51(3)	55(3)	73(4)	8(3)	-11(3)	0(3)
C(18)	56(3)	39(3)	54(3)	22(2)	-15(2)	-15(2)
C(19)	52(3)	55(3)	73(4)	25(3)	-19(3)	-18(3)
C(20)	44(3)	46(3)	69(3)	17(2)	-8(2)	-3(2)
C(21)	68(4)	57(4)	59(3)	21(3)	-19(3)	-18(3)

Table C.13. Hydrogen coordinates (x 10^4) and isotropic displacement parameters ($Å^2$x 10^3) for pcm-7(Li) (**17**).

	x	y	z	U(eq)
H(1C)	4685	5513	7450	79
H(1B)	4120	5187	7084	79
H(1A)	4245	5743	6434	79
H(2A)	3748	6114	11009	65
H(3A)	3864	5665	12876	65
H(5A)	4313	4363	10973	61
H(6A)	4192	4808	9071	58
H(9A)	2812	5529	9498	67
H(10A)	1850	5574	8818	70
H(12A)	2343	6377	5734	67
H(13A)	3314	6310	6370	68
H(16A)	3386	6844	9034	67
H(17A)	3719	7691	9378	72
H(19A)	5349	7193	8812	72
H(20A)	5010	6343	8347	63
H(7A)	5182(17)	4422(17)	15610(20)	92
H(7B)	4682(16)	4130(20)	16921(17)	92

Table C.14. Crystal data and structure refinement for PCM-7(Na) (**18**).

Identification code	PCM-7	
Empirical formula	C59 H81 N5 Na0 O26 P2 Zn3	
Formula weight	1534.33	
Temperature	180(2) K	
Wavelength	0.71073 Å	
Crystal system	Monoclinic	
Space group	P 21/c	
Unit cell dimensions	a = 14.3103(2) Å	a= 90°.
	b = 23.9089(3) Å	b= 104.1910(10)°.
	c = 24.2854(3) Å	g = 90°.
Volume	8055.53(18) $Å^3$	
Z	4	
Density (calculated)	1.265 Mg/m^3	
Absorption coefficient	0.997 mm^{-1}	
F(000)	3192	
Crystal size	0.150 x 0.120 x 0.120 mm^3	
Theta range for data collection	3.515 to 24.000°.	
Index ranges	-16<=h<=16, -27<=k<=26, -23<=l<=27	
Reflections collected	37489	
Independent reflections	12507 [R(int) = 0.0426]	
Completeness to theta = 24.000°	98.9 %	
Refinement method	Full-matrix least-squares on F^2	
Data / restraints / parameters	12507 / 53 / 743	
Goodness-of-fit on F^2	1.047	
Final R indices [I>2sigma(I)]	R1 = 0.0756, wR2 = 0.2142	
R indices (all data)	R1 = 0.0874, wR2 = 0.2241	
Extinction coefficient	n/a	
Largest diff. peak and hole	1.681 and -0.977 $e.Å^{-3}$	

Table C.15. Atomic coordinates (x 10^4) and equivalent isotropic displacement parameters ($Å^2$x 10^3) for PCM-7(Na) (**18**). U(eq) is defined as one third of the trace of the orthogonalized U^{ij} tensor.

	x	y	z	U(eq)
Zn(1)	4859(1)	6923(1)	2495(1)	28(1)
Zn(2)	-2867(1)	8633(1)	-2238(1)	28(1)
Zn(3)	2666(1)	6285(1)	2261(1)	27(1)
P(1)	2560(1)	6885(1)	-1272(1)	25(1)
P(2)	-2804(1)	7994(1)	1253(1)	26(1)
O(1)	2598(4)	4124(2)	-1849(2)	55(1)
O(2)	2646(3)	4456(2)	-2687(2)	42(1)
O(3)	-1602(3)	8287(2)	-2103(2)	43(1)
O(4)	-2233(3)	7429(2)	-2135(2)	45(1)
O(5)	4118(3)	6885(2)	1594(2)	44(1)
O(6)	2803(3)	6352(2)	1472(2)	40(1)
O(7)	-3098(3)	8556(2)	-1471(2)	40(1)
O(8)	-4382(3)	7980(2)	-1622(2)	36(1)
O(9)	-2466(3)	10758(2)	1822(2)	48(1)
O(10)	-2562(3)	10448(2)	2666(2)	40(1)
O(11)	1349(3)	6569(2)	2144(2)	42(1)
O(12)	1954(3)	7425(2)	2126(2)	50(1)
O(13)	3832(3)	6562(2)	2740(2)	34(1)
O(14)	5918(3)	6568(2)	2281(2)	38(1)
O(15)	4775(3)	7761(2)	2408(2)	45(1)
C(1P)	3392(4)	7327(2)	-1497(2)	34(1)
C(1)	2604(4)	6186(2)	-1537(2)	28(1)
C(2P)	-3656(4)	7580(3)	1489(2)	37(1)
C(2)	2666(5)	5734(3)	-1175(2)	48(2)
C(3)	2677(6)	5196(3)	-1386(3)	51(2)
C(4)	2605(4)	5106(2)	-1963(2)	34(1)
C(5)	2522(5)	5558(3)	-2317(2)	40(1)

C(6)	2520(5)	6101(3)	-2109(2)	39(1)
C(7)	2611(4)	4519(3)	-2173(3)	39(1)
C(8)	1354(4)	7141(2)	-1529(2)	26(1)
C(9)	1193(4)	7714(2)	-1588(2)	34(1)
C(10)	241(4)	7905(2)	-1763(3)	39(1)
C(11)	-522(4)	7541(2)	-1868(2)	30(1)
C(12)	-352(4)	6968(2)	-1808(2)	36(1)
C(13)	579(4)	6765(2)	-1641(2)	34(1)
C(14)	-1542(4)	7760(3)	-2050(2)	34(1)
C(15)	2820(4)	6842(2)	-511(2)	26(1)
C(16)	2095(4)	6704(3)	-251(2)	47(2)
C(17)	2292(4)	6635(3)	327(2)	45(2)
C(18)	3199(4)	6713(2)	657(2)	29(1)
C(19)	3930(4)	6847(3)	403(2)	42(2)
C(20)	3747(4)	6900(3)	-182(2)	44(2)
C(21)	3400(4)	6647(2)	1299(2)	31(1)
C(22)	-3073(4)	8011(2)	490(2)	26(1)
C(23)	-2349(4)	8153(3)	230(2)	45(2)
C(24)	-2553(4)	8228(3)	-349(2)	44(2)
C(25)	-3476(4)	8138(2)	-677(2)	28(1)
C(26)	-4189(4)	7989(3)	-419(2)	37(1)
C(27)	-4004(4)	7933(3)	165(2)	37(1)
C(28)	-3682(4)	8229(2)	-1315(2)	30(1)
C(29)	-2796(4)	8698(2)	1508(2)	29(1)
C(30)	-2873(5)	9149(2)	1145(2)	42(2)
C(31)	-2770(5)	9684(3)	1355(3)	44(2)
C(32)	-2626(4)	9780(2)	1933(2)	31(1)
C(33)	-2561(4)	9335(2)	2298(2)	38(1)
C(34)	-2642(4)	8784(2)	2091(2)	35(1)
C(35)	-2541(4)	10369(3)	2150(2)	36(1)
C(36)	-1607(4)	7724(2)	1512(2)	26(1)
C(37)	-1457(4)	7152(2)	1580(2)	35(1)
C(38)	-526(4)	6949(2)	1754(2)	37(1)

C(39)	250(4)	7311(2)	1862(2)	32(1)
C(40)	102(4)	7881(3)	1799(2)	36(1)
C(41)	-830(4)	8090(2)	1626(2)	34(1)
C(42)	1275(4)	7088(3)	2056(2)	36(1)
O(100)	4666(5)	3393(3)	1668(3)	85(2)
N(100)	3286(6)	3409(4)	955(3)	92(2)
C(100)	3778(6)	3286(4)	1478(3)	74(2)
C(101)	2311(8)	3273(6)	783(6)	138(5)
C(102)	3751(9)	3608(6)	561(5)	129(4)
O(110)	4778(6)	9169(3)	979(3)	112(2)
N(110)	4805(5)	9735(3)	1743(3)	65(2)
C(110)	4785(9)	9647(5)	1207(4)	116(4)
C(111)	4843(10)	10278(4)	1934(5)	121(4)
C(112)	4797(10)	9300(5)	2109(5)	124(4)
O(120)	2365(5)	9112(3)	1312(3)	102(2)
N(120)	2317(6)	9764(3)	618(3)	85(2)
C(120)	2447(8)	9248(4)	824(4)	93(3)
C(121)	2367(12)	9846(6)	61(5)	162(6)
C(122)	2060(11)	10195(5)	917(6)	139(5)
O(130)	4812(14)	5469(9)	329(8)	313(10)
N(130)	3924(7)	5185(4)	913(4)	96(2)
C(130)	3903(13)	5266(8)	379(6)	182(7)
C(131)	3165(11)	4959(8)	1082(7)	186(7)
C(132)	4719(12)	5302(9)	1340(7)	203(8)
O(140)	68(15)	5734(7)	-760(8)	147(7)
N(140)	211(10)	4746(5)	-767(6)	78(4)
C(140)	466(14)	5263(6)	-657(9)	95(6)
C(141)	-670(13)	4528(9)	-987(11)	125(8)
C(142)	928(13)	4350(8)	-592(9)	106(7)
O(150)	155(18)	4380(9)	3407(9)	172(8)
N(150)	11(9)	5080(5)	2779(5)	55(3)
C(150)	30(30)	4539(7)	2816(11)	192(15)
C(151)	110(30)	5292(12)	3366(8)	199(16)

C(152)	-90(15)	5518(7)	2476(7)	96(7)
O(200)	3091(4)	8098(2)	1680(2)	73(2)
O(201)	4107(5)	8122(3)	779(3)	89(2)
O(202)	-3643(8)	6304(4)	853(4)	141(3)
O(203)	5024(7)	9404(4)	-103(4)	126(3)
O(204)	2803(8)	8230(5)	-333(5)	160(4)
O(205)	3783(6)	6258(3)	4014(4)	115(3)

Table C.16. Bond lengths [Å] and angles [°] for PCM-7(Na) (**18**).

Zn(1)-O(14)	1.916(4)	P(2)-C(22)	1.799(5)
Zn(1)-O(13)	1.920(4)	O(1)-C(7)	1.231(8)
Zn(1)-O(15)	2.016(4)	O(2)-C(7)	1.272(7)
Zn(1)-O(8)#1	2.166(4)	O(2)-Zn(2)#5	2.008(4)
Zn(1)-O(5)	2.189(4)	O(3)-C(14)	1.269(7)
Zn(2)-O(14)#2	1.903(4)	O(4)-C(14)	1.242(7)
Zn(2)-O(3)	1.943(4)	O(5)-C(21)	1.238(7)
Zn(2)-O(7)	1.978(4)	O(6)-C(21)	1.257(7)
Zn(2)-O(2)#3	2.008(4)	O(7)-C(28)	1.268(7)
Zn(3)-O(13)	1.904(4)	O(8)-C(28)	1.244(7)
Zn(3)-O(11)	1.956(4)	O(8)-Zn(1)#2	2.166(3)
Zn(3)-O(6)	1.981(4)	O(9)-C(35)	1.247(7)
Zn(3)-O(10)#4	2.019(4)	O(10)-C(35)	1.273(7)
P(1)-C(1P)	1.775(5)	O(10)-Zn(3)#6	2.019(4)
P(1)-C(8)	1.793(5)	O(11)-C(42)	1.259(7)
P(1)-C(15)	1.795(5)	O(12)-C(42)	1.242(7)
P(1)-C(1)	1.798(5)	O(13)-H(13)	0.94(2)
P(2)-C(2P)	1.771(6)	O(14)-Zn(2)#1	1.903(4)
P(2)-C(36)	1.793(5)	O(14)-H(14)	0.95(2)
P(2)-C(29)	1.793(5)	O(15)-H(15X)	1.00(2)

O(15)-H(15Y)	1.00(2)	C(17)-C(18)	1.361(8)
C(1P)-H(1PA)	0.9800	C(17)-H(17A)	0.9500
C(1P)-H(1PB)	0.9800	C(18)-C(19)	1.376(8)
C(1P)-H(1PC)	0.9800	C(18)-C(21)	1.523(7)
C(1)-C(6)	1.378(8)	C(19)-C(20)	1.386(8)
C(1)-C(2)	1.385(8)	C(19)-H(19A)	0.9500
C(2P)-H(2PA)	0.9800	C(20)-H(20A)	0.9500
C(2P)-H(2PB)	0.9800	C(22)-C(27)	1.384(7)
C(2P)-H(2PC)	0.9800	C(22)-C(23)	1.382(8)
C(2)-C(3)	1.385(9)	C(23)-C(24)	1.376(8)
C(2)-H(2A)	0.9500	C(23)-H(23A)	0.9500
C(3)-C(4)	1.395(8)	C(24)-C(25)	1.381(8)
C(3)-H(3A)	0.9500	C(24)-H(24A)	0.9500
C(4)-C(5)	1.368(8)	C(25)-C(26)	1.368(8)
C(4)-C(7)	1.494(8)	C(25)-C(28)	1.522(7)
C(5)-C(6)	1.393(8)	C(26)-C(27)	1.384(7)
C(5)-H(5A)	0.9500	C(26)-H(26A)	0.9500
C(6)-H(6A)	0.9500	C(27)-H(27A)	0.9500
C(8)-C(9)	1.390(8)	C(29)-C(30)	1.380(8)
C(8)-C(13)	1.402(8)	C(29)-C(34)	1.396(8)
C(9)-C(10)	1.399(8)	C(30)-C(31)	1.371(9)
C(9)-H(9A)	0.9500	C(30)-H(30A)	0.9500
C(10)-C(11)	1.371(8)	C(31)-C(32)	1.386(8)
C(10)-H(10A)	0.9500	C(31)-H(31A)	0.9500
C(11)-C(12)	1.392(8)	C(32)-C(33)	1.374(8)
C(11)-C(14)	1.510(8)	C(32)-C(35)	1.498(8)
C(12)-C(13)	1.383(8)	C(33)-C(34)	1.404(8)
C(12)-H(12A)	0.9500	C(33)-H(33A)	0.9500
C(13)-H(13A)	0.9500	C(34)-H(34A)	0.9500
C(15)-C(20)	1.379(8)	C(36)-C(37)	1.388(8)
C(15)-C(16)	1.380(8)	C(36)-C(41)	1.389(8)
C(16)-C(17)	1.372(8)	C(37)-C(38)	1.384(8)
C(16)-H(16A)	0.9500	C(37)-H(37A)	0.9500

C(38)-C(39)	1.381(8)	C(120)-H(12B)	0.9500
C(38)-H(38A)	0.9500	C(121)-H(12C)	0.9800
C(39)-C(40)	1.380(8)	C(121)-H(12D)	0.9800
C(39)-C(42)	1.523(8)	C(121)-H(12E)	0.9800
C(40)-C(41)	1.390(8)	C(122)-H(12F)	0.9800
C(40)-H(40A)	0.9500	C(122)-H(12G)	0.9800
C(41)-H(41A)	0.9500	C(122)-H(12H)	0.9800
O(100)-C(100)	1.267(9)	O(130)-C(130)	1.422(15)
N(100)-C(100)	1.326(9)	N(130)-C(130)	1.303(12)
N(100)-C(102)	1.379(11)	N(130)-C(132)	1.366(13)
N(100)-C(101)	1.392(11)	N(130)-C(131)	1.363(12)
C(100)-H(10B)	0.9500	C(130)-H(13C)	0.9500
C(101)-H(10C)	0.9800	C(131)-H(13D)	0.9800
C(101)-H(10D)	0.9800	C(131)-H(13E)	0.9800
C(101)-H(10E)	0.9800	C(131)-H(13F)	0.9800
C(102)-H(10F)	0.9800	C(132)-H(13G)	0.9800
C(102)-H(10G)	0.9800	C(132)-H(13H)	0.9800
C(102)-H(10H)	0.9800	C(132)-H(13I)	0.9800
O(110)-C(110)	1.269(11)	O(140)-C(140)	1.260(15)
N(110)-C(110)	1.312(10)	N(140)-C(140)	1.297(14)
N(110)-C(112)	1.369(10)	N(140)-C(141)	1.348(14)
N(110)-C(111)	1.375(10)	N(140)-C(142)	1.384(14)
C(110)-H(11A)	0.9500	C(140)-H(14A)	0.9500
C(111)-H(11B)	0.9800	C(141)-H(14B)	0.9800
C(111)-H(11C)	0.9800	C(141)-H(14C)	0.9800
C(111)-H(11D)	0.9800	C(141)-H(14D)	0.9800
C(112)-H(11E)	0.9800	C(142)-H(14E)	0.9800
C(112)-H(11F)	0.9800	C(142)-H(14F)	0.9800
C(112)-H(11G)	0.9800	C(142)-H(14G)	0.9800
O(120)-C(120)	1.262(10)	O(150)-C(150)	1.454(18)
N(120)-C(120)	1.328(10)	N(150)-C(152)	1.268(13)
N(120)-C(122)	1.362(11)	N(150)-C(150)	1.296(15)
N(120)-C(121)	1.387(11)	N(150)-C(151)	1.489(16)

C(150)-H(15B)	0.9500	C(1P)-P(1)-C(1)	110.9(3)
C(151)-H(15C)	0.9800	C(8)-P(1)-C(1)	107.9(2)
C(151)-H(15D)	0.9800	C(15)-P(1)-C(1)	107.4(2)
C(151)-H(15E)	0.9800	C(2P)-P(2)-C(36)	111.1(3)
C(152)-H(15F)	0.9800	C(2P)-P(2)-C(29)	111.1(3)
C(152)-H(15G)	0.9800	C(36)-P(2)-C(29)	107.0(2)
C(152)-H(15H)	0.9800	C(2P)-P(2)-C(22)	110.9(3)
		C(36)-P(2)-C(22)	108.3(2)
O(14)-Zn(1)-O(13)	126.86(19)	C(29)-P(2)-C(22)	108.4(2)
O(14)-Zn(1)-O(15)	116.30(19)	C(7)-O(2)-Zn(2)#5	104.5(4)
O(13)-Zn(1)-O(15)	116.73(18)	C(14)-O(3)-Zn(2)	118.5(4)
O(14)-Zn(1)-O(8)#1	94.49(15)	C(21)-O(5)-Zn(1)	136.6(4)
O(13)-Zn(1)-O(8)#1	88.76(15)	C(21)-O(6)-Zn(3)	127.2(4)
O(15)-Zn(1)-O(8)#1	90.01(17)	C(28)-O(7)-Zn(2)	127.7(4)
O(14)-Zn(1)-O(5)	86.06(16)	C(28)-O(8)-Zn(1)#2	132.5(4)
O(13)-Zn(1)-O(5)	94.08(15)	C(35)-O(10)-Zn(3)#6	104.7(4)
O(15)-Zn(1)-O(5)	86.21(17)	C(42)-O(11)-Zn(3)	113.8(4)
O(8)#1-Zn(1)-O(5)	176.01(16)	Zn(3)-O(13)-Zn(1)	126.17(19)
O(14)#2-Zn(2)-O(3)	132.02(18)	Zn(3)-O(13)-H(13)	115(4)
O(14)#2-Zn(2)-O(7)	102.47(17)	Zn(1)-O(13)-H(13)	118(4)
O(3)-Zn(2)-O(7)	99.57(18)	Zn(2)#1-O(14)-Zn(1)	127.5(2)
O(14)#2-Zn(2)-O(2)#3	109.37(18)	Zn(2)#1-O(14)-H(14)	124(8)
O(3)-Zn(2)-O(2)#3	105.72(18)	Zn(1)-O(14)-H(14)	108(8)
O(7)-Zn(2)-O(2)#3	104.03(17)	Zn(1)-O(15)-H(15X)	121(4)
O(13)-Zn(3)-O(11)	129.62(18)	Zn(1)-O(15)-H(15Y)	106(7)
O(13)-Zn(3)-O(6)	106.47(16)	H(15X)-O(15)-H(15Y)	129(4)
O(11)-Zn(3)-O(6)	98.76(18)	P(1)-C(1P)-H(1PA)	109.5
O(13)-Zn(3)-O(10)#4	111.25(17)	P(1)-C(1P)-H(1PB)	109.5
O(11)-Zn(3)-O(10)#4	105.52(18)	H(1PA)-C(1P)-H(1PB)	109.5
O(6)-Zn(3)-O(10)#4	101.02(17)	P(1)-C(1P)-H(1PC)	109.5
C(1P)-P(1)-C(8)	110.5(3)	H(1PA)-C(1P)-H(1PC)	109.5
C(1P)-P(1)-C(15)	111.5(3)	H(1PB)-C(1P)-H(1PC)	109.5
C(8)-P(1)-C(15)	108.5(2)	C(6)-C(1)-C(2)	120.0(5)

C(6)-C(1)-P(1)	119.8(4)	C(11)-C(10)-H(10A)	119.3
C(2)-C(1)-P(1)	120.0(4)	C(9)-C(10)-H(10A)	119.3
P(2)-C(2P)-H(2PA)	109.5	C(10)-C(11)-C(12)	119.6(5)
P(2)-C(2P)-H(2PB)	109.5	C(10)-C(11)-C(14)	120.3(5)
H(2PA)-C(2P)-H(2PB)	109.5	C(12)-C(11)-C(14)	120.2(5)
P(2)-C(2P)-H(2PC)	109.5	C(13)-C(12)-C(11)	120.6(5)
H(2PA)-C(2P)-H(2PC)	109.5	C(13)-C(12)-H(12A)	119.7
H(2PB)-C(2P)-H(2PC)	109.5	C(11)-C(12)-H(12A)	119.7
C(3)-C(2)-C(1)	119.6(5)	C(12)-C(13)-C(8)	119.3(5)
C(3)-C(2)-H(2A)	120.2	C(12)-C(13)-H(13A)	120.3
C(1)-C(2)-H(2A)	120.2	C(8)-C(13)-H(13A)	120.3
C(2)-C(3)-C(4)	120.8(6)	O(4)-C(14)-O(3)	125.7(5)
C(2)-C(3)-H(3A)	119.6	O(4)-C(14)-C(11)	120.0(5)
C(4)-C(3)-H(3A)	119.6	O(3)-C(14)-C(11)	114.2(5)
C(5)-C(4)-C(3)	118.8(5)	C(20)-C(15)-C(16)	118.9(5)
C(5)-C(4)-C(7)	122.3(5)	C(20)-C(15)-P(1)	121.2(4)
C(3)-C(4)-C(7)	118.9(5)	C(16)-C(15)-P(1)	119.7(4)
C(4)-C(5)-C(6)	121.0(5)	C(17)-C(16)-C(15)	120.6(5)
C(4)-C(5)-H(5A)	119.5	C(17)-C(16)-H(16A)	119.7
C(6)-C(5)-H(5A)	119.5	C(15)-C(16)-H(16A)	119.7
C(1)-C(6)-C(5)	119.7(5)	C(18)-C(17)-C(16)	120.8(6)
C(1)-C(6)-H(6A)	120.1	C(18)-C(17)-H(17A)	119.6
C(5)-C(6)-H(6A)	120.1	C(16)-C(17)-H(17A)	119.6
O(1)-C(7)-O(2)	123.1(5)	C(17)-C(18)-C(19)	119.3(5)
O(1)-C(7)-C(4)	119.9(5)	C(17)-C(18)-C(21)	120.1(5)
O(2)-C(7)-C(4)	116.9(5)	C(19)-C(18)-C(21)	120.6(5)
C(9)-C(8)-C(13)	120.6(5)	C(18)-C(19)-C(20)	120.5(5)
C(9)-C(8)-P(1)	119.6(4)	C(18)-C(19)-H(19A)	119.8
C(13)-C(8)-P(1)	119.7(4)	C(20)-C(19)-H(19A)	119.8
C(8)-C(9)-C(10)	118.5(5)	C(15)-C(20)-C(19)	119.9(5)
C(8)-C(9)-H(9A)	120.8	C(15)-C(20)-H(20A)	120.0
C(10)-C(9)-H(9A)	120.8	C(19)-C(20)-H(20A)	120.0
C(11)-C(10)-C(9)	121.5(5)	O(5)-C(21)-O(6)	127.0(5)

O(5)-C(21)-C(18)	117.7(5)	C(33)-C(32)-C(35)	120.9(5)
O(6)-C(21)-C(18)	115.3(5)	C(31)-C(32)-C(35)	119.5(5)
C(27)-C(22)-C(23)	119.8(5)	C(32)-C(33)-C(34)	120.7(5)
C(27)-C(22)-P(2)	121.2(4)	C(32)-C(33)-H(33A)	119.7
C(23)-C(22)-P(2)	118.8(4)	C(34)-C(33)-H(33A)	119.7
C(24)-C(23)-C(22)	120.3(5)	C(29)-C(34)-C(33)	118.6(5)
C(24)-C(23)-H(23A)	119.9	C(29)-C(34)-H(34A)	120.7
C(22)-C(23)-H(23A)	119.9	C(33)-C(34)-H(34A)	120.7
C(23)-C(24)-C(25)	120.1(5)	O(9)-C(35)-O(10)	123.1(5)
C(23)-C(24)-H(24A)	119.9	O(9)-C(35)-C(32)	119.1(5)
C(25)-C(24)-H(24A)	119.9	O(10)-C(35)-C(32)	117.8(5)
C(26)-C(25)-C(24)	119.5(5)	C(37)-C(36)-C(41)	120.3(5)
C(26)-C(25)-C(28)	121.6(5)	C(37)-C(36)-P(2)	120.2(4)
C(24)-C(25)-C(28)	118.9(5)	C(41)-C(36)-P(2)	119.6(4)
C(25)-C(26)-C(27)	121.1(5)	C(38)-C(37)-C(36)	119.4(5)
C(25)-C(26)-H(26A)	119.4	C(38)-C(37)-H(37A)	120.3
C(27)-C(26)-H(26A)	119.4	C(36)-C(37)-H(37A)	120.3
C(22)-C(27)-C(26)	119.2(5)	C(39)-C(38)-C(37)	120.5(5)
C(22)-C(27)-H(27A)	120.4	C(39)-C(38)-H(38A)	119.7
C(26)-C(27)-H(27A)	120.4	C(37)-C(38)-H(38A)	119.7
O(8)-C(28)-O(7)	127.6(5)	C(38)-C(39)-C(40)	120.2(5)
O(8)-C(28)-C(25)	117.9(5)	C(38)-C(39)-C(42)	120.5(5)
O(7)-C(28)-C(25)	114.5(5)	C(40)-C(39)-C(42)	119.3(5)
C(30)-C(29)-C(34)	120.1(5)	C(39)-C(40)-C(41)	119.9(5)
C(30)-C(29)-P(2)	121.5(4)	C(39)-C(40)-H(40A)	120.1
C(34)-C(29)-P(2)	118.3(4)	C(41)-C(40)-H(40A)	120.1
C(31)-C(30)-C(29)	120.5(5)	C(40)-C(41)-C(36)	119.7(5)
C(31)-C(30)-H(30A)	119.8	C(40)-C(41)-H(41A)	120.1
C(29)-C(30)-H(30A)	119.8	C(36)-C(41)-H(41A)	120.1
C(30)-C(31)-C(32)	120.4(6)	O(12)-C(42)-O(11)	125.9(5)
C(30)-C(31)-H(31A)	119.8	O(12)-C(42)-C(39)	118.4(5)
C(32)-C(31)-H(31A)	119.8	O(11)-C(42)-C(39)	115.7(5)
C(33)-C(32)-C(31)	119.6(5)	C(100)-N(100)-C(102)	120.6(9)

C(100)-N(100)-C(101)	119.6(9)	H(11E)-C(112)-H(11G)	109.5
C(102)-N(100)-C(101)	119.4(9)	H(11F)-C(112)-H(11G)	109.5
O(100)-C(100)-N(100)	123.6(8)	C(120)-N(120)-C(122)	122.1(9)
O(100)-C(100)-H(10B)	118.2	C(120)-N(120)-C(121)	117.6(9)
N(100)-C(100)-H(10B)	118.2	C(122)-N(120)-C(121)	120.0(10)
N(100)-C(101)-H(10C)	109.5	O(120)-C(120)-N(120)	123.8(9)
N(100)-C(101)-H(10D)	109.5	O(120)-C(120)-H(12B)	118.1
H(10C)-C(101)-H(10D)	109.5	N(120)-C(120)-H(12B)	118.1
N(100)-C(101)-H(10E)	109.5	N(120)-C(121)-H(12C)	109.5
H(10C)-C(101)-H(10E)	109.5	N(120)-C(121)-H(12D)	109.5
H(10D)-C(101)-H(10E)	109.5	H(12C)-C(121)-H(12D)	109.5
N(100)-C(102)-H(10F)	109.5	N(120)-C(121)-H(12E)	109.5
N(100)-C(102)-H(10G)	109.5	H(12C)-C(121)-H(12E)	109.5
H(10F)-C(102)-H(10G)	109.5	H(12D)-C(121)-H(12E)	109.5
N(100)-C(102)-H(10H)	109.5	N(120)-C(122)-H(12F)	109.5
H(10F)-C(102)-H(10H)	109.5	N(120)-C(122)-H(12G)	109.5
H(10G)-C(102)-H(10H)	109.5	H(12F)-C(122)-H(12G)	109.5
C(110)-N(110)-C(112)	121.3(8)	N(120)-C(122)-H(12H)	109.5
C(110)-N(110)-C(111)	118.4(8)	H(12F)-C(122)-H(12H)	109.5
C(112)-N(110)-C(111)	120.3(8)	H(12G)-C(122)-H(12H)	109.5
O(110)-C(110)-N(110)	125.1(10)	C(130)-N(130)-C(132)	122.5(11)
O(110)-C(110)-H(11A)	117.4	C(130)-N(130)-C(131)	122.1(11)
N(110)-C(110)-H(11A)	117.4	C(132)-N(130)-C(131)	115.4(11)
N(110)-C(111)-H(11B)	109.5	N(130)-C(130)-O(130)	109.7(13)
N(110)-C(111)-H(11C)	109.5	N(130)-C(130)-H(13C)	125.2
H(11B)-C(111)-H(11C)	109.5	O(130)-C(130)-H(13C)	125.2
N(110)-C(111)-H(11D)	109.5	N(130)-C(131)-H(13D)	109.5
H(11B)-C(111)-H(11D)	109.5	N(130)-C(131)-H(13E)	109.5
H(11C)-C(111)-H(11D)	109.5	H(13D)-C(131)-H(13E)	109.5
N(110)-C(112)-H(11E)	109.5	N(130)-C(131)-H(13F)	109.5
N(110)-C(112)-H(11F)	109.5	H(13D)-C(131)-H(13F)	109.5
H(11E)-C(112)-H(11F)	109.5	H(13E)-C(131)-H(13F)	109.5
N(110)-C(112)-H(11G)	109.5	N(130)-C(132)-H(13G)	109.5

N(130)-C(132)-H(13H)	109.5	H(14E)-C(142)-H(14G)	109.5
H(13G)-C(132)-H(13H)	109.5	H(14F)-C(142)-H(14G)	109.5
N(130)-C(132)-H(13I)	109.5	C(152)-N(150)-C(150)	149.6(15)
H(13G)-C(132)-H(13I)	109.5	C(152)-N(150)-C(151)	104.2(13)
H(13H)-C(132)-H(13I)	109.5	C(150)-N(150)-C(151)	106.1(12)
C(140)-N(140)-C(141)	129.8(14)	N(150)-C(150)-O(150)	109.0(16)
C(140)-N(140)-C(142)	115.9(13)	N(150)-C(150)-H(15B)	125.5
C(141)-N(140)-C(142)	114.1(13)	O(150)-C(150)-H(15B)	125.5
O(140)-C(140)-N(140)	136.0(18)	N(150)-C(151)-H(15C)	109.5
O(140)-C(140)-H(14A)	112.0	N(150)-C(151)-H(15D)	109.5
N(140)-C(140)-H(14A)	112.0	H(15C)-C(151)-H(15D)	109.5
N(140)-C(141)-H(14B)	109.5	N(150)-C(151)-H(15E)	109.5
N(140)-C(141)-H(14C)	109.5	H(15C)-C(151)-H(15E)	109.5
H(14B)-C(141)-H(14C)	109.5	H(15D)-C(151)-H(15E)	109.5
N(140)-C(141)-H(14D)	109.5	N(150)-C(152)-H(15F)	109.5
H(14B)-C(141)-H(14D)	109.5	N(150)-C(152)-H(15G)	109.5
H(14C)-C(141)-H(14D)	109.5	H(15F)-C(152)-H(15G)	109.5
N(140)-C(142)-H(14E)	109.5	N(150)-C(152)-H(15H)	109.5
N(140)-C(142)-H(14F)	109.5	H(15F)-C(152)-H(15H)	109.5
H(14E)-C(142)-H(14F)	109.5	H(15G)-C(152)-H(15H)	109.5
N(140)-C(142)-H(14G)	109.5		

Symmetry transformations used to generate equivalent atoms:

#1 x+1,-y+3/2,z+1/2 #2 x-1,-y+3/2,z-1/2 #3 -x,y+1/2,-z-1/2

#4 -x,y-1/2,-z+1/2 #5 -x,y-1/2,-z-1/2 #6 -x,y+1/2,-z+1/2

Table C.17. Anisotropic displacement parameters ($Å^2$x 10^3)for PCM-7(Na) (**18**) . The anisotropic displacement factor exponent takes the form: $-2p^2[h^2a^{*2}U^{11} + ... + 2 h k a^* b^* U^{12}]$.

	U^{11}	U^{22}	U^{33}	U^{23}	U^{13}	U^{12}
Zn(1)	28(1)	30(1)	25(1)	1(1)	4(1)	-1(1)
Zn(2)	28(1)	26(1)	28(1)	4(1)	6(1)	3(1)
Zn(3)	27(1)	28(1)	26(1)	2(1)	4(1)	1(1)
P(1)	27(1)	25(1)	20(1)	-1(1)	2(1)	3(1)
P(2)	26(1)	29(1)	20(1)	1(1)	1(1)	2(1)
O(1)	86(4)	30(2)	54(3)	-7(2)	24(3)	-3(2)
O(2)	48(2)	33(2)	45(3)	-13(2)	12(2)	-2(2)
O(3)	34(2)	37(2)	55(3)	9(2)	7(2)	12(2)
O(4)	34(2)	41(2)	52(3)	-3(2)	-2(2)	4(2)
O(5)	41(2)	62(3)	23(2)	2(2)	-2(2)	-12(2)
O(6)	45(2)	46(2)	27(2)	3(2)	5(2)	-10(2)
O(7)	52(3)	40(2)	27(2)	1(2)	10(2)	-10(2)
O(8)	35(2)	46(2)	23(2)	3(2)	1(2)	0(2)
O(9)	61(3)	33(2)	53(3)	4(2)	19(2)	3(2)
O(10)	45(2)	34(2)	38(2)	-5(2)	8(2)	0(2)
O(11)	32(2)	42(3)	50(2)	8(2)	6(2)	12(2)
O(12)	33(2)	56(3)	58(3)	13(2)	4(2)	6(2)
O(13)	31(2)	46(2)	23(2)	4(2)	2(2)	-7(2)
O(14)	32(2)	54(3)	25(2)	-5(2)	4(2)	4(2)
O(15)	61(3)	31(2)	41(2)	2(2)	11(2)	-1(2)
C(1P)	33(3)	38(3)	29(3)	2(2)	5(2)	-5(2)
C(1)	26(3)	26(3)	31(3)	-2(2)	3(2)	4(2)
C(2P)	32(3)	46(3)	33(3)	8(3)	6(2)	0(3)
C(2)	83(5)	33(3)	27(3)	-2(3)	13(3)	10(3)
C(3)	80(5)	31(3)	40(4)	4(3)	15(3)	9(3)
C(4)	31(3)	34(3)	37(3)	-9(2)	10(2)	1(2)
C(5)	49(4)	43(4)	30(3)	-8(3)	13(3)	-4(3)

C(6)	59(4)	36(3)	23(3)	0(2)	10(3)	4(3)
C(7)	36(3)	38(3)	45(4)	-9(3)	12(3)	1(3)
C(8)	28(3)	30(3)	20(2)	-1(2)	1(2)	1(2)
C(9)	32(3)	29(3)	37(3)	-1(2)	0(2)	2(2)
C(10)	39(3)	31(3)	45(3)	2(3)	4(3)	12(3)
C(11)	30(3)	36(3)	20(2)	0(2)	-1(2)	5(2)
C(12)	30(3)	36(3)	38(3)	-1(2)	-2(2)	2(2)
C(13)	31(3)	29(3)	37(3)	-2(2)	0(2)	5(2)
C(14)	36(3)	41(3)	24(3)	2(2)	4(2)	10(3)
C(15)	28(3)	25(3)	25(3)	-1(2)	3(2)	6(2)
C(16)	28(3)	81(5)	28(3)	7(3)	-1(2)	-3(3)
C(17)	32(3)	72(5)	31(3)	5(3)	9(2)	-2(3)
C(18)	30(3)	31(3)	23(3)	-4(2)	3(2)	3(2)
C(19)	30(3)	67(4)	24(3)	0(3)	-5(2)	-11(3)
C(20)	32(3)	71(5)	27(3)	1(3)	4(2)	-14(3)
C(21)	37(3)	31(3)	24(3)	-3(2)	5(2)	8(3)
C(22)	30(3)	28(3)	18(2)	1(2)	2(2)	3(2)
C(23)	25(3)	82(5)	25(3)	1(3)	0(2)	-3(3)
C(24)	28(3)	72(4)	32(3)	5(3)	8(2)	-5(3)
C(25)	31(3)	28(3)	22(3)	1(2)	1(2)	4(2)
C(26)	31(3)	53(4)	22(3)	2(2)	-2(2)	-5(3)
C(27)	29(3)	52(4)	28(3)	3(3)	4(2)	-10(3)
C(28)	36(3)	27(3)	25(3)	4(2)	5(2)	9(2)
C(29)	26(3)	34(3)	26(3)	-1(2)	5(2)	4(2)
C(30)	65(4)	32(3)	28(3)	2(2)	8(3)	11(3)
C(31)	64(4)	32(3)	35(3)	7(3)	12(3)	11(3)
C(32)	27(3)	30(3)	34(3)	-4(2)	7(2)	2(2)
C(33)	47(4)	41(3)	26(3)	1(2)	7(2)	5(3)
C(34)	50(4)	29(3)	25(3)	2(2)	5(3)	7(3)
C(35)	30(3)	38(3)	40(3)	-3(3)	7(2)	6(2)
C(36)	29(3)	26(3)	22(2)	0(2)	3(2)	3(2)
C(37)	33(3)	34(3)	37(3)	-1(2)	4(2)	0(2)
C(38)	34(3)	29(3)	43(3)	5(2)	2(3)	8(2)

C(39)	34(3)	37(3)	23(3)	5(2)	5(2)	7(2)
C(40)	25(3)	40(3)	39(3)	2(3)	-1(2)	-1(2)
C(41)	38(3)	28(3)	32(3)	0(2)	3(2)	2(2)
C(42)	26(3)	49(4)	29(3)	4(3)	0(2)	4(3)

Table C.18. Hydrogen coordinates (x 10^4) and isotropic displacement parameters (Å^{2}x 10^3) for PCM-7(Na) (**18**).

	x	y	z	U(eq)
H(1PA)	4046	7181	-1353	50
H(1PB)	3236	7338	-1913	50
H(1PC)	3352	7705	-1349	50
H(2PA)	-4303	7736	1343	56
H(2PB)	-3638	7196	1351	56
H(2PC)	-3499	7579	1906	56
H(2A)	2701	5791	-783	57
H(3A)	2735	4886	-1136	61
H(5A)	2465	5501	-2711	48
H(6A)	2462	6411	-2359	47
H(9A)	1716	7970	-1512	41
H(10A)	122	8295	-1809	47
H(12A)	-880	6715	-1882	43
H(13A)	693	6373	-1602	40
H(16A)	1454	6658	-474	56

H(17A)	1788	6530	499	54
H(19A)	4565	6903	631	51
H(20A)	4260	6976	-356	53
H(23A)	-1708	8200	452	54
H(24A)	-2058	8341	-524	52
H(26A)	-4823	7924	-645	44
H(27A)	-4508	7841	340	44
H(30A)	-2999	9089	747	51
H(31A)	-2798	9991	1103	53
H(33A)	-2460	9400	2694	46
H(34A)	-2592	8476	2344	43
H(37A)	-1990	6902	1508	43
H(38A)	-419	6558	1799	44
H(40A)	637	8129	1874	43
H(41A)	-935	8482	1585	40
H(10B)	3447	3107	1724	89
H(10C)	2056	3391	388	207
H(10D)	2233	2867	812	207
H(10E)	1960	3464	1027	207
H(10F)	3279	3676	200	194
H(10G)	4082	3958	699	194
H(10H)	4224	3331	503	194
H(11A)	4776	9965	972	139
H(11B)	4854	10281	2339	182
H(11C)	5427	10459	1877	182
H(11D)	4275	10482	1721	182
H(11E)	4815	9448	2488	187
H(11F)	4209	9079	1972	187
H(11G)	5362	9063	2128	187
H(12B)	2611	8964	591	112
H(12C)	2259	10242	-38	243
H(12D)	3006	9734	20	243
H(12E)	1873	9620	-193	243

H(12F)	2001	10539	692	209
H(12G)	1440	10110	1003	209
H(12H)	2553	10245	1273	209
H(13C)	3362	5198	71	218
H(13D)	3325	4934	1497	279
H(13E)	2596	5197	952	279
H(13F)	3030	4584	919	279
H(13G)	4585	5212	1707	305
H(13H)	5265	5078	1290	305
H(13I)	4876	5700	1330	305
H(14A)	1118	5293	-447	114
H(14B)	-618	4121	-1017	187
H(14C)	-1097	4618	-740	187
H(14D)	-936	4686	-1366	187
H(14E)	661	3976	-694	158
H(14F)	1451	4421	-778	158
H(14G)	1178	4373	-179	158
H(15B)	-22	4287	2507	230
H(15C)	192	4976	3631	299
H(15D)	673	5539	3471	299
H(15E)	-471	5502	3384	299
H(15F)	-20	5849	2721	144
H(15G)	403	5526	2258	144
H(15H)	-731	5519	2214	144
H(13)	3950(40)	6450(20)	3121(11)	38(16)
H(14)	5750(90)	6520(60)	1882(11)	160(50)
H(15X)	5090(50)	8010(30)	2730(20)	70(20)
H(15Y)	4630(140)	7830(50)	1990(9)	270(90)

Table C.19. Crystal data and structure refinement for PCM-8(K) (**19**).

Identification code	PCM-8	
Empirical formula	C53 H54 K N3 O17 P2 Zn2	
Formula weight	1236.77	
Temperature	180(2) K	
Wavelength	71.073 pm	
Crystal system	Orthorhombic	
Space group	P b c n	
Unit cell dimensions	a = 2162.62(2) pm	a= 90°.
	b = 2557.15(3) pm	b= 90°.
	c = 2408.87(2) pm	g = 90°.
Volume	13.3214(2) nm^3	
Z	8	
Density (calculated)	1.233 Mg/m^3	
Absorption coefficient	0.891 mm^{-1}	
F(000)	5104	
Crystal size	0.230 x 0.200 x 0.100 mm^3	
Theta range for data collection	3.539 to 23.999°.	
Index ranges	-22<=h<=24, -29<=k<=29, -27<=l<=26	
Reflections collected	51725	
Independent reflections	10406 [R(int) = 0.0599]	
Completeness to theta = 23.999°	99.3 %	
Refinement method	Full-matrix least-squares on F^2	
Data / restraints / parameters	10406 / 40 / 664	
Goodness-of-fit on F^2	1.066	
Final R indices [I>2sigma(I)]	R1 = 0.0889, wR2 = 0.2310	
R indices (all data)	R1 = 0.1117, wR2 = 0.2476	
Extinction coefficient	n/a	
Largest diff. peak and hole	2.311 and -0.991 $e.Å^{-3}$	

Table C.20. Atomic coordinates (x 10^4) and equivalent isotropic displacement parameters (pm^2x 10^{-1}) for PCM-8(K) (**19**). U(eq) is defined as one third of the trace of the orthogonalized U^{ij} tensor.

	x	y	z	U(eq)
Zn(1)	-2156(1)	16775(1)	1935(1)	25(1)
Zn(2)	-2602(1)	16262(1)	3116(1)	30(1)
K(1)	-4008(1)	16511(1)	2353(1)	45(1)
P(1)	-3561(1)	16799(1)	-1426(1)	26(1)
P(2)	-1455(1)	13443(1)	1512(1)	24(1)
O(1)	-2462(2)	16889(2)	1183(2)	40(1)
O(2)	-3469(2)	16812(2)	1385(2)	39(1)
O(3)	-6302(2)	17974(2)	-1919(2)	42(1)
O(4)	-6617(2)	17145(2)	-1893(2)	49(1)
O(5)	-3354(3)	14192(2)	-1867(2)	46(1)
O(6)	-3462(3)	14463(2)	-2739(3)	65(2)
O(7)	-2055(3)	15733(2)	2778(2)	47(1)
O(8)	-1965(2)	16007(2)	1891(2)	40(1)
O(9)	-2522(3)	13626(2)	-1095(2)	51(2)
O(10)	-1567(3)	13398(2)	-1298(2)	54(2)
O(11)	1325(2)	12373(2)	2071(2)	47(1)
O(12)	1630(2)	13171(2)	1809(2)	50(2)
O(13)	-2651(2)	16822(2)	2590(2)	27(1)
C(1)	-3420(3)	16836(3)	-693(3)	30(2)
C(1P)	-3030(3)	17209(3)	-1785(3)	32(2)
C(2)	-2820(4)	16844(6)	-508(4)	91(5)
C(2P)	-1971(3)	13022(3)	1866(3)	33(2)
C(3)	-2697(4)	16853(6)	57(4)	87(4)
C(4)	-3169(3)	16857(3)	442(3)	33(2)
C(5)	-3757(4)	16866(4)	249(3)	53(2)
C(6)	-3891(3)	16862(4)	-315(3)	51(2)
C(7)	-3037(3)	16841(3)	1058(3)	33(2)

C(8)	-4337(3)	17002(3)	-1569(3)	25(1)
C(9)	-4474(3)	17523(3)	-1652(3)	36(2)
C(10)	-5073(3)	17680(3)	-1755(3)	36(2)
C(11)	-5547(3)	17311(3)	-1771(3)	31(2)
C(12)	-5421(3)	16794(3)	-1681(4)	44(2)
C(13)	-4814(3)	16633(3)	-1580(4)	44(2)
C(14)	-6212(3)	17479(3)	-1868(3)	33(2)
C(15)	-3484(3)	16133(3)	-1650(3)	30(2)
C(16)	-3478(4)	16030(3)	-2214(3)	41(2)
C(17)	-3457(4)	15513(3)	-2398(3)	45(2)
C(18)	-3443(3)	15106(3)	-2027(3)	34(2)
C(19)	-3438(4)	15207(3)	-1466(3)	48(2)
C(20)	-3462(4)	15721(3)	-1281(3)	51(2)
C(21)	-3423(4)	14543(3)	-2236(4)	44(2)
C(22)	-1576(3)	14104(3)	1742(3)	29(2)
C(23)	-1501(4)	14520(3)	1376(3)	40(2)
C(24)	-1611(4)	15016(3)	1552(3)	43(2)
C(25)	-1792(3)	15115(3)	2088(3)	34(2)
C(26)	-1847(3)	14705(3)	2456(3)	37(2)
C(27)	-1745(3)	14200(3)	2287(3)	34(2)
C(28)	-1949(3)	15667(3)	2265(3)	35(2)
C(29)	-1604(3)	13416(3)	778(3)	32(2)
C(30)	-2194(4)	13539(4)	591(3)	52(2)
C(31)	-2314(4)	13548(4)	31(3)	53(2)
C(32)	-1855(4)	13442(3)	-350(3)	36(2)
C(33)	-1272(4)	13322(3)	-160(3)	42(2)
C(34)	-1135(3)	13313(3)	399(3)	39(2)
C(35)	-1975(4)	13486(3)	-965(3)	40(2)
C(36)	-669(3)	13265(3)	1636(3)	24(1)
C(37)	-501(3)	12741(3)	1632(3)	32(2)
C(38)	109(3)	12599(3)	1718(3)	35(2)
C(39)	555(3)	12976(3)	1801(3)	31(2)
C(40)	387(3)	13492(3)	1799(3)	37(2)

C(41)	-222(3)	13645(3)	1725(3)	35(2)
C(42)	1228(3)	12825(3)	1897(3)	37(2)
O(100)	-4917(7)	16240(5)	3176(6)	168(3)
N(100)	-5058(8)	15434(6)	3632(7)	168(3)
C(100)	-4923(10)	15946(6)	3629(8)	168(3)
C(101)	-4939(10)	15134(7)	4099(7)	168(3)
C(102)	-5098(10)	15173(7)	3126(7)	168(3)
O(110)	-3433(8)	14250(6)	1112(7)	94(5)
N(110)	-3186(9)	15021(6)	655(7)	78(5)
C(110)	-3232(11)	14709(7)	1109(8)	85(7)
C(111)	-3282(18)	14840(11)	147(9)	148(13)
C(112)	-3025(18)	15522(8)	777(12)	151(13)
O(120)	145(10)	12739(8)	-58(9)	135(7)
N(120)	785(14)	13465(10)	-216(13)	187(14)
C(120)	499(14)	13019(10)	-394(12)	127(11)
C(121)	500(20)	13752(15)	193(16)	230(20)
C(122)	1098(17)	13745(12)	-608(14)	164(15)
O(130)	750(20)	16271(12)	2123(18)	273(19)
N(130)	353(13)	15420(9)	2183(10)	149(10)
C(132)	590(30)	15238(16)	1703(17)	300(30)
C(130)	437(16)	15905(10)	2372(13)	146(13)
C(131)	0	15081(9)	2500	142(9)
O(140)	-3860(20)	14323(13)	-310(19)	300(20)
N(140)	-4029(16)	13424(11)	-364(13)	178(13)
C(140)	-3870(30)	13877(13)	-611(17)	320(40)
C(141)	-3857(16)	12963(12)	-583(13)	144(13)
C(142)	-4210(20)	13431(14)	183(13)	178(17)
O(50)	1730(9)	14047(7)	1196(8)	105(5)
O(51)	-1126(16)	14875(13)	49(14)	206(13)

Table C.21. Bond lengths [pm] and angles [°] for PCM-8(K) (**19**).

Zn(1)-O(13)	191.0(4)	O(5)-Zn(2)#6	200.0(5)
Zn(1)-O(1)	195.0(5)	O(5)-K(1)#6	296.1(6)
Zn(1)-O(3)#1	195.6(5)	O(6)-C(21)	123.2(10)
Zn(1)-O(8)	201.0(5)	O(6)-K(1)#6	276.6(6)
Zn(2)-O(13)	191.6(4)	O(7)-C(28)	126.8(9)
Zn(2)-O(9)#2	193.1(5)	O(8)-C(28)	125.2(9)
Zn(2)-O(7)	197.2(5)	O(9)-C(35)	127.4(9)
Zn(2)-O(5)#2	200.0(5)	O(9)-Zn(2)#6	193.1(5)
Zn(2)-K(1)	361.0(2)	O(10)-C(35)	121.4(9)
K(1)-O(11)#3	270.1(6)	O(11)-C(42)	124.8(9)
K(1)-O(2)	271.7(5)	O(11)-K(1)#7	270.1(6)
K(1)-O(6)#2	276.6(6)	O(12)-C(42)	125.9(10)
K(1)-O(100)	287.7(15)	O(13)-H(13)	100.00
K(1)-O(5)#2	296.1(6)	C(1)-C(6)	136.7(10)
K(1)-O(13)	309.4(5)	C(1)-C(2)	137.3(11)
K(1)-C(21)#2	313.8(8)	C(1P)-H(1PA)	98.00
K(1)-K(1)#4	435.0(4)	C(1P)-H(1PB)	98.00
P(1)-C(1P)	177.8(7)	C(1P)-H(1PC)	98.00
P(1)-C(8)	179.0(6)	C(2)-C(3)	138.7(12)
P(1)-C(1)	179.4(7)	C(2)-H(2A)	95.00
P(1)-C(15)	179.5(7)	C(2P)-H(2PA)	98.00
P(2)-C(2P)	177.2(7)	C(2P)-H(2PB)	98.00
P(2)-C(36)	178.4(6)	C(2P)-H(2PC)	98.00
P(2)-C(22)	179.7(7)	C(3)-C(4)	137.8(12)
P(2)-C(29)	179.9(7)	C(3)-H(3A)	95.00
O(1)-C(7)	128.4(9)	C(4)-C(5)	135.6(10)
O(2)-C(7)	122.4(9)	C(4)-C(7)	151.1(9)
O(3)-C(14)	128.8(9)	C(5)-C(6)	138.8(11)
O(3)-Zn(1)#5	195.6(5)	C(5)-H(5A)	95.00
O(4)-C(14)	122.4(9)	C(6)-H(6A)	95.00
O(5)-C(21)	127.1(9)	C(8)-C(9)	137.9(10)

C(8)-C(13)	139.8(10)	C(29)-C(30)	138.8(10)
C(9)-C(10)	137.8(10)	C(29)-C(34)	138.9(10)
C(9)-H(9A)	95.00	C(30)-C(31)	137.4(11)
C(10)-C(11)	139.4(10)	C(30)-H(30A)	95.00
C(10)-H(10A)	95.00	C(31)-C(32)	138.0(11)
C(11)-C(12)	136.8(10)	C(31)-H(31A)	95.00
C(11)-C(14)	151.8(10)	C(32)-C(33)	137.5(11)
C(12)-C(13)	139.8(11)	C(32)-C(35)	150.9(10)
C(12)-H(12A)	95.00	C(33)-C(34)	137.9(10)
C(13)-H(13A)	95.00	C(33)-H(33A)	95.00
C(15)-C(20)	138.0(10)	C(34)-H(34A)	95.00
C(15)-C(16)	138.3(10)	C(36)-C(41)	138.8(10)
C(16)-C(17)	139.5(10)	C(36)-C(37)	138.9(9)
C(16)-H(16A)	95.00	C(37)-C(38)	138.3(10)
C(17)-C(18)	137.2(10)	C(37)-H(37A)	95.00
C(17)-H(17A)	95.00	C(38)-C(39)	137.9(10)
C(18)-C(19)	137.5(10)	C(38)-H(38A)	95.00
C(18)-C(21)	152.8(10)	C(39)-C(40)	137.0(10)
C(19)-C(20)	138.9(11)	C(39)-C(42)	152.2(10)
C(19)-H(19A)	95.00	C(40)-C(41)	138.5(10)
C(20)-H(20A)	95.00	C(40)-H(40A)	95.00
C(21)-K(1)#6	313.8(8)	C(41)-H(41A)	95.00
C(22)-C(27)	138.4(9)	O(100)-C(100)	132.6(14)
C(22)-C(23)	139.3(10)	N(100)-C(100)	134.2(15)
C(23)-C(24)	135.8(10)	N(100)-C(101)	138.6(14)
C(23)-H(23A)	95.00	N(100)-C(102)	139.2(15)
C(24)-C(25)	137.3(10)	C(100)-H(10B)	95.00
C(24)-H(24A)	95.00	C(101)-H(10C)	98.00
C(25)-C(26)	138.0(10)	C(101)-H(10D)	98.00
C(25)-C(28)	151.2(10)	C(101)-H(10E)	98.00
C(26)-C(27)	137.2(10)	C(102)-H(10F)	98.00
C(26)-H(26A)	95.00	C(102)-H(10G)	98.00
C(27)-H(27A)	95.00	C(102)-H(10H)	98.00

O(110)-C(110)	125.2(16)	C(131)-H(13H)	98.00
N(110)-C(111)	132.5(16)	O(140)-C(140)	135(2)
N(110)-C(110)	135.8(15)	N(140)-C(141)	134.4(17)
N(110)-C(112)	135.9(16)	N(140)-C(140)	134.8(18)
C(110)-H(11A)	95.00	N(140)-C(142)	137.5(18)
C(111)-H(11B)	98.00	C(140)-H(14A)	95.00
C(111)-H(11C)	98.00	C(141)-H(14B)	98.00
C(111)-H(11D)	98.00	C(141)-H(14C)	98.00
C(112)-H(11E)	98.00	C(141)-H(14D)	98.00
C(112)-H(11F)	98.00	C(142)-H(14E)	98.00
C(112)-H(11G)	98.00	C(142)-H(14F)	98.00
O(120)-C(120)	132.4(18)	C(142)-H(14G)	98.00
N(120)-C(120)	136.5(18)		
N(120)-C(122)	136.5(18)	O(13)-Zn(1)-O(1)	124.6(2)
N(120)-C(121)	138.0(19)	O(13)-Zn(1)-O(3)#1	121.6(2)
C(120)-H(12B)	95.00	O(1)-Zn(1)-O(3)#1	104.7(2)
C(121)-H(12C)	98.00	O(13)-Zn(1)-O(8)	102.7(2)
C(121)-H(12D)	98.00	O(1)-Zn(1)-O(8)	99.6(2)
C(121)-H(12E)	98.00	O(3)#1-Zn(1)-O(8)	97.1(2)
C(122)-H(12F)	98.00	O(13)-Zn(2)-O(9)#2	123.0(2)
C(122)-H(12G)	98.00	O(13)-Zn(2)-O(7)	105.9(2)
C(122)-H(12H)	98.00	O(9)#2-Zn(2)-O(7)	117.0(2)
O(130)-C(130)	130.5(19)	O(13)-Zn(2)-O(5)#2	113.7(2)
N(130)-C(130)	133.4(17)	O(9)#2-Zn(2)-O(5)#2	97.9(2)
N(130)-C(132)	135.0(18)	O(7)-Zn(2)-O(5)#2	95.7(2)
N(130)-C(131)	138.6(16)	O(13)-Zn(2)-K(1)	58.96(14)
C(132)-H(13B)	98.00	O(9)#2-Zn(2)-K(1)	123.38(18)
C(132)-H(13C)	98.00	O(7)-Zn(2)-K(1)	114.62(16)
C(132)-H(13D)	98.00	O(5)#2-Zn(2)-K(1)	55.07(17)
C(130)-C(130)#8	199(6)	O(11)#3-K(1)-O(2)	95.50(17)
C(130)-H(13E)	95.00	O(11)#3-K(1)-O(6)#2	131.5(2)
C(131)-H(13F)	98.00	O(2)-K(1)-O(6)#2	90.20(18)
C(131)-H(13G)	98.00	O(11)#3-K(1)-O(100)	91.4(3)

O(2)-K(1)-O(100)	162.3(3)	C(1P)-P(1)-C(1)	109.7(3)
O(6)#2-K(1)-O(100)	97.4(3)	C(8)-P(1)-C(1)	109.4(3)
O(11)#3-K(1)-O(5)#2	92.41(16)	C(1P)-P(1)-C(15)	110.7(3)
O(2)-K(1)-O(5)#2	120.79(16)	C(8)-P(1)-C(15)	107.7(3)
O(6)#2-K(1)-O(5)#2	45.57(17)	C(1)-P(1)-C(15)	109.3(3)
O(100)-K(1)-O(5)#2	75.0(3)	C(2P)-P(2)-C(36)	111.4(3)
O(11)#3-K(1)-O(13)	56.15(14)	C(2P)-P(2)-C(22)	109.3(3)
O(2)-K(1)-O(13)	71.25(14)	C(36)-P(2)-C(22)	109.1(3)
O(6)#2-K(1)-O(13)	80.91(18)	C(2P)-P(2)-C(29)	109.7(3)
O(100)-K(1)-O(13)	125.7(3)	C(36)-P(2)-C(29)	109.0(3)
O(5)#2-K(1)-O(13)	65.56(13)	C(22)-P(2)-C(29)	108.3(3)
O(11)#3-K(1)-C(21)#2	115.5(2)	C(7)-O(1)-Zn(1)	122.1(5)
O(2)-K(1)-C(21)#2	109.93(19)	C(7)-O(2)-K(1)	153.7(5)
O(6)#2-K(1)-C(21)#2	22.99(18)	C(14)-O(3)-Zn(1)#5	117.8(5)
O(100)-K(1)-C(21)#2	81.4(3)	C(21)-O(5)-Zn(2)#6	119.3(5)
O(5)#2-K(1)-C(21)#2	23.84(18)	C(21)-O(5)-K(1)#6	85.9(5)
O(13)-K(1)-C(21)#2	77.29(17)	Zn(2)#6-O(5)-K(1)#6	91.30(19)
O(11)#3-K(1)-Zn(2)	70.02(12)	C(21)-O(6)-K(1)#6	95.7(5)
O(2)-K(1)-Zn(2)	97.19(12)	C(28)-O(7)-Zn(2)	127.0(5)
O(6)#2-K(1)-Zn(2)	61.46(15)	C(28)-O(8)-Zn(1)	130.4(5)
O(100)-K(1)-Zn(2)	100.5(3)	C(35)-O(9)-Zn(2)#6	111.5(5)
O(5)#2-K(1)-Zn(2)	33.63(10)	C(42)-O(11)-K(1)#7	152.1(5)
O(13)-K(1)-Zn(2)	32.05(8)	Zn(1)-O(13)-Zn(2)	117.9(2)
C(21)#2-K(1)-Zn(2)	49.29(16)	Zn(1)-O(13)-K(1)	111.26(18)
O(11)#3-K(1)-K(1)#4	100.29(12)	Zn(2)-O(13)-K(1)	89.00(16)
O(2)-K(1)-K(1)#4	124.29(13)	Zn(1)-O(13)-H(13)	112.2
O(6)#2-K(1)-K(1)#4	115.71(15)	Zn(2)-O(13)-H(13)	112.2
O(100)-K(1)-K(1)#4	38.1(3)	K(1)-O(13)-H(13)	112.2
O(5)#2-K(1)-K(1)#4	111.54(12)	C(6)-C(1)-C(2)	119.1(7)
O(13)-K(1)-K(1)#4	154.92(10)	C(6)-C(1)-P(1)	122.1(5)
C(21)#2-K(1)-K(1)#4	110.26(14)	C(2)-C(1)-P(1)	118.8(6)
Zn(2)-K(1)-K(1)#4	138.42(7)	P(1)-C(1P)-H(1PA)	109.5
C(1P)-P(1)-C(8)	110.0(3)	P(1)-C(1P)-H(1PB)	109.5

H(1PA)-C(1P)-H(1PB)	109.5	C(8)-C(9)-H(9A)	119.7
P(1)-C(1P)-H(1PC)	109.5	C(9)-C(10)-C(11)	119.9(7)
H(1PA)-C(1P)-H(1PC)	109.5	C(9)-C(10)-H(10A)	120.0
H(1PB)-C(1P)-H(1PC)	109.5	C(11)-C(10)-H(10A)	120.0
C(1)-C(2)-C(3)	120.0(8)	C(12)-C(11)-C(10)	120.2(6)
C(1)-C(2)-H(2A)	120.0	C(12)-C(11)-C(14)	119.1(7)
C(3)-C(2)-H(2A)	120.0	C(10)-C(11)-C(14)	120.7(7)
P(2)-C(2P)-H(2PA)	109.5	C(11)-C(12)-C(13)	120.0(7)
P(2)-C(2P)-H(2PB)	109.5	C(11)-C(12)-H(12A)	120.0
H(2PA)-C(2P)-H(2PB)	109.5	C(13)-C(12)-H(12A)	120.0
P(2)-C(2P)-H(2PC)	109.5	C(12)-C(13)-C(8)	119.9(7)
H(2PA)-C(2P)-H(2PC)	109.5	C(12)-C(13)-H(13A)	120.1
H(2PB)-C(2P)-H(2PC)	109.5	C(8)-C(13)-H(13A)	120.1
C(4)-C(3)-C(2)	121.3(8)	O(4)-C(14)-O(3)	124.9(7)
C(4)-C(3)-H(3A)	119.4	O(4)-C(14)-C(11)	119.3(7)
C(2)-C(3)-H(3A)	119.4	O(3)-C(14)-C(11)	115.8(7)
C(5)-C(4)-C(3)	117.6(7)	C(20)-C(15)-C(16)	119.2(7)
C(5)-C(4)-C(7)	121.0(7)	C(20)-C(15)-P(1)	122.2(6)
C(3)-C(4)-C(7)	121.4(7)	C(16)-C(15)-P(1)	118.4(5)
C(4)-C(5)-C(6)	122.1(7)	C(15)-C(16)-C(17)	119.4(7)
C(4)-C(5)-H(5A)	119.0	C(15)-C(16)-H(16A)	120.3
C(6)-C(5)-H(5A)	119.0	C(17)-C(16)-H(16A)	120.3
C(1)-C(6)-C(5)	119.8(7)	C(18)-C(17)-C(16)	120.9(7)
C(1)-C(6)-H(6A)	120.1	C(18)-C(17)-H(17A)	119.6
C(5)-C(6)-H(6A)	120.1	C(16)-C(17)-H(17A)	119.6
O(2)-C(7)-O(1)	126.4(6)	C(17)-C(18)-C(19)	119.9(7)
O(2)-C(7)-C(4)	119.3(6)	C(17)-C(18)-C(21)	120.1(7)
O(1)-C(7)-C(4)	114.2(6)	C(19)-C(18)-C(21)	120.0(7)
C(9)-C(8)-C(13)	119.3(6)	C(18)-C(19)-C(20)	119.5(7)
C(9)-C(8)-P(1)	120.6(5)	C(18)-C(19)-H(19A)	120.2
C(13)-C(8)-P(1)	120.0(5)	C(20)-C(19)-H(19A)	120.2
C(10)-C(9)-C(8)	120.7(7)	C(15)-C(20)-C(19)	121.1(7)
C(10)-C(9)-H(9A)	119.7	C(15)-C(20)-H(20A)	119.5

C(19)-C(20)-H(20A)	119.5	C(29)-C(30)-H(30A)	120.1
O(6)-C(21)-O(5)	125.5(7)	C(30)-C(31)-C(32)	120.8(7)
O(6)-C(21)-C(18)	118.5(7)	C(30)-C(31)-H(31A)	119.6
O(5)-C(21)-C(18)	116.0(7)	C(32)-C(31)-H(31A)	119.6
O(6)-C(21)-K(1)#6	61.3(4)	C(33)-C(32)-C(31)	118.8(7)
O(5)-C(21)-K(1)#6	70.2(4)	C(33)-C(32)-C(35)	120.2(7)
C(18)-C(21)-K(1)#6	154.6(5)	C(31)-C(32)-C(35)	120.9(7)
C(27)-C(22)-C(23)	119.7(7)	C(32)-C(33)-C(34)	121.8(7)
C(27)-C(22)-P(2)	119.9(5)	C(32)-C(33)-H(33A)	119.1
C(23)-C(22)-P(2)	120.4(5)	C(34)-C(33)-H(33A)	119.1
C(24)-C(23)-C(22)	119.8(7)	C(33)-C(34)-C(29)	118.7(7)
C(24)-C(23)-H(23A)	120.1	C(33)-C(34)-H(34A)	120.6
C(22)-C(23)-H(23A)	120.1	C(29)-C(34)-H(34A)	120.6
C(23)-C(24)-C(25)	121.0(7)	O(10)-C(35)-O(9)	124.4(7)
C(23)-C(24)-H(24A)	119.5	O(10)-C(35)-C(32)	120.6(7)
C(25)-C(24)-H(24A)	119.5	O(9)-C(35)-C(32)	115.0(7)
C(24)-C(25)-C(26)	119.3(7)	C(41)-C(36)-C(37)	119.7(6)
C(24)-C(25)-C(28)	120.2(7)	C(41)-C(36)-P(2)	120.6(5)
C(26)-C(25)-C(28)	120.6(6)	C(37)-C(36)-P(2)	119.6(5)
C(27)-C(26)-C(25)	120.7(7)	C(38)-C(37)-C(36)	120.1(6)
C(27)-C(26)-H(26A)	119.6	C(38)-C(37)-H(37A)	120.0
C(25)-C(26)-H(26A)	119.6	C(36)-C(37)-H(37A)	120.0
C(26)-C(27)-C(22)	119.4(7)	C(39)-C(38)-C(37)	120.4(7)
C(26)-C(27)-H(27A)	120.3	C(39)-C(38)-H(38A)	119.8
C(22)-C(27)-H(27A)	120.3	C(37)-C(38)-H(38A)	119.8
O(8)-C(28)-O(7)	127.0(7)	C(40)-C(39)-C(38)	119.1(6)
O(8)-C(28)-C(25)	116.9(6)	C(40)-C(39)-C(42)	119.9(7)
O(7)-C(28)-C(25)	116.1(7)	C(38)-C(39)-C(42)	121.0(6)
C(30)-C(29)-C(34)	120.1(6)	C(39)-C(40)-C(41)	121.8(7)
C(30)-C(29)-P(2)	118.4(5)	C(39)-C(40)-H(40A)	119.1
C(34)-C(29)-P(2)	121.4(5)	C(41)-C(40)-H(40A)	119.1
C(31)-C(30)-C(29)	119.8(7)	C(40)-C(41)-C(36)	118.9(7)
C(31)-C(30)-H(30A)	120.1	C(40)-C(41)-H(41A)	120.5

C(36)-C(41)-H(41A)	120.5	H(11B)-C(111)-H(11D)	109.5
O(11)-C(42)-O(12)	126.3(7)	H(11C)-C(111)-H(11D)	109.5
O(11)-C(42)-C(39)	116.5(7)	N(110)-C(112)-H(11E)	109.5
O(12)-C(42)-C(39)	117.2(7)	N(110)-C(112)-H(11F)	109.5
C(100)-O(100)-K(1)	135.3(14)	H(11E)-C(112)-H(11F)	109.5
C(100)-N(100)-C(101)	120.2(14)	N(110)-C(112)-H(11G)	109.5
C(100)-N(100)-C(102)	118.4(13)	H(11E)-C(112)-H(11G)	109.5
C(101)-N(100)-C(102)	117.3(14)	H(11F)-C(112)-H(11G)	109.5
O(100)-C(100)-N(100)	124.0(15)	C(120)-N(120)-C(122)	116.6(19)
O(100)-C(100)-H(10B)	118.0	C(120)-N(120)-C(121)	117.6(19)
N(100)-C(100)-H(10B)	118.0	C(122)-N(120)-C(121)	116.0(19)
N(100)-C(101)-H(10C)	109.5	O(120)-C(120)-N(120)	122(2)
N(100)-C(101)-H(10D)	109.5	O(120)-C(120)-H(12B)	119.2
H(10C)-C(101)-H(10D)	109.5	N(120)-C(120)-H(12B)	119.2
N(100)-C(101)-H(10E)	109.5	N(120)-C(121)-H(12C)	109.5
H(10C)-C(101)-H(10E)	109.5	N(120)-C(121)-H(12D)	109.5
H(10D)-C(101)-H(10E)	109.5	H(12C)-C(121)-H(12D)	109.5
N(100)-C(102)-H(10F)	109.5	N(120)-C(121)-H(12E)	109.5
N(100)-C(102)-H(10G)	109.5	H(12C)-C(121)-H(12E)	109.5
H(10F)-C(102)-H(10G)	109.5	H(12D)-C(121)-H(12E)	109.5
N(100)-C(102)-H(10H)	109.5	N(120)-C(122)-H(12F)	109.5
H(10F)-C(102)-H(10H)	109.5	N(120)-C(122)-H(12G)	109.5
H(10G)-C(102)-H(10H)	109.5	H(12F)-C(122)-H(12G)	109.5
C(111)-N(110)-C(110)	121.8(15)	N(120)-C(122)-H(12H)	109.5
C(111)-N(110)-C(112)	124.7(16)	H(12F)-C(122)-H(12H)	109.5
C(110)-N(110)-C(112)	113.5(14)	H(12G)-C(122)-H(12H)	109.5
O(110)-C(110)-N(110)	125.6(17)	C(130)-N(130)-C(132)	124.1(17)
O(110)-C(110)-H(11A)	117.2	C(130)-N(130)-C(131)	117.9(16)
N(110)-C(110)-H(11A)	117.2	C(132)-N(130)-C(131)	118.0(17)
N(110)-C(111)-H(11B)	109.5	N(130)-C(132)-H(13B)	109.5
N(110)-C(111)-H(11C)	109.5	N(130)-C(132)-H(13C)	109.5
H(11B)-C(111)-H(11C)	109.5	H(13B)-C(132)-H(13C)	109.5
N(110)-C(111)-H(11D)	109.5	N(130)-C(132)-H(13D)	109.5

H(13B)-C(132)-H(13D)	109.5	C(140)-N(140)-C(142)	119.1(17)
H(13C)-C(132)-H(13D)	109.5	N(140)-C(140)-O(140)	119(2)
O(130)-C(130)-N(130)	125(2)	N(140)-C(140)-H(14A)	120.3
O(130)-C(130)-C(130)#8	130(3)	O(140)-C(140)-H(14A)	120.3
N(130)-C(130)-C(130)#8	89(2)	N(140)-C(141)-H(14B)	109.5
O(130)-C(130)-H(13E)	117.3	N(140)-C(141)-H(14C)	109.5
N(130)-C(130)-H(13E)	117.3	H(14B)-C(141)-H(14C)	109.5
C(130)#8-C(130)-H(13E)	47.6	N(140)-C(141)-H(14D)	109.5
N(130)-C(131)-H(13F)	109.5	H(14B)-C(141)-H(14D)	109.5
N(130)-C(131)-H(13G)	109.5	H(14C)-C(141)-H(14D)	109.5
H(13F)-C(131)-H(13G)	109.5	N(140)-C(142)-H(14E)	109.5
N(130)-C(131)-H(13H)	109.5	N(140)-C(142)-H(14F)	109.5
H(13F)-C(131)-H(13H)	109.5	H(14E)-C(142)-H(14F)	109.5
H(13G)-C(131)-H(13H)	109.5	N(140)-C(142)-H(14G)	109.5
C(141)-N(140)-C(140)	120.5(19)	H(14E)-C(142)-H(14G)	109.5
C(141)-N(140)-C(142)	117.9(18)	H(14F)-C(142)-H(14G)	109.5

Symmetry transformations used to generate equivalent atoms:
#1 x+1/2,-y+7/2,-z #2 x,-y+3,z+1/2 #3 x-1/2,y+1/2,-z+1/2
#4 -x-1,y,-z+1/2 #5 x-1/2,-y+7/2,-z #6 x,-y+3,z-1/2
#7 x+1/2,y-1/2,-z+1/2 #8 -x,y,-z+1/2

Table C.22. Anisotropic displacement parameters ($pm^2 x\ 10^{-1}$)for PCM-8(K) (**19**). The anisotropic displacement factor exponent takes the form: $-2p^2[\ h^2a^{*2}U^{11} + ... + 2\ h\ k\ a^*\ b^*\ U^{12}\ ]$.

	U^{11}	U^{22}	U^{33}	U^{23}	U^{13}	U^{12}
Zn(1)	23(1)	27(1)	24(1)	-1(1)	-1(1)	0(1)
Zn(2)	41(1)	26(1)	23(1)	-1(1)	-2(1)	4(1)
K(1)	47(1)	42(1)	47(1)	7(1)	2(1)	-2(1)

P(1)	26(1)	28(1)	25(1)	-1(1)	-6(1)	3(1)
P(2)	21(1)	29(1)	23(1)	-3(1)	-1(1)	5(1)
O(1)	37(3)	58(4)	25(3)	-2(2)	-8(2)	6(2)
O(2)	37(3)	48(3)	30(3)	-1(2)	-2(2)	4(2)
O(3)	23(3)	53(4)	49(3)	5(3)	-1(2)	12(2)
O(4)	21(3)	63(4)	64(4)	-8(3)	-6(2)	-8(3)
O(5)	59(4)	32(3)	47(3)	5(3)	11(3)	13(3)
O(6)	115(6)	34(3)	46(4)	-8(3)	6(3)	-2(3)
O(7)	65(4)	41(3)	36(3)	-10(2)	-7(3)	24(3)
O(8)	52(3)	27(3)	41(3)	-4(2)	7(2)	6(2)
O(9)	51(4)	74(4)	28(3)	5(3)	-9(2)	-2(3)
O(10)	74(4)	60(4)	28(3)	-4(3)	0(3)	15(3)
O(11)	38(3)	47(4)	57(3)	-7(3)	-14(3)	17(3)
O(12)	25(3)	55(4)	72(4)	-1(3)	-8(3)	2(3)
O(13)	30(2)	23(2)	28(2)	0(2)	2(2)	2(2)
C(1)	31(4)	32(4)	27(4)	-5(3)	-8(3)	6(3)
C(1P)	20(3)	34(4)	41(4)	4(3)	-2(3)	-2(3)
C(2)	30(5)	216(15)	27(5)	-26(6)	-1(4)	17(6)
C(2P)	29(4)	32(4)	39(4)	-7(3)	2(3)	-1(3)
C(3)	28(5)	198(14)	35(5)	-17(6)	-19(4)	19(6)
C(4)	33(4)	37(4)	28(4)	-5(3)	-5(3)	6(3)
C(5)	28(4)	107(8)	24(4)	3(4)	0(3)	5(4)
C(6)	22(4)	95(7)	35(4)	-3(4)	-2(3)	0(4)
C(7)	40(4)	30(4)	29(4)	-4(3)	-9(3)	9(3)
C(8)	22(3)	31(4)	22(3)	0(3)	-6(3)	0(3)
C(9)	25(4)	29(4)	54(5)	2(3)	0(3)	-1(3)
C(10)	23(4)	31(4)	54(5)	10(3)	-3(3)	3(3)
C(11)	29(4)	46(4)	16(3)	-2(3)	-6(3)	3(3)
C(12)	26(4)	39(5)	67(5)	0(4)	-11(4)	-9(3)
C(13)	39(5)	29(4)	65(6)	-2(4)	-15(4)	0(3)
C(14)	26(4)	54(5)	20(3)	-4(3)	-1(3)	8(4)
C(15)	28(4)	27(4)	33(4)	1(3)	-4(3)	4(3)
C(16)	70(6)	27(4)	26(4)	-2(3)	-5(4)	0(4)

C(17)	71(6)	35(4)	30(4)	-2(3)	1(4)	8(4)
C(18)	33(4)	29(4)	41(4)	-1(3)	-1(3)	9(3)
C(19)	72(6)	32(4)	39(5)	5(4)	-12(4)	12(4)
C(20)	85(6)	38(5)	29(4)	-4(3)	-9(4)	13(4)
C(21)	46(5)	31(4)	55(5)	-1(4)	16(4)	5(3)
C(22)	26(4)	33(4)	28(4)	-5(3)	-3(3)	6(3)
C(23)	54(5)	32(4)	33(4)	2(3)	13(3)	9(4)
C(24)	56(5)	36(4)	37(4)	1(3)	11(4)	7(4)
C(25)	30(4)	36(4)	35(4)	-4(3)	2(3)	9(3)
C(26)	45(4)	39(4)	29(4)	-6(3)	2(3)	14(3)
C(27)	38(4)	41(4)	24(4)	-1(3)	-2(3)	8(3)
C(28)	32(4)	33(4)	40(4)	-8(3)	-3(3)	6(3)
C(29)	35(4)	40(4)	22(3)	-7(3)	-5(3)	7(3)
C(30)	30(4)	99(7)	28(4)	-10(4)	-5(3)	21(4)
C(31)	34(4)	83(7)	41(5)	-1(4)	-12(4)	14(4)
C(32)	48(5)	36(4)	24(4)	-2(3)	-1(3)	8(3)
C(33)	42(5)	56(5)	28(4)	-4(4)	5(3)	11(4)
C(34)	27(4)	63(5)	28(4)	-6(4)	-5(3)	12(3)
C(35)	54(5)	37(4)	29(4)	-1(3)	-4(4)	6(4)
C(36)	21(3)	30(4)	21(3)	1(3)	-2(3)	2(3)
C(37)	30(4)	31(4)	35(4)	3(3)	-6(3)	-2(3)
C(38)	40(4)	29(4)	34(4)	-1(3)	-4(3)	13(3)
C(39)	31(4)	40(4)	22(3)	-1(3)	-3(3)	7(3)
C(40)	25(4)	40(4)	45(4)	-8(3)	-6(3)	4(3)
C(41)	32(4)	25(4)	47(4)	-1(3)	-5(3)	5(3)
C(42)	31(4)	39(5)	41(4)	-9(4)	-9(3)	10(4)

Table C.23. Hydrogen coordinates (x 10^4) and isotropic displacement parameters (pm^2x 10^{-1}) for PCM-8(K) (**19**).

	x	y	z	U(eq)
H(13)	-2618	17173	2771	40
H(1PA)	-2606	17095	-1705	48
H(1PB)	-3106	17185	-2185	48
H(1PC)	-3084	17571	-1662	48
H(2A)	-2488	16844	-766	109
H(2PA)	-2398	13129	1790	50
H(2PB)	-1909	12662	1738	50
H(2PC)	-1893	13041	2266	50
H(3A)	-2281	16856	182	104
H(5A)	-4089	16875	507	64
H(6A)	-4308	16877	-438	61
H(9A)	-4153	17776	-1638	43
H(10A)	-5162	18040	-1814	43
H(12A)	-5746	16544	-1687	52
H(13A)	-4725	16274	-1519	53
H(16A)	-3488	16310	-2474	49
H(17A)	-3452	15442	-2785	54
H(19A)	-3419	14927	-1207	57
H(20A)	-3464	15790	-893	61
H(23A)	-1373	14457	1005	48
H(24A)	-1562	15299	1299	52
H(26A)	-1958	14773	2831	45
H(27A)	-1789	13919	2542	41
H(30A)	-2513	13615	849	63
H(31A)	-2719	13630	-96	63
H(33A)	-956	13242	-420	51
H(34A)	-728	13238	523	47

H(37A)	-805	12479	1570	39
H(38A)	221	12239	1720	41
H(40A)	695	13752	1850	44
H(41A)	-332	14005	1734	42
H(10B)	-4825	16108	3973	202
H(10C)	-5065	14772	4030	252
H(10D)	-4496	15145	4184	252
H(10E)	-5173	15274	4414	252
H(10F)	-5199	14805	3191	252
H(10G)	-5422	15334	2898	252
H(10H)	-4701	15198	2931	252
H(11A)	-3100	14851	1453	102
H(11B)	-3227	15124	-122	223
H(11C)	-2985	14561	67	223
H(11D)	-3703	14702	119	223
H(11E)	-2981	15560	1180	227
H(11F)	-2631	15606	597	227
H(11G)	-3346	15761	643	227
H(12B)	556	12907	-766	152
H(12C)	747	14060	282	349
H(12D)	88	13864	62	349
H(12E)	448	13536	526	349
H(12F)	1283	14055	-435	245
H(12G)	1425	13528	-769	245
H(12H)	811	13855	-901	245
H(13B)	471	14873	1651	443
H(13C)	441	15449	1392	443
H(13D)	1047	15261	1718	443
H(13E)	251	15992	2717	175
H(13F)	-24	14741	2314	212
H(13G)	192	15038	2866	212
H(13H)	-417	15224	2544	212
H(14A)	-3763	13883	-994	382

H(14B)	-4013	12678	-351	216
H(14C)	-4028	12930	-958	216
H(14D)	-3405	12946	-601	216
H(14E)	-4324	13789	289	267
H(14F)	-4570	13201	232	267
H(14G)	-3871	13309	418	267

Table C.24 Crystal data and structure refinement for pcm-9(Cs) (**21**).

Identification code	PCM-9	
Empirical formula	C49 H51 N O21 P2 Zn3	
Formula weight	1247.95	
Temperature	180(2) K	
Wavelength	0.71073 Å	
Crystal system	Triclinic	
Space group	P -1	
Unit cell dimensions	a = 11.24380(10) Å	a= 85.2120(10)°.
	b = 13.8860(2) Å	b= 85.8650(10)°.
	c = 24.7223(3) Å	g = 66.6450(10)°.
Volume	3528.09(8) $Å^3$	
Z	2	
Density (calculated)	1.175 Mg/m^3	
Absorption coefficient	1.117 mm^{-1}	
F(000)	1280	
Crystal size	0.100 x 0.100 x 0.100 mm^3	
Theta range for data collection	3.515 to 24.000°.	
Index ranges	-12<=h<=12, -15<=k<=15, -28<=l<=27	
Reflections collected	24954	
Independent reflections	10875 [R(int) = 0.0309]	
Completeness to theta = 24.000°	98.3 %	
Refinement method	Full-matrix least-squares on F^2	

Data / restraints / parameters	10875 / 16 / 673
Goodness-of-fit on F^2	1.070
Final R indices [I>2sigma(I)]	R1 = 0.0691, wR2 = 0.2030
R indices (all data)	R1 = 0.0810, wR2 = 0.2118
Extinction coefficient	n/a
Largest diff. peak and hole	1.113 and -0.624 e.Å^{-3}

Table C.25. Atomic coordinates (x 10^4) and equivalent isotropic displacement parameters (Å^{2}x 10^3) for pcm-9(Cs) (**21**). U(eq) is defined as one third of the trace of the orthogonalized U^{ij} tensor.

	x	y	z	U(eq)
Zn(1)	-5495(1)	17707(1)	2337(1)	37(1)
Zn(2)	-3293(1)	15381(1)	2398(1)	36(1)
Zn(3)	-2684(1)	17433(1)	2794(1)	37(1)
P(1)	-4398(1)	16476(1)	-1071(1)	36(1)
P(2)	-9272(2)	13627(1)	3806(1)	37(1)
O(1)	-5332(4)	17310(3)	1580(1)	43(1)
O(2)	-3355(4)	15995(3)	1619(1)	40(1)
O(3)	-5873(5)	21503(3)	-1981(2)	55(1)
O(4)	-6825(5)	21037(3)	-2607(2)	56(1)
O(5)	1340(4)	14809(3)	-2442(2)	41(1)
O(6)	1143(4)	13262(3)	-2316(2)	45(1)
O(7)	-6678(4)	16944(3)	2623(2)	49(1)
O(8)	-5188(4)	15408(3)	2367(2)	43(1)
O(9)	-7550(5)	9777(4)	2053(2)	67(1)
O(10)	-6395(5)	8933(3)	2758(2)	64(1)
O(11)	-7942(5)	12807(3)	6467(2)	51(1)
O(12)	-6182(9)	13044(8)	6138(3)	133(3)
O(13)	-3952(4)	16779(3)	2772(1)	36(1)

O(14)	-2570(5)	13727(4)	2187(2)	70(1)
O(15)	-3075(5)	14282(4)	3071(2)	67(1)
C(1P)	-5455(6)	15837(5)	-1166(2)	47(1)
C(1)	-4295(6)	16545(4)	-356(2)	39(1)
C(2P)	-10976(6)	14360(5)	3824(2)	44(1)
C(2)	-3247(6)	15882(5)	-80(2)	45(1)
C(3)	-3243(6)	15908(5)	490(2)	46(1)
C(4)	-4295(5)	16623(4)	763(2)	36(1)
C(5)	-5349(8)	17293(7)	484(3)	79(3)
C(6)	-5367(8)	17255(7)	-76(3)	87(3)
C(7)	-4316(6)	16639(4)	1369(2)	37(1)
C(8)	-4993(5)	17780(4)	-1388(2)	36(1)
C(9)	-4632(7)	18532(5)	-1205(2)	49(2)
C(10)	-5000(7)	19502(5)	-1470(2)	50(2)
C(11)	-5756(6)	19751(4)	-1919(2)	41(1)
C(12)	-6105(7)	19004(5)	-2106(2)	52(2)
C(13)	-5732(6)	18009(5)	-1844(2)	45(1)
C(14)	-6158(6)	20846(5)	-2186(2)	46(2)
C(15)	-2812(5)	15758(4)	-1370(2)	36(1)
C(16)	-1965(6)	16251(5)	-1485(2)	48(2)
C(17)	-801(6)	15753(5)	-1752(2)	47(1)
C(18)	-463(5)	14747(4)	-1916(2)	37(1)
C(19)	-1279(6)	14219(4)	-1785(2)	41(1)
C(20)	-2462(6)	14724(4)	-1515(2)	42(1)
C(21)	783(5)	14231(4)	-2245(2)	38(1)
C(22)	-8443(5)	14334(4)	3421(2)	35(1)
C(23)	-8966(6)	15435(4)	3378(2)	41(1)
C(24)	-8254(6)	15964(4)	3108(2)	43(1)
C(25)	-7023(5)	15405(4)	2881(2)	38(1)
C(26)	-6518(6)	14315(5)	2922(3)	48(2)
C(27)	-7209(6)	13778(4)	3186(2)	46(1)
C(28)	-6233(6)	15958(4)	2603(2)	40(1)
C(29)	-8817(6)	12420(4)	3477(2)	39(1)

C(30)	-9236(6)	12481(5)	2957(2)	49(2)
C(31)	-8742(7)	11598(5)	2659(3)	53(2)
C(32)	-7837(6)	10680(5)	2860(2)	44(1)
C(33)	-7469(9)	10626(5)	3388(3)	72(2)
C(34)	-7949(8)	11485(5)	3694(3)	66(2)
C(35)	-7230(6)	9727(5)	2516(3)	50(2)
C(36)	-8679(7)	13371(5)	4487(2)	51(2)
C(37)	-9369(8)	13144(6)	4906(3)	65(2)
C(38)	-8876(8)	12959(6)	5441(3)	62(2)
C(39)	-7744(8)	13039(7)	5504(3)	73(2)
C(40)	-7071(12)	13319(16)	5099(3)	175(8)
C(41)	-7537(11)	13453(14)	4579(4)	148(6)
C(42)	-7261(8)	12839(10)	6100(4)	95(3)
C(43)	-2664(9)	13489(7)	2725(4)	82(2)
C(44)	-2367(13)	12388(8)	2930(5)	118(4)
O(100)	-2700(20)	8636(17)	-273(9)	172(8)
N(100)	-1683(14)	7669(11)	458(6)	83(4)
C(100)	-2740(30)	8410(20)	256(10)	191(14)
C(101)	-1600(20)	7515(19)	997(8)	122(8)
C(102)	-770(50)	6960(40)	159(14)	350(40)
O(110)	1480(30)	8420(20)	787(10)	221(11)
N(110)	180(20)	8947(18)	1568(8)	144(8)
C(110)	1320(20)	8384(19)	1323(9)	126(8)
C(111)	30(30)	8980(30)	2104(10)	168(12)
C(112)	-700(30)	9690(30)	1251(12)	233(19)
O(200)	1520(8)	1404(6)	1251(3)	117(2)
O(201)	8332(16)	2411(13)	4505(7)	243(6)
O(202)	8947(15)	2596(12)	1381(6)	227(6)
O(203)	5660(20)	3784(17)	4055(9)	162(7)
O(204)	-5950(20)	11819(18)	6144(8)	154(7)
O(205)	8220(20)	3082(18)	376(9)	167(7)
O(206)	5080(30)	6020(20)	3790(11)	197(10)

Table C.26. Bond lengths [Å] and angles [°] for pcm-9(Cs) (**21**).

Zn(1)-O(10)#1	1.944(4)	O(5)-Zn(2)#3	2.116(4)
Zn(1)-O(1)	1.972(4)	O(6)-C(21)	1.265(7)
Zn(1)-O(13)	2.023(4)	O(6)-Zn(3)#3	1.975(4)
Zn(1)-O(7)	2.060(4)	O(7)-C(28)	1.262(7)
Zn(1)-O(3)#2	2.308(5)	O(8)-C(28)	1.252(7)
Zn(2)-O(2)	2.034(4)	O(9)-C(35)	1.213(8)
Zn(2)-O(13)	2.058(4)	O(10)-C(35)	1.267(8)
Zn(2)-O(5)#3	2.116(4)	O(10)-Zn(1)#5	1.944(4)
Zn(2)-O(15)	2.119(4)	O(11)-C(42)	1.153(10)
Zn(2)-O(8)	2.123(4)	O(11)-Zn(3)#4	1.960(4)
Zn(2)-O(14)	2.206(5)	O(12)-C(42)	1.364(12)
Zn(2)-C(43)	2.512(9)	O(12)-O(204)	1.62(2)
Zn(3)-O(11)#4	1.960(4)	O(13)-H(13)	1.0000
Zn(3)-O(6)#3	1.975(4)	O(14)-C(43)	1.351(11)
Zn(3)-O(13)	1.977(4)	O(15)-C(43)	1.361(11)
Zn(3)-O(4)#2	1.994(4)	C(1P)-H(1PA)	0.9800
P(1)-C(1P)	1.781(6)	C(1P)-H(1PB)	0.9800
P(1)-C(1)	1.791(5)	C(1P)-H(1PC)	0.9800
P(1)-C(8)	1.794(5)	C(1)-C(2)	1.362(8)
P(1)-C(15)	1.801(6)	C(1)-C(6)	1.399(9)
P(2)-C(2P)	1.778(6)	C(2P)-H(2PA)	0.9800
P(2)-C(22)	1.783(6)	C(2P)-H(2PB)	0.9800
P(2)-C(29)	1.794(6)	C(2P)-H(2PC)	0.9800
P(2)-C(36)	1.812(6)	C(2)-C(3)	1.413(8)
O(1)-C(7)	1.263(7)	C(2)-H(2A)	0.9500
O(2)-C(7)	1.260(7)	C(3)-C(4)	1.379(8)
O(3)-C(14)	1.236(8)	C(3)-H(3A)	0.9500
O(3)-Zn(1)#2	2.308(5)	C(4)-C(5)	1.373(9)
O(4)-C(14)	1.273(8)	C(4)-C(7)	1.498(7)
O(4)-Zn(3)#2	1.994(4)	C(5)-C(6)	1.391(9)
O(5)-C(21)	1.250(7)	C(5)-H(5A)	0.9500

C(6)-H(6A)	0.9500	C(27)-H(27A)	0.9500
C(8)-C(9)	1.380(8)	C(29)-C(34)	1.372(9)
C(8)-C(13)	1.388(8)	C(29)-C(30)	1.385(8)
C(9)-C(10)	1.366(8)	C(30)-C(31)	1.381(8)
C(9)-H(9A)	0.9500	C(30)-H(30A)	0.9500
C(10)-C(11)	1.382(8)	C(31)-C(32)	1.359(9)
C(10)-H(10A)	0.9500	C(31)-H(31A)	0.9500
C(11)-C(12)	1.368(9)	C(32)-C(33)	1.384(10)
C(11)-C(14)	1.511(8)	C(32)-C(35)	1.526(8)
C(12)-C(13)	1.391(8)	C(33)-C(34)	1.368(10)
C(12)-H(12A)	0.9500	C(33)-H(33A)	0.9500
C(13)-H(13A)	0.9500	C(34)-H(34A)	0.9500
C(15)-C(16)	1.380(8)	C(36)-C(37)	1.341(9)
C(15)-C(20)	1.401(8)	C(36)-C(41)	1.369(13)
C(16)-C(17)	1.364(8)	C(37)-C(38)	1.434(10)
C(16)-H(16A)	0.9500	C(37)-H(37A)	0.9500
C(17)-C(18)	1.382(8)	C(38)-C(39)	1.342(11)
C(17)-H(17A)	0.9500	C(38)-H(38A)	0.9500
C(18)-C(19)	1.392(8)	C(39)-C(40)	1.336(13)
C(18)-C(21)	1.509(8)	C(39)-C(42)	1.571(11)
C(19)-C(20)	1.385(8)	C(40)-C(41)	1.394(12)
C(19)-H(19A)	0.9500	C(40)-H(40A)	0.9500
C(20)-H(20A)	0.9500	C(41)-H(41A)	0.9500
C(22)-C(23)	1.401(8)	C(42)-O(204)	1.59(2)
C(22)-C(27)	1.403(8)	C(43)-C(44)	1.482(12)
C(23)-C(24)	1.390(8)	C(44)-H(44A)	0.9800
C(23)-H(23A)	0.9500	C(44)-H(44B)	0.9800
C(24)-C(25)	1.394(8)	C(44)-H(44C)	0.9800
C(24)-H(24A)	0.9500	O(100)-C(100)	1.321(19)
C(25)-C(26)	1.388(8)	N(100)-C(100)	1.323(18)
C(25)-C(28)	1.488(8)	N(100)-C(101)	1.335(16)
C(26)-C(27)	1.375(9)	N(100)-C(102)	1.338(19)
C(26)-H(26A)	0.9500	C(100)-H(10B)	0.9500

C(101)-H(10C)	0.9800
C(101)-H(10D)	0.9800
C(101)-H(10E)	0.9800
C(102)-H(10F)	0.9800
C(102)-H(10G)	0.9800
C(102)-H(10H)	0.9800
O(110)-C(110)	1.325(19)
N(110)-C(111)	1.325(17)
N(110)-C(110)	1.335(18)
N(110)-C(112)	1.354(19)
C(110)-H(11A)	0.9500
C(111)-H(11B)	0.9800
C(111)-H(11C)	0.9800
C(111)-H(11D)	0.9800
C(112)-H(11E)	0.9800
C(112)-H(11F)	0.9800
C(112)-H(11G)	0.9800

O(10)#1-Zn(1)-O(1)	138.90(19)
O(10)#1-Zn(1)-O(13)	105.48(19)
O(1)-Zn(1)-O(13)	112.52(15)
O(10)#1-Zn(1)-O(7)	94.86(19)
O(1)-Zn(1)-O(7)	96.32(17)
O(13)-Zn(1)-O(7)	95.74(16)
O(10)#1-Zn(1)-O(3)#2	88.17(19)
O(1)-Zn(1)-O(3)#2	80.89(16)
O(13)-Zn(1)-O(3)#2	84.12(16)
O(7)-Zn(1)-O(3)#2	176.89(16)
O(2)-Zn(2)-O(13)	97.22(15)
O(2)-Zn(2)-O(5)#3	91.23(15)
O(13)-Zn(2)-O(5)#3	91.75(15)
O(2)-Zn(2)-O(15)	160.90(19)
O(13)-Zn(2)-O(15)	101.77(19)
O(5)#3-Zn(2)-O(15)	90.22(17)
O(2)-Zn(2)-O(8)	91.45(15)
O(13)-Zn(2)-O(8)	92.88(15)
O(5)#3-Zn(2)-O(8)	174.33(15)
O(15)-Zn(2)-O(8)	85.63(18)
O(2)-Zn(2)-O(14)	95.75(18)
O(13)-Zn(2)-O(14)	167.03(18)
O(5)#3-Zn(2)-O(14)	87.99(17)
O(15)-Zn(2)-O(14)	65.3(2)
O(8)-Zn(2)-O(14)	86.77(17)
O(2)-Zn(2)-C(43)	128.1(3)
O(13)-Zn(2)-C(43)	134.6(3)
O(5)#3-Zn(2)-C(43)	89.3(2)
O(15)-Zn(2)-C(43)	32.8(3)
O(8)-Zn(2)-C(43)	85.1(2)
O(14)-Zn(2)-C(43)	32.5(3)
O(11)#4-Zn(3)-O(6)#3	105.95(18)
O(11)#4-Zn(3)-O(13)	107.90(17)
O(6)#3-Zn(3)-O(13)	111.03(16)
O(11)#4-Zn(3)-O(4)#2	105.36(18)
O(6)#3-Zn(3)-O(4)#2	104.29(18)
O(13)-Zn(3)-O(4)#2	121.25(18)
C(1P)-P(1)-C(1)	108.5(3)
C(1P)-P(1)-C(8)	110.9(3)
C(1)-P(1)-C(8)	109.3(2)
C(1P)-P(1)-C(15)	110.2(3)
C(1)-P(1)-C(15)	110.1(3)
C(8)-P(1)-C(15)	107.7(2)
C(2P)-P(2)-C(22)	111.1(3)
C(2P)-P(2)-C(29)	112.2(3)
C(22)-P(2)-C(29)	105.2(2)
C(2P)-P(2)-C(36)	110.2(3)
C(22)-P(2)-C(36)	107.4(3)

C(29)-P(2)-C(36)	110.5(3)	H(2PA)-C(2P)-H(2PC)	109.5
C(7)-O(1)-Zn(1)	123.9(4)	H(2PB)-C(2P)-H(2PC)	109.5
C(7)-O(2)-Zn(2)	128.8(3)	C(1)-C(2)-C(3)	120.1(5)
C(14)-O(3)-Zn(1)#2	128.1(4)	C(1)-C(2)-H(2A)	120.0
C(14)-O(4)-Zn(3)#2	104.6(4)	C(3)-C(2)-H(2A)	120.0
C(21)-O(5)-Zn(2)#3	129.7(3)	C(4)-C(3)-C(2)	119.7(5)
C(21)-O(6)-Zn(3)#3	119.2(4)	C(4)-C(3)-H(3A)	120.2
C(28)-O(7)-Zn(1)	117.9(4)	C(2)-C(3)-H(3A)	120.2
C(28)-O(8)-Zn(2)	130.8(4)	C(5)-C(4)-C(3)	120.2(5)
C(35)-O(10)-Zn(1)#5	116.9(4)	C(5)-C(4)-C(7)	119.6(5)
C(42)-O(11)-Zn(3)#4	120.2(5)	C(3)-C(4)-C(7)	120.1(5)
C(42)-O(12)-O(204)	63.9(10)	C(4)-C(5)-C(6)	120.3(6)
Zn(3)-O(13)-Zn(1)	111.27(17)	C(4)-C(5)-H(5A)	119.9
Zn(3)-O(13)-Zn(2)	115.60(18)	C(6)-C(5)-H(5A)	119.9
Zn(1)-O(13)-Zn(2)	103.12(16)	C(5)-C(6)-C(1)	119.8(6)
Zn(3)-O(13)-H(13)	108.9	C(5)-C(6)-H(6A)	120.1
Zn(1)-O(13)-H(13)	108.9	C(1)-C(6)-H(6A)	120.1
Zn(2)-O(13)-H(13)	108.9	O(2)-C(7)-O(1)	126.3(5)
C(43)-O(14)-Zn(2)	86.3(5)	O(2)-C(7)-C(4)	118.6(5)
C(43)-O(15)-Zn(2)	89.6(4)	O(1)-C(7)-C(4)	115.1(5)
P(1)-C(1P)-H(1PA)	109.5	C(9)-C(8)-C(13)	119.9(5)
P(1)-C(1P)-H(1PB)	109.5	C(9)-C(8)-P(1)	119.9(4)
H(1PA)-C(1P)-H(1PB)	109.5	C(13)-C(8)-P(1)	120.0(4)
P(1)-C(1P)-H(1PC)	109.5	C(10)-C(9)-C(8)	120.2(6)
H(1PA)-C(1P)-H(1PC)	109.5	C(10)-C(9)-H(9A)	119.9
H(1PB)-C(1P)-H(1PC)	109.5	C(8)-C(9)-H(9A)	119.9
C(2)-C(1)-C(6)	120.0(5)	C(9)-C(10)-C(11)	120.7(6)
C(2)-C(1)-P(1)	121.8(4)	C(9)-C(10)-H(10A)	119.6
C(6)-C(1)-P(1)	118.1(5)	C(11)-C(10)-H(10A)	119.6
P(2)-C(2P)-H(2PA)	109.5	C(12)-C(11)-C(10)	119.3(5)
P(2)-C(2P)-H(2PB)	109.5	C(12)-C(11)-C(14)	122.6(6)
H(2PA)-C(2P)-H(2PB)	109.5	C(10)-C(11)-C(14)	118.1(5)
P(2)-C(2P)-H(2PC)	109.5	C(11)-C(12)-C(13)	120.9(6)

C(11)-C(12)-H(12A)	119.6	C(24)-C(23)-H(23A)	120.1
C(13)-C(12)-H(12A)	119.6	C(22)-C(23)-H(23A)	120.1
C(8)-C(13)-C(12)	119.0(6)	C(23)-C(24)-C(25)	120.4(5)
C(8)-C(13)-H(13A)	120.5	C(23)-C(24)-H(24A)	119.8
C(12)-C(13)-H(13A)	120.5	C(25)-C(24)-H(24A)	119.8
O(3)-C(14)-O(4)	124.1(5)	C(26)-C(25)-C(24)	119.3(5)
O(3)-C(14)-C(11)	119.5(6)	C(26)-C(25)-C(28)	119.5(5)
O(4)-C(14)-C(11)	116.3(6)	C(24)-C(25)-C(28)	121.2(5)
C(16)-C(15)-C(20)	119.8(5)	C(27)-C(26)-C(25)	121.1(5)
C(16)-C(15)-P(1)	119.6(4)	C(27)-C(26)-H(26A)	119.5
C(20)-C(15)-P(1)	120.5(4)	C(25)-C(26)-H(26A)	119.5
C(17)-C(16)-C(15)	120.8(5)	C(26)-C(27)-C(22)	119.9(5)
C(17)-C(16)-H(16A)	119.6	C(26)-C(27)-H(27A)	120.1
C(15)-C(16)-H(16A)	119.6	C(22)-C(27)-H(27A)	120.1
C(16)-C(17)-C(18)	120.1(6)	O(8)-C(28)-O(7)	125.5(5)
C(16)-C(17)-H(17A)	119.9	O(8)-C(28)-C(25)	117.4(5)
C(18)-C(17)-H(17A)	119.9	O(7)-C(28)-C(25)	117.1(5)
C(17)-C(18)-C(19)	120.1(5)	C(34)-C(29)-C(30)	120.0(5)
C(17)-C(18)-C(21)	119.8(5)	C(34)-C(29)-P(2)	121.9(5)
C(19)-C(18)-C(21)	120.1(5)	C(30)-C(29)-P(2)	117.5(4)
C(20)-C(19)-C(18)	119.7(5)	C(31)-C(30)-C(29)	119.0(6)
C(20)-C(19)-H(19A)	120.1	C(31)-C(30)-H(30A)	120.5
C(18)-C(19)-H(19A)	120.1	C(29)-C(30)-H(30A)	120.5
C(19)-C(20)-C(15)	119.4(5)	C(32)-C(31)-C(30)	121.5(6)
C(19)-C(20)-H(20A)	120.3	C(32)-C(31)-H(31A)	119.2
C(15)-C(20)-H(20A)	120.3	C(30)-C(31)-H(31A)	119.2
O(5)-C(21)-O(6)	125.8(5)	C(31)-C(32)-C(33)	118.4(6)
O(5)-C(21)-C(18)	116.9(5)	C(31)-C(32)-C(35)	121.3(6)
O(6)-C(21)-C(18)	117.2(5)	C(33)-C(32)-C(35)	120.3(6)
C(23)-C(22)-C(27)	119.5(5)	C(34)-C(33)-C(32)	121.3(6)
C(23)-C(22)-P(2)	121.2(4)	C(34)-C(33)-H(33A)	119.3
C(27)-C(22)-P(2)	119.2(4)	C(32)-C(33)-H(33A)	119.3
C(24)-C(23)-C(22)	119.8(5)	C(33)-C(34)-C(29)	119.6(6)

C(33)-C(34)-H(34A)	120.2	O(15)-C(43)-Zn(2)	57.5(4)
C(29)-C(34)-H(34A)	120.2	C(44)-C(43)-Zn(2)	176.8(8)
O(9)-C(35)-O(10)	125.9(6)	C(43)-C(44)-H(44A)	109.5
O(9)-C(35)-C(32)	120.2(6)	C(43)-C(44)-H(44B)	109.5
O(10)-C(35)-C(32)	113.9(6)	H(44A)-C(44)-H(44B)	109.5
C(37)-C(36)-C(41)	119.5(7)	C(43)-C(44)-H(44C)	109.5
C(37)-C(36)-P(2)	120.9(6)	H(44A)-C(44)-H(44C)	109.5
C(41)-C(36)-P(2)	119.6(6)	H(44B)-C(44)-H(44C)	109.5
C(36)-C(37)-C(38)	119.3(7)	C(100)-N(100)-C(101)	118.7(14)
C(36)-C(37)-H(37A)	120.3	C(100)-N(100)-C(102)	123.6(16)
C(38)-C(37)-H(37A)	120.3	C(101)-N(100)-C(102)	116.9(16)
C(39)-C(38)-C(37)	118.4(7)	O(100)-C(100)-N(100)	116(2)
C(39)-C(38)-H(38A)	120.8	O(100)-C(100)-H(10B)	121.8
C(37)-C(38)-H(38A)	120.8	N(100)-C(100)-H(10B)	121.8
C(40)-C(39)-C(38)	123.6(8)	N(100)-C(101)-H(10C)	109.5
C(40)-C(39)-C(42)	120.3(8)	N(100)-C(101)-H(10D)	109.5
C(38)-C(39)-C(42)	116.0(7)	H(10C)-C(101)-H(10D)	109.5
C(39)-C(40)-C(41)	117.1(11)	N(100)-C(101)-H(10E)	109.5
C(39)-C(40)-H(40A)	121.5	H(10C)-C(101)-H(10E)	109.5
C(41)-C(40)-H(40A)	121.5	H(10D)-C(101)-H(10E)	109.5
C(36)-C(41)-C(40)	121.9(10)	N(100)-C(102)-H(10F)	109.5
C(36)-C(41)-H(41A)	119.0	N(100)-C(102)-H(10G)	109.5
C(40)-C(41)-H(41A)	119.0	H(10F)-C(102)-H(10G)	109.5
O(11)-C(42)-O(12)	123.4(8)	N(100)-C(102)-H(10H)	109.5
O(11)-C(42)-C(39)	121.1(7)	H(10F)-C(102)-H(10H)	109.5
O(12)-C(42)-C(39)	112.3(8)	H(10G)-C(102)-H(10H)	109.5
O(11)-C(42)-O(204)	108.4(11)	C(111)-N(110)-C(110)	122.0(17)
O(12)-C(42)-O(204)	65.8(9)	C(111)-N(110)-C(112)	119.5(17)
C(39)-C(42)-O(204)	110.4(10)	C(110)-N(110)-C(112)	116.3(15)
O(14)-C(43)-O(15)	118.8(7)	O(110)-C(110)-N(110)	121.4(19)
O(14)-C(43)-C(44)	120.3(9)	O(110)-C(110)-H(11A)	119.3
O(15)-C(43)-C(44)	120.9(9)	N(110)-C(110)-H(11A)	119.3
O(14)-C(43)-Zn(2)	61.2(4)	N(110)-C(111)-H(11B)	109.5

N(110)-C(111)-H(11C)	109.5	N(110)-C(112)-H(11F)	109.5
H(11B)-C(111)-H(11C)	109.5	H(11E)-C(112)-H(11F)	109.5
N(110)-C(111)-H(11D)	109.5	N(110)-C(112)-H(11G)	109.5
H(11B)-C(111)-H(11D)	109.5	H(11E)-C(112)-H(11G)	109.5
H(11C)-C(111)-H(11D)	109.5	H(11F)-C(112)-H(11G)	109.5
N(110)-C(112)-H(11E)	109.5	C(42)-O(204)-O(12)	50.3(8)

Symmetry transformations used to generate equivalent atoms:
#1 x,y+1,z #2 -x-1,-y+4,-z #3 -x,-y+3,-z
#4 -x-1,-y+3,-z+1 #5 x,y-1,z

Table C.27. Anisotropic displacement parameters ($Å^2$x 10^3)for pcm-9(Cs) (**21**). The anisotropic displacement factor exponent takes the form: $-2p^2[h^2a^{*2}U^{11} + ... + 2 h k a^* b^* U^{12}]$.

	U^{11}	U^{22}	U^{33}	U^{23}	U^{13}	U^{12}
Zn(1)	44(1)	32(1)	30(1)	-2(1)	-3(1)	-8(1)
Zn(2)	41(1)	36(1)	28(1)	-1(1)	-3(1)	-11(1)
Zn(3)	46(1)	29(1)	29(1)	-4(1)	-8(1)	-7(1)
P(1)	46(1)	31(1)	26(1)	0(1)	0(1)	-12(1)
P(2)	50(1)	38(1)	23(1)	-5(1)	-2(1)	-16(1)
O(1)	46(2)	44(2)	28(2)	-3(2)	-3(2)	-6(2)
O(2)	41(2)	40(2)	32(2)	0(2)	-3(2)	-11(2)
O(3)	86(3)	37(2)	42(2)	2(2)	-4(2)	-24(2)
O(4)	74(3)	36(2)	44(2)	4(2)	-8(2)	-8(2)
O(5)	38(2)	41(2)	36(2)	3(2)	-4(2)	-8(2)
O(6)	54(2)	36(2)	36(2)	-2(2)	4(2)	-11(2)
O(7)	51(2)	41(2)	53(2)	-5(2)	6(2)	-15(2)
O(8)	39(2)	45(2)	43(2)	-10(2)	3(2)	-14(2)

O(9)	77(3)	52(3)	68(3)	-27(2)	1(3)	-18(2)
O(10)	71(3)	38(2)	65(3)	-10(2)	12(2)	-4(2)
O(11)	65(3)	49(2)	30(2)	0(2)	-5(2)	-13(2)
O(12)	134(7)	183(9)	79(5)	-4(5)	-18(4)	-58(6)
O(13)	44(2)	33(2)	27(2)	-1(2)	-3(2)	-11(2)
O(14)	63(3)	49(3)	86(4)	-10(3)	-20(3)	-7(2)
O(15)	81(4)	67(3)	62(3)	22(3)	-27(3)	-40(3)
C(1P)	59(4)	44(3)	41(3)	0(3)	1(3)	-25(3)
C(1)	48(3)	34(3)	26(3)	0(2)	-1(2)	-9(3)
C(2P)	47(3)	49(3)	39(3)	-6(3)	4(3)	-21(3)
C(2)	51(4)	46(3)	30(3)	-1(2)	5(2)	-11(3)
C(3)	39(3)	51(4)	37(3)	3(3)	-5(2)	-6(3)
C(4)	47(3)	35(3)	27(3)	1(2)	0(2)	-17(3)
C(5)	72(5)	84(5)	33(3)	-12(3)	-5(3)	22(4)
C(6)	70(5)	97(6)	36(4)	-6(4)	-10(3)	29(4)
C(7)	45(3)	40(3)	28(3)	0(2)	-3(2)	-20(3)
C(8)	43(3)	34(3)	26(3)	1(2)	-2(2)	-10(2)
C(9)	67(4)	37(3)	44(3)	2(3)	-21(3)	-18(3)
C(10)	65(4)	39(3)	47(3)	-1(3)	-13(3)	-21(3)
C(11)	50(3)	30(3)	38(3)	0(2)	4(3)	-12(3)
C(12)	65(4)	48(4)	38(3)	7(3)	-14(3)	-16(3)
C(13)	62(4)	41(3)	35(3)	1(2)	-13(3)	-22(3)
C(14)	52(4)	36(3)	38(3)	3(3)	4(3)	-6(3)
C(15)	48(3)	33(3)	25(3)	-2(2)	-4(2)	-13(2)
C(16)	57(4)	42(3)	48(3)	-16(3)	16(3)	-22(3)
C(17)	58(4)	38(3)	49(3)	-8(3)	8(3)	-23(3)
C(18)	44(3)	38(3)	22(2)	1(2)	-5(2)	-10(2)
C(19)	50(3)	35(3)	36(3)	-5(2)	-1(3)	-13(3)
C(20)	50(3)	42(3)	35(3)	2(2)	-1(2)	-20(3)
C(21)	40(3)	40(3)	31(3)	-1(2)	-6(2)	-11(3)
C(22)	40(3)	35(3)	30(3)	-7(2)	0(2)	-14(2)
C(23)	43(3)	35(3)	38(3)	-9(2)	5(2)	-8(3)
C(24)	44(3)	31(3)	46(3)	-9(2)	1(3)	-6(3)

C(25)	42(3)	40(3)	33(3)	-4(2)	-4(2)	-17(3)
C(26)	38(3)	41(3)	55(4)	-12(3)	11(3)	-7(3)
C(27)	52(4)	30(3)	49(3)	-4(2)	-2(3)	-9(3)
C(28)	45(3)	40(3)	35(3)	-7(2)	-1(2)	-15(3)
C(29)	52(3)	35(3)	32(3)	-4(2)	1(2)	-19(3)
C(30)	56(4)	42(3)	38(3)	-10(3)	-13(3)	-5(3)
C(31)	67(4)	43(4)	44(3)	-14(3)	-10(3)	-13(3)
C(32)	43(3)	39(3)	50(4)	-11(3)	5(3)	-16(3)
C(33)	95(6)	32(3)	71(5)	7(3)	-23(4)	-5(4)
C(34)	105(6)	38(3)	40(3)	-1(3)	-21(4)	-10(4)
C(35)	52(4)	41(4)	57(4)	-7(3)	9(3)	-19(3)
C(36)	64(4)	57(4)	26(3)	-10(3)	-2(3)	-16(3)
C(37)	81(5)	79(5)	35(3)	8(3)	-7(3)	-31(4)
C(38)	81(5)	70(5)	40(4)	-8(3)	6(3)	-35(4)
C(39)	59(5)	100(6)	54(4)	-27(4)	0(3)	-22(4)
C(40)	119(9)	400(30)	33(5)	28(8)	-12(5)	-138(13)
C(41)	105(8)	320(20)	42(5)	0(8)	-19(5)	-105(11)
C(42)	45(4)	164(10)	62(5)	-10(6)	-10(4)	-24(5)
C(43)	78(6)	72(6)	93(7)	17(5)	-34(5)	-24(5)
C(44)	158(11)	97(8)	127(9)	38(7)	-58(8)	-82(8)

Table C.28. Hydrogen coordinates (x 10^4) and isotropic displacement parameters ($Å^2$x 10^3) for pcm-9(Cs) (**21**).

	x	y	z	U(eq)
H(13)	-4262	16665	3152	43
H(1PA)	-5522	15793	-1556	70
H(1PB)	-5110	15127	-991	70
H(1PC)	-6317	16238	-1005	70
H(2PA)	-11408	13955	4037	66
H(2PB)	-11177	15025	3991	66
H(2PC)	-11282	14504	3453	66
H(2A)	-2517	15402	-270	54
H(3A)	-2521	15436	685	56
H(5A)	-6069	17784	673	95
H(6A)	-6105	17710	-267	104
H(9A)	-4126	18376	-893	59
H(10A)	-4734	20011	-1345	60
H(12A)	-6608	19167	-2419	63
H(13A)	-5980	17495	-1974	54
H(16A)	-2195	16945	-1378	58
H(17A)	-222	16098	-1826	57
H(19A)	-1026	13514	-1881	49
H(20A)	-3031	14373	-1429	50
H(23A)	-9804	15818	3533	49
H(24A)	-8609	16710	3078	51
H(26A)	-5681	13933	2766	57
H(27A)	-6851	13031	3209	55
H(30A)	-9855	13122	2807	59
H(31A)	-9041	11633	2305	64
H(33A)	-6871	9979	3540	86

H(34A)	-7684	11435	4055	79
H(37A)	-10175	13106	4849	79
H(38A)	-9340	12785	5743	74
H(40A)	-6309	13423	5163	210
H(41A)	-7048	13605	4280	177
H(44A)	-2485	12358	3326	176
H(44B)	-2953	12130	2772	176
H(44C)	-1468	11949	2825	176
H(10B)	-3488	8760	479	229
H(10C)	-771	6946	1086	184
H(10D)	-1661	8162	1151	184
H(10E)	-2314	7326	1151	184
H(10F)	-77	6490	392	527
H(10G)	-1148	6547	-16	527
H(10H)	-402	7321	-121	527
H(11A)	2023	7948	1538	151
H(11B)	-864	9433	2202	251
H(11C)	231	8269	2267	251
H(11D)	623	9262	2237	251
H(11E)	-452	9556	868	349
H(11F)	-1555	9666	1334	349
H(11G)	-738	10385	1322	349

Table C.29. Crystal data and structure refinement for Nd-PCM-21 (**23**).

Identification code	sh11027
Empirical formula	C88 H60 Cl N0 Nd3 O28.50 P4
Formula weight	2165.41
Temperature	293(2) K
Wavelength	0.71075 Å
Crystal system	Trigonal
Space group	R -3 c :H

Unit cell dimensions	a = 14.157(3) Å	a= 90°.
	b = 14.157(3) Å	b= 90°.
	c = 104.37(3) Å	g = 120°.
Volume	18116(9) $Å^3$	
Z	6	
Density (calculated)	1.191 Mg/m^3	
Absorption coefficient	1.404 mm^{-1}	
F(000)	6438	
Crystal size	0.150 x 0.250 x 0.090 mm^3	
Theta range for data collection	3.514 to 24.997°.	
Index ranges	-13<=h<=16, -13<=k<=12, -67<=l<=123	
Reflections collected	14867	
Independent reflections	3526 [R(int) = 0.0817]	
Completeness to theta = 24.997°	99.1 %	
Refinement method	Full-matrix least-squares on F^2	
Data / restraints / parameters	3526 / 0 / 195	
Goodness-of-fit on F^2	1.101	
Final R indices [I>2sigma(I)]	R1 = 0.0890, wR2 = 0.2768	
R indices (all data)	R1 = 0.1177, wR2 = 0.3027	
Extinction coefficient	n/a	
Largest diff. peak and hole	1.464 and -1.658 $e.Å^{-3}$	

Table C.30. Atomic coordinates (x 10^4) and equivalent isotropic displacement parameters ($Å^2$x 10^3) for Nd-PCM-21 (**23**). U(eq) is defined as one third of the trace of the orthogonalized U^{ij} tensor.

	x	y	z	U(eq)
Nd(1)	0	0	0	42(1)
Nd(2)	0	0	375(1)	42(1)
P(1)	-3333	3333	369(1)	50(1)
P(2)	3333	6667	715(1)	43(1)
O(1)	-1662(5)	221(6)	61(1)	62(2)
O(2)	-338(5)	965(5)	203(1)	48(1)
O(3)	123(5)	1384(4)	536(1)	44(1)
O(4)	1497(5)	1922(5)	401(1)	51(2)
CP1	-3333	3333	541(2)	57(5)
C(1)	-2741(7)	2551(7)	311(1)	51(2)
C(2)	-3230(11)	1828(14)	211(2)	118(6)
CP2	3333	6667	887(2)	51(4)
C(3)	-2705(11)	1302(15)	161(1)	130(7)
C(4)	-1751(7)	1417(7)	214(1)	49(2)
C(5)	-1378(12)	2061(12)	313(1)	99(5)
C(6)	-1859(12)	2634(12)	365(1)	97(5)
C(7)	-1249(8)	818(8)	156(1)	50(2)
C(8)	2689(7)	5293(7)	655(1)	45(2)
C(9)	1650(8)	4521(7)	699(1)	52(2)
C(10)	1115(8)	3501(7)	647(1)	47(2)
C(11)	1624(7)	3215(8)	551(1)	45(2)
C(12)	2639(8)	3969(8)	509(1)	67(3)
C(13)	3182(8)	5027(8)	559(1)	60(3)
C(14)	1064(7)	2094(8)	492(1)	45(2)
Cl(1)	1820(20)	8230(20)	174(3)	135(11)
O(50)	5310(30)	4580(30)	599(4)	106(13)
O(51)	6667	5490(30)	833	148(12)

O(52)	3280(50)	1900(50)	672(6)	159(19)

Table C.31. Bond lengths [Å] and angles [°] for Nd-PCM-21 (**23**).

Nd(1)-O(1)#1	2.604(6)	P(1)-C(1)#7	1.797(10)
Nd(1)-O(1)#2	2.604(6)	P(1)-C(1)	1.797(10)
Nd(1)-O(1)#3	2.604(6)	P(2)-C(8)	1.797(9)
Nd(1)-O(1)#4	2.604(6)	P(2)-C(8)#8	1.797(9)
Nd(1)-O(1)#5	2.604(6)	P(2)-C(8)#9	1.797(9)
Nd(1)-O(1)	2.604(6)	P(2)-CP2	1.802(16)
Nd(1)-O(2)	2.687(6)	O(1)-C(7)	1.238(11)
Nd(1)-O(2)#1	2.687(6)	O(2)-C(7)	1.295(11)
Nd(1)-O(2)#2	2.687(6)	O(3)-C(14)	1.287(10)
Nd(1)-O(2)#5	2.687(6)	O(4)-C(14)	1.223(10)
Nd(1)-O(2)#3	2.687(6)	CP1-HP1A	0.8200
Nd(1)-O(2)#4	2.687(6)	C(1)-C(6)	1.322(14)
Nd(2)-O(2)#4	2.445(6)	C(1)-C(2)	1.379(15)
Nd(2)-O(2)#2	2.445(6)	C(2)-C(3)	1.390(16)
Nd(2)-O(2)	2.445(6)	C(2)-H(2)	0.9300
Nd(2)-O(4)#4	2.491(6)	CP2-HP2A	0.8200
Nd(2)-O(4)#2	2.491(6)	C(3)-C(4)	1.389(15)
Nd(2)-O(4)	2.491(6)	C(3)-H(3)	0.9300
Nd(2)-O(3)	2.524(5)	C(4)-C(5)	1.307(14)
Nd(2)-O(3)#2	2.525(5)	C(4)-C(7)	1.480(14)
Nd(2)-O(3)#4	2.525(5)	C(5)-C(6)	1.404(16)
Nd(2)-C(14)	2.846(10)	C(5)-H(5)	0.9300
Nd(2)-C(14)#4	2.847(10)	C(6)-H(6)	0.9300
Nd(2)-C(14)#2	2.847(10)	C(8)-C(13)	1.379(12)
P(1)-CP1	1.793(17)	C(8)-C(9)	1.399(12)
P(1)-C(1)#6	1.797(10)	C(9)-C(10)	1.361(12)

C(9)-H(9)	0.9300	O(1)#4-Nd(1)-O(2)#1	106.9(2)
C(10)-C(11)	1.405(11)	O(1)#5-Nd(1)-O(2)#1	111.5(2)
C(10)-H(10)	0.9300	O(1)-Nd(1)-O(2)#1	68.5(2)
C(11)-C(12)	1.368(12)	O(2)-Nd(1)-O(2)#1	115.4(2)
C(11)-C(14)	1.506(13)	O(1)#1-Nd(1)-O(2)#2	131.0(2)
C(12)-C(13)	1.400(13)	O(1)#2-Nd(1)-O(2)#2	49.0(2)
C(12)-H(12)	0.9300	O(1)#3-Nd(1)-O(2)#2	106.9(2)
C(13)-H(13)	0.9300	O(1)#4-Nd(1)-O(2)#2	73.1(2)
		O(1)#5-Nd(1)-O(2)#2	68.5(2)
O(1)#1-Nd(1)-O(1)#2	180.0(5)	O(1)-Nd(1)-O(2)#2	111.5(2)
O(1)#1-Nd(1)-O(1)#3	114.18(12)	O(2)-Nd(1)-O(2)#2	64.6(2)
O(1)#2-Nd(1)-O(1)#3	65.82(12)	O(2)#1-Nd(1)-O(2)#2	180.0(3)
O(1)#1-Nd(1)-O(1)#4	65.82(12)	O(1)#1-Nd(1)-O(2)#5	73.1(2)
O(1)#2-Nd(1)-O(1)#4	114.18(12)	O(1)#2-Nd(1)-O(2)#5	106.9(2)
O(1)#3-Nd(1)-O(1)#4	180.0(4)	O(1)#3-Nd(1)-O(2)#5	111.5(2)
O(1)#1-Nd(1)-O(1)#5	114.18(12)	O(1)#4-Nd(1)-O(2)#5	68.5(2)
O(1)#2-Nd(1)-O(1)#5	65.82(12)	O(1)#5-Nd(1)-O(2)#5	49.0(2)
O(1)#3-Nd(1)-O(1)#5	114.18(12)	O(1)-Nd(1)-O(2)#5	131.0(2)
O(1)#4-Nd(1)-O(1)#5	65.82(12)	O(2)-Nd(1)-O(2)#5	180.00(15)
O(1)#1-Nd(1)-O(1)	65.83(12)	O(2)#1-Nd(1)-O(2)#5	64.6(2)
O(1)#2-Nd(1)-O(1)	114.17(12)	O(2)#2-Nd(1)-O(2)#5	115.4(2)
O(1)#3-Nd(1)-O(1)	65.83(12)	O(1)#1-Nd(1)-O(2)#3	111.5(2)
O(1)#4-Nd(1)-O(1)	114.17(12)	O(1)#2-Nd(1)-O(2)#3	68.5(2)
O(1)#5-Nd(1)-O(1)	180.0	O(1)#3-Nd(1)-O(2)#3	49.0(2)
O(1)#1-Nd(1)-O(2)	106.9(2)	O(1)#4-Nd(1)-O(2)#3	131.0(2)
O(1)#2-Nd(1)-O(2)	73.1(2)	O(1)#5-Nd(1)-O(2)#3	73.1(2)
O(1)#3-Nd(1)-O(2)	68.5(2)	O(1)-Nd(1)-O(2)#3	106.9(2)
O(1)#4-Nd(1)-O(2)	111.5(2)	O(2)-Nd(1)-O(2)#3	115.4(2)
O(1)#5-Nd(1)-O(2)	131.0(2)	O(2)#1-Nd(1)-O(2)#3	64.6(2)
O(1)-Nd(1)-O(2)	49.0(2)	O(2)#2-Nd(1)-O(2)#3	115.4(2)
O(1)#1-Nd(1)-O(2)#1	49.0(2)	O(2)#5-Nd(1)-O(2)#3	64.6(2)
O(1)#2-Nd(1)-O(2)#1	131.0(2)	O(1)#1-Nd(1)-O(2)#4	68.5(2)
O(1)#3-Nd(1)-O(2)#1	73.1(2)	O(1)#2-Nd(1)-O(2)#4	111.5(2)

O(1)#3-Nd(1)-O(2)#4	131.0(2)	O(4)#4-Nd(2)-O(3)#2	129.40(18)
O(1)#4-Nd(1)-O(2)#4	49.0(2)	O(4)#2-Nd(2)-O(3)#2	52.28(18)
O(1)#5-Nd(1)-O(2)#4	106.9(2)	O(4)-Nd(2)-O(3)#2	75.9(2)
O(1)-Nd(1)-O(2)#4	73.1(2)	O(3)-Nd(2)-O(3)#2	80.23(18)
O(2)-Nd(1)-O(2)#4	64.6(2)	O(2)#4-Nd(2)-O(3)#4	90.80(19)
O(2)#1-Nd(1)-O(2)#4	115.4(2)	O(2)#2-Nd(2)-O(3)#4	150.7(2)
O(2)#2-Nd(1)-O(2)#4	64.6(2)	O(2)-Nd(2)-O(3)#4	125.9(2)
O(2)#5-Nd(1)-O(2)#4	115.4(2)	O(4)#4-Nd(2)-O(3)#4	52.28(18)
O(2)#3-Nd(1)-O(2)#4	180.0(5)	O(4)#2-Nd(2)-O(3)#4	75.9(2)
O(2)#4-Nd(2)-O(2)#2	72.0(2)	O(4)-Nd(2)-O(3)#4	129.40(18)
O(2)#4-Nd(2)-O(2)	72.0(2)	O(3)-Nd(2)-O(3)#4	80.23(18)
O(2)#2-Nd(2)-O(2)	72.0(2)	O(3)#2-Nd(2)-O(3)#4	80.23(18)
O(2)#4-Nd(2)-O(4)#4	76.6(2)	O(2)#4-Nd(2)-C(14)	155.3(2)
O(2)#2-Nd(2)-O(4)#4	139.0(2)	O(2)#2-Nd(2)-C(14)	99.1(2)
O(2)-Nd(2)-O(4)#4	73.75(19)	O(2)-Nd(2)-C(14)	83.4(2)
O(2)#4-Nd(2)-O(4)#2	73.75(19)	O(4)#4-Nd(2)-C(14)	98.6(2)
O(2)#2-Nd(2)-O(4)#2	76.6(2)	O(4)#2-Nd(2)-C(14)	127.7(2)
O(2)-Nd(2)-O(4)#2	139.0(2)	O(4)-Nd(2)-C(14)	25.4(2)
O(4)#4-Nd(2)-O(4)#2	118.81(5)	O(3)-Nd(2)-C(14)	26.9(2)
O(2)#4-Nd(2)-O(4)	139.0(2)	O(3)#2-Nd(2)-C(14)	76.0(2)
O(2)#2-Nd(2)-O(4)	73.75(19)	O(3)#4-Nd(2)-C(14)	105.5(2)
O(2)-Nd(2)-O(4)	76.6(2)	O(2)#4-Nd(2)-C(14)#4	83.4(2)
O(4)#4-Nd(2)-O(4)	118.81(5)	O(2)#2-Nd(2)-C(14)#4	155.3(2)
O(4)#2-Nd(2)-O(4)	118.81(5)	O(2)-Nd(2)-C(14)#4	99.1(2)
O(2)#4-Nd(2)-O(3)	150.7(2)	O(4)#4-Nd(2)-C(14)#4	25.4(2)
O(2)#2-Nd(2)-O(3)	125.9(2)	O(4)#2-Nd(2)-C(14)#4	98.6(2)
O(2)-Nd(2)-O(3)	90.80(19)	O(4)-Nd(2)-C(14)#4	127.7(2)
O(4)#4-Nd(2)-O(3)	75.9(2)	O(3)-Nd(2)-C(14)#4	76.0(2)
O(4)#2-Nd(2)-O(3)	129.41(18)	O(3)#2-Nd(2)-C(14)#4	105.5(2)
O(4)-Nd(2)-O(3)	52.27(18)	O(3)#4-Nd(2)-C(14)#4	26.9(2)
O(2)#4-Nd(2)-O(3)#2	125.9(2)	C(14)-Nd(2)-C(14)#4	102.7(2)
O(2)#2-Nd(2)-O(3)#2	90.80(19)	O(2)#4-Nd(2)-C(14)#2	99.1(2)
O(2)-Nd(2)-O(3)#2	150.7(2)	O(2)#2-Nd(2)-C(14)#2	83.4(2)

O(2)-Nd(2)-C(14)#2	155.3(2)	C(3)-C(2)-H(2)	120.7
O(4)#4-Nd(2)-C(14)#2	127.7(2)	P(2)-CP2-HP2A	109.5
O(4)#2-Nd(2)-C(14)#2	25.4(2)	C(4)-C(3)-C(2)	122.5(10)
O(4)-Nd(2)-C(14)#2	98.6(2)	C(4)-C(3)-H(3)	118.7
O(3)-Nd(2)-C(14)#2	105.5(2)	C(2)-C(3)-H(3)	118.7
O(3)#2-Nd(2)-C(14)#2	26.9(2)	C(5)-C(4)-C(3)	115.1(10)
O(3)#4-Nd(2)-C(14)#2	76.0(2)	C(5)-C(4)-C(7)	125.6(9)
C(14)-Nd(2)-C(14)#2	102.7(2)	C(3)-C(4)-C(7)	119.3(9)
C(14)#4-Nd(2)-C(14)#2	102.7(2)	C(4)-C(5)-C(6)	124.6(11)
CP1-P(1)-C(1)#6	109.8(3)	C(4)-C(5)-H(5)	117.7
CP1-P(1)-C(1)#7	109.8(3)	C(6)-C(5)-H(5)	117.7
C(1)#6-P(1)-C(1)#7	109.1(3)	C(1)-C(6)-C(5)	119.5(10)
CP1-P(1)-C(1)	109.8(3)	C(1)-C(6)-H(6)	120.3
C(1)#6-P(1)-C(1)	109.1(3)	C(5)-C(6)-H(6)	120.3
C(1)#7-P(1)-C(1)	109.1(3)	O(1)-C(7)-O(2)	120.2(9)
C(8)-P(2)-C(8)#8	108.7(3)	O(1)-C(7)-C(4)	121.1(8)
C(8)-P(2)-C(8)#9	108.7(3)	O(2)-C(7)-C(4)	118.6(8)
C(8)#8-P(2)-C(8)#9	108.7(3)	O(1)-C(7)-Nd(1)	58.6(5)
C(8)-P(2)-CP2	110.3(3)	O(2)-C(7)-Nd(1)	62.6(5)
C(8)#8-P(2)-CP2	110.3(3)	C(4)-C(7)-Nd(1)	168.0(6)
C(8)#9-P(2)-CP2	110.3(3)	C(13)-C(8)-C(9)	120.1(9)
C(7)-O(1)-Nd(1)	97.5(6)	C(13)-C(8)-P(2)	119.7(7)
C(7)-O(2)-Nd(2)	130.2(6)	C(9)-C(8)-P(2)	119.9(6)
C(7)-O(2)-Nd(1)	92.1(5)	C(10)-C(9)-C(8)	120.7(8)
Nd(2)-O(2)-Nd(1)	99.2(2)	C(10)-C(9)-H(9)	119.6
C(14)-O(3)-Nd(2)	90.6(5)	C(8)-C(9)-H(9)	119.6
C(14)-O(4)-Nd(2)	93.8(5)	C(9)-C(10)-C(11)	119.5(9)
P(1)-CP1-HP1A	109.5	C(9)-C(10)-H(10)	120.2
C(6)-C(1)-C(2)	119.3(10)	C(11)-C(10)-H(10)	120.2
C(6)-C(1)-P(1)	120.7(8)	C(12)-C(11)-C(10)	119.9(9)
C(2)-C(1)-P(1)	119.9(8)	C(12)-C(11)-C(14)	118.8(8)
C(1)-C(2)-C(3)	118.5(11)	C(10)-C(11)-C(14)	121.3(8)
C(1)-C(2)-H(2)	120.7	C(11)-C(12)-C(13)	120.9(8)

C(11)-C(12)-H(12)	119.6	O(4)-C(14)-C(11)	118.5(8)
C(13)-C(12)-H(12)	119.6	O(3)-C(14)-C(11)	118.1(7)
C(8)-C(13)-C(12)	118.9(8)	O(4)-C(14)-Nd(2)	60.9(5)
C(8)-C(13)-H(13)	120.6	O(3)-C(14)-Nd(2)	62.5(4)
C(12)-C(13)-H(13)	120.6	C(11)-C(14)-Nd(2)	178.5(6)
O(4)-C(14)-O(3)	123.3(9)		

Symmetry transformations used to generate equivalent atoms:
#1 x-y,x,-z #2 -x+y,-x,z #3 y,-x+y,-z #4 -y,x-y,z
#5 -x,-y,-z #6 -x+y-1,-x,z #7 -y,x-y+1,z
#8 -x+y,-x+1,z #9 -y+1,x-y+1,z

Table C.32. Anisotropic displacement parameters ($Å^2$x 10^3)for Nd-PCM-21 (**23**). The anisotropic displacement factor exponent takes the form: $-2p^2[h^2a^{*2}U^{11} + ... + 2 h k a^* b^* U^{12}]$.

	U^{11}	U^{22}	U^{33}	U^{23}	U^{13}	U^{12}
Nd(1)	43(1)	43(1)	41(1)	0	0	22(1)
Nd(2)	41(1)	41(1)	42(1)	0	0	21(1)
P(1)	48(2)	48(2)	53(2)	0	0	24(1)
P(2)	45(2)	45(2)	37(2)	0	0	23(1)
O(1)	52(4)	70(5)	66(4)	-11(3)	-3(3)	32(4)
O(2)	41(3)	47(4)	58(3)	9(3)	1(3)	24(3)
O(3)	44(4)	33(3)	57(3)	5(2)	6(3)	22(3)
O(4)	42(4)	42(4)	58(4)	-2(3)	13(3)	12(3)
CP1	58(7)	58(7)	56(10)	0	0	29(4)
C(1)	46(6)	50(6)	61(5)	7(4)	7(4)	26(5)
C(2)	88(9)	168(15)	147(13)	-98(11)	-50(9)	99(11)
CP2	53(7)	53(7)	46(9)	0	0	27(3)
C(3)	81(9)	205(18)	133(12)	-118(12)	-55(8)	93(11)

C(4)	36(5)	42(5)	65(6)	0(4)	-2(4)	15(4)
C(5)	117(10)	114(10)	115(10)	-60(9)	-66(9)	94(9)
C(6)	113(10)	106(10)	118(10)	-64(8)	-63(8)	89(9)
C(7)	43(5)	50(6)	55(5)	1(4)	0(4)	21(5)
C(8)	56(6)	39(5)	43(4)	8(4)	6(4)	27(4)
C(9)	58(6)	42(5)	52(5)	-5(4)	6(4)	23(5)
C(10)	45(6)	50(6)	52(5)	7(4)	11(4)	27(5)
C(11)	45(6)	47(6)	47(5)	-1(4)	3(4)	25(5)
C(12)	57(7)	57(7)	71(6)	-15(5)	23(5)	15(5)
C(13)	44(6)	43(6)	81(7)	-4(5)	27(5)	12(5)
C(14)	34(5)	50(6)	52(5)	3(4)	1(4)	20(4)

Table C.33. Hydrogen coordinates (x 10^4) and isotropic displacement parameters ($Å^2$x 10^3) for Nd-PCM-21 (**23**).

	x	y	z	U(eq)
HP1A	-2705	3606	567	86
H(2)	-3895	1695	178	142
HP2A	2703	6331	913	76
H(3)	-3005	855	90	156
H(5)	-749	2146	352	119
H(6)	-1560	3068	438	116
H(9)	1320	4708	763	62
H(10)	419	2997	675	57
H(12)	2972	3776	445	81
H(13)	3864	5542	528	73

Table C.34. Crystal data and structure refinement for Fe-TCM-1 (**24**).

Identification code	SH16045	
Empirical formula	C12 H8 Fe N2 O4 S2	
Formula weight	364.17	
Temperature	100 K	
Wavelength	0.71073 Å	
Crystal system	Monoclinic	
Space group	P 21/n	
Unit cell dimensions	a = 3.6490(6) Å	a= 90°.
	b = 12.257(2) Å	b= 95.646(10)°.
	c = 13.661(3) Å	g = 90°.
Volume	608.02(19) $Å^3$	
Z	2	
Density (calculated)	1.989 Mg/m^3	
Absorption coefficient	1.601 mm^{-1}	
F(000)	368	
Crystal size	0.300 x 0.010 x 0.010 mm^3	
Theta range for data collection	3.647 to 25.179°.	
Index ranges	-3<=h<=4, -14<=k<=14, -15<=l<=16	
Reflections collected	5349	
Independent reflections	1076 [R(int) = 0.0848]	
Completeness to theta = 25.179°	98.2 %	
Refinement method	Full-matrix least-squares on F^2	
Data / restraints / parameters	1076 / 0 / 92	
Goodness-of-fit on F^2	1.062	
Final R indices [I>2sigma(I)]	R1 = 0.0515, wR2 = 0.1161	
R indices (all data)	R1 = 0.0730, wR2 = 0.1239	
Extinction coefficient	n/a	
Largest diff. peak and hole	0.702 and -0.539 $e.Å^{-3}$	

Table C.35. Atomic coordinates (x 10^4) and equivalent isotropic displacement parameters ($Å^2$x 10^3) for Fe-TCM-1 (**24**). U(eq) is defined as one third of the trace of the orthogonalized U^{ij} tensor.

	x	y	z	U(eq)
Fe(1)	0	0	0	12(1)
S(1)	4337(3)	-718(1)	-1169(1)	12(1)
O(1)	920(9)	-1375(3)	767(2)	15(1)
N(1)	4576(10)	-2667(3)	-1936(3)	12(1)
O(2)	2276(9)	-3026(3)	1360(2)	17(1)
C(2)	3860(13)	-2126(4)	-1105(3)	11(1)
C(3)	2825(12)	-2765(4)	-327(4)	11(1)
C(4)	2548(14)	-3884(4)	-457(4)	17(1)
C(5)	3201(16)	-4388(4)	-1327(4)	23(1)
C(6)	4268(14)	-3750(4)	-2063(4)	18(1)
C(7)	1973(13)	-2352(4)	676(4)	13(1)

Table C.36. Bond lengths [Å] and angles [°] for Fe-TCM-1 (**24**).

Fe(1)-O(1)	1.995(3)	N(1)-C(6)	1.342(6)
Fe(1)-O(1)#1	1.995(3)	N(1)-C(2)	1.363(6)
Fe(1)-S(1)	2.5146(13)	N(1)-H(1A)	0.8600
Fe(1)-S(1)#1	2.5146(13)	O(2)-C(7)	1.245(6)
Fe(1)-S(1)#2	2.6351(12)	C(2)-C(3)	1.401(6)
Fe(1)-S(1)#3	2.6351(12)	C(3)-C(4)	1.385(7)
S(1)-C(2)	1.738(5)	C(3)-C(7)	1.522(7)
S(1)-Fe(1)#4	2.6351(12)	C(4)-C(5)	1.381(7)
O(1)-C(7)	1.267(6)	C(4)-H(4A)	0.9300

C(5)-C(6)	1.360(7)
C(5)-H(5A)	0.9300
C(6)-H(6A)	0.9300
O(1)-Fe(1)-O(1)#1	180.0
O(1)-Fe(1)-S(1)	87.36(10)
O(1)#1-Fe(1)-S(1)	92.64(10)
O(1)-Fe(1)-S(1)#1	92.64(10)
O(1)#1-Fe(1)-S(1)#1	87.36(10)
S(1)-Fe(1)-S(1)#1	180.0
O(1)-Fe(1)-S(1)#2	96.75(10)
O(1)#1-Fe(1)-S(1)#2	83.25(10)
S(1)-Fe(1)-S(1)#2	90.21(4)
S(1)#1-Fe(1)-S(1)#2	89.79(4)
O(1)-Fe(1)-S(1)#3	83.25(10)
O(1)#1-Fe(1)-S(1)#3	96.75(10)
S(1)-Fe(1)-S(1)#3	89.79(4)
S(1)#1-Fe(1)-S(1)#3	90.21(4)
S(1)#2-Fe(1)-S(1)#3	180.00(7)
C(2)-S(1)-Fe(1)	104.08(16)
C(2)-S(1)-Fe(1)#4	112.18(16)
Fe(1)-S(1)-Fe(1)#4	90.21(4)
C(7)-O(1)-Fe(1)	141.6(3)
C(6)-N(1)-C(2)	124.6(4)
C(6)-N(1)-H(1A)	117.7
C(2)-N(1)-H(1A)	117.7
N(1)-C(2)-C(3)	116.6(4)
N(1)-C(2)-S(1)	114.4(3)
C(3)-C(2)-S(1)	129.0(4)
C(4)-C(3)-C(2)	118.6(5)
C(4)-C(3)-C(7)	115.2(4)
C(2)-C(3)-C(7)	126.2(4)
C(5)-C(4)-C(3)	122.4(5)
C(5)-C(4)-H(4A)	118.8
C(3)-C(4)-H(4A)	118.8
C(6)-C(5)-C(4)	117.7(5)
C(6)-C(5)-H(5A)	121.1
C(4)-C(5)-H(5A)	121.1
N(1)-C(6)-C(5)	120.0(5)
N(1)-C(6)-H(6A)	120.0
C(5)-C(6)-H(6A)	120.0
O(2)-C(7)-O(1)	124.0(4)
O(2)-C(7)-C(3)	116.4(4)
O(1)-C(7)-C(3)	119.6(4)

Symmetry transformations used to generate equivalent atoms:

#1 -x,-y,-z #2 x-1,y,z #3 -x+1,-y,-z #4 x+1,y,z

Table C.37. Anisotropic displacement parameters ($Å^2 x\ 10^3$)for Fe-TCM-1 (**24**). The anisotropic displacement factor exponent takes the form: $-2p^2[\ h^2 a^{*2} U^{11} + ... + 2\ h\ k\ a^*\ b^*\ U^{12}\ ]$.

	U^{11}	U^{22}	U^{33}	U^{23}	U^{13}	U^{12}
Fe(1)	9(1)	10(1)	15(1)	2(1)	0(1)	4(1)
S(1)	10(1)	10(1)	16(1)	1(1)	-1(1)	0(1)
O(1)	18(2)	8(2)	18(2)	1(2)	1(1)	3(1)
N(1)	11(2)	13(2)	13(2)	4(2)	0(2)	-2(2)
O(2)	24(2)	13(2)	14(2)	3(2)	3(2)	6(2)
C(3)	5(2)	9(2)	19(3)	0(2)	-1(2)	-1(2)
C(4)	17(3)	18(3)	14(3)	1(2)	1(2)	-4(2)
C(5)	31(3)	13(3)	24(3)	-3(3)	4(3)	-4(2)
C(6)	21(3)	18(3)	15(3)	-6(2)	-3(2)	-2(2)
C(7)	4(2)	19(3)	14(3)	1(2)	-1(2)	-3(2)

Table C.38. Hydrogen coordinates ($x\ 10^4$) and isotropic displacement parameters ($Å^2 x\ 10^3$) for Fe-TCM-1 (**24**).

	x	y	z	U(eq)
H(1A)	5276	-2288	-2414	15
H(4A)	1898	-4311	61	20
H(5A)	2921	-5138	-1407	27
H(6A)	4784	-4065	-2653	22

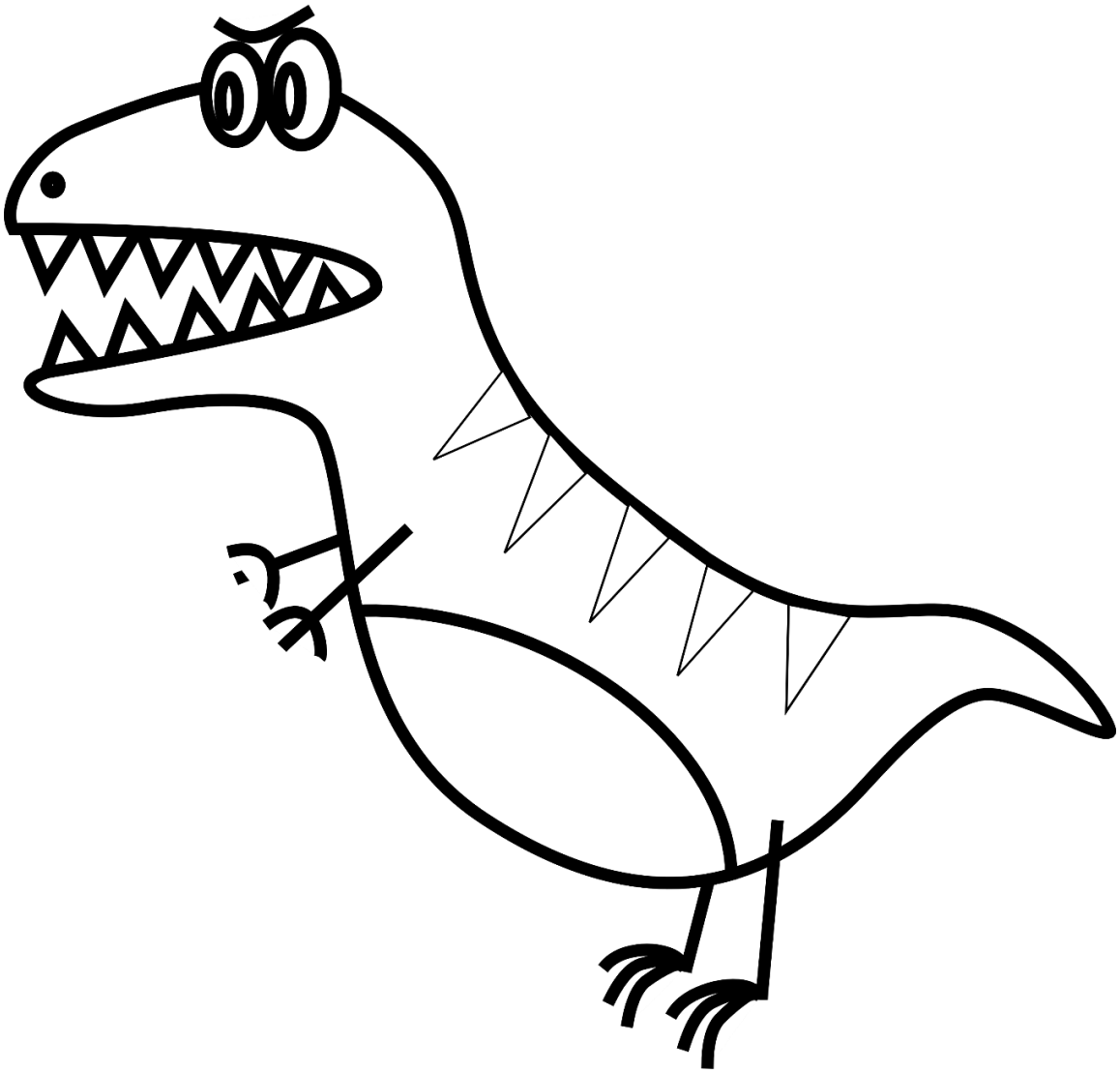

Figure A3.1. Tyranasourous rex coloring template (A realistic representation).

Bibliography

- Abdelhameed, R. M.; Carlos, L. D.; Silva, A. M. S.; Rocha, J. *Chem. Commun.* **2013**, *49* (44), 5019–5021.
- Abdur-Rashid, K.; Lough, A. J.; Morris, R. H. *Organometallics* **2000**, *19* (14), 2655–2657.

- Alduhaish, O.; Li, B.; Nesterov, V.; Chen, B. *Inorg Chem.* **2014**, *45*, 89-92.
- Alkordi, M. H.; Liu, Y.; Larsen, R. W.; Eubank, J. F.; Eddaoudi, M. *J. Am. Chem. Soc*. **2008**, *130* (38), 12639–12641.
- Allendorf, M. D.; Houk, R. J. T.; Andruszkiewicz, L.; Talin, A. A.; Pikarsky, J.; Choudhury, A.; Gall, K. A.; Hesketh, P. J. *J. Am. Chem. Soc.* **2008**, *130* (44), 14404–14405.
- Anwar, M. U.; Tandon, S. S.; Dawe, L. N.; Habib, F.; Murugesu, M.; Thompson, L. K. *Inorg. Chem.* **2012**, *51* (2), 1028–1034.
- Bailar Jr, J. C. *Prep. Inorg. React.* **1964**, *1*, 1-27.
- Bansal, R. C.; Goyal, M. *Activated Carbon Adsorption*; CRC Press, 2005.
- Barman, S.; Khutia, A.; Koitz, R.; Blacque, O.; Furukawa, H.; Iannuzzi, M.; Yaghi, O. M.; Janiak, C.; Hutter, J.; Berke, H. *J. Mater. Chem. A* **2014**, *2* (44), 18823–18830.
- Barman, S.; Khutia, A.; Koitz, R.; Blacque, O.; Furukawa, H.; Iannuzzi, M.; Yaghi, O. M.; Janiak, C.; Hutter, J.; Berke, H. *J. Mater. Chem. A* **2014**, *2*, 18823–18830.
- Bartolomé, E.; Bartolomé, J.; Arauzo, A.; Luzón, J.; Badía, L.; Cases, R.; Luis, F.; Melnic, S.; Prodius, D.; Shova, S.; Turta, C. *J. Mater. Chem. C* **2016**, *4* (22), 5038–5050.
- Batten, S. R.; Champness, N. R.; Chen, X.-M.; Garcia-Martinez, J.; Kitagawa, S.; Öhrström, L.; O'Keeffe, M.; Paik, S. M.; Reedijk, J. *Pure Appl. Chem.* **2013**, *85* (8), 1715–1724.
- Beck, J. S.; Vartuli, J. C.; Kennedy, G. J.; Kresge, C. T.; Roth, W. J.; Schramm, S. E. *Chem. Mater.* **1994**, *6* (10), 1816–1821.
- Benelli, C.; Gatteschi, D. *Introduction to Molecular Magnetism: From Transition Metals to Lanthanides*; John Wiley & Sons, **2015**.

- Bensch, W.; Sander, B.; Kremer, R. K.; Kockelmann, W. *J. Solid State Chem.* **2001**, *158* (2), 198–207.
- Bernt, S.; Guillerm, V.; Serre, C.; Stock, N. *Chem. Commun.* **2011**, *47* (10), 2838–2840.
- Bhunia, A.; Lan, Y.; Mereacre, V.; Gamer, M. T.; Powell, A. K.; Roesky, P. W. *Inorg. Chem.* **2011**, *50* (24), 12697–12704.
- Blanchard, G.; Maunaye, M.; Martin, G. *Water Res.* **1984**, *18* (12), 1501–1507.
- Bogani, L.; Wernsdorfer, W. *Nat Mater* **2008**, *7* (3), 179–186.
- Bohnsack, A. M. Novel Multifunctional Porous Coordination Polymers from Pre-synthetically Modified Organophosphorous Ligands, The University of Texas at Austin, TX, May 2015.
- Bohnsack, A. M.; Ibarra, I. A.; Bakhmutov, V. I.; Lynch, V. M.; Humphrey, S. M. *J. Am. Chem. Soc.* **2013**, *135* (43), 16038–16041.
- Bonaccorso, F.; Colombo, L.; Yu, G.; Stoller, M.; Tozzini, V.; Ferrari, A. C.; Ruoff, R. S.; Pellegrini, V. *Science* **2015**, *347* (6217), 1246501.
- Bowes, C. L.; Ozin, G. A. *Adv. Mater.* **1996**, *8* (1), 13–28.
- Brunauer, S.; Emmett, P. H.; Teller, E. *J. Am. Chem. Soc.* **1938**, *60* (2), 309–319.
- Canivet, J.; Vandichel, M.; Farrusseng, D. *Dalton Trans.* **2016**, *45* (10), 4090–4099.
- Casey, C. P.; Whiteker, G. T. *Isr. J. Chem.* **1990**, *30*, 299-304.
- Cavenati, S.; Grande, C. A.; Rodrigues, A. E. *J. Chem. Eng. Data* **2005**, *50*, 369-376.
- Cecen, F.; Aktas, Ö. *Activated Carbon for Water and Wastewater Treatment*: Integration of Adsorption and Biological Treatment; John Wiley & Sons, 2011.
- Čejka, J.; Morris, R. E.; Serrano, D. P. *Catal. Sci. Technol.* **2016**, *6* (8), 2465–2466.
- Cepeda, J.; Balda, R.; Beobide, G.; Castillo, O.; Fernández, J.; Luque, A.; Pérez-Yáñez, S.; Román, P.; Vallejo-Sánchez, D. *Inorg. Chem.* **2011**, *50* (17), 8437–8451.

- Chae, H. K.; Siberio-Pérez, D. Y.; Kim, J.; Go, Y.; Eddaoudi, M.; Matzger, A. J.; O'Keeffe, M.; Yaghi, O. M. *Nature* **2004**, *427* (6974), 523–527.
- Chang, G.; Wen, H.; Li, B.; Zhou, W.; Wang, H.; Alfooty, K.; Bao, Z.; Chen, B. *Cryst. Growth Des.* **2016**, *16* (6), 3395–3399.
- *Chapter 1: Crystal Growth and Nucleation*, Cubillas, P.; Anderson, M. W. In Zeolites and Catalysis; Čejka, J., Corma, A., Zones, S., Eds.; Wiley-VCH Verlag GmbH & Co. KGaA, 2010; pp 1–55.
- *Chemistry of Transition Metal Cyanide Compounds: Modern Perspectives - Progress in Inorganic Chemistry*, Volume 45, Dunbar, K.R.; Heintz, R. A., John Wiley & sons, Inc., 2007.
- Kardanpour, R.; Tangestaninejad, S.; Mirkhani, V.; Moghadam, M.; Mohammadpoor-Baltork, I.; Zadehahmadi, F. J. *Solid State Chem.* **2016**, *235*, 145–153.
- Chen, B.; Eddaoudi, M.; Reineke, T. M.; Kampf, J. W.; O'Keeffe, M.; Yaghi, O. M. *J. Am. Chem. Soc.* **2000**, *122* (46), 11559–11560.
- Chen, B.; Ockwig, N. W.; Millward, A. R.; Contreras, D. S.; Yaghi, O. M. *Angew. Chem., Int. Ed.* **2005**, *44* (30), 4745–4749.
- Chen, B.; Wang, L.; Zapata, F.; Qian, G.; Lobkovsky, E. B. *J. Am. Chem. Soc.* **2008**, *130* (21), 6718–6719.
- Chen, B.; Wang, X.; Zhang, Q.; Xi, X.; Cai, J.; Qi, H.; Shi, S.; Wang, J.; Yuan, D.; Fang, M. *J. Mater. Chem.* **2010**, *20* (18), 3758–3767.
- Chen, C. T.; Suslick, K. S. *Coord. Chem. Rev.* **1993**, *128* (1-2), 293-322.
- Chen, L.; Zheng, H.; Zhu, X.; Lin, Z.; Guo, L.; Qiu, B.; Chen, G.; Chen, Z.-N. The *Analyst* **2013**, *138* (12), 3490.
- Chen, M.; Zhao, H.; Sañudo, E. C.; Liu, C.-S.; Du, M. *Inorg. Chem.* **2016**, *55* (8), 3715–3717.

- Chen, Y.; Ma, S. *Rev. Inorg. Chem.* **2012**, *32* (2–4), 81–100.
- Chevreau, H.; Devic, T.; Salles, F.; Maurin, G.; Stock, N.; Serre, C. *Angew. Chem. Int. Ed.* **2013**, *52* (19), 5056–5060.
- Choi, H. J.; Suh, M. P. *J. Am. Chem. Soc.* **2004**, *126* (48), 15844–15851.
- Chorazy, S.; Rams, M.; Nakabayashi, K.; Sieklucka, B.; Ohkoshi, S. *Chem. Eur. J.* **2016**, *22* (22), 7371–7375.
- Christou, G.; Gatteschi, D.; Hendrickson, D. N.; Sessoli, R. *MRS Bullet.* **2000**, *25* (11), 66–71.
- Chui, S. S.-Y.; Lo, S. M.-F.; Charmant, J. P. H.; Orpen, A. G.; Williams, I. D. *Science* **1999**, *283* (5405), 1148–1150.
- Claus, P. *Appl. Catal., A* **2005**, *291* (1–2), 222–229.
- Clérac, R.; Miyasaka, H.; Yamashita, M.; Coulon, C. *J. Am. Chem. Soc.* **2002**, *124* (43), 12837–12844.
- Coe, B. J.; Chery, M.; Beddoes, R. L.; Hope, H.; White, P. S. *Dalton Trans.* **1996**, *No. 20*, 3917–3924.
- Comotti, A.; Bracco, S.; Sozzani, P.; Horike, S.; Matsuda, R.; Chen, J.; Takata, M.; Kubota, Y.; Kitagawa, S. *J. Am. Chem. Soc.* **2008**, *130* (41), 13664–13672.
- Cook, T. R.; Zheng, Y.-R.; Stang, P. J. *Chem. Rev.* **2013**, *113* (1), 734–777.
- Cooper, D. R.; D'Anjou, B.; Ghattamaneni, N.; Harack, B.; Hilke, M.; Horth, A.; Majlis, N.; Massicotte, M.; Vandsburger, L.; Whiteway, E.; Yu, V.; *Int. Scholarly Res. Not.* **2012**.
- Cooper, E. R.; Andrews, C. D.; Wheatley, P. S.; Webb, P. B.; Wormald, P.; Morris, R. E. *Nature* **2004**, *430* (7003), 1012–1016.
- Corma, A. *Chem. Rev*. **1997**, *97* (6), 2373–2420.
- Cormas, A.; García, H.; Llabrés i Xamena, F. X. *Chem. Rev.* **2010**, *110* (8), 4606–4655.

- Coronado, E.; Espallargas, G. M. *Chem. Soc. Rev.* **2013**, *42* (4), 1525–1539.
- Coronado, E.; Gaviña, P.; Tatay, S. *Chem. Soc. Rev.* **2009**, *38* (6), 1674–1689.
- Coronado, E.; Giménez-Marqués, M.; Mínguez Espallargas, G. *Inorg. Chem.* **2012**, *51* (7), 4403–4410.
- Cotton, S. *Lanthanide and Actinide Chemistry*; John Wiley & Sons: Hoboken, **2013**; 2-3.
- Coulon, C.; Miyasaka, H.; Clérac, R. *Single-Molecule Magnets and Related Phenomena*; Winpenny, R., Ed.; *Structure and Bonding*; Springer Berlin Heidelberg, **2006**; pp 163–206.
- Cui, Y.; Xu, H.; Yue, Y.; Guo, Z.; Yu, J.; Chen, Z.; Gao, J.; Yang, Y.; Qian, G.; Chen, B. *J. am. Chem. Soc.* **2012**, *134* (9), 3979–3982.
- Cui, Y.; Xu, H.; Yue, Y.; Guo, Z.; Yu, J.; Chen, Z.; Gao, J.; Yang, Y.; Qian, G.; Chen, B. *J. Am. Chem. Soc.* **2012**, *134* (9), 3979–3982.
- D'Alessandro, D. M.; Smit, B.; Long, J. R. *Angew. Chem., Int. Ed.* **2010**, *49* (35), 6058–6082.
- de Pater, J. J. M.; Maljaars, C. E. P.; de Wolf, E.; Lutz, M.; Spek, A. L.; Deelman, B.-J.; Elsevier, C. J.; van Koten, G. *Organometallics* **2005**, *24* (22), 5299–5310.
- Dhakshinamoorthy, A.; Garcia, H. *Chem. Soc. Rev.* **2012**, *41* (15), 5262–5284.
- Dietzel, P. D. C.; Georgiev, P. A.; Eckert, J.; Blom, R.; Strässle, T.; Unruh, T. *Chem. Commun.* **2010**, *46* (27), 4962–4964.
- Dincă, M.; Dailly, A.; Long, J. R. *Chem. Eur. J.* **2008**, *14* (33), 10280–10285.
- Ding, B.; Liu, S. X.; Cheng, Y.; Guo, C.; Wu, X. X.; Guo, J. H.; Liu, Y. Y.; Li, Y. *Inorg. Chem.* **2016**, *55* (9), 4391–4402.
- Ding, R.; Huang, C.; Lu, J.; Wang, J.; Song, C.; Wu, J.; Hou, H.; Fan, Y. *Inorg. Chem.* **2015**, *54* (4), 1405–1413.

- Dinh, T.-V.; Choi, I.-Y.; Son, Y.-S.; Kim, J.-C. *Sens. Actuators, B* **2016**, *231*, 529–538.
- Donahue, C. M.; McCollom, S. P.; Forrest, C. M.; Blake, A. V.; Bellott, B. J.; Keith, J. M.; Daly, S. R. *Inorg. Chem.* **2015**, *54* (12), 5646–5659.
- Douglas, P. G.; Feltham, R. D.; Metzger, H. G. *J. Chem. Soc. 1970*, *No. 14*, 889b–890.
- Drew, D.; Doyle, J. R.; Shaver, A. G. In *Inorganic Syntheses*; Angelici, R. J., Ed.; John Wiley & Sons, Inc., **1990**; pp 346–349.
- Driver, M. S.; Hartwig, J. F. *J. Am. Chem. Soc.* **1996**, *118* (30), 7217–7218.
- Drung, D.; Abmann, C.; Beyer, J.; Kirste, A.; Peters, M.; Ruede, F.; Schurig, T. *IEEE Trans. Appl. Supercond.* **2007**, *17* (2), 699–704.
- Du, M.; Jiang, X.-J.; Zhao, X.-J. *Inorg. Chem.* **2007**, *46* (10), 3984–3995.
- Du, P.-Y.; Gu, W.; Liu, X. *Inorg. Chem.* **2016**, *55* (16), 7826–7828.
- Duan, X.; Zhang, Q.; Cai, J.; Yang, Y.; Cui, Y.; He, Y.; Wu, C.; Krishna, R.; Chen, B.; Qian, G. *J. Mater. Chem. A* **2014**, *2* (8), 2628–2633.
- Dunning, S. D.; Nuñez, A. J.; Moore, M. D.; Waggoner, N. W.; Lytwak, L. A.; Steiner, A.; Lynch, V. M.; Holliday, B. J.; Humphrey, S. M. *J. Am. Chem. Soc.* **2016**, in draft.
- Eddaoudi, M.; Kim, J.; Rosi, N.; Vodak, D.; Wachter, J.; O'Keeffe, M.; Yaghi, O. M. *Science* **2002**, *295* (5554), 469–472.
- Emsley, J. Nature's Building Blocks: An A-Z Guide to the Elements; OUP Oxford, 2011.
- Falkowski, J. M.; Sawano, T.; Zhang, T.; Tsun, G.; Chen, Y.; Lockard, J. V.; Lin, W. *J. Am. Chem. Soc.* **2014**, *136* (14), 5213–5216.
- Fang, Q.; Zhu, G.; Xue, M.; Wang, Z.; Sun, J.; Qiu, S. *Cryst. Growth Des.* **2008**, *8* (1), 319–329.
- Fang, W.-H.; Cheng, L.; Huang, L.; Yang, G.-Y. *Inorg. Chem.* **2013**, *52* (1), 6–8.

- Faraday, M. *Experimental Researches in Chemistry and Physics*, Richard Taylor and William Francis: London, U.K., 1859.
- Farha, O. K.; Mulfort, K. L.; Hupp, J. T. *Inorg. Chem.* **2008**, *47* (22), 10223–10225.
- Farha, O. K.; Spokoyny, A. M.; Mulfort, K. L.; Hawthorne, M. F.; Mirkin, C. A.; Hupp, J. T. *J. Am. Chem. Soc.* **2007**, *129*, 12680-12681.
- Ferbinteanu, M.; Miyasaka, H.; Wernsdorfer, W.; Nakata, K.; Sugiura, K.; Yamashita, M.; Coulon, C.; Clérac, R. *J. Am. Chem. Soc.* **2005**, *127* (9), 3090–3099.
- Forman, G. S.; Ohkuma, T.; Hems, W. P.; Noyori, R. *Tetrahedron Lett.* **2000**, *41* (49), 9471–9475.
- Forrest, K. A.; Pham, T.; Georgiev, P. A.; Embs, J. P.; Waggoner, N. W.; Hogan, A.; Humphrey, S. M.; Eckert, J.; Space, B. *Chem. Mater.* **2015**, *27* (22), 7619–7626.
- Fuchikami, T.; Ohishi, K.; Ojima, I. *J. Org. Chem.* **1983**, *48* (21), 3803–3807.
- Fujita, M.; Kwon, Y. J.; Washizu, S.; Ogura, K. *J. Am. Chem. Soc.* **1994**, *116* (3), 1151–1152.
- Furukawa, H.; Ko, N.; Go, Y. B.; Aratani, N.; Choi, S. B.; Choi, E.; Yazaydin, A. Ö.; Snurr, R. Q.; O'Keeffe, M.; Kim, J.; Yaghi, O. M. *Science* **2010**, *329* (5990), 424–428.
- Gaffney, T. R. *Current Opinion in Solid State and Materials Science* **1996**, *1* (1), 69–75.
- Gatteschi, D.; Sessoli, R. *Angew. Chem., Int. Ed.* **2003**, *42* (3), 268–297.
- Gensow, M.-N. B.; Freixa, Z.; van Leeuwen, P. W. N. M. *Chem. Soc. Rev.* **2009**, *38* (4), 1099–1118.
- Goodenough, J. *Scholarpedia* **2008**, *3* (10), 7382.
- Gotthardt, M. A.; Grosjean, S.; Brunner, T. S.; Kotzel, J.; Gänzler, A. M.; Wolf, S.; Bräse, S.; Kleist, W. *Dalton Trans.* **2015**, *44* (38), 16802–16809.

- Gouma, P. -I., *Nanomaterials for Chemical Sensors and Biotechnology*, Pan Stanford Publishing, Singapore, 2009.
- Gründler, P., *Chemical Sensors*; Springer Berlin Heidelberg: Berlin, Heidelberg, 2007.
- Guo, Z.; Xu, H.; Su, S.; Cai, J.; Dang, S.; Xiang, S.; Qian, G.; Zhang, H.; O'Keeffe, M.; Chen, B. *Chem. Commun.* **2011**, *47* (19), 5551–5553.
- H. A. Kramers, *Physica,* **1934**, *1*, 182-192.
- Halder, G. J. *Science* **2002**, *298* (5599), 1762–1765.
- Hallman, P. S.; Stephenson, T. A.; Wilkinson, G. In *Inorganic Syntheses*; Parry, R. W., Ed.; John Wiley & Sons, Inc., **1970**; pp 237–240.
- Hamann, B. C.; Hartwig, J. F. *J. Am. Chem. Soc.* **1997**, *119* (50), 12382–12383.
- Haque, E.; Khan, N. A.; Park, J. H.; Jhung, S. H. *Chem. Eur. J.* **2010**, *16* (3), 1046–1052.
- Harbuzaru, B. V.; Corma, A.; Rey, F.; Atienzar, P.; Jordá, J. L.; García, H.; Ananias, D.; Carlos, L. D.; Rocha, J. *Angew. Chem., Int. Ed.* **2008**, *47* (6), 1080–1083.
- Harbuzaru, B. V.; Corma, A.; Rey, F.; Jordá, J. L.; Ananias, D.; Carlos, L. D.; Rocha, J. *Angew. Chem., Int. Ed.* **2009**, *48* (35), 6476–6479.
- Hausdorf, S.; Baitalow, F.; Böhle, T.; Rafaja, D.; Mertens, F. O. R. L. *J. Am. Chem. Soc.* **2010**, *132* (32), 10978–10981.
- He, J.; Waggoner, N. W.; Dunning, S. D.; Stiener, A.; Lynch, V. M.; Humphrey, S. M. *Angew. Chem., Int. Ed.* **2016**, accepted.
- He, Y.; Xiang, S.; Zhang, Z.; Xiong, S.; Fronczek, F. R.; Krishna, R.; O'Keeffe, M.; Chen, B. *Chem. Commun.* **2012**, *48* (88), 10856–10858.
- Henschke, J. P.; Burk, M. J.; Malan, C. G.; Herzberg, D.; Peterson, J. A.; Wildsmith, A. J.; Cobley, C. J.; Casy, G. *Adv. Synth. Catal.* **2003**, *345* (1–2), 300–307.
- Herrmann, J.-M. *Top. Catal.* **2005** *34* (1–4), 49–65.

- Horike, S.; Dincă, M.; Tamaki, K.; Long, J. R. *J. Am. Chem. Soc.* **2008**, *130* (18), 5854–5855.
- Hoskins, B. F.; Robson, R. *J. Am. Chem. Soc.* **1989**, *111* (15), 5962–5964.
- Hosseini, H.; Ahmar, H.; Dehghani, A.; Bagheri, A.; Tadjarodi, A.; Fakhari, A. R. *Biosens. Bioelectron.* **2013**, *42*, 426–429.
- Hu, A.; Ngo, H. L.; Lin, W. *J. Am. Chem. Soc.* **2003**, *125* (38), 11490–11491.
- Hu, Y.; Ding, M.; Liu, X.-Q.; Sun, L.-B.; Jiang, H.-L. *Chem. Commun.* **2016**, *52* (33), 5734–5737.
- Huang, X.-C.; Lin, Y.-Y.; Zhang, J.-P.; Chen, X.-M. *Angew. Chem., Int. Ed.* **2006**, *45* (10), 1557–1559.
- Huang, Y.-G.; Jiang, F.-L.; Hong, M.-C. *Coord. Chem. Rev.* **2009**, *253* (23–24), 2814–2834.
- Humphrey, S. M.; Allan, P. K.; Oungoulian, S. E.; Ironside, M. S.; Wise, E. R. *Dalton Trans.* **2009**, *No. 13*, 2298–2305.
- *Hysteresis in Magnetism: For Physicists, Materials Scientists, and Engineers*, Bertotti, G.; Gulf Professional Publishing USA, **1998**.
- Ibarra, I. A.; Tan, K. E.; Lynch, V. M.; Humphrey, S. M., *Dalton Trans.* **2012**, *41* (14), 3920–3923.
- Ibarra, I. A.; Yoon, J. W.; Chang, J.-S.; Lee, S. K.; Lynch, V. M.; Humphrey, S. M. *Inorg. Chem.* **2012**, *51* (22), 12242–12247.
- Ishikawa, N.; Sugita, M.; Ishikawa, T.; Koshihara, S.; Kaizu, Y. *J. Am. Chem. Soc.* **2003**, *125* (29), 8694–8695.
- Ishiyama, T.; Murata, M.; Miyaura, N. *J. Org. Chem.* **1995**, *60* (23), 7508–7510.
- Issleib, K; Müller D. W. *Chem. Ber.* **1959**, *92*, 3175-3182.

- Jackson, S. L.; Rananaware, A.; Rix, C.; Bhosale, S. V.; Latham, K. *RSC Adv.* **2015**, *5* (102), 84134–84141.
- Jami, A. K.; Baskar, V.; Sañudo, E. C. *Inorg. Chem.* **2013**, *52* (5), 2432–2438.
- Jessop, P. G.; Hsiao, Y.; Ikariya, T.; Noyori, R. *J. Am. Chem. Soc.* **1996**, *118* (2), 344–355.
- Jessop, P. G.; Ikariya, T.; Noyori, R. *Chem. Rev.* **1995**, *95* (2), 259–272.
- Jiang, D.; Keenan, L. L.; Burrows, A. D.; Edler, J. *Chem. Commun.* **2012**, *48* (99), 12053-12055.
- Jiang, H.-L.; Akita, T.; Ishida, T.; Haruta, M.; Xu, Q. *J. Am. Chem. Soc.* **2011**, *133* (5), 1304–1306.
- Jiang, J.-J.; Pan, M.; Liu, J.-M.; Wang, W.; Su, C. *Inorg. Chem.* **2010**, *49* (21), 10166–10173.
- Jiang, M.; Ning, P.; Wang, Z. H.; Bai, Y. W.; Chen, W.; Zhang, W.; Wang, R. B. *Adv. Mater. Res.* **2012**, *476–478*, 1862–1866.
- Jiang, N.; Ragauskas, A. J. *Tetrahedron Let.* **2006**, *47* (2), 197–200.
- Jiang, Z.-X.; Liu, J.-L.; Chen, Y.-C.; Liu, J.; Jia, J.-H.; Tong, M.-L. *Chem. Commun.* **2016**, *52* (37), 6261–6264.
- Julien, P. A.; Užarević, K.; Katsenis, A. D.; Kimber, S. A. J.; Wang, T.; Farha, O. K.; Zhang, Y.; Casaban, J.; Germann, L. S.; Etter, M.; Dinnebier, R. E.; James, S. L.; Halasz, I.; Friščić, T. *J. Am. Chem. Soc.* **2016**, *138* (9), 2929–2932.
- Kaczmarek, S. M.; Tomaszewicz, E.; Moszyński, D.; Jasik, A.; Leniec, G. *Mat. Chem. Phys.* **2010**, *124* (1), 646–651.
- Kagan, H. B.; Dang-Tuan-Phat. *J. Am. Chem. Soc.* **1972**, *94* (18), 6429–6433.
- Kahn, O. *Molecular magnetism*, Wiley-VCH, Chichester, **1993**.

- Kahrovic, E.; Orioli, P.; Bruni, B.; Di Vaira, M.; Messori, L. *Inorg. Chim. Acta* **2003**, *355*, 420–423.
- Kajiwara, T.; Nakano, M.; Kaneko, Y.; Takaishi, S.; Ito, T.; Yamashita, M.; Igashira-Kamiyama, A.; Nojiri, H.; Ono, Y.; Kojima, N. *J. Am. Chem. Soc.* **2005**, *127* (29), 10150–10151.
- Kaltsoyannis, N. *J. Chem. Soc., Dalton Trans.* **1997**, No. 1, 1–12.
- Kandiah, M.; Nilsen, M. H.; Usseglio, S.; Jakobsen, S.; Olsbye, U.; Tilset, M.; Larabi, C.; Quadrelli, E. A.; Bonino, F.; Lillerud, K. P. *Chem. Mater.* **2010**, *22* (24), 6632–6640.
- Kesanli, B.; Cui, Y.; Smith, M. R.; Bittner, E. W.; Bockrath, B. C.; Lin, W. *Angew. Chem., Int. Ed.* **2005**, *44* (1), 72–75.
- Khoshaman, A. H.; Bahreyni, B. *Sens. Actuators, B* **2012**, *162* (1), 114–119.
- Kim, H.-J.; Kang, B.-S.; Kim, M.-J.; Park, Y. M.; Kim, D.-K.; Lee, J.-S.; Lee, K.-Y. *Catal. Today* **2004**, *93–95*, 315–320.
- Kitagawa, S.; Kitaura, R.; Noro, S. *Angew. Chem., Int. Ed.* **2004**, *43* (18), 2334–2375.
- Knowles, W. S. *Angew. Chem., Int. Ed.* **2002**, *41* (12), 1998–2007.
- Ko, N.; Choi, P. G.; Hong, J.; Yeo, M.; Sung, S.; Cordova, K. E.; Park, H. J.; Yang, J. K.; Kim, J. *J. Mater. Chem. A* **2015**, *3* (5), 2057–2064.
- Kobalz, M.; Lincke, J.; Kobalz, K.; Erhart, O.; Bergmann, J.; Lässig, D.; Lange, M.; Möllmer, J.; Gläser, R.; Staudt, R.; Krautscheid, H. *Inorg. Chem.* **2016**, *55* (6), 3030–3039.
- Kodama, R. H. *Magn. Magn. Mater.* **1999**, *200*, 359-372.
- Korotcenkov, G. *Chemical Sensors: Comprehensive Sensor Technologies*, Vol 6, Chemical Sensors Applications; Momentum Press: New York, 2011**.**
- Kreno, L. E.; Hupp, J. T.; Van Duyne, R. P. *Anal. Chem.* **2010**, *82* (19), 8042–8046.

- Kreno, L. E.; Leong, K.; Farha, O. K.; Allendorf, M.; Van Duyne, R. P.; Hupp, J. T. *Chem. Rev.* **2012**, *112* (2), 1105–1125.
- Kröcher, O.; Köppel, R. A.; Baiker, A. *Chem. Commun.* **1997**, *No. 5*, 453–454.
- Kubas, G. J.; Ryan, R. R.; Swanson, B. I.; Vergamini, P. J.; Wasserman, H. J. *J. Am. Chem. Soc.* **1984**, *106* (2), 451–452.
- Kuznetsov, D. A.; Fedyanin, I. V.; Komarova, N. S.; Shilov, G. V.; Martynenko, V. M.; Vasilev, S. G.; Krivenko, A. G.; Lyssenko, K. A.; Bazhenova, T. A. *Eur. J. Inorg. Chem.* **2015** (*4*), 715–724.
- Landau, S. E.; Morris, R. H.; Lough, A. J. *Inorg. Chem.* **1999**, *38* (26), 6060–6068.
- *Lanthanides and actinides in molecular magnetism*, First edition.; Layfield, R. A., Murugesu, M., Eds.; Wiley-VCH Verlag GmbH & Co. KGaA: Weinheim, Germany, **2015**.
- Layfield, R. A. *Organometallics* **2014**, *33* (5), 1084–1099.
- Lebernegg, S.; Schmitt, M.; Tsirlin, A. A.; Janson, O.; Rosner, H. *Phys. Rev. B* **2013**, *87* (15), 155111.
- Lee, C. Y.; Farha, O. K.; Hong, B. J.; Sarjeant, A. A.; Nguyen, S. T.; Hupp, J. T. *J. Am. Chem. Soc.* **2011**, *133* (40), 15858–15861.
- Lee, D.-H.; Patel, B. P.; Crabtree, R. H.; Clot, E.; Eisenstein, O. *Chem. Commun.* **1999**, *No. 3*, 297–298.
- Lee, J.; Farha, O. K.; Roberts, J.; Scheidt, K. A.; Nguyen, S. T.; Hupp, J. T. *Chem. Soc. Rev.* **2009**, *38* (5), 1450–1459.
- Li, B.; Zhang, Z.; Li, Y.; Yao, K.; Zhu, Y.; Deng, Z.; Yang, F.; Zhou, X.; Li, G.; Wu, H.; Nijem, N.; Chabal, Y. J.; Lai, Z.; Han, Y.; Shi, Z.; Feng, S.; Li, J. *Angew. Chem. Int. Ed.* **2012**, *51* (6), 1412–1415.

- Li, H.-Y.; Wei, Y.-L.; Dong, X.-Y.; Zang, S.-Q.; Mak, T. C. W. *Chem. Mater.* **2015**, *27* (4), 1327–1331.
- Li, J.-R.; Kuppler, R. J.; Zhou, H.-C. *Chem. Soc. Rev.* **2009**, *38* (5), 1477–1504.
- Li, J.-R.; Ma, Y.; McCarthy, M. C.; Sculley, J.; Yu, J.; Jeong, H.-K.; Balbuena, P. B.; Zhou, H.-C. *Coord. Chem. Rev.* **2011**, *255* (15–16), 1791–1823.
- Li, M.-X.; Zhang, Y.-F.; He, X.; Shi, X.-M.; Wang, Y.-P.; Shao, M.; Wang, Z.-X. *Cryst.Growth Des.* **2016**, *16* (5), 2912–2922.
- Li, Y.; Xue, M.; Guo, L.; Huang, L.; Chen, S.; Qiu, S. *Inorg. Chem. Commun.* **2013**, *28*, 25–30.
- Li, Y.; Zhang, S.; Song, D. *Angew. Chem. Int. Ed.* **2013**, *52* (2), 710–713.
- Liang, L.-L.; Ren, S.-B.; Zhang, J.; Li, Y.-Z.; Du, H.-B.; You, X.-Z. *Dalton Trans.* **2010**, *39* (33), 7723.
- Lin, Y.; Kong, C.; Chen, L. *RSC Adv.* **2016**, *6* (39), 32598–32614.
- Lin, Y.-C.; Huber, G. W. *Energy Environ. Sci.* **2008**, *2* (1), 68–80.
- Lisnyi, B.; Strečka, J. *J. Magn. Magn. Mater.* **2015**, *377*, 502–510.
- Liu, B.; Shioyama, H.; Akita, T.; Xu, Q. *J. Am. Chem. Soc.* **2008**, *130* (16), 5390–5391.
- Liu, D.; Wu, H.; Wang, S.; Xie, Z.; Li, J.; Lin, W. *Chem. Sci.* **2012**, *3* (10), 3032–3037.
- Liu, J.; Chen, L.; Cui, H.; Zhang, J.; Zhang, L.; Su, C.-Y. *Chem. Soc. Rev.* **2014**, *43* (16), 6011–6061.
- Liu, K.; Li, H.; Zhang, X.; Shi, W.; Cheng, P. *Inorg. Chem.* **2015**, *54* (21), 10224–10231.
- Liu, K.; Zhang, X.; Meng, X.; Shi, W.; Cheng, P.; Powell, A. K. *Chem. Soc. Rev.* **2016**, *45* (9), 2423–2439.
- Liu, Y.; Eubank, J. F.; Cairns, A. J.; Eckert, J.; Kravtsov, V. C.; Luebke, R.; Eddaoudi, M. *Angew. Chem., Int. Ed.* **2007**, *46* (18), 3278–3283.

- Liu, Y.; Kravtsov, V. C.; Eddaoudi, M. *Angew. Chem., Int. Ed.,* **2008**, *47* (44), 8446–8449.
- Lu, G.; Li, S.; Guo, Z.; Farha, O. K.; Hauser, B. G.; Qi, X.; Wang, Y.; Wang, X.; Han, S.; Liu, X.; DuChene, J. S.; Zhang, H.; Zhang, Q.; Chen, X.; Ma, J.; Loo, S. C. J.; Wei, W. D.; Yang, Y.; Hupp, J. T.; Huo, F. *Nat. Chem.* **2012**, *4* (4), 310–316.
- Lu, X.; Zhang, W.; Wang, C.; Wen, T.-C.; Wei, Y. *Prog. Polym. Sci.* **2011**, *36* (5), 671–712.
- Luebke, R.; Weseliński, Ł. J.; Belmabkhout, Y.; Chen, Z.; Wojtas, Ł.; Eddaoudi, M. *Crys. Growth Des.* **2014**, *14* (2), 414–418.
- Ma, J.; Huang, X.; Song, X.; Liu, W. *Chem. Eur. J.* **2013**, *19* (11), 3590–3595.
- Ma, L.; Abney, C.; Lin, W. *Chem. Soc. Rev.* **2009**, *38* (5), 1248–1256.
- Ma, S.; Sun, D.; Ambrogio, M.; Fillinger, J. A.; Parkin, S.; Zhou, H.-C. *J. Am. Chem. Soc.* **2007**, *129* (7), 1858–1859.
- Maignan, A.; Hardy, V.; Hébert, S.; Drillon, M.; Lees, M. R.; Petrenko, O.; Paul, D. M. K.; Khomskii, D. *J. Mater. Chem.* **2004**, *14* (8), 1231–1234.
- Manna, B.; Chaudhari, A. K.; Joarder, B.; Karmakar, A.; Ghosh, S. K. *Angew. Chem., Int. Ed.* **2013**, *52* (3), 998–1002.
- Manna, K.; Zhang, T.; Greene, F. X.; Lin, W. *J. Am. Chem. Soc.* **2015**, *137* (7), 2665–2673.
- Marx, S.; Kleist, W.; Baiker, A. *J. Catal.* **2011**, *281* (1), 76–87.
- Meng, W.; Li, H.; Xu, Z.; Du, S.; Li, Y.; Zhu, Y.; Han, Y.; Hou, H.; Fan, Y.; Tang, M. *Chem. Eur. J.* **2014**, *20* (10), 2945–2952.
- Miller, J. S.; Gatteschi, D. *Chem. Soc. Rev.* **2011**, *40* (6), 3065–3066.
- Millward, A. R.; Yaghi, O. M. *J. Am. Chem. Soc.* **2005**, *127* (51), 17998–17999.

- Mingalieva, L. V.; Voronkova, V. K.; Galeev, R. T.; Sukhanov, A. A.; Melnik, S.; Prodius, D.; Turta, K. I. *Appl. Magn. Reson.* **2009**, *37* (1–4), 737–750.
- Miyaura, N.; Ishiyama, T.; Sasaki, H.; Ishikawa, M.; Sato, M.; Suzuki, A. *J. Am. Chem. Soc.* **1989**, *111* (1), 314–321.
- Miyaura, N.; Ishiyama, T.; Sasaki, H.; Ishikawa, M.; Sato, M.; Suzuki, A. *J. Am. Chem. Soc.* **1989**, *111* (1), 314–321.
- Molander, G. A.; Biolatto, B. *J. Org. Chem.* **2003**, *68* (11), 4302–4314.
- *Molecular nanomagnets and related phenomena*; Gao, S., Affronte, M., Eds.; Structure and Bonding; Springer: Berlin, **2015**.
- Mondal, S. S.; Thomas, A.; Holdt, H.-J. *Microporous Mesoporous Mater.* **2015**, *216*, 2–12.
- Motokawa, N.; Matsunaga, S.; Takaishi, S.; Miyasaka, H.; Yamashita, M.; Dunbar, K. R. *J. Am. Chem. Soc.* **2010**, *132* (34), 11943–11951.
- Mukherjee, P. S.; Maji, T. K.; Mostafa, G.; Mallah, T.; Chaudhuri, N. R. *Inorg. Chem.* **2000**, *39* (22), 5147–5150.
- Murray, L. J.; Dincă, M.; Long, J. R. *Chem. Soc. Rev.* **2009**, *38* (5), 1294–1314.
- Murray, L. J.; Dinca, M.; Yano, J.; Chavan, S.; Bordiga, S.; Brown, C. M.; Long, J. R. *J. Am. Chem. Soc.* **2010**, *132* (23), 7856–7857.
- Myers, A. L.; Prausnitz, J. M. *AIChE* **1965**, *11* (1), 121–127.
- Natarajan, S.; Mahata, P. *Chem. Soc. Rev.* **2009**, *38* (8), 2304–2318.
- Norby, P.; Fjellvåg, H. *Zeolites* **1992**, *12* (8), 898–908.
- Nouar, F.; Eckert, J.; Eubank, J. F.; Forster, P.; Eddaoudi, M. *J. Am. Chem. Soc.* **2009**, *131* (8), 2864–2870.
- Nugent, P.; Pham, T.; McLaughlin, K.; Georgiev, P. A.; Lohstroh, W.; Embs, J. P.; Zaworotko, M. J.; Space, B.; Eckert, J. *J. Mater. Chem. A* **2014**, *2* (34), 13884–13891.

- Nuñez, A. J.; Chang, M. S.; Ibarra, I. A.; Humphrey, S. M. *Inorg. Chem.* **2014**, *53* (1), 282–288.
- Nuzhdin, A. L.; Dybtsev, D. N.; Bryliakov, K. P.; Talsi, E. P.; Fedin, V. P. *J. Am. Chem. Soc.* **2007**, *129* (43), 12958–12959.
- O'Keeffe, M. O.; Yaghi, O. M. *Chem. Rev.* **2012**, *112* (2), 675-702.
- Orchard, A. F. *Magnetochemistry*, Oxford University Press: New York, USA, 2003.
- Ozturk, Z.; Kose, D. A.; Sahin, Z. S.; Ozkan, G.; Asan, A. *Int. J. Hydrogen Energy* **2016**, *41* (28), 12167–12174.
- Pagot, M.; Toniolo, L.; Antonetti, C.; Forte, C.; Galletti, A. M. R. *J. Mol. Catal. A: Chem.* **2015**, *410*, 202–208.
- Park, H. J.; Suh, M. P. *Chem. Commun.* **2010**, *46* (4), 610–612.
- Parkes, M. V.; Greathouse, J. A.; Hart, D. B.; Gallis, D. F. S.; Nenoff, T. M. *Phys. Chem. Chem. Phys.* **2016**, *18* (16), 11528–11538.
- Parnham, E. R.; Morris, R. E. *Acc. Chem. Res.* **2007**, *40* (10), 1005–1013.
- Pedersen, K. S.; Ariciu, A.-M.; McAdams, S.; Weihe, H.; Bendix, J.; Tuna, F.; Piligkos, S. *J. Am. Chem. Soc.* **2016**, *138* (18), 5801–5804.
- Peters, D.; McCulloch, I. P.; Selke, W. *Phys. Rev. B* **2009**, *79* (13), 132406.
- Pirngruber, G. D.; Llewellyn, P. L. In Metal-Organic Frameworks; Farrusseng, D., Ed.; Wiley-VCH Verlag GmbH & Co. KGaA, 2011; pp 99–119.
- Plabst, M.; Köhn, R.; Bein, T. *CrystEngComm* **2010**, *12* (6), 1920–1926.
- Poudeu, P. F. P.; Takas, N.; Anglin, C.; Eastwood, J.; Rivera, A. *J. Am. Chem. Soc.* **2010**, *132* (16), 5751–5760.
- Punji, B.; Mague, J. T.; Balakrishna, M. S. *Inorg. Chem.* **2007**, *46* (24), 10268–10275.
- Quinby, M. S.; Feltham, R. D. Inorg. Chem. 1972, 11 (10), 2468–2476.

- Robinson, A. L.; Stavila, V.; Zeitler, T. R.; White, M. I.; Thornberg, S. M.; Greathouse, J. A.; Allendorf, M. D. *Anal. Chem.* **2012**, *84* (16), 7043–7051.
- Rocha, J.; Carlos, L. D.; Paz, F. A. A.; Ananias, D. *Chem. Soc. Rev.* **2011**, *40* (2), 926–940.
- Rollmann, L. D.; Valyocsik, E. W.; Shannon, R. D. In *Inorganic Syntheses*; Murphy, D. W., Interrante, L. V., Eds.; John Wiley & Sons, Inc., 1995; pp 227–234.
- Rowsell, J. L. C.; Eckert, J.; Yaghi, O. M. *J. Am. Chem. Soc.* **2005**, *127* (42), 14904–14910.
- Rowsell, J. L. C.; Yaghi, O. M. *Angew. Chem., Int. Ed.* **2005**, *44* (30), 4670–4679.
- Rowsell, J. L. C.; Yaghi, O. M. *J. Am. Chem. Soc.* **2006**, *128* (4), 1304–1315.
- Rui, Z.; James, J. B.; Kasik, A.; Lin, Y. S. *AIChE J.* **2016**, ahead of print.
- Saccoccia, B.; Bohnsack, A. M.; Waggoner, N. W.; Cho, K. H.; Lee, J. S.; Hong, D.-Y.; Lynch, V. M.; Chang, J.-S.; Humphrey, S. M. *Angew. Chem. Int. Ed.* **2015**, *54* (18), 5394–5398.
- Sakai, T.; Takahashi, M. *Phys. Rev. B* **1998**, *50* (9), 6277-6288.
- Salih, Z. I.; Guo, Y.-J.; Zheng, J.-J.; Zhao, X. *Comput. Theor. Chem.* **2015**, *1058*, 28–33.
- Samouei, H.; Miloserdov, F. M.; Escudero-Adán, E. C.; Grushin, V. V. *Organometallics* **2014**, *33* (24), 7279–7283.
- Samui, A.; Chowdhuri, A. R.; Mahto, T. K.; Sahu, S. K. *RSC Adv.* **2016**, *6* (71), 66385–66393.
- Sava Gallis, D. F.; Parkes, M. V.; Greathouse, J. A.; Zhang, X.; Nenoff, T. M. *Chem. Mater.* **2015**, *27* (6), 2018–2025.
- Sawano, T.; Lin, Z.; Boures, D.; An, B.; Wang, C.; Lin, W. *J. Am. Chem. Soc.* **2016**, *138* (31), 9783–9786.

- Sawano, T.; Thacker, N. C.; Lin, Z.; McIsaac, A. R.; Lin, W. *J. Am. Chem. Soc.* **2015**, *137* (38), 12241–12248.
- Schaate, A.; Klingelhöfer, S.; Behrens, P.; Wiebcke, M. *Cryst. Growth Des.* **2008**, *8* (9), 3200–3205.
- Schäfer, P.; Veen, M. A. van der; Domke, K. F. *Chem. Commun.* **2016**, *52* (25), 4722–4725.
- Sessoli, R.; Gatteschi, D.; Caneschi, A.; Novak, M. A. *Nature* **1993**, *365* (6442), 141–143.
- Sessoli, R.; Powell, A. K. *Coord. Chem. Rev.* **2009**, *253* (19–20), 2328–2341.
- Sheldon, R. A.; Downing, R. S. *Appl. Catal., A* **1999**, *189* (2), 163–183.
- Sing, K. Colloids and Surfaces A: Physicochemical and Engineering Aspects 2001, 187–188, 3–9.
- Sing, K. S. W. *Adv. Colloid Interface Sci.* **1998**, *76–77*, 3–11.
- Singh-Wilmot, M. A.; Sinclair, R. A.; Andrews, M.; Rowland, C.; Cahill, C. L.; Murugesu, M. *Polyhedron* **2013**, *53*, 187–192.
- *Single-Molecule Magnets and Related Phenomena*; Winpenny, R., Ed.; Structure and Bonding; Springer-Verlag: Berlin/Heidelberg, 2006; Vol. 122, pp 164-206.
- Siriwardane, R. V.; Shen, M.-S.; Fisher, E. P.; Poston, J. A. *Energy Fuels* **2001**, *15* (2), 279–284.
- Siu, P. W.; Brown, Z. J.; Farha, O. K.; Hupp, J. T.; Scheidt, K. A. *Chem. Commun.* **2013**, *49* (93), 10920–10922.
- Skumryev, V.; Stoyanov, S.; Zhang, Y.; Hadjipanayis, G.; Givord, D.; Nogués, J. *Nature* **2003**, *423* (6942), 850–853.
- Southon, P. D.; Price, D. J.; Nielsen, P. K.; McKenzie, C. J.; Kepert, C. J. *J. Am. Chem. Soc.* **2011**, *133* (28), 10885–10891.

- Standfest-Hauser, C. M.; Mereiter, K.; Schmid, R.; Kirchner, K. *Organometallics* **2004**, *23* (9), 2194–2196.
- Stock, N.; Biswas, S. *Chem. Rev.* **2012**, *112* (2), 933–969.
- Su, L.; Song, W.-C.; Zhao, J.-P.; Liu, F.-C. *Chem. Commun.* **2016**, *52* (56), 8722–8725.
- Su, S.; Wang, S.; Song, X.; Song, S.; Qin, C.; Zhu, M.; Hao, Z.; Zhao, S.; Zhang, H. *Dalton Trans.* **2012**, *41* (16), 4772–4779.
- Subramani, V.; Gangwal, S. K. *Energy Fuels* **2008**, *22* (2), 814–839.
- Sumida, K.; Rogow, D. L.; Mason, J. A.; McDonald, T. M.; Bloch, E. D.; Herm, Z. R.; Bae, T.-H.; Long, J. R. *Chem. Rev.* **2012**, *112* (2), 724–781.
- Sun, H.-L.; Wang, Z.-M.; Gao, S. *Chem. Eur. J.* **2009**, *15* (7), 1757–1764.
- Sun, H.-L.; Wang, Z.-M.; Gao, S. *Coord. Chem. Rev.* **2010**, *254* (9–10), 1081–1100.
- Tafipolsky, M.; Amirjalayer, S.; Schmid, R. *Microporous Mesoporous Mater.* **2010**, *129* (3), 304–318.
- Takei, I.; Nishibayashi, Y.; Ishii, Y.; Mizobe, Y.; Uemura, S.; Hidai, M. *J. Organomet. Chem.* **2003**, *679* (1), 32–42.
- Tanabe, K. K.; Cohen, S. M. *Chem. Soc. Rev.* **2011**, *40* (2), 498–519.
- Taylor, K. M. L.; Jin, A.; Lin, W. *Angew. Chem., Int. Ed.* **2008**, *47* (40), 7722–7725.
- Thallapally, P. K.; Tian, J.; Radha Kishan, M.; Fernandez, C. A.; Dalgarno, S. J.; McGrail, P. B.; Warren, J. E.; Atwood, J. L. *J. Am. Chem. Soc.* **2008**, *130* (50), 16842–16843.
- Thompson, D. A.; Best, J. S. *IBM J. Res. Develop.* **2000**, *44* (3), 311-322.
- Tian, Y.-Q.; Zhao, Y.-M.; Chen, Z.-X.; Zhang, G.-N.; Weng, L.-H.; Zhao, D.-Y. *Chem. Eur. J.* **2007**, *13* (15), 4146–4154.
- Timofeeva, M. N.; Panchenko, V. N.; Jun, J. W.; Hasan, Z.; Matrosova, M. M.; Jhung, S. H. *Appl. Catal., A* **2014**, *471*, 91–97.

- Tsivion, E.; Long, J. R.; Head-Gordon, M. *J. Am. Chem. Soc.* **2014**, *136* (51), 17827–17835.
- U. S. Energy Information Administration; http://www.eia.gov/energy_in_brief/article/major_energy_sources_and_users.cfm. (accessed: August 1, 2016)
- Valenzano, L.; Civalleri, B.; Chavan, S.; Bordiga, S.; Nilsen, M. H.; Jakobsen, S.; Lillerud, K. P.; Lamberti, C. *Chem. Mater.* **2011**, *23* (7), 1700–1718.
- Vaz, M. G. F.; Cassaro, R. A. A.; Akpinar, H.; Schlueter, J. A.; Lahti, P. M.; Novak, M. A. *Chemistry **2014,** 20* (18), 5460–5467.
- Vaz, M. G. F.; Cassaro, R. A. A.; Akpinar, H.; Schlueter, J. A.; Lahti, P. M.; Novak, M. A. *Chemistry* **2014**, *20* (18), 5460–5467.
- Venkatasubramanian, A.; Lee, J.-H.; Stavila, V.; Robinson, A.; Allendorf, M. D.; Hesketh, P. J. *Sens. Actuators, B* **2012**, *168*, 256–262.
- Verma, P.; Maurice, R.; Truhlar, D. G. *J. Phys. Chem. C* **2015**, *119* (51), 28499–28511.
- Verma, P.; Maurice, R.; Truhlar, D. G. *J. Phys. Chem. C* **2015**, *119* (51), 28499–28511.
- Vermoortele, F.; Bueken, B.; Le Bars, G.; Van de Voorde, B.; Vandichel, M.; Houthoofd, K.; Vimont, A.; Daturi, M.; Waroquier, M.; Van Speybroeck, V.; Kirschhock, C.; De Vos, D. E. *J. Am. Chem. Soc.* **2013**, *135* (31), 11465–11468.
- Volkringer, C.; Henry, N.; Grandjean, S.; Loiseau, T. *J. Am. Chem. Soc.* **2012**, *134* (2), 1275–1283.
- Waggoner, N. W.; Allen, P. K.; Lynch, V. M.; Kornfuehrer, T.; Humphrey, S. M. *Chem. Sci.* **2016**, in draft.
- Waggoner, N. W.; Bohnsack, A. M.; Humphrey, S. M. Metal-organic frameworks for applications as sensing materials. In *Functional Metallosupramolecular Materials*, Hardy, J. G., Schacher, F. H., Eds.; Royal Society of Chemistry, Cambridge, United Kingdom, 2015, 192-245.

- Waggoner, N. W.; Saccoccia, B.; Ibarra, I. A.; Lynch, V. M.; Wood, P. T.; Humphrey, S. M. *Inorg. Chem.* **2014**, *53* (24), 12674–12676.
- Wang, B.; Lv, X.-L.; Feng, D.; Xie, L.-H.; Zhang, J.; Li, M.; Xie, Y.; Li, J.-R.; Zhou, H.-C. *J. Am. Chem. Soc.* **2016**, *138* (19), 6204–6216.
- Wang, C.; Lee, M.; Liu, X.; Wang, B.; Chen, J. P.; Li, K. *Chem. Commun.* **2016**, *52* (57), 8869–8872.
- Wang, C.; Liu, D.; Lin, W. *J. Am. Chem. Soc.* **2013**, *135* (36), 13222–13234.
- Wang, C.; Xie, Z.; deKrafft, K. E.; Lin, W. *J. Am. Chem. Soc.* **2011**, *133* (34), 13445–13454.
- Wang, H.-M.; Liu, H.-P.; Chu, T.-S.; Yang, Y.-Y.; Hu, Y.-S.; Liu, W.-T.; Ng, S. W. *RSC Adv.* **2014**, *4* (27), 14035–14041.
- Wang, J.; Lin, Y.; Yue, Q.; Tao, K.; Kong, C.; Chen, L. *RSC Adv.* **2016**, *6* (58), 53017–53024.
- Wang, S.; Cao, T.; Yan, H.; Li, Y.; Lu, J.; Ma, R.; Li, D.; Dou, J.; Bai, J. *Inorg. Chem.* **2016**, *55* (11), 5139–5151.
- Wang, Z.; Cohen, S. M. *J. Am. Chem. Soc.* **2007**, *129* (41), 12368–12369.
- Wee, L. H.; Alaerts, L.; Martens, J. A.; De Vos, D. In *Metal-Organic Frameworks*; Farrusseng, D., Ed.; Wiley-VCH Verlag GmbH & Co. KGaA: Weinheim, Germany, 2011; pp 191–212.
- Wei, X.; Zheng, L.; Luo, F.; Lin, Z.; Guo, L.; Qiu, B.; Chen, G. *J. Mater. Chem. B* **2013**, *1* (13), 1812.
- Weihe, H.; Güdel, H. U. *Inorg. Chem.* **1997**, *36* (17), 3632–3639.
- Weitkamp, E. A.; Lambe, A. T.; Donahue, N. M.; Robinson, A. L. *Environ. Sci. Technol.* **2008**, *42* (21), 7950–7956.
- Weller, D.; Moser, A. *IEEE Trans. Magn.* **1999**, *35* (6), 4423-4439.

- Wikipedia, the free encyclopedia; https://en.wikipedia.org/wiki/Coordination_polymer (accessed: July 27, 2016).
- Woodruff, D. N.; Winpenny, R. E. P.; Layfield, R. A. *Chem. Rev.* **2013**, *113* (7), 5110–5148.
- Wu, C.-D.; Hu, A.; Zhang, L.; Lin, W. *J. Am. Chem. Soc.* **2005**, *127* (25), 8940–8941.
- Wu, H.; Chua, Y. S.; Krungleviciute, V.; Tyagi, M.; Chen, P.; Yildirim, T.; Zhou, W. *J. Am. Chem. Soc.* **2013**, *135* (28), 10525–10532.
- Wu, P.; Guo, X.; Cheng, L.; He, C.; Wang, J.; Duan, C. *Inorg. Chem.* **2016**, *55* (16), 8153-8159.
- Wu, Y.-L.; Guo, F.-S.; Yang, G.-P.; Wang, L.; Jin, J.-C.; Zhou, X.; Zhang, W.-Y.; Wang, Y.-Y. *Inorg. Chem.* **2016**, *55* (13), 6592–6596.
- Xi, W.; Liu, Y.; Xia, Q.; Li, Z.; Cui, Y. *Chem. Eur. J.* **2015**, *21* (36), 12581–12585.
- Xie, W.; Peng, H.; Chen, L. *Appl. Catal., A* **2006**, *300* (1), 67–74.
- Xu, L.; Luo, Y.; Sun, L.; Pu, S.; Fang, M.; Yuan, R. -X.; Du, H. -B. *Dalton Trans.* **2016**, *45* (20), 8614-8621.
- Yamamoto, S.; Miyashita, S. *Phys. Rev. B* **1994**, *50* (9), 6277–6288.
- Yang, C.; Wang, X.; Omary, M. A. *J. Am. Chem. Soc.* **2007**, *129* (50), 15454–15455.
- Yang, J.; Ye, H.; Zhao, F.; Zeng, B. ACS *Appl. Mater. & Interfaces* **2016**, *8* (31), 20407–20414.
- Yang, J.; Zhou, L.; Cheng, J.; Hu, Z.; Kuo, C.; Pao, C.-W.; Jang, L.; Lee, J.-F.; Dai, J.; Zhang, S.; Feng, S.; Kong, P.; Yuan, Z.; Yuan, J.; Uwatoko, Y.; Liu, T.; Jin, C.; Long, Y. *Inorg. Chem.* **2015**, *54* (13), 6433–6438.
- Yang, R. T., *Adsorbents: Fundamentals and Applications*, John Wiley & Sons, Hoboken, 2003.
- Yu, Q. L.; Ballari, M. M.; Brouwers, H. J. H. *Appl. Catal., B* **2010**, *99* (1–2), 58–65.

- Yuan, S.; Chen, Y.-P.; Qin, J.-S.; Lu, W.; Zou, L.; Zhang, Q.; Wang, X.; Sun, X.; Zhou, H.-C. *J. Am. Chem. Soc.* **2016**, *138* (28), 8912–8919.
- Zacher, D.; Shekhah, O.; Wöll, C.; Fischer, R. A. *Chem. Soc. Rev.* **2009**, *38* (5), 1418–1429.
- Zhang, P.; Guo, Y.-N.; Tang, J. *Coord. Chem. Rev.* **2013**, *257* (11–12), 1728–1763.
- Zhang, R.; Ji, S.; Wang, N.; Wang, L.; Zhang, G.; Li, J.-R. *Angew. Chem., Int. Ed.* **2014**, *53* (37), 9775–9779.
- Zhang, S.; Wang, L.; Feng, X.; Bao, M. *Org. Biomol. Chem.* **2014**, *12* (37), 7233–7237.
- Zhang, X.; Vieru, V.; Feng, X.; Liu, J.-L.; Zhang, Z.; Na, B.; Shi, W.; Wang, B.-W.; Powell, A. K.; Chibotaru, L. F.; Gao, S.; Cheng, P.; Long, J. R. *Angew. Chem. Int. Ed.* **2015**, *54* (34), 9861–9865.
- Zhao, B.; Peng, X.; Wang, Z.; Xia, C.; Ding, K. *Chem. Eur. J.* **2008**, *14* (26), 7847–7857.
- Zhao, Y.-P.; Li, Y.; Cui, C.-Y.; Xiao, Y.; Li, R.; Wang, S.-H.; Zheng, F.-K.; Guo, G.-C. *Inorg. Chem.* **2016**, *55* (15), 7335–7340.
- Zhou, H. -C.; Long, J. R.; Yaghi, O. M. *Chem. Rev.* **2012**, *112* (2), 673-674.
- Zhou, X.; Xia, S.; Tanner, P. A. J. Phys. Chem. B 2007, 111 (30), 8677–8679.
- Zhu, Q.; Shen, C.; Tan, C.; Sheng, T.; Hu, S.; Wu, X. *Chem. Commun.* **2012**, *48* (4), 531–533.